

UNCLASSIFIED

AD NUMBER

AD410522

NEW LIMITATION CHANGE

TO

Approved for public release, distribution
unlimited

FROM

Distribution authorized to U.S. Gov't.
agencies and their contractors;
Administrative/Operational Use; Jan 1963.
Other requests shall be referred to the
Office of Civil Defense, Washington, DC.

AUTHORITY

OCD D/A ltr, 23 Jun 1969

THIS PAGE IS UNCLASSIFIED

UNCLASSIFIED

410522

DEFENSE DOCUMENTATION CENTER

FOR

SCIENTIFIC AND TECHNICAL INFORMATION

CAMPUS STATION, ALEXANDRIA, VIRGINIA



Best Available Copy

UNCLASSIFIED

NOTICE: When government or other drawings, specifications or other data are used for any purpose other than in connection with a definitely related government procurement operation, the U. S. Government thereby incurs no responsibility, nor any obligation whatsoever; and the fact that the Government may have formulated, furnished, or in any way supplied the said drawings, specifications, or other data is not to be regarded by implication or otherwise as in any manner licensing the holder or any other person or corporation, or conveying any rights or permission to manufacture, use or sell any patented invention that may in any way be related thereto.

410521

EDC

Volume 1

FALLOUT AND RADIOLOGICAL COUNTERMEASURES

Prepared for:

OFFICE OF CIVIL DEFENSE
DEPARTMENT OF DEFENSE
WASHINGTON, D.C.

STANFORD RESEARCH INSTITUTE

MENLO PARK, CALIFORNIA

410522



40-522
January 1963

Volume 1

FALLOUT AND RADIOLOGICAL COUNTERMEASURES

Prepared for:

OFFICE OF CIVIL DEFENSE
DEPARTMENT OF DEFENSE
WASHINGTON, D.C.

By: Carl E. Miller

SRI Project No. IM-4021

Approved:

Robert A. Harker
ROBERT A. HARKER, DIRECTOR
MANAGEMENT SCIENCES DIVISION

This report has been reviewed in the
Office of Civil Defense and approved
for publication. Approval does not
signify that the contents necessarily
reflect the views and policies of the
Office of Civil Defense.

CONTENTS

1	THE NATURE OF FALLOUT	1
1.1	Background	1
1.2	A General Description of Fallout	3
1.3	Characteristic Types of Fallout	4
1.4	Potential Hazards from Fallout	4
1.5	Radioactive Decay	7
1.6	The Standard Intensity and Contour Properties	9
	Chapter 1 References	11
2	FORMATION OF FALLOUT PARTICLES	13
2.1	General Definition of the Process	13
2.2	Mass-Chain Yields for the Fission of U-235, U-238 and Pu-239	17
2.3	The Structure and Composition of Individual Fallout Particles	28
2.3.1	Low Yield, Surface Shot, Silicate Soil	28
2.3.2	Low Yield, Underground Shot, Silicate Soil	31
2.3.3	Large Yield, Surface Shot, Coral	31
2.3.4	Tower Shot, Silicate Soil	38
2.3.5	Tower Shot, Coral Soil	41
2.3.6	Surface Shot, Ocean (Sea Water)	43
2.3.7	Inferences on Fallout-Particle Formation Processes	48
2.4	Properties of Small Fallout Particles from Detonations at Weapons Tests	72
2.5	Redistribution of Deposited Fallout	78
2.6	The Collection and Retention of Fallout Particles by Plant Foliage	81
	Chapter 2 References	83

CONTENTS

3	A THERMODYNAMIC MODEL OF FALLOUT FORMATION	97
3.1	The Condensation Process	97
3.1.1	Gas-Liquid Phase Condensation	99
3.1.2	Gas-Liquid Phases: Material Balance Constraints and Fractionation Numbers	106
3.1.3	Gas-Liquid Phase Condensation--Particle-Size Effects	111
3.2	The Dependence of Fireball Parameters on Weapon Yield and Time After Detonation	115
3.3	Estimates of Fireball Parameters for a Model Surface Burst on a Soil Consisting of Silicate Minerals	130
3.4	Process for Estimating the Concentration of Liquid Soil in the Fireball of a Model Surface Burst and the Fractionation Numbers of the Radionuclides	146
3.5	Computing the Decay Rates of Fission Product Mixtures	177
	Chapter 3 References	201
4	DISTRIBUTION OF FALLOUT PARTICLES FOLLOWING A NUCLEAR DETONATION	203
4.1	General Description of the Fallout Distribution Process	203
4.1.1	The Particle Source Geometry	203
4.1.2	The Particle Fall Trajectory	203
4.1.3	Radiological Factors	204
4.2	Mathematical Descriptions of the Fallout Distribution Process	204
4.2.1	Scaling Methods	204
4.2.2	Mathematical Models	204
4.3	Descriptive Features of a Simplified Fallout Scaling System for Land Surface Detonations	206
4.3.1	General Description of the Scaling Method	206
4.3.2	Particles Falling from Cloud Altitudes	207
4.3.3	Particles Falling from Stem Altitudes	211
4.3.4	Methods for Estimating the Dynamics of the Fallout Deposition	220
4.3.5	Estimation of Ionization Rate and Exposure Dose	223
	Chapter 4 References	227

CONTENTS

B CORRELATION OF BOMBING MODEL PARAMETERS WITH OBSERVED FALLOUT-PATTERN FEATURES	220
B.1 General Description of Fallout Patterns from Land Surface Detonations	220
B.2 General Conditions to Which the Source Data Apply	231
B.3 Scaling Functions for Fallout Pattern Features of Interest	232
B.3.1 Intensity Ridge Near Ground Zero	232
B.3.2 Location of the Downwind Standard Intensity Contour for Fallout from Stem Altitudes	237
B.3.3 Stem Pattern Half-Width	239
B.3.4 The Distance to Fallout Pattern Features for Fallout from Cloud Altitudes	239
B.3.5 The Intensity Levels of Pattern Features for Fallout from Cloud Altitudes	241
B.3.6 The Maximum Pattern Width	243
B.3.7 Areas and Fraction of Total Activity Within Intensity Contours	245
B.4 Summary of Derived Idealized Fallout Pattern Scaling Functions	246
B.5 Illustrative Computations for the Use of the Simplified Fallout Scaling System	255
B.5.1 Construction of Idealized Fallout Patterns	255
B.5.2 Fallout Arrival Rate and Exposure Dose During Fallout Arrival	260
B.5.3 Method for Estimating the Particle Sizes in the Fallout at a Given Location	270
B.6 The Effect of Cross-Wind Shear on the Fallout Pattern Scaling System	288
B.7 Comparison of Several Fallout Pattern Computations	298
Chapter B References	300
C IONIZATION RATE CONTOUR RATIOS AND COMPOSITION OF FALLOUT	301
C.1 Definition and Use of Ionization Rate Contour Ratios	301
C.2 Dependence of the Mass Contour Ratio on Detonation Conditions and Other Parameters	302

CONTENTS

6.2	Continued	
6.2.1	Dependence on Weapon Type and Yield	302
6.2.2	Dependence on Downwind Distance from Shot Point	304
6.2.3	Dependence on Height or Depth of Burst	320
6.2.4	Mass Contour Ratio for Fallout from a Surface Detonation on Deep Sea Water	327
6.2.5	Mass Contour Ratio for Fallout from Detonations in Harbors	330
6.2.6	Mass Contour Ratio for Fallout from a 1-MT Detonation at Several Detonation Geometries	335
6.3	Fission-Product and Fraction-of-Device Contour Ratios	338
6.4	Foltage-Contamination Factor Contour Ratio	339
6.4.1	Insoluble-Nuclide Fractions	341
6.4.2	Soluble-Nuclide Fractions	342
6.4.3	Variation of the Foltage-Contamination Factor with Particle Size	343
	Chapter 6 References	349

ILLUSTRATIONS

Figure		Page
2.1	Thin Section and Radiograph of Some Fallout Particles from a Small-Yield Surface Shot at the Nevada Test Site	29
2.2	Thin Section and Radiograph of a Fallout Particle from a Small-Yield Surface Shot at the Nevada Test Site	33
2.3	Thin Section and Radiograph of an Angular Fallout Particle from a Large-Yield Surface Shot at the Eniwetok Proving Ground	34
2.4	Section of a Fallout Particle from a Large-Yield Surface Shot at the Eniwetok Proving Ground	35
2.5	Thin Section and Radiograph of a Spherical Fallout Particle from a Large-Yield Surface Shot at the Eniwetok Proving Ground	37
2.6	Two Fallout Particles from a Tower Shot at the Nevada Test Site	39
2.7	Thin Section and Radiograph of a Fallout Particle from a Moderate-Yield Tower Shot at the Nevada Test Site	40
2.8	Thin Section and Radiograph of a Fallout Particle from a Moderate-Yield Tower Shot at the Eniwetok Proving Ground	40
2.9	Thin Section and Radiograph of a Fallout Particle from a Moderate-Yield Tower Shot at the Eniwetok Proving Ground	44
2.10	Photomicrograph of a Dichromate Reagent Film of an Individual Liquid Fallout Particle from a Large-Yield Barge Shot at the Eniwetok Proving Ground	46

ILLUSTRATIONS

Figure	Page
2.11 Electromicrograph of the Radioactive Nails in the Liquid Fallout Particles from a Large-Yield Barge Shot at the Enewetak Proving Ground	47
2.12 Calculated Fraction of Mass Chain 89, 90, 137, and 140 Condensed as a Function of Time after Fission with Indicated Non-condensing Elements	64
2.13 Plot of Calculated r_n (λ) Values for Mass Numbers 89, 137, and 140 against Those of Mass Number 89 for the Assumption that Only the Alkali Metal Elements and Alkaline Earth Elements in the Chain Condense	65
2.14 Reduction in the Ionization Rate at the Center of 10th Street and at the Center of the Plaza, Camp Parks, California	82
2.15 Accumulated Distribution of Number of Particles Having Different Diameters on Foliage	83
2.16 Distribution of Activity as a Function of Particle Diameter for Local Collections of Fallout from Tower-Mounted Detonations	86
3.1 Fraction of Nitrogen Molecules Dissociated as a Function of Temperature and Total Pressure	122
3.2 Fraction of Oxygen Molecules Dissociated as a Function of Temperature and Pressure	123
3.3 The Calculated Variation of n/W , P_A , n_A/n , and n_A/W with Assumed Values of $T_A(a)$ for the Model Surface-Burst Fireball	140
3.4 Comparison of Calculations of the Activity and Photon Emission Rate of the Fission Products from 14-Mev Neutron Fission of U-238 with Those from 8-Mev Neutron Fission of U-238 Given as a Ratio of the Two with Time after Fission	183

ILLUSTRATIONS

Figure	Page
3.6 The Gross Air Ionization Rate Fractionation Number, r_{ip} , Relative to the Ionization Rate of the Fission Products from Thermal Neutron Fission of U-235, for the Fission Product Mixtures from Other Fissile Nuclides and Neutron Energies	185
3.6 The Gross Air Ionization Rate Fractionation Number, r_{ip} , Relative to the Ionization Rate of the Fission Products from Thermal Neutron Fission of U-235, for the Fission Product Mixtures from Other Fissile Nuclides and Neutron Energies	186
3.7 The Number of Photons per Disintegration for the Normal Mixture of Fission Products from 8-Mev Neutron Fission of U-238	188
3.8 The Average Energy of the Photons from the Normal Mixture of Fission Products from 8-Mev Neutron Fission of U-238	189
3.9 The Relative Response of the AN/PDR-38(T1B) Portable Radiac Held by a Man at 3 Feet above An Extended Plane Area Contaminated with Fission Products from Thermal Fission of U-235	191
3.10 Variation of r_{ip} with Time after Fission for the Fractionated Mixture of Fission Products from 8-Mev Neutron Fission of U-238	193
3.11 The Observed Variation of r_{ip} with Time after Fission for Close-in Fallout from a Low Tower Shot at the Nevada Test Site	195
3.1 Schematic Outline for the Intensity Profile Downwind from Ground Zero along the Axis of the Fallout Pattern ($y = 0$) as Used in the Simplified Fallout Pattern Scaling System	233
3.2 Intensity-Distance Plots for Construction of an Idealized Fallout Pattern for a 1-MT Yield Surface Detonation for a Wind Speed of 10 mph	267

ILLUSTRATIONS

Figure	Page
5.3 Identified Fallout Pattern for a 1-MT Yield Surface Burst for a Wind Speed of 15 mph and 100 Percent Pluton	268
5.4 First Estimate of the Dependence of $K_0(1)A_\alpha$ on α for a 1-MT Surface Detonation and Wind Speed of 15 mph	269
5.5 Variation of $K_0(1)A_\alpha(\alpha)$ with α at $X = 1.87 \times 10^3$ ft for $W = 10^3$ KT and a Wind Speed of 15 mph	270
5.6 Time of Arrival of the Various Particle Groups Designated by α For a Wind Speed of 15 mph	271
5.7 Rate of Activity Deposition on the Ground as a Function of α at $X = 1.87 \times 10^3$ ft, for $W = 10^3$ KT and a Wind Speed of 15 mph	272
5.8 Rate of Fallout Arrival as a Function of Time after Detonation at $X = 1.87 \times 10^3$ ft for $W = 10^3$ KT and a Wind Speed of 15 mph	273
5.9 Variation of Ionization Rate with Time after Detonation at $X = 1.87 \times 10^3$ ft for $W = 10^3$ KT and a Wind Speed of 15 mph	274
5.10 Variation of α_{\max} and α_{\min} with Downwind Distance for a 1-MT Yield Surface Detonation and Wind Speed of 15 mph	275
5.11 First Estimate of $K_0(1)A_\alpha$ as a function of α for Fallout from Stem Altitudes for a 10^3 KT Yield Surface Burst and a Wind Speed of 15 mph	276
5.12 Variation of the Ionization Rate with Time after Detonation at $X = 3.80 \times 10^3$ ft for $W = 10^3$ KT and a Wind Speed of 15 mph	277
5.13 Vertical Component of the Velocity for Spherical Particles Falling from Various Altitudes to Sea Level	278
	279

ILLUSTRATIONS

Figure	Page
5.14 Accumulated Activity Distribution as a Function of Particle Size at $X = 3.35 \times 10^4$ ft and 1.87×10^5 ft Downwind from the 1-MT Yield Surface Burst for a Wind Speed of 15-mph	286
5.15 Comparison of the Gross Activity Distribution on Particles of Various Diameters Derived from the Simplified Fallout Model to Distributions Used in Other Mathematical Fallout Models	287
5.16 Plot of Particle Fall Trajectory Components Relative to Estimated Pattern Center Line for Castle Bravo Winds	292
5.17 Variation of the Calculated Infinite (ideal Plane Standard) Intensity with Downwind Distance (Center Line of Pattern) for a 10-MT Yield Surface Detonation (100 percent Fission)	297
6.1 Calculated Ionization Rate as a Function of Time after Detonation for Assumed Condensations up to 60,174 and 408 Seconds after Fission of Fission Products from 8-Mev Neutron Emission of U-238 and an Assumed Surface Burst Total Yield of 14-MT	314
6.2 Estimated Percent of the Fission Product Activity in r/hr at 1 hr from the Fission Products Condensed on Particle Groups with α Values (15-mph Wind Speed) Less than a Stated Value	330
6.3 Proposed Curve for the Variation of $f(\alpha)$ with α for a 15-mph Wind Speed	334
6.4 Proposed Mass Correction Curve to the Mass Contour Ratio as a Function of the Nuclear Scaled Depth of Burst	338
6.5 Proposed Crater Depth Correction Curve for the Mass Contour Ratio as a Function of the Nuclear Scaled Depth	338
6.6 Variation of α_L with Calculated Values of α_n	346
6.7 Variation of the Median Particle Diameter of Fallout on Foliage with α_n of the Deposited Fallout	347

TABLES

Number		Page
2.1	Fractional Chain Yields for Mass 89 for U-235 Fission	19
2.2	Fractional Chain Yields for Mass 140 for U-235 Fission	19
2.3	Cumulative Mass-Chain Yields of Fission Products	20
2.4	Calculation of Relative Activity Ratios from Kimura's Data on Coral Fallout ²³	51
2.5	Percentage Activities in Ion Exchange Peaks of Different Chemical Groups in Coral Fallout Sample ²⁴	53
2.6	Summary of Estimated Fractionation Numbers for Beta-Emitting Nuclides in Coral Fallout from No. 8 Fukuryu Maru at D+21 and D+25	54
2.7	Radiochemical Data on Coral Type Fallout Particles from a Large Yield Surface Detonation	57
2.8	Summary of Fractionation Numbers for Mass Numbers 89 and 140 in Coral Fallout Particles	61
2.9	Summary of Fractionation Numbers Relative to Mass Number 89 for Coral and Seawater Fallout Corrected for Appropriate Fission Yields	65
2.10	Comparison of Empirical Fractionation-Correlation Parameters with Those Estimated for Condensation of Alkali and Alkaline Earth Elements of Mass Chains 89, 132, 137, and 140, at Specified Times after Fission	70
2.11	Relative Radionuclide Concentrations in Jack Rabbit Bone Tissue at about 20 Days after Detonation of Shot Smoky, Operation Plumbbob, in 1957	76
2.12	Average Fractionation Numbers of Radionuclides in Fallout from Tower- and Balloon-Supported Detonations at the Nevada Test Site	77
2.13	Gross Solubility of Activity from Small Fallout Particles	77

TABLES

Number		Page
2.14	Gross Solubility of Activity from Small Fallout Particles Lodged on Plant Foliage	79
2.15	The Size Distribution and Amount of Fallout Particles Lodged on the Foliage of Different Species of Plants	87
2.16	Collection and Retention of Fallout by Some Forage Crops	88
2.17	The Decontamination of Fallout Particles from Foliage	89
2.18	Summary of Averaged Foliage Contamination Factors for Native Foliage Exposed to Fallout from Tower- and Balloon-Mounted Detonations at the Nevada Test Site	91
3.1	Thermal Properties of Nitrogen and Oxygen as Ideal Gases	124
3.2	The Change in Energy Content and Number of Moles of Gas in Heating 1 Mole of Air as an Ideal Gas from 290°K and 1 Atmospheric Pressure to T°K at Pressures of 1 to 20 Atmospheres	126
3.3	Summary of Values of the Fireball Energy and Gas Content Related to Total Pressure, Volume, and Temperature for Heating Air from 295°K to 8300°K	127
3.4	Summary of Values of n_T/W and p_e for the Model Air Burst	136
3.5	Thermal Data for Ideal Soil Constituents of Composition $\text{Na}_2\text{O} \cdot \text{Al}_2\text{O}_3 \cdot 6\text{SiO}_2$	136
3.6	Summary of Calculations for $T_2(n)$ Based on the Assumption of Equal Vapor Densities at the Second Temperature Maximum for the Model Air- and Surface-Burst Fireballs	139
3.7	Summary of Fireball Conditions at the Second Temperature Maximum for the Model Surface Burst of Different Yields Using Eq. 3.192 for $T_2(n)$	141
3.8	Summary of Model Fireball Parameter Values for Various Yields of the Model Surface Burst	147
3.9	Summary of Fireball Parameters and Thermal Data for the 14-MT Yield Model Surface-Burst Fireball	149
3.10	Summary of Estimates of $n(\ell)/V$ for the Model Surface Burst of Different Yields at the Time the Fireball Temperature is 1673°K	153

TABLE III

Number		Page
3.11	Summary of Estimates of $n(r)/V$ or $n(\infty)V$ Based on Fission Content of Fallout	160
3.12	Summary of Empirical Constants for Vaporization Reactions of Fission Products and Other Elements	160
3.13	Summary of Raoult's Law Constants for the Gaseous Species of the Fission Product and Other Elements at 1673° K	160
3.14	Calculated Partial Pressures and Equilibrium Partial Pressures of Some of the More Abundant Fission Product Elements Dispersed Uniformly in the Model Surface-Burnt Fireball at 1673° K for a Fission Yield of 14-MT	167
3.15	Summary of $r_v(A)$ Values at 9 and 60 Seconds after Fission for Fission Product Nuclides that Contribute to the Gross Activity at 48.8 Minutes and Longer Times after Fission	169
3.16	Summary of Disintegration Multipliers for the Fission Product and Other Radionuclides ^a	171
3.17	Decay of Normal Fission Products from U-238, U-235, and Pu-239	178
3.18	Summary of H+1 Ionization Rates of Normal Fission Products ^a	187
3.19	Early-Time Ionization Rate, Photon Energy Emission Rate, and Average Photon Energy for Fission Products from Thermal Neutron Fission of U-238	192
3.20	Ionization Rate for Fission Products Condensed on Ideal Soil at 1400°C at 9 Seconds (84-KT) and 60 Seconds (14-MT) after Fission of U-238 (8-Mev Neutrons) and Ratio to That for the Normal Mixture from Fission of U-238 (Thermal Neutrons)	194
3.21	Activity from U-237 for 10^4 Atoms at Zero Time ^a ; C(U-237) = 1	197
3.22	Activity from U-239 for 10^4 Atoms at Zero Time ^a ; C(U-239) = 1	198
3.23	Activity from Np-239 for 10^4 Atoms of U-239 at Zero Time ^a ; C(U-239) = 1	199
3.24	Activity from Np-240 for 10^4 Atoms of U-240 at Zero Time ^a ; C(U-240) = 1	200

TABLES

Number		Page
4.1	Values of Stem and Fireball-Cloud Geometry Constants for Several Weapon Yields	214
5.1	Equation Parameter Values for the Variation of $\Delta z_{\theta, \alpha}$ with Wind Speed and Derived Values of $K_{\theta, \alpha} A_r$	237
5.2	Summary of the Relative Wind Speed Shear Factor $S(v_w)$, for the Fallout Pattern Maximum Half-width and Associated Standard Ionization Rate, for Several Wind Speeds	244
5.3	Summary of Fallout Pattern Features and Fallout Scaling System Parameter Values for an Assumed Effective Wind Speed of 15 mph	254
5.4	Comparison of Fallout Pattern Data for a 1-MT Yield Obtained from the Simplified Scaling System Functions and from the ENW Method	260
5.5	Calculation of Fallout Arrival Rate at $X = 1.87 \times 10^3$ feet, $y = 0$, from a 1-MT Surface Burst for a Wind Speed of 15 mph	261
5.6	Summation of Fallout Rates for α Groups Arriving at the Same Time and Accumulation of Activity and Exposure Dose during the Fallout Period	264
5.7	First Estimate of $K(1) A'_\alpha$ as a Function of α for a 1-MT Yield Surface Detonation	274
5.8	Calculated Arrival Times and Dose Rates during the Fallout Period and up to 1.8 hour at the Downwind Distance of 0.8 Miles from a 1-MT Surface Detonation	276
5.9	Diameters of Spherical Particles for Various α Groups Falling at 1.87×10^3 feet and 0.88×10^4 feet Downwind from a 1-MT Yield Surface Detonation Assuming a Wind Speed of 15 mph	284
5.10	Wind Data and Particle Fall Trajectory Components for Jangle "B" Shot	286

TABLES

Number		Page
6.11	Summary of "Equivalent" Uniform Wind Shear from Relative Pattern Spread for the Simple Fallout Scaling System Patterns (Wind Speed of 15 mph)	298
6.12	Ratio of Areas within Stated Standard Intensity Contours for Fallout Patterns Computed	299
6.1	Summary of Fission Product Nuclide $r/(A)$ Values for 84-KT and 14-MT Yield Surface Detonations	307
6.2	Equation Constants for Air Ionization Rates from 0.76 to 1.12 Hours after Fission and Fraction of the Total Ionization Rate at H+1 from Fission Products Condensed on Particles at Given Times after Detonation of an 84-KT and a 14-MT Yield Land Surface Burst	311
6.3	Calculated Ionization Rates of Condensed Fission Product Mixtures from U-238 (8-Mev Neutrons) Fission at Selected Condensation Times	313
6.4	Fractionation Numbers for U-238 (8-Mev Neutrons) Fission Products Relative to the Normal Mixture of U-238 (Thermal Neutrons) Fission Products as Calculated for the End of the First Period of Condensation and at 408 Seconds after Detonation	318
6.5	Computation of Particle Size Parameters for Various Condensation Times of the 84-KT and 14-MT Yield Land Surface Detonations	319
6.6	Calculation of $f(\alpha)$ from $M_p(1)$ Data from Operation Jangle Shot "B"	322
6.7	Computation of M_p for Several Detonation Conditions of a 1-MT Fission Weapon	326
6.8	Computation of $M_p(1)$ for Several Detonation Conditions of a 1-MT Yield Fission Weapon at Selected Downwind Distances	327
6.9	Summary of Shot Conditions for Estimating the Median Particle-Diameter Designator	343
6.10	Calculation of α_0 for Some Fallout Locations from Shots Apple II and Smoky	344

Chapter 1

THE NATURE OF FALLOUT

1.1 Background

On the 16th day of August in 1945 the first nuclear explosion, Shot Trinity, was detonated at Alamogordo, New Mexico. The nuclear device was mounted on a tower at a height of about 100 feet and the energy of the explosion was equivalent to that of 19,000 tons of TNT. The explosion, as all nuclear explosions, produced radioactive materials that combined with other materials engulfed by the forces of the explosion. The product of the combination has been given the name fallout.

From most nuclear explosions, fallout is in the physical form of particles. After Shot Trinity some of these particles deposited on pastures and on the backs of cows at some distance from the point of detonation, and the nuclear radiations from the particles caused burn-like injuries on the cows' backs. Other than this the exposure had no ostensible influence on the life of the animals or their offspring.

The incident, however, initiated interest and concern among some scientists and engineers. Both the fate of radioactive substances produced in nuclear explosions and the biological consequences of their interaction with living matter came under study.

In Operation Crossroads, in 1946, ships exposed to the effects of an underwater nuclear detonation, were found to be contaminated with radioactive substances, and military--especially Navy--interest in the fallout phenomenon was aroused. The results of that test initiated the recognition of fallout as one of the primary phenomena of nuclear explosions and one that could have a profound influence on military operations using nuclear weapons.

The recognition and acceptance of the implications of fallout on military operations, however, was at first limited to a rather small group of scientists, engineers, and military people. Additional evidence and data on fallout were obtained in subsequent tests, especially in Operations Greenhouse and Buster-Jangle in 1951 and in Upshot-Knothole in 1953. But it was not until the detonation of Shot Bravo in Operation Castle in 1954 that general recognition of the fallout phenomenon was established.

Two of the better-known incidents that influenced (or forced) such recognition were the exposure of the Marshall Islanders on the Rongelap Atoll and of the Japanese fishermen in their boat at sea to the radiations from fallout. But even after the Shot Bravo experience there remained a few who wanted to believe that a "fluke" had occurred and that fallout was not of military significance.

Now, several years and many test detonations later, there are no remaining doubts about the production of fallout in nuclear explosions. Present studies are directed to quantitative evaluations of the degree to which fallout is significant in the military applications of nuclear explosives. Thus it is no longer of interest simply to note that radioactive atoms are produced in nuclear explosions. The problem is to determine the quantity of the radioactive atoms produced, what physical processes they are subjected to, where they go, and how their disposition may affect the operations and the lives of people.

Because fallout contains radioactive atoms, and because radioactive atoms emit nuclear radiations that can cause damage in the cells of living tissues, the presence of fallout in the environment is usually equated with a potential radiological hazard to living matter. The core of the present-day interest in fallout, therefore, consists of evaluating the biological consequences to humans, animals, and plants of the exposure to nuclear radiations from fallout.

The degree and nature of possible exposures of living matter to nuclear radiation depend upon many physical parameters and these begin with the initial production of the fallout in a nuclear explosion. The nature of the exposure is more fundamentally connected with physical processes than is the degree of the exposure. In terms of degree, it is known that possible radiation exposures would be highest, and therefore the biological consequences most severe, for nuclear explosives used in a large-scale war. This degree of exposure is of concern to many.

After the fallout is in an environment, the degree of this radiological hazard can be measured. But the kind and amount of hazard in a nuclear war situation, at least before the fact, cannot be evaluated without a reasonably detailed description of the history of the radioactive atoms produced in nuclear explosions. Such a history, to be useful, must reveal the essential details of the physical processes in which the radioactive atoms participate, from the instant they are formed up to any desired later time.

The major purpose of this report, therefore, is to outline and discuss these physical processes and the important parameters on which they depend. The data, data analyses, data correlation schemes, and discussions presented here are organized to emphasize basic principles so that an appropriate methodology can be applied in evaluating the radiological consequences of nuclear war.

1.2 A General Description of Fallout

An explosion of any kind, detonated near the surface of the earth, causes material to be thrown up or drawn into a chimney of hot rising gases and raised aloft. In a nuclear explosion, two important processes occur: (1) radioactive elements, which are produced and vaporized in the process, condense into or on this material; and (2) a large amount of non-radioactive material, rises thousands of feet into the air before the small particles begin to fall back. This permits the winds to scatter them over large areas of the earth's surface. Thus, when the particles reach the surface of the earth they are far from their place of origin and contain, within or on their surface, radioactive elements. Whether they are solid particles produced from soil minerals, or liquid (salt-containing) particles produced from sea water, they are called fallout.

The composition of fallout can be described in terms of two or three components. One is the inactive carrier; this consists of the environmental material at the location of the detonation and is the major component in a near-surface detonation. The second component includes all the radioactive elements in the fallout.

These radioactive elements can be subclassified into two groups by source. The first group contains the fission-product elements that are produced in the fission process that initiates the explosion. The second group consists of the elements produced by the capture of neutrons released in both fission and fusion. The kinds and amounts of these neutron-induced radioactive elements in the fallout differ from one detonation to another depending upon the type of weapon used and the chemical elements in the environment at the point of detonation.

Occasionally, a third fallout component group is considered. This consists of the bomb's structural materials and is a major component in air-burst fallout.

The word fallout is occasionally preceded by "close-in" (or "local") and "long-range" (or "world-wide"). These terms have never been precisely defined except for operational purposes. The terms imply some arbitrary differentiation of the fallout, or the radioactivity, on the basis of distance from the point of detonation or time required for the material to fall to the earth's surface. However, as is discussed in the following chapters, the gradual changes in the properties of the fallout with distance make precise definition of these terms impossible, except for the extremes of each fallout classification. Therefore, except for these extreme cases, these descriptions are not used further as definitive terms in discussing the nature and properties of fallout.

1.3 Characteristic Types of Fallout

The characteristic types of fallout are determined by the environment at the point of detonation. They are generally classified as being either land, sea water, harbor, or air fallout.

The major component of the fallout from detonations near the surface of land is the soil particles. In detonations near the surface of the ocean the major component is the sea water residues (salts and water). The fallout from detonations in harbors, rivers, and shallow lakes may contain materials from the bottom as well as water and/or sea water salts; the relative amounts of each depend on the depth of the water, the height or depth of the burst, and the energy released during the explosion.

From an air burst (not near the surface of the earth) the major fallout component is the structural materials, such as iron and aluminum, etc., of the bomb or missile war head. When the mass of these materials is not too large, and when it is all vaporized, only very small fallout particles are formed. The properties of air burst fallout are those most often associated with the terms long-range or world-wide.

The fallout from the near-surface bursts consists of large particles that fall rapidly to the earth; these fallout types result in much higher deposit densities than those from the air burst. Because of this large difference in fallout deposit density and the associated radiological hazard, only the first three characteristic types of fallout (land, sea, and harbor) are discussed at length in the following chapters.

1.4 Potential Hazards from Fallout

The potential hazards from fallout are mentioned briefly here to identify them, to indicate their relationship with physical quantities that can be measured, and to emphasize the fact that interest in knowledge about fallout has been aroused mainly because of those hazards.

The radioactive elements within or on the surface of the fallout particles emit gamma and X-rays and/or beta or alpha particles. The gamma and X-rays are the same except that the gamma rays are more energetic; they are often termed the penetrating or long-range radiations because gamma and X-rays travel long distances in air and in other low-density materials. The beta and alpha particles are often termed short-range radiations because they do not travel very far even in air and are stopped by small thicknesses of more dense material. Of the two, the alpha particles are the easier to stop.

The potential hazard from the three types of nuclear radiations lies in the capability of the different types of radiation to penetrate material, both living and inanimate, especially when the radioactive source is not in contact with the material irradiated. Thus, from fallout particles deposited on the ground, the gamma rays are the only ones emitted that can penetrate large distances into the human body. The shorter-range beta particles can penetrate a short distance into material when their source is either in contact with its surface or is part of the material (i.e., an internal source). In general, alpha particles are not a fallout hazard because the alpha emitters are so extremely diluted and long-lived.

The gamma rays, then, constitute an external hazard; the beta particles are often termed a contact and an internal hazard; and the alpha rays constitute an internal hazard, if any. But since the major source of alpha particles in fallout is from the decay of unreneted uranium or plutonium, which are very long-lived radionuclides, the alpha-particle hazard is negligible compared with that of the gamma and beta rays derived from other radionuclides. Hence the alpha-particle hazard is not considered further.

The two radionuclie emissions that are of concern in fallout, therefore, are the gamma radiations (including the X-rays) as an external source of hazard, and the beta particles as a contact or internal source of hazard. The significance of this differentiation between the two types of radiations as hazard sources is discussed in later chapters. Both types of radiations cause injury to living organisms by producing ionization along their paths through living tissue. In other words, the rays or particles transfer energy to the electrons of the atoms in the material they penetrate. This causes the electrons to leave their orbits around the nucleus of the atom so that the atom takes on, for a short time, a positive charge.

A specified amount of energy is required to ionize an atom; for every ion pair formed by the passing of a gamma ray or beta particle near an atom, the ray or particle loses an equivalent amount of energy. The amount is not the same for all materials penetrated because the energy required to ionize an atom differs from one chemical element to another. The roentgen is the defined unit for measuring the energy absorbed from gamma and X-rays in air. The value of the r unit is based on the energy required to ionize the nitrogen and oxygen atoms of air to form, in one cubic centimeter of air at standard conditions, one pair of ions. By this definition, the r unit is equivalent to the absorption of about 87 ergs of energy per gram of air.

Since this unit, the r, is defined on the basis of air ionization, it cannot be related to the number of radionuclie atoms that emit gamma rays unless both the energy of the rays passing through a given volume of air and the geometric configuration of the emitting sources are known. These

relationships, for a complicated mixture of radionuclides such as would be present in fallout, have only been calculated for a few very simple source geometries. An example is the calculation for the air ionization rate at three feet above an infinite smooth plane covered with a uniform distribution of fission products.^{1*}

The air ionization rate, in roentgens per hour, is often called the intensity, or the radiation intensity; when used, these terms always refer to the magnitude of the air ionization rate. Another term often used is dose rate; however, this one is more practically associated with the rate of energy absorption, from the radiations, in living tissue rather than in air, since dose rate has a biological connotation. In common usage, the three terms (intensity, radiation intensity, and dose rate) are used interchangeably; when their units are r per hour, they are, in fact, air ionization rates.

The total amount of energy absorbed in a volume of air over a period of time is the radiation dose. When the accumulated air ionization rate (i.e., the dose) is associated with biological hazard from an unmodified fallout deposit, the restrictive terms potential dose or exposure dose are often used. Such use actually involves two restrictive concepts or assumptions. The first is that this dose is the total amount of air ionization, per unit volume, that a person or object is exposed to by staying in the specified location for the length of time that the stated energy is being absorbed by the air. The second concept is that the dose, or the energy absorbed by the air, is proportional to the amount of energy absorbed by the person or object.

The terms, dose, potential dose, or exposure dose are used only in reference to the air ionization in the following chapters. While the biological effects of a radiation dose are outside the scope of this discussion, arbitrary values of dose limits are used occasionally; they illustrate the methodology that can be used to solve exposure-control problems.

The dose-limit values used in this report are selected on the basis of assumed relations between air ionization doses and biological effects. These selections, when applicable, include the concept that some biological effects have a threshold dose while others do not, and that, when the dose is absorbed over a long period of time, the biological effect of the dose is decreased due to bodily repair of tissue damaged during the exposure.

*References are listed at the end of each chapter.

The ionization rate and the dose from beta rays are usually defined in terms of the energy absorbed by the ionization of the atoms or molecules in tissue. Since the beta particles do not penetrate very far into the tissue, the dose from beta emitters on the surface of tissue, such as the skin, is absorbed largely in the skin's outer layers. Because of the complicated manner in which the energy of the beta particles is distributed, there is no simple method for estimating the energy absorbed in various thicknesses of a tissue having a deposit of a mixture of radioactive atoms on its surface. Even when the radioactive atoms are uniformly distributed through a tissue, as may be the case for several ingested radio-elements, the methods for estimating the absorbed dose are fairly complicated.² In this case, the rates of accumulation in, and elimination from, the tissue must also be considered.

In most of the fallout conditions described in the following chapters, the beta radiation exposure turns out to be the less dominant fallout hazard. However, some times and situations where beta radiation can be a significant hazard are discussed.

The main immediate hazard from fallout when it arrives on the surface on the earth after a nuclear explosion is due to the gamma, or penetrating, radiation. These nuclear radiations can travel long distances, and their summed, or integrated, intensity completely dominates the radiation hazard. This is the case even for persons or objects contaminated with falling particles, since the contribution of the beta particles to the exposure dose is only from those particles that are deposited on exposed tissue.

The ingestion of radionuclides from fallout over a long period of time, however, becomes the predominant hazard after a period of time. The magnitude of this internal-hazard depends on the fallout's chemical nature, which uniquely determines both the availability of the radionuclides for ingestion and the period of their retention in living tissue.

1.8 Radioactive Decay

Evaluation of the hazards from fallout so that the necessary degree of protection from the nuclear radiations can be specified requires knowledge of how the air ionization rate decreases with time. The integral, or accumulated, dose is determined from a curve giving the variation of the air ionization rate with time, and, since some value of the dose is known to produce undesirable biological effects, the ratio of the two is used to determine the desired protection factor of either a safety procedure or radiological defense countermeasure, or both.

In a nuclear detonation, the fission process produces about 90 fission-product mass chains, consisting of about 40 different elements. In each mass chain produced in the fission of fissile materials, one or more radionuclides are produced. These parent-daughter pairs decay one to the next until finally a single stable nuclide is formed. The decay of this mixture of radionuclides can be calculated from (a) the initial yield of the nuclides in each mass chain, (b) the half-life of each nuclide, and (c) the abundance of the gamma rays produced when each nuclide decays. The details of such calculations as these are discussed in Chapter 2.

In a nuclear detonation, the fission products are initially vaporized; they condense later as the fireball cools. Of the approximately 40 elements present, some are volatile and not usually in a condensed state even at ordinary temperatures. Some elements are refractory and condense at high temperatures. The remainder condense at intermediate temperatures.

Because there is such a large range in the thermal stability of the condensates of the fission-product radionuclides, the normal abundance ratios of the fission-product radionuclides in fallout are altered. It is found that, in the larger fallout particles, the relative concentration of the volatile radionuclides (and their daughters) is low and that the concentration of the more refractory radionuclides is high. Any such alteration in the abundance ratios of the fission products, relative to the original fission-yield abundance ratios, is called fractionation. In most types of fallout, the fission-product radionuclides are found to be fractionated.

Neutron-induced activities are also found in fallout. These induced activities are produced by neutron capture in materials present in the weapon itself and in other environmental materials at the point of detonation. Perhaps the most important of the induced activities are those produced by neutron capture in the elements of the weapon's construction materials. These induced activities result from neutron activation of uranium-238, iron, manganese, and other construction materials. In soil and sea water, manganese and sodium are perhaps the most likely elements to be neutron-activated in highest abundance.

The gross decay, or variation in air ionization rate with time, of the nuclear radiations from fallout is the sum of the contributions of all the radionuclides present in the radiation source. Thus, to specify or even to estimate the gross decay rate of the radioactivity in fallout, both fractionation and neutron-induced activities must be considered.

3.0 The Standard Intensity and Contour Properties

The term standard intensity is defined here as the magnitude of the air ionization rate at three feet above an extended open area covered with fallout, corrected to a stated time after detonation; conventionally the stated time is one hour. This reference-time originated when the "nominal" detonation yield of nuclear weapons was 20 kilotons (KT), and when data on fallout were available only for small-yield weapons, since for such yields the fallout process was essentially complete by one hour after detonation, at least in areas receiving significant amounts of fallout. Of course, the heavy deposition of fallout from megaton (MT) yield explosions is not complete even after several hours. In such cases, the observed radiation intensity at one hour after detonation is not the same as that calculated from a measurement of the intensity after the fallout ceases to arrive and must be decay-corrected to one hour after detonation.

The standard intensity values are used in constructing charts of areas on which fallout has been deposited. A chart showing a fallout pattern consists of a series of iso-intensity contours. These contours are not lines of equal potential hazard until after the fallout has ceased to arrive at the farthest downwind location on a given contour. The charts are very useful, however, in evaluating the area-coverage of fallout with regard to both the potential radiation hazard and the kinds of protection needed to reduce that hazard to a desired level.

The determination of the standard intensities requires measurements of the intensity, over time, at a series of locations during and after the fallout is deposited, and, in addition, measurements of the ionization rate, over time, on samples collected when the fallout first starts to arrive. A heavily shielded detector is required for the latter. However, for locations where the fallout arrival time is greater than one hour, correcting the obtained data to the conventional time of one hour requires a decay-correction factor for the period between the time of the first measurement and the standard time of one hour. Measurements of the intensity over areas covered with fallout particles, the contaminated areas, have been made, in most cases, with portable ion chambers. The accuracy of the measurements made with most of the presently available portable instruments is not very high; however, if the ion chambers are kept in excellent repair, are carefully handled, and are kept calibrated, accuracies of about 20 percent can be obtained.

The intensity due to the fallout particles depends on (a) the number or mass of the particles deposited, per unit surface area, and (b) the specific activity, or concentration, of the radionuclides in the particles. To reduce the intensity of the fallout from a land detonation by intention, either the particles must be moved away from the location of interest or shielding must be placed between the particles and the location of interest.

Moving the particles efficiently and effectively requires some knowledge of the properties of the particles; also, the removal procedure or decontamination method must be designed to remove fallout particles. Because of these requirements on the performance of decontamination methods, relationships are needed among (a) the mass of the particles, per unit area (b) their specific activity, and (c) their radiation intensity. Such relationships are extremely useful, because intensity measurements, which are easy to make, can then be used to deduce the fallout properties that influence decontamination.

These relationships between the radiation intensity and the related fallout properties are called contour ratios; they are discussed in detail in Chapter 6. The values of these ratios, and the mathematical form of the relationships among these ratios and the other parameters, depend on two major factors. One is the type of chemical system produced under the given conditions of temperature, pressure, and concentrations of various constituent elements in the fireball. The other factor is the manner in which the particles become distributed, both in the forming cloud and in their fall through the atmosphere back to earth.

Definition of the chemical systems formed in these processes, as well as of the chemical systems formed when the fallout particles contaminate surfaces, is important in devising appropriate decontamination procedures. To be useful, such procedures must be designed to operate on any chemical systems that contain radioactive substances.

CHAPTER 1 REFERENCES

1. Miller, C. F., and P. Losb, Ionization Rate and Photon Pulse Decay of Fission Products from the Slow Neutron Fission of U-238, USNRDL-TR-247 (1958)
2. Morgan, K. Z., and M. R. Ford, Nucleonics, 12, 6, 52 (1954)

Chapter 2

FORMATION OF FALLOUT PARTICLES

2.1 General Definition of the Process

The process of radioactive fallout formation is initiated when fissile material undergoes fission. In each fission event, about 200 million electron volts (Mev) of energy are released; also, two neutron-rich radioactive elements, or particles, plus two to four or five neutrons, and several gamma rays are produced. If the resulting two particles carried all the released energy before colliding with another atom, the average initial energy would correspond to a kinetic temperature of about 10^{15} degrees Kelvin ($^{\circ}$ K).

The released energy is initially in the form of electromagnetic and kinetic energy whose immediate and rapid transmission to nearby surrounding materials causes the latter to vaporize at high pressure. Thus when many fission events occur in a small volume in a short period of time a high-pressure shock wave forms and a nuclear explosion results.

The two fission-product atoms formed from a heavy-element atom contain more neutrons than do stable elements having the same atomic mass. Therefore, the initial fission-product atoms progress to stability by emitting beta particles and/or neutrons. This beta decay of many of the fission-product radionuclides results in the simultaneous release of gamma rays. Also, the capture of neutrons by nearby atoms results in the release of gamma rays. At detonation, therefore, the gamma ray pulse includes gamma rays from (a) the fission reaction itself, (b) neutron capture by elements in the surrounding media, and (c) the decay of fission products.

In the so-called fusion, or thermonuclear, weapons, the high temperature created by the fission process is utilized to fuse the light elements such as deuterium, tritium, and lithium. In this combining of the lighter elements to form helium or other heavier nuclei, additional energy and neutrons are released. Such neutrons, having higher energies than those produced by fission, are able to cause the fission of uranium-238 or, when captured by the nuclei of other elements near the explosion, to cause the latter elements to become radioactive.

As the thermal and shock waves travel outward from the detonation point, the materials enveloped are also heated to high temperatures; crystal bonds are broken, chemical compounds are decomposed, molecules dissociate, and atoms become thermally ionized. The result is the highly luminous mass of gaseous material called the fireball.

This transfer of energy by the shock wave and radiant processes to these materials and to other substances occurs at the expense of the initial energy of the fission fragments; their kinetic temperature falls extremely fast, by collision with other atoms, as they diffuse outward from the center of the explosion. The rate at which the energy is transferred to the materials being enveloped by the expanding fireball also decreases rapidly as the thermal exchange proceeds, and as the temperature of the materials on the interior of the gas volume decreases. As the temperature decreases, positive ions regain their electrons and become atoms, atoms recombine to form molecules, molecules condense to form liquid droplets, and, finally, when the temperature is low enough, the droplets solidify.

In the cooling of the fireball the important stage in the formation of fallout begins with the time and temperature at which the first liquid drops form. This formation process continues until after the materials involved have cooled to about the temperature of the surrounding air. While the condensing process probably never actually ceases, such a large fraction of the radioactive and other elements have condensed by about five to ten minutes after detonation that the process is essentially complete.

The highest fireball temperature to be considered in the formation of fallout is the boiling point of the most refractory material present in sufficient quantity to form a macroscopic liquid phase. For most materials this temperature is between 3000 and 4000°K.

By the time the fireball temperature cools to 3000 or 4000°K, it has risen some height into the air and, for near-surface bursts, crater materials consisting of liquid and/or solid soil particles have entered the fireball. At first some of these are melted and vaporized; as the gas temperature decreases, fewer and fewer of the crater material particles are melted, until finally those that actually reach the altitude of the rising cloud are only slightly warmed. The melted particles dissolve, aggregate, and occlude the smaller vapor-condensed particles formed by direct vapor condensation even before the mass

of larger particles enters the fireball.* Whether melted or solid, the entering particles present an extremely large amount of surface area upon which the gas atoms or molecules can condense.

There are several basic characteristics of the fallout formation process in the developing fireball. The first is that, of the fission products alone, about 40 different radioactive elements are produced in a given yield, or order of abundance, that results in a set of partial pressures of vaporized species whose values are initially ranked in the same order as the abundance values. The second characteristic is that the chemical reactivity and the equilibrium vapor pressure of each element in the fireball differ from those of the other elements; thus the fraction of each element in a condensed state at a given temperature is also different from the fractions of the other elements.

The third characteristic is the presence of inert (nonradioactive) substances; these furnish either (a) an available surface area that the dilute vapors can condense on or interact with, or (b) a dense vapor that condenses to form a macroscopic liquid phase with which the less abundant radioactive elements can interact. The role of the condensation process, both in fallout formation and in fractionation, is discussed in detail later in this chapter. Condensation is one of several causes of observed fractionation in fallout.

An example of the dense-vapor condensation process is a detonation on sea water. In this type of detonation many of the fission-product elements condense, along with the bomb casing materials and the salts, before the water does, but the fission-product elements are occluded or dissolved by the water when it condenses. Such inert materials, that serve to carry the radioactive elements back to earth, are called the carrier or the carrier materials.

The amount of each radioactive element that is actually found in fallout, relative to some standard of measure, depends on five main factors:

1. The original fission yields, that is, the relative abundance of the fission products;

*A more complete general description of the fireball and its behavior is given in The Effects of Nuclear Weapons (designated ENW hereafter). Certain data from that volume are utilized here; generally these are confined to input information required to describe the fallout formation process. Data on the size, temperature, and position of the fireball are important in estimating its energy content, and in establishing an appropriate standard reference time for estimating fireball parameters for different nuclear yields.

2. The capture of neutrons by the fission products themselves;
3. The degree to which each fission product condenses into or onto the carrier particles;
4. The neutron emissions in the decay chain; and
5. The radiochemical standards used in measuring the relative abundances of the fission products.

The relative abundance of each fission product element originally produced at detonation depends on the fissile material used; i.e., whether the material is U-235, U-238, Pu-239, or some other substance. The fission-chain yields also depend on the energy spectrum of the incident neutrons.

In general, in the change of energy of the incident neutrons, the fission yields of the nuclides in the lighter-mass ($A = 90$ to 100) peak tend to shift more with mass number than do those in the heavier-mass ($A = 131$ to 144) peak. In the fission of the heavier fissile elements, the center of the lighter-mass group moves toward the higher-mass numbers. As the incident-neutron energy increases, the yields of the mass chains that appear in the valley between the two yield peaks rise, and the yields of the highest- and lowest-mass numbers also rise; also, the neutron yield per fission increases. This increase in neutron yield per fission tends to spread the two peaks farther apart and, again, the lighter-mass group is shifted more than the heavy-mass group.

Neutron capture by the fission-product elements results in a general shift of the whole fission-yield curve to the higher-mass numbers. This causes a decrease in the yields of the elements of both mass groups that have the smaller mass numbers (the left sides of the peaks), and an increase in the yields of the elements of both mass groups that have larger mass numbers. In the yields of the elements in the peaks relatively little change results except for those elements that have extremely high neutron-capture cross-sections. The subject is not discussed further because of insufficient data.

During the decay process, neutron emission results in a product nuclide that has a mass number that is a single-unit less than its parent. This chain "shift" can be accounted for if the decay scheme of the radionuclide is known. For many of the short-lived radionuclides, however, there is insufficient data presently available for giving further consideration to decay by-neutron emission.

The experimental measure of fractionation is most often given as an "R" factor, or "R" value, that is relative to the fission yields in the thermal-neutron fission of U-238 and of a selected radionuclide. The most commonly

selected radionuclide for comparison in Mo-98. However, a radio-chemical assay of a fallout sample that gives an R value different from unity does not necessarily mean that the nuclide in question has, in fact, been fractionated with respect to some other nuclide or element. The true initial fission yields must be known, both to correct the observed assay data and to determine whether fractionation has, in fact, occurred.

2.2 Mass-Chain Yields for the Fission of U-235, U-238, and Pu-239

One major factor that determines the amount of a fission product that condenses with the carrier up to a given time and temperature is the amount of that element present in each of the mass chains. In this section, data on the fission-mass yields are summarized, and estimates of undetermined yields are presented, so that calculations of the fraction of the fission products that condense to form fallout may be made.

The independent yields of all radionuclides, for thermal-neutron fission of U-235, have been calculated by Bollen and Ballou³, according to the theories of independent fission yields of Glendenin⁴ and of Present.⁵ The fractional chain yields from these calculations, for times from zero to 180 seconds, are given in Table 2.1, for mass 89; and, in Table 2.2, for mass 140. Much chain contains a rare gas (Kr and Xe) element.

The two mass chains selected lie on the outer edge of the two yield points. In each case, the independent yield distribution from the Glendenin theory is the broader, and the short-lived, lowest-Z, elements are the more heavily weighted. This difference diminishes as the mass number approaches the value 118.

The fractional yields themselves indicate what might be expected during condensation with respect to the fractionation of the chain members. For example, if only the rare gas member is considered, the maximum loss (minimum amount condensed) should occur between 19 and 28 seconds for mass 89, according to Glendenin; for mass 140, according to both theories of yield, the fraction not condensed should decrease as the time period of the condensation process increases.

Computational estimates of the independent nuclide yields have not yet been made for fission of U-235 and Pu-239 with fission-spectrum neutrons, nor for fission of U-238 with 8-Mev broad-band spectrum neutrons; the latter would be more applicable to nuclear detonations. Moreover, the mass chain yields for even Pu-239 and U-238 fission are not very well known. Available chain yield data and estimates of unmeasured yields are summarized in Table 2.3 for the fission of U-235, U-238 and Pu-239. The bulk of the data are taken from the summary by Katzoff,⁶ other references are included in the table.

Table 2.1
FRACTIONAL CHAIN YIELDS FOR MASS 99 FOR U-235 FISSION

T (sec)	Present ^a						Henderson ^b			
	Se	Br	Kr	Rb	Sr	Se	Br	Kr	Rb	Sr
0	0.05	0.172	0.223	0.109	0	0.178	0.420	0.343	0.057	0
1	0.125	0.371	0.164	0.104	0	0.121	0.410	0.399	0.070	0
2	0.239	0.512	0.198	0.108	0	0.087	0.390	0.452	0.071	0
3	0.345	0.544	0.171	0.111	0	0.052	0.362	0.302	0.074	0
4	0.422	0.573	0.115	0.115	0	0.034	0.322	0.547	0.077	0
5	0.493	0.720	0.121	0.121	0	0.022	0.266	0.629	0.083	0
6	0.562	0.754	0.133	0.133	0	0.016	0.183	0.726	0.090	0
7	0.635	0.779	0.147	0.147	0	0.012	0.106	0.736	0.105	0.012
8	0.692	0.793	0.166	0.166	0	0.011	0.041	0.838	0.124	0.020
9	0.745	0.794	0.195	0.195	0	0.011	0.011	0.832	0.135	0.022
10	0.791	0.784	0.232	0.232	0	0.002	0.009	0.890	0.192	0.020
11	0.827	0.767	0.283	0.283	0	0.007	0.004	0.744	0.249	0.015
12	0.853	0.737	0.347	0.347	0	0.015	0.007	0.670	0.316	0.012
13	0.871	0.701	0.436	0.436	0	0.025	0.025	0.539	0.419	0.022
14	0.889	0.663	0.529	0.529	0	0.037	0.037	0.455	0.384	0.014
15	0.905	0.624	0.625	0.625	0	0.057	0.057	0.380	0.380	0
16	0.919	0.584	0.725	0.725	0	0.087	0.087	0.316	0.316	0
17	0.931	0.544	0.825	0.825	0	0.127	0.127	0.250	0.250	0
18	0.941	0.504	0.925	0.925	0	0.177	0.177	0.188	0.188	0
19	0.949	0.464	0.925	0.925	0	0.237	0.237	0.128	0.128	0
20	0.956	0.424	0.925	0.925	0	0.307	0.307	0.078	0.078	0
21	0.962	0.384	0.925	0.925	0	0.387	0.387	0.038	0.038	0
22	0.967	0.344	0.925	0.925	0	0.477	0.477	0.018	0.018	0
23	0.971	0.304	0.925	0.925	0	0.577	0.577	0.008	0.008	0
24	0.974	0.264	0.925	0.925	0	0.687	0.687	0.003	0.003	0
25	0.976	0.224	0.925	0.925	0	0.807	0.807	0.001	0.001	0
26	0.977	0.184	0.925	0.925	0	0.937	0.937	0.000	0.000	0
27	0.978	0.144	0.925	0.925	0	1.077	1.077	0.000	0.000	0
28	0.978	0.104	0.925	0.925	0	1.227	1.227	0.000	0.000	0
29	0.978	0.064	0.925	0.925	0	1.387	1.387	0.000	0.000	0
30	0.978	0.024	0.925	0.925	0	1.557	1.557	0.000	0.000	0
31	0.978	-0.016	0.925	0.925	0	1.737	1.737	0.000	0.000	0
32	0.978	-0.056	0.925	0.925	0	1.927	1.927	0.000	0.000	0
33	0.978	-0.116	0.925	0.925	0	2.127	2.127	0.000	0.000	0
34	0.978	-0.176	0.925	0.925	0	2.337	2.337	0.000	0.000	0
35	0.978	-0.236	0.925	0.925	0	2.557	2.557	0.000	0.000	0
36	0.978	-0.296	0.925	0.925	0	2.787	2.787	0.000	0.000	0
37	0.978	-0.356	0.925	0.925	0	3.027	3.027	0.000	0.000	0
38	0.978	-0.416	0.925	0.925	0	3.277	3.277	0.000	0.000	0
39	0.978	-0.476	0.925	0.925	0	3.537	3.537	0.000	0.000	0
40	0.978	-0.536	0.925	0.925	0	3.807	3.807	0.000	0.000	0
41	0.978	-0.596	0.925	0.925	0	4.087	4.087	0.000	0.000	0
42	0.978	-0.656	0.925	0.925	0	4.377	4.377	0.000	0.000	0
43	0.978	-0.716	0.925	0.925	0	4.677	4.677	0.000	0.000	0
44	0.978	-0.776	0.925	0.925	0	5.007	5.007	0.000	0.000	0
45	0.978	-0.836	0.925	0.925	0	5.357	5.357	0.000	0.000	0
46	0.978	-0.896	0.925	0.925	0	5.727	5.727	0.000	0.000	0
47	0.978	-0.956	0.925	0.925	0	6.117	6.117	0.000	0.000	0
48	0.978	-1.016	0.925	0.925	0	6.527	6.527	0.000	0.000	0
49	0.978	-1.076	0.925	0.925	0	6.957	6.957	0.000	0.000	0
50	0.978	-1.136	0.925	0.925	0	7.407	7.407	0.000	0.000	0
51	0.978	-1.196	0.925	0.925	0	7.877	7.877	0.000	0.000	0
52	0.978	-1.256	0.925	0.925	0	8.367	8.367	0.000	0.000	0
53	0.978	-1.316	0.925	0.925	0	8.877	8.877	0.000	0.000	0
54	0.978	-1.376	0.925	0.925	0	9.407	9.407	0.000	0.000	0
55	0.978	-1.436	0.925	0.925	0	9.967	9.967	0.000	0.000	0
56	0.978	-1.496	0.925	0.925	0	10.557	10.557	0.000	0.000	0
57	0.978	-1.556	0.925	0.925	0	11.177	11.177	0.000	0.000	0
58	0.978	-1.616	0.925	0.925	0	11.827	11.827	0.000	0.000	0
59	0.978	-1.676	0.925	0.925	0	12.507	12.507	0.000	0.000	0
60	0.978	-1.736	0.925	0.925	0	13.217	13.217	0.000	0.000	0
61	0.978	-1.796	0.925	0.925	0	13.957	13.957	0.000	0.000	0
62	0.978	-1.856	0.925	0.925	0	14.727	14.727	0.000	0.000	0
63	0.978	-1.916	0.925	0.925	0	15.527	15.527	0.000	0.000	0
64	0.978	-1.976	0.925	0.925	0	16.357	16.357	0.000	0.000	0
65	0.978	-2.036	0.925	0.925	0	17.227	17.227	0.000	0.000	0
66	0.978	-2.096	0.925	0.925	0	18.127	18.127	0.000	0.000	0
67	0.978	-2.156	0.925	0.925	0	19.057	19.057	0.000	0.000	0
68	0.978	-2.216	0.925	0.925	0	20.027	20.027	0.000	0.000	0
69	0.978	-2.276	0.925	0.925	0	21.027	21.027	0.000	0.000	0
70	0.978	-2.336	0.925	0.925	0	22.057	22.057	0.000	0.000	0
71	0.978	-2.396	0.925	0.925	0	23.127	23.127	0.000	0.000	0
72	0.978	-2.456	0.925	0.925	0	24.227	24.227	0.000	0.000	0
73	0.978	-2.516	0.925	0.925	0	25.357	25.357	0.000	0.000	0
74	0.978	-2.576	0.925	0.925	0	26.527	26.527	0.000	0.000	0
75	0.978	-2.636	0.925	0.925	0	27.727	27.727	0.000	0.000	0
76	0.978	-2.696	0.925	0.925	0	28.957	28.957	0.000	0.000	0
77	0.978	-2.756	0.925	0.925	0	30.227	30.227	0.000	0.000	0
78	0.978	-2.816	0.925	0.925	0	31.527	31.527	0.000	0.000	0
79	0.978	-2.876	0.925	0.925	0	32.857	32.857	0.000	0.000	0
80	0.978	-2.936	0.925	0.925	0	34.227	34.227	0.000	0.000	0
81	0.978	-2.996	0.925	0.925	0	35.627	35.627	0.000	0.000	0
82	0.978	-3.056	0.925	0.925	0	37.057	37.057	0.000	0.000	0
83	0.978	-3.116	0.925	0.925	0	38.527	38.527	0.000	0.000	0
84	0.978	-3.176	0.925	0.925	0	40.027	40.027	0.000	0.000	0
85	0.978	-3.236	0.925	0.925	0	41.557	41.557	0.000	0.000	0
86	0.978	-3.296	0.925	0.925	0	43.127	43.127	0.000	0.000	0
87	0.978	-3.356	0.925	0.925	0	44.727	44.727	0.000	0.000	0
88	0.978	-3.416	0.925	0.925	0	46.357	46.357	0.000	0.000	0
89	0.978	-3.476	0.925	0.925	0	48.027	48.027	0.000	0.000	0
90	0.978	-3.536	0.925	0.925	0	49.727	49.727	0.000	0.000	0
91	0.978	-3.596	0.925	0.925	0	51.457	51.457	0.000	0.000	0
92	0.978	-3.656	0.925	0.925	0	53.227	53.227	0.000	0.000	0
93	0.978	-3.716	0.925	0.925	0	55.027	55.027	0.000	0.000	0
94	0.978	-3.776	0.925	0.925	0	56.857	56.857	0.000	0.000	0
95	0.978	-3.836	0.925	0.925	0	58.727	58.727	0.000	0.000	0
96	0.978	-3.896	0.925	0.925	0	60.627	60.627	0.000	0.000	0
97	0.978	-3.956	0.925	0.925	0	62.557	62.557	0.000	0.000	0
98	0.978	-4.016	0.925	0.925	0	64.527	64.527	0.000	0.000	0
99	0.978	-4.076	0.925	0.925	0	66.527	66.527	0.000	0.000	0
100	0.978	-4.136	0.925	0.925	0	68.557	68.557	0.000	0.000	0
101	0.978	-4.196	0.925	0.925	0	70.627	70.627	0.000	0.000	0
102	0.978	-4.256	0.925	0.925	0	72.727	72.727	0.000	0.000	0
103	0.978	-4.316	0.925	0.925	0	74.857	74.857	0.000	0.000	0
104	0.978	-4.376	0.925	0.925	0	77.027	77.027	0.000	0.000	0
105</										

Table 2.2
FRACTIONAL CHAIN YIELDS FOR MASS 140 FOR U-235 FISSION

t (sec)	Present ^a						Glaeser ^b					
	I	Xe	Cs	Ba	La	T	Xe	Cs	Ba	La		
0	0.071	0.193	0.229	0.034	0	0.138	0.408	0.355	0.055	0		
1	0.047	0.198	0.115	0.079	0	0.057	0.111	0.380	0.092	0		
2	0.029	0.195	0.133	0.043	0	0.035	0.153	0.395	0.097	0		
3	0.019	0.135	0.129	0.058	0	0.024	0.154	0.412	0.100	0		
4	0.012	0.173	0.116	0.032	0	0.022	0.147	0.426	0.105	0		
6	0.006	0.138	0.093	0.064	0	0.008	0.123	0.433	0.115	0		
9	0.001	0.139	0.031	0.073	0	0.002	0.377	0.491	0.139	0		
13	0.023	0.371	0.192	0	0	0.315	0.531	0.571	0			
19	0.232	0.659	0.139	0	0	0.246	0.569	0.635	0			
28	0.170	0.632	0.192	0	0	0.167	0.592	0.741	0			
41	0.097	0.619	0.284	0	0	0.095	0.584	0.721	0			
60	0.033	0.559	0.462	0	0	0.041	0.525	0.633	0			
85	0.013	0.438	0.548	0	0	0.012	0.416	0.572	0			
129	0.002	0.234	0.764	0	0	0.002	0.278	0.729	0			
159	0.001	0.157	0.942	0	0	0.001	0.149	0.551	0			

Table 2.3

CUMULATIVE MASS-CHAIN YIELDS OF FISSION PRODUCTS
(VALUES ARE IN PERCENT OF FISSION/NH)

Mass Number	U-238		U-235		Pu-239	
	Thermal Neutrons*	Fission Neutrons	Fission Neutrons	8-Mev Neutrons	Thermal Neutrons	Fission Neutrons
72	1.0x10 ⁻⁶	4.6x10 ⁻⁴	5.0x10 ⁻⁶	-	1.8x10 ⁻⁴ *	-
73	1.1x10 ⁻⁵	0.0012	0.7x10 ⁻⁵	-	0.2x10 ⁻⁴	-
74	(0.2x10 ⁻⁵)**	0.0084	1.1x10 ⁻⁴	0.001	4.1x10 ⁻⁴	0.0011
75	(0.8x10 ⁻⁵)**	0.0082	8.3x10 ⁻⁵	0.0040	7.0x10 ⁻⁴	0.0028
76	(0.0029)	0.012	0.0012	0.0078	0.0014	0.0061
77	0.0088	0.028	0.0088*	0.014	0.0026	0.011
78	0.021	0.048	0.0095	0.026	0.0049	0.025
79	(0.041)	0.096	0.019	0.053	0.0090	0.048
80	(0.077)	0.19	0.045	0.096	0.018	0.076
81	0.14	0.21	0.088	0.18	0.080	0.14
82	(0.29)	0.50	0.20	0.35	0.056	0.26
83	0.544	0.80	0.40*	0.66	0.10	0.07
84	1.00	1.0	0.56*	1.08	0.17	0.00
85	1.00	1.85	0.80	1.45	0.28	0.02
86	2.02	2.5	1.85*	1.8	0.48	1.15
87	(2.94)	3.0	1.00	2.85	0.70	1.0
88	(3.02)	4.0	2.45	2.7	1.2	1.0
89	4.70	5.1	3.9*	3.17	1.0*	0.4
90	5.77	5.5	3.2*	3.7	0.4	0.0
91	5.84	5.85	3.0	4.0	0.0	0.7
92	6.03	6.0	4.1	4.8	0.7	4.4
93	0.45	0.4	4.85	5.0	1.0	5.0
94	0.40	0.4	5.0	5.45	0.5	0.4
95	0.27	0.3	5.7*	5.6	0.9*	0.6
96	0.80	0.8	5.8	5.7	0.7	0.0
97	0.00	0.1	5.7	5.84	0.6*	0.2*
98	5.78	5.8	5.7	5.6	0.4	0.4
99	0.08	0.1**	5.0*	5.2**	0.0*	0.0*
100	0.80	0.7	6.1	6.4	0.0	0.4
101	0.0	5.3	5.0	5.0	0.0	0.0

Table 8.9 (continued)

**CUMULATIVE-MASS-CHAIN YIELDS OF FISSION PRODUCTS
(VALUES ARE IN PERCENT OF FISSIONS)**

Mass Number	U-238		U-235		Pu-239	
	Thermal Neutrons*	Fission Neutrons	Fission Neutrons	H-Mev Neutrons	Thermal Neutrons	Fission Neutrons
102	4.1	2.0	5.0	0.0	5.0	5.0
103	0.0	1.7	0.0	0.0	0.8*	4.0
104	1.8	0.95	0.4	0.2	0.0	0.5
105	0.00	0.54	0.0	0.2	0.0*	0.2
106	0.08	0.30	2.7*	1.5	0.0*	0.0
107	0.10	0.17	1.85	1.0	4.0	3.1
108	(0.085)	0.008	0.07	0.70	3.0	2.0
109	(0.089)	0.058***	0.32*	0.48	1.0*	1.0*
110	(0.020)	0.000	0.18	0.30	0.00	0.81
111	(0.018)	0.022***	0.073	0.28***	0.27*	0.34
112	(0.018)	0.020***	0.046*	0.10	0.10*	0.14*
113	(0.018)	0.018	0.040	0.17	0.055	0.000
114	(0.011)	0.017	0.041	0.16	0.040	0.075
115	0.0104	0.017***	0.040*	0.18***	0.041*	0.000*
116	(0.010)*	0.017*	0.000	0.14	0.030	0.000
117	(0.010)	0.017	0.030	0.14*	0.038	0.065
118	(0.010)	0.017	0.040*	0.14	0.038*	0.004*
119	(0.011)	0.017	0.041	0.14	0.030	0.004
120	(0.011)	0.018	0.042	0.15	0.041	0.060
121	(0.018)	0.020	0.044	0.10	0.044*	0.066
122	(0.018)	0.022	0.040	0.17	0.047	0.069
123	(0.015)	0.030	0.050	0.19	0.032	0.070
124	(0.017)	0.030	0.055	0.00	0.038	0.088
125	0.021	0.095	0.072	0.00	0.072*	0.14
126	(0.058)	0.17	0.175	0.48	0.175	0.05
127	(0.145)	0.80	0.89	0.70	0.39*	0.80
128	0.07	0.54	0.77	1.0	0.77	1.0
129	0.00	0.05	1.45	1.5	1.40	2.5
130	2.0	1.7	2.0	2.2	2.0	3.2
131	(2.88)	2.0	0.2*	0.2	0.8*	0.8

Table 2.8 (continued)
 CUMULATIVE MASS-CHAIN YIELDS OF FISSION PRODUCTS
 (VALUES ARE IN PERCENT OF FISSIONS)

Mass Number	U-235		U-238		Pu-239	
	Thermal Neutrons*	Fission Neutrons	Fission Neutrons	8-Mev Neutrons	Thermal Neutrons	Fission Neutrons
132	(4.31)	4.0	4.7*	4.4	5.0	4.0
133	(6.46)	6.1	5.5*	5.4	5.27*	4.0
134	(7.80)	7.0	6.0*	6.5	5.08*	5.2
135	(6.40)	6.0	6.0*	6.0	5.03*	5.1
136	(6.86)	6.4	5.9*	5.8	5.00*	5.0
137	(6.05)	6.0	6.2	5.85	5.24*	6.4*
138	5.74	5.7	6.4	6.0	5.5	5.4
139	(6.84)	6.4	6.5	6.0	5.7*	5.9
140	6.44	6.4	5.7*	5.6	5.08*	5.0*
141	(6.80)	6.8	6.7	6.6	5.2*	4.7
142	(5.85)	5.9	5.7	5.4	5.00*	4.0
143	(5.87)	5.8	5.6	4.07	5.4*	5.0
144	5.67	5.1**	4.0*	4.0**	5.30*	4.8
145	5.95	4.2	5.7	5.7	4.84*	4.4
146	5.07	5.3	5.1	5.17	5.63*	5.7
147	5.88	2.6**	2.6**	2.7**	5.02*	5.0
148	1.70	1.85	2.0	2.27	2.98*	2.86
149	1.13	1.8**	1.48	1.0**	1.70	1.80
150	0.07	0.80	1.05	1.45	1.38*	1.48
151	0.40	0.00	0.74	1.02	1.00	1.10
152	0.285	0.01	0.50	0.00	0.88*	0.08
153	0.15	0.10**	0.82	0.41**	0.52	0.00
154	0.077	0.000	0.10	0.25	0.32*	0.07
155	0.030	0.048	0.11	0.15	0.20	0.23

Table 2.8 (concluded)

**CUMULATIVE MASS-CHAIN YIELDS OF FISSION PRODUCTS
(VALUES ARE IN PERCENT OF FISSIONS)**

Mass Number	U-235		U-238		Pu-239	
	Thermal Neutrons*	Fission Neutrons	Fission Neutrons	8-Mev Neutrons	Thermal Neutrons	Fission Neutrons
156	0.014	0.028**	0.086*	0.092**	0.12*	0.14
157	0.0078	0.012	0.034	0.057	0.084	0.075
158	0.009	0.0082	0.016	0.082	0.084	0.048
159	0.00107	0.0084**	0.0090**	0.017**	0.020****	0.025
160	8.5x10 ⁻⁴	0.0018	0.0096	0.0085	0.0092	0.011
161	7.6x10 ⁻⁶	4.6x10 ⁻⁶ ***	9.4x10 ⁻⁴	0.0044**	0.0035****	0.0051

* Seymour Katcoff, Fission-Product Yields From U, Th and Pu, Nucleonics, Vol. 18, No. 4, p. 78-85 (1958).

** L. R. Bunney, E. M. Scadden, J. O. Abriam, and N. E. Ballou, Radiochemical Studies of the Fast Neutron Fission of U-235 and U-238, Second UN International Conference on the Peaceful Uses of Atomic Energy, A/Conf. 16/P/648, USA, June 1958.

*** G. P. Ford, J. S. Gilmore, et al., Fission Yields, LA-DC-8088, 1958.

**** L. R. Bunney, E. M. Scadden, J. O. Abriam, and N. E. Ballou, Fission Yields in Neutron Fission of Pu-239, USNRDL-TR-268, 1958, Uncl.

a. Parentheses indicate estimated values or where Katcoff's value was altered in order to adjust the yields to a gross sum of 100 in each peak.

b. Line indicates division of two peaks that was used for individual peak sums.

The yield curve for thermal-neutron fission of U-235 gives an average value of 2.5 neutrons per fission. For fission-spectrum neutron fission of U-238, an average value of 3.1 neutrons per fission is obtained. These two values, together with the referenced data in Table 2.8, are used to derive a set of stylized yield curves for the fission-neutron fission of U-238 and Pu-239 and for the 8-Mev neutron fission of U-238.

In each case, the fission by fission neutrons is assumed to yield about 3 neutrons per fission and the 8-Mev fission to yield 4 neutrons per fission. For such a variation with neutron energy in the neutron yield per fission, 14-Mev neutron fission gives about 4.8 neutrons per fission. At a given mass chain yield, the increase in the neutron energy from thermal to fission-spectrum energies shifts the right side of the heavy-element peak to the heavier masses by about a 1/4-mass unit. Where there are no data to indicate any possible changes in the fine-structure shape of the yield curve at the peak, the general shape of the thermal-neutron yield curves is retained, but is adjusted in height so that the total yield in each peak is reasonably near 100.

The large discrepancy between Katcoff's values and those given by Bunney (see Table 2.8) in the rare earth yields for thermal-neutron fission of Pu-239 may be due to persistent errors in the counter calibration. The yield values given by Bunney are lower by a factor of 1.5 at mass number 144 and approach Katcoff's values as the mass increases; at mass number 186, Bunney's value is only about 20 percent lower. Katcoff's values give a peak sum nearer 100; therefore are used in Table 2.8.

Comparison of the cumulative chain yields at the two peaks ($A = 90$ to 100 and $A = 181$ to 144) for these types of fission indicates that no very large differences in the gross decay rates of the fission products from the three fission nuclides should be expected. The mass-chain yields for fission-neutron fission of Pu-239 appear to differ most from the yields of the thermal-neutron fission of U-238. For mass numbers such as 140 and 98, whose radioisotopes may contribute more than 80 percent of the total gamma radiation at specific times after fission, the largest difference is 28 percent for mass number 140 and 11 percent for mass number 98. The yield of mass number 90, however, is significantly lower for U-238 (8-Mev neutrons) and Pu-239 (fission neutrons); the differences are 36 and 48 percent, respectively.

The yields of mass number 187 are all more nearly alike. The largest chain yield differences occur between the peaks and the yields that appear at the highest and lowest mass numbers. But even for U-238 fission (8-Mev neutrons), where the yields of the mass numbers near 118 are more than a factor of ten larger than the yield for U-238 fission (thermal neutrons), the contribution of these "valley" elements is a small fraction of the total radioactivity of the fission products.

To use the mass chain-yield values in computations of the amount of each element that is condensed to form fallout and in calculating the gross decay rate of the mixture requires some estimate of the independent yield of each chain member. Partly for convenience, the independent yields calculated by Hollow and Ballou² for thermal-neutron fission of U-235 are converted to fractional chain yields so that they may be applied directly to all the cumulative mass-chain yields for each type of fission.

Although it appears that Glendenin's symmetrical charge-distribution curve is generally applicable for all fission nuclides in low energy neutron fission, it has been shown⁶ that the most probable charge, Z_p , (for a given mass distribution) shifts toward stability with increasing neutron energy. That is, the higher fractional yields appear farther to the right (toward a higher Z-number) in any decay chain. Pappas⁷ used a discontinuous function for Z_p and considered the primary fragments before neutron boil-off; however, Wahl⁸ has shown empirically that the Z_p function in thermal fission of U-235 is continuous, as was originally postulated by Glendenin et al.⁹ Harrington¹⁰ proposes two charge-distribution curves, one for the even-neutron nuclides and another, showing a lower yield, for the odd-neutron nuclides.

It is clear that there is no unequivocal choice among methods for estimating the independent yields of the chain members, even for thermal-neutron fission of U-235. For the independent yields of higher-energy fission, the experimental data are rarer yet. It is therefore assumed that the fractional independent yields for thermal fission of U-235 calculated by Hollow and Ballou on Glendenin's postulate are not too inappropriate for any kind of fission with low-energy neutrons. When more data become available on the total chain yields and on the independent yields for each fission nuclide, the indicated corrections can be easily applied to the computations.

The total energy released in the fission process can be calculated by using the mass packing-fraction curves, for the final stable nuclide in each mass chain, for the fission nuclide involved, and for the fractional mass-chain yields. The calculated energy releases are:

199 Mev per fission for fission-neutron U-235 fission,

204 Mev per fission for 8-Mev neutron fission of U-235, and

209 Mev per fission for fission-neutron fission of Pu-239.

By use of the value 1.10×10^{12} calories per kiloton of TNT, and the value 8.697×10^{-14} calories per Mev, the number of fissions that release the same energy as 1 kiloton of TNT can be obtained. These are:

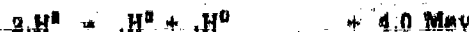
$$1 \text{ KT} = 1.44 \times 10^{20} \text{ fissions (U-235, fission-neutrons)}$$

$$1 \text{ KT} = 1.41 \times 10^{20} \text{ fissions (U-238, 8-Mev neutrons)}$$

$$1 \text{ KT} = 1.08 \times 10^{20} \text{ fissions (Pu-239, fission-neutrons).}$$

All of the original computations in which this number-of-fissions conversion factor is used are made by using the value 1.45×10^{20} fissions per KT, without reference to the type of fissile material the computation applies to.¹¹ The excess neutrons, produced by the fission process only, were 0.48 moles per KT for U-235 (fission neutrons), 0.47 moles per KT for U-238 (Mev-neutrons), and 0.46 moles per KT for Pu-239 (fission neutrons).

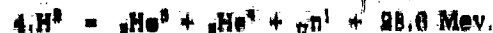
The energy and neutron yields that are possible for some thermonuclear reactions can be estimated from the reactions given in ENW (p. 16). These include, for deuterium combinations:



and



The sum of these reactions is



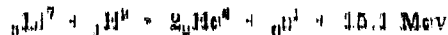
The indicated energy release is 0.80 KT per mole of deuterium molecules; the neutron yield is 1.7 moles per KT.

For the tritium reaction,



The energy release for this reaction is 0.28 KT per mole of tritium molecules; the neutron yield is 0.4 moles per KT.

For the combination of light elements, such as lithium and deuterium, a reaction such as



can occur. In this reaction, the energy released is 0.92 KT per mole of lithium deuteride, with a neutron yield of 2.1 moles per KT. Several other reactions can be formulated for the fusion of these light elements; most of them give reaction energies in the range of 10 to 25 Mev, and neutron yields of between zero and 2 for each reaction. Thus, for the energy-release and the neutron yields of thermonuclear reactions, a reasonable estimate seems to be that about 0.8 KT of energy per mole of reactant is released, and about 2.5 moles of neutrons per KT are produced.

In all thermonuclear weapons, the total yield of the explosion is the sum of the energy released by both the fission and the fusion processes. However, the amount of radioactive fission products produced depends only on the fission yield. Thus, in considering fallout, the ratio of fission to total yield is an important quantity; the concentration of the fission products is directly proportional to the ratio of the fission yield to the total weapon yield. For example, if the fission and fusion yields of a thermonuclear weapon are equal, the radiation from the fallout would be about half that of a pure fission weapon of the same yield.

The number of neutrons produced is also of interest in fallout. Since all the neutrons released are captured by some nearby atom, a considerable amount of additional radioactivity may result. It may be noted that in the fission of U-238 the amount of radioactive fission-product elements produced is 0.47 moles/KT. If all of the excess neutrons were captured by some substance to produce a radioactive product, the total initial radioactive yield would be 1.17 moles/KT. In the same situation, but for a pure thermonuclear yield, the neutron activations alone would amount to 2.5 moles/KT. Thus, in a sense, a pure thermonuclear, or so-called "clean", weapon could have a radiological capability twice that of a pure fission weapon.

But, it would be a rare occurrence that this capability would be realized, because many of the naturally occurring elements that are in large abundance (such as hydrogen, silicon, oxygen, and aluminum) can capture neutrons to produce either another stable nuclide or a very short-lived radionuclide. On the other hand, if a thermonuclear explosion took place where such elements as sodium (mild), manganese, cobalt, and so on, were concentrated in large quantities, the radioactive yield of these elements could be expected to be high.

2.5 The Structure and Composition of Individual Fallout Particles

Information on the structure and composition of individual fallout particles is obtained mainly from two types of observations: (1) petrographic and radiographic analyses of thin sections of fallout particles and (2) radiochemical and chemical analyses of fallout particles. The results of analyses of single fallout particles contribute more to the understanding of the fallout formation process than any other type of analysis. The major limitation in the analyses of single particles is that the methods are not applicable to the study of particles of less than about 100 microns in diameter (and usually larger) for the petrographic methods, and of particles with less than a given radioactive content for the radiochemical methods. The pertinent results from the petrographic and radiographic studies are summarized here, and a description of the experimental techniques follows the summary.

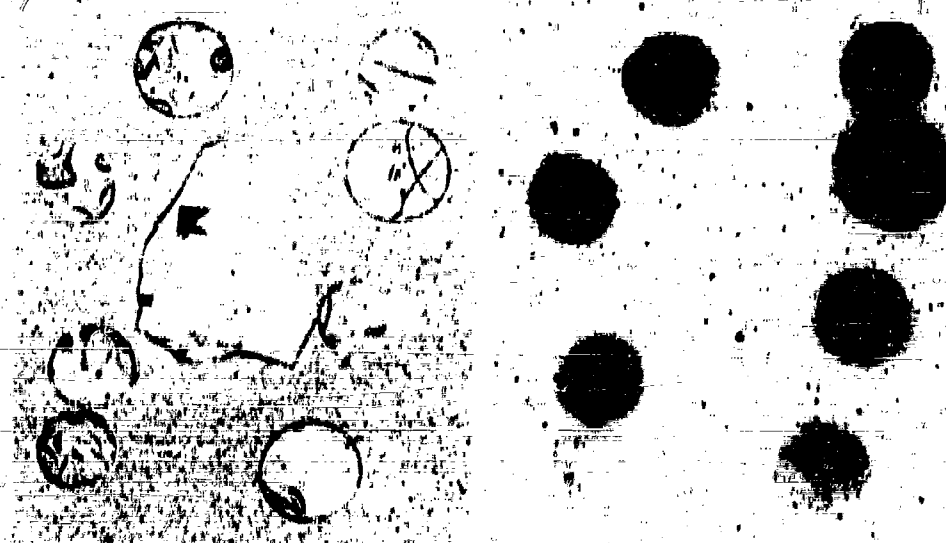
2.5.1 Low Yield, Surface Soil, Silicate Soil

Particles from Operation Jangle in 1961 were analyzed by Adams, Poppoff, and Wallace¹¹ of the U.S. Naval Radiological Defense Laboratory (NRDL) and by others.^{11,14,15} The results of these analyses are the only ones available on fallout from a detonation on the surface of a silicate soil. The particles studied ranged in size from 500 to 10,000 microns in diameter and were selected on the basis of activity content. Thus the results apply to the larger and most highly radioactive of the fallout particles. The observations were made on thin sections about 30 microns thick taken from the central region of the particles (see Figure 2.1).

The findings are summarized as follows:

1. In this section, almost all of the fallout particles consisted throughout of a transparent glass (i.e., a fused silicate mass). Many contained fragments of unmelted mineral grains and air bubbles inside the glass. The mineral grains composed perhaps a few percent of the volume of a particle and the bubbles or voids composed something like two to four times the volume of the mineral grains. Some particles, in the glass phase, contained neither mineral grains nor air bubbles and no radioactivity was found in the unmelted mineral grains.
2. Most of the mineral grains in the glass particles were too small to be easily identified with the petrographic

Figure 2.1
THIN SECTIONS AND RADIOPHOTOGRAPHS OF SOME FALLOUT PARTICLES FROM A SMALL-YIELD SURFACE SHOT AT THE NEVADA TEST SITE. THE PARTICLES ARE A TRANSPARENT, GREEN-YELLOW GLASS WITH THE RADIOACTIVITY DISTRIBUTED MORE OR LESS UNIFORMLY THROUGHOUT THEIR VOLUMES



microscope. Those that were large enough were identified as quartz or feldspar; about 75 percent of the soil at the shot point consisted of these two minerals. Most of the grains were smaller than that of the native soil, appeared to be shattered, generally gave no appearance of being melted, and generally were found scattered at random throughout the glass phase.

3. A fairly large fraction of the particles were spherical or spheroidal; some were true spheres of about 500 microns diameter. The smaller of the particle sizes studied contained fewer mineral grains and voids than the larger irregularly-shaped particles.
4. The exterior appearance of the spherical particles varied from a transparent yellow-green color to a light brown color, and the radioactivity was distributed more or less homogeneously throughout their volume. Many of the spheres had smaller spheres attached or partially fused to their surfaces.
5. The exterior appearance of the irregular particles was the same as that of the native soil mineral grains, but in the glass phase the radioactivity was distributed in an irregular manner throughout the irregular particle.

The study indicated that the large glass particles containing significant amounts of radioactivity could not have been formed by direct vapor condensation of the silicate glass. Electron micrographs of fallout collected on air filters revealed the presence of spheres having diameters of the order of 0.1 micron. Theoretical calculations such as those of Stewart¹⁶ on the condensation of such materials as iron and fission products (in air) in the cooling fireball give particle diameters of the order 0.1 micron. In his calculation, Stewart assumed a fireball containing 20 tons of iron in a radius of 500 feet and that the growth of the particles was a combination of condensation and coagulation. Stewart obtained a modal diameter of 0.2 micron for the iron oxide particles.

Simple kinetic theory equations that describe the growth of particles by collision processes give particle-diameter values, for the formation of particles of a given size in the vapor condensation process, that range from about 0.001 to 0.1 micron, depending on various assumed values of the initial vapor density. Thus the small spherical particles in the NRDL study, with diameters of the order 0.1 micron, probably resulted from direct vapor condensation plus some growth by particle impaction in the liquid state.

The larger spherical particles (containing radioactivity but very few or no mineral grains and no voids) were most likely either mineral grains heated to temperatures near the boiling point of the glass so that the glass became very fluid, or were from a layer of liquid soil, at a point nearest the initial fireball gases, that formed particles when the crater material was violently pulled upward as the fireball rose in the air. The more irregular particles containing the shattered but unmelted mineral grains could have been formed by the violent mixing of the molten glass with the grains of soil minerals that were originally outside the melted zone. The voids also could have been produced in this violent mixing process, as well as by the partial vaporization of volatile constituents in the melted soil that was not sufficiently hot and fluid to permit the escape of these gases.

2.3.2 Low Yield, Underground Shot, Silicate Soil

Particles from a low-yield underground shot were also examined by Adams, Popoff, and Wallace. None of the larger particles were spherical. However, fused glass spheres in the small size range (less than 100 microns in diameter) were observed. Superficially most of the radioactive particles looked like the original soil minerals of the detonation area. They were usually a light brown in color, and opaque. In thin section they were transparent and colorless, had the glass structure found for the surface-shot fallout, but contained a much higher concentration of unmelted mineral grains and voids.

2.3.3 Large Yield, Surface Shot, Coral

Particles available for analysis from detonations of large-yield weapons on the surface of land areas are restricted to those of the fallout produced from coral atolls. The coral reefs are, of course, composed largely of calcium carbonate in the form of aragonite.¹⁷ The findings of C. E. Adams,¹⁸ from analyses of particles obtained from the Mike Shot of Operation Ivy, the first large thermonuclear detonation, are summarized as follows:

1. The particles available for study were grains of a solid white material whose diameters range from about 0.012 microns to less than 25 microns. (Those selected for petrographic and radiographic analyses had diameters between about 750 and 1,500 microns.)
2. The principal constituents, as determined from X-ray diffraction patterns of powders prepared from a group

of particles, were calcium carbonate, in both the calcite and aragonite forms, and calcium hydroxide. Sodium chloride and magnesium oxide were also present but the calcium carbonate and hydroxide compounds were in highest abundance. Small amounts of calcium nitrate were also found on the exterior of some particles.

3. Most of the particles were composed of calcium hydroxide, with a surface layer of calcium carbonate of the calcite structure. The thickness of the surface calcium carbonate layer, on particles exposed to the open air, increased with time. These particles were generally angular in shape.
4. A few particles consisted of only calcium carbonate (aragonite structure).
5. The radiographs of the thin sections of the particles showed that the radioactivity was usually concentrated in a band near the outer surface of the particle (see Figure 2.3). However, a significant fraction of the particles studied had radioactivity distributed more or less uniformly throughout their volumes. These distributions were not found to be related to the chemical or physical structure of the particles.

This information on fallout from detonations on coral was later added to; analyses were made of particles collected from other thermonuclear detonations and by improved sampling methods and coverage. A general discussion of all the results was given by Adams, Maslow, and Scheel.¹⁰ The findings pertinent to fallout from large detonations on coral are:

1. The angular particles found predominating in the Operation Ivy Mike shot fallout were always observed. Variations in this general type of angular particles included some particles containing a core of unaltered calcium carbonate and others with many small reddish-orange-to-black spheres adhering to the particle surface.
2. Occasionally, unaltered oval particles were found that had small black spheres attached to their surfaces (see Figure 2.4). The size of the small spheres generally ranged from submicroscopic up to about 40 microns in diameter.

Figure 2.2
THIN SECTION AND RADIOPHOTOGRAPH OF A FALLOUT PARTICLE FROM A SMALL-YIELD SURFACE SHOT AT THE NEVADA TEST SITE. THE PARTICLE IS A TRANSPARENT YELLOW-BROWN GLASS WITH MANY INCLUSIONS OF GAS BUBBLES AND UNMELTED MINERAL GRAINS. THE RADIONACTIVITY IS DISTRIBUTED IRREGULARLY THROUGHOUT THE GLASS PHASE OF THE PARTICLE

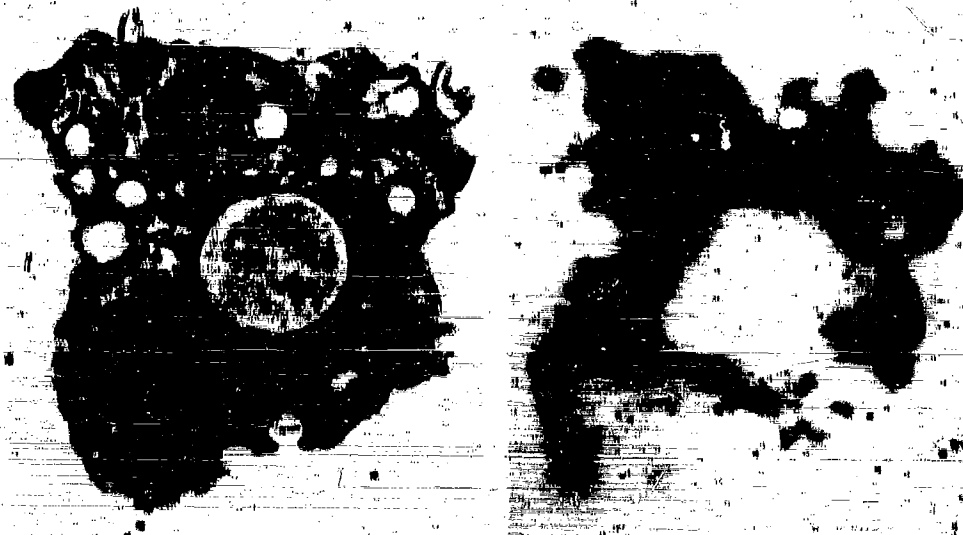


Figure 2.3

THIN SECTION AND RADIOPHOTOGRAPH OF AN ANGULAR FALLOUT PARTICLE FROM A LARGE-YIELD SURFACE SHOT AT THE ENIWETOK PROVING GROUNDS. THIS PARTICLE IS COMPOSED ALMOST ENTIRELY OF CALCIUM HYDROXIDE WITH A THIN OUTER LAYER OF CALCIUM CARBONATE. THE RADIONACTIVITY HAS COLLECTED ON THE SURFACE AND HAS DIFFUSED A SHORT DISTANCE INTO THE PARTICLE

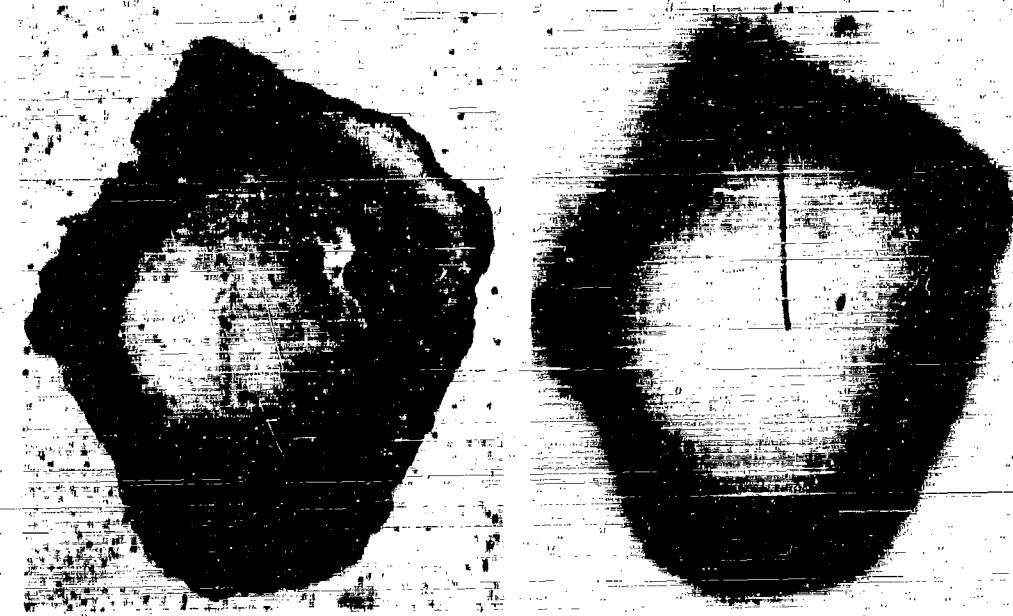


Figure 2.4

**SECTION OF A FALLOUT PARTICLE FROM A LARGE-YIELD SURFACE SHOT AT THE
ENIWETOK PROVING GROUND. THE SMALL, BLACK, RADIOACTIVE SPHERES SHOWN
ADHERING TO THE SURFACE OF A CORAL SAND GRAIN ARE FORMED BY VAPOR
CONDENSATION, WITH SUBSEQUENT GROWTH BY COAGULATION, OF MATERIALS
VAPORIZED IN THE FIREBALL**



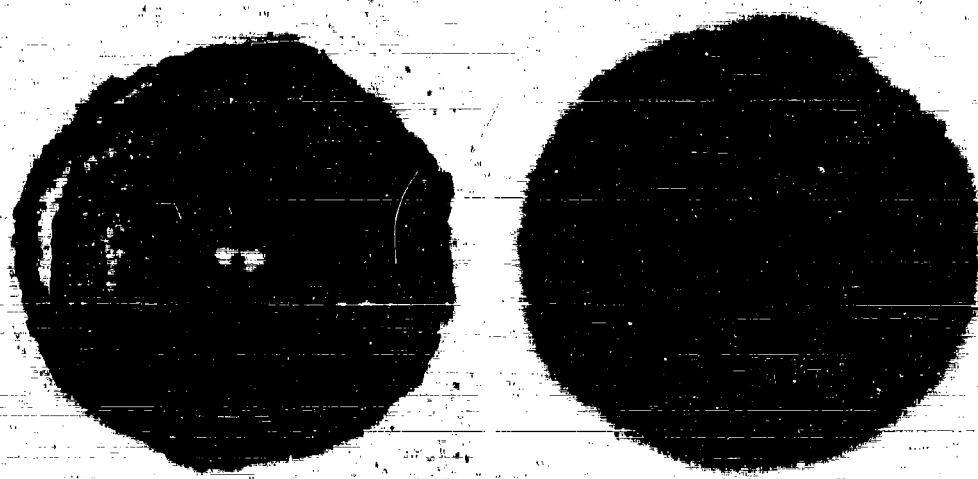
3. The third general type of particle found was spherical; it was composed of calcium oxide that, by the time of analysis, had partially hydrated to calcium hydroxide. The surface was covered with a thin layer of calcium carbonate in the calcite form. In these spherical forms the radioactivity was usually distributed more or less uniformly throughout the particle (see Figure 2,5).
4. The fourth general type of particle found was a very fragile fluffy particle similar to a snow-flake. (Most of these apparently broke easily, either on landing in the collectors or in the handling and shipping of the samples.)

The angular particles, the ones having the irregular shape of fractured coral grains, must have been heated to temperatures higher than 800 to 900°C, since this range of temperatures decarbonates the calcium carbonate. However, the angular particles did not reach the temperature of 2590°C required to melt the calcium oxide. The microporous calcium oxide was hydrated by atmospheric water after it cooled and during its fall to the earth. The calcium carbonate layer in the calcite form must have been formed from the carbon dioxide of the atmosphere after the particle had cooled, since calcite is the stable structure formed by this reaction at temperatures less than 30°C.

The small orange-red-to-black spheres were vapor-condensed particles consisting of a mixture of calcium, iron, and fission-produced oxides. Since it was later found that a large fraction of the activity was in ionic form and could be leached from the angular particles lacking the spheres on their surfaces, it is likely that these radioactive fission products were present in molecular or ionic form in the structure of the particle. The band of activity around the edge of the particle indicates that some inward diffusion must have occurred.

The small particles on the surfaces of the larger ones, however, did not lose activity by diffusion. Hence, some of the activity in these irregular particles must have been collected by the vapor condensation of fission-product elements in their molecular form and some from collisions with vapor-condensed solid (or liquid) particles ranging from molecular size to 10 microns in diameter. The solid calcium oxide, in the presence of carbon dioxide, can exist between 800°C and 2590°C, and many of the fission-product oxides can condense from a vapor phase in this temperature range. The iron, for production of the vapor-condensed spheres, came from the structures around the test device, and the calcium oxide from the vaporized coral at shot point.

Figure 2.5
THIN SECTION AND RADIOPHOTOGRAPH OF A SPHERICAL FALLOUT PARTICLE FROM A
LARGE-YIELD SURFACE SHOT AT THE ENIWETOK PROVING GROUND. THIS PARTICLE
IS COMPOSED ALMOST ENTIRELY OF CALCIUM OXIDE WITH A THIN SURFACE LAYER
OF CALCIUM HYDROXIDE AND CALCIUM CARBONATE. THE RADIOACTIVITY IS
DISTRIBUTED MORE OR LESS UNIFORMLY THROUGHOUT THE VOLUME OF THE PARTICLE



The spherical particles were formed from coral particles heated to temperatures between 2800°C, the melting point of calcium oxide, and about 3500°C, its boiling point (in the presence of about one atmosphere of oxygen). Since this temperature range is not large and would be of short duration, spherical particles were neither formed nor found in great abundance or in large size ranges in coral fallout. Also, melting would destroy the porous structure of the calcium oxide, so that the hydration process would be much slower, hence in these spherical coral particles a large fraction of the oxide would not be converted to hydroxide until after a long exposure to humid atmospheric conditions.

Hydration of the fused calcium oxide involves an increase by a factor of 2 in the volume of the solid, resulting in a rupture of the crystal to the crumbly, fluffy structure. Hence the fragile fluffy particles may have formed from small vapor-condensed calcium oxide particles that hydrated as they fell and agglomerated with other similar particles. Some of these particles may have been formed from larger melted particles that collided with water drops in their fall and thus completely hydrated to the observed structure.

2.8.4 Tower Shot, Silicate Soil

Fallout particles from tower shots over both coral and silicate soils have been collected and analyzed. The results of analyses on particles from a tower detonation over silicate soils by C.E. Adams and J.P. Wittman²⁰ are summarized as follows:

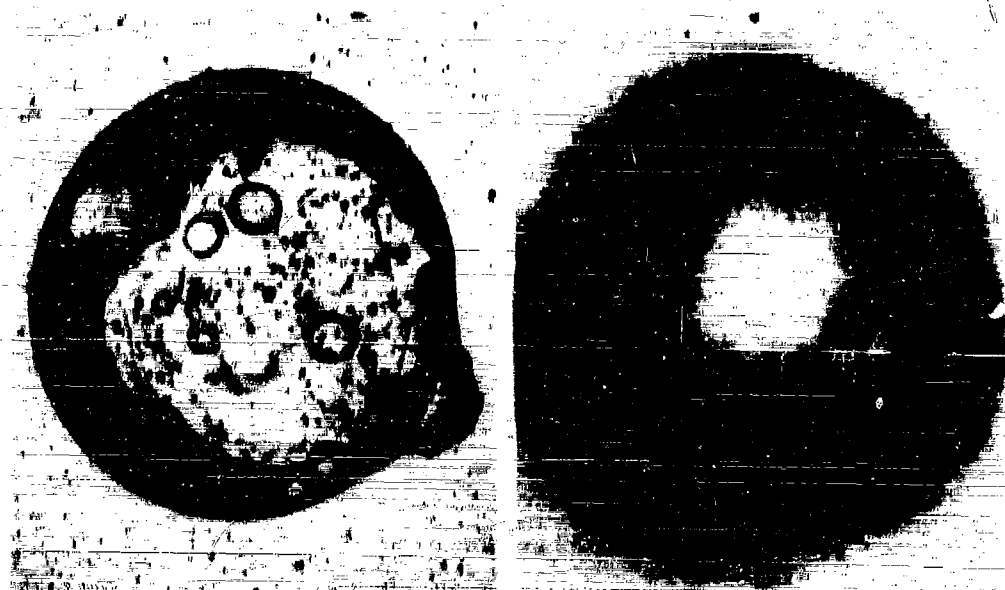
1. The particle sizes used in the study ranged from 140 to 1750 microns in diameter. Most of the particles were brown-to-black spheres or spheroids, but some were irregular in shape (see Figure 2.6). Most of them were magnetic. The surface luster was between dull metallic and a brilliant gloss. Their measured densities were between 1.4 and 3.9 gm/cm³. Many of the particles had smaller spheres fused onto their surfaces.
2. In thin section the central core of the particles was transparent glass with a color ranging from light brown to colorless (see Figure 2.7). The core was surrounded by an irregular thickness of dark brown (or black) opaque glass.
3. The glass occasionally had flow lines and in many cases a fairly large number of voids; the latter were responsible for the extreme variation in the observed densities. A few mineral grains were observed in the glass matrix.

Figure 2.6

TWO FALLOUT PARTICLES FROM A TOWER SHOT AT THE NEVADA TEST SITE. THE PARTICLE ON THE LEFT IS A PERFECT SPHERE WITH A HIGHLY GLOSSY SURFACE; THE ONE ON THE RIGHT HAS MANY PARTIALLY-ASSIMILATED SMALLER SPHERES ATTACHED TO ITS SURFACE. BOTH PARTICLES ARE BLACK AND MAGNETIC AND HAVE A SUPERFICIAL METALLIC APPEARANCE. THE INTERIOR STRUCTURE OF THIS TYPE OF PARTICLE IS SHOWN IN FIGURE 2.7



Figure 2.7
THIN SECTION AND RADIOPHOTOGRAPH OF A FALLOUT PARTICLE FROM A MODERATE-YIELD
TOWER SHOT AT THE NEVADA TEST SITE. THIS PARTICLE IS COMPOSED OF A
TRANSPARENT GLASS CORE WITH A DARKLY COLORED IRON OXIDE GLASS OUTER
ZONE. MOST OF THE RADIOACTIVITY IS CONCENTRATED IN THE OUTER ZONE



4. The radiographs showed that the radioactivity was usually more highly concentrated in the opaque glass around the core. In some particles the core was inactive; in others the radioactivity was distributed in a more or less random manner throughout the particle.

The strong magnetic property of these particles was due to the iron oxide (opaque) glass around the central core. The smaller particles tended to be more opaque throughout their volumes; i.e., without the transparent central core. The amount of iron oxide glass varied somewhat with weapon yield and with the tower's size or mass; the heavier tower types resulted in particles containing as much as an average of 8 percent iron by weight.

2.8.8 Tower Shot, Coral Soil

The results of analyses of particles from a tower detonation over coral soils by C.E. Adams and J.D. O'Connor¹¹ are summarized as follows:

1. Three general types of radioactive particles were found.
2. The most abundant type was dull black, spheroidal, weakly magnetic, and cracked and veined with white crystalline material. The sizes analyzed had diameters from about 300 to 1000 microns. The thin sections (see Figure 2.8) showed that these particles had a central core--originally calcium oxide but partially converted to calcium hydroxide and calcium carbonate by the time of sectioning--that was surrounded by a thick layer of black opaque material identified as dicalcium ferrite ($3\text{CaO}\cdot\text{Fe}_2\text{O}_3$). The white material in the veins was found to be a mixture of calcite and vaterite, the two low-temperature crystal forms of calcium carbonate. The radioactivity was always concentrated in the dicalcium ferrite phase.
3. The second most abundant type was a magnetic black spherical particle with a glossy luster. The particles in the samples analyzed were between 300 and 600 microns in diameter, and were composed mostly of magnetite (Fe_3O_4) along with some hematite (Fe_2O_3). The radioactivity was found to be more or less uniformly distributed throughout the particle volume (see Figure 2.9).
4. The third type, not very abundant, was white and irregular in shape and looked much like grains of the original coral. The

thin sections showed these particles to be composed either of unaltered coral or of calcium hydroxide with a thin coating of calcium carbonate. Many small black spheres with diameters about 10 microns or less were found attached to the surface of these least abundant particles. The radioactivity, as shown by radiographs, was concentrated in these attached small black spheres.

The most abundant type of particles contained dicalcium ferrite; these could only have been formed either by the reaction between liquid calcium oxide particles and iron vapor in the presence of oxygen or by the impaction and solution of small drops of liquid iron oxide to form the dicalcium ferrite. Since the calcium oxide has a two-fold volume increase on hydration to the hydroxide, the veins must have formed after the particles solidified under internal pressure resulting from the hydration of the inner core of calcium oxide. In this process, some of the hydroxide apparently diffused into the fissures where it was carbonated by atmospheric carbon dioxide.

The second most abundant type, the iron oxide particles, were probably formed during the cooling of the fireball by the oxidation of liquid iron drops (from the steel tower). Both the vaporized iron and some of the fission-product elements apparently condensed more or less simultaneously to form these particles; apparently they solidified without colliding with molten calcium oxide particles.

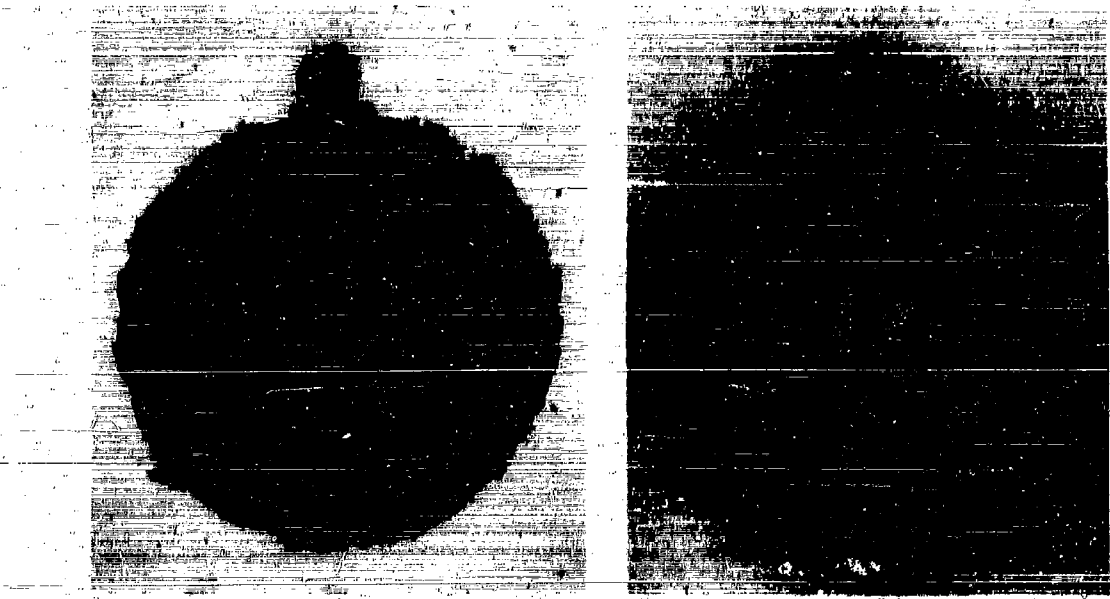
Since the melting temperature of magnetite is 1600°C and that of the calcium oxide is 2890°C, the two would not be present in liquid form in the temperature range 1600°C to 2890°C. In fact, the more stable liquid iron oxide (in the presence of about one atmosphere of oxygen at temperatures above the melting point) is FeO; under these conditions, its boiling point is about 3300°C. Thus the temperature range over which both liquid calcium oxide and iron oxide may exist is between about 2600°C and 3300°C. The iron came from the tower; it was located nearer to the center of the detonation than the calcium oxide that was originally coral at the base of the tower; the presence of the pure iron oxide particles indicates that the two materials did not mix homogeneously in the fireball by the time it cooled to 2600°C. The absence of calcium in the particles also indicates that the amount of calcium oxide vaporized was very small.

The third type of particle was apparently formed by collisions between the small vapor-condensed iron oxide particles and grains of coral not heated to 2600°C. Thus these least-abundant particles must have formed at later times than the other two types. The fact that the small attached particles were as large as 10 microns indicates that the initial vapor condensation process continued long enough to permit considerable coagulation.

Figure 2.8
THIN SECTION AND RADIOPHOTOGRAPH OF A FALLOUT PARTICLE FROM A MODERATE-YIELD
TOWER SHOT AT THE ENIWETOK PROVING GROUND. THE GRAY CENTRAL AREA AND
VEINS ARE REMNANTS OF THE ORIGINAL INACTIVE MELTED CALCIUM OXIDE PARTICLE.
THE DARK AREAS ARE THE DICALCIUM FERRITE IN WHICH THE RADIOACTIVITY IS
CONCENTRATED



Figure 2.9
THIN SECTION AND RADIOPHOTOGRAPH OF A FALLOUT PARTICLE FROM A MODERATE-YIELD
TOWER SHOT AT THE ENIWETOK PROVING GROUND. THIS PARTICLE IS COMPOSED
ENTIRELY OF MAGNETITE AND THE RADIOACTIVITY IS DISTRIBUTED UNIFORMLY
THROUGHOUT ITS VOLUME



That the pure iron oxide particles were not observed in the fallout from tower shots over silicate soil does not prove their nonexistence, but that, if produced, their abundance in the fallout was very low. This is best explained by the fact that the glass from silicate minerals can exist in a liquid (i.e., fluid) state at temperatures even lower than those at which the pure iron oxide solidifies. This would permit more time for mixing in the fireball and for coagulation of the liquid drops of iron oxide and the silicate minerals. Since many of the silicate glass particles had small spheres attached or fused onto their surfaces, the process of coagulation must have continued until the surface of the particles was very viscous.

Weapon yield, the height and mass of the tower, and the boiling temperatures of the various substances are all factors in determining whether ground-surface materials are vaporized, and, if they are vaporized, in determining the quantities that enter the fireball in vapor form. Most of the fallout particles from tower shots are undoubtedly derived from grains of original soil. However, in one or two cases, where the surface soil contained an appreciable amount of substances that melt at low temperatures, such as sodium carbonate, that could act as a fluxing agent, evidence of liquid puddling on the surface of the soil under the tower was observed.

2.8.6 Surface Shot, Ocean (Sea Water)

Only a few fallout particles or liquid drops from detonations on or near the surface of the ocean have been analyzed, mainly due to the fact that special analytical techniques not available early in the weapons test series had to be developed. However, special reagent films developed by Farlow²² for analyzing liquid drops were used on a few collected samples (see Figure 2.10). The particles, collected at a single location from a detonation on a barge anchored in the lagoon at Bikini Atoll, consisted of a saturated solution of sea water salts, some suspended crystals of sodium chloride, and some insoluble solids.

Most of the insoluble solid materials were found to be agglomerates of small reddish-orange-to-black spheres. Some of these were as large as 30 microns in diameter (see Figure 2.11). From their X-ray diffraction pattern, the spheres were identified as being composed of dicalcium ferrite. In these particular samples, only about 15 percent of the activity diffused into the reagent films; the remainder was associated with the solids. The iron came from the large steel barge and the calcium came from the coral sand used as ballast in the barge.

Figure 2.10
PHOTOMICROGRAPH OF A DICHROMATE REAGENT FILM OF AN INDIVIDUAL LIQUID FALLOUT PARTICLE FROM A LARGE-YIELD BARGE SHOT AT THE ENIWETOK PROVING GROUND. THE SOLUBLE CHLORIDE IN THE DROP HAS REACTED WITH THE REAGENT FILM, FORMING A WHITE CIRCULAR AREA INDICATING THE AMOUNT OF CHLORIDE IN THE DROP. THE AREA OF THE CENTRAL ELLIPTICAL TRACE COVERED BY SMALL SOLIDS IS A MEASURE OF THE WATER CONTENT OF THE DROP. THE SOLIDS IN THE CENTER ARE SMALL SPHERES FORMED BY THE CONDENSATION OF THE VAPORIZED BARGE AND BALLAST MATERIALS.

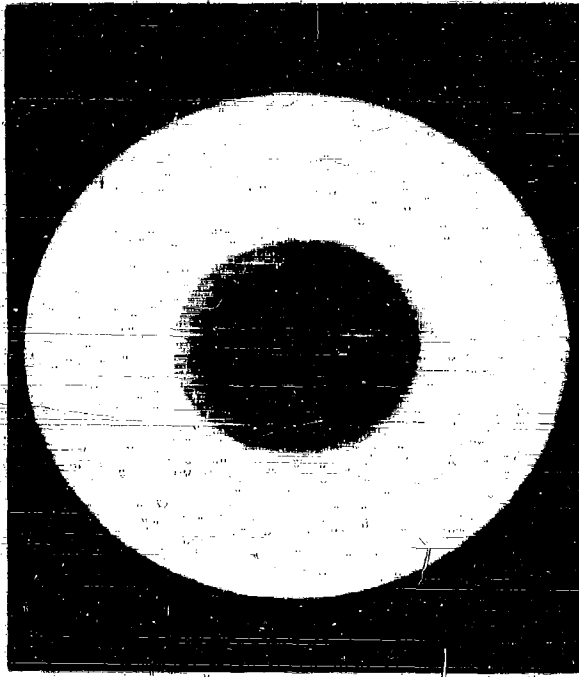


Figure 2.11

ELECTRONMICROGRAPH OF THE RADIOACTIVE SOLIDS IN THE LIQUID FALLOUT PARTICLES FROM A LARGE-YIELD BARGE SHOT AT THE CHISETOK PROVING GROUND. THIS AGGLOMERATION OF VERY SMALL SPHERES, EACH FORMED FROM THE CONDENSATION OF THE VAPORIZED BARGE AND BALLAST MATERIALS, IS COMPOSED LARGELY OF DICALCIUM FERRITE



For these sea water fallout particles, the association of the results of the analyses with possible high-temperature reactions is not quite as straightforward as for the completely solid particles from the other types of detonations. Because of the presence of water, the droplet or particle can change in size. Perhaps changes in the relative amounts of various chemical constituents also occur during the fall of the droplet through the atmosphere. These changes are due to evaporation of water in the drop or to the condensation of atmospheric water vapor, as well as to a continual process of accretion of neighboring particles.

Certainly a large amount of sea water would be vaporized initially along with the fission-product elements and the solid materials of the bomb structure (including the barge and ballast in the test shots). The iron and calcium oxide vapors condense, to form the small calcium ferrite particles, in much the same way as was observed in the fallout from the coral surface and tower detonations. These oxides and some of the more refractory fission-product oxides would condense first, at the higher temperatures. The next substances to condense are the sodium chloride and the less refractory fission products (oxides, hydroxides, or chlorides). And finally, at temperatures around 100°C, the water vapor condenses. It is likely that the first particles to be formed serve as nuclei or surfaces upon which the remaining vapor condenses, although this may not be the only process involved. The same final particle could be formed by separate condensation of the various substances, and by particle growth by impaction, especially when the water drops are present in liquid form and in high concentration.

The water content of the final particle would depend on the humidity and temperature conditions of the atmosphere through which it falls. While the final water content of the particle would be determined to a large degree by these conditions in the latest part of their fall trajectory near the earth, the particles carried to great altitudes would fall through air layers at temperatures less than 0°C. In these layers the particles would be solid, and the time that they would remain in the solid state from a large yield detonation would be a large fraction of their total fall time. The loss and/or gain in water content during the fall would result in corresponding changes in particle size and density as well as in fall velocity of the particle.

2.3.7 Inferences on Fallout Particle Formation Processes

The consistent inferences of the data, with regard to the formation of the fallout particles in the cooling fireball, are:

1. The vapor-condensation of small particles begins at the highest temperature at which a macroscopic liquid phase can exist in equilibrium with its saturated vapor. The

substance forming this initial liquid phase is always a non-radioactive material, such as the metal oxides from the structural components of the weapon and/or the decomposition products of the wotto. These substances are the ones, nearest the point of detonation, whose vapors are intimately mixed with the fission-product gas atoms. Some of the fission product atoms or molecules condense to form a dilute solution in these particles.

2. Heated soil (and tower) materials are drawn into the fireball as it rises; some of those form particles from the disintegration of a bulky layer of liquid material or are otherwise melted before they enter the cooling fireball. Certain other particles are melted after they enter the fireball, some are only partially melted, and some are not melted at all. The degree of heat treatment received by the various types of particles depends upon the time the particle entered the fireball, its trajectory through the hot gases, the temperatures along that trajectory, and the particle's velocity.
3. The larger of the melted particles collide with and dissolve the small vapor-condensed particles, thus acquiring the radioactive elements they contain.
4. Radioactive elements that remain in the gaseous state during the time these melted particles exist--that is, when the fireball temperature is between the melting and boiling points of the particles--vapor-condense directly onto the particle surfaces to form dilute solutions of the mutually-soluble oxides or compounds. The elements may solidify as separate phases in the particles if the concentration is sufficiently large, or remain essentially as an impurity site in the crystal or glass phase of the larger melted particles.
5. The latest solid particles to arrive in the fireball collide with and scavenge some of the remaining small particles, which then remain on the surface of the larger (unmelted) particles. Since these solid particles collect on their surfaces other particles as large as 10 microns in diameter, they can also vapor-condense on their surfaces the more volatile of the radioactive atoms not previously condensed into the liquid particles. And, since some of the fission products are rare gas elements, this latter type of condensation proceeds as long as the particles and gas atoms remain together.

The particle thin-section analyses, although giving much information on the structures of fallout particles and on the way they are formed, give no quantitative data on the radio-chemical composition of the particles, and only a limited amount of unclassified information is available from radio-chemical analyses of fallout particles. The first information of this kind was reported by Kimura³⁵ et al., who presented analyses of the fallout from Shot Bravo, detonated on March 1, 1954. The fallout for these analyses contaminated the Japanese boat No. 5 Fukuryu Maru. Some of the particles, called ash or dust because of the white color of calcium carbonate or hydroxide, were collected by the crew of the ship who carried the material back to the Japanese mainland where the analyses were made.

In the report, Kimura chose to refer his data to the thermal-neutron fission of Pu-239. The data were reanalyzed on the basis of 8-Mev neutron fission of U-238 because of the reported high abundance of the nuclide, U-237, presumably produced by a ($n, 2n$) reaction on U-238. In this instance, the Pu-239 was presumably produced by a (n, γ) reaction on U-238 in which the initial product, U-239, had, to a great degree, decayed to Np-239 and then to Pu-239 by the time of the analyses. Kimura's data are compared with the calculated activities for U-238 fission at D + 25 (25 days after detonation) and summarized in Table 2.4. The ratios of the observed percentages to those calculated for the rare earth nuclides, Y-91 and Nb-95, are greater than one. It is clear that the percentage of fission product activity missing is greater than the 17.4 percent unaccounted for in the sample analyses. To check the reality of the high yield for Nd-147 and the low yield for Ce-141, the two ion-exchange elution curves given by Kimura for the rare earth nuclides at D + 40 were integrated, giving the following percentages: Y-91, 18-21 percent; Pm-147, Nd-147, 3-12 percent; Pr-143, 15-30 percent; and Ce-141, Ce-144, Pr-144, 40-50 percent. These values agree with the calculated percentages of Y-91, 21 percent; Nd-147, 10 percent; Pr-143, 25 percent; and Ce-141, Ce-144, Pr-144, 45 percent, at D + 40. Thus it was concluded that the ratios 0.88 and 2.00 in Table 2.4, for Ce-141 and Nd-147 respectively, do not indicate a depletion of Ce-141 and an enrichment of Nd-147.

Assuming that the rare earth elements, yttrium, zirconium, and niobium are in the correct ratios for U-238 fission, their gross contribution to the activity may be used as a basis for estimating the relative depletion or enrichment of other fission-product nuclides. The data of Bolles and Ballou³⁶ for U-238 fission products (with adjustment to the fission yields of Table 2.3) were used to calculate the percentage of activity at D + 25 for U-238 fission with 8-Mev neutrons. The indicated unfractionated nuclides contribute 46.9 percent of the beta activity, whereas the observed percentage was 65.0 percent; hence only 72 percent of the normal fission-product mixture activity must have been present in the sample. The remaining 28 percent was then either with another group of particles or did not condense on any large fallout particles.

Table 2.4
CALCULATION OF RELATIVE ACTIVITY RATIOS FROM KIMURA'S DATA ON CORAL FAULTURE²

Nucleide	Half-Life	Percent Of Total Activity On D-25	Percent Of Fission Product Activity On D-25	Percent Of Activity For U-238 For U-238 On D-25	Ratio (%) For U-238 (% Observed)	Adjusted Percent Of Fission Products To Failure	Fraction- ation Number $r_e(A)$
Sr-89	3.8	1.95	1.25	4.01	0.31	0.90	0.27
Sr-90	28.5	0.02±0.01	0.025	0.053	0.47	0.018	0.34
Y-90	61.5	0.02±0.01	0.025	0.053	0.47	0.018	0.34
Y-91	37.0	B-3	10.0	5.39	1.70*	7.22	(1.0)
Zr-93	65.2	3.2	6.25	6.24	0.98*	4.51	(1.0)
Zr-95	35.0	3.1	3.75	3.65	1.23*	2.71	(1.0)
Po-140	12.3d	5.1	6.35	11.92	0.32	4.51	0.35
La-140	1.6h	6.1	7.35	15.68	0.55	3.41	0.46
Ce-141	3.1d	7.5	8.75	19.55	0.83*	6.31	(1.0)
Ce-144	26.2d	2.1	2.50	1.49	1.68*	1.80	(1.0)
Pr-143	13.7d	15.5	20.0	12.02	1.65*	14.4	(1.0)
Pr-144	17.5d	2.1	2.5	1.49	1.63*	1.80	(1.0)
Nd-147	11.3d	3.4	11.25	5.46	2.86*	3.12	(1.0)
T-237	6.75d	28.10	(4.2x10 ⁻⁴)	-	-	-	-
Pu-239	24.36d	5.0	32.35	W.45	-	-	-
		Missing					

* Nucleides with these ratios are assumed to be in correct relative abundance; the ratio of their sums (65.1% of FP activity observed, 46.5% of FP activity for Normal U-238 mixture) is 0.72. The values of $r_e(A)$ are calculated from the ratios of the values of Column 6 to those of Column 4, except for the elements which are assumed to have $r_e(A)$ values of unity.

The ion exchange elution curves reported by Kimura for a gross sample on D + 20 to 22 were also integrated and adjusted to the percentages of the total activity lying under the curve at D + 21. The results are given in Table 2.5, along with the data from Table 2.4 for comparison. In this case, the observed percentage for the rare earth (yttrium, zirconium, and niobium) nuclides is 66.4 percent and the calculated fraction is 48.4 percent; this indicates that, at D + 21, 66 percent of the total activity of the normal mixture was present in the sample. The percentages at the two times differ a little; they would, of course, be expected to change with time.

The estimated fractionation numbers, $r_0(A)$, given in Table 2.6 for various nuclides in the fallout were compiled from the data of Tables 2.4 and 2.5 and other sources as noted. In addition to the rare gas elements and their daughter products, the important elements in the fallout that were depleted include Ru, Te, and I. Other elements undoubtedly were also fractionated but are not listed because they would not contribute significant amounts of activity at D + 21 and D + 25. The summed beta activity for the unfractionated mixture of activities at D + 25 is 7.61×10^{10} disintegrations per second (d/s) per fission. Since only 72 percent of this amount is present in the fallout sample, the equivalent beta activity at D + 25 is 5.49×10^9 d/s per fission.

Pu-239, with a 24,300-year half-life and formed from the decay of U-239 and Np-239, has a decay rate ($1/\lambda$) value of 1.11×10^{-18} atoms of Pu-239 per d/s. At D + 25, the reported ratio of the Pu-239 activity to the fission product activity is 5.0×10^{-6} . The product of these values gives 0.8 atoms Pu-239 per fission. This is essentially equal to the number of U-239 atoms formed at zero time.

The ratio of the activity of the U-237 to the fission products at D + 25 is given as 20/80. For the 6.75-day half-life, $1/\lambda$ is 8.49×10^{-6} atoms U-237 per d/s; hence the relative capture number, C, is

$$C(237) = (20/80) \times 0.8 \times 10^8 \times 8.49 \times 10^{-6} / \exp \left[\frac{-0.698 \times 25}{6.75} \right] \quad (2.1)$$

= 0.15 atoms/fission

Since the alpha-counting technique and separation methods might result in low values of Pu-239 activity relative to the total, the yield of U-239 (or Pu-239) in the sample could well have been larger than 0.8 atoms per fission. For a broad energy band of neutrons centering at about 8-Mev, the yield from a (n, γ) reaction on U-238 could be as much as 5 times the yield of the $(n, 2n)$ reaction.

Table 2.5

PERCENTAGE ACTIVITIES IN ION EXCHANGE PEAKS OF DIFFERENT
CHEMICAL GROUPS IN CORAL FALLOUT SAMPLE Σ_{Cs}

Peak No.	Elements	Percent Of Total Activity At D=21	Percent Of FP Activity At D=21	Adjusted Percent Of FP Activity At D=21	Adjusted Percent Of FP Activity At D=25
1	Sr, Te, La, Ba, Nb, Mo Zr, Nb U	13.5 8.3 21.3	17.2 18.6 -	19.8 8.25 -	11.4 7.9 -
2	Y, Ce, La, Pr, Nb, Pb Sr (T)	39.4	62.7(51.8)* 1.6	35.2 3.61**	39.7 1.06
3	Ba (Lg)	6.2	7.9(5.8)*	25.1	16.5
4					9.9
5					
6					

*7.9% for La-140 is added to Peak 6 and subtracted from Peak 4 for calculating the fraction of normal fission-product activity present.

**Includes Sr-82 and Pb as contributing to Sr-fraction.

Table 2.0
SUMMARY OF ESTIMATED FRACTIONATION NUMBERS
FOR BETA-EMITTING NUCLIDES IN CORAL FAULTURE
FROM NO. 8 FUNIRYU MARU AT D-21 AND D-25

Fractionation Number, $r_n(\Delta)$				
Nuclide	Note	D-21 data	D-25 data	Selected Value
Kr-85	1	(0)	(0)	0
Sr-89		0.27	0.22	0.22
Br-90		0.27	0.34	0.34
Y-90		0.27	0.34	0.34
Y-91		1.0	1.0	1.0
Zr-95		1.0	1.0	1.0
Nb-95		1.0	1.0	1.0
Mo-99	1	(1.0)	(1.0)	1.0
Ru-100	1	(1.0)	(1.0)	1.0
Ru-106	2	0.14	0.41	0.41
Rh-106	2	0.14	0.41	0.41
Ag-111	1	(1.0)	(1.0)	1.0
Cd-115	1	(1.0)	(1.0)	1.0
Cd-116	1	(1.0)	(1.0)	1.0
In-115	1	(1.0)	(1.0)	1.0
Sn-120	1	(1.0)	(1.0)	1.0
Sn-122	1	(1.0)	(1.0)	1.0
Sb-125	1	(1.0)	(1.0)	1.0
Sb-127	1	(1.0)	(1.0)	1.0
Tc-127	1	(1.0)	(1.0)	1.0
Tc-130	2	0.00	0.27	0.27
Tc-132	2	0.06	0.19	0.19
I-131	2	0.08	0.24	0.24
I-132	2	0.06	0.10	0.10
Xe-133	1	(0)	(0)	0
Cm-187	3	--	0.20	0.20
Ba-140		0.40	0.30	0.40
Ta-140		0.40	0.39	0.40
Co-141		1.0	1.0	1.0
Ge-144		1.0	1.0	1.0
Pr-143		1.0	1.0	1.0

Table 2.0 (concluded)

**SUMMARY OF ESTIMATED FRACTIONATION NUMBERS
FOR BETA-EMITTING NUCLIDES IN CORAL FALL-OUT
FROM NO. 6 FUKUROYU MARU AT DIRE AND DEWE**

Fractionation Number, r_0 (Δ)				
Nuclide	Note	D21 data	D125 data	Selected Value
Nd-147		1.0	1.0	1.0
Pm-147		1.0	1.0	1.0
Bm-141		1.0	1.0	1.0
Bm-143		1.0	1.0	1.0
Bu-158		1.0	1.0	1.0
Bu-160		1.0	1.0	1.0

Note 1: Estimated

Note 2: Estimated from ion exchange elution peak activity percentage and from data of Section 2.8, giving the relative fractions condensate of mass numbers 182, 181, 180, and 100, considered to be in the ratio of 1 : 1.0 : 1.4 : 2.2.

Note 3: From a plot of r_0 (Δ) versus the half-life of parent-gamma progenitor.

It may be noted that, at D + 25, the relative activity of 50-hour Np-239 is 2.00×10^{-6} d/s per atom of U-238 produced initially, and for 0.76-day U-237 it is 0.18×10^{-6} d/s per atom of U-237. Thus, even at a 1-to-1 yield ratio, the activity of the Np-239 at D + 25 would be only 1/8 of the U-237 activity and would be difficult to detect. The factor of 8 would give a capture number, C(239), value of 0.75 atoms per fission.

The second set of unclassified data on the radiochemical content of radionuclides particles was reported by Mnokin and coworkers at NRD.²⁴ The sample particles were obtained from detonations on coral islands at the Eniwetok Proving Grounds in 1960. In this case, analyses are made for only a few radionuclides: Mo-90, Sr-89, Ba-140, and Np-239. However, no Np-239 data are reported. In addition, the gross activity of the particles is measured by using a well-crystal-(WC) NaI(Tl) scintillation counter and a 4× high-pressure argon gas (at a pressure of 600 psig) gamma ionization chamber.²⁵

Many of the particles were weighed so that specific activities could be determined, and some data on gross samples were obtained. The Mo-90 radionuclide was utilized as the "fission" tracer with the assumed yield of 6.1 percent; this yield value is sufficiently close to the yield for the 8-Mev neutron fission of U-238 that no adjustment of the reported values was required. Some of the data are summarized in Table 2.7. The particle type designations "altered" and "unaltered" used by the authors have been changed to "fused" particles and "irregular" particles as the first classification of the particles as the first classification of the particle type since the thin-section analyses showed that most of the irregular particles have been calcined.

Because of analytical requirements, only the more highly radioactive particles were used in the reported analyses. This means that the results are applicable only to a description of the larger particles. However, even with this bias, the results are useful in illustrating the possible range in values of all the measured quantities.

The counting-rate and ion-current measurements were corrected to 14470 hours before the apparent average ionization rates, WC-rates per fission, ion-current per fission, and the specific ionization rate were computed. The decay corrections for the WC measurements were obtained from the reported decay curves for the two types of particles; the ionization rate decay corrections were obtained from unpublished data on particles from the same set of samples. It is quite likely that each particle had its own decay rate, differing to some degree from other particles of the same general type. Therefore, with a single type of decay curve, the corrections to it common time are only approximate.

The variability of the ratio of the ion current to the WC count-rate of the set of particles is the first indication of a gross difference in the relative abundances of the emitted gamma rays of different energies, hence of a

Table A.7

RADIOCHEMICAL DATA ON CORAL-TYPE FALL-OUT PARTICLES FROM A LARGE MILD SURFACE IRADIATION

Collecting Source	Particle Description	Diameter (μ)	Crystalline Weight Concentration Weight × 10 ⁻¹⁰ to H + Zn	Oxygen Isotopic Concentration O/H Atom Weight × 10 ⁻¹⁰ to H + Zn	1 Diameter × 10 ⁻¹⁰	Particle Weight Weight Weight × 10 ⁻¹⁰	Average Average Isotopic H + Zn Weight × 10 ⁻¹⁰	W/O at H + Zn Weight/D × 10 ⁴ Weight/D × 10 ⁴	W/O at H + Zn Weight/D × 10 ⁴ Weight/D × 10 ⁴	Average Isotopic H + Zn Weight × 10 ⁻¹⁰
A. Point Particles										
Ship	WI	70	0.017	1.00	70	1.00	0.07	100.7	0.004	0.00
	WI	70	0.0007	1.00	7	1.00	—	101.2	—	—
	WI	70	0.001	1.00	68	1.00	0.78	88	0.404	04.7
	WI	70	0.007	1.00	41	1.00	1.4	78	0.070	00.6
	VI	71	0.006	1.01	69	1.01	0.60	109	0.009	00.8
	WI	70	0.007	1.00	19	1.00	0.49	80	0.403	00.7
	WI	70	0.010	1.00	10	1.00	0.70	90	0.071	00.9
	WI	74	0.120	1.00	16	1.07	—	—	—	—
Island	VI	100	0.500	1.00	407	1.00	20.0	2.100	0.000	00.0
	YH	104	1.17	1.46	128	1.04	—	104	—	0.01
	YH	104	10.0	1.46	1,020	1.08	76.0	0.046	00.0	0.010
	YH	119	0.78	1.08	811	1.08	17.0	0.008	0.007	00.0
Island	YH	800	37.0	1.00	1,000	0.800	—	6.00	70	0.004
	YH	950	07.8	1.00	1,000	0.800	—	17.0	108	0.010
	YH	950	06.6	1.00	1,720	0.800	—	6.70	80	0.000
	YH	950	0.00	1.00	344	1.00	—	47.2	—	—
	YH	950	0.00	1.00	408	1.00	—	6.00	—	—
	YH	950	0.00	1.00	1,400	0.800	—	7.10	20	0.000
	YH	950	0.00	1.00	400	0.800	—	8.00	00.0	0.000
	YH	950	0.00	1.00	164	1.00	40.0	1.76	70	0.047
	YH	950	0.00	1.00	400	0.800	—	6.10	80	0.000
	YH	950	0.00	1.00	1,720	0.800	—	88.8	70	0.000
	YH	950,401	0.70	01.0	860	1.00	180.0	0.76	0.011	00.0
	YH	950,401	1.04	01.0	180	1.00	180.0	1.78	0.008	00.0
B. Irregular Particles										
Ship	WI	70	0.006	1.00	80	1.00	0.07	140	0.034	14.6
	WI	70,71	0.0411	1.03	8	1.03	—	482	—	—
	WI	70,74	0.000	1.04	68	1.04	0.04	109	0.010	00.0
	WI	70,74	0.0173	1.04	8	1.04	—	178	—	—
Island	OI	98	0.01	1.00	408	1.00	0.4	10,440	1.7	0.700
	OI	98	1.71	1.81	168	1.89	—	0.110	174	41.0
	WI	98	0.08	1.81	178	1.89	1.8	0.000	00.9	0.000
	WI	98	0.48	1.00	816	1.40	8.7	0.170	158	0.000
	WI	100	0.0001	1.06	8	1.44	—	0.000	00.7	—
	WI	100	0.000	1.06	87	1.44	8.0	0.000	00.7	—
	WI	100	0.000	1.06	141	1.44	1.0	4.100	101	1.00
	WI	100,100	1.18	1.00	87	1.44	8.0	0.191	124	0.000
	WI	100,100	1.18	1.00	141	1.44	1.0	4.100	101	0.000
	WI	100,100	0.0048	1.06	4	1.40	—	0.191	124	0.000
	OI	108	0.701	1.00	88	1.47	0.04	0.000	106	0.000
	OI	108	0.000	1.00	84	1.47	—	1.000	108	0.000
	WI	108	0.000	1.00	118	1.47	0.07	0.072	108	0.000
	WI	110	0.114	1.00	58	1.03	—	0.000	108	0.000
	WI	110	0.110	1.00	10	1.03	—	0.000	108	0.000
	OI	110	0.000	1.00	10	1.03	—	1.700	108	0.000
	OI	110	0.480	1.00	64	1.03	—	1.010	101	0.000
	OI	110	0.007	1.00	58	1.03	—	1.010	101	0.000
Island	WI	100	0.49	0.00	800	0.00	40.1	207	—	00.0
	WI	100	0.101	0.00	800	0.00	11.8	(100)	—	4.400
	WI	100	1.04	0.00	820	0.00	40.0	100	0.477	00.1
	WI	100	0.00	0.00	820	0.00	40.0	100	—	100
	OI	9444	0.000	0.00	81	0.00	40.0	104	—	4.000
	OI	9444	0.000	0.00	81	0.00	40.0	104	—	4.000
	WI	9444	1.70	0.00	100	0.00	800.0	107	—	1.000
	WI	9444	1.11	0.00	100	0.00	400.0	110	—	1.700
	WI	9444	0.071	0.00	85	0.00	8.0	(100)	—	4.000
	WI	9444	1.07	14.0	880	15.0	44	11.00	100	0.000
	WI	9444	1.07	14.0	880	15.0	44	11.00	100	M.0

T. Radiochemical type description of experimental items

x. Relatively spherical, predominantly formed by coagulation of small active particles and large inactive particles.

YH - yellowish sphere

WI - white sphere

VI - yellowish irregular

OI - pyramidal irregular

WL - white irregular

YH - yellowish irregular

WI - white irregular

VI - yellowish irregular

OI - pyramidal irregular

WL - white irregular

Point Particles

Irregular Particles (I)

Irregular Particles (II)

Average R/R - epd	R/R × 10 ⁻¹⁷	R/R × 10 ⁻¹⁷	R/R × 10 ⁻¹⁷
Mean epd /	0.0000 × 10 ⁻¹⁷ (+ 0.00)	0.0000 × 10 ⁻¹⁷ (+ 0.00)	—
Stdev epd /	0.0000 × 10 ⁻¹⁷ (+ 0.00)	116.6 × 10 ⁻¹⁷ (+ 0.00)	—
Avg R/R - epd	803 × 10 ⁻¹⁷ (+ 0.00)	84.4 × 10 ⁻¹⁷ (+ 0.00)	2.00 × 10 ⁻¹⁷ (+ 0.00)
Avg Particle Mass, mg	—	0.00	0.0
Specific Activity, f. m.c.	26.0 × 10 ⁻¹⁰	0.471 × 10 ⁻¹⁰	0.0000 × 10 ⁻¹⁰

variation in the constituent radionuclides. Although the ratios of the two measurements of the gross activity in the fused particles (i.e., spheres or broken spheres) and the irregular particles have values that average 83×10^{-17} ma/epm and 132×10^{-17} ma/epm, respectively, there are overlapping values in each particle group. Perhaps if the number of particles analyzed had been doubled, this ratio, as a second particle-type classification or distinction between the two groups, might be less marked. In any case, at H=70 the activity in or in the irregular particles emitted more high-energy gamma rays than the activity emitted by the fused particles.

The third type of classification of the two types of particles is the comparison count per minute (cpm) per fission of the Mo value or the mma per fission ratios. Of the two, the ion current per fission gives the larger differentiation, since it is a more sensitive measure of the total photon energy emitted from the mixture. The unfractionated fission-product mixture from the thermal-neutron fission of U-238 gives an ion current of 89.1×10^{-21} ma/fission²⁰ at H=70. This should be within a few percent of the ion current per fission for the unfractionated fission products from 8-Mev neutron fission of U-238. The value, 80.8×10^{-21} ma/fission for the fused particles indicates that if Mo-99 is a good fission indicator the relative abundance of many other nuclides in these particles is low. The value, 110.6×10^{-21} ma/fission for the irregular particles indicates that the relative abundance of the other nuclides is high. The fact that the two values do not have a mean value near 89.1×10^{-21} ma/fission must be due, in part, to the presence of induced activation.

Assuming that the two types of particles together condense essentially all of the gamma-emitting radionuclides that contribute at H=70, and that all the excess ionization is due to Np-239, the capture number, C(239), for U-238 can be estimated from

$$r_{fp}(70) 39.1 \times 10^{-21} + 27.4 \times 10^{-21} C(239) = 80.8 \times 10^{-21} \quad (2.2)$$

where $r_{fp}(70)$ is the gross fission-product ionization-rate fractionation number at H=70, which for the combination of both particle sets is approximately equal to one; 27.4×10^{-21} is the ion current at H=70 per atom of U-238 at zero time; and 80.8×10^{-21} mma per fission is the geometric mean value for the two types of particles.

Setting $r_{fp}(70)$ equal to one gives C(239) equal to 0.70. Since the authors indicate that C(239) is about the same for both particle types, $r_{fp}(70)$ can be back-computed for each type. For the fused particles $r_{fp}(70)$ is 0.20 and for the irregular particles it is 2.43. The fission-product nuclides in the irregular particles, therefore, emit about 0.3 times more gamma energy per fission (relative to Mo-99) than the spherical particles at H=70. When calculated

per unit fission, the reported decay curves of the two types of particles tend to approach each other at about 6000 hours after fission. At these times most of the ionization is due to Zr and Nb nuclides. Hence, these two elements cannot be fractionated with respect to Mo-99; and, further, at about 6000 hours after fission there are no differences in the radiations emitted from the two types of particles.

The fourth comparison between the spherical and irregular types of particles is by their specific activity. At 11470, the ion current per milligram (mg) of the fused particles is about 15 times larger than that of the irregular particles. In this classification, the sample set of irregular particles is given an additional arbitrary subclassification by selection; the particles with a very low specific activity are separated out. The particles so selected for elimination are of the type found in the thin-section analyses where a small native particle is observed to be attached to a larger inactive coral grain. It is also possible that, had more particles been analyzed, the number distribution in specific activities could have filled in the intermediate values to give a broader single distribution.

The specific activity of the fused particles in terms of fissions per gram, based on Mo-99 yields, is about 55 times that of the irregular particles. Since the ion current per fission of the two types of particles becomes equal at about 6000 hours after fission, the ion current from the fused particles is, on the average, 55 times larger than that of the irregular particles.

In a sense, the comparisons given should be taken with some reservation because of the small sampling. On the other hand, the large errors indicated by the standard deviations do not in themselves influence the validity of the conclusions from the data. These deviations rather indicate the breadth of the distributions in the radioactive content of the fallout particles or any other parameter of concern. Thus, the single-particle data of this type are very useful; they provide detailed information on the likely nature of large-sample distributions.

The fractionation numbers for mass numbers 80 and 140, for some of the coral particles, are given in Table 2.8. The values given by Macklin and coworkers¹⁴ are corrected to correspond to the yields from U-238 fission with 8-Mev neutrons. The original R_{80}^A values are defined by

$$R_{80}^A \text{ (U-235 fission)}$$

$$\frac{\text{(Content of Mass } A \text{ in Sample}) / (\text{Content of Mass 99 in Sample})}{(\text{Yield of Mass } A \text{ in U-235 fission}) / (\text{Yield of Mass 99 in U-235 fission})}$$

(2.8)

Table 2.8

**SUMMARY OF FRACTIONATION NUMBERS* FOR MASS NUMBERS
80 AND 140 IN CORAL FALLOUT PARTICLES**

Particle Description	GIC/f at H+70 (ma/f) x 10 ⁻³	R ⁸⁰ ₉₀	R ¹⁴⁰ ₉₀	R ¹⁴⁰ / ₉₀ R ⁸⁰
A. Fumed Particles				
WB	18.8	0.024	0.015?	0.625
B	18.8	0.012	0.080	2.50
YB	25.2	0.20	-	-
YB	26.0	0.026	0.028	1.08
B	29.0	0.0088?	0.018?	0.14
YI	32.6	0.046	0.14	3.04
YB	34.7	0.026	-	-
YI	35.0	0.041	0.14	3.41
WI	38.8	0.114	0.88	2.81
WI	40.7	0.88	-	-
WB	58.0	0.040	0.20	5.00
Geometric Mean	-	0.050(±180%)	0.10(±180%)	-
B. Irregular Particles				
WI	54.0	1.81	0.82	0.455
WI	75.7	0.04	1.6	2.81
WI	88.0	0.86	-	-
GI	98.1	0.82	2.7	0.29
WI	120	1.0	4.0	4.00
WI	126	1.7	2.6	1.53
I	140	0.82	0.89	1.71
WI	208	2.0	9.6	1.56
GI	218	2.8	4.0	1.74
Geometric Mean	-	1.05(±98%)	9.19(±94%)	-

$$\frac{R^{80}}{R^{90}} \text{ (U-238 fission)} = 1.54 \times \frac{R^{80}}{R^{90}} \text{ (U-235 fission)}$$

$$\frac{R^{140}}{R^{90}} \text{ (U-238 fission)} = 1.17 \times \frac{R^{140}}{R^{90}} \text{ (U-235 fission)}$$

? Questionable values, not used to calculate means.

where the content and yields are given in terms of activity at a given time or of number of atoms at zero time, or, in terms of a count rate, from a calibrated analytical procedure in which a foil of U-235 is bombarded with thermal neutrons. The values in the table show that, relative to mass 00, mass 80 was very much depleted in the fused particles and was enriched in some of the irregular particles. For mass 140, the enrichments in the irregular particles were as high as a factor of 4.

The corrected fractionation numbers for the gross-fallout sample collected near the barge-sample particles are 0.061 for mass 80 and 0.12 for mass 140. These values indicate that most of the activity in the gross sample was from the fused (spherical) particles. Because most of the reported data was obtained from large particles, it is not known whether the high fractionation numbers are applicable to small irregular particles and hence to locations further away from ground zero. At least, in the samples further from ground zero, the relative abundance of the fused particles was decreased.

In the irregular particles, the relative amounts of Sr-89 and Ba-140 were higher by factors of 21.0 and 21.9, respectively, than they were in the fused particles. These ratios are not comparable to the ratio of the r_{10} (70) values for the two types of particles, since the latter refers to the relative ionization rate at H+70 hours only, and, of course, the r_{10} values change with time. The fractionation numbers for the irregular particles appear to decrease with particle mass (or size); no comment can be made on the dependence of the fractionation numbers on particle mass for the fused particles because of the small range (1.7 to 3.8 mg) of particle sizes used.

Correlations of fractionation numbers for fallout from relatively high-yield detonations on the surface of coral islands and on sea water are reported by Freiling¹⁷. In the report, Freiling mentions the identification of the induced activities of Na-24, S-35, Ca-48, Br-89, U-237, U-240, and Np-239 although no yields are given. The presence of the last three nuclides suggests that much of the fission yield was due to the fission of U-238. The correlations indicate some relationship among the fractionation numbers namely, that, relative to the refractory elements, the fractionation numbers of the volatile elements increase or decrease more or less as a group. This could be due to the relative composition of the gross samples with respect to the two types of particles, as suggested by the data of Maskin for the coral fallout. It could also result from a time, concentration, and temperature dependence of the condensation process for each particle or particle group. The correlations, therefore should depend on weapon yield and on type of environmental carrier material in forming the particles.

Precisely, a treatment in correlating all the data, irrespective of yield or carrier material, neglects these effects. The methods of using the ratio of the fractionation numbers to a highly fractionated nuclide in the correlations is an attempt to spread out the data on a graph but, unfortunately, the technique does not give reliable statistical data. Converted to fractionation numbers relative to mass numbers 88 or 90 and corrected to U-238 fission yields, the data are reproduced in Table 2.0. The mass number 90 is used as the reference nuclide. For the samples in which the relative yields of the other refractory elements (Zr, Os, Ti) are appreciably different from unity, indicating possible error in the data for mass number 90, one of the other refractory elements could be the chosen reference nuclide.

With corrections, the data indicate that:

1. Within experimental error, the mass numbers 88, 90, 144, 187, and 230 are present in their original ratios in all samples.
2. Only mass numbers with rare gas elements in the chain are fractionated in non water fallout.
3. For the large yield detonation on the surface of deep non water, the mass numbers with rare gas elements in the chain are not fractionated to a significant degree.
4. The fractionation numbers increase with (downwind) distance from shot point and therefore must decrease with the mean particle size, and
5. The mass number 188 with the elements Sr, Sb, Te, and I in the decay chain has fractionation numbers in the non water fallout that are nearly equal to those for mass number 90.

Some idea of what occurred in the fallout formation process for mass numbers 88, 90, 144, and 187 can be deduced from the curves of Figure 2.12. These show the fraction of each chain that could have condensed at a given time after fission with the exception of the indicated elements. For the four rare gas members only, the minimum fractionation numbers for the four mass numbers are: 88, 0.10; 90, 0.36; 144, 0.24; and 187, 0.85. In this treatment, the fractionation numbers are relative to the independent yields of the chain, and not to another mass chain yield; therefore values larger than 1 are not possible. However, these minima occur at different times; therefore they do not all occur for a given group of particles.

Figure 2.12
**CALCULATED FRACTION OF MASS CHAINS 89, 90, 137, AND 140 CONDENSED AS A FUNCTION
 OF TIME AFTER FISSION WITH INDICATED NON-CONDENSING ELEMENTS.
 (Based on Glendenen's Postulate of Independent Yields.)**

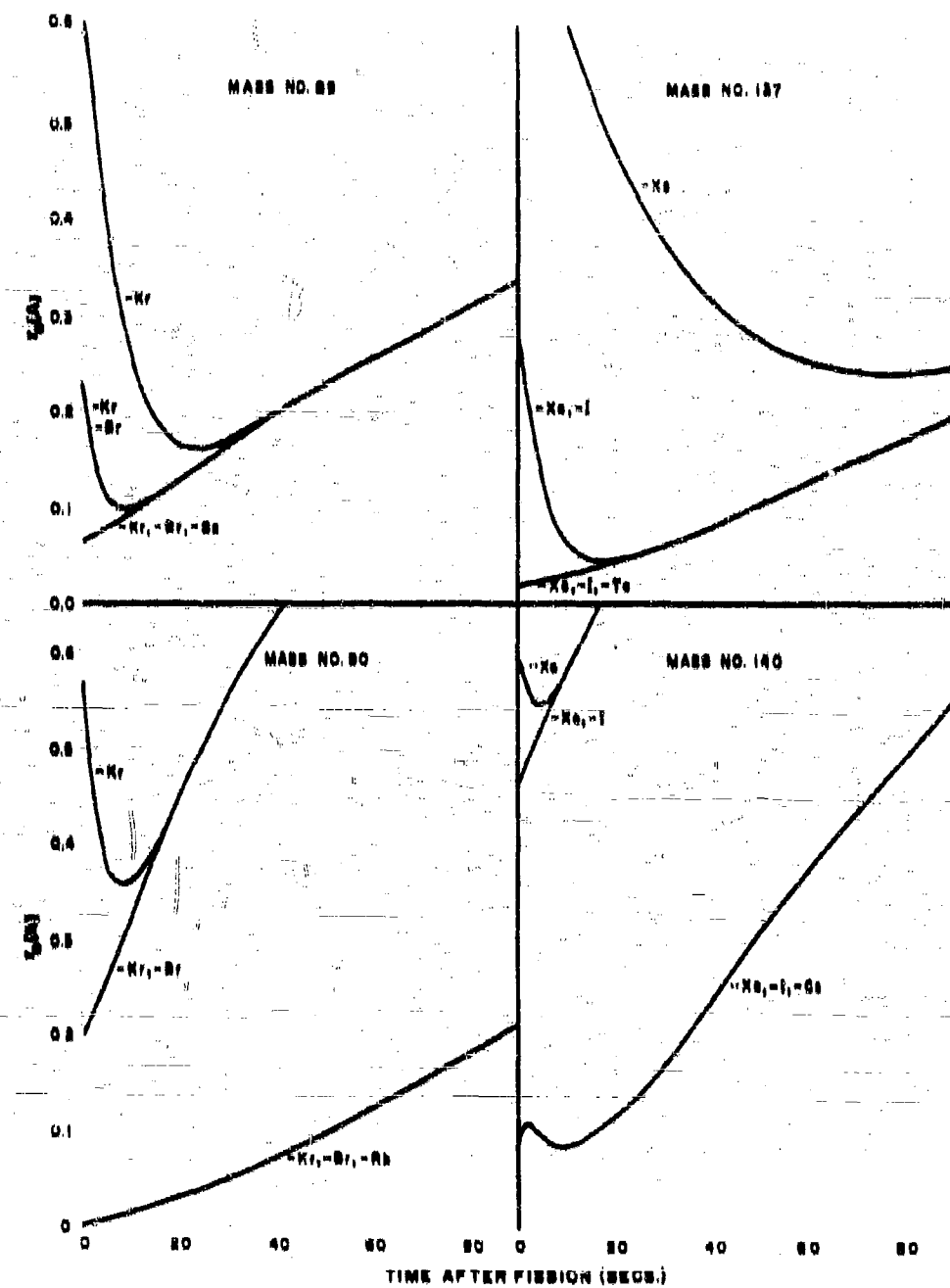


Table 2.9
**SUMMARY OF FRACTIONATION NUMBERS RELATIVE TO MASS NUMBER 99 FOR
 CORAL AND SEAWATER FALLOUT CORRECTED FOR APPROPRIATE FISSION YIELDS**

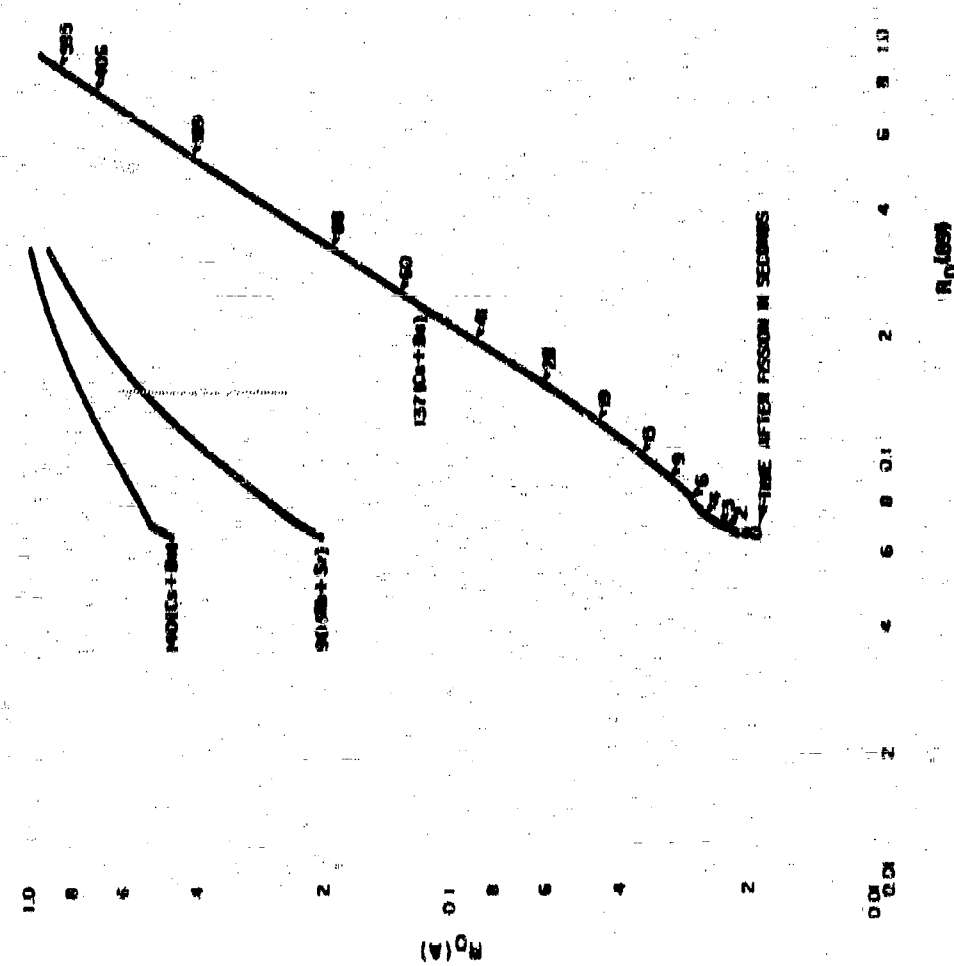
Relative Sample Location	Mass Number							
	99	99	95	90	132	137	140	144
A. Larger Yield (10¹² Rads) Coral Surface Detonation								
Cloud Sample	5.1	4.9	2.1	0.9	2.5	3.3	4.2	2.0
1	0.83	0.97	1.6	(1.6)	1.3	-	-	1.2
0.38	0.44	1.0	(1.6)	0.69	0.22	0.98	1.5	0.91
0.031	0.079	0.94	(1.6)	0.12	0.026	0.14	0.96	0.57
0.13	0.24	0.82	(1.6)	0.45	0.046	-	0.85	0.71
0.55	0.88	1.0	(1.6)	0.15	0.013	-	0.65	0.73
								0.51
B. Large Yield (10¹² Rads) Shallow Water-Surface Detonation (Coral Bottom)								
Cloud Sample	2.1	2.1	1.4	0.6	1.5	1.7	2.2	1.2
1	0.52	0.57	1.1	(1.6)	0.94	0.37	-	1.0
0.65	0.74	1.5	(1.6)	1.3	0.20	-	1.6	0.57
0.38	0.49	0.92	(1.6)	0.81	0.13	0.36	-	1.1
0.82	-	0.51	(1.6)	0.27	-	-	0.60	0.56
0.24	0.36	0.34	(1.6)	0.49	0.13	-	0.81	0.76
0.12	0.18	0.34	(1.6)	0.34	0.032	0.32	0.76	0.71

a. Values for 237 and 239 are not corrected for yields.

Table 2.9 (continued)

Relative Sample Location	Mass Number									
	59	50	55	59	132	137	140	144	237	239
C. Medium Field (50 ft Range) Surface Detonation on Deep Water										
Cloud Sample	2.6	1.7	0.98	(0.9)	1.0	2.5	1.6	0.96	1.0	0.95
1	0.73	-	1.0	0.59	1.1	0.52	-	1.1	1.0	0.97
	0.73	0.78	0.94	0.97	0.97	0.38	-	0.90	0.99	0.94
	0.46	0.47	1.3	0.95	0.98	-	0.70	1.1	1.1	0.98
	0.31	0.51	1.0	0.99	1.0	0.20	0.98	0.94	1.0	1.1
	0.39	0.37	1.1	0.99	0.99	-	1.0	1.1	0.95	-
D. Large Field (100 ft Range) Surface Detonation on Deep Water										
Cloud Sample	1.1	-	1.2	0.59	0.77	-	1.0	1.0	0.95	1.0
1	1.2	0.98	1.1	0.59	1.0	-	-	1.3	0.94	0.97
	0.36	0.38	1.1	0.99	0.95	0.41	-	0.92	0.96	0.96
	0.30	0.34	0.92	0.99	1.0	1.0	-	1.0	1.1	1.1
	0.33	0.38	1.5	0.99	1.0	1.2	-	1.1	0.64	0.71
	0.39	1.2	1.3	0.99	1.1	-	-	1.4	0.72	0.74
	1.6	1.2	0.95	-	1.0	-	-	0.94	0.72	0.74

Figure 2.13
PLOT OF CALCULATED $\langle A \rangle$ VALUES FOR MASS NUMBERS 90, 137, AND 140 AGAINST THOSE OF MASS NUMBER 19 FOR THE ASSUMPTION THAT ONLY THE ALKALI METAL ELEMENTS AND ALKALINE EARTH ELEMENTS IN THE CHAIN CONDENSE



If the independent yields from Glendenin's postulate for U-236 fission are reasonably accurate estimates for the yields from a nuclear weapon, then, for condensation times up to 60 seconds, it appears from the data that only the alkaline earth members of the chain (Sr, Ba) and a fraction of the alkali metal elements (Rb, Cs) condense in the core particles falling nearest to shot point. For the condensation of the fractions of each element at any time up to 60 seconds after fission, the curves indicate that the fractionation number for mass number 89 should be larger than for mass number 80, and that its value for mass number 140 should be larger than for mass number 137.

The effect of increasing weapon yield on the condensation is to extend both the time and time-period over which the condensation occurs, since the rate of decrease of the fireball temperature decreases as the yield increases. On the average, the fallout from larger yield weapons, therefore, is less fractionated in mass numbers 80, 89, and 140 and even perhaps in mass number 137. The maximum amount of fractionation of those mass numbers results from condensation occurring between about 10 and 20 seconds after fission.

A plot of calculated $r_0(A)$ values for mass numbers 80, 137, and 140, based on the independent yields of the chain members and the complete condensation of the alkali and alkaline earth nuclides, as a function of the $r_0(A)$ values for mass number 89, is shown in Figure 2.18. The shape of the curves suggests possible correlations among the fractionation numbers, especially if the condensation period is short. For times longer than about 60 seconds after fission, the curves for mass numbers 80 and 140 represent the case for noncondensation of only the rare gas chain members. If the condensation takes place over a relatively short time interval, the fractionation numbers are related according to

$$r_0(A) = r_0(89) [r_0(89)]^n \quad (2.8)$$

where $r_0(A)$ and n are constants; the constant n is the slope of the curve for a short period of time.

The empirical correlation constants for Eq. 2.8 are given in Table 2.10, along with the mean values of the condensation times taken from a plot of $r_0^*(A)$ and n as derived from the tangents to the $r_0(A)$ curves in Figure 2.18, with time after fission; $r_0^*(A)$ is the coefficient for the observed data. The mean times of condensation range from about 25 to 60 seconds after fission and agree reasonably well considering the scatter in the data. More precise data would permit estimating the fractionalized condensation of the alkali metal elements and even perhaps of iodine in the case of mass

number 197. However, the results of the treatment give reasonable values of the moment which the condensation occurred.

The main feature of this type of data condensation is the fact that the fractionation numbers of the volatile elements vary in some unknown manner, so that if one element is fluorinated all other elements are also fluorinated to a degree specified by the empirical correlations. Unfortunately, the method requires the fractionation number of at least one major element in addition to the analysis of a reference sample before it can be used to make estimates of the fractionation numbers of other nuclides. In addition, a sufficient number of mass numbers correlations are not reported from which to estimate the gross decay and the potential dose from fallout.

The chief interest in fractionation in fallout concerns the uptake of radionuclides in fallout from weapons other than from ground and detonations. Since the radionuclides melt at lower temperatures than calcium oxide, the elements condensed into the fused particles should, for the same weapon yield, have a different composition. Therefore the radioactive mixture in fallout fallout should exhibit a different distribution ratio decay than that in ground fallout.

The petrographic and radiochemical analyses described in this section, as well as other analyses of fallout, were made on samples of fallout collected from test weapons detonated at the Nevada Test Site and the Trinity Proving Grounds. The collection methods and devices varied considerably. The more crude methods used a shovel and pail or a bin to sweep up a surface layer of contaminated soil. Others used sheets of canvas spread on the ground, a sweater and coat tube, pants, jeans, pajamas (with or without plastic liners), bags, and gummed paper. The more elaborate methods consisted of collectors that opened and closed automatically by use of radio signals and timing devices and were sealed against the weather when not open for fallout collection. Others were designed to collect a large number of fallout samples rapidly and automatically, for a pre-set short time, on prewired trays or on special films. Still others were designed to collect the particles directly from the air by drawing them into filters. The analyses described here were made on fallout samples collected by a variety of these methods.

Since each method has its own peculiar collection bias with respect to the surrounding terrain, probably none gave a more representative sample than the shovel. However, the shovel and the exposed device gave samples that contained much non-fallout debris. These samples were not useful, except for certain types of analyses, since it is obviously impossible to separate cleanly the fallout from the background material in a reasonable period of time.

Table 2.10

**COMPARISON OF EMPIRICAL FRACTIONATION-CORRELATION
PARAMETERS WITH THOSE ESTIMATED FOR CONDENSATION
OF ALKALI AND ALKALINE EARTH ELEMENTS OF MASS
CHAINS 90, 132, AND 140, AT SPECIFIED
TIMES AFTER FISSION**

Mass Number	Data Source	$\tau_{\text{c}}(\text{A})$	τ	(sec)	$\tau_{\text{c}}(\text{A})$
90	Shot A	1.12	0.77	56 ^a	2.26
	Shot B	1.05	0.82	51 ^a	2.43
	Shot C	0.91	0.86	47 ^a	1.83
132	Shot A	1.81	0.80	-	-
	Shot B	1.79	0.75	-	-
137	Shot A	0.80	1.40	56 ^a , 56 ^b	0.80, 0.88
	Shot B	0.71	1.19	55 ^b	0.71
	Shot C	0.67	1.00	55 ^a	1.08
140	Shot A	1.60	0.78	58 ^b	1.60
	Shot B	1.44	0.88	52 ^a	1.44
	Shot C	1.29	0.42	38 ^a	1.08

4. From $\tau_{\text{c}}(\text{A})$ vs t (t is the estimated time of condensation)
 5. From $\tau_{\text{c}}(\text{A})$ vs t

The single particle analyses, as mentioned previously, were made on samples further biased with regard to minimum particle size, minimum radioactivity content, and numerical numbers. These analyses were also biased as to the limitations of the practicability of the procedure as well as because of lack of time.

Two methods were used to identify and select the radioactive particles from among inactive particles mixed with soil materials. One method was to subdivide the sample and check each fraction with a portable survey meter or gamma scintillation counter until the subdivided fractions containing the radioactive particles could be viewed easily under a low-power binocular microscope. The radioactive particle or particles could then be identified by their distinctive appearance and manually removed and surveyed for activity.

The second method, better for very small particles, involved distributing the particles on the backs of photographic sheet film sprayed with liquid plastic. After allowing an appropriate exposure time, the film was developed and fixed by brushing the developing and fixing solutions on the emulsion side of the film without disturbing the particles on the reverse side. The radioactive particles then were located with a low-power binocular microscope by the dark areas of the exposed film. Both stripping film and single-coated X-ray film were found suitable for this method.

The thin sections of individual fallout particles were made by casting the particles in plastic cylinders, using paraffin molds, and bake-hardened at 60°C. One end of the cylinder was then ground down with a motor driven iron wheel using carborundum abrasive until the center portion of the particle was exposed. The exposed surface was then polished on a glass plate and cemented with Canada Balsam to a glass microscope slide. Then the other end of the cylinder was ground down until the thin section of particle and plastic remaining was about 50 microns thick. The thickness of the thin section was estimated by observing, with the petrographic microscope, the birefringence of grains of quartz placed in the plastic along with the fallout particles. At the required thickness, the quartz shows a greyish-white or grey interference color.

The distribution of the radioactivity within the thin section was determined by radiograph techniques using Eastman NTE stripping films. For this, the thin section was cemented with a gelatin-alum cement or taped to the back of the film during exposure.

The petrographic microscope with and without polarized light was used to give information on the crystal structure and, in some cases, the chemical composition of the particles. The crystal structures were also identified by X-ray diffraction analysis.

The size and composition of sea water fallout particles, was determined by use of a special reagent film developed by Farlow¹¹ which served both as a collecting surface and analytical device. One of its advantages was that the particles could be analyzed *in situ*, and involved no sample recovery problems. In order to keep the film from being saturated with water drops, pieces of the film were usually exposed by use of a cycling collector and each piece of film surface was exposed serially for a pre-set time; these collectors used a circular piece of film about 3-in. in diameter.

The reagent film for determining the amount of soluble chloride present in a liquid particle was prepared by impregnating one side of a commercial gelatin-coated film (such as Eastman Type K-509) with rod silver dichromate. The film area over which the reaction occurs was easily measured with a microscope. Since the reaction area for a given film preparation was found to be proportional to the amount of soluble chloride present in a drop

of fallout, it was possible to determine a calibration curve for each film preparation and thus to determine the amount of chloride in other drops. The method was useful in the determination of 1 to 10^{-6} micrograms (μg) of sodium chloride.

The chloride-sensitive reagent film was also useful in determining the water content of the drops. The measurement depends upon the presence of some very small insoluble particles, suspended in the drop. Each drop spreads over an area of the film related to its volume and, when dry, the solid residues remaining (called an "artifact") forms an outline of the maximum spread of the drop such as that shown in Figure 2.10. The film can be calibrated by suspending some insoluble solid particles in standard chloride solutions and aspirating the mixture on the film. The chloride-reaction area determines the water content of the drop; the area of the artifact is then measured. This technique measures water volumes as small as 0.1 micromicroliter (μl). Comparative visual standards use aluminum oxide suspensions prepared for estimating the amount of solids present in the residue.

2.4 Properties of Small Fallout Particles from Detonations at Weapons Tests

Several properties of fallout particles can be inferred from the interactions of the radionuclides with biological systems such as the uptake of certain fission-product elements by plants and animals. Data on these biological reactions, the physical properties of the fallout particles, and ground distribution of the smaller fallout particles from nuclear detonations (mainly from tower and balloon-supported test devices) have been summarized by Larson and Neal²⁸ and Nishita, Romney, and Larson²⁹. The basic information was derived from data such as those reported by Bellamy,³⁰ Rainey,³¹ and Lindberg.³² (See References 28 and 29 for a more complete bibliography of works contributing to the data on these subjects.)

The physiochemical properties of the fallout particles inferred from these data that are of main interest here are those that describe the fallout formation process with respect to the disposition of individual radionuclides in the fallout particles for different conditions of detonation. Data describing the contamination processes are also very important in understanding the entire fallout process, including the major factors that determine the fate of the radionuclides. Radionuclides which are condensed on the surface of fallout particles (i.e., are not fused in the interiors of the particles) are available for uptake by plants and animals; thus information and data on uptake processes also provide information about the fallout formation process and the contamination process.

There are three major paths by which a radionuclide carried by fallout particles becomes incorporated into animal tissue. One involves dissolution in water, transfer to the root zone of plants, uptake through the root system to the plant tops, and thence into the animal that eats any part of the plant. The second path involves the direct assimilation of the radionuclide by the plant leaves which are then eaten by an animal. The third path is the direct intake, when eaten by the animal, of the fallout particles that remain on the surface of plant leaves or other parts of the plant.

In general, the dissolution process for the incorporation of a radionuclide into the parts of plants occurs in neutral (or at most slightly acidic) water systems. The possible exception to this process is radiotelluride, which, in air, tends to volatilize as rapidly as it is formed by the decay of the tellurium parent. In the vapor state radiotelluride can react with any nearby organic material, especially by addition to unsaturated hydrocarbons such as a leaf surface or decayed organic matter. This behavior should dilute the radiotelluride concentrations in the plants (relative to the other elements) and spread it by transfer through the air.

By contrast, the dissolution process for the uptake path involving direct intake into an animal that eats the plant parts on which the fallout particles are deposited proceeds in acidic water systems of the animal's digestive tract. Because the stomach fluids are acidic, this direct path should result in a maximum transfer of radionuclides from a fallout particle (or group of particles) into the body tissues of the animal.

The gross fission-product uptake by redshanks from a subsurface detonation at the Nevada Test Site, is found by Nishita, Romney, and Larson²⁰ to vary from 0.001 to 0.010 percent (based on beta activity measurements). These authors also report the uptake by red clover grown in soil contaminated by fallout from a 100-foot tower detonation; the uptake varied from about 0.001 to 0.01 percent. In the latter case, the red clover uptake was greater from the soil contaminated at the larger distance from ground zero (i.e., where the smaller fallout particles landed). As might be expected, amount of uptake was found to be dependent on the plant species and the soil type.

In the areas on and adjacent to the Nevada Test Site, vegetation retained predominately particles with diameters less than 44 microns. Also, the gross solubility of the fission products carried by these particles from tower-mounted detonations was found to vary from 5 to 35 percent in 0.1 normal HCl (0.1 normal HCl is approximately the acidity of digestive fluids).^{21,22} (In this basis, the uptake in animals foraging on clover whose leaves were contaminated by fallout, as compared to foraging on new clover grown on contaminated ground (Nevada Test Site tower detonation), would range from about 0,000/1 to 0,000/1 if the clover covered 100 percent of the ground and the particles were 44 microns or less in diameter.

The value of the relative uptake would vary with (a) the time after detonation and period of exposure, (b) the particle size, (c) the fraction of area covered by fallout, and (d) the weather conditions prevailing during the period under consideration. The data on particle retention by fallout are discussed more fully in Section 2.6. Although the data apply only to a tower-type detonation, the magnitude of the relative uptake, even at a maximum, suggests that the direct-uptake path would also predominate for fallout from large-yield surface detonations.

The major contributing radionuclides found in the tissue of rabbits and rodents taken from areas near the Nevada Test Site on which small fallout particles deposited within the first day after a test detonation include fallout, strontium, yttrium, ruthenium, osmium, barium, and cerium.²⁰ The radionuclide concentrations increased with distance from shot point up to a maximum and then decreased again.²¹ The maximum tissue concentrations generally occurred at locations where the fallout arrival time was about 2 to 3 hours after detonation. These data indicate that the fraction of the radionuclides on the exterior of the particles available for uptake increased with decreasing particle size more rapidly than the total amount of fallout deposited decreased with distance, up to some distance. At farther distances, the decrease in the deposit level predominated, and the amount of uptake also decreased with downwind distance.

Radiodiodine was found to be 80 to 90 percent of the activity in the thyroid tissue of native rodents.²² The radionuclides found in the bone tissue of Jack rabbits at about 20 days after a tower shot are listed in Table 2.11 in which a few of the data given by Larson and Neel²³ have been converted to number of atoms and approximate fission equivalents taken up and deposited in the bone tissue. The relatively low uptake factor of yttrium, ruthenium, and cerium (last column of the table) is probably due to both a lower solubility in the rabbit digestive tract (especially if the r_s (A) values are assumed to be correct) and a lower retention of these elements in the bone tissue of rabbits.

The main point of the data is that the listed radionuclides were dissolved by the acidic digestive tract fluids from small fallout particles that pass through the gut. Other radionuclides in fallout, but not listed, presumably were not dissolved in appreciable or significant amounts. The listed elements are those expected to be depleted in the larger fallout particles, and enriched in the smaller fallout particles, relative to the other refractory type fission product elements.

The effects of detonation conditions on the properties of fallout can be illustrated by comparisons between the data on fallout from balloon-supported devices (i.e., low air bursts) and tower-mounted devices (i.e., near-surface bursts).²⁴ The total amount of local fallout deposited, up to about 200 meters from ground zero at the Nevada Test Site, from tower detonations, has been observed to be 30 to over 100 times the amount observed for air bursts. Those

Table 2.11

**RELATIVE RADIONUCLIDE CONCENTRATIONS IN JACK RABBIT BONE
TISSUE AT ABOUT 30 DAYS AFTER DETONATION
OF SODIUM OPERATION PLATINUMBOB, IN 1957.**

Radionuclide	$A_{23}^{(23)}$ days) (d/m)	N_{23} (days) (atoms/ gm bone)	N_1 (21 days) (atoms/ fission fission)	$1 - r_0 / (A)^e$ (availability factor)	A_b (fissions gm bone)	U_f^e exposure factor
Sr-89	30	2×10^7 (1.7) ^b	0.0339	0.30	7.2×10^6	1.9
Sr-90	35	3×10^7 (3.6) ^b	0.0516	0.97	7.2×10^6	1.9
Sr-90Y-91	35	1×10^6	0.0120	0.30	1.1×10^6	0.1
Ru-103/Ru-105 ^c	4.5	3×10^6	0.0225	0.65	0.2×10^6	0.65
Cs-137 ^d	1.7	1×10^6	0.0517	0.99	9.33×10^5	1.9
Ba-140	700	1×10^7	0.0195	0.36	11.1×10^6	1.9
Ce-141(Ce-144) ^e	1.9	2×10^6	0.0384	0.32	0.17×10^6	0.02

- a. Possible partial chain fission prior to 26 days
- b. Estimated from assumption of 7.2×10^6 fissions/gm bone and $U_f = 1.0$
- c. For fission products from thermal fission of U-235 (see reference 2)
- d. $r_0 / (A)^e$ taken from Table 2.23 for 34 keV surface burst without correction for yield and type of detonation
- e. Relative uptake factor assuming value of 1.6 for Sr, Cs, and Ba

lower fallout depositions from the air burst reflect the fact that the sizes of the fallout particles formed in the air burst are very small compared to those formed in the near-surface burst. For example, in some fallout samples from tower detonations, about 80 percent of the sample activity is found on particles with diameters less than 44 microns, and as much as 18 percent on particles with diameters less than 5 microns. In samples from a balloon-supported detonation, of similar yield and burst height, about 70 percent of the activity is found on particles with diameters less than 44 microns, and as much as 58 percent on particles with diameters less than 5 microns.

The average fractionation numbers of some radionuclides in fallout from some tower and balloon-supported detonations are given in Table 2.12, relative to the refractory Zr-95 nuclide and to the mass chain yields for thermal neutron fission of U-235. The values were derived from the data of Larson and Neel¹⁸ and presumably apply to particles with diameters less than about 100 or 200 microns having mean diameters of about 50 microns. The values of the fractionation numbers for the fallout from the tower-mounted explosions suggest that the Zr-95 condensed more completely than the other nuclides on the larger particles, and that the nuclides Sr-89, Sr-90 and Ru-103(100) did not condense completely on the particle-size groups in the observed samples. The fractions of these three elements not condensed would then be concentrated on the very small particles and carried to much greater distances away.

The same general statement applies to the fractionation numbers for the fallout from the balloon-supported detonations, except that the mean diameters of the particles in the samples must have been smaller and that the Zr-95 is more depleted. Thus there may be even a higher degree of separation between the very refractory and the volatile fission product elements in the fallout particles from an air-burst than in the near-surface burst fallout particles. Possible causes of this separation are (1) a lower concentration of available liquid or solid surfaces in the air-burst fireball, and (2) a corresponding delay, due to lower vapor pressures, in the selective condensation.

The gross solubility data in terms of gross beta count-rate measurements of the radioactivity in some gross fallout samples under several different detonation conditions, from the data of Larson and Neel¹⁸, are given in Table 2.13. Although the time of measurement was not given, but is presumed to be about 2 weeks or so after detonation, the general magnitudes of the fraction of the activity which was soluble clearly show that the nuclides in the fallout from the air-burst detonation were the more soluble. The higher solubility of the activity in water, for the air-burst fallout, suggests that many more of the fission-product radionuclides were condensed on the surfaces of the particles.

Table 2.12

**AVERAGE FRACTIONATION NUMBER OF RADIONUCLIDES IN FALLOUT
FROM TOWER AND BALLOON-SUPPORTED DTONATIONS AT THE
NEVADA TEST SITE**

Nuclide	R(DD) ^a	
	Tower	Balloon
Br-80	0.82	1.8
Br-80	0.05	-
Y-88	1.4	2.8
Zr-96	1.0	1.0
Ru-108(108)	0.40	3.2
Ba-140	1.4	3.8
Ce-141(144)	1.4	0.8

^a. Relative to the yields for thermal neutron fission of U-238.

Table 2.13

GROSS SOLUBILITY OF ACTIVITY FROM SMALL, FALLOUT PARTICLES

Type of Detonation	Percent Activity Soluble ^a		Particle Size (microns)
	In H ₂ O	In 0.1N HCl	
Underground	5.4	85	0-44
Tower-Mounted	2	14 to 30	0-44
	1	0	44-on 100
Balloon-Supported	14	60	0-44
	81	80	44-on 100

^a. Based on beta count-rate measurements (presumably at about 8 weeks after detonation).

than were condensed in this manner in the tower detonation. The higher solubility of the activity in acid, especially for the air burst fallout, may be partially due to dissolution of the primary iron oxide or alumina particles. However, the very high solubility in both water and acid of the radioactivity on the larger particles from the air burst suggests almost complete surface

condensation of the radionuclides on these larger particles at late times, since a significant fraction of these particles were grains of soil, of which some had been melted. The solubility of the activity on the particles from the tower-mounted detonations, on the other hand, decreased with increasing particle size. Fallout particles with diameters of 200 to 2000 microns from low tower detonations often have negligible solubility, in water or even in strong acids.¹¹

The gross solubility data on the radioactivity from small fallout particles lodged on foliage after some tower detonations, as taken from Romney and coworkers,¹² are given in Table 2.14. The solubility was measured by suspending 0.5 gm samples of dry plant material in 10 ml of 0.1 normal HCl after the samples have been radioassayed. The suspension was then shaken for 20 minutes, centrifuged for 15 minutes, and the supernatant solution separated by filtration.

Since the data do not indicate a consistent trend in solubility with distance from ground zero, averages were calculated. The average fraction of the activity dissolved was the same (24 percent) for the Apple shot detonated on 500-foot towers; it was smaller (16 percent) for the Met shot detonated on a 400-foot tower. The data suggest that the particle size retained by the different plants was about the same; that is, the type of foliage was not a dominant factor in either the gross solubility or biological uptake potential of the retained fallout.

2.8 Redistribution of Deposited Fallout

The redistribution of deposited fallout should depend on (1) the type of surface on which the particles land, (2) the size of the particles, (3) the amount and frequency of rainfall, and (4) the surface wind conditions. The combined effect is often called "weathering." On land areas, the combined effects of weathering processes are found to be rather small, even for the small fallout particles from which a larger fraction of the radionuclides are soluble. After nine years on undisturbed soil, fallout from the Trinity Shot (New Mexico) was still confined to the surface two inches of soil.¹³

Resurvey data from the surface and underground shots at Operation Jangle (Nevada Test Site), after exposure to winter winds, snow, and spring rains, indicated no significant change other than that due to radioactive decay.¹⁴ Radiation measurements taken during Operation Castle (Enewetak Proving Grounds) in 1954 on the islands of several atolls (before and during heavy rains for several months) show no decrease that could not be accounted for on the basis of radioactive decay.¹⁵ Dunning¹⁶ and Lapp¹⁷ erroneously attribute the rapid decrease in the gamma radiations during the first year to a

Table 2.14

**CHRONIC SOLUBILITY OF ACTIVITY FROM SMALL FALLOUT
PARTICLES LODGED ON PLANT FOLIAGE**

Plant Type	Distance From Ground Zero (miles)	Fraction Dissolved ^a in 0.1N HCl
1. Shot Apple I (14 KT on 500 ft. Tower)		
Artemesia (Beebrush)	12	0.50
Ephedra (Mormon tea bush)	40	0.27
Ephedra (Mormon tea bush)	80	0.15
Juniperus (Juniper)	165	0.02
	Average	0.24
2. Shot Met (29 KT on 400 ft. Tower)		
Larrea (Creosote bush)	80	0.26
Larrea (Creosote bush)	88	0.08
Medicago (Alfalfa)	140	0.14
	Average	0.16
3. Shot Apple II (89 KT on 500 ft. Tower)		
Triticum (wheat)	7	0.10
Triticum (wheat)	40	0.17
Triticum (wheat)	106	0.35
	Average	0.24

a. Based on beta count-rate measurements.

weathering factor of 0.4 due to the first heavy rains 10 to 20 days after the first detonation, apparently by comparison with an inappropriate decay curve. This misinterpretation has also been noted by Knupp¹⁹ in discussions of this subject.

Experimental measurements reported by Miller and Bottometer¹⁰ on soluble radionuclides deposited on soils through which water has passed gave an average leaching depth, for Sr-89, of 0.75 inch after passing 30 inches of water, and 1.5 inches after passing 300 inches of water. The movement of Cs-137 is found to be only 0.25 inch after passage of 300 inches of water, even in sandy soil. Larson and Neel²⁰ report penetrations up to 0.5 inch after the passage of 84 inches of water; the source of the activity used in the experiments was not specified.

These data show that the soluble radionuclides, in almost all cases, would be absorbed by the top inch or two of soil particles and remain there unless the whole layer eroded away in heavy rains. But even in this case the nuclides would remain attached to the particles; the fraction of the nuclide soluble in water in such conditions would be negligibly small. The studies of Thornehalo, Mather, and Nakamura²¹ show that many rain cycles would be needed to transport the activity farther than about two inches below the surface of the soil. Since most of the radioactivity on the larger fallout particles would be fused into the particles, the only way it could move into the soil is by mechanical mixing, as occurs in the plowing or tilling of agricultural lands.

The translocation of fallout particles on land areas by wind occurs to a small degree. The experience in the Nevada Test Site, (under dry conditions) where excursions in the fallout area were made by experimental crews to recover fallout samples, was that, for entries during the first day after a detonation, clothes became contaminated with small fallout particles due to the stirring up of surface dusts and brushing against desert plants, but that, for entries after the second day or so, only the bottom parts of shoes (or boots) picked up fallout particles. Apparently the small particles become adsorbed or physically attached to larger particles, or otherwise become mechanically trapped by the surface soil grains.

Movement of large particles by the wind is usually small because the larger gravity force retards such movement. However, particles in the size range of about 100 to 800 microns drift more easily than particles of other diameters if the surface wind speed is in excess of about 10 mph. These particles, if dislodged, may carry with them small attached fallout particles. Data from experiments at Camp Parks, California, reported by Harter and Owens²² in which particles with diameters from 150 to 800 microns (tagged with Ba(133)-140) were deposited on various types of surfaces showed that the movement of the particles on unpaved areas and on tar and gravel roofs is insignificant, even for wind speeds up to 20 mph. The movement of the particles on and from paved

area is found to be quite large; the particles apparently moved in the wind by hopping and by rolling over the smooth surfaces, although very few particles were raised higher than 3 or 4 inches. They did not jump over curbs but were deposited along the gutters and in depressions and behind low obstructions.

The fraction of the original ionization rate remaining, as measured in the center of a street and in the center of a rather large area of asphaltic concrete, is plotted in Figure 2.14 as a function of the total wind vector (including only winds in excess of 10 mph) that occurred over a ten-day period. Further data of this kind on other particle sizes are needed to establish whether the data of Figure 2.14 are representative of the reductions that could occur generally in the ionization rate at locations of interest. The reduction in the ionization rate for both areas in the first four days (wind vector of 200 miles) was equivalent to a decontamination of about 50 percent; some of this, of course, was due to shielding, since the particles concentrated in surface depressions and along barriers.

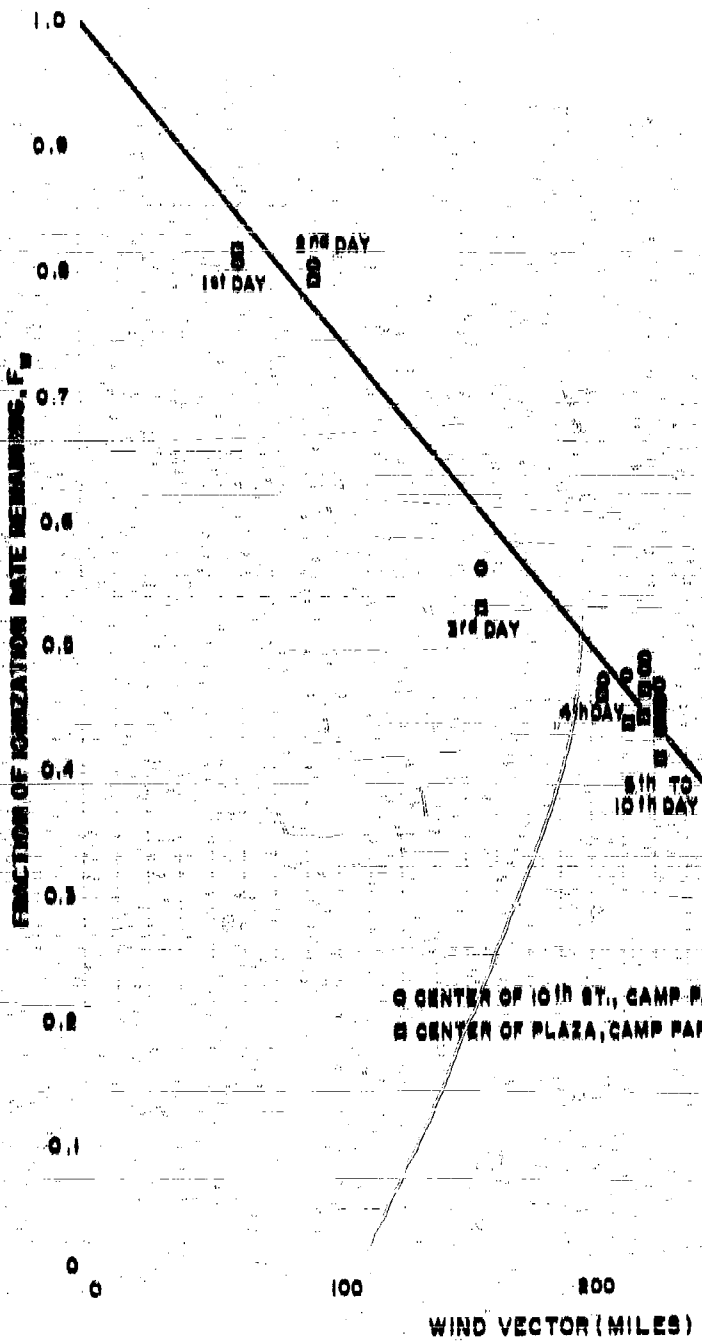
2.6 The Collection and Retention of Fallout Particles by Plant Foliage

Some of the data obtained at weapons' tests on the collection and retention of fallout particles by foliage are reported by Romney, Lindberg, Hawthorne, Bystrom, and Larson.⁵⁵ Their stated findings, with respect to the ability of the outer surface of leaves to trap and retain fallout particles, were that the size-range of particles lodged on the foliage was predominately less than 100 microns in diameter and that the best correlations of the amount of activity (beta count-rate) on the foliage was with the fraction of the total activity carried by particles having diameters less than 44 microns that landed at the same location. These two findings suggest that the foliage of most plants is selective in trapping only the smaller sizes of fallout particles. Some of the reported data are given in Table 2.16, as converted from curie units at H+12 to the equivalent number of fissions by use of the factor, 8.67×10^9 fissions/micro-curie.⁵⁶ The median particle diameters are taken from the plotted particle-size distributions in Figure 2.15.

It is interesting that the median particle diameter increased with fallout arrival time up to arrival-times of 4 to 5 hours after detonation. However, since the data are for different plant species, part of this increase also may be due to the plant species selected for analysis. The spread of the distributions, however, tend to decrease with time of fallout arrival or with decreasing particle size of the arriving fallout. The upper-limit particle diameter cut-off is fairly sharp at diameters larger than 88 microns, excepting for the bush-mallow foliage sample. The higher retention levels and larger particles on the bushmallow foliage is probable due to the high density of stellate hairs on the leaves which would serve to trap and hold particles onto the surface.

Figure 2.14

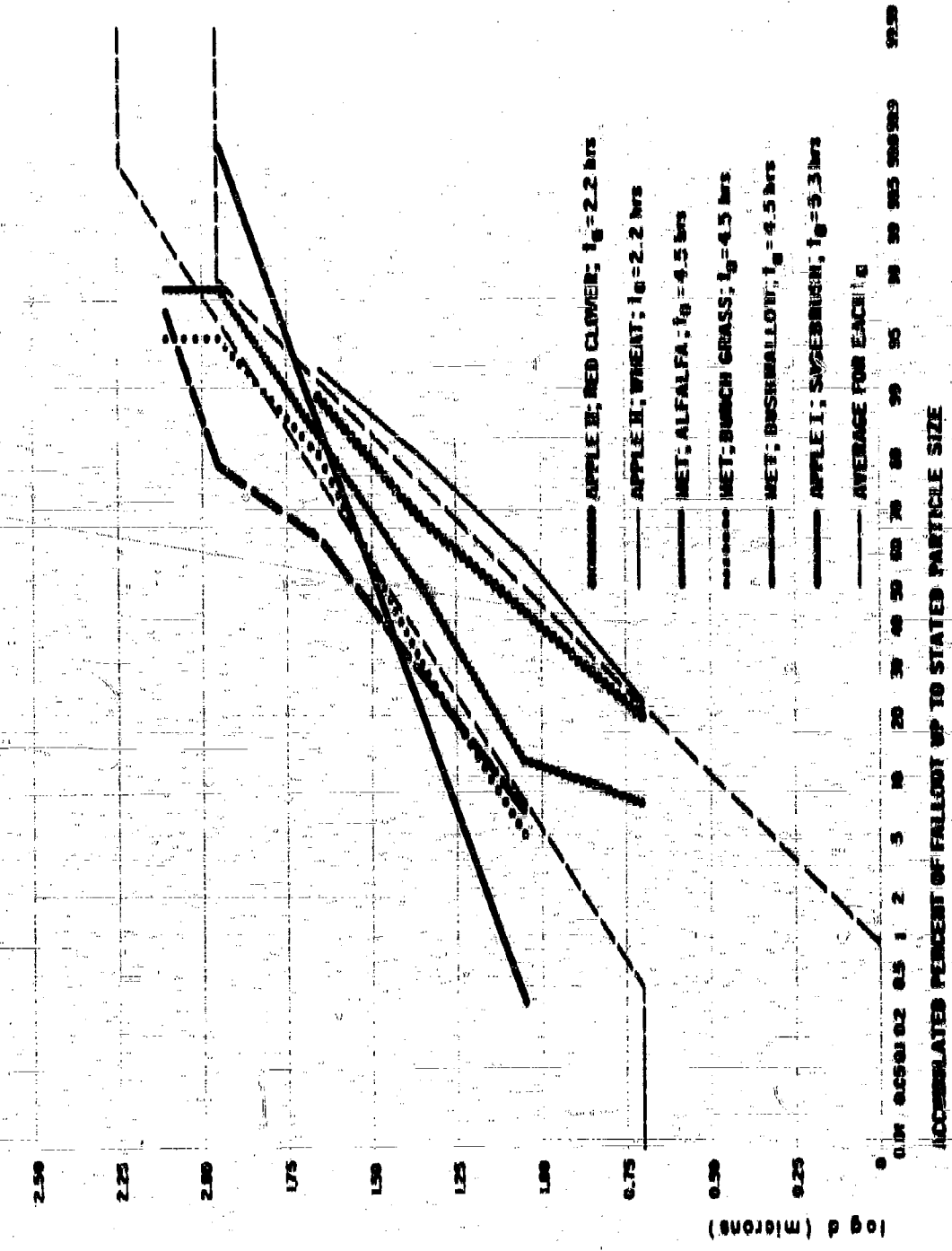
REDUCTION IN THE IONIZATION RATE AT THE CENTER OF 10TH STREET AND AT THE CENTER OF THE PLAZA, CAMP PARKS, CALIFORNIA, AS A FUNCTION OF THE WIND VECTOR (sum of the products of wind speed \cdot time) FOR WINDS IN EXCESS OF 10 MPH OVER A 10-DAY PERIOD. THE TAGGED PARTICLES WERE 150 TO 300 MICRONS IN DIAMETER



© CENTER OF 10TH ST., CAMP PARKS, CALIFORNIA

© CENTER OF PLAZA, CAMP PARKS, CALIFORNIA

**Figure 2.15
ACCELERATED DISTRIBUTION OF THE NUMBER OF PARTICLES WITH DIFFERENT
DIAMETERS ON FOLIAGE**



Data on the collection of the fallout from Apple II shot and Smoky shot tower detonations by some forage crops are given in Table 2.10. The fractions of the deposited fallout retained by red clover (in flats) increased with time of fallout arrival from about 0.1 percent at 7 miles downwind from the Apple II shot to about 1 percent at 100 miles away. For wheat, the fractions retained increased from about 0.2 percent to about 8 percent over the same range in distance. The highest fraction retained, of these data, was for alfalfa foliage at 200 miles away from shot Smoky. The distributions of the activity on the fallout particles that were deposited at several of the locations are plotted in Figure 2.10. The values of the median diameters decreased with time of arrival as would be expected but the spread of the various activity-size distributions appears to be roughly the same in logarithmic units. In all the collected samples,

The major conclusion from the data of Romney and coworkers is that the fraction of the deposited fallout collected and retained by forage is rather small even when the diameters of the arriving particles are small enough to be trapped by the hairs and resins on the leaves. Thus large trees and shrubs cannot be considered as significant sources of radiation where heavy fallout deposits from land surface detonations occur and where the particle diameters are in excess of about 50 microns.

There are no good data on the decontamination of fallout particles from foliage (neglecting data on the very fine material of world-wide fallout). Romney and coworkers,¹⁰ however, do report data on the decontamination of fallout particles from foliage; these can be used to indicate at least the upper limit of a decontamination by a heavy rain. The results of the experiments, using the decontamination reagents water, 0.1 normal HCl and 5 percent EDTA, are summarized in Table 2.11. The water decontamination data would be most representative of the decontamination that could result in a heavy rain. The desert foliage decontaminated generally to levels between about 30 and 40 percent of the initial deposit. However, the smooth-leaf annual was decontaminated to 9 percent and growing wheat was decontaminated to about 20 percent of the initial level. The latter value should be representative of most grass-type foliage.

The foliage contamination data appear to show that all the leaves on a plant retain about the same level of contamination on all the foliage. If exceptions to this rather uniform distribution on plant foliage can occur, they obviously would be most predominant in foliage growths such as a very dense tall growth of grass. This interpretation of the contamination process at least agrees better with the observations than a process in which only the exposed surfaces of the exterior or upper leaves are assumed to be the only collecting surfaces. The use of the assumption of uniform contamination of all the foliage on a plant allows correlation of the fallout particle retention data in terms of the mass of the collecting foliage on a plant. The correlation of the fallout retained per unit

of dry plant (leaf) mass with the total amount of fallout deposited at a location can then be used to evaluate the internal radiological hazard from the intake of radionuclides in the fallout retained on foliage. To make the correlations, a foliage contamination factor, a_L , is defined as the ratio of the number of fissions per gram of dry plant (foliage) to the number of fissions of total fallout per sq. ft. of soil surface. If the plant or foliage surface density is defined as w_L in grams of dry foliage per sq. ft. of soil surface, the fraction of the fallout retained by foliage is

$$F_L = a_L w_L \frac{(\text{fissions}/\text{ft}^2 \text{ on foliage})}{(\text{fissions}/\text{ft}^2 \text{ on soil})} \quad (3.5)$$

The denominator quantity, fissions/ ft^2 on soil is the total fallout deposit uncorrected for the amount on the foliage. The value of w_L is a measure of the density of plants growing on the land. The values of a_L and a^{*L} (for only particles with diameters less than 44 microns) reported by Romney and co-workers¹¹ are given in Table 3-18 for native desert-type foliage. The independence of the values of a^{*L} on distance from ground zero is further evidence of the selectivity of the foliage in retaining only the smaller particles. The high values of a^{*L} for the fallout from Shots Met, Diablo, and Bhurta could be due either to higher humidity conditions and early post-shot plant collections or to the fact that the fallout from these detonations contained a fairly large fraction of the activity on particles with diameters between 44 and 88 microns which were retained by the foliage.

For general use, the value of a_L is a more important quantity than a^{*L} . The dependence of the values of a_L on several detonation parameters and further analysis of the data presented in this section are given in Chapter 6 in the form of fallout contour ratio weighting functions. In most of the data of Table 3-18, the values of a_L increase with distance from ground zero.

It was previously mentioned that, for 100 percent retention of the fallout on clover, the predominance of the direct uptake path for animals eating uncontaminated clover might be on the order of 3000 to 5000 times greater than that of eating new clover on contaminated soil. However, for foliage conditions where the value of a_L is 1.0×10^{-6} and w_L is 10, the factor of predominance for the direct-uptake path is reduced to the order of 50 to 50. Thus the direct-uptake path, at least for exposure times of about a year, can be expected to be the predominating source of an internal hazard to animals and humans after a nuclear war in which land-surface explosions take place.

Figure 2.16
DISTRIBUTION OF ACTIVITY AS A FUNCTION OF PARTICLE DIAMETER FOR LOCAL
COLLECTIONS OF FALLOUT FROM THREE COUNTED DETONATIONS

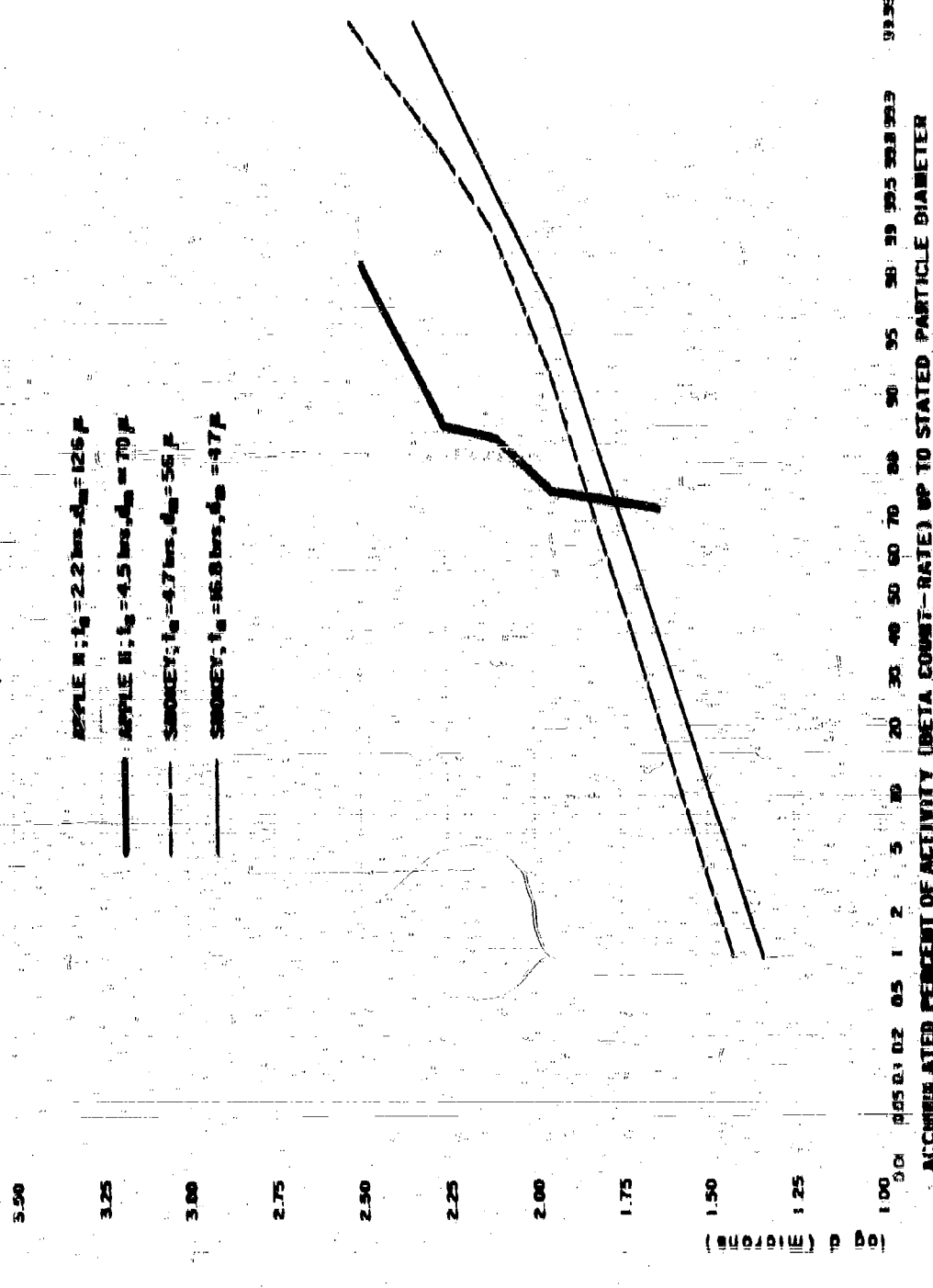


TABLE 2.15

SIZE DISTRIBUTION AND AVERAGE OF POLLUTION PARTICLES LOADED ON THE SURFACE OF DIFFERENT SPECIES OF PLANTS

Key	Description of Plant	Diameter (microns)					Mean Diameter (microns)	Mean Coverage of surface	Weight
		2.5	5.0	7.5	10.0	12.5			
Number Sheet	Apple I	2.5	7.5	10.0	12.5	12.5	Apple II	Apple III	
Field (AII)	2.5	2.5	2.5	2.5	2.5	2.5	2.5	2.5	
Type of Sheet	Tree	2.5	2.5	2.5	2.5	2.5	Tree	Tree	
Height of Sheet (ft)	30	30	30	30	30	30	30	30	
Nett Weight of Clean (kg)	37.00	37.00	37.00	37.00	37.00	37.00	37.00	37.00	
L. (ft) + W. (ft)	32	32	32	32	32	32	32	32	
Particles/cm. ² of Leaf Surface	3000 ^a	3000 ^a	3000 ^a	3000 ^a	3000 ^a	3000 ^a	3000 ^a	3000 ^a	
Fractional Particle (Percent)	3.00 ^b	3.00 ^b	3.00 ^b	3.00 ^b	3.00 ^b	3.00 ^b	3.00 ^b	3.00 ^b	
Mean Particle Diameter	12.5	12.5	12.5	12.5	12.5	12.5	12.5	12.5	
Particle Number (a)									
0 to 5	0	0	0	0	0	0	0	0	
6 to 11	5.9	5.9	5.9	5.9	5.9	5.9	5.9	5.9	
12 to 16	13.2	13.2	13.2	13.2	13.2	13.2	13.2	13.2	
17 to 22	21.5	21.5	21.5	21.5	21.5	21.5	21.5	21.5	
23 to 28	31.3	31.3	31.3	31.3	31.3	31.3	31.3	31.3	
29 to 35	41.0	41.0	41.0	41.0	41.0	41.0	41.0	41.0	
36 to 42	51.8	51.8	51.8	51.8	51.8	51.8	51.8	51.8	
43 to 49	62.5	62.5	62.5	62.5	62.5	62.5	62.5	62.5	
50 to 56	73.2	73.2	73.2	73.2	73.2	73.2	73.2	73.2	
57 to 63	83.9	83.9	83.9	83.9	83.9	83.9	83.9	83.9	
64 to 70	94.6	94.6	94.6	94.6	94.6	94.6	94.6	94.6	
71 to 77	105.3	105.3	105.3	105.3	105.3	105.3	105.3	105.3	
78 to 84	116.0	116.0	116.0	116.0	116.0	116.0	116.0	116.0	

2. Numbers in parentheses are the averages of coverage at the location.

TABLE 3 IS
COLLECTION AND RETENTION OF FALLOUT BY SOME SURFACE CROPS

Crops	Collection		Retention		Summary
	Surface	Root	Surface	Root	
Yield (kg)	29	—	—	—	
Type of Soil	—	—	—	—	
Height of Crop (m)	0.3	—	—	—	
Net Weight of Crop (kg)	2.2	—	—	—	
1.0 (15 + 10%)	—	—	—	—	
Yield (kg) from 1 ha	7	—	—	—	
Yield (kg) from 1 ha (15%)	6.3	—	—	—	
Fallout Deposition (kg/m ²)	1.750*	—	—	—	
Root Collection	—	—	—	—	
Whole	1.350**	—	—	—	
Arable	1.350**	—	—	—	
Forest Grounds	—	—	—	—	
Total Collection	1.350**	—	—	—	
Root	—	—	—	—	
Arable	—	—	—	—	
Forest Grounds	—	—	—	—	
Total	—	—	—	—	
Root Collection	15.5	5.1	—	—	Surface Density of Retained Radioactivity (kg/m ²) of soil surface
Whole	15.5	5.1	—	—	15.5
Arable	15.5	5.1	—	—	15.5
Forest Grounds	—	—	—	—	15.5
Total	15.5	5.1	—	—	15.5
Root Collection	32.5	—	—	—	Percent of Activity (Net Collected) by a Single Particle Retained
Whole	32.5	—	—	—	32.5
Arable	32.5	—	—	—	32.5
Forest Grounds	—	—	—	—	32.5
Total	32.5	—	—	—	32.5
Percent of Activity (Net Collected) Retained by the Total Particle Retained	—	—	—	—	Percent of Activity (Net Collected) Retained by the Total Particle Retained
Particle Diameter (μ)	—	—	—	—	41.32
0.10-25	0.5	0.5	0.11	0.11	No. of Particles
0.10-55	0.5	0.5	0.23	0.23	Fallout
0.10-125	0.5	0.5	0.38	0.38	Source
0.10-175	0.5	0.5	0.54	0.54	
0.10-250	0.5	0.5	0.51	0.51	
0.10-500	0.5	0.5	0.55	0.55	
0.10-1000	0.5	0.5	0.50	0.50	

* Plants were grown in plots of land situated at London Royal Holloway.

** Plants were collected from fields in the same area.

TABLE 2.17
THE INCINERATION OF FALLOUT PARTICLES FROM FOLIAGE

Plant	Distance From Ground Zero (miles)	Fraction of Gross Activity Remaining on the Foliage, After Decay Correction ^a		
		Reagent	0.1N HCl	5% EDTA
1. SANTA FE (22 KT at a 400 ft Tower)				
Larrea (Creosote bush)	29	0.52	0.34	0.33
Lepidium (Peppergrass)	33	0.19	0.10	0.05
Artemisia (Sagebrush)	19	0.64	0.51	0.46
2. SANTA FE (22 KT at a 200 ft Tower)				
Broad-leaved Coleogyne (Black Locust)	7	0.022	0.016	0.02
Triticum (Wheat)	7	0.25	0.18	0.35
Artemisia (Sagebrush)	45	0.18	0.10	0.19
Artemisia Trifolia (Sage)	45	0.32	0.16	0.17
Chrysothamnus (Sagebrush)	45	0.33	0.39	0.14
Atriplex (Saltbush)	105	0.25	0.29	0.10
Caryothamnus (Sagebrush)	105	0.49	0.26	0.21
3. SANTA FE (22 KT at a 200 ft Tower)				
Broad-leaved Coleogyne (Black Locust)	7	0.022	0.016	0.02
Triticum (Wheat)	7	0.25	0.18	0.19
Artemisia (Sagebrush)	45	0.18	0.10	0.17
Artemisia Trifolia (Sage)	45	0.32	0.39	0.14
Chrysothamnus (Sagebrush)	45	0.33	0.29	0.10
Atriplex (Saltbush)	105	0.25	0.26	0.21
Caryothamnus (Sagebrush)	105	0.49	0.26	0.11

^a Based on beta count-rate.

Table 2.17 (continued)

Leaf Surface Properties
<i>Lemna</i> - very-resinous
<i>Lepidium</i> - glabrous and glaucous
<i>Artemisia</i> - dense, naked, unbranched hairs and glands
<i>Broad-leaved annual</i> - smooth, velvety, sparse hairs
<i>Coleosia</i> - coarse, fine hairs
<i>Trifolium</i> - rows of short hairs, parallel to veins
<i>Clypeola</i> - dense, soft, wooly hairs
<i>Atriplex</i> - starry surface
<i>Ephedra</i> - scale-like, meristematic branches
<i>Isocoma</i> - scale-like, indurated
<i>Oryzopsis</i> - sparse, hair-like hairs
<i>Sphaeralcea</i> - dense, stellate hairs
<i>Trifolium (lower)</i> - rough, with scattered, unbranched hairs

Table 2.18

**SUMMARY OF AVERAGED FOLIAGE CONTAMINATION FACTORS FOR
NATIVE FOLIAGE EXPOSED TO FALLOUT FROM TOWER- AND
BALLOON-MOUNTED DTONATIONS AT THE NEVADA TEST SITE**

Shot	Distance from Ground Zero (miles)	$10^{10} \text{ } \mu\text{L}$	
		fallouts/gm of dry plant	fallouts/gm of dry plant
Tsunami, 1956	12	0.008	2.99
	60	0.418	8.81
	79	0.480	8.80
	98	0.584	8.00
Apple I, 1956	12	0.368	2.78
	40	0.328	2.00
	80	0.408	2.02
	140	0.295	18.04
Met, 1956	20	0.026	18.00
	80	0.07	18.28
	140	0.05	18.28
	200	0.008	2.00
Apple II, 1956	7	0.720	2.82
	48	0.720	2.00
	100	0.07	2.00
	140	4.80	5.00
Priscilla, 1957 ^a	7	0.28	7.27
	64	0.18	0.48
	128	0.30	0.40
	184	4.80	0.16
	180	1.01	20.0
	12	1.70	0.00
	18	1.88	17.8
Diablo, 1957	40	0.28	18.0
	60	12.0	10.5
	15	1.52	11.0
	44	1.87	7.72
	70	2.81	0.60
	172	8.10	0.42
Smoky, 1957	48	0.480	2.08
	80	0.070	2.52
	100	0.280	2.88
	120	0.008	2.00

Table 2.18 (concluded)

Shot	Distance from Ground Zero (miles)	$10^6 \frac{\text{fissions}}{\text{gm of dry plant}}$	
		$\frac{\text{fissions}/\text{gm of dry plant}}{\text{fissions}/\text{ft}^2 \text{ of total fallout}}$	$\frac{\text{fissions}/\text{gm of dry plant}}{\text{fissions}/\text{ft}^2 \text{ of } \approx 44 \mu\text{ fallout}}$
	100	0.529	2.76
	108	1.40	3.18
	170	1.20	2.00
	206	0.002	0.88

a. Balloon-mounted detonation

CHAPTER 8 REFERENCES

1. The Effects of Nuclear Weapons, U.S. Government Printing Office, Washington 25, D.C.(1957)
2. Bolles, R. C., and N. E. Ballou, Calculated Abundances of U-235 Fission Products, USNRDL-488, 1960.
3. Glendenin, L. E., Technical Report No. 85, Massachusetts Institute of Technology, Cambridge, Mass., 1949
4. Present, R. D., Phys. Rev., 72, 7 (1947)
5. Katcoff, Seymour, Nucleonics, 16, 4, 78 (1958)
6. Steinberg, E. P., L. E. Glendenin, International Conference on The Peaceful Uses of Atomic Energy, 7, 9 (1956)
7. Pappas, A. C., International Conference on The Peaceful Uses of Atomic Energy, Vol. 18, 583 (1958)
8. Wahl, A. C., J. Inorg. Nucl. Chem. 6, 263 (1955)
9. Glendenin, L. E., C. D. Coryell, and R. R. Edwards, Radiochemical Studies: The Fission Products, NNSA, Plutonium Project Record, Div. IV, D. 489, McGraw Hill, New York, N.Y., 1951
10. Herrington, A. C., Massachusetts Institute of Technology, Laboratory for Nuclear Science, Annual Progress Report, p. 87, June 1957-June 1958
11. Miller, C. F., A Theory of Formation of Fallout, USNRDL-TR-485, 1960
12. Adams, C. E., I. G. Popoff, and N. R. Wallace, The Nature of Individual Radioactive Particles, I. Surface and Underground ABD Particles from Operation Jangle, USNRDL-874, 1952
13. Maxwell, Ray D., Project 2.0-S Report, Operation Jangle, 1952
14. Schorr, M. G., and B. S. Gilligan, Project 2.0 Report, Operation Jangle, 1952

15. Alexander, L. T., J. M. Blume, and M. E. Jefferson, Project 2.8 Report, Operation Jangle, 1952
16. Stewart, K., Trans. Faraday Soc. 52, 101 (1956)
17. Pettijohn, F. J., Sedimentary Rocks, Harper Brothers, New York, N.Y., 1949
18. Adams, C. E., The Nature of Individual Radioactive Particles, II. Fallout Particles from M-Shot, Operation Ivy, UBNRDL-408, 1954
19. Adams, C. E., N. H. Farlow, and W. R. Schell, Geochimica et Cosmochimica, 18, 18 (1960)
20. Adams, C. E., and J. P. Wittman, The Nature of Individual Radioactive Particles from An ABD of Operation Upshot-Knothole, UBNRDL-440, 1954
21. Adams, C. E., and J. D. O'Connor, The Nature of Individual Radioactive Particles. VI. Fallout Particles from a Tower Shot, Operation Redwing, UBNRDL-TR-209, 1958
22. Farlow, N. H., Analyt. Chem. 29, 888 (1957)
23. Kenjiro Kimura, Geneva Conference on The Peaceful Uses of Atomic Energy, 7, 196 (1956)
24. Mackin, J., P. Zigman, D. Love, D. McDonald, and D. Bam, J. Inorg. Nucl. Chem., 18, 20 (1960)
25. Jones, J. W., and R. T. Overman, AECD-2867, 1948
26. Miller, G. F., and P. Loeb, Ionization Rate and Photon Pulse Decay of Fission Products from The Slow Neutron Fission of U-235, UBNRDL-TR-247, 1958
27. Freling, E. C., Fractionation Correlations, UBNRDL-TR-885, 1959
28. Larson, K. H., J. W. Neel, et al., Summary Statement of Findings to the Distribution, Characterization, and Biological Availability of Fallout Debris Originating from Testing Programs at the Nevada Test Site, UCLA-488, 1960
29. Nishita, Hideo, E. M. Romney, and K. H. Larson, Agricultural and Food Chemistry, 9, 2, 101 (1961)

30. Bellamy, A. W., et al., The 1948 Radiological and Biological Survey of Areas in New Mexico Affected by the First Atomic Bomb Detonation, UCLA-92, 1949.
31. Rainey, C. T., et al., Distribution and Characterization of Fallout at Distances Greater Than Ten Miles from Ground Zero, March and April, 1950, Operation Upshot/Knothole, WT-811, 1954.
32. Lindberg, R. G., et al., The Factors Influencing the Biological Fate and Persistence of Radioactive Fallout, Operation Teapot, WT-1177, 1950.
33. Romney, R. G., Lindberg, H. A., Hawthorne, B. G., Bystrom, and K. H. Larson, Health Physics (to be published).
34. Fuller, R. K., unpublished data, USNRDL, 1960.
35. Heiman, W. T., and R. L. Swanson, unpublished data, USNRDL, 1962.
36. Miller, C. F., Analysis of Fallout Data, II: Radioactive Decay, UENRDL-TR-221, Del. 1958.
37. Dunning, Gordon M., Ed., Radioactive Contamination of Certain Areas in the Pacific Ocean from Nuclear Test Washington, D.C. Atomic Energy Commission, August 1957.
38. Lapp, Ralph E., Local Fallout Radiocactivity, Bulletin Atomic Scientists, XV, 5, 181, 1959.
39. Knapp, H. A., External Gamma Doses and Dose Rates from the Fallout from Nuclear Detonations, Civil Defense, Hearings before a Sub-committee of the Committee on Government Operations, U.S. Congress, 1960.
40. Miller, J. R., and R. F. Reitemeier, Rate of Leaching through Soils by Simulated Rain and Irrigation Waters, ARS Report No. 800, 1957.
41. Thornthwaite, C. W., J. R. Mather, and J. K. Nakamura, Science, 131, 1015 (1960).
42. Bartor, J. D., and W. L. Owens, Radiological Recovery of Land Target Components, Complex I and II, UENRDL-TR (in preparation), 1961.

Chapter 2

A THERMODYNAMIC MODEL OF FALLOUT FORMATION

3.1 The Condensation Process

The essential features of the fallout formation process deduced from the final structures, compositions, and general properties of fallout particles as described in Sections 2.3 and 2.4 are that:

1. Some portion of the radioactive elements condenses into liquid particles.
2. Some portion condenses onto the surface of solid particles.
3. If a time limit is placed on the process, some fraction of some of the radioactive elements will be still in the vapor phase.

Even in the case where the bulk carrier is sea water, the first two statements are valid for the fallout from a moderately high-yield detonation near the sea surface, since the temperature of the drops, at the altitude of the cloud, will at some time fall below freezing.

The general condensation process can be divided into two general time periods. The first period of the process is characterized by the presence of gas and liquid phases and the second period by the existence of gas and solid phases. The first period of condensation ends when the bulk carrier particle solidify. There is probably no real precise instant at which this occurs in the fireball since temperature gradients must certainly exist; the different sizes of particles cool and solidify at different rates and times.

One most important aspect of the condensation of the radioactive fission products into the liquid phase is that the fission-product elements and compounds are dissolved to form a very dilute solution. Because of this dilution, the solution process can be treated with neglect of (a) surface saturation effects and (b) interactions among the various radioactive elements in the formation of the solution.

In a glassy matrix, i.e., after solidification, the dissolved or compound fission products should not be able to escape. With concentrations of the order

of 10^{-10} moles of fission products per mole of glass, the vapor pressure would be extremely low and the diffusion of the elements through the solid glass would be very slow.

The fraction of each fission product that is condensed into the liquid carrier particles when they solidify will be determined by (a) the melting point of the carrier and (b) the time after fission at which the solidification occurs. If the melting point of the carrier is high, the fractions that are condensed will be smaller than those in carrier materials having low melting points. For some of the larger particles, the fractions that are condensed will be determined by the time at which solidification of the particle occurs. In the case where the carrier can exist in the liquid state over a relatively large temperature range, and the yield is reasonably large so that fireball does not cool too rapidly, the larger particles can not only enter but can leave the fireball volume before the interior gases cool to the temperature at which the particles solidify.

The fraction of each fission product that is not condensed into the liquid phase of the carrier can still condense on or react with the surface of the solid particles. The solid particles available could consist of (a) the smaller of the melted particles (since these do not fall out of the cloud volume as soon or as rapidly as the larger particles) or (b) of unmelted particles that enter the gas volume at later times.

The best illustration of the latter type of particle is the irregular particles found in the coral fallout. Because of the high melting point of calcium oxide, the number of the more active (fused, spherical) particles found was usually, but not always, smaller than the number of irregular unmelted particles. Even though the fused particles had higher specific activities, they carried a fraction of the total radioactivity produced that was much smaller than the fraction carried by the irregular unmelted particles.

The reverse was true for the particles of the lower-melting silicate glasses. There is no doubt that both unfused and sintered grains of soil and the smaller fused spheres carried radioactivity on their surfaces; various amounts of activity were leached from the samples of these particles in water and dilute acids. However, in the presence of the larger fused spheres in heavy-fallout regions the irregular soil grains contributed only a rather small fraction of the total radioactive content of the fallout deposit.

In the second period of condensation, i.e., after the particles solidify, the fission-product elements may condense by (a) sublimation on the surface of solid particles or (b) they may react directly with the carrier substance. In the case of a more or less open or porous crystal structure, the fission products could diffuse well into the body of the particle. This process was evidenced by the layer of activity in the irregular coral particles.

The previously-mentioned vapor-condensation computations using simple kinetic theory, or the more complicated method used by Stewart¹, both indicate that condensation-vaporization equilibrium can be established within a fraction of a second at temperatures around 3000°K. The finding of the small spheres confirms the nature of this early direct vapor-condensation. When equilibrium is established the gaseous species of each fission product element can either (a) react with the vapor or liquid products of the bulk carrier, or (b) dissolve into the liquid phase according to Henry's law of dilute solutions. These solutions of fission product elements or compounds in the liquid phase should be (a) sufficiently dilute to result in no change in the free energy of the liquid carrier, and (b) so dilute that the free energy of solution of each element is independent of the concentration of all other fission-product elements.

3.1.1 Gas-Liquid Phase Condensation

Because of the extreme dilution of the fission product elements in the fallout particles, it is possible to consider the gas-liquid phase condensation and the solubility of each fission product element in the carrier as an independent two-component system. Moreover, there should be no appreciable surface loading (due to large excess surface concentrations during the condensation process) if the temperature range over which the liquid carrier exists exceeds 200 or 300°C. Concentration gradients in particles may occur, however; particles that are not heated very much above the softening temperature and are not very fluid, or larger particles that may not have been melted in their center by the time the surface temperature falls below the melting point, would each contain concentration gradients when solidified.

Two general types of gas-liquid phase condensation processes may be considered. One is Henry's law of dilute solution; the other is compound formation with carrier material. Henry's law of dilute solution is given by

$$P_j = k_j N_j \quad (3.1)$$

in which N_j is the mole fraction of element j in the liquid phase, k_j is the Henry's law constant, and P_j is the partial pressure of the gaseous species of element j . For a mixture of gases,

$$P_j = N_j^* P \quad (3.2)$$

in which N_j^* is the mole fraction of the gaseous species of element j in the vapor and P is the total pressure. Combining Eq. 3.1 and 3.2 gives

$$N_j^*/N_j = k_j/P \quad (3.3)$$

In the thermodynamic treatment, the dependence of k_j on P will be assumed too small for all elements. The dependence of k_j on temperature is described by $k_j^0 e^{-\Delta H_v/RT}$ where k_j^0 is a constant and ΔH_v is given by

$$\Delta H_v = L_j^g - L_j^l \quad (8.4)$$

where L_j^g is the relative partial molar heat content of element j in the gas phase and L_j^l is its relative partial molar heat content in the liquid phase. For an ideal gas and an ideal solution, ΔH_v is the heat of vaporization of the condensing species of element j .

It may be noted from Eq. 8.3 that a decrease in the total pressure, P , results in an increase in the ratio, N_j^g/N_j^l , or a decrease in the mole fraction of the minor constituent, j , in the liquid phase relative to its mole fraction in the gas phase. Because of this, N_j^g/N_j^l depends on the vapor pressures of the various major constituents in the fireball.

For early-time condensations (as would occur with a high-melting-temperature carrier and when the temperature is high and gas volume not fully expanded) the total pressure should also be high. The high pressure would tend to decrease the value of N_j^g/N_j^l . However, the high temperature would tend to increase the value of N_j^g/N_j^l by the term $e^{-\Delta H_v/RT}$. Since both the pressure and temperature decrease with time, the one should tend to cancel or balance the effect of the other on producing changes in N_j^g/N_j^l with time, although over a long period of time the effect of the temperature decrease will generally prevail in the cooling of the fireball.

If the liquid soil particles are assumed to be more or less uniformly distributed throughout the fireball volume, and the temperature is also assumed to be somewhat uniform, then all the liquid particles may be considered as a single liquid phase in contact with the gas at a given temperature and time. Although a given pair of values of P and T at a given time would be valid only for some small increment of the fireball volume, it is obvious that these cannot be given a uniform or average value for the whole volume if assumed in the treatment.

Without specifying the number or size of particles, the mole fraction of element j in the liquid phase is given by

$$N_j^l = n_j/n(\#) \quad (8.5)$$

where n is the number of moles of element j dissolved in $n(\#)$ moles of liquid carrier where $n_j \leq n(\#)$. The mole fraction of element j in the vapor phase is given by

$$N_j^g = n_j^g/n \quad (8.6)$$

where n_j^0 is the number of moles of element j mixed with n moles of vapor and $n_j^0 \ll n$.

If the perfect-gas law is assumed for all the gaseous species comprising the n moles of gas, then Eq. 8.6 can be written as

$$N_j^0 = n_j^0 RT / PV \quad (8.7)$$

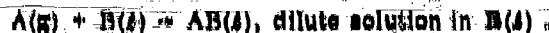
Substituting Eqs. 8.5 and 8.7 into Eq. 8.3 gives

$$n_j^0 = \frac{n_j k_j}{[n(t)/V] RT} \quad (8.8)$$

The ratio, n_j^0/n_j , in Eq. 8.8 depends on the values of k_j , T , and $n(t)$ per unit volume in the fireball at the time.

Because the mole fractions are small, the value of n_j^0/n_j is independent of the total amount of the element present. Therefore the same fraction of an element should be condensed at a given time and temperature for a 100 percent fission weapon as for a "clean" thermonuclear weapon of the same total yield. The value of $n(t)/V$ depends on the total yield and time after detonation, since the amount of carrier material liquefied depends on (a) how the total energy is utilized in the process and (b) the rate of the in-flow and spatial distribution of the carrier material passing through the fireball volume.

Compound formation of an element with the carrier in the gas phase, followed by condensation of the heavier gas molecule into a liquid solution with the mated carrier material, can also be described by use of Henry's law for the dilute solution. However, when the compound is formed with the (bulk) liquid carrier, then the free energy of formation of the compound and its heat of vaporization must be considered. The over-all reaction for a direct combination of fission product element A with carrier material B to form the compound AB may be written as follows:



This reaction may be written as a sum of three or four separate reactions depending on whether the combination of A and B occurs as A condenses or when B is in the vapor phase prior to condensation.

There should be no difference in the two processes with regard to the total change in free energy between the same initial and final thermodynamic

states. The difference, if any, would be in the kinetics of the process. In the first process, the separate reactions and the standard free-energy changes are:

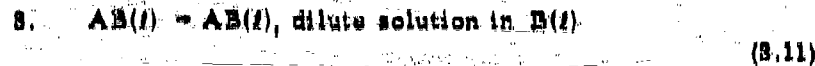


$$\Delta F_1^\circ = RT \ln p_A$$



$$\Delta F_2^\circ = -RT \ln K_{AB}$$

where K_{AB} is the equilibrium constant for the formation of $AB(l)$ from $A(l)$ and $B(l)$ at the temperature, T . The solution reaction is



$$\Delta F_3^\circ = -RT \ln \gamma_{AB}$$

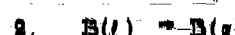
where γ_{AB} is the thermodynamic activity of $AB(l)$ in $B(l)$ and is equal to $N_{AB} k_{AB}$ if N_{AB} is the mole fraction and k_{AB} is the Henry's law constant or activity coefficient. The sum of the standard free-energy changes for the three reactions, or the free energy of the over-all reaction, is

$$\Delta F^\circ = RT \ln \frac{p_A}{N_{AB} k_{AB} \gamma_{AB}} \quad (B.12)$$

In the second process, the separate reactions and the standard free-energy changes are:



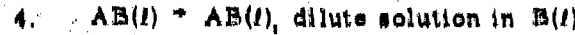
$$\Delta F_1^\circ = -RT \ln \frac{P_{AB}}{P_A P_B} \quad (B.13)$$



$$\Delta F_2^\circ = -RT \ln p_B \quad (B.14)$$



$$\Delta F_3^\circ = RT \ln \gamma_{AB} \quad (B.15)$$



$$\Delta F^\circ = -RT \ln N_{AB} k_{AB} \quad (B.16)$$

The sum of the standard free-energy changes for these four reactions is

$$\Delta F^{\circ} = 10F/n \frac{p_A}{N_{AB} K_{AB}} \quad (3.17)$$

The free-energy changes given by Eqs. 3.12 and 3.17 would be equal if $p_A/N_{AB} K_{AB}$ of Eq. 3.12 is equal to p_A/N_{AB} of Eq. 3.17, or if K_{AB} is unity. If the perfect-gas law is used to estimate the number of moles of A, n_A in the gas volume from p_A in Eqs. 3.12 or 3.17 and if N_{AB} is replaced by $N_{AB}/n(A)$, the two equations become

$$n_A = \frac{N_{AB} k_{AB} K_{AB} e^{-\Delta F^{\circ}/RT}}{[n(t)/V] RT} \quad (3.18)$$

and

$$n_A = \frac{N_{AB} k_{AB} e^{-\Delta F^{\circ}/RT}}{[n(t)/V] RT} \quad (3.19)$$

respectively. Replacing either $k_{AB} K_{AB} e^{-\Delta F^{\circ}/RT}$ (Eq. 3.18) or $k_{AB} e^{-\Delta F^{\circ}/RT}$ (Eq. 3.19) by k_{AB} reduces the two equations to the same form as Eq. 3.8. The same computational treatment would therefore apply except that the standard free-energy functions, when available, could be used to calculate the free-energy change for the compound-formation reaction.

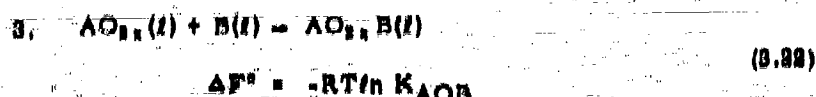
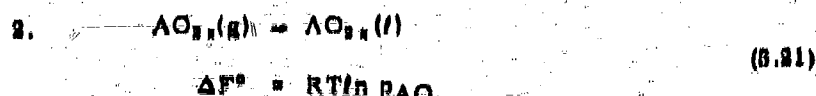
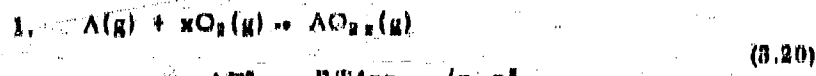
The first compound-formation reaction described above did not include any reaction between the atmospheric oxygen and the element A in the condensation process. Of course, even in the presence of oxygen many of the fission-product oxides are partially or completely dissociated in the vapor phase. For those that are completely dissociated at the temperatures where the carrier material exists as a liquid, the above reaction(s) is applicable. Also, if the oxides are completely associated, A(g) may be taken to represent the oxide molecule, and Eq. 3.18 or 3.19 can be applied. However, for the elements in which the oxide molecule is partially dissociated in the vapor state and associates further with oxygen in the condensed state, the oxygen partial pressure will influence the relative amounts of the element in the liquid and the gas phases.

The over-all reaction for this condensation process is

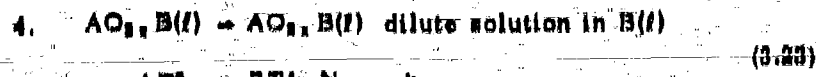


in which x is the number of oxygen molecules that combine with each atom of

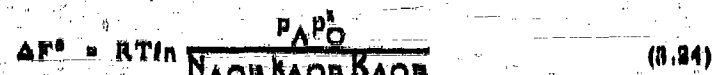
element A. Separate reactions for this over-all reaction can be set up in the same way as above, but for this over-all reaction to be different from the one above (or competing with it), the gas atoms of A and O_x must be in equilibrium with the oxide of element A in the vapor state. The oxide molecules then either (a) react with B(?) as they condense or (b) they react with B(g) in the vapor before the larger oxide molecules condense to form the dilute solution. In the first of these two processes, the separate reactions and the standard free-energy changes are:



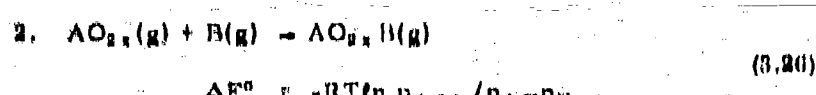
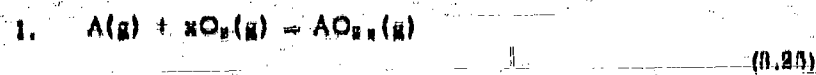
where K_{AOB} is the equilibrium constant for the formation of $AO_{x,x}B(l)$ from the two liquid compounds at the temperature, T.



The sum of these reactions and their standard free-energy changes give



In the second process, the separate reactions and the standard free-energy changes are:





$$\Delta F^\circ = -RT/n \ln p_{II}$$



$$\Delta F^\circ = RT/n \ln \frac{p_{B(l)}}{p_{B(g)}}$$



$$\Delta F^\circ = -RT/n \ln \frac{p_{B(l)}}{k_{AOB} p_{AOB}}$$

The sum of the five standard free-energy changes is

$$\Delta F^\circ = RT/n \ln \frac{p_{AOB}}{\frac{k_{AOB} p_{AOB}}{k_{AOB} k_{AOB}}} \quad (0.30)$$

Equations 0.24 and 0.30, when solved for n_A by use of the perfect-gas law, give

$$n_A = \frac{\Delta F^\circ / RT}{\left[n(l)/V \right] - RT \frac{p_0}{p_l}} \quad (0.31)$$

and

$$n_A = \frac{\Delta F^\circ / RT}{\left[n(l)/V \right] - RT \frac{p_0}{p_l}} \quad (0.32)$$

respectively.

The values of n_A in Eqs. 0.31 and 0.32 are sensitive to the oxygen partial-pressure. If p_0 is greater than 1 atmosphere, the value of n_A will be decreased (most with largest x value) and the amount of element A condensed is increased. If p_0 is less than 1 atmosphere, the value of n_A will be increased (most with largest x value) and the amount of element A condensed is decreased. If p_0 is incorporated into the k_{AOB} in the same way as was done for the factors of Eqs. 0.18 and 0.19, then Eqs. 0.31 and 0.32 can also be reduced to the same form as Eq. 0.8 for material balance and other general summation formulas.

Equations 8.30 to 8.38 are perhaps more rigorous in the definition of the condensation process than that given by Eq. 8.8 which describes the process only in terms of Henry's law. In a real case, the carrier material is not an inert substance but is capable of forming compounds with many of the fission product elements. Also, the Eqs. 8.30 to 8.38 will be applicable for elements that react with the carrier in the solid state. For these, the notation only need be changed from (7) to (8) to refer to the solid rather than the liquid state.

Before considering the second period of condensation, the material-balance equations (in terms of fission yields and fractionation numbers) for the first period of condensation are presented. Although the form of Eq. 8.8 for Henry's law of dilute solution is used in the treatment, the final material-balance equations would be identical for the compound-formation processes.

8.1.2 Gas-Liquid Phase Material-Balance Constraints and Fractionation Numbers

Since the condensing elements are radioactive, the number of moles of each is constantly changing; therefore the material balance of a given element also changes with time. On the other hand, the fission yield of a given mass-chain (except for neutron emitters) is constant. If the amount of a radionuclide of element J and mass number A present at the time, t, after fission is given by $y_{JA}(t)$, then the total amount of element J present at time t is

$$Y_J(t) = \sum_A y_{JA}(t) \text{ atoms or moles} \quad (8.33)$$

The corresponding sum for the chain yield of mass number A is

$$Y_A = \sum_J y_{JA}(t) \text{ atoms or moles} \quad (8.34)$$

In which Y_A is constant except for the mass chains containing neutron emitters. The material balance for the amounts element J in the gas and liquid phases is

$$Y_J(t) = n_J^g(t) + n_J^l(t) \quad (8.35)$$

where the time dependence of n_J^g and n_J^l of Eq. 8.8 is indicated.

If n_J^g and n_J^l are taken for the amounts of each nuclide in the gas and liquid-phases, respectively, the material balance for each element is

$$\sum_A y_{JA}(t) = \sum_A n_J^g(t) + \sum_A n_J^l(t) \quad (8.36)$$

If k_f^0 is used for $k_f / [(n(t)/V)Rt]$, substitution of Eq. 8.8 in Eq. 8.30 gives

$$\sum_{A'} n_{JA'}(t) = (1 + k_f^0) \sum_{A'} n_{JA}(t) \quad (8.37)$$

and, since $(1 + k_f^0)$ is the multiplier for each of the $n_{JA}(t)$ terms, the terms for each nuclide can be separated out. The separated terms then give the amount of each nuclide condensed, which is

$$n_{JA}(t) = \frac{y_{JA}(t)}{1 + k_f^0} \quad (8.38)$$

The fraction of the mass chain that is condensed, or the absolute fractionation number (i.e., referred to the fission yield rather than to another nuclide), $r_n(A, t)$, for the end chain-members is defined by

$$r_n(A, t) = \frac{1}{Y_A} \sum_{A'} n_{JA'}(t) \quad (8.39)$$

Substitution of Eq. 8.38 and replacing the $y_{JA}(t)/Y_A$ ratio by $y_j(A, t)$ in Eq. 8.39 gives, for the fractionation number of each mass number,

$$r_n(A, t) = \sum_j \frac{y_j(A, t)}{1 + k_f^0} \quad (8.40)$$

In which $y_j(A, t)$ is the fraction of the chain yield of element j having mass number A . According to Eq. 8.40, the fraction of the chain that is condensed in the liquid phase depends only on k_f^0 and the fractions of the chain yield of the elements present. The use of this equation, therefore, requires values of the independent yields of each member element of the chain at times from a few seconds after fission, or at least for the time of the end of the first period of condensation that may be applicable to the first group of particles that leave the fireball in the liquid state.

The experimental radiochemical fractionation number for a given sample of fallout (or quantity of mixed fission products) is usually defined as the ratio of the number of atoms of a given mass number that are present to the number of atoms of mass number 99 that are present, divided by the expected value of the ratio for thermal neutron fission of U-235. In mathematical notation, this is

$$R^{99}(A) = \frac{n(A)}{K_0(A) n(99)} \quad (8.41)$$

Ordinarily, count-rate ratios are used, along with the appropriate decay corrections from the time of analysis to zero time, with a corresponding value of $K_n(\Delta)$ that has been previously determined from an analysis of a sample of U-238 bombarded with thermal neutrons. For analyses made more than several days after fission, only the last or last two members of a decay chain of most mass numbers will be present in appreciable amount.

Since the observed "R" factors give an over-all measure of variation from U-238 thermal-neutron fission, another factor is needed to account only for that part of the variation that is due to the first period of the condensation process. For this, let

$$r^{99}(A) = \frac{n(A)}{K(A) n(99)} \quad (B.42)$$

In which $K(A)$ is the true yield ratio, Y_A/Y_{99} , of mass number A to that of mass number 99, which varies with the kind of fissioning nuclide and incident neutron spectrum (the same definition holds if some mass number other than 99 is selected as the reference nuclide).

The value of the ratio, $n(A)/n(99)$, should be the same as the ratio of the sum over j of the respective $n_j(A,t)$ terms. The fractionation number from the material balance equations referred to a standard nuclide (in this case mass number 99) becomes

$$r^{99}(A) = \frac{\sum_j y_j(A,t)/(1+k^j)}{\sum_j y_j(99,t)/(1+k^j)} \quad (B.43)$$

when $K(A)$ is replaced with Y_A/Y_{99} . It is possible for $r^{99}(A)$ to have values greater than one; the values of $r_0(A)$ cannot be greater than one.

In the second period of condensation, the fraction of each element not condensed from the gas phase (when the fireball temperature has fallen below the melting point of the carrier material) can begin plating out on the surface of solid particles. The available particles for this period of condensation can be the smaller solidified particles that have not settled out of the radioactive gas volume plus the unmelted soil grains that entered the fireball late and were not heated to their melting temperature.

Although it is possible that a variety of gas-solid state reactions may occur for the different elements, depending on the physical and chemical properties of the carrier particles, only one simple and idealized process is considered here. This is that the fraction of each element that is condensed, up

to some stated time after fission, is related to that element's total sublimation pressure. Further, it is assumed that the carrier surface acts as if it were the pure solid compound of the condensing species. Under these conditions, the computational values of the amounts condensed reflects the relative volatility of the (assumed) constituent gaseous molecules at all temperatures at which this kind of condensation can occur.

If an excess of solid-surface area is presented to the condensing molecules, the number of molecules condensed by the process (assuming the process to be reversible) at any time after the solidification of the carrier is defined by

$$n_j^c = n_j^0 + n_j^v \quad (8.44)$$

where n_j^c is the amount of element j condensed on the surface of the solid particles, n_j^0 is the amount of the element remaining in the gas phase when the carrier particles solidified, and n_j^v is the amount in the vapor phase at any later time. Because of radioactive decay, all three amounts depend on the time after fission.

If the perfect-gas law is assumed for each gaseous species, then

$$n_j^v = \frac{P_j^v V}{RT} \quad (8.45)$$

where V is the gas volume containing the n_j^v moles and P_j^v is the equilibrium sublimation pressure which, in turn, is given by

$$P_j^v = e^{-\Delta F_j^\circ / RT} \quad (8.46)$$

in which ΔF_j° is the free energy of sublimation. If uniform mixing in the fireball volume is assumed for the particles and gaseous species at all times, then V is the fireball (or cloud) volume. The time-dependent material balance for element j is

$$Y_j(t) = n_j(t) + n_j^c(t) + n_j^v(t) \quad (8.47)$$

where n_j is the number of moles condensed in the liquid phase.

One of Eq. 8.48 for n_j^c and Eq. 8.46 for n_j^v , combined with Eq. 8.47, gives

$$n_j^c = \frac{k_j^0 Y_j}{1 + k_j^0} = \frac{V P_j^v}{R T} \quad (8.48)$$

or, for all mass numbers of a given element,

$$\sum_{A} n_{JA} \frac{k^0}{1+k^0} \sum_{A} Y_{JA} = \frac{V}{RT} \sum_{A} p_{JA}^0 \quad (8.40)$$

Repeating out the terms for each nuclide results in

$$n_{JA}^0 = \frac{k^0 Y_{JA}}{1+k^0} = \frac{V p_{JA}^0}{RT} \quad (8.50)$$

In this case the partial pressure of each nuclide is proportional to its abundance at the time and is given by

$$p_{JA}^0 = (Y_{JA}/Y) p_{JA}^0 \quad (8.51)$$

The fractionation number of the end-chain member of each mass chain, or, the fraction of the chain that is condensed up to a given time in the second period of condensation, $r_0(A,t)$, is defined by

$$r_0(A,t) = \sum_i \frac{Y_i(A,t)k^0}{1+k^0} = \frac{V}{RT} \sum_i p_i^0(A,t) \quad (8.52)$$

In which

$$p_i^0(A,t) = \frac{p_{JA}^0}{0.241 Y_A B W} \quad (8.53)$$

where y_A is the fractional chain yield in atoms per fission, B is the ratio of fission to total yield, and W is the total yield in kiloton; the total chain yield is $0.841 y_A B W$ moles.

In Eq. 8.52, the k^0 values are, as in Eq. 8.40, evaluated at the temperature of the end of the first period of condensation; this is different from the temperature, T , in the second term. Thus the fractions of each element not condensed during the first period of condensation (given by the first term of Eq. 8.52) must be decay-corrected to the time of interest to determine y_A and Y , applicable to Eq. 8.51.

In assuming the condensation to be independent of the nature of the particle surface, and in neglecting solid-solution-compound or formation with the carrier material, the components and equations for each element have to be reduced by one. Therefore the fractional partial pressures become yield

dependent, as shown in Eq. 9.38. The dependence of $r_0'(A,t)$ on weapon yield, however, will be determined by the variation of V/W with yield.

In summary, the over-all fallout particle formation process, from the above treatment, may be described as follows. In the first period of condensation, when the liquid and gas phases predominate in the fireball, the more refractory elements are dissolved into the liquid phase of the carrier material. The larger fallout particles, which fall away from the fireball while they are in the liquid state, will contain only those more refractory radionuclides. These particles will land nearest to the point of detonation.

The smaller particles, that stay with the rising fireball for a longer time, may condense out radionuclides during both periods of condensation. These, as well as the particles that enter the fireball late, should carry radionuclides that were condensed on their surfaces. The smallest of the particles would make up the world-wide fallout or would be deposited at large distances from ground zero.*

The intermediate size particles, that deposit at intermediate distances from ground zero, should contain radionuclides that were condensed during both periods of condensation. In fallout of a given particle size in which a fraction of a mass chain had condensed during the first period of condensation and the remainder of the mass chain during the second period, the gross fractionation number of the fallout sample would be given by

$$R_0(A) = x(t') \left[1 - \frac{V}{RT} \sum_i m_i'(A,t') \right] \quad (9.44)$$

In which $x(t')$ is the fraction of the element not carried out of the fireball by larger particles prior to t' . No single value of $r_0'(A)$ or $R_0(A)$ would apply to all the particles since the fraction condensed depends on the time period that each particle spends in the gas volume.

9.1.3 Gas-Liquid Phase Condensation - Particle-Size Effects

In the discussion of the condensation processes, some attention must be given to the effect of particle size on the amount of the element condensed. The vapor pressure over the liquid drops can depend on the size of the drop, especially at the higher temperatures. The relationship between

*The world-wide fallout from air, sea water, tower, and surface bursts also contains vapor-condensed particles which have activity more or less uniformly distributed through their volumes.

drop size and vapor pressure is given by

$$RT\ln p/p_0 = 4\gamma M/d \quad (3.55)$$

In which p_0 is the vapor pressure of the carrier material over the liquid with a flat surface; p is the pressure over the drop of diameter, d ; γ is the surface tension of the drop (assumed independent of T); M is the molecular weight of the carrier; and ρ is the density of the liquid. For Al_2O_3 at 2050°C and SiO_2 at 1800°C , the value of γ is 800 dynes/cm and 307 dynes/cm, respectively.¹⁰

The value of the ratio, p/p_0 , for these values of γ is not very different from unity for particles having diameters larger than a few tenths of a micron. Hence, unless the carrier material has a surface tension that is larger than that of these two oxides by more than two orders of magnitude, the increased vapor pressure of the carrier material over the larger drops should not be enough to influence the condensation process.

If the surface tension of the carrier material were extremely large, the fission product elements most likely to be preferentially condensed on the smaller particles are those elements whose volatilities are the same as, or lower than, that of the carrier itself. These would co-condense with the volatilized carrier molecules as soon as the temperature dropped to the carrier boiling point, since at this time the vapor pressure of the carrier material should be a significant fraction of the total pressure. At the melting point of the carrier, its own vapor pressure would be no small a fraction of the total pressure that it could not influence the mole-fraction ratio even if the surface tension were extremely large.

Thus the variations with distance, or with particle size, that are found in the fractionation numbers in the data (see Sections 3.3 and 3.4) must arise from two causes. The first cause is the gradual shift with downwind distance in the mixing of the melted with the irregular particles or of the particles present during both periods of condensation. The second cause is the difference in the period of time that the different-sized particles stay in the gas volume.

For particles with a fairly large range in sizes, the mole fraction, N_i , needs to be precisely defined (see p. 99). Carrier materials such as silicate rocks containing metal oxides are refractory materials with low heat conductivity. But a particle need not be completely melted throughout its volume in order to condense and dissolve gaseous molecules; only a thin liquid layer on its exterior is required for the process. Because of its low thermal conductivity, some maximum-size carrier particle or group of particles should exist that melts completely when exposed to a given thermal cycle. This partial melting

of the larger particles would limit the penetration of the condensing elements and of those collected through collision with the very small liquid particles.

The penetration of the condensates into the liquid drop, and the rate of distribution of these condensates throughout the volume of the drop, would be more rapid if caused by turbulence and convection rather than by simple diffusion, especially in penetrating or distributing through the peripheral regions of the liquid particles. The general uniformity of the radionuclide concentration in the silicate fallout particles--especially from the low-tower shots--indicates that diffusion is not the controlling process. The condensates are often found deposited more or less to a given depth from the surface of the very largest particles and in a more or less uniform concentration throughout the medium-size and smaller particles. Although there are no data for verification, the more volatile elements may form solutions in particles with the larger-surface concentration excesses by condensing in relatively large amounts just as the particles are solidifying.

If the average depth of the surface layer containing the condensates is designated as h and is assumed to be the same for all particles, then the number of moles of carrier per (spherical) particle involved in forming the dilute solution is given by

$$n(t, p) = \frac{\pi ph}{M} [d(d-2h) + (4/3)h^3], \quad d > 2h \quad (0.50)$$

in which $n(t, p)$ is the number of moles of the carrier (that was melted) in the surface layer of the particle and d is the particle diameter. For dilute solutions, $n_j(p)$, the number of moles of element j in the particle is given by

$$n_j(p) = N_j \frac{\pi ph}{M} [d(d-2h) + (4/3)h^3], \quad d > 2h \quad (0.57)$$

If $n_0(p)$ is taken as the total number of moles of the carrier in the particle, then

$$n_j(p)/n_0(p) = 6.00 N_j h \frac{[d(d-2h) + (4/3)h^3]}{d^3}, \quad d > 2h \quad (0.58)$$

or

$$n_j(p)/n_0(p) = N_j \cdot d - 2h \quad (0.59)$$

The mole fraction in Eq. 8.60 is for the particles that had been completely melted. The relative concentration of the solute, $n_1(p)/n_0(p)N_1$, becomes proportional to $1/d$ for $d > 2h$; this occurrence would be equivalent to the condensation of amounts of activity in proportion to the surface area of the particle.

There are two additional factors that could have some bearing on the relative amount of an element that condenses into the liquid particles. First, the larger particles may fall out of the gaseous volume before they solidify and, second, they may be melted only on one side (not sufficiently melted to form a spherical particle). Both of these two groups of particles would condense smaller amounts of all elements per particle than would be estimated from Eq. 8.68.

The origins of the melted particles in the fireball may be several in number. The small vapor-condensed particles originating from vaporized soil have been mentioned. Others are the particles that were originally lying on the ground out to some distance from shot point, some of which probably are warmed and perhaps melted by the heat absorbed from the radiant energy emitted at detonation. These particles are then drawn into the fireball as it rises.

In low air bursts, where a very small crater is formed, the latter mechanism probably is the dominant process by which particles enter the fireball. In this case the size distribution of the fallout particles that are produced should be the same as the original size distribution of the surface soil. In the detonation, the blast wave would powder the surface layer of soil to some depth and the resulting dust particles, like the surface-melted particles, would retain their size in the formation process. However, these particles would not be melted until after they entered the fireball.

For surface detonations, two other major mechanisms may occur that cause particles to enter the fireball. One is the "jetting" of the soil where the blast or shock wave hits the soil surface; this should occur at very early times after detonation. The soil grains in the jets may be partially heated or even melted by absorption of energy from the blast wave and then vaporized as they penetrate into the hot fireball gases at high velocity. Following this ejection of the surface-layers of soil material, new exposed but thin layers of soil may be melted. It seems reasonable that such a liquid layer of soil would intervene between the vapor in the fireball and the layer of shock-powdered earth as long as the fireball remained in contact with the earth's surface. If enough "fluxing" material (such as the carbonates) is present, a rather large amount of fluid material could be formed. The other major mechanism takes place as the fireball lifts; the liquid is broken up into drops that enter the fireball, followed by

the powdered soil. The mechanism break-up of the fluid mass should produce about the same size distribution of particles from all liquids that have about the same surface tension.

8.2 The Dependence of Fireball Parameters on Weapon Yield and Time After Detonation

A descriptive mathematical model of the fireball--giving its size, temperature, rate of rise, energy content, and other characteristics--is needed to specify the boundary conditions for use in the condensation equations. Specifically, the mathematical description of the fireball should be designed to yield estimates of the quantity, $n(t)/V$, in addition to the others.

The descriptive models presented here, although crude and much oversimplified, are organized to bring together the major parameters that are involved. It should be understood that improvements in the model can be made when more details of the basic data are declassified.

The basic reference data from UNW used here deals mainly with the description of air and/or tower detonations. To develop the model presented in this report for the surface detonation the parameters describing the air burst case were organized first. Then the major differences and similarities in the parameters, for the two types of detonations, were noted or assumed. From those, new parameter values for the surface burst case were established. The air-burst fireball model is identified for a detonation at sea level without an air-sea interface. For the surface-burst model presented here, the interface is added.

Condensation reactions occur during the cooling of the fireball; therefore the highest temperature observed in the final cooling curve of the fireball is used as a reference point in temperature and time. This reference point is the time of the second-maximum in the observed (exterior) fireball temperature, which occurs just after the blast wave breaks away from the fireball. At this point the energy of the shock wave has decreased to a level at which it is no longer able to cause ionization of the air molecules.

The descriptive models are developed according to the following format:

1. At the starting reference time, the fraction of the released energy is specified for:

- a. The fireball
- b. The blast wave
- c. The amount of energy lost by thermal radiation

2. The original state of the materials in the fireball is taken as their standard thermodynamic state at 208°K and 1 atmosphere.
3. Where materials are heated sufficiently to cause dissociation, the energies are calculated as if dissociation occurred at 208°K and as if the dissociated atoms had been heated as ideal gases.
4. The internal energy of the gas atoms in the fireball is utilized or released during cooling by:
 - a. The heating of inflowing air and/or soil material
 - b. The expanding of the gases against the external atmosphere (at 1 atm)
 - c. The radiating of energy into the atmosphere
5. The second reference point for establishing a thermal balance is taken at the time at which the solidification temperature of the carrier occurs.

A more refined treatment would consider these parameters for the whole temperature range over which the liquid carrier material can exist. Also, except for energy lost through radiation, ionization energies are not considered.

The distribution of the released energy for the air burst, according to IENW, p.9, is 10 percent for nuclear radiation, 80 percent for thermal radiation (IENW occasionally terms this thermal energy), and 10 percent for blast and shock. The time or time period after the detonation at which these values apply is not given, nor is energy allotted for the processes enumerated above. Certainly the distribution of the total energy among the various forms is time dependent, and eventually all of the released energy does become thermal or heat energy. But for the purposes of the descriptive model used here, the initial specification of the energy distribution is required for the time of the second temperature maximum. Therefore, of the energy distribution values given by IENW, only the 10 percent for nuclear radiation is assumed to be unavailable for use in other processes. The remaining 80 percent, then, is to be distributed among

1. The energy lost by radiation
2. The energy carried beyond the fireball perimeter by the blast wave
3. The energy content of the fireball.

In making the estimates of the energy distribution among these three quantities, data for the 20-KT air burst from KNW is used. The energy conversion factor, 1.11×10^{18} calories/KT (calories per kiloton), is adopted so that a 20-KT yield is equal to an energy release of 2.22×10^{19} calories. Of this, 1.80×10^{18} calories is available for division into three parts.

In the following treatment it is assumed that the air molecules in the blast wave as it leaves the fireball move outward at least as fast as the fireball expands; they are not enveloped by the fireball prior to the second temperature maximum. Since those molecules absorb some of the energy in the blast wave, envelopment of a good fraction of them would increase the energy content of the fireball relative to that carried away by the blast wave.

The energy lost from the fireball by radiation prior to the time of the second temperature maximum is estimated to be 8 percent of the total energy (see below). For a 20-KT air burst, the radiant energy lost up to this time is then 1.8×10^{18} calories. This leaves 1.71×10^{18} calories for both formation of the fireball and dispersal by the blast wave.

The energy carried away by the blast wave as it separates from the fireball should consist of

- a. The internal energy content of the air molecules expressed as a temperature rise,
- b. The compression energy (i.e., the dynamic pressure of the pulse), and
- c. The potential energy or work expressed in terms of the outward velocity of the wave. For a 20-KT yield weapon the measured fireball temperature decrease prior to the second maximum (see KNW, p. 80) is taken to be the decrease of the air temperature within the blast wave itself.

The temperature curve in this period of time, expressed as an increase in the air temperature from that of the ambient atmosphere can be represented by

$$\Delta T = 204t^{-0.423} \quad (8.80)$$

for t in seconds and ΔT in °K. For an apparent breakaway time (i.e., the time the blast wave is no longer incandescent) of 0.015 seconds, ΔT is 1800°K. For this temperature rise, the change in internal energy, ΔE , for air is 10,800 calories per molecule.

The peak over-pressure (from ENW, p. 100), for a 20-KT air burst can be represented in part, by

$$p = 1.20 \times 10^{10} r^{-2.31}, \quad r = 2.4 \times 10^4 \text{ to } 5.0 \times 10^4 \quad (8.01)$$

where r is the fireball radius in cm and p is the over-pressure in psi. The variation of the fireball radius with time up to the breakaway (from ENW, p. 85) can be represented by

$$r_{\text{ao}} = 1.98 \times 10^4 t^{0.372}, \quad t = 10^{-3} \text{ to } 0.015 \quad (8.02)$$

for r in cm and t in seconds. At 0.015 second, r is 1.04×10^4 cm, and extrapolating Eq. 8.01 to 1.04×10^4 cm, p is 820 psi (48 atmospheres). The corresponding value of the peak dynamic pressure is 1880 psi, which is equal to 2.19 cal/cm^2 ($1 \text{ psi} = 1.05 \times 10^{-6} \text{ cal/cm}^2$). For a temperature of 8100°K (1800°C), the number of moles of gas atoms per cm^3 at a pressure of 48 atmospheres, by use of the perfect gas law, is 2.4×10^{-4} . The energy absorbed by the gas due to the compression is then $0.1 \times 10^9 \text{ cal/mole}$.

The outward velocity of the blast-wave is obtained by differentiating Eq. 8.02 to give

$$v_p = 1.85 \times 10^{11} t^{-0.628} \quad (8.03)$$

Using the gross kinetic energy, $1/2 m v_p^2$, as a measure of the potential work of the wave in moving the air molecules outward, and converting this measure to number of moles of air and to caloric units, the energy content at 0.015 second is

$$Q_p = 2.28 \times 10^4 n_1 \quad (8.04)$$

Where n_1 is number of moles of air in the blast wave at the breakaway. The total energy in the blast wave is then approximately

$$Q_1 = 1.09 \times 10^4 n_0 + 0.91 \times 10^4 n_0 + 2.28 \times 10^4 n_1 \quad (8.05)$$

$$\approx 4.28 \times 10^4 n_0$$

The energy content of the fireball at the second maximum should be equal to the energy utilized in its formation. That is, it consists of

- a. The internal energy for a temperature close to 8100°K (see ENW, p. 80)

- b. The dissociation of a certain number of air molecules
- c. The work of expanding the gases to the fireball volume at the second maximum

The thermodynamic first law energy balance for this process, assuming ideal behavior of the gases, is

$$Q_d = (\Delta E_{T_f} + \frac{n'}{n} \Delta E_D) n_0 + P_0 V_0 + n_0 R T_0 \quad (0.06)$$

In which n_0 is the number of moles of undissociated air molecules, n' is the number of moles of dissociated atoms, ΔE_T is the change in internal energy, $E_{T_f} + E_{D_m}$ per mole of air molecules for the final mixture of gases, ΔE_D is the average dissociation energy per mole of dissociated atoms, V_0 is the fireball volume at the second maximum, $n_0 R T_0$ is a substitution for $P_0 V_0$ where V_0 is the original volume of the heated air molecules, T_0 is taken as 200°K, and P_0 is taken as 1 atmosphere.

From the curve given in ENW, p. 60, for the 20-KT burst, the fireball radius at the second temperature maximum at 0.10 seconds is 620 feet or 1.80×10^4 cm. The volume, V_0 , is then 2.80×10^{11} cm³ and hence $P_0 V_0$ is 0.80×10^{11} cal (1 cal = 41.80 cm-atmos).

The values of ΔE_T , ΔE_D , n_0 and n' depend upon the internal pressure because the degree of dissociation of the oxygen and nitrogen are pressure sensitive. For example, with pure nitrogen where the dissociation reaction is defined by



the fraction of the $N_2(g)$ molecules dissociated is

$$\frac{x}{n_0(N_2)} = \frac{K_p^{1/2}}{\sqrt{4P + K_p}}$$

where K_p is the dissociation constant in terms of the partial pressures, $n_0(N_2)$ is the total amount of nitrogen in terms of $N_2(g)$ and x is the amount of $N_2(g)$ dissociated.

The relationship between the fraction of the molecules dissociated in a mixture of gases and the total pressure is more complicated than that given by Eq. 3.07. The equilibrium distribution equations for N_2 and O_2 in a mixture of 0.8 n_0 of $\text{N}_2(\text{g})$ and 0.2 n_0 of $\text{O}_2(\text{g})$, are

$$K_N = \frac{4P^2y^2}{(n_0 + x + y)(0.8n_0 - x)} \quad (3.08)$$

and

$$K_O = \frac{4P^2y^2}{(n_0 + x + y)(0.2n_0 - y)} \quad (3.09)$$

in which K_N and K_O are the K_p for nitrogen and oxygen, respectively; x and y are the respective amounts dissociated, and P is the total pressure.

The solution for x and y can be simplified over much of the temperature range of interest from inspection of the thermal data on the two gases shown in Table 3.1. The values of $G_{\text{f}}^{\circ} - G_{\text{f},298}$ and K_p were derived mainly from the data of K.K. Kelley¹ and Shull and Linke.² Conversion from the heat content data was made using the relation

$$\Delta H_T = \Delta H_{298} + RT - (H_{298} - R(T-298)) \quad (3.70)$$

The dissociation constant values indicate that oxygen is almost completely dissociated at 4000°K and above for pressures up to 30 atmosphere. Also, at temperatures below 4000°K, nitrogen is dissociated to a negligible degree. For these two temperature ranges Eqs. 3.08 and 3.09 can be solved to give

$$\frac{x/n_0(\text{N}_2)}{1-x/n_0(\text{N}_2)} = \frac{1.8PK_N}{(4P+K_N)} \left[\sqrt{1 + 3.8T/K_N} - 0.20 \right], \quad T > 6000^\circ\text{K} \quad (3.71)$$

$$\frac{y/n_0(\text{O}_2)}{1-y/n_0(\text{O}_2)} = \frac{PK_O}{(4P+K_O)} \left[\sqrt{T + 2.2P/K_O} - 2.2 \right], \quad T > 4000^\circ\text{K} \quad (3.72)$$

Approximate solutions for the temperature range 4000 to 8000°K and for cases where other gases besides nitrogen and oxygen are present are

$$x = \frac{n_T K_N}{8P} \left[\sqrt{1 + \frac{12.8 P n_o}{n_T K_N}} - 1 \right] \quad (3.73)$$

and

$$y = \frac{n_T K_o}{8P} \left[\sqrt{1 + \frac{3.2 P n_o}{n_T K_o}} - 1 \right] \quad (3.74)$$

where n_T is the total number of moles of gas present. These equations can be solved by a series of approximations. The change in energy content (including dissociation energy and number of moles of gas in heating air as an ideal gas) from the above equations are given in Table 3.2; the E_T-E_{gas} values are to be identified with $\Delta E_T - \frac{1}{2} \Delta E_D$ of Eq. 3.00. The fractions of the nitrogen and oxygen molecules dissociated as a function of temperature and pressure are shown in Figures 3.1 and 3.2.

At the temperature of the second maximum of the 20-KT fireball, 8300°K, the curves show, as previously stated, that the oxygen molecules are 100 percent dissociated at pressures up to 20 atmospheres or greater. However, the nitrogen molecules are not; at 20 atmospheres, less than 50 percent are dissociated. And, since the dissociation energy is large, compared to the $C_v dT$ contributions, an estimate of the internal gas pressure (at the second maximum) is needed to obtain a reasonable value of the total change in energy.

Since the fireball volume and temperature at the second maximum are specified, the ratio of the number of moles of gas to the pressure, by assuming the perfect gas law is

$$n_T/P = 4.15 \times 10^7 \quad (3.75)$$

Figure 3.1
FRACTION OF NITROGEN MOLECULES DISSOCIATED AS A FUNCTION OF
TEMPERATURE AND TOTAL PRESSURE

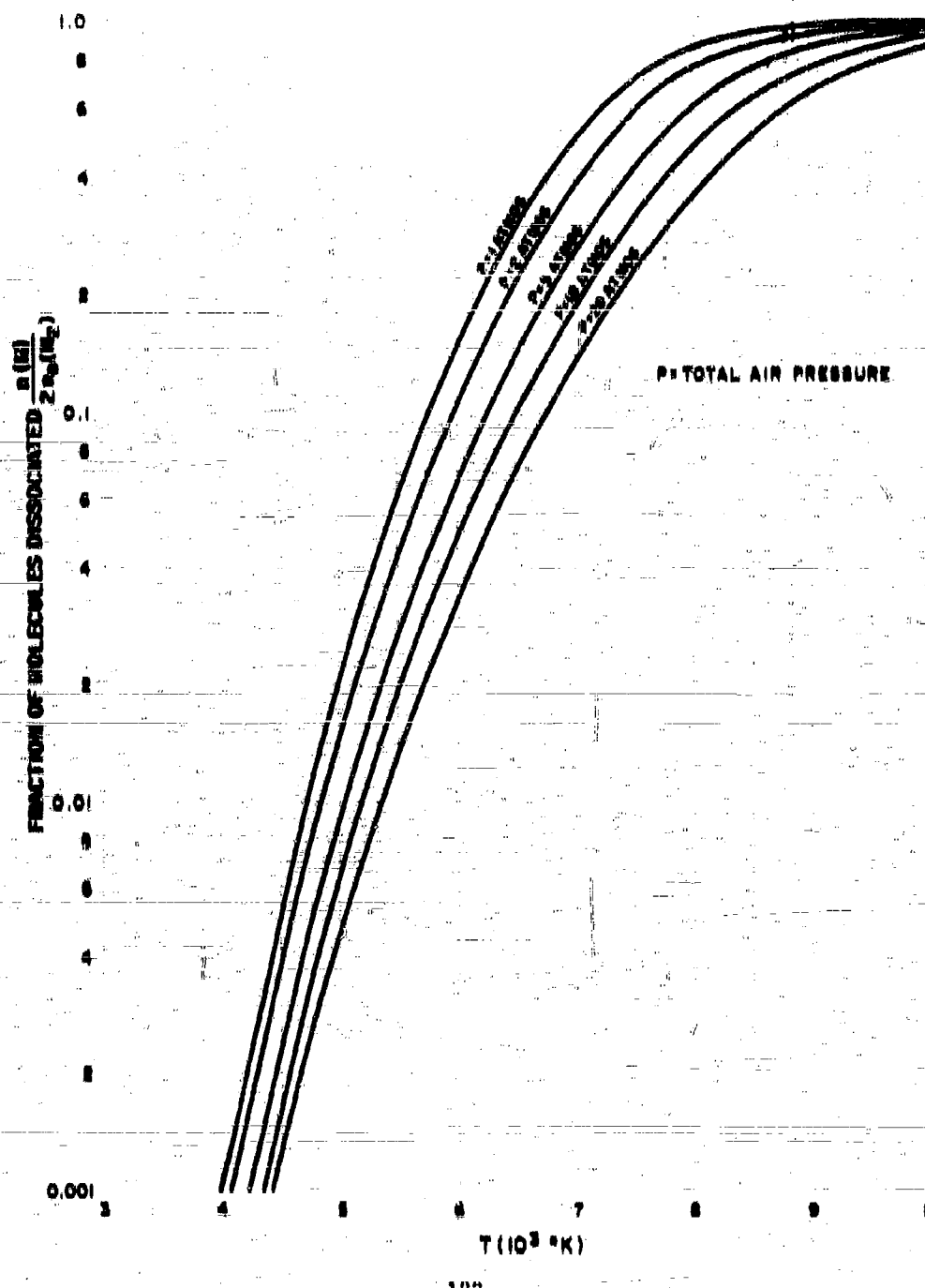


Figure 3.2
FRACTION OF OXYGEN MOLECULES DISSOCIATED AS A FUNCTION OF
TEMPERATURE AND PRESSURE

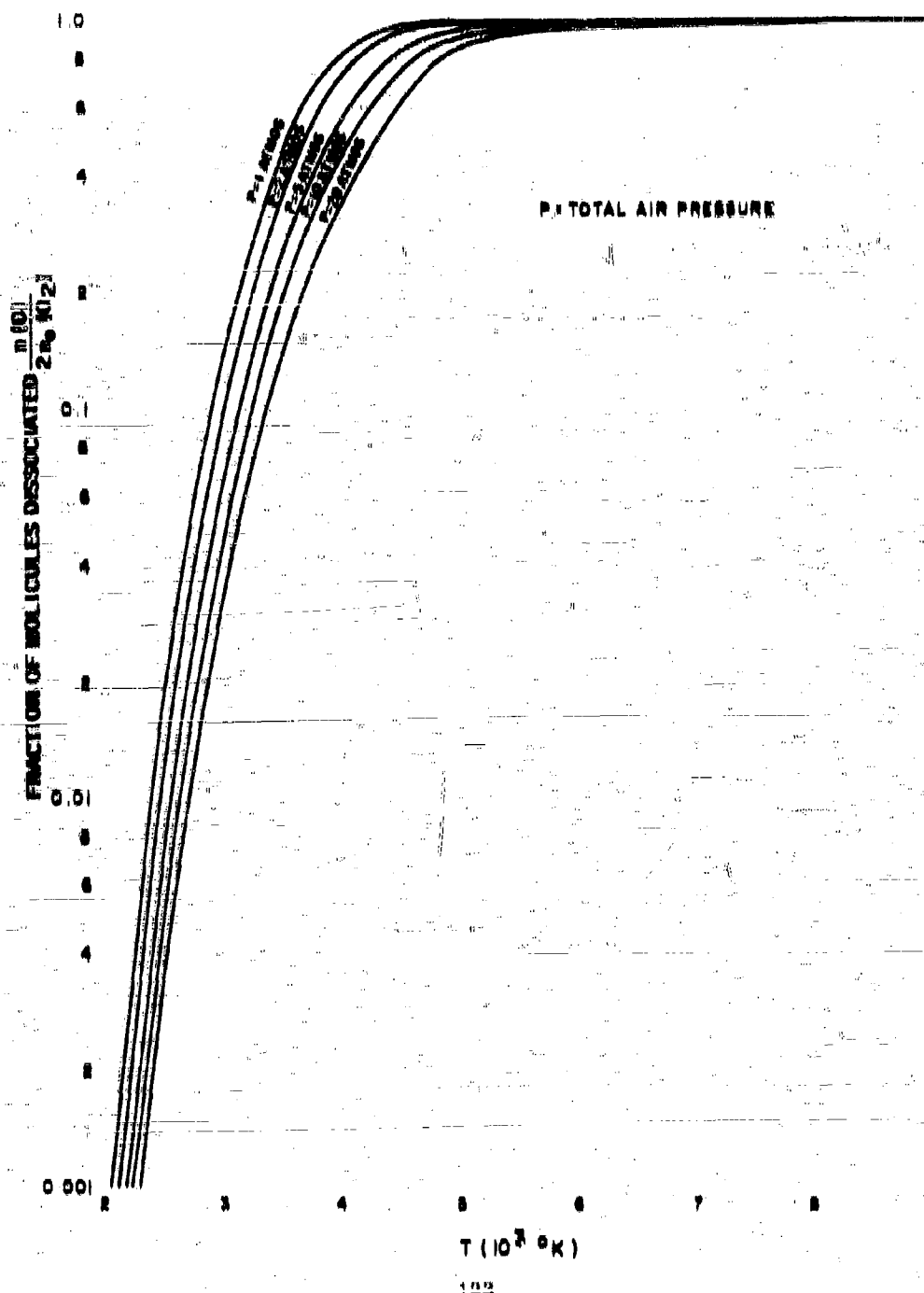


Table 3.1
THERMAL PROPERTIES OF NITROGEN AND OXYGEN AS IDEAL GASES

T°K	N _n (g)	N(g)	O _n (g)	O(g)	Dissociation Constant, K _d	
					Nitrogen	Oxygen
298	0	0	0	0	-	-
500	1,001	602	1,055	787	-	-
1,000	3,734	2,092	4,052	2,150	-	-
1,573	7,902	4,101	8,490	4,179	-	-
2,000	10,050	5,089	10,780	5,168	7.94×10^{-20}	4.40×10^{-7}
3,000	18,890	8,569	14,550	8,652	8.85×10^{-14}	3.07×10^{-4}
4,000	16,800	8,069	18,070	8,159	1.88×10^{-10}	1.28×10^{-6}
5,000	28,750	11,190	25,850	11,320	2.10×10^{-6}	2.17
6,000	30,810	14,000	32,810	14,380	1.09×10^{-3}	4.58×10^{-4}
7,000	37,850	18,440	42,060	17,880	5.58×10^{-2}	8.84×10^{-2}
8,000	44,950	22,910	50,880	21,040	0.970	1.71×10^{-1}
9,000	52,250	27,590	58,850	24,000	0.47	5.28×10^{-5}
10,000	59,650	32,340	67,850	28,000	4.78×10^{-4}	1.84×10^{-3}
	67,350	37,200	76,870	31,840	1.88×10^{-2}	9.51×10^{-4}

A. For reactions $N_2(g) \rightarrow 2N(g)$, $O_2(g) \rightarrow 2O(g)$. Values of ΔH_f° used were 112,540 cal/mole for the heat of formation of N(g) and 58,988 cal/mole for the heat of formation of O(g). The values of ΔE_f° at 298 of formation are 112,088 cal/mole of N(g) and 59,860 cal/mole of O(g).

The other facts seem apparent. First, the fireball is still expanding at the second/maximum; therefore, the internal pressure must be greater than 1 atmosphere. Second, the blast wave separated at a pressure of around 40 atmospheres at 0.018 second; therefore the internal pressure of the fireball must be less than this and would have decreased considerably, by both cooling and expanding, up to 0.18 second. For example, the gas volume at the break-away, from r_{bg} , is $4.7 \times 10^{12} \text{ cm}^3$; thus the fireball volume increased by a factor of 6 between 0.018 and 0.18 second so that, on volume expansion alone, the pressure would have decreased from 40 to 6 atmospheres.

The values of the ratio of the total number of gas molecules (associated plus dissociated air molecules) to the number of original (associated) gas molecules, n_t/n_0 , for heating air ($0.8N_2 + 0.2O_2$) from 20K to 8300°K, and the energy change per molecule of the original air molecules along with the compatible values of P and n_p from Eq. 3.76 are shown in Table 3.8.

The total energy required for heating and dissociating the air, $n_t(10^6\text{ ergs})$, for each value of P shows that all the available energy for both the blast wave and the fireball would be required if the internal pressure were as much as 3.0 atmospheres. In this case, the original volume of the air, according to the perfect-gas law, would be about $2.8 \times 10^{-10} \text{ cm}^3$, or about half the volume enclosed by the blast wave at the time of breakaway ($4.7 \times 10^{-10} \text{ cm}^3$). Hence it seems reasonable to assume that the original air molecules at a given location would not be subject to forces tending to move them away from the center of the explosion prior to the arrival of the blast wave, a reasonably good estimate of the original air molecules involved in both the formation of the fireball and in the blast wave shock is that they are those enclosed within the volume of the latter at breakaway. The perfect-gas law estimate, for air at 800°K and 1 atmosphere ($V = 4.7 \times 10^{-10} \text{ cm}^3$), gives the number of air molecules for n_1 , the number of air molecules in the blast wave, and n_2 , the number of air molecules in the fireball, to be

$$n_1 + n_2 = 1.92 \times 10^{10} \quad (3.78)$$

The calculated values of n_p are shown in the last column of Table 3.8. A plot of n_p and n_2 against the compatible values of P give an intercept at $n_p = 4.87 \times 10^{-10}$ mole of air and $P = 1.00$ atmosphere. At this pressure, $10^6\text{ ergs}/\text{mole}$ is 220,000 cal/mole of air molecules, so that the energy absorbed by the air for the 20-KT yield fireball is 1.01×10^{10} calories. Hence, Q_p is 1.08×10^{10} calories, or 40 percent of the total energy, and \bar{Q}_p is 0.86×10^{10} calories or 28 percent of the total energy.

The yield-dependent functions (scaling relationships) for the fireball temperature, radius, and other parameters can be derived from the information given in RENW, pp. 88, 89 and 890-HB. In the treatment here some adjustment is made to obtain consistency among the various functions.

The thermal power of the fireball, assuming black-body conditions, is given by

$$P = 1.73 \times 10^{11} T^4 R^2 \quad (3.77)$$

for P in calories per second, T in °K, and R , the fireball radius, in cm. The

Table 8.9

THE CHANGE IN ENERGY CONTENT AND NUMBER OF MOLES OF OXID
IN HEATING 1 MOLE OF AIR AS AN IDEAL GAS FROM 208°K AND 1
ATMOSPHERIC PRESSURE TO T°K AT PRESSURES OF 1 TO 20
ATMOSPHERES

1. $(E_T - E_{208})$ cal/mole of air*

T°K	Total Pressure, Atmospheres				
	1	2	5	10	20
500	1020	1020	1020	1020	1020
1000	3800	3800	3800	3800	3800
2000	10,810	10,810	10,800	10,800	10,800
3000	18,840	18,850	18,750	18,680	18,650
4000	19,800	19,870	18,340	17,970	17,710
5000	19,700	19,810	18,400	18,770	19,400
6000	57,400	53,110	54,310	52,740	50,000
7000	80,210	78,030	78,820	80,100	80,820
8000	137,500	136,300	138,700	131,100	131,700
9000	231,400	214,000	184,600	161,800	140,000
10,000	201,500	200,000	242,600	220,000	204,500
	275,000	274,000	269,700	268,800	261,800

2. n_h/n_o moles gms/mole air

	1,000	1,000	1,000	1,000	1,000
3000	1.003	1.002	1.001	1.001	1.001
4000	1.081	1.017	1.011	1.008	1.000
5000	1.160	1.130	1.100	1.083	1.000
6000	1.210	1.208	1.195	1.180	1.166
7000	1.212	1.200	1.201	1.200	1.220
8000	1.000	1.001	1.002	1.040	1.000
9000	1.084	1.007	1.070	1.070	1.480
10,000	1.074	1.001	1.000	1.021	1.720
	1.003	1.000	1.068	1.040	1.001

* $n_h = 0.8n(N_2) + 0.2n(O_2)$; E_{qp} includes energy of dissociation.

Table 3.3
**SUMMARY OF VALUES OF THE FIREBALL ENERGY AND GAS CONTENT RELATED TO TOTAL PRESSURE,
 VOLUME, AND TEMPERATURE FOR HEATING AIR FROM 298K TO 390K**

P (atmos)	n_1/n_0 (mole air) mole air	$E_T - E_{298}$ (cal/mole air)	n^* (moles gas)	$n_0(E_T - E_{298})$ (cal)	$n_0(E_T - E_{298})$ $\zeta_{1,2}^{**}$	$n_0(E_T - E_{298})$ $\zeta_{1,2}^{***}$
1	1.00	242,500	4.15x10 ⁷	2.16x10 ⁷	3.25x10 ⁷	0.315
2	1.564	229,800	8.36x10 ⁷	4.45x10 ⁷	1.02x10 ⁸	0.622
5	1.06	205,800	2.36x10 ⁸	1.18x10 ⁸	2.43x10 ⁸	1.45
10	1.03	182,800	4.15x10 ⁸	2.51x10 ⁸	4.57x10 ⁸	2.73
20	1.02	159,100	8.30x10 ⁸	5.33x10 ⁸	8.68x10 ⁸	5.17

- * for $n_1 = 4.15x10^7 \text{ P}$
- ** $Q_{1,2} = 1.64x10^{13} = \rho_1 \cdot Q_1 + Q_2 = 6.15x10^{11} \cdot n_0 (E_T - E_{298}) / Q_{1,2} = 1.0 \text{ at } 3.33 \text{ seconds, where } n_1 = 1.38x10^8.$
- *** $n_0 = 7.62x10^7$
- **** from $n_2 = 8.2x10^{12} / (E_T - E_{298} - 2.309)$

radiant energy emitted is convenient to use to adjust the derived scaling relationships since experimental measurements indicate that the total amount of energy radiated is, at least approximately, proportional to the released energy. The radiant energy lost up to the time of the second temperature maximum, t_{g_2} , is

$$q_1(n) = \int_0^{t_{g_2}} P dt \quad (8.78)$$

A similar expression can be written for $q_2(n)$, the energy radiated from t_{g_2} to some later time, t .

Integration to times when incandescence no longer occurs should be equivalent to the total measured amount of radiated energy. Integration of the P/P_0 curve given in ENW, p. 880, gives $q_2(n)$ equal to $0.67 P_0 t_{g_2}$ calories. The value of $q_2(n)$ is found to be given by

$$q_2(n) = P_0 t_{g_2} \left[0.345 + 1.28 \int_{1.4}^{10} (t/t_{g_2})^{-1.590} d(t/t_{g_2}) + 10q_2'' \right] \quad (8.79)$$

where P_0 is the thermal power at the second maximum, t_{g_2} is the time of the second maximum, and $10q_2''$ is the energy radiated after $t/t_{g_2} = 10$. The second term of Eq. 8.79 was derived from the curve of ENW and given a fairly precise representation of the P/P_0 curve between the t/t_{g_2} values of 1.4 and 10. By use of Eq. 8.77, it can be written

$$T^4 R^2 = 1.28 T_0^4 R_0^2 (1/t_{g_2})^{-1.590}, \quad 1.4 \leq t/t_{g_2} \leq 10 \quad (8.80)$$

If R is assumed to be constant in this interval of time and equal to the maximum fireball radius, R_m , then we have that

$$R_m = 1.13 R_0, \quad 1.4 \leq t/t_{g_2} \leq 10 \quad (8.81)$$

and

$$T = T_0 (t/t_{g_2})^{-0.398}, \quad 1.4 \leq t/t_{g_2} \leq 10 \quad (8.82)$$

However, the curve of temperature with time given in ENW (p. 69) is represented only approximately by Eq. 8.82 in this relative time period when plotted against t/t_0 using 0.18 seconds for t_0 .

On the other hand, for t/t_0 values greater than 10 the temperature curve is well represented by a function of the form $T_0 \exp(-kt/t_0)$, (T_0 and k being constants) which joins smoothly to the curve from earlier times. This suggests that, for times greater than t/t_0 of 10, an exponential temperature-time function should give a better representation of the temperature variation with time than Eq. 8.82. The function, fitted to join Eq. 8.82 smoothly at $t/t_0 = 10$ is

$$T = 0.595 T_0 e^{-0.0398t/t_0}, \quad t/t_0 > 10 \quad (8.83)$$

The value of $10q_s^*$ can be evaluated by use of either temperature equation by noting that, experimentally, q is not measurable at temperatures lower than about $0.1 T_0$ (i.e., between 800 and 1000K) when the assumption is made that the fireball radius remains constant for a very long period of time. When $0.1 T_0$ is substituted for T in Eq. 8.82, t/t_0 is 326 and with Eq. 8.83, it is 45. The times for the temperature to drop to $0.1 T_0$ for a t_0 of 0.18 seconds ($20-KT$) are 48 seconds and 7 seconds, respectively. Because of the obvious overestimate, from use of Eq. 8.82, of the time for the temperature to fall to $0.1 T_0$, a high value of $10q_s^*$ would result from its use even without considering an increase in the fireball radius after $10t_0$.

However, in proceeding further with these assumptions, it is found that the two respective values of $10q_s^*$ are $0.48 P_0 t_0$ for Eq. 8.82 and $0.312 P_0 t_0$ for Eq. 8.83, indicating that Eq. 8.82 would give about twice as much radiant energy emitted after $10t_0$ as would Eq. 8.83. The total energy radiated is then

$$Q_{T_0}(n) = 2.63 P_0 t_0 \quad (8.84)$$

by use of Eq. 8.82 for T from $t/t_0 = 10$ to 820 or

$$Q_T(n) = 2.36 P_0 t_0 \quad (8.85)$$

by use of Eq. 8.83 to T from $t/t_0 = 10$ to 45.

If the information of BNW (p.881) is used to solve for the coefficient of $P_{p,T}$ with q_T equal to $W/8$, a coefficient of 2.00 is obtained; this corresponds to the result of Eq. 8.84 with the excessively large value of $10q_p$. The coefficient of $P_{p,T}$ can be solved with respect to the total available energy by $q_T(a)$ equal to $1.11 \times 10^4 f_n W$ in calories, where f_n is the fraction of the total energy released. For P_p in terms of R_p and T_p , the above equations can be rearranged to give

$$f_n = 1.56 \times 10^{20} T_p^4 R_p^2 t_p a W^{-1} \quad (8.86)$$

where a is the coefficient of $P_{p,T}$ in Eqs. 8.84 and 8.85. If the previously used values, $R_p = 1.89 \times 10^4$ cm, $T_p = 8800^\circ K$, $t_p = 0.15$ seconds, and $W = 80\text{-KT}$, are substituted, f_n is then 0.198 so that for an a value of 2.00, f_n is 0.52 and, for the value of 2.36 it is 0.47. The value of a , 2.00, calculated from the BNW data by using an f_n value of 0.888 to begin with, gives back the value, 0.815, for a . It may be concluded from this value that the curves for R and T for the 80-KT yield and the information on q_T , P_p , and t_p as given in BNW are not consistent.

The dependence of T_p on yield can be evaluated by rearranging Eq. 8.86 to give

$$T_p^4 R_p^2 t_p = 6.41 \times 10^{20} f_n W/a \quad (8.87)$$

If the values of R_p ($= R_m/1.18$), t_p , T_p , and a obtained from BNW are substituted, the value of T_p is found to be $8800 W^{-0.079}$. This function gives a T_p value of $6800^\circ K$ for a 80-KT yield and of $4880^\circ K$ for a 1-MT yield. Thus, T_p , as derived from the BNW scaling functions, is 1000° lower than the "observed" curve in BNW for the 80-KT yield and decreases much too rapidly with yield.

To obtain more reasonable and more internally consistent information for use in the idealized air burst fireball model, the various parameter functions from BNW were adjusted to a set that was consistent with respect to their functional form and numerical values. The resulting set of functions was derived from the energy utilizations given by

$$q_T(a) = 0.50 W/KT \quad (8.88)$$

$$q_r(a) = 0.08 W/KT \quad (8.89)$$

$$q_u(a) = 0.42 W/KT \quad (8.90)$$

$$Q_p = 0.49 W/KT \quad (8.91)$$

The utilization of the fractions of the total energy (0.28 for blast, 0.15 for nuclear radiation, and 0.57 in the fireball up to the second maximum, including the 0.08 lost by radiation up to that time) leaves, from the above separations, 0.07 of the total energy for such processes as heating and mixing of air that enters the fireball after the second maximum and for expansion of the heated gas against the atmosphere.

The expansion of the fireball from t_0 to time of maximum expansion, t_m , is represented by the ratio

$$R_m/R_0 = 1.24 \quad (3.82)$$

This ratio is the value obtained from the data for the 20-KT yield in ENW and replaces the value derived from the P/P_0 function.

The radiant energy from Eq. 3.80 in terms of $P_0 t_0$, is given by

$$q_T(a) = 2.52 P_0 t_0 \quad (3.83)$$

in which

$$q_i(a) = 0.40 P_0 t_0 \quad (3.84)$$

$$1.0q_i^{(B)}(a) = 1.68 P_0 t_0 \quad (3.85)$$

$$10q_i^{(B)}(a) = 0.44 P_0 t_0 \quad (3.86)$$

The $P_0 t_0$ multiplier for $q_i(a)$ was reduced from 0.57 to 0.40 so as to retain about the same ratio between $q_i(a)/q_T(a)$ as that given in ENW. The value of $1.0q_i^{(B)}(t/t_0 = 1$ to 10) was increased by a factor of 1.2 due to the change to the R_m/R_0 ratio given in Eq. 3.82. The remainder of the 2.52 is the multiplier for $10q_i^{(B)}$. Since the temperature decrease after about $10t_0$ is probably better described by Eq. 3.85 than Eq. 3.82, the larger multiplier for $10q_i^{(B)}(a)$ can only be obtained by accounting for an increase in the fireball radius with t/t_0 after $10t_0$. A suitable function for such a variation of the fireball radius with t/t_0 , when selected for convenience of integration as well as for expressing an appropriate acceleration of volume expansion, is

$$R = 0.71 R_m e^{0.038t/t_0}, \quad 10 \leq t/t_0 \leq 45 \quad (3.87)$$

when the constants are evaluated. A function of this form must be restricted as an estimate of the fireball radius for t/t_0 values less than 45. In this time period, T will decrease to the order of $0.1T_0$ and the increase in R is about a factor of 3.6.

The increase in the mean cloud radius to essentially full expansion at 0 to 8 minutes is between 8000 to 10,000 times R_{in} . In the model fireburst, the fireball radius increases from R_p at t_0 to R_m at $1.4t_0$, remaining constant from $1.4t_0$ to $10t_0$ and then begins to increase again to form the large cloud about the time the firendence disappears.

The relation among T_p , R_p , t_p and W , using 0.50 W for $Q_p(0)$, is

$$T_p^4 R_p^3 t_p = 1.27 \times 10^{38} W \quad (B.98)$$

In which

$$T_p = 10^4 W^{0.020} \text{ K} \quad (B.99)$$

$$t_p = 0.080 W^{0.413} \text{ sec} \quad (B.100)$$

and

$$R_p = 5.04 \times 10^8 W^{0.333} \text{ cm} \quad (B.101)$$

In obtaining the above functions, the first assumption is that the 80 percent of the energy lost by radiation is independent of yield. The corollary assumption is that the fireball volume is proportional to the yield, or that simple geometric scaling applies. The remaining residual difference in the exponent on W , namely -0.107, was distributed in equal parts to t_p and T_p^4 (using the ENW dependence of t_p as being proportional to $W^{0.4}$ to start with) and that, for Q_p and $q_p(n)$ to be directly proportional to the yield, T_p should be almost independent of yield.

The coefficient for T_p was taken from a logarithmic extrapolation of the temperature curve in ENW for the 20-kT yield along a line with the slope -0.4, and using the temperatures from the curve between the t/t_0 values of 2 and 8. The coefficient for t_p was obtained by adjusting the values of t_0 from the ENW curve to give the same percentage difference at yields of 20-kT and 1-MT. In doing this, t_0 for 20-kT is increased from 0.10 to 0.17 second and for 1-MT it is decreased from 1.0 to 0.80 second. The coefficient of R_p was finally derived from Eq. B.98.

The corresponding values of the fireball parameters of interest are

$$T = 10^4 W^{-0.020} (t/t_0)^{-0.398} \text{ K}, \quad t_p = t \pm 10t_0 \quad (B.102)$$

$$R_p = 5.04 \times 10^8 W^{0.144} t^{-0.398} \text{ cm}, \quad t_0 = t \pm 10t_0 \quad (B.103)$$

$$T = 5.95 \times 10^4 W^{-0.020} \exp(-0.0398t/t_m) ^\circ K, t \geq 10t_m \quad (3.104)$$

$$= 5.95 \times 10^4 W^{-0.020} \exp(-0.79 W^{-0.413t}) ^\circ K, t \geq 10t_m \quad (3.105)$$

$$t_m = 0.070 W^{0.413} \text{ sec} \quad (3.106)$$

$$R_m = 6.25 \times 10^4 W^{0.333} \text{ cm}, t_m \leq t \leq 10t_m \quad (3.107)$$

and

$$R = 4.41 \times 10^4 W^{0.333} \exp(0.70 W^{-0.413t}) \text{ cm}, 10t_m \leq t \leq 45t_m \quad (3.108)$$

The adjustments, in general, result in a displacement or shifting of the parameter values between 10 and 25 percent from those given in ENW, except for the fireball radius. For example, the adjusted values of the radius R_c are 10 percent less at 1-MT and 44 percent less at 1-MT than those given by the ENW functions. This decrease in the radius from that of ENW is in agreement with the observations of other authors. Lappie⁴, for example, writes that the true fireball radius may actually be as small as half of that given in ENW.

3.3 Estimates of Fireball Parameters for a Model Surface Detonation in Soil Consisting of Silicate Minerals

The fireball parameter scaling functions for the model surface detonation are derived on the basis of assumed differences or similarities with the fireball from the model air burst. In this model, the soil-air interface is introduced.

The main assumptions used in the derivation of the parameter scaling functions are:

1. In the model surface burst, half the energy in the fireball at the second maximum is used to heat, dissociate, and expand the gas molecules from the air and half the energy is used to vaporize, dissociate, and expand the gaseous products from the soil;
2. The vapor density of the fireball at the time of the second temperature maximum is the same for both air and surface types of bursts;
3. The blast and shock wave carry away 28 percent of the released energy (as for the air burst), and 15 percent of the fission yield goes into nuclear radiation;

4. The fireball volume at the second maximum for the surface burst is the same as that of the air burst except that it has a hemispherical rather than spherical shape.

Taking the last assumption first,

$$R_2(s)/R_2(a) = 2^{1/3} \approx 1.26 \quad (3.109)$$

where $R_2(s)$ is the fireball radius for the surface burst and $R_2(a)$ is that for the air burst. The ratio of the energies radiated into the air space around the two fireballs at the time of the second maximum is

$$q_1(s)/q_1(a) = 0.794 [T_2(s)/T_2(a)]^4 \quad (3.110)$$

where $q_1(s)$ is the radiated energy and $T_2(s)$ is the temperature at the second maximum for the surface burst, and $q_1(a)$ and $T_2(a)$ are for the air burst. But since much of the energy is lost before the second maximum occurs and at much higher temperatures, before the blast wave breaks away, the amount lost by radiation up to this time should be insensitive to the ratio of the two values of T_2 . Therefore, the fraction of energy radiated into the air space is taken to be 0.86 percent, or 6 percent.

The total surface area of the surface burst fireball under the equal volume assumption is 1.19 times that of the air burst, so that the amount radiated through all surfaces would be nearly 10 percent of the total energy with 4 percent of this amount being radiated into the ground surface. However, since the whole bottom of the fireball is in direct thermal contact with the ground, some additional energy would be absorbed by the latter. An additional 5 percent is therefore assumed to be lost, or not contained within the gaseous phase of the fireball at the second maximum. With these assumptions, the model surface burst fireball contains 49 percent of the released energy at the time of the second temperature maximum.

The assumption of equal vapor densities and fireball volumes leads to the equality of the number of gas molecules heated to the respective values of T_2 per unit of yield, since the fireball volume scaling function is proportional to the yield. The combination of all the assumptions permits the estimation of $T_2(s)$ for the surface burst.

The first law of thermodynamics for the utilization of 49 percent of the released energy in heating air as an ideal gas, in the model air burst, is

$$Q_2 = n_a(E_T - E_{298}) + p_a(V_2 - V_1) \quad (3.111)$$

In which n_a is the number of moles of air heated to T_0 (°), $E_T - E_{298}$ is the change in energy, including dissociation, of the air molecules in cal/mole of air, p_a is the external pressure (1 atmose.), V_0 is the volume of the fireball at second maximum, V_0 is the original volume of the air molecules, and Q_0 is 6.44×10^{11} W-sec (or W in KT). For a spherical fireball, V_0 from Eq. 8.111 is

$$V_0 = 5.36 \times 10^{11} \text{ W cm}^3 \quad (8.112)$$

With the ideal-gas law, $p_a V_0$ is replaced by $n_a R T_0$, or 0.02 n_a cal/s. Also, $p_a V_0$ is equal to 1.3×10^{11} W-sec. Replacing the appropriate equalities in Eq. 8.111 results in

$$\frac{n_a / W}{(E_T - E_{298} - 592)} = \text{moles air/KT} \quad (8.113)$$

Assuming the perfect gas law to estimate the number of moles of gas in the fireball results in

$$n_T / W = 6.53 \times 10^5 W^{0.02} p_a \text{ moles/KT} \quad (8.114)$$

when Eqs. 8.00 and 8.112 are substituted for T_0 and V_0 , respectively; p_a is the total internal pressure at t_0 . Combination of Eqs. 8.113 and 8.114 gives

$$n_T / n_a = 1.23 \times 10^7 \cdot W^{0.02} p_a (E_T - E_{298} - 592) \quad (8.115)$$

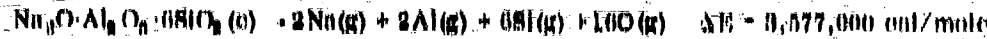
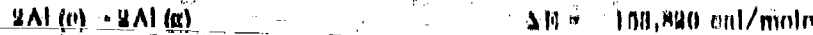
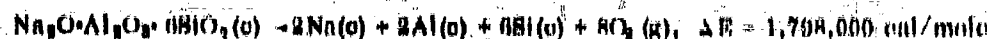
In which the compatible values of n_T/n_a , p_a , and $(E_T - E_{298} - 592)$ are obtained from the thermal data on air at a given temperature and can be determined by calculating p_a of Eq. 8.115 and then plotting the calculated values as a function of p ; the equation is satisfied at the point where $p = p_a$. A single value of p results for each selected value of W . The solutions of Eq. 8.115 for different values of W are shown in Table 8.4 along with the corresponding values of n_T/W .

In order to make a similar computation for the model surface burst, the thermal properties of an "ideal" soil must be specified. For this, the thermal properties of the mineral albite or anorthoclase ($\text{Na}_2\text{O} \cdot \text{Al}_2\text{O}_5 \cdot 6\text{SiO}_4$), with a selected melting point of 1400°C, are assumed. One mole of the soil, upon complete dissociation, produces 26 moles of gas atoms; the molecular weight of the compound is 524 and its heat of formation at 200°K is 1,800 kcal/mole.

Table 3.4
SUMMARY OF VALUES OF n_{p}/W AND p_0 FOR THE MODEL AIR BURST

$W(\text{RT})$	$T_0 (\text{°K})$	$p_0 (\text{atmos})$	$n_{\text{p}}/W (\text{mole}/\text{RT})$
1	10,000	0.00	3.80×10^6
10	9,000	5.85	4.00×10^6
10^2	9,120	5.79	4.14×10^6
10^3	8,710	5.70	4.32×10^6
10^4	8,320	5.80	4.00×10^6
10^5	7,940	6.11	5.02×10^6

The data of K.K. Kelly¹ and Stull and Binko² were used to calculate the energy changes of the following reactions at 2000°K.



107,700 cal/mole
of gas atoms

Where appropriate, the heat content data were corrected to ΔE by subtraction of the quantity ΔnRT , Δn being the change in the number of moles for the gaseous species. The values of $E_T-E_{T,0}$ for the ideal soil, and some of its decomposition products at higher temperatures, are given in Table 3.5. The values for the soil composition assume complete dissociation of all the oxide products and of the oxygen molecule.

The first law of thermodynamics for the conversion of 48 percent of the released energy, for the model surface burst at the second temperature maximum, is

$$4.66 \times 10^{11} W = n_a (\Delta E_a - 592) + n_s \Delta E_s + 1.30 \times 10^{10} W \quad (B.116)$$

In which ΔE_a and ΔE_s are the $\Delta E_p - E_{200}$ values, including dissociation, for the air and soil, respectively; n_a is the number of gas atoms from the soil, and $1.30 \times 10^{10} W$ is the $p_0 V_k$ term as before. According to the definition of the ideal surface burst, the equal portions of the energy for heating soil and air that remain after subtraction of $p_0 V_k$ are

$$2.266 \times 10^{11} W = n_a (\Delta E_a - 592) \quad (B.117)$$

and

$$2.266 \times 10^{11} W = n_s \Delta E_s \quad (B.118)$$

Since the oxygen molecules are essentially all dissociated at the temperatures of interest, n_a and ΔE_s can be determined for given temperatures, as they were in the case of the air burst, by estimating n_a (g), the number of moles of gas from the air, on assumption of the perfect gas law. In this case

$$n_a = \frac{p_a V_k}{R T_k(n)} = 6.53 \times 10^6 W p_a / T_k(n) \quad (B.119)$$

where p_a is the sum of the partial pressures of N_2 (g), N (g), O_2 (g), and O (g) from the original air, and T_k (n) is the temperature at the second maximum.

Combining Eqs. B.117 and B.119 gives

$$n_a / n_o = 2.88 \times 10^{-8} p_a (E_a - 592) / T_k(n) \quad (B.120)$$

The values of n/W , given by

$$n/W = n_a/W + n_s/W \quad (B.121)$$

were determined at several assumed values of T_k (n). The values of T_k (n) for different values of W were then determined, from a smoothed plot of n/W vs. T_k (n), by reading off T_k (n) at the corresponding n/W values for the air burst, for each yield. The results of these calculations are summarized in Table B.6.

Table 3.8

**TERMAL DATA FOR TOTAL BOLT CONSTITUENTS OF
COMPOSITION $\text{Na}_2\text{O}(\text{Al}_2\text{O}_5\text{SiO}_4)_2$ mol/mole**

$\frac{\partial H}{\partial T} \Big|_{20R}$, cal/mole

T(K)	N _O (g)	N _{Al} (g)	N _{Si} (g)	Bolt Composite ^a	Bolt Composite ^b	Bolt (g)	Bolt (g)
208	0	0	0	0	0	0	0
1,000	-	-	-	-	-	22,780	23,180
1,100	-	-	-	-	-	22,440	24,440
1,200	2,080	2,720	2,770	-	-	207,440	210,440
1,300	3,280	3,820	3,880	-	-	129,080	130,700
1,400	3,480	3,920	3,980	-	-	108,120	113,800
1,500	3,680	4,010	4,065	-	-	100,720	106,180
1,600	3,880	4,110	4,110	-	-	100,440	107,440
1,700	4,170	4,210	4,210	-	-	105,840	105,100
1,800	5,080	5,110	5,280	-	-	201,080	210,000
2,000	5,000	5,100	5,050	-	-	-	-
3,000	11,410	11,080	11,100	-	-	-	-
5,000	15,080	14,180	13,700	14,770	152,800	-	-
6,000	22,420	17,150	10,220	18,880	180,100	-	-
7,000	30,080	21,980	20,780	22,420	180,100	-	-
8,000	40,000	26,180	26,080	27,040	104,700	-	-
9,000	42,810 ^c	28,010 ^c	28,010 ^c	32,020 ^c	179,100 ^c	-	-
10,000	100,700 ^c	41,700 ^c	36,100 ^c	38,080 ^c	170,400 ^c	-	-

a. Estimated from extrapolation of heat capacity data

b. Cal/mole gas atoms basis, gpm at 20R^K

c. Cal/mole gas atoms basis, $\text{Na}_2\text{O}(\text{Al}_2\text{O}_5\text{SiO}_4)$ at 20R^K

Table 8.6

SUMMARY OF CALCULATIONS FOR $T_g(s)$ BASED ON THE ASSUMPTION OF EQUAL VAPOR DENSITIES AT THE SECOND TEMPERATURE MAXIMUM FOR THE MODEL AIR AND SURFACE-BURST FIREBALLS

$T_g(s)$ (°K)	P_s (atmos.)	n_s/W (10^6 moles/KT)	n_s/W (10^6 moles/KT)	n/W (10^6 moles/KT)	W (KT)
6000	0.54	0.60	1.452	0.31	--
6300	0.55	0.49	1.441	4.00	--
6600	0.54	0.11	1.400	4.54	--
6900	2.96	0.74	1.419	4.10	--
7200	2.07	0.42	1.407	0.80	--
7140	2.72	0.45	1.41	0.80	1
7080	2.81	0.58	1.42	4.00	10^4
6910	2.80	0.72	1.42	4.14	10^4
6770	3.00	0.50	1.43	4.00	10^4
6550	0.17	0.17	1.40	4.00	10^4
6220	0.40	0.58	1.44	0.02	10^4

The derived $T_g(s)$ values are represented quite well from 10^4 to 10^6 KT by the scaling function

$$T_g(s) = 7200 W^{-0.010} \cdot K \quad (8.122)$$

for W in KT. It should be noted that this equation is used in estimating $T_g(s)$ in all following computations rather than the values given in Table 8.6; this is done to maintain consistency among the various parameters derived from use of the $T_g(s)$ value. The model surface-burst fireball conditions, using the smoothed values of $T_g(s)$, are summarized in Table 8.7. The parameter values are tabulated with more significant numbers than are warranted by the assumptions merely to aid in interpolation to other values of W . Interpolations to other yields can be made by plotting the parameters against $T_g(s)$, which is related to W by Eq. 8.122 as is shown in Figure 8.8. The values of ΔE_0 and ΔE_{-500} can be then calculated by use of Eqs. 8.118 and 8.117. It should be mentioned that the recalculated values of n/W do not quite conform to the assumption of equal vapor densities in the model air and surface bursts at all yields.

Figure 3.3
CALCULATED VARIATION OF n_w , P_w , n_e , n_i , AND $n_w w$ WITH ASSUMED VALUES
OF $T_2(z)$ FOR THE MODEL SURFACE-BURST FIREBALL.

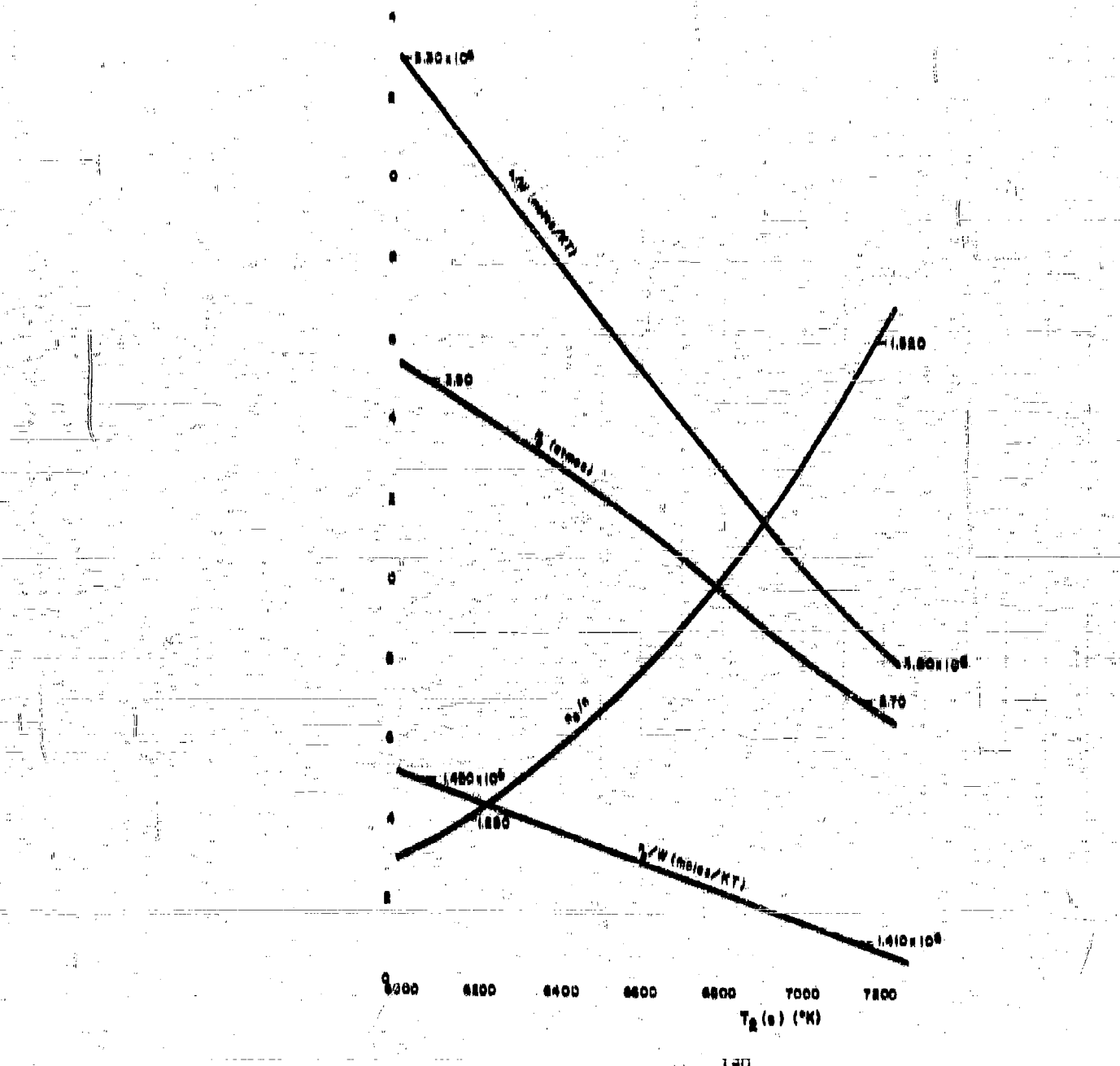


Table 8.7

**SUMMARY OF FIREBALL CONDITIONS AT THE SECOND TEMPERATURE MAXIMUM
FOR THE MODEL SURFACE BURST OF DIFFERENT YIELDS
USING EQ. 8.188 FOR t_0 (8)**

Quantity	W(KT)					
	1	10	10^2	10^3	10^4	10^5
T_0 (°K)	7,800	7,040	6,880	6,720	6,570	6,420
p_a , atmos	2.087	2.780	3.008	3.087	3.158	3.204
p_{air} , atmos	4.818	4.804	4.800	4.470	4.080	4.006
n_e/n_i	1.028	1.470	1.422	1.381	1.347	1.320
n_e/W , 10^6 moles/KT	1.407	1.414	1.420	1.428	1.431	1.438
n_e/W , 10^6 moles/KT	2.420	2.870	2.762	2.651	2.140	3.010
n/w , 10^6 moles/KT	0.827	0.990	4.182	4.876	4.571	4.755
ΔN_e , cal/mole gas atoms	101,080	100,280	100,010	100,000	100,000	100,000
$(\Delta E_{K0} - 500)$ cal/mole air	143,100	120,820	110,060	100,000	97,800	90,110

The assumptions that given fractions of the released energy are contained in the fireball, carried away by the blast wave, and lost by thermal radiation, and the corollary assumption that the time dependence of the various parameters can be given in terms of the time relative to t_0 , as was done for the model air burst, lead to the mathematical requirement that, for the model surface burst, t_0 must vary as $W^{0.478}$. By adjusting the t_0 values for the model air burst to give the same percentage deviation at 20-KT and 1-MT, the model surface burst scaling function for t_0 that results is

$$t_0 = 0.61 W^{0.478} \text{ sec.} \quad (8.188)$$

This gives 0.10 seconds for 20-KT and 0.80 seconds for the 1-MT yield. The lower values of T_0 (m) and t_0 (higher yields) for the surface burst would indicate that the surface burst fireball either cools more rapidly than the air burst fireball at the very early times or that it never was as hot, or both.

At t_0 the model surface-burst fireball is in the shape of a hemisphere centered at the point of detonation; in the model it remains in this position and shape until it reaches full expansion at t_m . After t_m , it begins to rise and in doing so takes on the shape of a sphere as it separates from the earth's surface at t_s . During this time, the volume remains constant; as in the case of the air burst, the fireball volume is assumed to remain essentially constant from

$t \leq 1.4t_g$ to $t = 10t_g$. Since the same fireball volumes are assumed for both types of bursts, the same type of equation for the increase in radius after $10t_g$ is used. The fallout predictions enter the fireball some time after t_g and, presumably to a larger degree, even after $10t_g$.

From the assumption of equal fireball volumes, the fireball radius for the model surface burst is

$$R_g = 6.35 \times 10^8 W^{0.333} \text{ cm} \quad (3.124)$$

$$R_m = 7.88 \times 10^8 W^{0.343} \text{ cm} \quad (3.125)$$

and

$$R_s = 6.25 \times 10^8 W^{0.333} \text{ cm} \quad (3.126)$$

In order to estimate the energy radiated to the atmosphere between t_m and t_s , the value of R_e , the effective radius for the surface of the fireball exposed to the atmosphere, is assumed to vary as $(t/t_g)^m$, where m is a constant that is independent of yield, so that the form of the integral of Pdt during this period is the same as for the period between t_s and $10t_g$. (The value of m can be evaluated from the height of the cloud for a 1-MT yield as given in ENW, p. 23.)

The curve can be represented, with a fair degree of precision, by

$$h_t = 4.24 \times 10^4 t^{0.704} \text{ cm}, \quad t = t_m \text{ to } 60 \text{ sec} \quad (3.127)$$

and

$$h_t = 6.46 \times 10^4 t^{0.600} \text{ cm} \quad t = 60 \text{ to } 390 \text{ sec} \quad (3.128)$$

For the model surface-burst fireball, h_t is equal to $2R_s$ at t_s .

For the 1-MT yield, $2R_s$ is 1.28×10^9 cm; t_s is then 4.00 seconds. Since t_g for this yield is 0.80 second, t_s/t_g is 5.00. Using the values of 0.70 R_m^0 and R_s^0 at t_m and t_s , respectively, the variation of R_e , the effective "spherical" radius, with t/t_g during t_m to t_s is

$$R_e = 5.42 \times 10^8 W^{0.333} (t/t_g)^{0.081} \text{ cm}, \quad t/t_g = 1.4 \text{ to } 5.8 \quad (3.129)$$

The estimates of t_m and t_s are given by

$$t_m = 0.088W^{0.373} \text{ sec} \quad (0.180)$$

$$t_s = 0.354W^{0.373} \text{ sec} \quad (0.181)$$

The fireball radius from $t/t_0 = 0.8$ to $t/t_0 = 10$ is assumed to be the same as R_m for the model air burst which is $0.25 \times 10^6 W^{0.383}$ cm as given by Eq. 0.120 for R_m .

The variation of the temperature with t/t_0 for the model surface burst is assumed to follow the same pattern of decrease with time as in the air burst. That is, it varies as $(t/t_0)^{-n}$ up to $t/t_0 = 10$ and thereafter varies as $\exp(-k(t/t_0))$ where n and k are yield-independent parameters. Since $T_0(n)$ is much lower than $T_0(0)$, it would appear that the temperature should be decreasing at a somewhat slower rate, at this time, for the surface burst. That is, the constant n should be less than 0.4.

A likely value of n can be determined from evaluation of the integrals for the radiant energy lost to the surrounding atmosphere, as was done for the air burst. Although the total amount of energy radiated to the atmosphere should be less than for the air burst (50 percent), the lower limit would certainly be about 20 percent, with an upper limit of around 40 percent. Allowing the estimate of 0 percent for the amount of energy lost up to T_0 and $0.30 \times 0.82 t_0$ (or 4 percent) from t_0 to t_m , as in the case of the air burst (but corrected for geometry and temperature), and assuming the same variation of T with t/t_0 after $10t_0$ as for the air burst case (as a first approximation), the integrals give 25 percent of the energy radiated to the atmosphere for $n = 0.80$ and about 40 percent lost for $n = 0.80$. On this basis, n was taken as 1/8. The estimate of the fireball temperature for the surface burst then is

$$T = 7.2 \times 10^6 W^{-0.010} (t/t_0)^{-1/8} \text{ K}, \quad t/t_0 = 1 \text{ to } 10 \quad (0.182)$$

$$T = 2.83 \times 10^6 W^{0.114} t^{-1/8} \text{ K}, \quad t = t_0 \text{ to } 10t_0 \quad (0.183)$$

$$T = 4.66 \times 10^6 W^{-0.010} \exp(-0.03346/t_0) \text{ K}, \quad t/t_0 = 10 \text{ to } 50 \quad (0.184)$$

$$T = 4.66 \times 10^6 W^{-0.010} \exp(-0.0516 W^{-0.373} t) \text{ K}, \quad t = 10t_0 \text{ to } 50t_0 \quad (0.185)$$

Because the main concern is with the surface burst, it is desirable to have a better estimate of the fireball radius and volume after $t/t_0 = 10$ than was obtained for the air-burst fireball. To do this, the work done in the expansion of the fireball against the atmosphere and in the heating of inflowing air, as well as thermal radiation losses, are taken into account in estimating the rate of expansion of the fireball after its initial rapid expansion to V_m or V_s . To a first

approximation, in these estimates, the presence of the soil need not be taken into account if the end point of the calculation for the energy balance for the expansion is taken at a sufficiently low temperature. In its solid form, the soil would not contribute to the volume, and, because of the high relative abundance of air molecules, the proportion of the fireball energy that is absorbed by the soil should be small.

First, the energy radiated to the air between $t/t_0 = 1$ and $t/t_0 = 10$ must be subtracted from the 4.08×10^{11} W units in the fireball at t_0 . The energy radiated to the air up to $t/t_0 = 10$ is summarized by

$$q^{1-10} = 6.66 \times 10^{10} \text{ W cal/s (6.0\%)} \quad (8.136)$$

$$1q^{1-10} = 4.44 \times 10^{10} \text{ W cal/s (4.0\%)} \quad (8.137)$$

$$1.4q^{1-10} = 0.92 \times 10^{10} \text{ W cal/s (8.9\%)} \quad (8.138)$$

$$5.8q^{1-10} = 4.06 \times 10^{10} \text{ W cal/s (2.8\%)} \quad (8.139)$$

The energy remaining, after subtracting the last three above quantities, is 2.70×10^{11} W units; it is available for the processes mentioned above. The mathematical form of the increase of the fireball radius after $t/t_0 > 10$ is assumed, as in the case of the air burst, to be

$$R = R_0 \exp -a(t/t_0 - 10) \quad (8.140)$$

In which the constant is yield-independent.

According to the variation of the temperature with t/t_0 (from Eqn. 8.132 to 8.135) a temperature between 800 and 900°K is reached at $t/t_0 = 50$, for all yields from 1- to 10^3 -KT. Since this is about the time the fireball is such that it should disappear, it was selected as the end point for evaluating the constant of Eq. 8.141 by means of an energy balance.

The work of expansion against the atmosphere is

$$q(\Delta V) = P(V_{50t_0} - V_{t_0}) = 2.48 \times 10^{10} \text{ W exp}(120a) + 1.36 \times 10^{10} \text{ W cal/s} \quad (8.141)$$

The number of moles of gas molecules present at the end point can be estimated by use of the perfect-gas law plus the assumption that the internal pressure of the gases, at $t = 50t_0$, is the same as the external pressure (1 atmosphere). The number of moles of air molecules present, at t_0 , ranges from 1.0×10^{10} W (for 1-KT) to 2.5×10^{10} W (for 10^3 -KT). The value 2.12×10^{10} W for 10^3 -KT is used as an average value to estimate the number of moles of air that have entered the fireball between t_0 and $50t_0$.

The estimate of the energy used in heating additional air to 800°K, with these provisions, is

$$\Delta E = \Delta n(E_{800} - E_{298}) = 4.74 \times 10^{10} W \exp(120a) - 6.44 \times 10^9 W \text{ cal/s} \quad (8.142)$$

In which Δn is the increase in number of moles of air between t_0 and $80t_0$, and $E_{800} - E_{298}$ is 8040 cal/mole.

The radiant energy lost is approximately

$$10q_r'' \approx 1.73 \times 10^{-11} t_0 \int_{10}^{50} T^4 R^3 d(t/t_0) = \frac{8.12 \times 10^9 W}{(0.133-2a)} \text{ cal/s} \quad (8.143)$$

Summing these energies and equating to $2.79 \times 10^{11} W \text{ cal/s}$ given

$$4.13 = \exp(120a) + \frac{0.071}{(0.133-2a)} \quad (8.144)$$

The equation is satisfied for $a = 0.0104$; this value of the constant is about a third of that obtained for the air burst where thermal radiation only was considered.

The estimated radius is now given by

$$R = 5.69 \times 10^9 W^{0.580} \exp(0.0104 t/t_0) \text{ cm}, t/t_0 = 10 \text{ to } 50 \quad (8.145)$$

or

$$= 5.69 \times 10^9 W^{0.580} \exp(0.170 W^{-0.070} t) \text{ cm}, t = 10t_0 \text{ to } 50t_0 \quad (8.146)$$

The radiant energy lost is

$$10q_r'' = 4.65 \times 10^{10} W \text{ cal/s} \quad (4.2\%) \quad (8.147)$$

Therefore the radiant energy lost to the atmosphere (surrounding air) is 35.9 percent of the total released.

The thermal power functions for the model surface burst from $1.4t_0$ to about $50t_0$ are

$$P = 8.13 \times 10^{10} W^{1.062-1.171} \text{ cal/s/sec}, t = 1.4t_0 \text{ to } 5.8t_0 \quad (8.148)$$

$$P = 4.33 \times 10^{10} W^{1.123-1.333} \text{ cal/s/sec}, t = 5.8t_0 \text{ to } 10t_0 \quad (8.149)$$

$$P = 2.64 \times 10^{11} W^{0.627} \exp(-1.84 W^{-0.373} t) \text{ cal/s/sec}, t = 10t_0 \text{ to } 50t_0 \quad (8.150)$$

In the evaluation of the constant, n , it would be preferable to integrate the energies to the time at which the gases reach ambient temperature. In such a case, the only energy lost would be in the work of expansion and in the radiant energy. In the real case, the cloud would have formed at higher altitudes by this time. In addition, the observed value for the increase in fireball volume would be required for the calculation. Even further, the additional energy released by the cooling of the original gas to lower temperatures than 208°K would have to be considered, as well as the decrease in the external pressure to below 1 atmosphere.

The times after burst of chief interest in the fallout formation are those when the temperature of the fireball has fallen below about 250°K. For the ideal soil, the end of the first period of condensation should occur at the soil-melting temperature, 167°K.

Some of the fireball temperatures and times, for yields between 1- and 10^{10} -KT, as calculated from the above scaling functions are summarized in Table 8.8. For most yields, the temperature range of interest occurs between $20t_g$ and $80t_g$. The times at which the temperature is estimated to decrease to 167°K varies from about 2 seconds for 1-KT to about 122 seconds for 10^{10} -KT. In scaled time, the change is only from $3t_g$ to $27t_g$ from 1- to 10^{10} -KT, respectively.

Because of the many assumptions involved in deriving the descriptive equations for the surface burst fireball, no reliability can be attached to the numerical values derived from them. However, the general trends in these values, as given by the functions with respect to time and yield, and with respect to the model air burst, are consistent with observations. Except on the point of accuracy, the descriptive value that can be placed on the development of the functions, and therefore their presentation here, is associated with pointing out what the important fireball parameters are, with respect to fallout formation, and how they are related to each other. When more data are made available, appropriate adjustments in the scaling function parameters can be made.

8.4 Process for Estimating the Concentration of Liquid Soil in the Fireball of a Model Surface Burst and the Fractionation Numbers of the Radionuclides

The use of the fireball scaling functions for estimating the value of $n(r)/V$ which is required in Eqs. 8.8, 8.10, or 8.82 in the evaluation of the $r_0(A)$ of each mass chain, is illustrated in this section. In the illustrative calculation, the

Table II.8

SUMMARY OF HOME FIREBALL PARAMETER VALUES FOR VARIOUS YIELDS
OF THE MODEL SURFACE BURST

Parameter	Weapon Yield					
	1	10	10 ²	10 ³	10 ⁴	10 ⁵
t ₀ (sec)	0.001	0.14	0.84	0.80	1.80	4.47
T at 10t ₀ ("K)	3340	3260	3100	3120	3050	2080
T at 20t ₀ ("K)	2800	2840	2280	2280	2180	2180
T at 30t ₀ ("K)	1720	1680	1040	1600	1570	1580
T at 40t ₀ ("K)	1280	1200	1170	1100	1120	1100
T at 50t ₀ ("K)	880	800	840	820	800	786
t/t ₀ at 1878°K	80.8	80.1	29.4	28.7	28.0	27.4
t at 1878°K (sec)	1.88	4.84	10.0	28.1	53.1	129

value of $n(t)/V$ is estimated at only one temperature for each of several weapon yields, and the temperature at which the liquid-volt multitudes is selected so that fractions of each element condensed may be calculated to apply at the time of the end of the first period of condensation.

Two times are selected for a complete computation of the $r_p(A)$ values. The first time, 80 seconds after burst, was selected so as to minimize, to a degree, any possible errors in the relative abundances of the short-lived fission products, and so as to make the computations apply to a land-surface burst in the megaton yield range. The second time, of 0 seconds, was used to determine the sensitivity of the results of the computation to the changes in relative abundance of the different nuclides due to decay and to the changes in the weapon yield.

The use of single values for temperature and time neglects both the possible variation of $n(t)/V$ with time and the possible losses of some of the fission products and volat from the fireball at earlier times. The computation of the liquid-volt concentration at a given time and fireball temperature by means of energy balances is not an optimum method because of the approximations used in the fireball scaling functions and because the calculations involve the determination of small differences in rather large numbers which themselves cannot be computed with accuracy.

The selection of the fireball temperature and the time of occurrence determines the yield, by use of Eqs. 8.183 or 8.186. Substitution of 1078°K and 80 seconds and solving for W gives a yield of 14,000-kT (14-MT); the yield for 0 seconds is 8d-kT. The method of computing the necessary quantities is discussed below for the 14-MT yield detonation.

To estimate, by means of energy balances, the molar concentration of the soil in the fireball requires estimates of the disposition of the energy contained in the fireball between the time of the second temperature maximum and 80 seconds. In this time period, the following processes must be considered:

1. Cooling to 1078°K, and recombination of the gases at $T_g(t)$ including liquefaction of the vaporized soil.
2. Loss of energy due to radiation from the fireball.
3. Loss of energy due to expansion of the fireball gases against the atmosphere.
4. Loss of energy in heating the additional air that enters the fireball.
5. Loss of energy in heating and melting a given amount of additional soil.

An estimate of the energy exchanged among the first four processes is required, in order to calculate the amount of soil that is both present and melted in the fireball at 1078°K.

The thermal data and parameters describing the 14-MT yield fireball, for use in the calculations, are summarized in Table 8.8. The values of n/W were taken from Figure 8.1, the other data were calculated from the cooling functions or from the interpolation of data in the tables and graphs of Section 8.8. In using the plotted data at odd values of $T_g(t)$, a check computation is required to assure that the energy sum at t_p is 48 percent of the yield. The data are interpolated from the curves plotted against temperature, after calculation of $T_g(t)$, rather than against yield, because the initial computations were made from such curves. The amount of soil vaporized and present at t_p would form, upon complete condensation at 80 seconds, 0.51×10^4 W moles in accounting for the 28 atoms per molecule.

Table 8.0

SUMMARY OF FIREBALL PARAMETERS AND THERMAL DATA
FOR THE 14-MT YIELD MODEL SURFACE-BURST FIREBALL.

Parameter	Value
t_b	8.14 sec
T_b	0.645°K
n_e/W	4.800×10^6 moles/KT
n_n/W	1.482×10^6 moles/KT
n_{γ}/W	0.168×10^6 moles/KT
V_b	0.80×10^{11} W cm ³
P_b	4.01 atmos
P_a	0.18 atmos
\bar{n}_e/n_n	1.042
n_e/W	2.801×10^6 moles/KT
$\Delta H_a - 502$	95,950 cal/mole air
ΔH_n	158,840 cal/mole solid/gas atom
$60/t_b$	28.04
$10q_b^{1/2} W$	8,08%

The energy released on cooling the gases from 8860°K to 1878°K, including association of the gas molecules, is calculated by the process of cooling to 298°K and reheating to 1878°K. Thus, for the air,

$$\text{Air, } 886^\circ\text{K} \rightarrow \text{Air, } 1878^\circ\text{K}, \Delta H = 8,080 \text{ cal/mole}$$

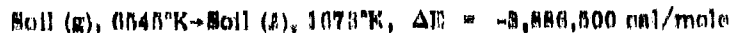
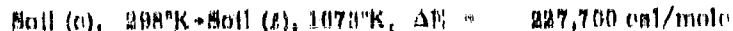
$$\text{Air, } 6845^\circ\text{K} \rightarrow \text{Air, } 298^\circ\text{K}, \Delta H = -85,000 \text{ cal/mole}$$

$$\text{Air, } 6845^\circ\text{K} \rightarrow \text{Air, } 1878^\circ\text{K}, \Delta H = -87,080 \text{ cal/mole}$$

Therefore the heat released on cooling and recombining the air is

$$Q_1 = -8.148 \times 10^{11} \text{ W cal/s} \quad (8.101)$$

For the soot, including melting at 1073°K.



Therefore the heat released on cooling, recombining, and liquifying the soot is

$$Q_1'' = -2.14 \times 10^{11} \text{ W cal/s} \quad (8.162)$$

Thus, the release of energy on cooling and recombining the fireball gasses is

$$Q_1' = -4.22 \times 10^{11} \text{ W cal/s} \quad (8.163)$$

The radiant energy lost from the fireball from t_0 to $10t_0$ is 15.7 percent; the additional amount from $10t_0$ to $28.6t_0$ is 8.8 percent for a total of 19.5 percent. Hence the total energy lost by radiation from t_0 to $28.6t_0$ is

$$Q_R = 2.14 \times 10^{11} \text{ W cal/s} \quad (8.164)$$

The spherical fireball volume, from Eq. 8.146 is

$$V = 7.72 \times 10^{11} \text{ W exp}(0.510W^{-0.373}) \text{ cm}^3, \quad t_0 \leq t \leq 10t_0 \text{ to } 50t_0 \quad (8.165)$$

Therefore the volume at 60 seconds, for 14-MT, is

$$V = 1.85 \times 10^{12} \text{ W cm}^3 \quad (8.166)$$

The change in volume from V_0 is therefore

$$\Delta V = V - V_0 = 1.31 \times 10^{12} \text{ W cm}^3 \quad (8.167)$$

The work energy used in expanding all the gases from V_0 to V against the external pressure of 1 atmosphere (1 cal = $41.25 \text{ cm}^3\text{-atmos}$) is

$$Q_W = 3.17 \times 10^{10} \text{ W cal/s} \quad (8.168)$$

In order to estimate the number of additional moles of air that have entered the fireball between t_0 and 28.0 t_0 , it is assumed that the internal pressure of the fireball at 28.0 t_0 is very close to 1 atmosphere. With this assumption and that of the perfect-gas law, the number of moles of gas in the 14-MT fireball at 60 seconds is

$$n_T = 1.35 \times 10^7 W \text{ moles} \quad (3.160)$$

The net gain in air molecules, neglecting the small amount of other gases, is

$$\Delta n = n_T - n_0 = 1.11 \times 10^7 W \text{ moles} \quad (3.160)$$

On this basis, about 80 percent of the fireball gas molecules at 60 seconds is from the air that entered after t_0 . The energy required to heat this air from 298°K to 1673°K is

$$Q_1 = 8.90 \times 10^{10} W \text{ cal/s} \quad (3.161)$$

Since the energy changes for all processes must equal zero, the remaining amount not accounted for is

$$Q_2 = 8.73 \times 10^{10} W \text{ cal/s} \quad (3.162)$$

Assuming that this remainder is utilized to heat and melt soil, the amount of soil that could be liquified (at the melting temperature) plus that condensed from the vapor is

$$n(t) = 3.83 \times 10^6 W + 5.51 \times 10^4 W \text{ moles} \quad (3.163)$$

$$= 4.38 \times 10^6 W \text{ moles}$$

Therefore at 1673°K, or 60 seconds after detonation of the 14-MT model surface burst, the gross concentration of the liquid soil is

$$n(t)/V = 2.37 \times 10^{-7} \text{ moles/cm}^3 \quad (3.164)$$

The results of similar computations of $n(t)/V$ at 1673°K for values of W from 1- to 10¹²-KT are summarized in Table 3.10. Over this large range in yields, the $n(t)/V$ values for the model surface burst vary only from about 1.8×10^{-7} to 2.5×10^{-7} moles of soil/cm³. The fractions of the energy required to melt these amounts of soil range from 7.5 to 9.2 percent of the total. For a low yield tower shot, Adams⁶ estimated that about 9 percent of the energy was used in heating the soil and tower materials. Since it is expected that a larger fraction of the energy would be utilized in a surface burst, the two estimates are in relative agreement.

In regard to the energy balance, it may appear during the development of the equations that 0 percent of the energy initially absorbed by the soil at t_g has been disregarded from the calculations. But some of the soil heated by this energy is certainly part of the $n(t)$ moles that are melted. This rendition of energy is partially, and arbitrarily, compensated for by not accounting for further losses to the underlying soil surface between t_g and t_s .

If these energy losses are considered to occur over the bottom of the fireball, and the readditions are considered to occur only for soil from the crater area, the fractional error in the neglect of the readditions can be estimated from the relative areas involved. The crater radius, from ENW, is $62.5W^{1/4}$ foot (or W in KT), or,

$$R_c = 1.90 \times 10^3 W^{1/4} \text{ cm} \quad (3.105)$$

The ratio of the surface area of the crater to the surface area covered by the fireball should give the fraction of energy recovered, assuming uniform losses from the surface of the fireball that is in contact with the earth. The ratio of R_c^2/R_f^2 is 0.09; hence the amount of energy recovered from this area only would be 0.81 percent of the total.

While it is possible that a large part of the energy losses to the soil could be near the center of the area covered by the fireball, these losses were not considered to occur before t_g . Because of the low thermal conductance of the soil minerals and the high temperatures of the liquid layer or boundary, if any, between the gases and the solid soil should be very thin. The final computation of $n(t)$ does not stipulate whether the energy losses to the soil after t_g result in the formation of a liquid layer or puddle in the crater which is thereafter disrupted and sucked up into the fireball or liquid particles by the direct melting of individual soil grains. Therefore, except for the averaging of the energy losses over the fireball surface up to t_g , no specification of the fate of the 0 percent of the energy lost to the soil can be given.

The final major assumption for the calculation of $n(t)/V$ is that the internal pressure of the fireball is 1 atmosphere. There is apparently no data to substantiate this assumption except the inference from the fact that the early expansion of the fireball has stopped at t_g , so that even at this early time the internal pressure cannot be very much larger than the external pressure. At the time the temperature has reached 1073°K, the fireball is quite high. For example, at 23 seconds the top of the fireball (or forming cloud) for the 1-MT yield, from Eq. 3.127 would be at an altitude of about 12,000 feet. At this altitude, the actual external pressure is considerably less than 1 atmosphere. The number of moles of air, as estimated by the use of the assumption, is about twice the original number of air atoms in the same volume at 1 atmosphere and

TABLE 3.10
**SUMMARY OF ESTIMATES OF M_3/V FOR THE MODEL SURFACE BURST OF DIFFERENT YIELDS
 AT THE TIME THE FIREBALL TEMPERATURE IS 1673°K**

Quantity	Units	Yield (kT)				
		1	10	10^2	10^3	10^4
n_e	10^{16} moles orig air	1.384	1.749	1.912	2.157	2.331
$\Delta E(T_2(s) \text{ to } 1673\text{K})$	cal/mole air	-135,480	-121,300	-108,620	-98,050	-89,190
$\Delta E(T_2(s) \text{ to } 1673\text{K})$	cal/mole soil	-152,350	-151,320	-150,350	-150,230	-149,630
	stones	-	-	-	-	-
Q_1	10^{10} W cal/s	-	2.140	-	2.110	-
Q_1'	10^{11} W cal/s	-	2.142	-	2.142	-
Q_1''	10^{12} W cal/s	-	2.154	-	2.152	-
Q_2	10^{10} W cal/s	-	2.182	-	2.196	-
Q_2	10^{11} W cal/s	-	2.159	-	2.156	-
$V, 1673\text{K}$	10^{12} W cm ³	2.162	2.159	2.156	2.151	2.147
ΔV	10^{12} W cm ³	2.167	2.173	2.162	2.152	2.141
Q_3	10^{10} W cal/s	0.359	0.348	0.338	0.328	0.318
$m_T, 1673\text{K}$	10^7 W moles air	1.465	1.438	1.407	1.378	1.348
Δn	10^7 W moles air	1.311	1.263	1.312	1.164	1.115
Q_4	10^{11} W cal/s	1.061	1.013	0.973	0.934	0.894
Q_5	10^{12} W cal/s	0.710	0.744	0.785	0.823	0.861
m_f	10^5 moles soil	3.659	3.311	3.938	4.162	4.231
m_f	10^{-5} moles soil/cm ³	1.81	1.36	2.57	2.20	2.34
m_f	10^{-4} gm soil/cm ³	0.951	1.01	1.08	1.15	1.23

208°K and, of course, the energy balance equations do not specify the origin of the gas atoms. Some of the additional air certainly comes from the volume swept out above the fireball as it rises; also, some must enter from the bottom along with the column of soil particles that is formed by the updrafts. The latter is particularly noticeable on the periphery of the columns of the larger yield detonations.

Some estimate of the amount of the crater material that is involved in the formation of $n(t)$ can be made, using the crater radius given above and the crater depth, $26W^{1/6}$ foot, as given in ENW. For the crater volume, a cone shape is used, which is somewhat more typical of the shape of craters from the larger yield nuclear weapons than the ellipsoid of revolution of ENW. Taking 110 lb/cu. ft for the soil density gives

$$M_c = 5.11 \times 10^6 W^{0.17} \text{ gm} \quad (8.100)$$

for the amount of soil removed from the crater (yields in the MT range leave no crater lip). The range in the mass of $n(t)$ from 1-KT to 10^3 -KT according to the model surface burst fireball (mol. wt. 824) is $1.08 \times 10^6 W$ gm to $2.35 \times 10^6 W$ gm; with the crater mass of Eq. 8.100, the corresponding range in the percentage of the crater mass that forms $n(t)$ is from 8.8 percent to 12 percent, respectively. In terms of the model, those are the fractions of the crater mass that have entered the fireball up to 1.0 and 122 seconds after detonation, providing no significant amounts of melted soil have fallen out of the fireball volume during this period.

It is clear that the $n(t)/V$ ratios, as calculated, assume that many soil particles have entered the fireball and that none have left. If a large number of particles have been ejected from the fireball during the period when the liquid soil can exist, then the computed values of $n(t)/V$ are too large. However, the assumption that only an insignificant fraction of the particles leave the fireball during the period when the more refractory fission products condense should be valid because of the short times involved. If it is further assumed that the mixing in the volume is rather uniform and that equilibrium conditions exist between the liquid particles and vapor, then estimates can be made of $n(t)$ (or of $n(s)$ if complete condensation of all the elements does not occur at temperatures above the melting point of the crater) from observed values of the concentration of fission product elements in fallout.

The condensation of the more refractory fission-product elements occurs independently of the state of the crater material. All that is required is the presence of a macroscopic condensed phase, liquid or solid, on which the vapor can condense. When complete condensation of one or more of the fission product

elements occurs, the ratio of the total amount of soil present in the fireball to the total amount of the element present in the fireball volume is equal to the ratio found in the fallout particles formed. In the more general case, this ratio is given by

$$n(t) = \frac{Y_A}{N_A} \sum_i \left(\frac{y_i(A, t)}{1 + \frac{y_i(A, t)}{n(t)/V} RT} \right) \quad (8.107)$$

In which Y_A is the total weapon yield of mass number A (in moles or fission equivalents), and N_A is the mole fraction or concentration of mass number A in the fallout particles in (moles or fissions)/(mole of gm of soil). For mass chains containing only elements whose gaseous species are less volatile than the carrier, the summation term is equal to one.

For investigating possible times and temperatures at which a given element condenses, radiochemical data on the fractionated mass chains are required. In this case, the better estimate of $n(t)/V$ would result when the summed term has values between 0.2 and 0.8. Unfortunately, no unspecified data are available on fractionated chains for use in solving Eq. 8.107. Some data, based on Mo-90 analyses in terms of fissions and other measurements, are available for making rough estimates of $n(t)$ or $n(s)$, assuming the mass Mo chain had completely condensed while all the fallout-forming particles were present; these data are summarized in Table 8.14.

The fireball volumes used to calculate the fission concentrations of Table 8.7 was the 1078°K volume for the model surface burst. The only data directly applicable for comparison with model surface burst calculations are those of the operation Jingle "B" shot. Some error is involved in the estimates of the factors used to convert the $M_x(t)$ values to $1/N_{A,i}$ values applicable to the refractory elements; also, some bias is introduced because the samples from which the $M_x(t)$ values were derived were known to contain some unknown fraction of background soil, not fallout, which would tend to make the calculated values of $n(t)$ or $n(s)$ high. The factor-of-two difference between the "data" and the model values could be accounted on this basis alone. The data from the other shots were included only to exhibit differences; no fireball model has been developed for them as yet.

For the underground shot, the fireball volume from the model surface burst is certainly larger than the actual gas volume was at 1078°K. Therefore the true value of $n(t)/V$ or $n(s)/V$ for an underground detonation would be even larger than that of Table 8.14. On the other hand, the samples from which the $M_x(t)$ values were determined contained more background soil, not fallout, than those from the surface shot. However, the excess was probably not a factor of two greater, so the larger value of $n(t)/V$ or $n(s)/V$ anticipated for the underground shot represents a real excess over that of the surface shot fallout, and it could be even larger.

Table 3.11
SUMMARY OF ESTIMATES OF Fe^{+3}/V (OR Fe^{+3}/Y) BASED ON FISSION CONTENT OF FAULTS

Type of Site	Fission Yield (10^{-3} fissions)	Total Yield (kT)	$1/\text{N}_{\text{Fe}}$		$\text{M}(A)$ or $\text{M}(S)$ (10^6 grams)	$\text{M}(A)$ or $\text{M}(S)$ (10^6 gm. cm^{-2})
			Mean	Range		
Jangle "S" - Land Surface ^a	1.50	1.1	3.1	1.5 - 5.0	4.9	2.2
Jangle "U" - Underground ^a	1.73	1.2	1.0	2 - 2.5	17	7.0
Low Tower Sheet Over Soil ^b	34.5	17	0.87	0.5 - 1.0	21	0.63
Surface Coral Detachments ^c	3,000	5,000	3.5	3 - 12	12,000	1.3
Surface Coral Detachments ^c	11,000	15,000	2.2	2 - 2.5	24,000	0.97

- a. From Reference 6 values of $\text{M}(I)$. The $1/\text{N}_{\text{Fe}}$ values are estimated by assuming a terrane factor of 0.75, a gross fissionation number of 0.3, and $\text{A} = \text{Fe}^{+3}$ (Fe^{+3} for 1 hr) / fission (sq. m.) for the ionization rate at 3 R. Note a smooth uniform, contaminated plane including an instrument response factor of 0.75.
- b. Based on data from fused silicate particles containing about 5 percent Fe in the silicate glass. The $1/\text{N}_{\text{Fe}}$ are average for gross sample of mixed particle sizes.
- c. Yields estimated sample weights are corrected to original coral composition based on sample analysis of CaO and MgO , data from References 7 and 8.

The friball volume of the low tower shot should be reasonably near that of the surface burst. The lower value of $n(t)/V$ (i.e., fixed particles) in this case is mainly due to height of burst; a true air burst at the same height would be expected to have even lower soil concentrations. Even with these differences, the calculated value of $n(t)/V$ is less than a factor of two from that of the model.

In the case of the coral detonations, the samples contained both fixed and irregular particles, hence a large fraction of the fission product elements present had condensed on the solid CaO particles. The model values of $n(t)/V$ again agree with the observed data (in this case $n(s)/V$) within a factor of two. All the observed data for the fallout from a near surface detonation where more than one sample or datum point is available, show the derived $n(t)/V$ or $n(s)/V$ values to have a spread of about a factor of two. Since the values calculated for the ideal surface burst friball model lie within this range one concludes that these concentrations can be estimated from the model with about the same reliability as they are known from the available data.

If the Henry's law constants for all the radionuclides in equilibrium with a silicate soil were available, the fractions of each that have condensed at a given temperature could be calculated by using the estimated values of $(n(t)/V)RT$. But while there are some thermal data on silicate compounds, they are not sufficiently extensive to include many fission-product elements. No comprehensive study has been made to correlate all the available thermal data on silicate materials at high temperatures, as has been made of other compounds. If this latter data were carefully studied, perhaps they and other data could be utilized to make reasonable estimates of the vapor pressures of many of the important fission-product elements over a molten soil mineral.

In order to test the model of the condensation process, and to estimate on a relative basis of the fractions that condensed, the following compromises with reality were made:

- (1) The fission product, its oxide or other compound, forms an ideal solution in the molten silicate glass during the first period of condensation;
- (2) The carrier material is non-reactive, so that no compound formation with the fission product elements or oxides occurs; and
- (3) The gaseous species of each fission-product element (with a few exceptions) is, in the presence of oxygen, the same as that which is in equilibrium with its own liquid or solid oxide.

For many of the fission-product elements, the first compromise, or species i , is perhaps reasonable, because many oxides do form solutions in silicon, e.g., see and, in this case, the solution is very dilute. The second and third compromises merely state the premise on which concentrations, in the liquid and vapor state, respectively, are computed. The simplification of the liquid-vapor phase system to a set of ideal solutions means that the solution behavior is defined by Raoult's law, rather than Henry's law, and that the vapor pressure of the gaseous species, i , of element i is given by

$$p_{ij} = N_j p_i^0 \quad (3.108)$$

where p_i^0 is the vapor pressure of the gaseous atom or molecule over the pure compound in the liquid or solid state at the same temperature, and N_j is the mole fraction of the pure compound in the molten salt.

In the real chemical system, many of the fission-product oxides or other compounds would certainly exhibit significant deviation from ideal behavior, even at low concentrations. In the case of the liquid silicon as a condensing surface, it might be expected that those elements whose ionic character differs most from that of Si⁴⁺ would probably deviate most from ideal behavior. The elements expected to deviate most would therefore be those of the alkali metals. However, similar oxides should give similar deviations, so that the relative values of p_{ij} for similar oxides should be in the same numerical order as the Henry's law constants.

There is one additional factor that eliminates, to some degree, the requirement for knowing the vapor pressures of all the elements over the condensed phase to a high degree of accuracy. In the condensation equations, the value of $R_0(A)$ varies inversely with $1 + p_{ij}/((n(r)/V)RT)$, where k_j is replaced by p_{ij} . The value of the sum of a series of these terms depends on the value of p_{ij} relative to the value of $(n(r)/V)RT$. If the ratio, given by the second term, is less than 0.001, then the element is essentially 100 percent condensed, and if the second term is more than about 300, the fraction condensed will be negligible (i.e., its contribution to the sum nettivity will be negligible). In the cases where the value of the second term is outside these limits, no accuracy in the actual value of p_{ij} is required. The greatest accuracy in the p_{ij} value is desired when the value of the ratio is near unity.

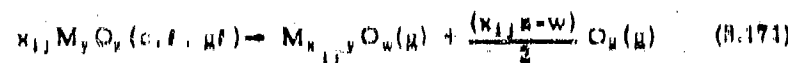
The vapor pressure data for the assumed vaporization, or condensation, reactions for the many elements considered are given, in Table 3.12, in terms of empirical constants for the equation

$$\log p_{ij} = \frac{A}{T} + B + C \quad (3.109)$$

where p_{11}^0 is in atmosphere, A and B are empirically-fitted constants, and

$$C = (x_{11} y - w) \log P(O_2) \quad (8.170)$$

based on the volatilization reaction of the condensed oxide, $M_y O_x$, according to



where $P(O_2)$ is the oxygen pressure in atmosphere and the x_{11} , y , w and x are numbers. The designation (c) is for crystal, (l) is for liquid, and (g) for gaseous. The constant, C, determines the effect of oxygen pressure on the amount of the gaseous species that condense. In all but a very few cases, the free energy data for the condensed phases of the oxides as reported by Coughlin⁸ were used in the evaluation of the constants of Eq. 8.169. The free energy data used for the elements was that of Stull and Sinker⁹. The other data sources used, mainly those of Brower and coworkers, are given in the table.

The empirical constants were evaluated from the free-energy data as near 1700°K as was feasible. Where tabulated data were available, the free-energy changes from the linear equation were calculated for comparison; in most cases the deviation of the values given by the equation from the tabulated data at extremes of the given temperature ranges were less than 500 cal/mole. The estimated equation constants were usually obtained from estimates of the free-energy functions of the gaseous molecules and from estimates of the heat capacities for the condensed phase.

Taking into account the effects of the oxygen pressure and of the dissociation and/or polymerization of the gas molecules requires some adjustment of the material balance equations that were developed for the application of Henry's law. From the generalized vaporization equation, the following quantities are defined:

$$N_j = n_j / y n(l) \quad (8.172)$$

for the mole fraction of the condensed oxide in solution and in equilibrium with one or more gaseous species, l;

$$N_{ij}^0 = n_{ij}^0 / y n \quad (8.173)$$

for the mole fraction of the gaseous species, and

$$p_{11} = N_{ij}^0 P \quad (8.174)$$

Table 3.12

SUMMARY OF EMPIRICAL CONSTANTS FOR VAPORIZATION REACTIONS OF JUNCTION PRODUCTS AND OTHER ELEMENTS

Reaction	Temperature Range (°K)	A ^a	B ^b	C ^c	M _d (°K)
1/2 Na ₂ O(<i>g</i>) → Na(<i>g</i>) + 1/2 O ₂ (<i>g</i>)	700-1,000	-10,900	8.848	-1/4 log P(O ₂ / <i>p</i>)	9,100
1/2 Na ₂ O(<i>f</i>) → Na(<i>g</i>) + 1/2 O ₂ (<i>g</i>)	0,000-1,000	-16,740	8.977	-1/4 log P(O ₂ / <i>p</i>)	
1/2 K ₂ O(<i>g</i>) → K(<i>g</i>) + 1/2 O ₂ (<i>g</i>)	700-1,000	-18,850	8.198	-1/4 log P(O ₂ / <i>p</i>)	8,878
1/2 Rb ₂ O(<i>g</i>) → Rb(<i>g</i>) + 1/2 O ₂ (<i>g</i>)	1,000-1,500	-38,280	7.988	-1/4 log P(O ₂ / <i>p</i>)	
1/2 Nb ₂ O(<i>g</i>) → Nb(<i>g</i>) + 1/2 O ₂ (<i>g</i>)	700-1,074	-10,000	7.180	-1/4 log P(O ₂ / <i>p</i>)	750
1/2 Rb ₂ O(<i>f</i>) → Rb(<i>g</i>) + 1/2 O ₂ (<i>g</i>)	074-1,000	-10,000	6.864	-1/4 log P(O ₂ / <i>p</i>)	
1/2 Ca ₂ O(<i>g</i>) → Ca(<i>g</i>) + 1/2 O ₂ (<i>g</i>)	700-1,000	-10,500	7.470	-1/4 log P(O ₂ / <i>p</i>)	768
1/2 Ca ₂ O(<i>f</i>) → Ca(<i>g</i>) + 1/2 O ₂ (<i>g</i>)	0,000-1,000	-10,180	7.049	-1/4 log P(O ₂ / <i>p</i>)	
MgO(<i>g</i>) → Mg(<i>g</i>) + 1/2 O ₂ (<i>g</i>)	0,000-1,000	-10,780	10.008	-1/2 log P(O ₂ / <i>p</i>)	8,025
MgO(<i>f</i>) → Mg(<i>g</i>) + 1/2 O ₂ (<i>g</i>)	0,000-1,000	-10,870	10.001	-1/2 log P(O ₂ / <i>p</i>)	
MgO(<i>l</i>) → Mg(<i>g</i>) + 1/2 O ₂ (<i>g</i>)	0,075-1,000	-10,850	7.977	-1/2 log P(O ₂ / <i>p</i>)	
CaCl(<i>g</i>) → Ca(<i>g</i>) + 1/2 Cl ₂ (<i>g</i>)	1,000-1,700	-43,000	10.000	-1/2 log P(Cl ₂ / <i>p</i>)	8,460
CaCl(<i>e</i>) → Ca(<i>g</i>) + 1/2 Cl ₂ (<i>g</i>)	1,700-2,000	-41,000	10.000	-1/2 log P(Cl ₂ / <i>p</i>)	
CaCl(<i>f</i>) → Ca(<i>g</i>) + 1/2 Cl ₂ (<i>g</i>)	2,000-6,000	-87,150	9.708	-1/2 log P(Cl ₂ / <i>p</i>)	
BrCl(<i>g</i>) → Br(<i>g</i>) + 1/2 Cl ₂ (<i>g</i>)	1,000-1,000	-88,260	9.808	-1/2 log P(Cl ₂ / <i>p</i>)	8,750
BrCl(<i>e</i>) → Br(<i>g</i>) + 1/2 Cl ₂ (<i>g</i>)	0,000-1,000	-88,030	9.808	-1/2 log P(Cl ₂ / <i>p</i>)	
BrCl(<i>n</i>) → BrCl(<i>g</i>)	0,000-1,000	-88,260	7.808		
BrCl(<i>f</i>) → Br(<i>g</i>) + 1/2 Cl ₂ (<i>g</i>)	1,700-1,000	-88,000	9.808	-1/2 log P(Cl ₂ / <i>p</i>)	
SnCl ₂ (<i>g</i>) → SnCl(<i>g</i>) + 1/2 O ₂ (<i>g</i>)	0,000-1,100	-80,700	9.808	-1/2 log P(O ₂ / <i>p</i>)	8,190
SnCl ₂ (<i>e</i>) → SnCl(<i>g</i>)	0,000-1,100	-80,700	9.808	-1/2 log P(O ₂ / <i>p</i>)	
SnCl ₂ (<i>f</i>) → SnCl(<i>g</i>) + 1/2 O ₂ (<i>g</i>)	0,000-1,000	-87,700	9.198	-1/2 log P(O ₂ / <i>p</i>)	
SnCl ₂ (<i>l</i>) → SnCl(<i>g</i>)	0,000-1,000	-80,000	9.808	-1/2 log P(O ₂ / <i>p</i>)	
ZnCl(<i>g</i>) → Zn(<i>g</i>) + 1/2 Cl ₂ (<i>g</i>)	1,000-1,000	-104,070	10.007	-1/2 log P(Cl ₂ / <i>p</i>)	12,000
ZnCl(<i>e</i>) → Zn(<i>g</i>)	1,000-1,000	(-104,070) ^a	(9,975) ^b	"	
CaClO ₂ (<i>g</i>) → CaCl(<i>g</i>) + 1/2 O ₂ (<i>g</i>)	0,000-1,000	-104,770	10.000	-1/2 log P(O ₂ / <i>p</i>)	
CaClO ₂ (<i>f</i>) → CaCl(<i>g</i>) + 1/2 O ₂ (<i>g</i>)	0,000-1,000	-104,770	10.000	-1/2 log P(O ₂ / <i>p</i>)	
LiOH + 1/2 H ₂ O → LiOH ₂ (<i>g</i>) + 1/2 O ₂ (<i>g</i>)	1,000-1,000	-105,580	10.000	-0.008 log P(O ₂ / <i>p</i>)	1,050
LiOH + 1/2 H ₂ O → LiOH ₂ (<i>g</i>) + 1/2 O ₂ (<i>g</i>)	0,000-1,000	-105,580	9.904	-0.008 log P(O ₂ / <i>p</i>)	
1/2 Pb ₂ O ₃ (<i>g</i>) → Pb(<i>g</i>) + 1/2 PbO ₂ (<i>g</i>)	1,000-1,070	-105,570	10.198	-1/2 log P(O ₂ / <i>p</i>)	1,270
1/2 Pb ₂ O ₃ (<i>f</i>) → Pb(<i>g</i>) + 1/2 PbO ₂ (<i>g</i>)	1,070-1,000	-107,140	10.000	-1/2 log P(O ₂ / <i>p</i>)	
1/2 Y ₂ O ₃ (<i>g</i>) → YO(<i>g</i>) + 1/2 O ₂ (<i>g</i>)	1,000-1,000	-114,000	10.000	-1/2 log P(O ₂ / <i>p</i>)	2,000
1/2 La ₂ O ₃ (<i>g</i>) → LaO(<i>g</i>) + 1/2 O ₂ (<i>g</i>)	1,000-1,000	-110,470	10.000	-1/2 log P(O ₂ / <i>p</i>)	2,600
1/2 Pr ₂ O ₃ (<i>g</i>) → PrO(<i>g</i>) + 1/2 O ₂ (<i>g</i>)	1,000-1,000	-110,470	10.000	-1/2 log P(O ₂ / <i>p</i>)	2,600
1/2 Nd ₂ O ₃ (<i>g</i>) → NdO(<i>g</i>) + 1/2 O ₂ (<i>g</i>)	1,000-1,000	-104,810	10.0047	-1/2 log P(O ₂ / <i>p</i>)	2,350

Table 3.12 (continued)

Reaction	Temperature Range (K)	A ^b	B ^b	C ^b	M.P.(K)
1/2 $\text{Pm}_2\text{O}_3(\text{s}) \rightarrow \text{Pm}(\text{g}) + 1/4 \text{O}_2(\text{g})$	1,000-8,000	(-81,870)	(8,010)	-1/4 log P(O ₂)	9,800
1/2 $\text{Nm}_2\text{O}_3(\text{s}) \rightarrow \text{Nm}(\text{g}) + 1/4 \text{O}_2(\text{g})$	1,000-8,000	(-27,850)	(8,810)	-1/4 log P(O ₂)	9,800
1/2 $\text{Al}_2\text{O}_3(\text{s}) \rightarrow \text{Al}(\text{g}) + 1/4 \text{O}_2(\text{g})$	1,000-8,000	-47,115	11,807	-1/4 log P(O ₂)	9,800
1/2 $\text{Al}_2\text{O}_3(\text{s}) \rightarrow \text{Al}_2\text{O}(\text{g}) + \text{O}_2(\text{g})$	1,000-8,000	-76,020	10,058	-log P(O ₂)	
1/2 $\text{Al}_2\text{O}_3(\text{s}) \rightarrow \text{Al}(\text{g}) + 3/4 \text{O}_2(\text{g})$	1,000-8,000	-65,750	14,848	-3/4 log P(O ₂)	
1/2 $\text{Al}_2\text{O}_3(\text{s}) \rightarrow \text{Al}_2\text{O}(\text{g}) + 1/8 \text{O}_2(\text{g})$	1,000-8,000	-64,050	14,708	-1/8 log P(O ₂)	
1/2 $\text{Al}_2\text{O}_3(\text{l}) \rightarrow \text{AlO}(\text{g}) + 1/4 \text{O}_2(\text{g})$	2,800-8,000	(-47,840)	(11,800)	-1/4 log P(O ₂)	
1/2 $\text{Al}_2\text{O}_3(\text{l}) \rightarrow \text{Al}_2\text{O}(\text{g}) + \text{O}_2(\text{g})$	2,800-8,000	(-70,800)	(10,760)	-log P(O ₂)	
1/2 $\text{Al}_2\text{O}_3(\text{l}) \rightarrow \text{Al}(\text{g}) + 3/4 \text{O}_2(\text{g})$	2,800-8,000	(-60,800)	(14,708)	-3/4 log P(O ₂)	
1/2 $\text{Ca}_2\text{O}_3(\text{s}) \rightarrow \text{CaO}(\text{g}) + 1/4 \text{O}_2(\text{g})$	1,000-1,000	-41,800	11,928	-1/4 log P(O ₂)	1,000
1/2 $\text{Ca}_2\text{O}_3(\text{s}) \rightarrow 3 \text{Ca}(\text{g}) + 5/4 \text{O}_2(\text{g})$	1,000-1,000	-45,150	14,600	-5/4 log P(O ₂)	
1/2 $\text{In}_2\text{O}_3(\text{s}) \rightarrow \text{InO}(\text{g}) + 1/4 \text{O}_2(\text{g})$	1,000-8,000	-48,000	11,405	-1/4 log P(O ₂)	1,500
1/2 $\text{In}_2\text{O}_3(\text{s}) \rightarrow \text{In}(\text{g}) + 5/4 \text{O}_2(\text{g})$	1,000-8,000	-46,570	13,940	-5/4 log P(O ₂)	
1/2 $\text{As}_2\text{O}_3(\text{s}) \rightarrow \text{As}_2\text{O}_3(\text{g})$	750-1,000	-8,878	8,020		ARC
1/2 $\text{As}_2\text{O}_3(\text{l}) \rightarrow \text{AsO}(\text{g}) + 1/4 \text{O}_2(\text{g})$	1,000-8,000	(-16,070)	(7,948)	-1/4 log P(O ₂)	
1/2 $\text{Bi}_2\text{O}_3(\text{s}) \rightarrow \text{Bi}_2\text{O}_3(\text{g})$	928-1,000	-8,894	8,298		ARC
1/2 $\text{Bi}_2\text{O}_3(\text{l}) \rightarrow \text{BiO}(\text{g}) + 1/4 \text{O}_2(\text{g})$	1,000-8,000	(-20,720)	(8,710)	-1/4 log P(O ₂)	
2 $\text{ZnO}_2(\text{s}) \rightarrow \text{Zn}_2\text{O}_3(\text{g})$	1,000-8,000	-60,800	18,468	-1/4 log P(O ₂)	8,000
2 $\text{ZnO}_2(\text{s}) \rightarrow \text{ZnO}_2(\text{g})$	1,000-8,000	-40,150	8,050		
2 $\text{CeO}_2(\text{s}) \rightarrow \text{CeO}(\text{g}) + 1/8 \text{O}_2(\text{g})$	1,000-8,070	(-40,610)	(14,801)	-1/4 log P(O ₂)	8,870
2 $\text{CeO}_2(\text{s}) \rightarrow \text{CeO}_2(\text{g})$	1,000-8,070	(-26,620)	(8,224)		
$\text{VO}_3(\text{s}) \rightarrow \text{VO}(\text{g}) + 1/2 \text{O}_2(\text{g})$	1,000-8,000	-48,070	12,048	-1/2 log P(O ₂)	8,000
$\text{VO}_3(\text{s}) \rightarrow \text{VO}_2(\text{g})$	1,000-8,000	-38,010	9,094		
$\text{VO}_3(\text{s}) + 1/2 \text{O}_2 \rightarrow \text{VO}_2(\text{g})$	1,000-8,000	-11,850	4,006	-1/2 log P(O ₂)	
$\text{SiO}_2(\text{s}) \rightarrow \text{SiO}(\text{g}) + 1/2 \text{O}_2(\text{g})$	1,000-1,000	-40,100	18,000	-1/2 log P(O ₂)	1,000
$\text{SiO}_2(\text{s}) \rightarrow \text{SiO}_2(\text{g})$	1,000-1,000	-28,980	8,005		
$\text{SiO}_2(\text{l}) \rightarrow \text{SiO}(\text{g}) + 1/2 \text{O}_2(\text{g})$	1,000-8,000	-38,780	12,268	-1/2 log P(O ₂)	
$\text{SiO}_2(\text{l}) \rightarrow \text{SiO}_2(\text{g})$	1,000-8,000	-37,810	8,049		
$\text{GeO}_2(\text{s}) \rightarrow \text{GeO}(\text{g}) + 1/2 \text{O}_2(\text{g})$	900-1,000	-89,800	18,000	-1/2 log P(O ₂)	1,000
$\text{GeO}_2(\text{s}) \rightarrow \text{GeO}_2(\text{g})$	900-1,000	-81,020	18,000	-1/2 log P(O ₂)	
$\text{RuO}_2(\text{s}) \rightarrow \text{RuO}(\text{g}) + 1/2 \text{O}_2(\text{g})$	1,000-1,000	-88,400	18,780	-1/2 log P(O ₂)	1,000
$\text{RuO}_2(\text{s}) \rightarrow \text{RuO}(\text{g}) + (1/8 \text{O}_2(\text{g}))$	1,000-1,000	-88,840	11,400	-1/8 log P(O ₂)	
$\text{RuO}_2(\text{s}) \rightarrow \text{RuO}(\text{g}) + 1/4 \text{O}_2(\text{g})$	1,000-1,000	(-20,610)	(18,007)	-1/4 log P(O ₂)	
$\text{RuO}_2(\text{s}) \rightarrow \text{Ru}(\text{g}) + \text{O}_2(\text{g})$	1,000-1,000	-45,000	18,000	-log P(O ₂)	
1/2 $\text{Rh}_2\text{O}_3(\text{s}) + 1/4 \text{O}_2(\text{g}) \rightarrow \text{RhO}(\text{g})$	1,000-8,000	(-19,000)	(0,010)	-1/4 log P(O ₂)	
1/2 $\text{Rh}_2\text{O}_3(\text{s}) + 3/4 \text{O}_2(\text{g}) \rightarrow \text{RhO}_2(\text{g})$	1,000-1,000	-12,000	1,000	-3/4 log P(O ₂)	
$\text{BeO}_2(\text{s}) \rightarrow \text{BeO}_2(\text{g})$	600-1,000	-4,500	7,044		ARC, sub
$\text{BeO}_2(\text{s}) \rightarrow \text{BeO}(\text{g}) + 1/2 \text{O}_2(\text{g})$	600-1,000	-10,710	10,704	-1/2 log P(O ₂)	
$\text{BeO}_2(\text{s}) \rightarrow \text{BeO}(\text{g}) + 1/8 \text{O}_2(\text{g})$	1,000-2,000	(-10,000)	(12,227)	-1/8 log P(O ₂)	

Table 8.12 (concluded)

Reaction	Temperature Range (K)	A ^b	B ^b	C ^b	M.P. (K)
TbO ₂ (s) → Tb(g) + 1/2 O ₂ (g)	700-1,000	+88,870	19,880	-1/2 log P(O ₂)	1,000
TbO ₂ (f) → TbO ₂ (g)	1,000-2,000	(-10,100)	(0,000)	"	
1/2 TbO ₂ (f) → Tb ₂ (g) + 2 O ₂ (g)	1,000-2,000	(-88,870)	(18,870)	-1/2 log P(O ₂)	
TbO ₂ (f) → TbO(g) + 1/2 O ₂ (g)	1,000-2,000	(-88,870)	(0,000)	-1/2 log P(O ₂)	
1/2 Nb ₂ O ₆ (n) → NbO(g) + 5/4 O ₂ (g)	1,000-1,780	-40,810	10,802	+5/4 log P(O ₂)	1,780
1/2 Nb ₂ O ₆ (n) → NbO ₂ (g) + 1/4 O ₂ (g)	1,000-1,780	-80,470	11,700	-1/4 log P(O ₂)	
1/2 Nb ₂ O ₆ (f) → NbO(g) + 5/4 O ₂ (g)	1,780-2,000	-40,800	14,820	+5/4 log P(O ₂)	
1/2 Nb ₂ O ₆ (f) → NbO ₂ (g) + 1/4 O ₂ (g)	1,780-2,000	-80,000	0,700	-1/4 log P(O ₂)	
0 MoO ₃ (n) → Mo ₂ O ₅ (g)	800-1,000	-17,600	14,887	"	1,000
4 MoO ₃ (n) → Mo ₄ O ₉ (g)	800-1,000	-80,400	17,040	"	
5 MoO ₃ (n) → Mo ₅ O ₁₁ (g)	800-1,000	-88,077	18,647	"	
MoO ₃ (f) → MoO(g) + O ₂ (g)	1,000-2,000	-61,600	10,888	-1/2 log P(O ₂)	
MoO ₃ (f) → MoO ₂ (g) + 1/2 O ₂ (g)	1,000-2,000	-84,780	10,140	-1/2 log P(O ₂)	
MoO ₃ (f) → Mo ₂ (g)	1,000-2,000	-17,810	7,870	"	
0 MoO ₃ (f) → Mo ₃ O ₄ (g)	1,000-2,000	-11,650	5,048	"	
0 MoO ₃ (f) → Mo ₄ O ₉ (g)	1,000-2,000	-4,700	0,880	"	
4 MoO ₃ (f) → Mo ₄ O ₉ (g)	1,000-2,000	-1,100	0,400	"	
5 MoO ₃ (f) → Mo ₅ O ₁₁ (g)	1,000-2,000	+1,081	-2,048	"	
MoO ₃ (f) → MoO ₂ (g)	1,000-2,000	-99,810	8,890	"	
MoO ₃ (n) + 1/2 O ₂ (g) → MoO ₂ (g)	1,000-2,000	-19,240	6,410	+1/2 log P(O ₂)	
2 MoO ₃ (n) + O ₂ (g) → Mo ₂ O ₅ (g)	1,000-2,000	-4,400	0,047	+ log P(O ₂)	
0 MoO ₃ (n) + 5/2 O ₂ (g) → Mo ₅ O ₁₁ (g)	1,000-2,000	+11,040	-0,061	+5/2 log P(O ₂)	
4 MoO ₃ (n) + 2 O ₂ (g) → Mo ₄ O ₉ (g)	1,000-2,000	+81,110	-4,100	+2 log P(O ₂)	
6 MoO ₃ (n) + 5/2 O ₂ (g) → Mo ₆ O ₁₃ (g)	1,000-2,000	+28,880	-7,700	+5/2 log P(O ₂)	
TbO ₃ (n,f) → TbO(g) + 1/2 O ₂ (g)	1,000-2,000	(-48,870)	(12,887)	-1/2 log P(O ₂)	
TbO ₃ (n,f) → TbO ₂ (g)	1,000-2,000	(-48,870)	(0,004)	"	
Tb ₂ O ₃ (f) → Tb ₂ O ₇ (g)	800-1,000	-8,000	0,280	"	800
Cu(l) → Cu(g)	800-1,000	-17,410	0,814	"	1,000
Cu(f) → Cu(g)	1,000-2,000	-16,680	0,881	"	
Ag(l) → Ag(g)	800-1,000	-14,680	0,844	"	1,000
Ag(f) → Ag(g)	1,000-2,000	-16,700	0,078	"	
Pd(l) → Pd(g)	1,000-1,880	-80,010	0,100	"	1,000
Pd(f) → Pd(g)	1,000-2,000	-10,180	0,640	"	
Kp(f) → Kp(g)	"	"	"	"	
Xe(f) → Xe(g)	"	"	"	"	
NaBr(f) → NaBr(g)	1,000-2,000	-8,010	0,840	"	1,000
NaI(f) → NaI(g)	900-1,000	-8,980	0,000	"	0.000

^a Values in parentheses are estimated values.^b See text.

Bibliography for Table 3.18

1. Coughlin, James P., Bureau of Mines, Bulletin 643, 1964.
2. Stull, D. R., and G. C. Blenko, *The Thermodynamic Properties of the Elements*, Am. Chem. Soc., Washington, D.C., 1959.
3. Kelley, K. K., Bureau of Mines, Bulletin 684, 1960.
4. Brewer, Leo, *Chem. Rev.*, **58**, 1 (1958).
5. Brewer, Leo, UCRL-2654 (rev.), 1955.
6. Brewer, Leo, UCRL-8886, 1958.
7. Brewer, Leo, and J. Drowart, UCRL-8086, 1959.
8. Chandrasekharan, M. S., and L. Brewer, UCRL-8786, 1960.
9. Brewer, L., and M. S. Chandrasekharan, UCRL-8718 (rev.), 1960.
10. Chupka, W. A., and J. Berkowitz, *J. Chem. Phys.*, **36**, 1207 (1967).
11. Burns, R. P., G. De Maria, J. Drowart, and R. T. Grimley, *J. Chem. Phys.*, **32**, 1860 (1960).
12. Drowart, J., G. De Maria, R. P. Burns, and M. G. Inghram, *J. Chem. Phys.*, **32**, 1866 (1960).
13. Chupka, W. A., M. G. Inghram, R. F. Porter, *J. Chem. Phys.*, **34**, 702 (1960).
14. De Maria, G., R. P. Burns, J. Drowart, and M. G. Inghram, *J. Chem. Phys.*, **32**, 1878 (1960).
15. Alcock, C. B., and G. W. Hooper, *Proc. Royal Society (London)*, **A204**, 601 (1950).
16. Soulton, J. R., P. Shapitananda, and J. L. Margrave, *J. Chem. Physics*, **39**, 189 (1963).

Combining these with Eq. 3.8 given

$$n_{ij}^0 = x_{ij} k_{ij}^0 \quad (3.175)$$

where k_{ij}^0 is substituted for $p_{ij}^0 / \{ (n(t)/V) k_{ij}^0 \}$.

These definitions, together with use of Raoult's law and the material balance requirements, result in the value of k_j^0 defined for Eq. 3.37 to be given by

$$k_j^0 = 2x_{ij} k_{ij}^0 \quad (3.176)$$

The values of x_{ij} are given by the individual reactions in Table 3.12.

At the temperature of the soil melting point i.e., at the end of first period of condensation, the gases that determine the total pressure are the nitrogen and oxygen of the air. The partial pressures of all the other materials are relatively small. In the model surface burst, relatively large amounts of soil are considered to be vaporized so that the vapor products of Al_2O_3 , Na_2O , and SiO_2 are introduced into the fireball. The Al_2O_3 , with a boiling point of about 3050°K (in 1 atmosphere of oxygen) could start vapor-condensing at this, or lower, temperature into liquid drops. In doing so the Al_2O_3 would co-condense some of the less volatile fission products which could not vapor-condense otherwise because their individual vapor pressure would be lower than that anticipated from the data of Table 3.12. These small vapor-condensed Al_2O_3 drops may solidify, when they cool to about 2800°K, or they may combine with the SiO_2 liquid drops, that are forming at about this temperature, to form alumino-silicate liquid drops.

Also, at these lower temperatures, larger soil particles entering the fireball can exist in the liquid state and would dissolve any of these small particles they collide with. In a very short time the majority of these small particles disappear. In the meantime, the more volatile fission-product elements are condensing into all the liquid particles present according to their vapor pressure equilibria with the liquid phase.

If one is interested in the equilibrium conditions at the higher temperatures when the partial pressures from the soil constituents are high, then these constituents must be considered and added to the partial pressures of N_2 , O_2 , and possibly CO_2 . However, if it is assumed that no particles leave the fireball before the end of the first period of condensation, then it suffices to compute the fractions of each endproduct condensed at that instant. At this time or temperature even the partial pressure of the Na_2O (or Na) can be neglected. This assumption was followed in the foregoing computations.

The weighted values of the Raoult's law constants, or vapor pressures, of all the elements of interest at 1073°K are summarized in Table 3.13; an oxygen pressure of 0.2 atmosphere was used in the calculation. The two rare gas elements have been assigned infinity values because it is expected that the fractions of those elements condensing in the molten glass would be negligible. The other elements that are indicated as not fully condensed in the ideal solution are Cr, As, Se, Br, Rb, Mo, Ru, Cd, Ni, Te, I, and Os.

If no carrier material were present in the fireball with the fission product elements and if all were in the vapor state at 1073°K, their partial pressures could be estimated from use of the perfect gas law using the calculated volume of the model surface burst fireball and the yield factor of 0.8 atoms of fission products per KT. The calculated partial pressures for a 14-MT yield surface burst fireball are shown in Table 3.14 for some of the more abundant fission product elements. The atom percent abundances were taken from the tabulations of Bollay and Ballou¹⁰. Of all the elements listed, only Br, La, and Zr would have condensed to a solid state at the indicated temperature and time.

In order to test the effect of weapon yield on the fractions of each fission product nuclide condensed in the ideal solution as previously stated, end-pointed times of 0 and 60 seconds were selected; these correspond to yields of about 84 and 14,000 KT, respectively. The $r_0(\Lambda)$ calculations were made by rearranging Eq. 3.40 for the independent nuclide yields in terms of 10^4 fissions so that the data of Bollay and Ballou¹⁰ could be used without conversion to fractions of the chain yield. The chain yields derived from Glendenin's postulate were used. The calculations were made from the chain summations according to

$$r_0(\Lambda, t) = \frac{\sum_j N_j(\Lambda, t)/(1 + k^j)}{\sum_i N_i(\Lambda, t)} \quad (3.177)$$

where $N_j(\Lambda, t)$ is the number of atoms of element, j , of mass number, Λ , per 10^4 fissions present at time, t , after fission. The values of $(n(t)/V)RT$, from the data of Table 3.23 are 2.89×10^{-6} atmosphere for the 84-KT yield and 3.26×10^{-6} atmosphere for the 14-MT yield. The calculated values of $r_0(\Lambda)$ for each nuclide contributing to the gross activity at 40.8 minutes after fission are given in Table 3.15. It may be noted that the fractions of the Kr and Xe isotopes condensed are not zero. This is because it was assumed that these, no decay products of Br and I, do not readily escape from the glass after it has solidified.

Table 3.19
SUMMARY OF RAOUFT'S LAW CONSTANTS FOR THE GASEOUS SPECIES
OF THE FISSION PRODUCT AND OTHER ELEMENTS AT 1073K

Element	$p_i^0(\text{atm})^a$	Element	$p_i^0(\text{atm})$
Cu	0.04×10^{-3}	Ag	2.70×10^{-3}
Zn	2.06×10^{-4}	Cd	0.902
Ga	0.76×10^{-11}	In	2.60×10^{-8}
Ge	0.420	Sn	1.82×10^{-4}
As	1.85×10^{-6}	Sb	1.84
Se	1.01×10^{-6}	Te	4.04
Br	1.04	I	2.80
Kr	(m) ^b	Xe	(m) ^b
Rb	0.606	Cs	1.88
Br	4.61×10^{-10}	Ba	2.04×10^{-6}
Y	8.76×10^{-16}	La	0.50×10^{-14}
Ze	4.54×10^{-16}	Ce	4.08×10^{-8}
Nb	2.07×10^{-7}	Pr	9.80×10^{-14}
Mo	18.02	Nd	5.20×10^{-11}
Ta	0.28×10^{-6}	Pm	1.94×10^{-10}
Ru	1.14	Bm	1.81×10^{-7}
Rh	1.08×10^{-11}	U	8.00×10^{-4}
Pd	1.00×10^{-6}		

$$a. p_i^0 = \sum_i x_i p_i^0$$

b. Taken to be large so that the fraction condensed is negligible.

Table 8-11
 CALCULATED PARTIAL PRESSURES AND EQUILIBRIUM PARTIAL
 PRESSURES OF SOME OF THE MORE ABUNDANT FISSION PRODUCT
 ELEMENTS DISPERSED UNIFORMLY IN THE MODELED
 SURFACE-BURST FIREBALL AT 1078°K FOR A
 FISSION YIELD OF 14-MT

Element	Percent Number of Atoms at 1 min.	Partial Pressure in Volume (10^{-6} atmos)	Partial Pressure Over Oxide (atmos)
Rb	0	1.0	1.2
Cl	0	1.0	3.8
Sr*	8	0.0	4.0×10^{-10}
Ba	7	2.0	2.0×10^{-9}
Ta*	4	1.2	0.58×10^{-10}
Ge	0	2.2	4.4×10^{-6}
Hg	4	1.5	0.02
Zr*	8	0.0	4.0×10^{-10}
Nb	0	2.2	5.0×10^{-7}
Mo	8	0.0	4.2
Po	0	2.2	1.0

*Elements that would have formed a condensed phase from the vapor at 1078°K

The most exact method of computing the amount of each radionuclide present (and its activity) for a given number of fissions would be to use the value of $y_1(\Delta)/(1/\kappa_f)$ for each and the appropriate decay formula for the production of the daughter products. But to simplify the computation process, the calculations were made by direct multiplication of the $r_n(\Delta)$ values and the single nuclide d/ π values per 10^4 fissions and the disintegration multipliers are given in Table 3.10. Although this procedure gives higher values for the daughter products in each chain, the error decreases with time. Compared to other possible errors involved in the computation, the error due to this approximation is rather insignificant.

For example, at 60 seconds the initial fraction for Sr-89 is 0.010 which increases, after Rb-89 decays out, to 0.0406; in the exact method of computation, the latter value is reached by 2.5 hours. The $r_n(00)$ value for Sr-89 is valid from 31.2 minutes and the $r_n(140)$ value for Ba-140 is essentially valid at 60 seconds. The multipliers of Table 3.10 are from decay scheme data available up to about 1000 as indicated by the references given in the table.

Table 8.1B

Summary Of ν_0 (A) Values At 0 and 80 Seconds After Fission For Fission Product Nuclides That Contribute To The Gross Activity At 46.8 Minutes And Longer Times After Fission

Nuclide	ν_0 (A)		Nuclide	ν_0 (A)		Nuclide	ν_0 (A)	
	(0 sec)	(80 sec)		(0 sec)	(80 sec)		(0 sec)	(80 sec)
Zn-79	0.004	0.004	Zr-95	0.080	1.00	In-115	0.004	
Zn-74	0.004	0.004	Zr-97	1.00	1.00	In-117	0.847	
Cu-79	0.006	0.004	Nb-96	0.080	1.00	In-118	0.748	
Cu-78	0.006	0.006	Nb ¹ -96	0.080	1.00	In-119	0.030	
Cu-74	0.097	0.004	Nb ² -97	1.00	1.00	In-120	0.008	
Os-76	0.042	0.006	Nb-98	1.00	1.00	Mn-121	0.304	
Os-77	0.074	0.140	Mo-99	0.057	0.764	Mn-123	0.000	
Os ² -78	0.424	0.0700	Mo-101	0.011	0.0287	Mn-126	0.000	
An-77	0.002	0.114	Mo-102	0.000	0.00007	Mn-127	0.000	
An-78	0.414	0.0700	Tc-99	0.057	0.764	Mn-128	0.000	
An-79	0.276	0.0160	Tc-101	0.010	0.0000	Mn-129	0.000	
Be ₁ -81	0.0830	0.000001	Tc-102	0.844	0.0804	Mn-130	0.000	
Be ₂ -81	0.0828	0.000168	Ru-108	0.060	0.500	Mn-131	0.000	
Be ₃ -80	0.00100	0.0	Ru-106	0.585	0.110	Mn-132	0.000	
Br-83	0.00176	0.00702	Ru-100	0.450	0.0270	Tc ₁ -126	0.000	
Br-84	0.00221	0.00000	Rh-108	0.060	0.500	Tc ₁ -127	0.044	
Kr-83	0.00176	0.00702	Rh-100	0.086	0.111	Tc ₂ -127	0.044	
Kr ₁ -83	0.0122	0.0258	Rh ¹ -105	0.585	0.112	Tc ₁ -129	0.000	
Kr ₂ -83	0.0122	0.0240	Rh ² -100	0.450	0.0270	Tc ₂ -101	0.0007	
Kr ² -87	0.0100	0.0197	Rh-107	0.040	0.167	Tc ₂ -101	0.0754	
Kr-88	0.0195	0.00168	Pd-100	0.400	0.000	Tc ₂ -102	0.0007	
Rb-88	0.0100	0.00226	Pd-111	0.801	0.000	Tc ₁ -100	0.0180	
Rb-80	0.00804	0.0128	Pd-112	0.010	1.00	Tc ₂ -100	0.0118	
Rb _p -81	0.00886	0.0004	Ag-100	0.400	0.000	Tc ₂ -104	0.00000	
Ir-80	0.00004	0.0001	Ag-111	0.001	0.000	I-101	0.0752	
Ir-90	0.00021	0.101	Ag-112	0.014	1.00	I-102	0.0052	
Ir-91	0.107	0.000	Ag-113	0.000	0.001	I-103	0.0110	
Ir-92	0.000	0.024	Ag-115	0.004	0.020	I-104	0.00000	
Ru-90	0.708	0.000	Cd ₁ -110	0.000	0.005	Xe ₁ -101	0.0752	
Y-90	0.0021	0.101	Cd ₂ -110	0.000	0.005	Xe ₁ -100	0.0110	
Y ₁ -91	0.107	0.000	Cd-117	0.847	0.408	Xe ₁ -100	0.0110	
Y ₂ -91	0.107	0.200	Cd-118	0.740	0.250	Xe ₂ -100	0.0101	
Y-92	0.008	0.026	Cd-120	0.584	0.0000	Xe ₂ -105	0.00004	
Y-93	0.724	0.008				Xe ₂ -108	0.00280	
Y-94	0.040	1.00				Cs-107	0.00720	
						Cs-108	0.00300	
						Cs-109	0.0110	



Table 3.1b

Summary Of r_0 (A) Values At 0 And 60 Seconds After Plutonium For Plutonium Product Nuclides That Contribute To The Gross Activity At 40.8 Minutes And Longer Times After Plutonium

Nuclide	r_0 (A)		Nuclide	r_0 (A)		Nuclide	r_0 (A)	
	(0 sec)	(60 sec)		(0 sec)	(60 sec)		(0 sec)	(60 sec)
Zr-96	0.080	1.00	Ta-116	0.064	0.020	Ba-137	0.00720	0.00098
Zr-97	1.00	1.00	Ta-117	0.847	0.400	Ba-139	0.0320	0.0010
Nb-96	0.080	1.00	Ta-118	0.748	0.283	Ba-140	0.187	0.442
Nb-97	0.080	1.00	Ta-120	0.058	0.144	Ba-141	0.570	0.001
Nb-98	1.00	1.00	Ru-121	0.084	0.618	Ta-140	0.187	0.342
			Ru-120	0.690	0.080	Ta-141	0.582	0.001
			Ru-125	0.803	0.000	Ta-142	0.870	1.00
Mo-98	1.00	1.00				Ta-148	0.086	1.00
Mo-99	0.057	0.704						
Mo-101	0.511	0.0207						
Mo-102	0.000	0.00507						
						Ce-141	0.482	0.001
						Ce-148	0.080	1.00
Te-99	0.057	0.704	Hg-120	0.000	0.000	Ce-144	1.00	
Te-101	0.513	0.0086	Hg-127	0.044	0.041	Ce-146	1.00	
Te-102	0.044	0.00804	Hg-128	0.580	0.0002	Ce-148	1.00	
			Hg-120	0.200	0.0178			
						Pr-148	0.080	1.00
Ru-100	0.088	0.080	Ru-131	0.0807	0.0174	Pr-144	1.00	
Ru-105	0.520	0.110				Pr-146	1.00	
Ru-106	0.450	0.0270	Tc-125	0.300	0.099			
			Tc-127	0.044	0.041	Pr-140	1.00	
			Tc-129	0.044	0.041			
Rh-108	0.000	0.500	Tc-127	0.044	0.041			
Rh-109	0.526	0.111	Tc-129	0.200	0.0177	Nd-147	1.00	
Rh-109	0.626	0.112	Tc-130	0.302	0.0170	Nd-149	1.00	
Rh-108	0.450	0.0270	Tc-131	0.0807	0.0100	Nd-151	1.00	
Rh-107	0.040	0.107	Tc-131	0.0754	0.0100			
			Tc-130	0.0057	0.0124	Pm-147	1.00	
Pd-100	0.409	0.009	Tc-130	0.0120	0.0105	Pm-149	1.00	
Pd-111	0.801	0.008	Tc-130	0.0112	0.0124	Pm-140	1.00	
Pd-119	0.910	1.00	Tc-134	0.00003	0.00061	Pm-140	1.00	
						Pm-151	1.00	
						Pm-152	1.00	
						Pm-148	1.00	
Ag-100	0.400	0.009	I-131	0.0752	0.0100	Pm-148	1.00	
Ag-111	0.801	0.000	I-130	0.0002	0.0104	Pm-150	1.00	
Ag-118	0.014	1.00	I-130	0.0118	0.0110	Hm-161	1.00	
Ag-119	0.008	0.001	I-131	0.00000	0.000681	Hm-168	1.00	
Ag-116	0.004	0.000	I-135	0.0100	0.0141	Hm-166	1.00	
						Hm-160	1.00	
						Hm-160	1.00	
Xe-116	0.000	0.000	Xe-131	0.0752	0.0100	Ba-168	1.00	
Xe-116	0.000	0.000	Xe-130	0.0113	0.0110			
Xe-117	0.847	0.408	Xe-130	0.0118	0.0110	Eu-155	1.00	
Xe-118	0.740	0.280	Xe-130	0.0101	0.0108	Eu-150	1.00	
Xe-120	0.084	0.0006	Xe-136	0.00084	0.0134	Eu-157	1.00	
			Xe-138	0.00280	0.0	Eu-158	1.00	
						Tl-131	1.00	
			Cs-137	0.00720	0.00303			
			Cs-138	0.00000	0.00201			
			Cs-139	0.0110	0.0130			

Table 3.16
SUMMARY OF DISINTEGRATION MULTIPLIERS
FOR THE FISSION PRODUCT AND OTHER RADIONUCLIDES^a

Nuclide	Betas (Betas/ dis)	Photons (Photons/ dis)	Photon Energy (MeV/dis)	Air Ionization (10^{-6} r/hr-ft 2 dis/sec)	Meter Response (10^{-6} r hr-ft 2 dis/sec)
Zn-72	1.00	0.85	1.24	0.75	0.18
Zn-74	1.00	1.00	0.70	4.22	0.28
Ga-72	1.00	2.07	2.61	14.3	10.7
Ga-73	1.00	0.62	0.850	2.11	1.30
Ga-74	1.00	1.80	2.57	12.4	9.07
Ga-75	1.00	0.186	0.0380	0.216	0.170
Ga-77	1.00	2.80	2.38	18.1	10.1
Ga-78	1.00	1.00	0.440	2.74	2.14
As-75	1.00	0.042	0.0109	0.0785	0.0520
As-76	1.00	0.885	0.486	2.81	1.78
As-78	1.00	0.0	0.0	0.0	0.0
Se-81m	0.0	1.00	0.0200	0.117	0.0448
Se-81	1.00	0.0	0.0	0.0	0.0
Se-83	1.00	0.04	2.28	12.8	10.2
Br-83	1.00	0.15	0.0029	0.0174	0.00426
Br-84	1.00	1.00	1.65	8.12	6.26
Kr-85m	0.0	0.00	0.0160	0.0959	0.0
Kr-85m	0.77	1.00	0.161	0.070	0.081
Kr-86	1.00	0.010	0.0062	0.0016	0.0247
Kr-87	1.00	1.00	1.41	7.03	5.20
Kr-88	1.00	1.00	1.50	7.40	5.48
Rb-88	1.00	0.088	0.861	4.80	0.28
Rb-89	1.00	1.71	2.30	12.0	9.08
Rb-91	1.00	1.00	1.20	6.67	5.11

Table 3.10 (continued)

Nuclide	Betas (Betas/ dis)	Photons (Photons/ dis)	Photon Energy (MeV/dis)	Air Ionization (10^{-6} r/hr-ft 2 dis/mo)	Meter Response (10^{-6} r hr-ft 2 dis/mo)
Sr-89	1.00	0.0	0.0	0.0	0.0
Sr-90	1.00	0.0	0.0	0.0	0.0
Sr-91	1.00	0.08	0.800	5.00	5.00
Sr-92	1.00	1.02	1.28	6.00	6.48
Sr-93	1.00	1.00	0.2	1.20	0.004
Y-90	1.00	0.0002	0.0001	0.008	0.006
Y-91m	0.0	1.00	0.528	0.84	2.52
Y-91	1.00	0.002	0.0024	0.0135	0.0102
Y-92	1.00	1.44	1.17	6.50	5.00
Y-93	1.00	0.100	0.150	0.817	0.000
Y-94	1.00	1.00	1.8	0.07	0.11
Zr-95	1.00	0.07	0.710	4.92	3.00
Zr-97	1.00	0.078	0.0801	0.040	0.268
Nb ₁ -95m	0.0	1.00	0.203	1.41	1.12
Nb ₁ -95	1.00	1.00	0.762	4.50	3.54
Nb ₁ -97m	0.0	1.00	0.700	4.42	3.42
Nb ₁ -97	1.00	1.00	0.060	4.02	0.10
Nb-98	1.00	1.00	2.7	11.7	0.10
Mo-99	1.00	0.410	0.180	0.772	0.007
Mo-101	1.00	1.70	0.814	0.80	0.07
Mo-102	1.00	0.0	0.0	0.0	0.0
Tc-99m	0.0	1.00	0.180	0.782	0.014
Tc-101	1.00	1.05	0.034	2.00	1.50
Tc-102	1.00	1.00	0.4	2.40	1.00
Ru-100	1.00	0.001	0.487	2.00	2.00
Ru-105	1.00	1.00	0.720	4.00	0.80
Ru-108	1.00	0.0	0.0	0.0	0.0

Table 3.10 (continued)

Nuclide	Betas (Betas/ dR)	Photons (Photons/ dR)	Photon Energy (MeV/dR)	Air Ionization $\left(\frac{10^{-6} \text{ e}/\text{hr} \cdot \text{ft}^3}{\text{dR}/\text{sec}} \right)$	Meter Response $\left(\frac{10^{-6} \text{ e}/\text{hr} \cdot \text{ft}^3}{\text{dR}/\text{sec}} \right)$
Rh-108m	0.0	1.00	0.0207	0.100	0.0102
Rh-105m	0.0	1.00	0.0472	0.388	0.154
Rh-106	1.00	0.90	0.0015	0.550	0.487
Rh-108	1.00	0.488	0.804	1.81	1.41
Rh-107	1.00	3.00	0.829	5.08	8.00
Pd-100	1.00	0.0	0.0	0.0	0.0
Pd-111	1.00	1.20	0.88	5.00	0.00
Pd-112	1.00	1.00	0.0087	0.0228	0.0
Ag-109m	0.0	1.00	0.0288	0.172	0.0002
Ag-111	1.00	0.11	0.0286	0.175	0.184
Ag-112	1.00	0.80	0.843	4.59	3.50
Ag-110	1.00	0.090	0.0268	0.158	0.0050
Ag-115	1.00	1.00	0.211	1.28	0.980
Cd-115	1.00	0.080	0.0828	0.187	0.144
Cd-116	1.00	0.088	0.180	1.11	0.863
Cd-117m	0.0	2.00	1.40	8.11	0.08
Cd-118	1.00	0.0	0.0	0.0	0.0
Cd-120	1.00	1.00	0.5	0.08	2.40
In-115	1.00	0.048	0.184	1.12	0.801
In-117	1.00	0.80	0.224	1.00	1.00
In-118	1.00	1.00	0.0	10.0	0.85
In-119	1.00	1.00	0.092	0.0871	0.0
Sn-121	1.00	0.0	0.0	0.0	0.0
Sn-120	1.00	0.0	0.0	0.0	0.0
Sn-125	1.00	1.71	1.05	0.10	4.82
Sn-120	1.00	0.0	0.0	0.0	0.0
Sn-127	1.00	1.00	0.0	0.08	0.40
Sb-125	1.00	1.05	0.455	2.78	2.08
Sb-126	1.00	0.00	2.82	16.1	12.4
Sb-127	1.00	1.00	0.440	2.70	2.05
Sb-128	1.00	2.00	2.4	18.0	9.05
Sb-129	1.00	2.05	1.00	0.10	4.70
Sb-131	1.00	1.00	0.0	0.00	2.80

Table 3.16 (continued)

Nuclide	Betas (Betas/ dpm)	Photons (Photons/ dpm)	Photon Energy (MeV/dpm)	Air Ionization (10^{-10} r hr-ft 2 dpm/sec)	Meter Response (10^{-10} r hr-ft 2 dpm/sec)
Te ₁ -125m	0.0	2.0	0.0862	0.0095	0.0054
Te ₁ -127	0.015	0.005	0.0276	0.181	0.0
Te ₂ -127	1.00	0.0120	0.0040	0.0240	0.0102
Te ₁ -129m	0.0	1.00	0.0670	0.098	0.280
Te ₂ -129	1.00	1.00	0.262	1.52	1.00
Te ₁ -131	0.780	3.12	1.40	8.42	8.48
Te ₂ -131	1.00	1.20	0.347	2.08	1.00
Te-132	1.00	2.00	0.258	1.52	1.18
Te ₁ -133m	0.0	1.00	0.128	0.790	0.544
Te ₂ -133	1.00	1.70	1.57	0.18	7.04
Te-134	1.00	1.00	1.80	7.80	6.00
I-131	1.00	1.05	0.890	2.38	1.85
I-132	1.00	2.77	2.22	18.0	10.0
I-133	1.00	1.08	0.890	8.50	8.80
I-134	1.00	1.70	1.68	9.68	7.42
I-135	1.00	1.40	1.78	9.80	7.17
Xe ₁ -131	0.0	1.00	0.0344	0.207	0.0273
Xe ₁ -130m	0.0	1.00	0.0682	0.410	0.311
Xe ₂ -130	1.00	1.00	0.0610	0.304	0.121
Xe ₁ -130m	0.0	1.00	0.487	2.60	2.07
Xe ₂ -135	1.00	1.00	0.284	1.55	1.31
Xe-136	1.00	1.00	1.5	7.50	6.00
Cs-137	1.00	0.0	0.0	0.0	0.0
Cs-138	1.00	1.71	2.15	11.2	8.47
Cs-139	1.00	2.00	0.787	4.75	3.73
Ba-130m	0.0	1.00	0.607	3.65	2.53
Ba-137	1.00	0.87	0.143	0.888	0.600
Ba-140	1.00	1.14	0.183	1.10	0.846
Ba-141	1.00	1.00	0.7	4.22	3.28
Ba-142	1.00	1.00	1.0	5.70	4.44

Tabel 8.10 (continued)

Nuclide	Betas (Betas /dis)	Photons (Photons /dis)	Photon Energy (MeV/dis)	Air Ionization (10^{-6} r/hr-ft 3 dis/sec)	Meter Response (10^{-6} r hr-ft 3 dis/sec)
La-140	1.00	2.66	2.42	13.0	0.93
La-141	1.00	0.08	0.0765	0.400	0.004
La-142	1.00	1.70	2.33	11.0	0.87
La-143	1.00	1.0	1.2	6.07	0.11
Ce-141	1.00	0.708	0.0778	0.470	0.353
Ce-143	1.00	1.66	0.890	2.04	1.79
Ce-144	1.00	0.481	0.0812	0.188	0.117
Ce-145	1.00	1.00	0.7	1.92	0.26
Ce-146	1.00	1.80	0.265	1.00	1.24
Pr-143	1.00	0.0	0.0	0.0	0.0
Pr-144	1.00	0.0258	0.0315	0.165	0.125
Pr-145	1.00	0.0	0.0	0.0	0.0
Pr-146	1.00	1.55	1.12	6.42	4.04
Nd-147	1.00	1.08	0.187	0.968	0.683
Nd-149	1.00	2.85	0.888	2.81	1.74
Nd-151	1.00	2.25	1.10	6.44	4.91
Pm-147	1.00	0.0	0.0	0.0	0.0
Pm-149	1.00	1.80	1.98	7.28	5.87
Pm-150	1.00	1.61	0.844	4.09	3.85
Pm-151	1.00	1.80	0.066	2.21	1.68
Pm-152	1.00	2.00	0.62	3.79	3.96
Pm-153	1.00	1.0	0.8	4.76	3.69
Bm-151	1.00	1.00	0.0000	0.0544	0.0
Bm-153	1.00	1.20	0.0766	0.458	0.271
Bm-155	1.00	2.00	0.001	1.80	1.80
Bm-156	1.00	1.0	0.2	1.80	0.004
Bm-158	1.00	1.0	0.6	0.08	2.40
Hu-155	1.00	1.44	0.0569	0.314	0.173
Hu-156	1.00	0.00	1.14	5.55	4.17
Hu-157	1.00	1.75	0.023	3.78	2.00
Hu-158	1.00	2.00	1.2	7.21	0.00

Table 8.10 (concluded)

Nuclide	Betas (Betas /dm)	Photons (Photons /dm)	Photon Energy (MeV/dm)	Air Ionization $\left(10^{-6} \text{ r hr ft}^2\right)$ dm/sec	Meter Response $\left(10^{-6} \text{ r hr ft}^2\right)$ dm/sec
Ck-150	1.00	0.288	0.0721	0.430	0.328
Tb-161	1.00	0.50	0.0207	0.123	0.0570
U-237	1.00	2.77	0.200	1.13	0.808
U-239	1.00	1.00	0.0641	0.388	0.215
U-240	1.00	0.0	0.0	0.0	0.0
Np-239	1.00	2.07	0.185	1.11	0.790
Np-240	1.00	0.48	0.052	2.07	1.00
Mn-56	1.00	1.47	1.76	8.40	7.17

a. References:

- (1) C. F. Miller, Response Curves for USNRDL 4-pi Ionization Chamber, USNRDL-TR-155 (1957)
- (2) C. F. Miller, Proposed Decay Schemes for Some Fission-Product and Other Radionuclides, USNRDL-TR-160 (1957)
- (3) C. F. Miller and P. Logh (Ref. 12)
- (4) P. D. La Riviere, private communication, (July 1960)

8.8 Computing the Decay Rates of Fission Product Mixtures

In making the decay rate computations, the data of Bolles and Ballou¹⁰ based on Glendenin's postulate of independent yields for the slow neutron fission of U-238 were used as the basic input data. As discussed in Section 8.4, it is assumed that the fractional chain yields are the same for all fissile nuclides so that the disintegration rate per fission of a given nuclide from each type of fission differs only by a constant. This constant is the ratio of the mass chain yield in a given type of fission to the mass chain yield in the slow neutron fission of U-238; this constant is here called the chain-yield multiplier.

Where the decay schemes of fission products are known, gamma ray characteristics can be calculated. In this case it is convenient to give multipliers in terms of the characteristic emissions per disintegration of each nuclide. The multipliers for the gamma ray energy emitted, in terms of Mev/dis and r/hr at 8 feet above an ideal plane per dis/sec per sq ft., given in Table 8.16, are ones of chief interest for use in these calculations.

The results of the computations of the disintegration rates, photon emission rates, photon energy emission rates, and air ionization rates, for times extending from 48.8 minutes to 25.7 years after fission for the fissile nuclides U-238, U-235, and Pu-239, are given in Table 8.17. The use of Katcoff's yields¹¹ (adjusted) for thermal fission give disintegration rates that are almost identical with those of Bolles and Ballou. The air ionization rate (U-238, thermal) is also very close to that of Reference 12; at 8.4 hours, it is about 8 percent higher and at 2.6 years it is about 10 percent lower (maximum fluctuation).

Dolan^{13,14} calculated the disintegration rates and photon emission rates for 14-Mev neutron fission of U-238. The ratios of the calculations for 5-Mev neutron fission of U-238 in Table 8.17 to Dolan's values for 14-Mev neutrons are given in Figure 8.4. It may be noted that the disintegration rates are within 5 percent of each other from 1 to about 850 hours; the agreement in the photon emission rates is not quite as good, with Dolan's values being more than 10 percent lower after 40 hours. The maximum spread is +8 percent at (75 hours) to -12 percent at (2,500 hours) for the disintegrations-per-second computations, and +8 percent at (7.8 hours) to -17 percent at (1,200 hours) for the photons-per-second computations. A few more photons were counted in the method by which the data in Table 8.17 were obtained than by the method used by Dolan; these photons were chiefly in the energy range 0 to 20 Kev.

Table 8.17

DECAY OF NORMAL FISSION PRODUCTS FROM U-235, U-238 AND Pu-239

1. In dis/sec for 10^4 fission (Glendenin)

Age			U-235		U-238		Pu-239	
Years	Days	Hours	Thermal	Fission	(8 Mev)	Thermal	Fission	
		0.768	1.018	1.018	1.898	1.898	1.898	
		1.12	1.072	1.072	1.048	1.048	1.001	
		1.64	0.6900	0.6900	0.6578	0.6258	0.6368	
		2.40	0.4861	0.4454	0.4152	0.3867	0.3936	
		3.52	0.3818	0.2908	0.2691	0.2473	0.2568	
		5.16	0.1847	0.1916	0.1780	0.1640	0.1734	
		7.26	0.1228	0.1271	0.1195	0.1117	0.1186	
		11.1	(1)8171	(1)8393	(1)8000	(1)7601	(1)8088	
		16.2	(1)8280	(1)8378	(1)8201	(1)8107	(1)8245	
		28.8	(1)8311	(1)8341	(1)8291	(1)8304	(1)8318	
		1.45	34.8	(1)8087	(1)2042	(1)2049	(1)2062	
		2.18	51.1	(1)1223	(1)1219	(1)1250	(1)1260	
		3.12	74.9	(2)7417	(2)7881	(2)7698	(2)7662	
		4.57	109.7	(2)4787	(2)4778	(2)4978	(2)4982	
		6.70	161	(2)8288	(2)8286	(2)8288	(2)8290	
		9.82	238	(2)2227	(2)2228	(2)2247	(2)2198	
		14.4	348.7	(2)1528	(2)1502	(2)1501	(2)1458	
		21.1	506	(2)1025	(2)1001	(2)1002	(2)9885	
		30.9	748	(2)8828	(2)8608	(2)8682	(2)8885	
		45.8	1,087	(2)4458	(2)4277	(2)4365	(2)4191	
		66.4	1,594	(2)3078	(2)2748	(2)2614	(2)2781	
		97.5	2,985	(2)1888	(2)1784	(2)1780	(2)1780	
		148	4,480	(3)1117	(3)1088	(3)1082	(3)1080	
		208	4,990	(4)6162	(4)6078	(4)5988	(4)6507	
		301	7,320	(4)8192	(4)8174	(4)8140	(4)8175	
1.2	488	10,820	(4)1078	(4)1066	(4)1710	(4)8506	(4)8186	
1.75	650	15,600	(5)8804	(5)8768	(4)1025	(4)1588	(4)1541	
2.60	949	22,780	(5)6010	(5)5978	(5)6886	(5)8663	(5)7926	
3.80	1387	38,500	(5)8715	(5)8782	(5)8740	(5)4617	(5)4400	
5.58	2037		(5)8478	(5)8586	(5)8859	(5)8882	(5)8470	
		8.18		(5)1015	(5)1087	(5)1701	(5)1448	(5)1688
		10.0		(5)1500	(5)1580	(5)1523	(5)1086	(5)1253
		17.6		(5)1189	(5)1201	(5)1027	(5)7922	(5)8719
		20.7		(5)9078	(5)9624	(5)7814	(5)6001	(5)7465

Table 8.17 (continued)

2. In betas/sec for 10^4 fissions (Glendelin)

Years	Days	Hours	Age		U-235		U-238		Pu-239	
			Thermal	Fission	(8 Mev)	Thermal	Fission	Thermal	Fission	
		0.768	1.544	1.548	1.587	1.482	1.406			
		1.18	1.008	1.015	0.9816	0.9432	0.9398			
		1.64	0.6358	0.6444	0.6070	0.5724	0.5707			
		2.40	0.3988	0.4081	0.3703	0.3457	0.3542			
		3.52	0.2547	0.2687	0.2402	0.2170	0.2272			
		6.10	0.1655	0.1782	0.1571	0.1420	0.1515			
		7.56	0.1088	0.1180	0.1042	(1)0556	0.1025			
		11.1	(1)7159	(1)7377	(1)6982	(1)6518	(1)6892			
		16.2	(1)4581	(1)4880	(1)4496	(1)4348	(1)4484			
		23.8	(1)3556	(1)3900	(1)2830	(1)2840	(1)2859			
		34.8	(1)1781	(1)1697	(1)1804	(1)1881	(1)1802			
		51.1	(1)1098	(1)1098	(1)1195	(1)1166	(1)1180			
		8.12	74.9	(2)6697	(2)7117	(2)6847	(2)7450	(2)7160		
		4.57		(2)4592	(2)4558	(2)4698	(2)4911	(2)4709		
		6.70		(2)8102	(2)8180	(2)8155	(2)8268	(2)8128		
		9.82		(2)9143	(2)2158	(2)2121	(2)2150	(2)2076		
		14.4		(2)1455	(2)1480	(2)1404	(2)1440	(2)1860		
		21.1		(2)9707	(2)9701	(2)9216	(2)9454	(2)9550		
		30.9		(2)6878	(2)8850	(2)5999	(2)6158	(2)6740		
		45.8		(2)4108	(2)4088	(2)5852	(2)5968	(2)6694		
		60.4		(2)9682	(2)8008	(2)2450	(2)2559	(2)2890		
		87.9		(2)1607	(2)1084	(2)1581	(2)1690	(2)1678		
		140		(2)1026	(2)1025	(2)9610	(2)1075	(2)8900		
		208		(2)5919	(2)5920	(2)5587	(2)6756	(2)6167		
		301		(4)8118	(4)8110	(4)8088	(4)4070	(4)8610		
	1.2	435		(4)1630	(4)1029	(4)1866	(4)2469	(4)8140		
	1.78	650		(5)9542	(5)9455	(5)8923	(4)1511	(4)1807		
	2.60			(5)5708	(5)5680	(5)8981	(5)8598	(5)7600		
	3.80			(5)9410	(5)9442	(5)9444	(5)4364	(5)7600		
	5.58			(5)2194	(5)2257	(5)2080	(5)2089	(5)8181		
	8.18			(5)1648	(5)1723	(5)1469	(5)1218	(5)1401		
	12.0			(5)1255	(5)1848	(5)1082	(5)8220	(5)8010		
	17.6			(5)9621	(5)1041	(5)8124	(5)6002	(5)7878		
	26.7			(5)7120	(5)7787	(5)8974	(5)4412	(5)8450		

Table B.17 (continued)

8. In photons/sec for 10⁴ fissions (Clarendon)

Age			U-235		U-238		Pu-239	
Years	Days	Hours	Thermal	Fission	(H Mev)	Thermal	Fission	
		0.768	1.007	1.004	1.028	1.005	1.021	
		1.12	1.280	1.278	1.259	1.269	1.250	
		1.64	0.8048	0.8068	0.7821	0.7688	0.7658	
		2.40	0.4908	0.4977	0.4751	0.4495	0.4581	
		3.52	0.2971	0.3030	0.2904	0.2654	0.2708	
		5.18	0.1815	0.1898	0.1810	0.1628	0.1770	
		7.56	0.1149	0.1204	0.1165	0.1052	0.1108	
		11.1	(1)7584	(1)7801	(1)7741	(1)7150	(1)7808	
		16.2	(1)4688	(1)5148	(1)3080	(1)4866	(1)5188	
		28.8	(1)8289	(1)8810	(1)8807	(1)8268	(1)8820	
1.48	84.8	(1)2108	(1)2140	(1)2151	(1)2180	(1)2157		
2.18	51.1	(1)1855	(1)1872	(1)1855	(1)1444	(1)1808		
		3.12	74.9	(2)5799	(2)8807	(2)9118	(2)9597	(2)9148
		4.57		(2)5836	(2)5968	(2)6115	(2)6461	(2)8097
		6.70		(2)8927	(2)8974	(2)4050	(2)4267	(2)8894
		9.52		(2)2668	(2)2590	(2)2626	(2)2758	(2)9551
		14.4		(2)1644	(2)1629	(2)1648	(2)1720	(2)1577
		21.1		(2)1020	(2)9949	(2)1019	(2)1064	(2)9640
		30.9		(2)6166	(2)6595	(2)6212	(2)6526	(2)6848
		45.8		(2)8878	(2)8884	(2)8865	(2)8895	(2)8467
		66.4		(2)8014	(2)8100	(2)1882	(2)2268	(2)2015
		97.8		(2)1168	(2)1088	(2)1218	(2)1880	(2)1188
		148		(4)6400	(4)8880	(4)6840	(4)7810	(4)6640
		208		(4)8842	(4)8179	(4)8838	(4)8810	(4)8460
		301		(4)1421	(4)1893	(4)1481	(4)1728	(4)1508
1.2	435			(5)5188	(5)5176	(5)5881	(5)7612	(5)8714
1.78	650			(5)8117	(5)8158	(5)8647	(5)8782	(5)8884
2.60				(5)1108	(5)1145	(5)1084	(5)2058	(5)1884
3.80				(6)8058	(6)8848	(6)8011	(6)1040	(6)1094
5.58				(6)8762	(6)8948	(6)8505	(6)8078	(6)8644
8.18				(6)8014	(6)8080	(6)8808	(6)8100	(6)8861
12.0				(6)2709	(6)2690	(6)8088	(6)8588	(6)8158
17.6				(6)2418	(6)2857	(6)2550	(6)2208	(6)2700
27.7				(6)2074	(6)2016	(6)2141	(6)1010	(6)2810

Table 3-17 (continued)

4. In photon Mev range for 10^6 fission

Age Years	Days	Hours	II-230		II-238		III-239	
			Thermal	Fission	(8 Mev)	Thermal	Fission	
		0.700	1.830	1.830	1.720	1.680	1.605	
		1.12	1.240	1.240	1.147	1.084	1.085	
		1.64	0.7757	0.7770	0.7187	0.6650	0.6550	
		2.40	0.4310	0.4004	0.4070	0.3813	0.3708	
		3.02	0.2580	0.2004	0.2070	0.1818	0.1770	
		5.00	0.1400	0.1020	0.1368	0.1190	0.1271	
		7.00	(1)8540	(0)8088	(0)8073	(0)7044	(1)7746	
		8.0	(1)6242	(0)5454	(0)5096	(0)4468	(1)6040	
		10.2	(1)5020	(0)4289	(0)4023	(0)3801	(1)3058	
		18.0	(1)3817	(0)3068	(0)2844	(0)1731	(1)1526	
0.40	84.8	(0)3008	(0)2070	(0)1608	(0)1008	(1)1008	(1)1008	
	9.00	50.0	(2)0228	(2)0181	(2)0121	(2)0103	(2)0095	
		0.02	74.0	(2)8807	(2)8074	(2)4064	(2)4284	(2)4034
		4.07		(2)8570	(2)8098	(2)2695	(2)2845	(2)2600
		6.70		(2)7150	(2)1800	(2)1807	(2)1908	(2)1778
		9.82		(2)5110	(2)2266	(2)1206	(2)1273	(2)1170
		14.4		(2)4000	(2)8039	(2)7026	(2)8147	(2)7480
		22.0		(2)3128	(2)5273	(2)4700	(2)4768	(2)4760
		30.0		(2)2220	(2)4220	(2)3225	(2)3202	(2)3200
		48.8		(2)1312	(2)3180	(2)1004	(2)1706	
		66.4		(2)0408	(2)1008	(2)0021	(2)1008	(2)9780
		97.8		(2)0070	(2)0000	(2)0076	(2)0007	(2)0046
		148		(2)0050	(2)0010	(2)0000	(2)0070	(2)0000
		208		(2)0000	(2)0000	(2)0000	(2)0070	(2)0070
		300		(2)0000	(2)0024	(2)7000	(2)8007	(2)8070
1.2	488		(2)2817	(2)2010	(2)2000	(2)1001	(2)8050	
0.78	650		(2)0080	(2)0485	(2)0400	(2)0488	(2)0812	
2.00			(2)0000	(2)0000	(2)0728	(2)0000	(2)7408	
3.80			(2)0000	(2)0445	(2)0000	(2)0500	(2)4460	
5.00			(2)0000	(2)0042	(2)0057	(2)0000	(2)2670	
		8.08		(2)1724	(2)1720	(2)1800	(2)1700	(2)2028
		12.0		(2)1670	(2)1602	(2)1600	(2)1644	(2)1620
		17.0		(2)1405	(2)1077	(2)1020	(2)1258	(2)1507
		25.7		(2)1408	(2)1168	(2)1280	(2)1040	(2)1200

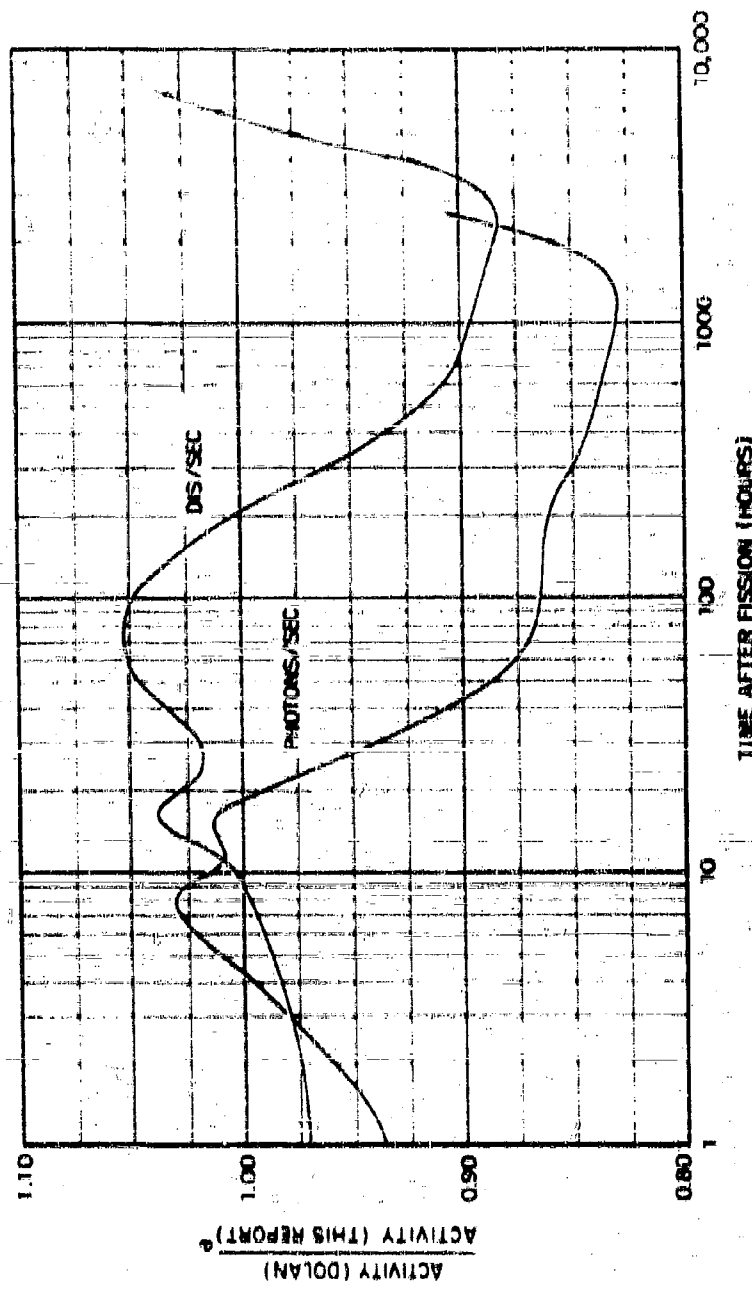
Table A-15 (continued)

5. The following table gives the cumulative probability for 100 frequencies per age.

Year	Days	Hours	Age		17-235		17-236		17-237	
			Thousands	Thousands	(1) Month	(2) Month	(3) Month	(4) Month	(5) Month	(6) Month
1940	1	0.700	0.700	(8)00777	(8)00770	(8)00729	(8)00707	(8)00700	(8)00750	(8)00701
		1.12	1.12	(8)00448	(8)00432	(8)00472	(8)00400	(8)00400	(8)00450	(8)00451
		1.44	1.44	(8)004140	(8)004138	(8)00427	(8)00400	(8)00400	(8)00417	(8)00417
		2.40	2.40	(8)02463	(8)02464	(8)02450	(8)02407	(8)02400	(8)02485	(8)02485
		3.52	3.52	(8)13410	(8)13409	(8)13402	(8)13400	(8)13400	(8)13450	(8)13450
		5.16	5.16	(9)00779	(9)00778	(9)00762	(9)00700	(9)00700	(9)00708	(9)00708
1941	1	7.56	7.56	(9)07786	(9)07784	(9)07787	(9)07000	(9)07000	(9)07008	(9)07008
		11.1	11.1	(9)02664	(9)02664	(9)02607	(9)02556	(9)02556	(9)02581	(9)02581
		16.2	16.2	(9)01604	(9)01600	(9)01702	(9)01626	(9)01626	(9)01701	(9)01701
		26.8	26.8	(10)00710	(10)00704	(10)00750	(10)00701	(10)00701	(10)00680	(10)00680
		41.6	41.6	(10)00400	(10)00428	(10)00300	(10)00295	(10)00295	(10)00300	(10)00300
		61.0	61.0	(10)01720	(10)01716	(10)02617	(10)02650	(10)02650	(10)02711	(10)02711
1942	1	74.0	74.0	(10)2270	(10)2210	(10)2300	(10)2470	(10)2300	(10)2300	(10)2300
		11.7	11.7	(10)1453	(10)1524	(10)1550	(10)1645	(10)1545	(10)1545	(10)1545
		17.0	17.0	(11)00766	(11)00731	(11)00300	(11)00900	(11)00900	(11)0021	(11)0021
		28.2	28.2	(11)00774	(11)00772	(11)00800	(11)02444	(11)00800	(11)00800	(11)00800
		44.4	44.4	(11)04400	(11)04587	(11)04602	(11)04550	(11)04550	(11)04220	(11)04220
		71.1	71.1	(11)00110	(11)00100	(11)02845	(11)02953	(11)02953	(11)02953	(11)02953
1943	1	80.0	80.0	(11)00110	(11)00107	(11)01702	(11)0227	(11)0227	(11)0227	(11)0227
		45.3	45.3	(11)00601	(11)00539	(11)00304	(11)0092	(11)0092	(12)0777	(12)0777
		66.4	66.4	(12)00656	(12)00607	(12)00100	(12)0300	(12)0300	(12)0728	(12)0728
		97.0	97.0	(12)00676	(12)00497	(12)00000	(12)0590	(12)0590	(12)0643	(12)0643
		143	143	(12)00170	(12)00000	(12)00700	(12)02320	(12)02320	(12)2200	(12)2200
		208	208	(12)01104	(12)01104	(12)01103	(12)01297	(12)01297	(12)1180	(12)1180
1944	1	261	261	(13)00774	(13)00700	(13)04730	(13)0707	(13)0707	(13)5170	(13)5170
		40.0	40.0	(13)00000	(13)00720	(13)00200	(13)0130	(13)0130	(13)1004	(13)1004
		77.8	77.8	(14)00004	(14)00768	(14)00517	(14)00683	(14)00683	(14)7000	(14)7000
		116.0	116.0	(14)00001	(14)00725	(14)00300	(14)01004	(14)01004	(14)4202	(14)4202
		181.0	181.0	(14)00444	(14)00432	(14)00213	(14)02692	(14)02692	(14)2504	(14)2504
		256.8	256.8	(14)00154	(14)00158	(14)00003	(14)01442	(14)01442	(14)1011	(14)1011
1945	1	304	304	(14)00020	(14)001021	(14)00000	(14)00071	(14)00071	(14)1226	(14)1226
		42.0	42.0	(15)00432	(15)00200	(14)00000	(14)00452	(14)00452	(14)1057	(14)1057
		77.6	77.6	(15)00310	(15)00211	(14)00000	(14)01377	(14)01377	(14)0160	(14)0160
		127.7	127.7	(15)00783	(15)00741	(14)00000	(14)02216	(14)02216	(14)07608	(14)07608

a. Number in parentheses is identification number of zeros between decimal and first digit.

Figure 24
COMPARISON OF CALCULATIONS OF THE ACTIVITY AND PHOTON EMISSION RATE OF THE
FISSION PRODUCTS FROM 14MeV NEUTRON FISSION OF U-235 (Data^{27,28}) WITH THOSE
FROM 8MeV NEUTRON FISSION OF U-238 (Table¹⁷) GIVEN AS A RATIO OF THE TWO WITH
TIME AFTER FISSION



The air ionization rate curves from each type of fission are of chief interest; these are compared in Figures 3.5 and 3.6 in terms of an air ionization rate "R" factor. The factor, r_{ip} , is the ratio of the air ionization rate from one type of fission to the rate from thermal neutron fission of U-238. The fluctuation in the curves of Figures 3.3 and 3.4 reflects the relative prominence of the important gamma emitters in each mixture.

The deviation in r_{ip} from the value 1 is a measure of the difference in the ionization rate from that of the U-238 thermal fission reference curve. The order in the r_{ip} deviations, from least to most, is:

1. fission neutron fission of U-238,
2. 8-Mev neutron fission of U-238,
3. fission-neutron fission of Pu-239, and
4. thermal-neutron fission of Pu-239.

The maximum relative deviation for the first three (combined), between 1 and 7000 hours after fission, is from -16 percent at 2.5 hours to +6.5 percent at 110 hours. However, between 2 and 3 years after fission the U-238 (8-Mev neutrons) r_{ip} value is almost 1.6 and the Pu-239 (fission neutrons) r_{ip} value is almost 0.8 because of the higher yields for the rare earth elements (heavy mass peak) in the fission products from the heavier fissile nuclides and larger neutron energy.

The two main factors that determine the gross decay of the normal product mixtures (besides the half-lives and the individual nuclide-decay schematics) are the mass chain yields and the independent yields of the isotopes in the chain. For times after fission of about 1 hour and greater, the Boiles-Baillou calculations¹⁰ show that the difference in the total disintegration rates, based on Present's yield theory, from those based on Glendenin's postulate is insignificant. This is due to the fact that, at these times after fission, most of the chains have decayed from the short-lived early members to the last one or two active members. The displacement from 1.00 in the curves of Figures 3.3, 3.5, and 3.6 therefore are due to differences in the chain yields. The curves show that, for times between about 1 hour and 1 year, the maximum error in the ionization rate by use of the data for thermal neutron fission of U-238 would be about 10 percent.

Figure 3.5
 GROSS AIR IONIZATION RATE FRACTIONATION NUMBER, $\frac{I_{\text{air}}}{I_{\text{U-235}}} \text{ RELATIVE TO THE}$
 $\text{IONIZATION RATE (in hours) OF THE FISSION PRODUCTS FROM THERMAL NEUTRON}$
 $\text{FISSION OF U-235, FOR THE FISSION PRODUCT MIXTURES FROM OTHER FISSILE}$
 $\text{NUCLEIDES AND NEUTRON ENERGIES}$

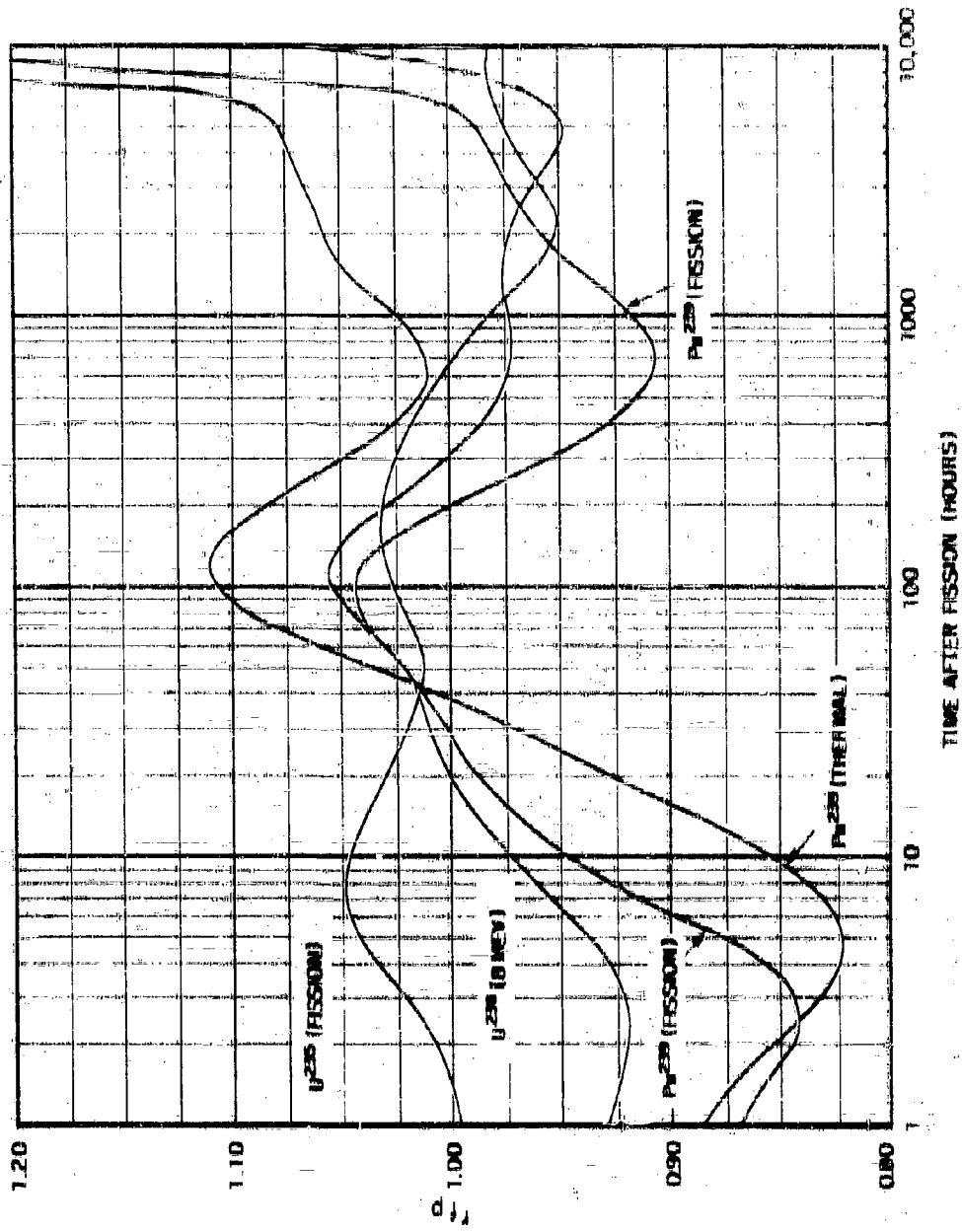
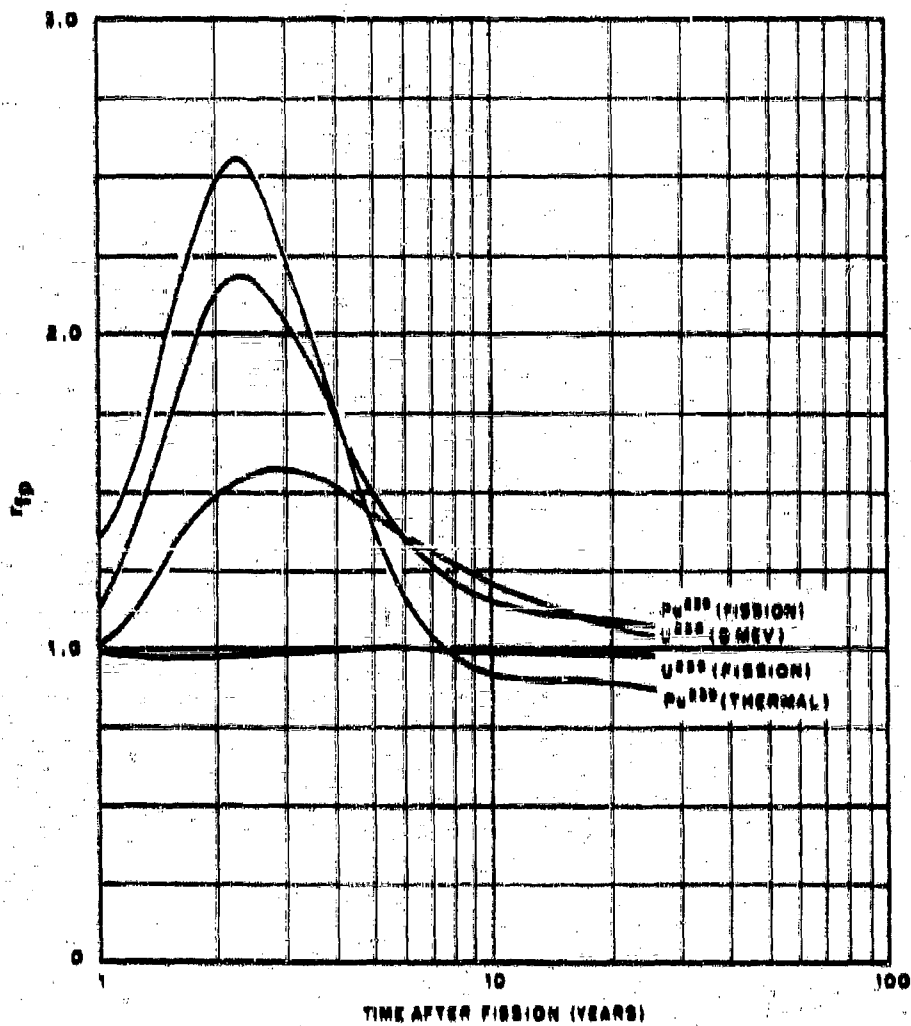


Figure 3.4
GROSS AIR IONIZATION RATE FRACTIONATION NUMBER, r_{10} , RELATIVE TO THE
IONIZATION RATE (in years) OF THE FISSION PRODUCTS FROM THERMAL NEUTRON
FISSION OF U-235, FOR THE FISSION PRODUCT MIXTURES FROM OTHER FISSILE
NUCLIDES AND NEUTRON ENERGIES



The H+1 ionization rates at 3 feet above an infinite smooth contaminated plane for a unit yield distribution of fission products per unit area are summarized in Table 3.18. The highest value is for the thermal neutron fission of U-235; the lowest is for fission-neutron fission of Pu-239.

Table 3.18

SUMMARY OF H+1 IONIZATION RATES OF NORMAL FISSION PRODUCTS*

Type of Fission	(H+1 Ionization Rate) (unit yield/unit area)	
	(r/hr at 1 hr) (fiss/sq ft)	(r/hr at 1 hr) (KT/sq mi)
U-235 (thermal)	7.60×10^{-13}	3050
U-235 (fission)	7.58×10^{-13}	3040
U-238 (9-Mev)	6.04×10^{-13}	3010
Pu-239 (thermal)	6.70×10^{-13}	3480
Pu-239 (fission)	6.84×10^{-13}	3400

a. Per unit yield per unit area, for 3 feet above an infinite smooth contaminated plane.

The same value, 1.46×10^{23} fissions/KT, was used to convert all the ratios from fissions to kilotonnes. The corresponding ionization rate factor derived from ENW is $(1240 \text{ r/hr at 1 hr}) / (\text{KT/sq mi})$ or about a factor of 3 lower than the values of Table 3.18. Other authors^{15, 16, 17, 18} have made similar calculations and comparisons of these factors and of the decay curves for the thermal neutron fission of U-235.

The number of photons per disintegration and the average energy of the photons for the normal mixture of fission products from 9-Mev-neutron fission of U-238 are shown as a function of time after fission in Figures 3.7 and 3.8, respectively.

Figure 3.7
NUMBER OF PHOTONS PER DISINTEGRATION FOR THE NORMAL MIXTURE OF
FISSION PRODUCTS FROM 8-MeV NEUTRON FISSION OF U-238

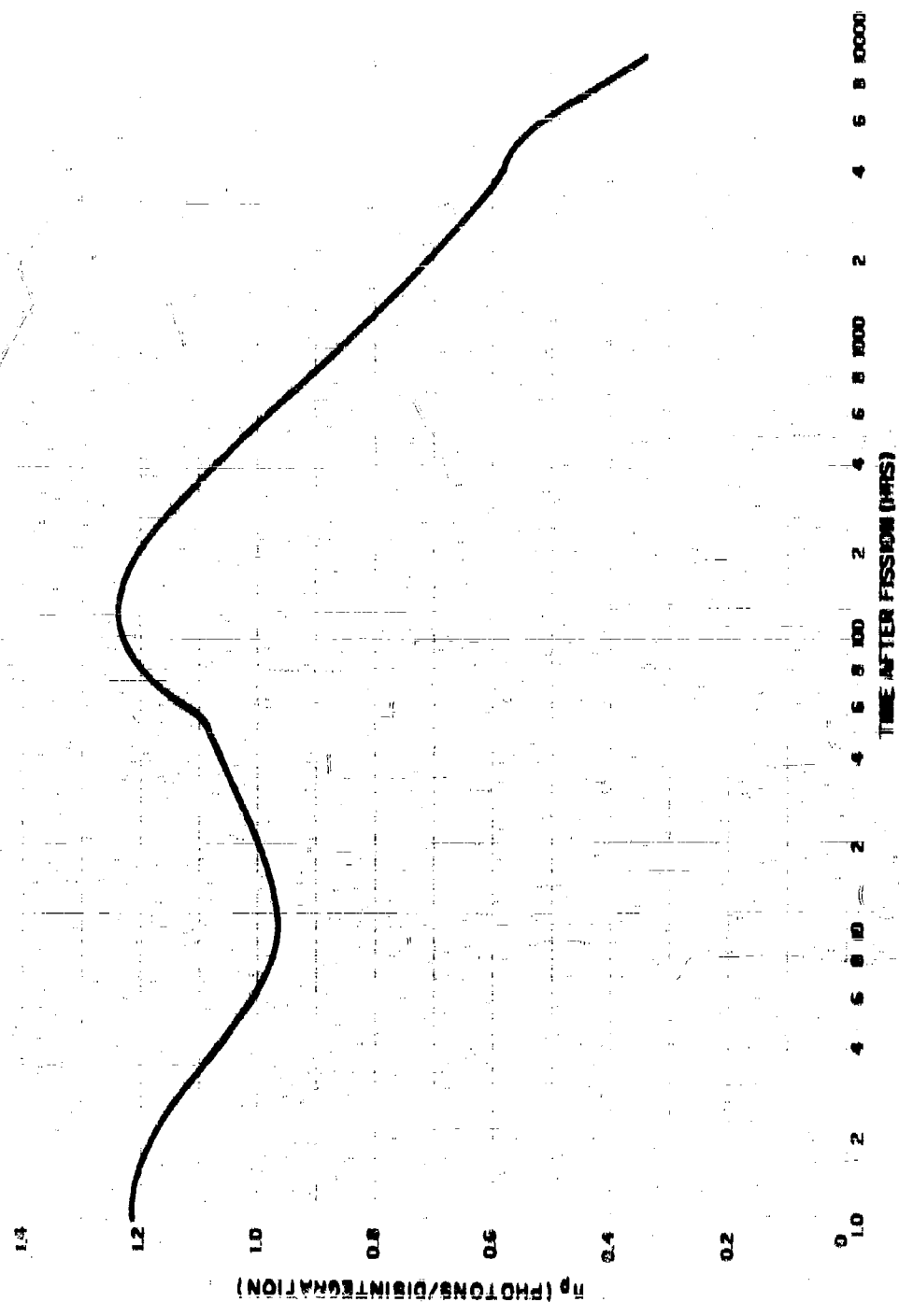
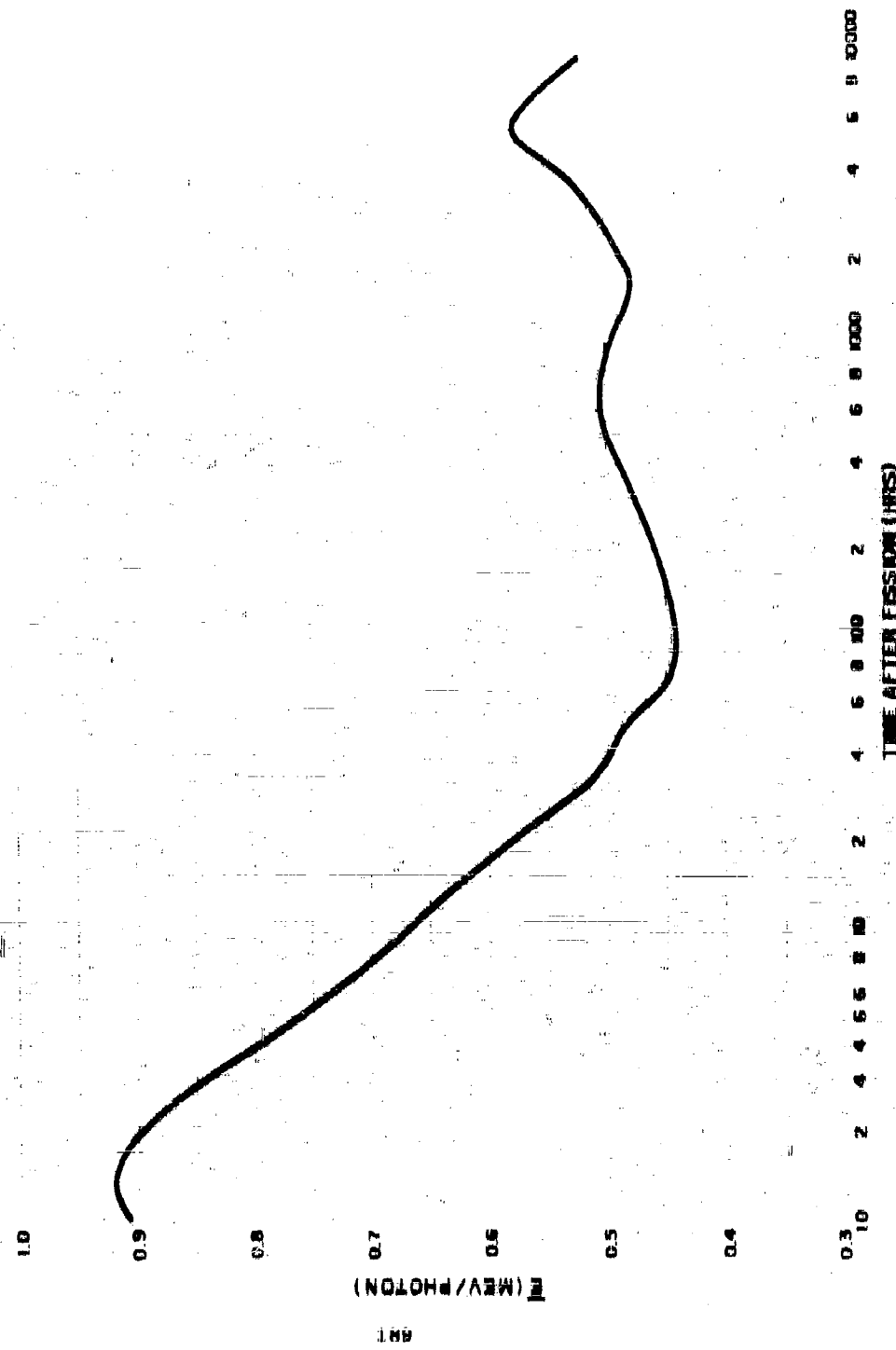


Figure 3.5
AVERAGE ENERGY OF THE PHOTONS FROM THE NORMAL MIXTURE OF FISSION
PRODUCTS FROM 8-MeV NEUTRON FISSION OF U-238



The ratio of the response of an AN/PDR-3B(PIB) radiois held by a man at about 3 feet above a uniform distribution of fission products over a plane area to the calculated site ionization rate is shown in Figure 8.10 as a function of time after fission. The instrument, for the indicated response, is held by a man and is calibrated with a Co-60 standard source.¹⁹ The ratio varies from about 73 to 77 percent; most of the reduction in the ionization rate measured is due to attenuation of the gamma rays by the person holding the instrument and by the batteries and other dense materials near the ion chamber of the instrument.

The only estimates of the ionization rate of mixed fission products at early times after fission available are those for the products of thermal neutron fission of U-235. The data, and calculations of the gamma energy release, from these fission products at early times after fission have been summarized by Zigman and Mackin.²⁰ This summary of the gamma ray abundances is converted to the ionization rates, photon energy emission rate, and average photon energies given in Table 8.19. To adjust the ionization rate values calculated from the data of Zigman and Mackin to those of Table 8.17 at 46.8 minutes, the former were increased by 22.8 percent; this adjustment provides a smooth join of the ionization rate decay curve from the early to the later times.

The computed ionization rates for the fission product elements condensed in the liquid of the ideal cell when it solidifies at 1400°C (end of the first period of condensation) for times of 0 seconds (84-KT) and 60 seconds (14-MT) are given in Table 8.20 for 8-Mev neutron fission of U-235. Also given are the r_{ip} values, with respect to the normal fission-product mixture from thermal neutron fission of U-235. The variation in Figure 8.10 of the computed values of r_{ip} with time after fission shows that the dependence of the fractionation on times of condensation of 0 seconds and 60 seconds (84-KT and 14-MT, respectively) is not large, but that between about 2 hours and 4000 hours after fission the mixture from the lower yield is more highly fractionated.

The minimum in the curve at 2 hours is due to major depletions in Cs and Te, whereas the minimum at about 200 hours is due to depletions in I-131 and Ba-140 - La-140. The maximum in the curve, at 3800 hours, results from the high abundance of Zr-93 - Nb-93, and the peaks at times longer than 10,000 hours are due to the high yields of the rare earth elements from 11-238 fission products with respect to the U-235 fission products.

The observed variation in r_{ip} with time after fission as measured with a standard ionization chamber, is shown in Figure 8.11 for the fallout from a low tower shot.²¹ The observed r_{ip} value at 1 hour after detonation is very close to the values computed for the larger yields and with the exception of some details in the curve that may be due in part to the response characteristics of the ion chamber and, in part, to the type of fission, the calculated curves follow the trend of the observed curve quite well.

Figure 3.9
RELATIVE RESPONSE OF THE AN/UPDR-3775 PORTABLE RADAC HELD BY A MAN AT
3 FEET ABOVE AN EXTENDED PLANE AREA CONTAMINATED WITH FISSION PRODUCTS
FROM THERMAL NEUTRON FISSION OF U-235

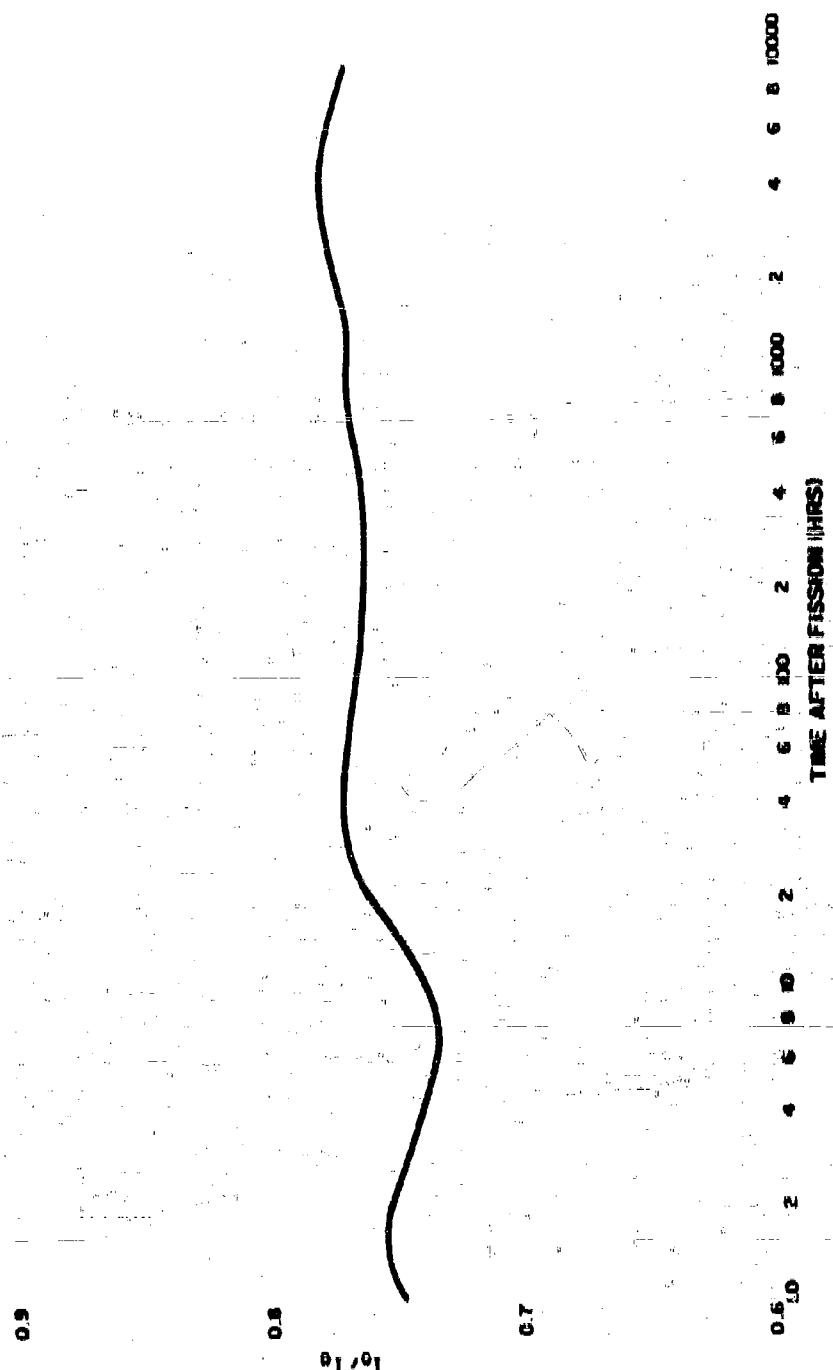


Table 3.10

**EARLY-TIME IONIZATION RATE, PHOTON ENERGY EMISSION RATE,
AND AVERAGE PHOTON ENERGY FOR FISSION PRODUCTS FROM
THERMAL NEUTRON FISSION OF U-235**

Time After Fission (secs)	Air Ionization Rate $(10^{-15} \text{ r hr}) / (\text{fission}/\text{sq ft})$	Photon Energy Emission Rate (MeV/sec) / (10^4 fissions)	Average Photon Energy (MeV/photon)
1	25,800	5,020	1.150
1.5	19,800	3,940	1.178
2	16,800	3,300	1.200
3	12,700	2,580	1.235
4	10,800	2,060	1.262
6	7,530	1,510	1.296
9	2,680	1,060	1.328
13	3,620	768	1.348
19	2,680	541	1.363
28	1,840	368	1.375
41	1,250	252	1.384
60	840	168	1.390
88	580	112	1.393
129	373	74.3	1.390
189	250	49.1	1.378
277	166	32.0	1.355
406	109	20.8	1.308
598	70.2	13.5	1.245
870	48.5	8.65	1.170
1250	33.6	6.42	1.074
1870	17.9	3.29	0.992
2750	10.6	1.92	0.958
4050	6.05	1.24	0.970
5900	4.15	0.776	0.964

Figure 3.10
VARIATION OF $\frac{^{133}\text{I}}{\text{TOTAL}}$ WITH TIME AFTER FISSION FOR THE FRACTIONATED MIXTURE
OF FISSION PRODUCTS FROM BORON NEUTRON FISSION OF U-238



Table 8.20

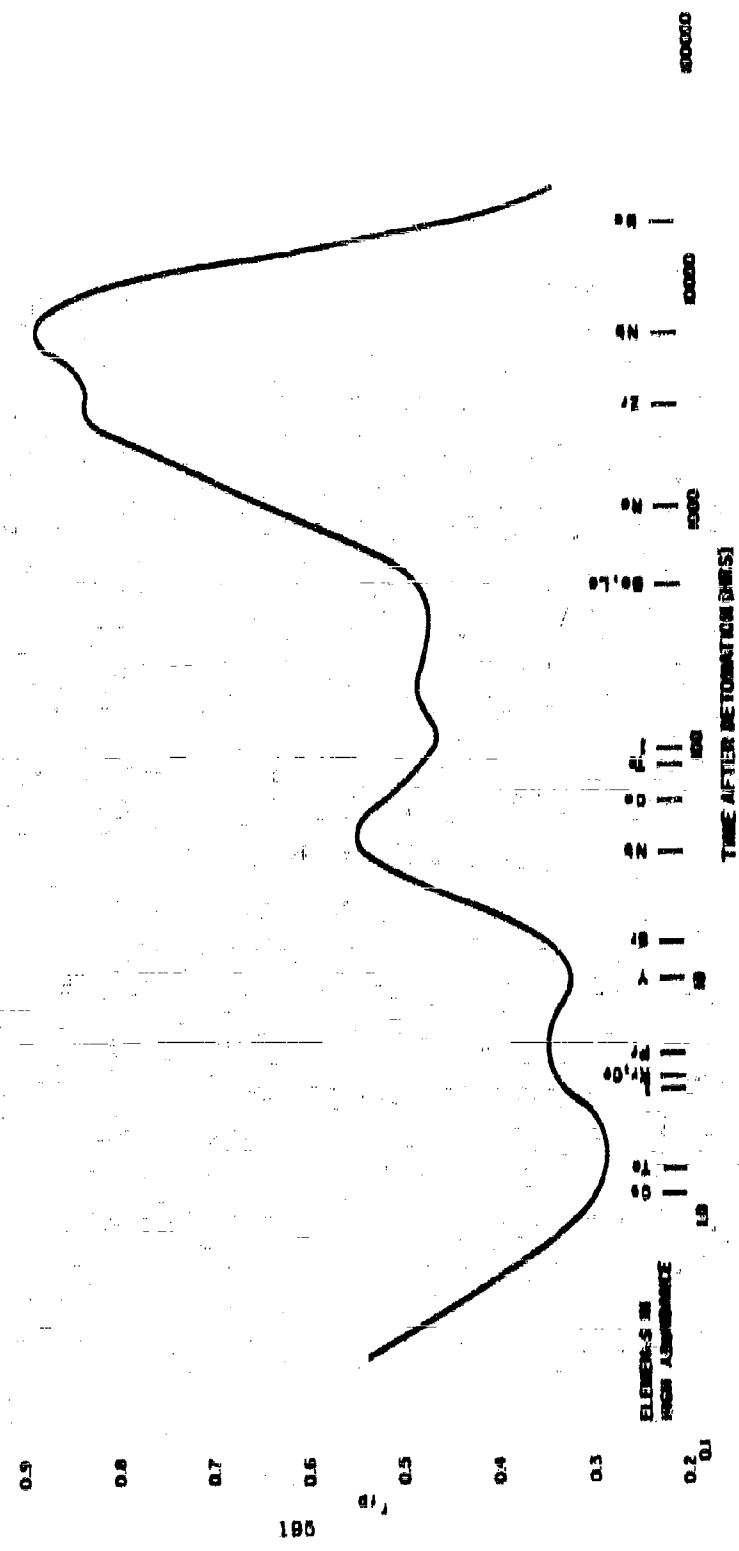
IONIZATION RATE FOR RIBBON PRODUCT CONDENSED ON IDEAL ROLL
 AT 1400°C AT 0 MICRODRIVE (0 KT) AND 60 SECONDS (14-MT)
 AFTER RIBBON FOR 0.58K (0.5 MEV NEUTRON) AND RATIO
 TO THAT FOR THE NORMAL MIXTURE FROM RIBBON
 OF U-235 (THERMAL, NEUTRONIC)

Years	Days	Hours	$\frac{I_{fp}}{I_{fp}^*}$		$\frac{I_{fp}}{I_{fp}^*}$		
			84-KT	14-MT	84-KT	14-MT	
		0.768	(8)871 ^b	(8)845	0.872	0.846	
		1.12	(8)810	(8)820	0.881	0.910	
		1.64	(8)119	(8)118	0.287	0.284	
		2.40	(9)842	(9)867	0.262	0.272	
		3.62	(9)898	(9)429	0.279	0.304	
		5.16	(9)874	(9)818	0.889	0.888	
		7.50	(9)107	(9)881	0.412	0.488	
		11.1	(9)187	(9)181	0.462	0.548	
		16.2	(10)890	(10)102	0.488	0.585	
		23.4	(10)844	(10)589	0.580	0.607	
		34.5	(10)823	(10)887	0.818	0.885	
		48.1	(10)188	(10)189	0.481	0.507	
		63.8	74.8	(11)865	(10)103	0.424	0.455
		4.87	110.	(11)808	(11)891	0.889	0.898
		6.70	161.	(11)889	(11)868	0.268	0.368
		9.82	236.	(11)162	(11)259	0.289	0.382
		14.4	346.	(11)110	(11)191	0.346	0.426
		21.1	500.	(12)823	(11)141	0.288	0.485
		30.8	748.	(12)659	(11)100	0.552	0.551
		45.8	1,087.	(12)498	(12)678	0.469	0.689
		66.4	1,594.	(12)887	(12)455	0.688	0.752
		97.8	2,885.	(12)298	(12)811	0.795	0.846
		143.	5,480.	(12)195	(12)200	0.915	0.922
		208.	4,900.	(12)110	(12)107	0.921	0.905
		301.	7,220.	(12)479	(12)488	0.982	0.995
1.80	455.	10,880.	(12)170	(12)180	1.015	0.992	
1.78	650.	18,600.	(14)877	(14)818	1.480	0.891	
2.60	949.	32,750.	(14)879	(14)128	1.075	0.680	
3.80	1,287.	58,000.	(14)158	(15)599	0.921	0.415	
5.08	2,087.	48,000.	(15)878	(15)284	0.498	0.246	
6.18	2,986.	71,700.	(15)298	(15)161	0.285	0.157	
12.0			(15)194	(15)111	0.300	0.118	
17.8			(15)158	(15)807	0.160	0.087	
25.7			(16)984	(16)607	0.180	0.086	

a. r^2/hr at 8 ft above an infinite smooth plane for 10^4 fissions per sq ft.

b. Number in parenthesis is number of decimal points between decimal point and first digit (see Figure 3.21).

Figure 3.11 VARIATION OF r_{γ} WITH TIME AFTER FISSION FOR CLOSE-IN FALLOUT
DESERVED FROM A LOW TOWER SHOT AT THE NEVADA TEST SITE



For an r_{10} of 38 percent at H+1, the ionization rate at 1 hour per KT per sq mi, would be 1100 for the mixture of fission products condensed up to the indicated times. If the fallout also contained neutron-induced activities that contribute at H+1, the ratio would be higher. The important likely (or possible) induced activities are those produced from neutron captures by U-238 as was found by Kimura⁷, Mackin⁸, Fretling⁹ and also reported by Stewart, Crooks and Fischer¹⁰.

The activities and ionization rates of the possible product nuclides, for a yield of 10^4 atoms at zero time and up to 100 days later, are summarized in Tables 8.21 to 8.24. For the case in which the tabulated activities are associated with the activities from 10^4 fissions, they are equivalent to a yield of one product-nuclide for each fission. Thus, for the case where one of the neutrons from each fission event results in a (n, γ) reaction with U-238, the ionization rate from the products U-239 and Np-239 at H+1 would be 0.857×10^{-10} r/hr per fission or about 180 r/hr per KT/sq mi. The ratio for the gross mixture is then 1870 r/hr at 1 hour per KT/sq mi.

If the relative yield of U-237 was that found by Kimura⁷, namely 0.15 atoms per fission, the additional activity at H+1 would be 0.0020×10^{-10} r/hr per fission or about 1 r/hr per KT/sq mi. A yield of 0.15 atoms per fission of U-240, however, would give a contribution at H+1 of about 20 r/hr per KT/sq mi. If this occurred, the ratio for the mixture would be 1900 r hr at 1 hour per KT/sq mi. The observed ratio for this mixture of radionuclides in fallout particles on an open real terrain would be less than this value, due to both the instrument response mentioned above and to shielding by the roughness of the terrain. If it is assumed that the instrument response to the final mixture is about the same as it is for the normal mixture of fission products, then a value of about 70 percent (see Figure 2.0) would be appropriate for the AN/PDR-50(TIB) or similar radiac instrument. An effective terrain attenuation of 75 percent with respect to the ideal smooth plane would give an observed value for the ratio of about 780 r/hr at 1 hour per KT/sq mi. This is lower than the value, 1840, obtained from the data of the ENW.

Additional discussions of how the condensation process may proceed at times longer than the end of the first period of condensation, and of how the radionuclide composition can vary with particle size and downwind distance, are given in Chapter 6.

Table 8.21
ACTIVITY FROM U-237 FOR 10⁴ ATOMS AT ZERO TIME^a
 $C(U-237) = 1$

Time After Fission	Λ (d/a)	I_a (r/hr $\times 10^6$)	I_o (r/hr $\times 10^6$)	$D_a(1)$ (r $\times 10^6$)
1h	(1)1183 ^b	(1)1880 ^b	(2)087 ^b	0
1.5h	(1)1181	(1)1880	(2)086	(2)000 ^b
2h	(1)1178	(1)1880	(2)082	(1)188
3h	(1)1178	(1)1880	(2)048	(1)207
4h	(1)1168	(1)1880	(2)044	(1)400
6h	(1)1158	(1)1810	(2)030	(1)644
8h	(1)1148	(1)1800	(2)028	(1)988
10h	(1)1138	(1)1888	(2)020	0.1180
12h	(1)1120	(1)1278	(2)913	0.1400
15h	(1)1114	(1)1201	(2)901	0.188
18h	(1)1100	(1)1245	(2)880	0.210
24h	(1)1072	(1)1210	(2)807	0.298
1.5d	(1)1018	(1)1168	(2)801	0.486
2d	(2)908	(1)1000	(2)780	0.570
3d	(2)873	(2)688	(2)700	0.821
4d	(2)780	(2)600	(2)658	1.040
6d	(2)640	(2)724	(2)618	1.400
8d	(2)520	(2)602	(2)420	1.740
10d	(2)426	(2)481	(2)844	2.005
15d	(2)264	(2)247	(2)206	2.407
20d	(2)158	(2)178	(2)180	2.788
30d	(2)647	(2)610	(2)448	2.087
40d	(2)108	(2)281	(2)100	2.040
60d	(4)252	(4)280	(4)204	0.190
80d	(5)828	(5)800	(5)201	0.180
100d	(8)414	(4)408	(8)808	0.108

- a. I_a , I_o and $D_a(1)$ are for the distribution of 10⁴ atoms per square foot over an infinite plane at zero time. I_a is in air ionization rates, I_o is in instrument response units.
- b. Number in parentheses is number of zeros between decimal point and first digit.

Table 8.32
ACTIVITY FROM U-238 FOR 10^4 ATOMS AT ZERO TIME^a (U-238) — 1

Time After Pluton	Λ (d/s)	I_a (r/hr $\times 10^6$)	I_n (r/hr $\times 10^6$)	$D_n(1)$ (e $\times 10^6$)
1h	0.0065	0.0040	0.1700	0
1.5h	0.0485	0.18202	(1)740	0.1680
2h	0.1420	(1)5603	(1)817	0.1627
3h	(1)240	(2)042	(2)522	0.1775
4h	(2)410	(2)180	(2)868	0.1830
6h	(3)120	(4)470	(4)202	0.1830
8h	(5)004	(5)120	(5)718	0.1830
10h	(0)161	(7)000	(7)217	0.1830
12h				0.1830
15h				0.1830
18h				0.1830
24h				0.1830
1.0d				0.1830
2d				0.1830
3d				0.1830
4d				0.1830
6d				0.1830
8d				0.1830
10d				0.1830
15d				0.1830
20d				0.1830
30d				0.1830
40d				0.1830
60d				0.1830
80d				0.1830
100d				0.1830

a. I_a , I_n , $D_n(1)$ are for the distribution of 10⁻⁴ atoms per square foot over an infinite plane at zero time.

b. Number in parentheses is number of zeros between decimal point and first digit.

Table 3.23
ACTIVITY FROM NP-239 FOR 10^4 ATOMS OF U-239 AT ZERO TIME^a
 $C(U-239) = 1$

Time After Fission	Λ (d/s)	I_{α} (r/hr $\times 10^6$)	I_{β} (r/hr $\times 10^6$)	$D_{\alpha}(1)$ (r $\times 10^6$)
1h	(1)8870 ^b	(1)8107 ^b	(1)8270 ^b	0 ₆
1.5h	(1)8182	(1)8541	(1)2618	(1)108
2h	(1)8288	(1)8050	(1)2897	(1)349
3h	(1)8023	(1)8008	(1)2620	(1)714
4h	(1)8204	(1)8044	(1)2600	0.1084
6h	(1)8216	(1)8570	(1)2040	0.1808
8h	(1)8307	(1)8401	(1)2477	0.2512
10h	(1)8060	(1)8400	(1)2417	0.020
12h	(1)2084	(1)8321	(1)2357	0.087
15h	(1)2877	(1)8202	(1)2278	0.486
18h	(1)2700	(1)8081	(1)2187	0.570
24h	(1)2573	(1)8808	(1)2082	0.707
1.5d	(1)2213	(1)8405	(1)1780	1.077
2d	(1)1910	(1)8125	(1)1500	1.001
3d	(1)1410	(1)1570	(1)1121	1.791
4d	(1)1084	(1)1174	(2)800	2.122
6d	(2)683	(2)648	(2)400	2.546
8d	(2)822	(2)658	(2)204	2.787
10d	(2)178	(2)108	(2)141	2.010
15d	(2)402	(2)447	(2)818	3.002
20d	(4)011	(2)101	(4)710	0.002
30d	(6)407	(6)510	(6)800	0.007
40d	(6)840	(6)807	(6)100	0.008
60d				0.008
80d				0.008
100d				0.008

a. I_{α} , I_{β} , and $D_{\alpha}(1)$ are for the distribution of 10^4 atoms per square foot over an infinite plane at zero time.

b. Number in parenthesis is number of zeros between decimal point and first digit.

Table 3.24

ACTIVITY FROM Np-230 FOR 10^4 ATOMS OF U-230 AT ZERO TIME^a
 $(\text{U-230}) = 1$

Time After Emission	Λ (d/s)	I_{α} (r/hr ² $\times 10^6$)	I_0 (r/hr $\times 10^6$)	$D_a(1)$ (r $\times 10^6$)
1h	0.1307	0.2705	0.2007	-0
1.5h	0.1270	0.2647	0.2002	0.184
2h	0.1244	0.2588	0.2002	0.205
3h	0.1180	0.2401	0.1997	0.518
4h	0.1131	0.2041	0.1845	0.758
5h	0.1080	0.1924	0.1645	1.212
8h	(3)028 ^b	0.1021	0.1489	1.611
10h	(3)843	0.1744	0.1982	1.978
12h	(1)760	0.1570	0.1224	2.812
15h	(1)668	0.1602	0.1055	2.754
18h	(1)569	0.1177	(1)019 ^b	8.130
24h	(1)424	(1)878 ^b	(1)680	8.780
1.5d	(1)200	(1)480	(1)377	4.847
2d	(1)100	(1)200	(1)208	4.080
3d	(2)400	(2)898	(2)642	5.372
4d	(2)123	(2)384	(2)107	6.484
6d	(3)116	(3)240	(3)180	6.680
8d	(4)110	(4)227	(4)170	6.680
10d	(5)104	(5)210	(5)167	6.688
15d	(8)986	(8)582	(8)489	6.688
20d				6.688
30d				6.688
40d				6.688
60d				6.688
80d				6.688
100d				6.688

a. I_{α} , I_0 , and $D_a(1)$ are for the distribution of 10^4 atoms per square foot over an infinite plane at zero time.

b. Number in parentheses is number of zeros between decimal point and first digit.

CHAPTER 3 REFERENCES

1. Stewart, K., *Trans. Faraday Soc.*, **52**, 101 (1956).
2. Kelley, K. K., *Contributions to the Data on Theoretical Metallurgy, XIII: High Temperature Heat-Content, Heat-Capacity, and Entropy Data for the Elements and Inorganic Compounds*, U.S. Bureau of Mines, Bulletin 584, 1960.
3. Still, D. R., and G. C. Sinko, *The Thermodynamic Properties of the Elements*, Am. Chem. Soc., Washington, D.C., 1956.
4. Lapple, C. E., *Fallout Control*, Stanford Research Institute, SRIA-8, 1958.
5. Adams, C. E., N. H. Farlow, W. R. Schell, *The Compositions, Structures, and Origins of Radioactive Fallout Particles*, USNRDL-TR-208, 1958.
6. Miller, C. F., *Analysis of Fallout Data, I: The Jangle "S" and "U" Shot Fallout Patterns*, USNRDL-TR-220, Del., 1958.
7. Kimura, Kenjiro, *Geneva Conference on the Peaceful Uses of Atomic Energy*, **2**, 190 (1950).
8. Mackin, J., P. Zigman, D. Love, D. McDonald, and D. Bam, *J. Inorg. Nucl. Chem.*, **15**, 20 (1960).
9. Coughlin, J. P., U.S. Bureau of Mines, Bulletin 549, 1954.
10. Bolles, R. G., and N. E. Ballou, *Calculated Abundances of U-235 Fission Products*, USNRDL-456, 1956.
11. Kalcoff, Seymour, *Nucleonics*, **10**, 4, 75 (1958).
12. Miller, C. F., and P. Loeb, *Ionization Rate and Photon-Pulse Decay of Fission Products from the Slow Neutron Fission of U-235*, USNRDL-TR-247, 1958.
13. Dolan, P. T., *Calculated Abundances and Activities of the High Energy Neutron Fission of Uranium-238*, DASA-525, 1959.
14. Dolan, P. T., *Gamma Spectra of Uranium-238 Fission Products at Various Times after Fission*, DASA-526, 1959.

16. Knupp, H. A., Oral Defense Hearings before a Subcommittee of the Committee on Government Operations, U.S. Congress, External Gamma Doses and Dose Rates from the Fallout from Nuclear Detonations, 1960.
16. Lapp, Ralph E., Local Fallout Radioactivity, Bulletin Atomic Scientists, XV, 5, 181, 1959.
17. Perkins, J. F., and R. W. King, Energy Release from the Decay of Fission Products, Nuclear Sci. and Eng., 9, 780, 1961.
18. Knabe, W. B., and G. E. Putnam, The Activity of the Fission Products of U-235, General Electric Co., APENX-44B, 1958.
19. Zigmahn, P., and J. Mackin, Early Time Decay of Fission Products, Health Physics, 5, 79, 1961.
20. Strope, W. B., Evaluation of Countermeasure System Components and Operational Plumbbob, WT-1464, 1968.
21. Stewart, N. G., R. N. Crooks, E. M. R. Fischer, Hearings of the Joint Committee on Atomic Energy, U.S. Congress, The Nature of Radioactive Fallout and Its Effects on Man, p.1600, June 1957.
22. Freiling, E. O., Fractionation Correlations, USNRDL-TR-980, 1960.

Chapter 4

DISTRIBUTION OF FALLOUT PARTICLES FOLLOWING A NUCLEAR DETONATION

4.1 General Description of The Fallout Distribution Process

4.1.1 The Particle Source Geometry

A very simple descriptive statement of the fallout process might be that a cloud of particles is formed rapidly as the result of an explosion and that this cloud is then dispersed by the wind and by the force of gravity acting on the particles to return them to the earth. Most investigators concerned with the distribution of fallout assume that the visible volume occupied by the nuclear cloud and stem above the point of detonation within a few minutes after explosion more or less defines the volume source of the fallout particles¹.

Anderson², however, considers a moving source volume which might be described as the air volume swept through by the rising fireball and stem. In either case the source volumes for the particles depend on total yield and, if other than surface detonations are considered, on the height or depth of burst. The yield dependent parameters which are used to define the particle source geometry include the cloud height, cloud thickness and radius, and, occasionally, the stem geometry. Anderson's studies include consideration of the time dependence of these parameters.

One important additional factor that is usually considered is the distribution, or spatial concentration, of the particles in the volume, and quantitative considerations have been given to internal circulations of the particles by several investigators.³

4.1.2 The Particle Fall Trajectory

The fall trajectory of a particle depends on its own properties and on meteorological factors. The various aspects of these factors have been discussed by Neuhert,⁴ Anderson² and others⁵. The major properties that influence a particle's fall rate through the atmosphere are its density, diameter or size, and shape. The major meteorological factors are the wind speed and direction, and the air density and viscosity.

The two air properties, of course, are dependent on the air pressure and temperature and these, in turn, change with altitude. The wind speed and direction are also highly variable quantities since each has both spatial and time variations. The vertical motions of the air and particle-group diffusion can influence the fall trajectory of particles, but are usually not taken into account in the study of the fallout distribution process.

4.1.3 Radiological Factors

The major radiological factors in the fallout distribution process are the fission yield and the variation with particle size of the gross radioactivity carried by particles of a given size. The first essentially determines the total radioactivity available for distribution on the particles; the second involves the distribution of that radioactivity among particles of different sizes.

Additional factors, such as neutron induced radioactivity, fractionation, and the biological availability of single fission-product elements, have not yet been incorporated into studies of the fallout distribution process in a systematic way by most investigators and fallout model designers.

4.2 Mathematical Descriptions of the Fallout Distribution Process

4.2.1 Scaling Methods

The original attempt to describe and/or predict the end result of the fallout distribution process--the fallout pattern--was made by C.F. Knandt and coworkers in 1955³. The original scaling method was based on the work of Laurino and Poppoff⁶ which described some fallout patterns from Operation Jangle in 1951 from low yield devices. The original scaling method was intended for predictions or estimates of fallout patterns from yields possibly as high as 10-KT. In 1958⁷ the method was expanded to include yields in the megaton range, without adequate explicit experimental documentation. This method was subsequently included in ENW.⁸ In some studies of fallout effects a scaling system is to be preferred over a complex mathematical model. Therefore, a scaling method for estimating fallout patterns is described in Section 4.3.

4.2.2 Mathematical Models

Mathematical models attempt to establish quantitative values for the several factors mentioned in Section 4.1 and to compute the activity deposited on the ground at various locations usually with use of electronic computers. The general approach used and the organizations and investigators involved in the

development and testing of these models up to 1957 is described in some detail by Kellogg.¹ Later developments include the work by Anderson,^{1,6} by Hugh and Galliano,¹⁷ by Callahan, et al.¹⁸ and by Rapp,¹⁹ to mention a few of the unclassified reported studies. A general comment on the results might be that none of the models agree with each other in several details, and that none of the models reproduce very accurately all of the few data in the yield range of 1-KT to 10-MT that are experimentally available.

The exact causes of the differences among the various models are difficult to isolate for at least two reasons: 1. Each model is different from any other in several of its assumptions about parameter values or in its manner of handling the many variables mathematically. 2. The reports describing the models generally do not include sufficient detailed information regarding the minor assumptions and the methods used in making the computations. If the input data in the mathematical models were all more reliably established experimentally, many of the differences among them would disappear. Whether better agreement with observations resulted would still have to be established.

Nonetheless, many of the features of the mathematical models are used in Section 4.3 which describes the derivation of a simplified scaling method. A few of the parameter values used in several of the mathematical models are discussed there to better describe the over-all process of fallout distribution as it might take place. In Chapter 6 some general concepts are described that could be utilized to derive a more refined mathematical model of fallout than is presently available. Some possible improvements in the treatment of the problem are also touched upon in this chapter.

In most mathematical models, after selecting the values of the source geometry, trajectory, and radiological factors, the computation is carried out by dividing the source geometry for each of several particle size ranges into horizontal discs of finite thickness. The location on the ground where these "particle discs" land, under the influence of the specified meteorological conditions, is then calculated. All the activity at each of a series of coordinate points is then summed, according to the number of different discs that land at the point and the amount of activity assigned to each disc.

No short summary of the work on the mathematical models should not be interpreted to mean that the efforts in the development of the mathematical models have been small and unfruitful. On the contrary, much has been learned about the fallout process through them, and most of the concepts employed by many of the mathematical model developments are covered in the remainder of this chapter. But to describe all the work and all the details of each model currently in use is not considered to be within the scope of this discussion.

4.3 Descriptive Features of a Simplified Fallout Scaling System for Land Surface Detonations

4.3.1 General Description of the Scaling Method

The fallout scaling system described here was developed for estimating standard intensities, potential exposure doses, and other radiological quantities by use of both manual and machine computational techniques. The system is based on corrected experimental data, on empirical relationships among the geometrical arrangement of the cloud and stem as the source of fallout particles, and on several of the observed features of the fallout pattern of radiation intensities on the ground. In the system, the cloud and stem dimensions are stylized as simple solid geometric configurations to facilitate the use of algebraic relationships among the model parameters and the dependence of the parameter values on weapon yield.

In making estimates of the hazards from fallout, for the purpose of establishing the nature and required degree of protection against these hazards, two major quantities requiring evaluation are (1) the exposure dose levels that can result at different distances from the detonation, and (2) the land surface areas in which the exposure dose is greater than a stated amount. To make these evaluations requires estimates of the amount of fallout that deposits at various locations, the time at which the fallout arrives, and the rate of its arrival.

Such general evaluations of hazard levels, and of the protection requirements for radiological countermeasures in defense planning, must first consider the possible levels of effect (or hazard) and, in a generalized manner, the feasibility of methods for protecting against these levels of possible hazard. For these purposes a rather simplified fallout scaling system can serve because no precise or accurate prediction of fallout under specified detonation and wind conditions is possible even with the most complicated fallout models at their present stage of development. Therefore in the following discussion the presentation is limited to the description of a simplified version of the fallout distribution process.

The mathematical derivations of the simplified fallout scaling system attempt to depict the fall of particles of different size-groups from a volume source in the air; the boundaries of that source are assumed to depend only on weapon yield. The problem is to describe mathematically the dependence of the fallout pattern features, in space and time, on—(a) the cloud and stem geometry, (b) the particle fall velocities, (c) the wind velocity, (d) the radionuclivity-particle size distributions, and (e) the weapon yield.

The geometrical configuration of the cloud is taken to be an oblate spheroid, and the configuration of the stem as the frustum of an exponential cone or horn whose larger base is approximately adjacent to the bottom of the spheroid. The fall of particles from each of these source volumes is considered separately.

4.3.2 Particles Falling from Cloud Altitudes

The descriptive equations for fallout from cloud altitudes are based on the following premises:

1. The cloud source of the particles (at about H+0 minutes to H+8 minutes after detonation) has the shape of an oblate spheroid where a is the major axis (parallel to the earth's surface) and b is the minor axis.
2. The particles of a given size-parameter, α , fall with a constant terminal velocity vector, v_t , from their position in the cloud to the ground.
3. The wind velocity, v_w , is constant with time and space through all altitudes from the ground to the top of the cloud.
4. The initial distribution of the particles of each size-parameter inside the cloud is uniform.
5. The fractional distribution of the total activity on each particle group can be determined from fallout pattern data as a function of that group's fall velocity parameter.

The outer dimensions of the cloud, according to the first premise, are defined by

$$\frac{x^2}{a^2} + \frac{y^2}{b^2} + \frac{z^2}{h^2} = 1 \quad (4.1)$$

where the origin of the x , y , z coordinate system is directly over ground zero at the altitude, h , at the center of the cloud.

A particle originating at the point x_0, y_0, z in the cloud moves along a line of slope, v_t/v_w , and lands on the ground at the downwind distance, X_t , given by

$$X_t = \alpha(h + u)^{1/2} s \quad (4.2)$$

where α is equal to v_w/v_t (v_w is independent of v_t).

The number of particles with a given value of α that fall at the downwind distance, X_t , from ground zero, for a uniform distribution in the cloud, are proportional to the length of the line given by Eq. 4.2 contained within the cloud. The total number of particles having size-parameter α is an $n_{\alpha} L \Delta t^2$, where n_{α} is the number per unit volume, L is the length along the line of fall in the cloud, and Δt^2 is the cross-sectional area along the line.

The area on the earth's surface intercepted by Δt^2 is $\Delta t \Delta X$ (Δt in y direction) such that

$$\Delta X = \sqrt{(1 + \alpha^2)} \Delta t \quad (4.3)$$

The number of particles per unit area at X_t is then

$$N_x = \frac{n_{\alpha} L}{\sqrt{1 + \alpha^2}} \quad (4.4)$$

Similarly, A_n is the activity per unit volume of cloud carried by the particles having the inverse fall velocity, or size-parameter, α . The amount of activity per unit area at X_t contained in the group is

$$\Lambda_x(\alpha) = \frac{A_n L}{\sqrt{1 + \alpha^2}} \quad (4.5)$$

where $\Lambda_x(\alpha)$ is the activity per unit area on the ground at the distance, X_t , that is carried by the particles having the size-parameter α .

The value of L is determined from the two intercepts of the line given by Eq. 4.2 with the spheroid described by Eq. 4.1 by use of

$$L^2 = \Delta x^2 + \Delta z^2 \quad (4.6)$$

Solving Eq. 4.6 for Δx and Δz given

$$\Delta x = \frac{4\alpha^2 b^2 (1 + \alpha^2) - [(a^2 + \alpha^2 b^2)(1 - v^2/a^2) - (X_t - \alpha h)^2]}{(a^2 + \alpha^2 b^2)^2} \quad (4.7)$$

The activity per unit area on the ground, $A_x(a)$, is then

$$A_x(a) = \frac{2\Delta_{\alpha}ab \sqrt{(a^2 + a^2 b^2)(1 - y^2/a^2) - (X - ah)^2}}{(a^2 + a^2 b^2)} \quad (4.8)$$

The activity contours on the ground surface for a given value of a therefore are ellipses; Eq. 4.8, in standard elliptical form, is

$$\frac{(X - ah)^2}{(a^2 + a^2 b^2) \left[1 + \frac{\Delta_x^2(a)(a^2 + a^2 b^2)}{4\Delta_{\alpha}^2 a^2 b^2} \right]} + \frac{y^2}{a^2 \left[1 + \frac{\Delta_x^2(a)(a^2 + a^2 b^2)}{4\Delta_{\alpha}^2 a^2 b^2} \right]} = 1 \quad (4.9)$$

The centers of the ellipses are at X equal to ah and at y equal to 0.

The total activity per unit area deposited at the location X, y (y is taken as the same lateral dimension on the ground as it is in the cloud) is determined by summing the contributions from all possible values of a ; it is given by

$$A_x = \int_{a(\min)}^{a(\max)} A_x(a) da \quad (4.10)$$

where $a(\max)$ and $a(\min)$ are given by the two respective values of

$$a_m = \frac{hX + \sqrt{X^2 b^2 (1 - y^2/a^2) + (a^2 - y^2) h^2} - b^2 (1 - y^2/a^2)}{h^2 + b^2 (1 - y^2/a^2)} \quad (4.11)$$

Equation 4.10 can be integrated graphically if the values of Δ_{α} and the other parameters are provided. From the data given by Pugh and Gallopo¹⁰ and by Schuert¹¹, the following empirical scaling functions were derived for the yield-dependent parameters of the above equations:

$$a = 2.34 \times 10^3 W^{0.431} ft, \quad W = 1-KT \text{ to } 10^6-KT \quad (4.12)$$

$$b = 1.40 \times 10^3 W^{0.300} ft, \quad W = 1-KT \text{ to } 10^6-KT \quad (4.13)$$

$$h = 0.60 \times 10^4 W^{0.445} ft, \quad W = 1-KT \text{ to } 28-KT \quad (4.14)$$

$$h = 1.68 \times 10^4 W^{0.164} ft, \quad W = 28-KT \text{ to } 10^6-KT \quad (4.15)$$

An approximation method for estimating A_{α} can be derived from information on the final fallout pattern itself. From Eqs. 4.12 and 4.13, the cloud volume for the ellipsoid of revolution about the minor axis is

$$V_p = 3.21 \times 10^{10} W^{1-10^8} \text{ cu. ft., } W = 1-\text{KT to } 10^8-\text{KT} \quad (4.16)$$

If the fraction of the total activity associated with the particles having the inverse falling velocity α is f_{α} , and those particles are uniformly distributed throughout the volume, then A_{α} is equal to $f_{\alpha} A_p / V_p$, where A_p is equal to $1.4 \times 10^{10} g_e$ BW fractions (B here is the ratio of the fission to total yield; g_e is the fraction of the total activity produced that is contained in the cloud; and W is the total yield in KT). The value of A_{α} is then given by

$$A_{\alpha} = 4.36 \times 10^{14} f_{\alpha} g_e BW^{0-10^8}, \quad W = 1-\text{KT to } 10^8-\text{KT} \quad (4.17)$$

where the dependence of g_e and f_{α} on W is unspecified.

From arbitrary distributions of A_{α} and from evaluations of $A_x(\alpha)$ and the difference, $\alpha_{\max} - \alpha_{\min}$, from Eq. 4.11, it was noted that (1) the difference, $\alpha_{\max} - \alpha_{\min}$, generally is not large, and (2) the maximum value of $A_x(\alpha)$ generally occurs near the value of α that is equal to X/h (designated here as α_0). The first estimate of the A_{α} values is obtained from experimental knowledge (or estimates) of A_x along the line $y = 0$ from field test data, and from the assumption of a constant value of $A_x(\alpha)$ evaluated at α_0 as a rectangular step function between α_{\min} and α_{\max} . With this approximation Eq. 4.16 becomes

$$A_{\alpha} = A_x(\alpha_0) (\alpha_{\max} - \alpha_{\min}) \quad (4.18)$$

Substituting X/h for α in Eqs. 4.8 and 4.11 gives

$$A_x(\alpha_0) = \frac{2 \pi b h A_x}{\sqrt{a^2 h^2 + b^2 X^2}} \quad (4.19)$$

and

$$\alpha_{\max} - \alpha_{\min} = \frac{2 \sqrt{b^2 X^2 + a^2 (h^2 - b^2)}}{(h^2 - b^2)} \quad (4.20)$$

so that Eq. 4.18 becomes, when solved for A_{α} ,

$$A_{\alpha} \approx \frac{(h^2 - b^2) A_x}{4 \pi b h \sqrt{1 - \frac{b^2}{h^2} + \frac{X^2}{a^2}}} \quad (4.21)$$

For all values of the constants, and for reasonable values of X, the value of the radicant in Eq. 4.21 is between 0.05 and 1.00, so that, within less than 5 percent,

$$A_x \approx \frac{(h - b)(h + b)}{4\pi b^2} A_x \quad (4.22)$$

The relationship between A_x and the observed intensity, $I_x(t)$, is discussed in Section 4.8.5.

4.8.3 Particles Falling from Stem Altitudes

The source volume for particles falling from the stem is described, in outline, by a figure that is circular in the plane parallel to the ground but whose radius increases exponentially with altitude. The lower radius is equal to that of the fireball (R_b) at the time the fireball leaves the ground; the height at this point is also R_b . The stem radius at the height, b , is the same as that of the cloud at full expansion. This geometry portrays a particle source volume that expands laterally, with increasing altitude as well as with fireball rise and expansion, until it forms the characteristic cloud. The entire volume or space through which the fireball (or cloud) passes in its rise is considered to be the source volume of the fallout particles from the stem.

The assumptions used for the model are listed below; some discussion of these assumptions is given in the following text. Many fundamental difficulties in the fallout models and in the basic understanding of fallout formation and its distribution could be removed if more information were available on the processes that actually occur during the cloud rise.

The descriptive equations for the fallout from the stem altitudes are based on the following assumptions:

1. The stem source of particles has the shape of an inverted exponential horn.
2. The spherical exponential horn-shaped volume has a radius, R_b , at the height R_b , and a radius, a , equal to the cloud radius at the height b .
3. The particle fall velocity vector, v_f , wind velocity, v_w , and their ratio, the particle size-parameter, α , are the same as for particles falling from cloud altitudes.

4. The volume and shape of the cloud, as it rises, are specified by the major radius (defined in 2 above) and a minor radius that also increases exponentially with altitude from R_0 , at the height R_0 , to the cloud half-thickness, b , at the height h .
5. To make hand computations feasible, the particles having a given value of α in the cloud volume at a given altitude are assumed to be concentrated on a horizontal plane through the center of the cloud volume.
6. The particles rise with a velocity that is equal to or greater than the rate of rise of the center of the cloud; they begin to fall earthward from the altitude at which their fall velocity (due to gravity forces) equals the rate of rise of the mass of air surrounding the particles. This altitude is assumed to be located in the region near or below the bottom of the rising cloud. Together with assumption 5, this assumption specifies that particle groups with a given value of α fall only from one altitude or altitude increment. Therefore the size-segregation with altitude, as described, is somewhat similar to that of an ideal fluidized bed of particles.
7. Particles having the same value of α fall in the downwind direction along the length of a high-intensity ridge near ground zero. The diameter of the stem at the altitude of origin of this group of particles is then equal to the length of the ridge.

The mathematical model for the shape of the volume of air that is swept out by the rising cloud is based on thermodynamic equations for the adiabatic expansion of an ideal gas, including a term for the change in free energy with altitude, and assuming that the external pressure is proportional to $\exp(-mgz/kT)$. In this stem-model approximation for the rising cloud (in which the number of moles of gas in the volume is increasing) only the exponential form of the equation is retained for empirical fit to the data. The volume of the stem is then represented by

$$V_s = V_{s0} e^{k_v z} \quad (4.20)$$

where V_{s0} and k_v are determined from a known volume at a minimum of two altitudes.

Since the stem volume must have the same shape as the cloud volume at full expansion, namely an elliptical spheroid of revolution about the z axis, the major semi-axis of the stem volume may be written as

$$a_x = a_0 e^{k_x h} \quad (4.24)$$

and its minor semi-axis as

$$b_x = b_0 e^{k_b h} \quad (4.25)$$

where V_0 is equal to $(4/3)\pi a_0^2 b_0$ and k_y is equal to $2k_x + k_b$.

The values of a_0 , k_x , b_0 , and k_b are determined from

$$\log a_0 = \log a - \frac{h \log a/R_s}{h - R_s} \quad (4.26)$$

$$k_x/2,303 = \frac{\log a/R_s}{h - R_s} \quad (4.27)$$

$$\log b_0 = \log b - \frac{h \log b/R_s}{h - R_s} \quad (4.28)$$

and

$$k_b/2,303 = \frac{\log b/R_s}{h - R_s} \quad (4.29)$$

Values of the stem and fireball-cloud geometry constants for several yields are listed in Table 4.1. The outer dimensions of the stem are defined by

$$x^2 + y^2 = a_x^2 \quad (4.30)$$

for which the center of the coordinate system is at surface zero.

The particle fall and accumulation equations for the stationary cloud could be used for the rising cloud in estimating the α groups arriving at a given downwind location. However, such computations would require the use of an electronic computer, and the more complicated treatment would not necessarily improve the accuracy of estimator ratio by using the simpler computation. These mathematical complications are eliminated when it is assumed that all the particles falling from the rising fireball or cloud are concentrated at the horizontal plane through its center. This assumption also eliminates spool-flection, except for the height, of the point of origin within the stem for any α group arriving at a particular point on the ground surface. If the α values for

Table 4.1
VALUES OF STEM AND FIREBALL-CLOUD CHROMATRY CONSTANTS
FOR SEVERAL WEAPON YIELDS

Yield (KT)	a_0 (ft)	$k_a/2.808$ (ft ⁻¹)	b_0 (ft)	$k_b/2.808$ (ft ⁻¹)
1	1.92×10^2	1.07×10^{-4}	1.06×10^2	1.20×10^{-4}
10	4.20×10^2	0.51×10^{-4}	4.28×10^2	4.40×10^{-4}
10^3	8.01×10^2	0.04×10^{-4}	9.20×10^2	2.10×10^{-4}
10^6	1.88×10^3	2.72×10^{-6}	1.04×10^3	1.40×10^{-6}
10^4	8.08×10^2	0.04×10^{-4}	4.05×10^2	0.71×10^{-4}
10^5	6.85×10^2	1.54×10^{-5}	8.04×10^2	0.08×10^{-5}

the particle groups falling from the downwind-edge of the stem α_{\min} and, those from the upwind-edge of the stem, α_{\max} , at a given downwind distance can be determined; then it is possible to sum up the activity deposited at that location. The simplest case is at the $y = 0$ plane; the solution can then be generalized by replacing a_0 with $\sqrt{a_0^2 - y^2}$.

To determine α_{\min} and α_{\max} , three equations are required in order to eliminate a_0 and x from the stem model equations with equation constants and yield-dependent parameters. Two of the three equations are

$$a_0 = \frac{4k_a}{x} e^{k_a x} \quad (4.01)$$

and

$$a_0 = X + \alpha y \quad (4.02)$$

where α is either α_{\min} or α_{\max} depending on the sign of a_0 .

The third required equation must give the α value of the particle group falling from a given altitude. An equation for this description was derived from the data of Anderson⁸ by the following technique. The altitude, z , is first defined as the mean altitude of location for the particles that have entered the fireball or cloud and have collected condensing radioactive elements at time, t , after detonation. The altitudes z_b , z_t , and z_c are the heights of the bottom, top, and center of the visible fireball or cloud at time, t , after detonation.

From a plot of Anderson's data on the rate of rise of the cloud for the 1.9-kT yield it is found that ratios of rates of rise, k_b , and k_t , could be represented quite accurately by a function of the form: constant times ($\exp - kt$) over a given period of time. The integration of the rates of rise with time should give the cloud height as a function of time. The function for v_h thus determined is

$$v_h = (h+b)(1 + e^{-0.0123t}), \quad t = 10 \text{ to } 250 \text{ sec} \quad (4.83)$$

where h is the height of the cloud and b its half-thickness at 8 to 10 minutes after detonation. The multiplier $(h+b)$ is 6 percent larger than that obtained directly from Anderson's data.

In the case of v_t , Anderson's data give values that are about 4000 feet greater at 5 minutes after detonation than can be obtained from Schuert's data⁴ for the 10-minute cloud expansion. Since Anderson's data give larger values, it is assumed that he either used uncorrected observed data or that his values were adjusted to the heights at the Nevada Test Site. Anderson's values, accordingly, were reduced by 30 percent to agree with the values of $h+b$ that would be obtained from Eqs. 4.13, 4.14, and 4.15, giving

$$v_t = 0.331(h+b)(1 + e^{-0.0626t}), \quad t = 5 \text{ to } 20 \text{ sec} \quad (4.84)$$

and

$$v_t = 0.893(h+b)(1.120 - e^{-0.00784t}), \quad t = 20 \text{ to } 200 \text{ sec} \quad (4.85)$$

To test whether the only yield-dependence of the equation is that in the parameters h and b , the rates of rise, k_{t1} , are computed for the 1-MT yield for comparison with the values given in BNW (p. 21). The calculated values of k_t are found to be from 0 to 15 percent lower, up to 1.8 minutes; but, by 8.8 minutes, the BNW rates of rise are 8 times larger. Also, the larger rates from the BNW data give integrated cloud heights that are larger than $h+b$ when the cloud rise-rates are integrated over the rise-time. Therefore, the rate of rise must decrease more rapidly at the longer times than is indicated by the cloud rise-rate data of BNW.

The height of the center of the cloud, v_c , is determined from the average of v_h and v_t , is approximated by

$$v_c = 0.915h(1.093 - e^{-0.00905t}), \quad t = 20 \text{ to } 200 \text{ sec} \quad (4.86)$$

If v_s is the falling rate of a particle at the height, z (v_s is the average fall velocity, v_f /t, from z to the ground), and k is the rate of rise of z of the air around the particle, the particle starts to fall earthward immediately after its normal fall rate equals the rate of rise of the surrounding air mass, or after

$$v_s = k \quad (4.87)$$

From Anderson's particle falling-rate data for spherical particles⁶, the following relations between v_s and v_f were determined:

$$\frac{v_s}{v_f} = 0.95 + 1.02 \times 10^{-6} z \quad (4.88)$$

$z = 5000 \text{ to } 50,000 \text{ ft,}$

$$d = 200 \text{ to } 1200 \text{ microns}$$

and

$$\frac{v_s}{v_f} = 0.58 + 1.74 \times 10^{-6} z \quad (4.89)$$

$z = 50,000 \text{ to } 110,000 \text{ ft,}$

$$d = 300 \text{ to } 1000 \text{ microns}$$

Equation 4.88, which is applicable to most of the altitude region of possible stem fallout, fits the plotted data extremely well in the altitude and particle-size range indicated. Even when applied to altitudes of 1000 and 60,000 feet and to particle diameters up to 8000 microns, the difference between the ratios calculated from the tabulated fall-rates and from the equation are less than 20 percent.

When the cloud rates of rise, k_1 , k_2 , or k_3 , and the particle-fall rates are used to compute the time of arrival of particles at locations very close to ground zero where fallout from stem altitudes should predominate, the calculated arrival times are quite consistently longer than the observed times when compared with the few available observed arrival times in which the particle sizes are also known. Actually, the same discrepancy is often observed for cloud fallout at larger distances.

This result, i.e., the longer arrival time computed for particles falling near ground zero, is not as general or comprehensive as might be desired because of the shortage of data for complete verification. But it suggests two deductions about the fallout process from stem altitudes, provided it is assumed that, at a given time, the values of the particle-fall rates are more accurately

known than is the rate of rise of the air surrounding the particles (this assumption is without doubt a good one). The first deduction is that the change in rate of rise of the cloud, with time, as given by the exponential terms in the equations for v_p , v_a , and x_{pa} , represents the change in rate of rise of the air around the particles more accurately than the rate of rise of the air itself is represented because of inaccuracies in the equation multipliers. If this were not the case, the discrepancies in the calculated and observed arrival times would not be consistently of the same sign.

The second deduction is that, when the rising cloud takes on a toroidal motion, the larger particles are involved in such a way that they experience downward accelerations for some rather extended period of time. Because the calculated fall rates include only accelerations due to gravity, the computed time of fall (neglecting downward accelerations) from the height of the cloud would always be longer than the true time. Conversely, when the fall rates are used, in order to estimate the height of origin of a particle from the time of its arrival on the ground (including its rise time), the computed height of origin is less than the cloud height.

This interpretation of the above-mentioned observations of particle-arrival time may be used to describe, in qualitative terms, the process of stem fallout. The rising cloud takes on toroidal circulation when the internal pressures and temperatures of the fireball approach those of the ambient air and a large-scale air circulation is established. Air and soil particles rise from directly below the cloud in a narrow visible stem or chimney, and the surrounding air is entrained over the whole length of this stem. This rising material flows into the bottom center of the cloud, and the countercurrent air flow, around the periphery of the cloud, is downward. The observable effect, upon occasion, is that the mass of particles appears to flow out from the top portion of the cloud and then downward.

When the toroidal circulation starts, a particle (or liquid drop) in the central region of the cloud could, by centrifugal force, be moved to the outer periphery of the cloud and then be accelerated downward at speeds greater than the particle's normal fall velocity; it would then be at a lower altitude than the cloud when its terminal fall velocity is reached. However, even if this centrifugal action and movement to the exterior of the rising cloud did not occur for the majority of the particles, they could still fall from lower altitudes, by virtue of the downward circulation around the periphery of the cloud, than would be calculated on the basis that gravity-pull alone was overcoming the gross rise-rate of the visible cloud.

However, even with toroidal motion the separation of fallout particles by their sizes because of gravity forces is still a valid concept. The smaller particles will not move outward by centrifugal forces as far as the

larger ones in the circulation and they could be swept back upward through the cloud as long as the velocity of the rising air is sufficiently large. To use this concept in a mathematical treatment requires a method of estimating the upward velocity of the air directly below the cloud, or a particle-altitude function for estimating the apparent origin of particles having a given value of α .

Assumption 7 and a few observed data were used to derive a particle-altitude function whose use gives a good representation of the input data on the particle arrival times and particle sizes used in its derivation. The best representation of the data is

$$n = n_0 (1 - e^{-k_x t}) \quad (4.40)$$

where k_x is 0.011 sec⁻¹, and n_0 is a yield-dependent multiplier whose evaluation by means of Assumption 7 is discussed later. The obtained value of k_x is between the values found for the n_a and n_b time-dependent functions. For use in the scaling system, the lower limit of application of Eq. 4.40 is assumed to be about 20 seconds and the upper limit about 8 minutes. The rate of rise of the air layer from which the particles fall, represented by the coordinate z , is

$$\dot{z} = n_0 k_x e^{-k_x t} \quad (4.41)$$

or

$$z = k_x (z_0 - n). \quad (4.42)$$

The particle size parameter α , for the particle groups falling from the apparent altitude, z , as defined by the ratio v_w/v_r , is obtained from the combination of Eqs. 4.37, 4.38 or 4.39, and 4.42, and is

$$\alpha = \frac{v_w(v_r + w_0 z)}{k_x(n_0 - n)} \quad (4.43)$$

where v_r and w_0 are the constants of Eqs. 4.38 and 4.39.

In the functions for the simplified fallout scaling system, the standard conditions adopted are that z is 5000 to 50,000 feet and that v_w is 18 mph or 22 feet/second. For these conditions $v_w v_r / k_x$ is 1000 feet and $v_w w_0 / k_x$ is 0.020. In cases where n_0 and n are greater than 50,000 feet, these parameters are 1100 feet and 0.035, respectively; where appropriate, they are substituted for the standard values in making computations.

Having found a suitable relationship between α and x , the values of α_{\min} and α_{\max} arriving at a given downwind distance along the center of the pattern can be determined from

$$\frac{k_a(x_0 \alpha_{\min} - 1900)}{2.303(\alpha_{\min} + 0.020)} = \log \left[X + \frac{\alpha_{\min}(x_0 \alpha_{\min} - 1900)}{(\alpha_{\max} + 0.020)} \right] - \log a_0 \quad (4.44)$$

and

$$\frac{k_a(x_0 \alpha_{\max} - 1900)}{2.303(\alpha_{\max} + 0.020)} = \log \left[\frac{\alpha_{\max}(x_0 \alpha_{\max} - 1900)}{(\alpha_{\max} + 0.020)} - X \right] - \log a_0 \quad (4.45)$$

The particle group arriving at the distance X from the center of the stem, α^* , under the same range of altitude and wind speed as in Eqs. 4.44 and 4.45, can be estimated from

$$\alpha^* = \frac{(X + 1900) + \sqrt{(X + 1900)^2 + 0.0816x_0 X}}{2x_0} \quad (4.46)$$

The height from which the group falls is

$$H = \frac{\sqrt{(X + 1900)^2 + 0.0816x_0 X} - (X + 1900)}{0.0408} \quad (4.47)$$

(For altitudes greater than 50,000, the constants 0.0816 and 0.0408 are 0.130 and 0.0000, respectively.)

Because the equations for α_{\min} and α_{\max} are not solved explicitly in terms of the equation constants and X , it is simpler to obtain α_{\min} and α_{\max} graphically computing a_x and α at selected values of x , calculating X from Eq. 4.46, and then plotting the two values of α as a function of X .

Since the atom fallout scaling system has been simplified to designate a spatial distribution of the α groups that are uniformly distributed in a horizontal plane at a given value of x , it is convenient to define the activity concentration of each group in terms of the number of fissions per unit cross-sectional area of the stem. If this concentration is designated as A'_x , then the total activity carried by each group is

$$A_x(\alpha) = \pi A'_x a_x^2 \quad (4.48)$$

The total activity per unit area accumulated on the ground at the downwind distance, X , is given by the sum of the A_α from α_{\min} to α_{\max} , or:

$$A_X = \int_{\alpha_{\min}}^{\alpha_{\max}} A_\alpha d\alpha \quad (4.40)$$

The procedure for estimating A_α for atom fallout is essentially the same as that for estimating A_α for cloud fallout. The method is based on the use of observed or estimated values of A_α , given as a function of X , to determine by successive approximations A_α as a function of α . The first approximation is obtained by calculating an average value of A_α for the value of α at each of a series of selected values of X along the center of the pattern ($y = 0$), by use of

$$A_\alpha = \frac{A_X}{\alpha_{\max} - \alpha_{\min}} \quad (4.50)$$

The appropriate values of α_{\min} , α , α_{\max} , and A_X , for a given yield, can be read from a plot of each with the downwind distance, X .

4.3.4 Methods for Estimating the Dynamics of the Fallout Deposition

The time of fallout arrival, time of fallout cessation, rate of deposition during fallout, variation of the dose-rate, and potential dose during the fallout period, can all be estimated by use of the simplified fallout scaling system. Association of particle sizes with the average fall rates from different altitudes will give the particle size ranges that fall at any location.

The assumption of a uniform distribution in the cloud of the particles having a given value of α implies that, at the location X, y , the first particles of the arriving group fell from the height of the bottom boundary of the cloud, h_1 , and that the particles (or activity) from each α group will accumulate on the ground at a constant rate until the last ones falling from the height of the top boundary of the cloud, h_2 , arrive.

For a constant value of the wind speed, or wind velocity vector from cloud to ground,

$$V_F = \frac{V_W}{\alpha} \quad (4.51)$$

so that the time of arrival, $t_a(\alpha)$, for the group is given by

$$t_a(\alpha) = \frac{\alpha h_1}{v_w} \quad (4.53)$$

where

$$h_1 = h + s_a \quad (4.54)$$

and the time of cessation, $t_c(\alpha)$, for the group is given by

$$t_c(\alpha) = \frac{\alpha h_2}{v_w} \quad (4.54)$$

where

$$h_2 = h + s_c \quad (4.55)$$

In these equations, s_a is the positive, or largest, value of s , and s_c is the negative, or smallest, value of the intercepts of the particle group trajectory with the cloud boundary. The intercepts are given by

$$s_a = \frac{a(X-h)b^2 + ab\sqrt{(h^2 + a^2b^2)(1 - y^2/a^2)} - (X-h)b^2}{a^2 + a^2b^2} \quad (4.56)$$

The time period over which the group arrives is

$$\Delta t(\alpha) = \frac{\alpha \Delta s(\alpha)}{v_w} \quad (4.57)$$

where

$$\Delta s(\alpha) = s_a - s_c \quad (4.58)$$

Since the total amount of particles or activity per unit area that arrives at X, y is given by $\Lambda_x(\alpha)$, the rate of arrival of the group is given by

$$\Lambda_x(\alpha)/\Delta t = \frac{v_w \Lambda_x(\alpha)}{\alpha \Delta s(\alpha)} \quad (4.59)$$

The total rate of arrival of fallout at any time after the first particles start arriving can be determined by summing the individual rates for all the α groups arriving at a given time. This sum is given by

$$(A_x/\Delta t)_t = \int_{\alpha_{min,t}}^{\alpha_{max,t}} \frac{A_x(\alpha)}{\Delta t(\alpha)} d\alpha \quad (4.00)$$

The $(\alpha_{min,t})$ and $(\alpha_{max,t})$ values are obtained from a plot of $t_n(\alpha)$ and $t_p(\alpha)$ as a function of α . The integration indicated by Eq. 4.00 can be carried out graphically from a plot of $A_x(\alpha)/\Delta t(\alpha)$ as a function of α .

The gross activity, or number of radioactive atoms per unit area, accumulated on the ground at any time after the first particles arrive is given by

$$A_x(t) = \int_{t_n(1)}^t (A_x/\Delta t)_t dt \quad (4.01)$$

where $t_n(1)$ is the time of arrival of the first group. When t is t_n of the last group to arrive, Eq. 4.01 is equal to the A_x of Eq. 4.10. For close-in locations, 8 minutes should be added to these times to account for the cloud-formation time.

The time of arrival of each particle group falling from the atom altitudes at a given downwind location is the sum of its rise time and fall time. The rise time of each group may be estimated from a combination of Eqs. 4.41, 4.42 and 4.43 which is

$$t_r (\text{sec}) = 209 [\log(\alpha + 0.020) - \log(1900/v_w + 0.020)], \quad (4.02)$$

When t_r is greater than 80 seconds the time required for the group to fall to the ground is

$$t_f = v/v_r = nv/v_w \quad (4.03)$$

or, with Eq. 4.03, the time of fall under the same conditions of wind speed and height of origin as in Eq. 4.02 is

$$t_f (\text{sec}) = \frac{\alpha(nv_w - 1900)}{22(\alpha + 0.020)} \quad (4.04)$$

The activity accumulated to any time can be determined from a plot of the integral (or sum),

$$\Delta_x(t) = \int_{t_{\min}}^t A_\alpha d\alpha \quad (4.05)$$

against the time of arrival of the α group as given by $t_x + t_f$. The rate of arrival of the α groups, if desired, can be determined for various times by taking slopes from the curve. The delay time due to particle circulation, as is discussed in Chapter 4, would increase the arrival times given by $t_x + t_f$.

4.8.5 Estimation of Ionization Rate and Exposure Dose

In order to estimate the air ionization rate and exposure dose from $A_x(t)$, both a conversion from fissions per unit area to r/hr and a decay curve for the gross radioactive mixture are needed. The conversion factor from fissions/sq.ft to r/hr is defined by

$$I_x(t) = K_x(t)A_x \quad (4.06)$$

and

$$K_x(t) = Dq_x [r_x(t)I_{fp}(t) + I_x(t)] \quad (4.07)$$

in which $I_{fp}(t)$ is the air ionization rate per fission at 8 feet above an infinite ideal plane for a uniform distribution of the normal fission product mixture, $I_x(t)$ is the same unit for neutron-induced activities, $r_x(t)$ is the gross fission product fractionation number, q_x is the terrain shielding factor, D is an instrument response factor, and t is the time after fission. The true air ionization rate, $I_x^0(t)$, is obtained when D is set equal to one.

Since most fallout data have been corrected to a standard time of $H + 1$ hr and reported in values as of this time (even though the fallout had not yet arrived at 1 hour), it is convenient to refer to the common-time data in r/hr by means of a decay correction factor, $d(t, 1)$, defined by

$$I_x(t) = d(t, 1)I_x(1) \quad (4.08)$$

where $I_x(t)$ is the air ionization rate corrected to $H = 1$. It is seen that

$$I_x(t) = K_x(t) A_x \quad (4.69)$$

and

$$I_x(t) = K_x(t) d(t, 1) A_x \quad (4.70)$$

The potential (exposure) dose from deposited fallout during fallout arrival is

$$D_{X,t} = \int_{t_0}^{t_1} I_x^*(t) dt \quad (4.71)$$

where t_0 and t_1 are the arrival and cessation times, respectively, for all values of α arriving at X . Equation 4.71 can be integrated from a plot of $I_x^*(t)$ as a function of time.

In order to estimate the dose rate contribution from the activity in the air as it falls, the air concentrations of all the particle groups are needed. Since a uniform volume distribution of the particle groups was assumed and a single velocity for the wind speed was taken, the concentration of particles for each value of α remains the same at all altitudes and is given by A_α .

From calculations made by Laumetzy¹¹ the air ionization rate at three feet inside a plane boundary of a semi-infinite volume containing a uniformly-distributed radiation source is given by

$$I_x(t) = 0.950 \times 10^{-6} A_t A_\alpha E_t \text{ in r/hr}^{-1} \quad (4.72)$$

in which A_t is the activity in dCi/sec per fission at the time, t , after fission, A_α is the concentration in $\text{fissions}/\text{ft}^3$ and E_t is the total gamma ray energy in MeV/dis .

At a given time, A_t and E_t are constant, so that the contributions from the particle groups of all α values arriving at a given time can be summed as in the case of the deposited material. Multiplication by the appropriate values of A_α and E_t for the designated time will convert the sum to r/hr . The sum for fallout from cloud altitudes is given by

$$I_x(t) = 0.950 \times 10^{-6} A_t E_t \int_1^{t_2} A_\alpha d\alpha \quad (4.73)$$

Values for A_{α} and B_{α} can be derived from the data of Bolles and Bellou¹⁴ LaRiviere,¹⁵ and Zigman and Mackin.¹⁶

The method of estimation for the ionization rate from the airborne particles arriving from the atom altitude is the same as for those from cloud altitude, except that the value of A_{α} in Eq. 4.72 must be estimated from

$$A_{\alpha} = \frac{1}{v_t} \frac{dA_{\alpha}}{dt} \quad (4.74)$$

where $v_t = v_w/\alpha$. In Eq. 4.74, the v_t applies to the α group arriving at the time t given by Eqs. 4.03 and 4.04. The ionization rate is given directly by Eq. 4.72 because the simple atom fallout scaling system gives only one particulate group as arriving at a given instant.

CHAPTER 4 REFERENCES

1. Kellogg, W. W., Hearings before the Special Subcommittee on Radiation of the Joint Committee on Atomic Energy, U.S. Congress, *The Nature of Radioactive Fallout And Its Effects on Man*, Part I, p. 104-41, 1957.
2. Anderson, A.D., *A Theory for Close In Fallout*, USNRDL-TR-249, 1958.
3. Kellogg, W.W., R.R. Rapp, and S.M. Greenfield, *J. Meteor.* 14, 1, 1-8 1957.
4. Schuert, E.A., *A Fallout Forecasting Technique With Results Obtained at the Eniwetok Proving Ground*, USNRDL-TR-139, 1957.
5. Ksanda, C.F., L. Minvielle, and A. Moskin, *Scaling of Contamination Patterns, Surface and Underground Detonations*, USNRDL-TR-1, 1958 (Classified).
6. Laurino, R.K., and I.G. Popoff, *Contamination Patterns at Operation Jangle*, USNRDL-899, 1959.
7. *Capabilities of Atomic Weapons*, Armed Forces Special Weapons Project, TM28-200, 1958 (Classified).
8. *The Effects of Nuclear Weapons*, U.S. Government Printing Office, Washington, D.C., 1957.
9. Anderson, A.D., *Application of "Theory for Close-In Fallout" To Low-Yield Land Surface and Underground Nuclear Detonations*, USNRDL-TR-289, 1958.
10. Pugh, G.E., and R.J. Callano, *An Analytic Model of Close-In Deposition of Fallout for Use in Operational-Type Studies*, Research Memorandum No. 10, Weapons Systems Evaluations Group, 1959.
11. Callahan, E.D., L. Rosenblum, J.D. Kaplan, and D.R. Batten, *The Probable Fallout Threat over the Continental United States*, TO-B60-18, 1000.
12. Rapp, R.R., *Summary Report of RAND Work on the AFNSWP Fallout Project*, RM-2884, 1960 (Classified).

13. Laumetz, E., Private Communication, USNRDL, 1960.
14. Boller, R.C., and N.E. Ballou, Calculated Abundances of U-235 Fission Products, USNRDL-400, 1960.
15. LaRiviere, P.D., Early-Time Gamma Ray Properties of U-235 Gross Fission Products, USNRDL-TM-89, 1968.
16. Zigman, P., and J. Mackin, Early Time Decay of Fission Product Mixtures --II Health Physics 5, 79 1961.

Chapter 8

CORRELATION OF SCALING MODEL PARAMETERS WITH OBSERVED FALLOUT PATTERN FEATURES

5.1 General Description of Fallout Patterns from Land Surface Detonations

Although observed data on fallout patterns from land surface shots of various yields are very meager, the processed data give indication in a qualitative way of a number of persistent characteristics. For example, the general shape of the fallout standard intensity contours (in R/hr at 1 hr) from shots where the wind structures were rather simple, resembles a shadow of the mushroom cloud and its stem on the ground.

Because of the shortage of reliable data on the fallout patterns from land surface detonations, any systematic method for scaling fallout patterns--i.e., methods for interpolating and/or extrapolating data from one weapon yield to another--must take full advantage of all such apparently persistent qualitative characteristics of the available patterns. In devising methods that can convert the qualitative characteristics to quantitative ones, the methods must, of course, be capable of at least reproducing the observed data that was used in obtaining the original scaling relationships, which are given as functions of weapon yield.

Some of the apparently persistent characteristics of the fallout patterns from surface detonations are:

1. In the region near ground zero, the intensity gradient in the upwind and crosswind directions is very steep
2. The high intensities near ground zero appear as an intensity ridge (rather than as a circular peak) displaced in the downwind direction
3. The length of this high intensity ridge appears to be proportional to the width of the lower portion of the stem
4. The peak intensity of the ridge increases with yield in the 1- to 10-KT yield range and decreases in the 100-KT to 10-MT yield range

6. The best simple empirical relationship for the variation of the intensity with upwind and crosswind distances from ground zero, from graphical plots of the data, is that of the form, $I_0 e^{-kx}$, where I_0 is the ridge peak intensity, k is a constant for a given yield, and x is the upwind and/or crosswind distance from the upwind shoulder of the ridge peak.
9. The contours downwind from ground zero appear to be parallel to the intensity ridge for its entire length.
7. At distances greater than the length of the ridge, the intensity contours directly downwind decrease with distance from ground zero.
8. At some distance downwind (or perhaps even upwind for very large yields), the low-valued intensity contours fan out and the intensities directly downwind from ground zero rise sharply with distance and then more slowly with distance to a peak value.
9. The distance from ground zero to this downwind peak intensity increases with weapon yield.
10. The magnitude of the peak intensity also appears to increase continuously with yield.
11. The distance between the lower-valued contours appears to be related to the width of the cloud (not considering wind shear differences) and the maximum width seems to occur farther downwind than the peak intensity.
12. The variation of the intensity with downwind distance from this outer pattern peak can be approximated within reasonable limits of error if the wind shear is not large by a function of the form $I_0 e^{-mx}$, where I_0 is the peak intensity, m is a yield dependent parameter, and x is the downwind distance from the peak.

The above listed fallout pattern characteristics are based on a combination of experimental observations and analysis of field test data. The most reliable of the group appear to be those numbered 1, 2, 4, 6, 7, 8, and 9.

6.2 General Conditions to Which the Source Data Apply

In deriving the empirical constants for the scaling functions of the fallout patterns, the available data were converted to the reference of 100 percent fission yield ($B = 1$), including 0.8 neutron captures per fission by U-238 to give the appropriate value of $I_x(1)$ in roentgens per hour at 1 hour.

Also, the $I_x(1)$ values (or standard intensities) correspond to radionuclide measurements taken at three feet above an extended open area contaminated with fallout as it existed when the measurements were taken. The reference radionuclide instrument for the $I_x(1)$ values is the AN/PDR-30(R1B) portable radiometer; it has a geometric and photon energy response of very nearly 70 percent of the true air ionization rate at three feet above a plane source of fission products uniformly distributed on the area. Therefore to obtain the true air ionization, in calculating exposure doses, the $I_x(1)$ values should be multiplied by 1.08.

The average value of the terrain shielding factor, which is automatically contained in the source data, is about 0.75. The data, in general, apply to U-238 fission, for which the $I_x(1)$ of Eq. 4.07 is 0.04×10^{-10} r/hr at 1 hr per fission/sq ft. The value of $I_x(1)$ for the indicated induced activity is 0.10×10^{-10} r/hr at 1 hr per fission/sq ft. With those numbers, Eq. 4.07 becomes

$$K_x(1) = 3.90 \times 10^{-10} [r_x(1) + 0.019] \frac{r/\text{hr at 1 hr}}{\text{fission/sq. ft.}} \quad (6.1)$$

The numerical coefficient is 0.40×10^{-10} in r/hr at 1 hr per KT/sq ft and 1000 in r/hr at 1 hr per KT/sq mi. However, $r_x(1)$ is also included in the observed data to some degree; just how much is unknown because most of these data were decay-corrected to H+1 by a single decay curve. The exact value and dependence of $r_x(1)$ on distance is not needed for developing the scaling functions since it is unnecessary to separate the product $K_x(1)\Lambda_x$ in the derivations. An average value of $r_x(1)$ is defined at the end of this section to account for the fraction of the total activity produced that falls within a given area on the ground.

The average wind speed, for the source data used, was between 10 and 15 mph. It may be assumed, therefore, that the scaling functions are for an average or effective wind speed of 10 mph.

5.8 Scaling Functions for Fallout Pattern Features of Interest

Some of the pattern features of interest along the downwind axis ($y = 0$) of the idealized fallout pattern are shown in Figure 5.1 as a schematic intensity profile. The numbers shown in the figure correspond to the number subscripts of the scaling functions. The evaluated scaling functions for those and other quantities are given in Section 6.4. The procedures and assumptions used in obtaining the numerical values are described below.

5.8.1 Intensity Ridge Near Ground Zero

This ridge is assumed to result from the deposition of particles from atom altitudes. Because (1) more data are available on the fallout deposited in the vicinity of ground-zero for surface-ground shots than for other downwind shots, and (2) the simplified fallout scaling system for the atom geometry could not be utilized in a straightforward manner to reproduce the observed intensities upwind from ground zero, the scaling function for $-X_{11}$, the upwind distance to the 1 r/hr at 1 hr intensity, was derived directly from the observed data.

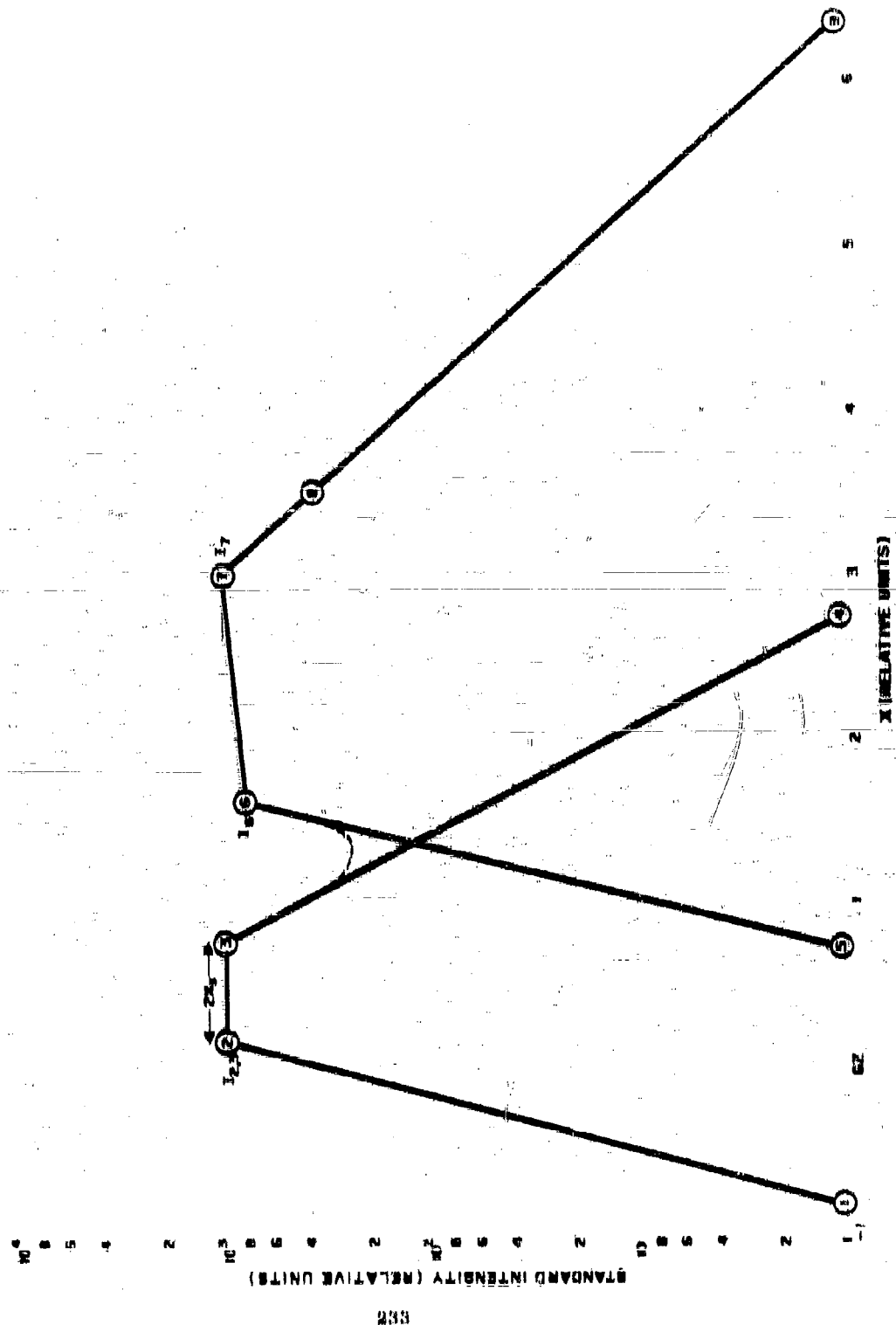
According to observation 5 in Section 6.4.1, the peak intensity near ground zero is given by

$$I_{g,0} = \exp k_{11,g} (X_g - X_1) \quad (6.8)$$

where $k_{11,g}$ is a yield-dependent parameter evaluated empirically from observed data. The parameter designated by X_g is the distance to the upwind shoulder of the intensity edge; this location generally does not coincide with that of the center at $X = 0$.

The length of the intensity ridge, $X_g - X_{11}$, is assumed to be equal to the diameter of the atom, $2a_{11}$, for the particle groups falling from a characteristic altitude, ν_{11} . One possible explanation for the observation of the intensity ridge is that a large number of fallout particles having a rather narrow size-range fall from a given small range of altitude after the fireball has some distance from the ground because a basic change in the initial circulation has occurred. The onset of toroidal motion, for example, might result in the rapid ejection of the larger particles in a short period of time. The dumping or ejection of a rather large number of big particles might also coincide with the time it takes the larger particles to make one pass through the rising fireball prior to their mass migration to the periphery regions where the air currents can accelerate their fall downward.

Figure 5.1
SCHEMATIC OUTLINE FOR THE INTENSITY PROFILE DOWNWARD FROM GROUND ZERO
ALONG THE AXIS OF THE FAULT PATTERN ($y = 0$) AS USED IN THE SIMPLIFIED
FAULT PATTERN SCALING SYSTEM



Since both R_x and g are proportional to W^a , where $a = \text{near } 1/3$, the same type of dependence on yield is assumed for $(X_p - X_n)/X_n$ or $\alpha_{p,n}$. Because the assumption requires that the particle groups falling from X_p are the minimum size group that arrives at X_p and the maximum size group that falls at X_p , the particles that fall from the center of the minimum band near X_p are $X_p/2$. The particle-size parameter indicator for these particles, therefore, can be defined by

$$\alpha_{p,n} = \frac{X_p + X_n}{2X_n} \quad (B.3)$$

where

$$2, 200 \cdot \log \alpha_{p,n} > \log \beta_0 \quad (B.4)$$

Once the yield-dependency of $\alpha_{p,n}$ is determined, the value can be calculated. It is then available to obtain estimation of X_p and X_n for any yield, by use of the relations

$$X_p = \beta_0 \cdot \alpha_{p,n} \cdot R_x \quad (B.5)$$

and

$$X_n = \beta_0 \cdot (1 - \alpha_{p,n}) \cdot R_x \quad (B.6)$$

The additional use of $\alpha_{p,n}$ is to evaluate the parameter v_p that defines the ratio-of-time function. Use of Eq. B.4B to make the substitution results in

$$\frac{v_w v_n}{R_x} = \frac{\alpha_{p,n} \cdot (v_w v_n / k_p) \beta_0}{(1 - \alpha_{p,n}) \cdot k_n} \quad (B.7)$$

which, for the 20 ft/age wind speed, 30,000 to 10,000 ft altitude, fall time range of 20 to 500 sec, is given by

$$\frac{1000}{R_x} = \frac{1000 \cdot (1 - 0.020) \beta_0}{(1 - 0.020) \beta_0 + 1000} \quad (B.8)$$

and, for use with z values greater than 50,000 ft, is given by

$$k_{s,z} = \frac{1160 + (a_{s,z} + 0.015)z}{a_{s,z}} \quad (5.9)$$

These evaluations of a_s assume that at z_0 the same upward force is acting on the particles that may go higher than 50,000 feet as is acting on those that fall back from lower altitudes. In a general way, the equation constants for the higher altitudes should not apply to yields for which z_0 itself is less than 50,000 feet. For the empirically-evaluated constants, the yields for which the high-altitude equations apply is actually near 10^3 -KT. The upper limit of z_0 is (h-b). This limit is exceeded for yields less than about 8- or 9-KT; therefore, for the lower yields, z_0 is replaced by (h-b).

In estimating the change in the relationship between $I_{s,z}$, X_s , and X_1 with change in wind speed, $k_{s,z}$ is assumed to remain constant. This means that the intensity levels in the upwind and crosswind directions increase or decrease with $I_{s,z}$ as the wind speed decreases or increases. In the model for fallout from atom altitudes, only one particle-size group is described as falling from a given altitude.

The inverse of the fall velocity of the group, from Eqs. 4.38 and 4.43, is

$$1/v_f = \frac{86.4 + 9.27 \times 10^{-4}z}{z_s + z} \quad (5.10)$$

The downwind distance at which the particle group falls from either edge of the stem is defined by

$$X = v_w z / v_f \approx z_s \quad (5.11)$$

where z_s is the stem radius at z , as given by Eq. 4.31, and v_w is the wind speed. By calculating the values of $1/v_f$, X , and a_s for a series of selected values of z , it is possible to construct a plot of the maximum and minimum values of $1/v_f$ against X for a selected wind velocity. When this is done, the two values of $1/v_f$ approach a central value as the wind speed increases and diverge as the wind speed decreases.

If the location $X_{s,z}$ at the center of the downwind intensity ridge is selected as the location at which the variation of $I_{s,z}$ with wind speed is to be estimated, and if it is assumed that an average value of the activity per unit volume can be assigned to a central particle group, then $I_{s,z}$ can be estimated

from

$$I_{g,0} = K_{g,0}(1) \bar{A}_f (n_g - n_e) \quad (5.18)$$

where \bar{A}_f is the average value of the concentration, in fractions per cu ft; $K_{g,0}(1)$ is a constant for conversion to r/hr at 1 hr; n_g is the altitude of origin of the largest particle size group arriving at $X_{g,0}$; and n_e is taken as the lowest altitude from which particles fall at $X_{g,0}$. In the yield range of from 100 to 50,000 KT, and for wind speeds from 7.5 to 15 mph, the dependence of $n_g - n_e$, or $\Delta n_{g,0}$, on wind speed can be represented by

$$\Delta n_{g,0} = \Delta n_{g,0} v_w^n \quad (5.19)$$

where $\Delta n_{g,0}^0$ and n are yield-dependent parameters. The values of these two parameters and the derived values of $K_{g,0}(1)\bar{A}_f$ are given in Table 5.1 at several values of weapon yield. In making the calculation, $X_{g,0}$ is estimated from

$$X_{g,0} = t_{g,0} v_w \quad (5.14)$$

Thus $X_{g,0}$ varies directly with wind speed, since $t_{g,0}$ is equal to $v_w/v_{g,0}$, where $v_{g,0}$ is the fall velocity of the central particle-size group that arrives at $X_{g,0}$.

The scaling system described above is designed to reproduce roughly, by means of the assumed particle source geometry, (1) the fall behavior of a given particle-size group, and (2) the variation in size-spread of the group as a function of wind speed and weapon yield. This general approach is repeated for other fallout pattern features in the following sections.

The variation of X_g and X_1 with wind speed is estimated by multiplying $n_{g,0}$ by $v_w/10$; n_e is assumed to be independent of wind. The indicated change of X_g with wind speed, from the assumption of a constant value of $k_{1,g}$, is

$$X_1 = X_g + \frac{2,303 \log I_{g,0}}{k_{1,g}} \quad (5.15)$$

where $I_{g,0}$ is given by Eq. 5.18. For X_g computed for the same value of v_w as $I_{g,0}$, the value of X_1 in Eq. 5.15 is for $I_g \approx 1$ r/hr at 1 hr.

Table 8.1

**EQUATION PARAMETER VALUES FOR THE VARIATION OF $\Delta K_{B,R}$ WITH
WIND SPEED^a AND DERIVED VALUES OF $K_{B,R} \bar{A}_I$**

W (KT)	$\Delta v_{B,R}^0$ (ft)	n	$K_{B,R}(1) \bar{A}_I$ (r/hr at 1 hr/ft)	$K_{B,R}(1) \bar{A}_I \Delta v_{B,R}^0$ (r/hr at 1 hr)
100	12,200	-0.78	83.0	802,000
200	12,700	-0.78	18.2	108,000
500	15,400	-0.77	5.80	312,000
1,000	18,800	-0.765	3.60	70,700
2,000	18,000	-0.76	3.84	64,800
5,000	14,000	-0.75	2.60	88,400
10,000	13,000	-0.74	1.92	28,500
20,000	13,100	-0.71	1.80	18,200
50,000	11,100	-0.69	0.638	10,200

a. Wind speed in mph.

**8.0.2 Location of the Downwind Standard Intensity Contour for Fallout
from Stem Altitude**

The particle-size group designator, α_4 , for particles falling at X_4 , is assigned to the group that originated from the center of the stem. This group, from Eq. 4.46 is specified by

$$\alpha_4 = (X_4 + 1900) + \sqrt{(X_4 + 1900)^2 + 0.0816 R_0 X_4} \quad (8.16)$$

and, given the yield-dependence of α_4 , X_4 can be estimated from

$$X_4 = \frac{\alpha_4(\alpha_4 R_0 + 1900)}{(\alpha_4 + 0.020)} \quad (8.17)$$

If R_0 , given by X_4/α_4 , is greater than 80,000 feet, the indicated equation constants are replaced by those previously given for the higher altitudes.

For wind speeds other than 10 mph, X_4 is directly proportional to the wind speed. If the fall velocity of the center particle-size group is designated v_4 , then Eq. 5.17 is

$$X_4 = \frac{v_w(v_0/v_4 - 86.36)}{(1 + 9.273 \times 10^{-4} v_4)} \quad (5.18)$$

The variation of the realization ratio at X_4 due to the narrowing of the particle size with wind speed is given by

$$I_4 = K_4(1)\tilde{\Delta}_1 \Delta x_4 \quad (5.19)$$

where Δx_4 is the span in altitude from which the particles fall to X_4 . The value of Δx_4 is given by

$$\Delta x_4 = \frac{(v_1 + v_2)(86.36 + 9.273 \times 10^{-4} v_0)}{(1 + 9.273 \times 10^{-4} v_1)(1 + 9.273 \times 10^{-4} v_2)} \quad (5.20)$$

In which v_1 and v_2 are the respective values of the largest and smallest particle fall rates for the groups that arrive at X_4 . Their values are determined by the method described for estimating the variation of $I_{4,a}$ with wind speed. Calculations of Δx_4 for yields from 500 to 50,000 KT, and for wind speeds from 0 to 40 mph, give

$$\Delta x_4 = 1720 W^{0.046} / v_w \quad (5.21)$$

Also, it was determined that

$$K_4(1)\tilde{\Delta}_1 = 8.72 \times 10^{-8} W^{-0.046} \quad (5.22)$$

so that, as might be expected, I_4 is inversely proportional to wind speed and is given by

$$I_4 = 18.0 / v_w \quad (5.23)$$

for v_w in mph. This result occurs because the span in altitude of origin for the particles arriving at X_4 is very narrow.

6.3.3 Stem Pattern Half-Width

The half-width of the stem fallout, designated Y_s , is the lateral distance from the center-line of the stem pattern ($y = 0$) to the 1 r/hr at 1 hr contour. Because of the geometry used for the stem, where the diameter of the upper portion of the stem becomes proportional to the cloud diameter, the ratio Y_s/a is assumed to vary uniformly with yield according to a function of the form: constant times W^n . The constants were evaluated empirically from observed data.

For wind speeds other than 15 mph, the r/hr at 1 hr contours may be estimated from

$$Y_s = \frac{Y_{s,0} \log I_{0,0}}{\log I_{0,W}} \quad (6.84)$$

where $Y_{s,0}$ is the half-width and $I_{0,0}$ is the ridge intensity for the 15 mph wind speed. This relationship assumes that the logarithmic slope from the intensity ridge in the y , or cross-wind, direction is independent of wind speed. The logarithmic slope, and $k_{1,0}$ assumed constant for a given yield of detonation, results in a slight reduction in the fraction of the total activity that is accounted for in the stem pattern with increasing wind velocity, since the decrease in the total activity that is due to the decrease in $I_{0,W}$ with wind speed is not quite compensated for by the increase in the distance $X_0 - X_s$.

An additional contributing factor is the neglect of any spread in $X_0 - X_s$ with wind speed. The over-all error in the areas enclosed by given contours, or in the total activity in a pattern, by this simplified treatment of the variation of Y_s with wind speed, however, is not large; the error should decrease with yield since the fraction of the total activity in the fallout pattern that comes from stem altitudes (according to the scaling system) decreases with increasing weapon yield. The shape of the so-called ground zero circular contours should tend to flatten on the sides and the radius should decrease toward the value of Y_s as the wind speed increases.

6.3.4 The Distance to Fallout Pattern Features for Fallout from Cloud Altitudes

The basic assumption in the scaling of the cloud fallout pattern features is that the distances from ground zero to various points in the pattern are approximately proportional to the height of the particle cloud source geometry. The second assumption is that all variations from a direct proportionality to cloud height for triangular scaling of distances, for example, involves a gradual

change, with weapon yield, in the particle-size groups that arrive at a location of interest.

The assumed form of the gradual change of the inverse fall-velocity designator, α_n , is $\alpha_0^n W^n$, where α_0^n and n are yield-independent parameters. In the central area of fallout from cloud altitudes, the above assumptions result in a distance-scaling function given by

$$X = 6.60 \times 10^4 W^{0.445} \alpha_0, \quad W = 1 \text{ to } 28\text{KT} \quad (5.25)$$

or

$$X = 1.68 \times 10^4 W^{0.164} \alpha_0, \quad W = 28\text{KT} \text{ to } 10^8\text{KT} \quad (5.26)$$

where α_0 is the particle-size designator for particles falling along a line from the center of the cloud to X since α_0 is equal to X/h . The distances designated X_h , X_s , X_{s1} , and X_p are scaled by use of these functions.

For locations underneath the cloud and near the upwind limit of the fallout from cloud altitudes, the distances are better determined by α_{max} because the peak value of $A_n(\alpha)$ tends to shift towards α_{max} as X becomes small. The location of interest in this case is the upwind point of the 1 r/hr at 1 hr standard intensity designated as X_p . The distance-scaling function for this location is

$$X_p = \frac{6.60 \times 10^4 W^{0.445}}{\alpha_0 + 1.40 \times 10^6 W^{0.300} \sqrt{3.06 W^{0.262} + \alpha_0}} \quad W = 1 \text{ to } 28\text{KT} \quad (5.27)$$

or

$$X_p = \frac{1.68 \times 10^4 W^{0.164}}{\alpha_0 + 1.40 \times 10^6 W^{0.300} \sqrt{3.06 W^{0.262} + \alpha_0}} \quad W = 28 \text{ to } 10^8\text{KT} \quad (5.28)$$

The scaling function for α_0 is assumed to be of the form, $\alpha_0^n W^n$. For lower weapon yields, X_p is larger than $\alpha_0 h$; at the yields and wind speeds where this occurs, the variation of X_p with yield is given by Eq. 5.25 or 5.26.

5.3.6.5 The Intensity Levels of Pattern Polygons for Plume from Cloud Altitudes

Functions for estimating the variation of the standard ionization ratio, or the radiation intensity, at the selected downwind locations are derived from the assumption that an average value of \bar{A}_x can be assigned to the particle groups conforming at α_0 , where the values of X or h are small. The average value of $\bar{A}_x(\alpha)$ for these conditions is

$$\bar{A}_x(\alpha) = \frac{2\bar{A}_{\text{pab}}}{\sqrt{a^2 + (\alpha/b)^2}} \quad (5.80)$$

The integral of $\bar{A}_x(\alpha)d\alpha$ is then given by

$$A_x = 2\bar{A}_{\text{pab}} \cdot \sin \left\{ \frac{\alpha_{\max} + \sqrt{a^2/b^2 + \alpha_{\min}^2}}{\alpha_{\min} + \sqrt{a^2/b^2 + \alpha_{\min}^2}} \right\} \quad (5.80)$$

where A_x is the total activity in the same units as \bar{A}_{pab} . Actually, the approximate integral of $\bar{A}_x(\alpha)d\alpha$ may be applied to the levels at locations where both X and h are small, as well as locations where the mid-range value of α is near α_0 . This application is for locations underneath the cloud where X is smaller than the cloud radius.

Although the values of α_{\max} and α_{\min} can be evaluated from Eq. 4(1) in terms of α_0 , it is more convenient, for hand computations, to evaluate the logarithmic term by approximating α_{\max} and α_{\min} from

$$\alpha_{\max} \approx \alpha_0 + a/b \quad (5.81)$$

or

$$\alpha_{\max} \approx \alpha_0 + a/h \quad (5.82)$$

and

$$\alpha_{\min} \approx \frac{X - a}{b} \quad (5.83)$$

or

$$\alpha_{\min} \approx \alpha_0 - a/h \quad (5.84)$$

variation of the three parameters with weapon yield or by the variation in α_0 with wind speed. Since the lower limit of α from the stem model is α_{\min} , and the lower limits of α for the cloud model are not specified without complete evaluation of A_α , the value of α_{\min} for locations at which $\alpha_0 + n/h$ is taken to be

$$\alpha_{\min} = \alpha_{\min}^* \quad (B.85)$$

Although the scaling functions for the different characteristics standard intensities at locations underneath the cloud where $\alpha_0 + n/h(X_0, a)$ are evaluated in Eq. B.8 by using α_{\min} for α_{\min} , better first estimates of A_α as a function of α are obtained when the quantity $X_0/(h-b)$ is substituted for α_{\min} , providing X_0 is less than X_b . The true values of α_{\min} for different weapon yields have not yet been determined.

With the above limits on α_0 , the scaling equations for the intensity levels at the selected locations are

$$I_1 = K_1(1) \bar{A}_\alpha n 4.606 \log \phi_1, \quad m^2 s/h \quad (B.86)$$

and

$$I_2 = K_2'(1) \bar{A}_\alpha n 4.606 \log \phi_2', \quad m^2 s/h \quad (B.87)$$

where

$$\phi_1 = \frac{(\alpha_0 + n/h) + \sqrt{n^2/b^2 + (\alpha_0 + n/h)^2}}{(\alpha_0 + n/h) + \sqrt{n^2/b^2 + (\alpha_0 + n/h)^2}}, \quad \alpha_0 \neq n/h \quad (B.88)$$

and

$$\phi_2' = \frac{(\alpha_0 + n/h) + \sqrt{n^2/b^2 + (\alpha_0 + n/h)^2}}{\alpha_0 n + \sqrt{n^2/b^2 + \alpha_0^2 n^2}}, \quad \alpha_0 \neq n/h \quad (B.89)$$

and n_1 is α_0 for the distance X_1 . In the case of X_b , however, α_0' is the upper limit. At X_b where $\alpha_0 + n/h$ is much larger than n/h , ϕ_2' reduces to

$$\phi_2' = \frac{\alpha_0 + n/h}{\alpha_0 - n/h} \quad (B.90)$$

The parameters $K_1(1)A_n$ and $K_1'(1)A_n'$ are assumed to be dependent on only the weapon yield and to have a yield-dependence of the form: constant times W^n . The effect of the wind speed on L_1 is determined by the change in $\log \phi_1$ caused by the increase or decrease in α_1 with wind speed, which is determined from

$$\phi_1(v_w) = (v_w/15)\phi_1(15) \quad (8.41)$$

for v_w in mph. The scaling functions of α_1 with weapon yield were evaluated from data for a presumed effective wind speed of 15 mph.

The scaling functions presented here could be used to evaluate A_n as a function of α as well as for the approximations that are given by Eqs. 4.32 and/or 4.30. Use of either set would require a series of recomputations of A_n to obtain a reasonably good fit to the general shape of the fallout pattern downwind intensity profile and to other pattern features.

8.3.6 The Maximum Pattern Width

The scaling function for the downwind distance, X_1 , to the maximum pattern half-width, Y_1 , is taken to be similar to those for X_1 and X_2 . The particle-group designator for this distance, α_1 , is taken to represent the case in which the maximum pattern width is measured between the 1 r/hr at 1 hr contours when the average wind speed is 15 mph. For some of the data used to determine scaling function parameters, the maximum half-width was found to be roughly proportional to the cloud radius as of 8 to 10 minutes after detonation.

The crosswind distances to given contours in the fallout area depend, first, on the lateral displacement of the particles during the rise of the cloud; second, on the wind directions at all altitudes from the bottom to the top of the cloud; and third, on the wind speeds. Thus, the observed half-widths result from the combination of the three.

The wind speed has two effects on the lateral displacement of an intensity contour. One is the displacement of particles, because of the relative horizontal distance traveled in a given period of time. The other is the decrease in surface density of a given size group with wind speed, because of the change in the angle of the particle trajectory. Hence, even for the case in which the wind direction is the same at all altitudes, a change in wind speed results in a change in the maximum cross-wind distance of a given intensity contour.

In general, the difference in direction of the horizontal components of particle-fall trajectories, because of the differences in direction and speed of the air flow from the bottom to the top of the fallout particle source volume,

is called the wind shear. Because of the difficulties in correcting fallout-pattern data, and because some of the available data have maximum pattern-widths roughly proportional to the cloud diameters for about the same wind speeds, the overall effect of the wind shear is assumed to be the same as for that group of data. The data, together with derived restrictions on the fraction of the total activity that is carried by fallout particles within a stated low intensity contour, were used to determine the variations of Y_s with weapon yield. The method used is given in Section 5.8.7.

The variation of Y_s with wind speed (for a given wind direction) is determined relative to Y_s for a wind speed of 15 mph. The representation for this variation is

$$Y_s(v_w) = Y_s(15) S(v_w) \quad (5.42)$$

in which $S(v_w)$ is the relative shear factor due to wind speed only.

The values of $S(v_w)$ determined from the fallout scaling system parameters for different wind speeds are essentially independent of yield. The indicated value of $Y_s(v_w)$ is for the particle groups falling at the downwind distance; the associated intensity contour, that passes through the location at $Y_s(v_w)$, X_s , is the same as that at X_s for the same wind speed. The intensity at the location is thus 1 r/hr at 1 hr when the wind speed is 15 mph. Values of $S(v_w)$ at several wind speeds, and the associated intensities, are given in Table 5.8.

Table 5.8

**SUMMARY OF THE RELATIVE WIND SPEED SHEAR FACTOR, $S(v_w)$,
FOR THE FALLOUT PATTERN MAXIMUM HALF-WIDTH
AND ASSOCIATED STANDARD IONIZATION RATE,
FOR SEVERAL WIND SPEEDS**

Wind Speed (mph)	$S(v_w)$	I_s (r/hr at 1 hr)
7.5	1.678	2
15	1	1
20	0.840	0.75
30	0.694	0.50
45	0.604	0.38

The value of Y_B for the 1 r/hr at 1 hr contour can be estimated from

$$Y_B(1) = \frac{Y_B(v_w) \log I_1}{\log I_1 / I_0} \quad (B.43)$$

where I_1 and I_0 are the intensities at X_1 and X_B ($y=0$) for a given value of v_w .

B.3.7 Areas and Fraction of Total Activity within Intensity Contours

With the simplified fallout scaling system and the stylized downwind intensity profile it is convenient to construct contours by using simple geometric forms which approximate to some degree the true shapes of the contours, and, within reasonable limits, account for the fraction of the activity produced that falls back to earth within their areas.

The assumed shape of the intensity contours for fallout from stem altitudes is a partial circle having its center at X_B and an elliptical contour about the intensity ridge whose major axis is down the length of the ridge and whose minor axis is crosswind. The center of the ellipse is at the intersection of the circle, centered about X_B with the major axis of the ellipse. Thus, the area within the 1 r/hr at 1 hr contour (10 mph wind speed) may be approximated by

$$SA(1) = 3.14(X_2 - X_1)^2 + 1.571 Y_{x_1}(1)(X_4 - 2X_3 + X_1) \quad (B.44)$$

This approximation gives an underestimate of the enclosed area because the ellipse is actually centered at a downwind distance of $X_B - X_1$; at that point the minor axis of the half-ellipse is tangent to the circle. The error in the area estimate is largest for the lower-valued contours and for the larger weapon yields. The maximum underestimate possible, for yields less than about 10MT, is 7 to 8 percent of the total area of the stem-pattern contour, based on the assumed geometric shape; the true error involved is unknown.

For the stem-fallout pattern, the area within contours other than the 1 r/hr at 1 hr contour can be estimated from the following functions. These are derived from the definitions of the idealized three-dimensional intensity surface. The functions are:

$$SA(1) = 3.14 (X_2 - X')^2 + 1.57 Y_{x_1}(X + X' - 2X_B) \quad (B.45)$$

where

$$X' = X_B - (2.303/k_{1,B}) \log (I_{B,B}/I) \quad (5.46)$$

$$X = X_B + \frac{(X_B - X_A) \log (I_{B,B}/I)}{\log (I_{B,B}/I_A)} \quad (5.47)$$

$$Y_B = (2.303/k_B) \log (I_{B,B}/I) \quad (5.48)$$

and

$$2.303/k_B = Y_B^2 / \log I_{B,B}^2 \quad (5.49)$$

where X' is the upwind distance between X_A and X_B , X is the downwind distance between X_A and X_B , and Y_B is the crosswind distance for the contour of intensity, I_B , for I values between I_A and $I_{B,B}$. The values of Y_B^2 and $I_{B,B}$ are those for a wind speed of 15 mph.

The shape of the 1 r/hr at 1 hr contour (15 mph wind speed) for fall-out from cloud altitudes is described by the smooth join of two ellipses at X_B , Y_B and centered at the point X_B on the pattern center line. The upwind half-ellipse for the 1 r/hr at 1 hr contour (15 mph wind speed) has a major axis of Y_B and a minor axis of $X_B - X_A$; the downwind half-ellipse has a major axis of $X_B - X_A$ and a minor axis of Y_B . Thus the area within this contour can be estimated from

$$CA(1) = 1.57 Y_B (1) (X_B - X_A) \quad (5.50)$$

For other contours, the areas can be estimated from

$$CA(I) = 1.57 Y (X - X') \quad (5.51)$$

where

$$Y = \frac{Y_B \log (I_B/I)}{\log (I_B/I_A)} \quad (5.52)$$

$$X = X_B + \frac{(X_B - X_A) \log (I_B/I)}{\log (I_B/I_A)} \quad (5.53)$$

and

$$X' = X_n + \frac{(X_0 - X_n) \log (I/I_n)}{\log (I_n/I_0)}, \quad I \leq I_n, \quad (B.54)$$

or

$$X' = X_n + \frac{(X_0 - X_n) \log (I/I_n)}{\log (I_n/I_0)}, \quad I_n \leq I \leq I, \quad (B.55)$$

In the above equations, X is the distance to the intensity I farther downwind than X_n , X' is the downwind distance between X_n and X_0 , and Y is the cross-wind distance. The variation of the distance Y with intensity is calculated from the assumption that $\log I$ decreases linearly with the distance between the points $(X_0, 0)$ and (X_n, Y_n) , and I is I_0 and I_n , respectively, at the two locations. The total area within some of the lower-valued contours for the combined fallout from both atom and cloud altitudes is less than the sum of $BA(I)$ and $CA(I)$ when the two overlap. The joint center of the ellipses moves from X_n toward X_0 as I is increased from I_n . For wind speeds other than 10 mph, I_0 and I_n (at X_n and X_0) are not 1 r/hr at 1 hr.

The activity produced by a detonation is about 1.4×10^{18} BW fissions where W is the total yield in KT and B is the ratio of fission to total yield. Some fraction of this total activity is contained within the fallout pattern. If the activity in a pattern is summed over the fallout area from the central high intensities down to a stated low-valued intensity contour enclosing the largest area, the fraction accounted for increases with yield. An ionization rate or intensity sum of a fallout pattern made in this way does not account for the activity deposited on the ground at lower intensities than the selected "lowest" contour, nor does it account for the fraction carried away on very small particles as world-wide fallout. The sum or integration of the activity over the fallout area can be used, however, to determine the fraction of the activity that is accounted for, in the fallout pattern, out to a stated low-level contour.

This fraction is defined by

$$C(I) \overline{K(I)} 1.4 \times 10^{18} BW \times \int_{I_n}^I I_n(1) dA \quad (B.56)$$

in which $C(I)$ is the true fraction of the number of fissions accounted for, and $K(I)$ is the average value of the ratio of r/hr at 1 hr to the number of fissions per unit area for all the activity within the area, A_n . The average or accumulated fractionation number, for the radioactive elements accounted for, may be

defined through $\bar{K}(1)$ by

$$\bar{K}(1) = Dq \left[r(1)k_{f_0}^0(1) + k_f^0(1) \right] \quad (B.07)$$

When the standard values of D , q , $k_{f_0}^0(1)$ and $k_f^0(1)$, from Eq. B.1 are substituted, the activity integral is

$$\int_0^\infty I_x(1) da = 5.46 \times 10^{-10} \left[r(1) + 0.19 \right] C(1) BW \quad (B.08)$$

For observed fallout patterns, the integration is carried out by replacing the integral with a sum, such as

$$\int_0^\infty I_x(1) da = \sum_j I_j A_{j+1} \quad (B.09)$$

where T_j is determined from

$$T_j = \frac{I_j - I_{j+1}}{2.303 \log I_j / I_{j+1}} \quad (B.10)$$

in which the designation j is for the successive decreasing values of $I_x(1)$ used in carrying out the summation, and A_{j+1} is the area between the contours I_j and I_{j+1} . This particular value of T_j results from the semilogarithmic approximation of the variation with distance of the intensity profile.

The activity integrals over the fallout areas obtained from the scaling system can be carried out, using the assumed shapes of the contours for the patterns from the stem and cloud fallout. The activity integral for the stem fallout pattern, designated $A_{s,1}$ for the sum out to $I_{s,1}$, can be estimated from

$$A_s = I_{s,1} \left\{ \frac{6.28}{k f_0} + \frac{1.87}{k_0} \left[\frac{2(X_4 - X_3)}{2.303 \log (I_{s,1}/I_4)} + X_3 - X_4 - \frac{2}{k f_0} \right] \right\} \quad (B.01)$$

for the case where $I_{s,1} \gg I_4$.

The activity integral for the cloud fallout pattern, designated A_0 , can be estimated from

$$A_0 = \frac{1.364 Y_R}{\log I_7} \left\{ \frac{(X_0 - X_7)}{\log(I_7/I_0)} + \frac{(X_7 - X_0)}{\log(I_7/I_0)} \right\} \times \left\{ 0.434(I_7 - I_0) + I_0 \log(I_7/I_0) \right\}$$

$$+ \frac{0.6822 Y_R I_0}{\log I_7} \left\{ \frac{(X_0 - X_7)}{\log(I_7/I_0)} [2 \log(I_7/I_0) + 0.868] \right\} \quad (6.62)$$

$$+ \frac{(X_0 - X_7)}{\log(I_0/I_7)} [\log(I_7/I_0) - \log(I_0/I_7) + 0.868] + X_7 - X_0 \}$$

for the case where $I_0 > I_7$.

The dependence of Y_R on wind speed is determined from these equations by computing the values of the various distances and intensities at several weapon yields and wind speeds and then solving for Y_R by keeping the sum of A_0 and A_0 constant for a given weapon yield. This procedure keeps constant, at least approximately, the fraction of the total activity that is carried by particle groups of a given minimum size. The integration is carried out to the low intensity, I_0 , and I_7 , whose dependence on wind speed is the same, so that the limit of integration is, in fact, changed with wind speed. The lower intensity limit used is the 1 r/hr at 1 hr for a wind speed of 18 mph; this defines the particle groups that are involved in the integrals for other wind speeds.

6.4 Summary of Derived Idealized Fallout Pattern Scaling Functions

The scaling functions given below contain constants evaluated from observed fallout pattern data. The number subscripts correspond to the notations given in Figure 6.1 on the descriptive plot of the standard intensity profile for the line directly downwind from ground zero. The functions apply to an effective wind speed of 18 mph and for a surface burst of 100 percent fission yield. All distances are in feet; all intensities are in r/hr at 1 hr; and the yield is in KT.

The scaling functions for the α values are:

$$\log \alpha_{2,0} = -0.600 + 0.070 \log W \quad , \quad W = 1 \text{ to } 10^6 \text{ KT}$$

$$\log \alpha_4 = 0.270 + 0.080 \log W \quad , \quad W = 1 \text{ to } 10^6 \text{ KT}$$

$$\log \alpha_6 = -0.170 + 0.022 \log W \quad , \quad W = 1 \text{ to } 10^6 \text{ KT}$$

$$\begin{aligned}
 \log \alpha_6 &= -0.084 + 0.000 \log W, & W &= 1 \text{ to } 10^6 \text{ KT} \\
 \log \alpha_7 &= 0.090 + 0.000 \log W, & W &= 1 \text{ to } 10^6 \text{ KT} \\
 \log \alpha_8 &= 0.049 + 0.141 \log W, & W &= 1 \text{ to } 10^6 \text{ KT} \\
 \log \alpha_9 &= 0.106 + 0.151 \log W, & W &= 1 \text{ to } 10^6 \text{ KT} \\
 \log \alpha_{10} &= 1.071 - 0.124 \log W, & W &= 1 \text{ to } 28 \text{ KT} \\
 \log \alpha_{11} &= 0.080 + 0.140 \log W, & W &= 28 \text{ to } 10^6 \text{ KT}
 \end{aligned}$$

The resulting functions for the distances are:

$$\begin{aligned}
 \log(-X_1) &= 0.308 + 0.400 \log W, & W &= 1 \text{ to } 28 \text{ KT} \\
 &= 0.504 + 0.310 \log W, & W &= 28 \text{ to } 10^6 \text{ KT}
 \end{aligned}$$

$$X_2 = \alpha_{12,n} R_n - R_n$$

$$X_3 = \alpha_{13,n} R_n + R_n$$

$$X_4 = \frac{\alpha_4(\alpha_{14} R_n - 1000)}{\alpha_4 + 0.020}$$

where

$$\log n_n = 0.880 + 0.048 \log W, \quad W = 1 \text{ to } 10^6 \text{ KT}$$

$$R_n = \frac{2,800(\log n_n - \log n_0)}{K_n}$$

$$\begin{aligned}
 \log n_0 &= \log n_n - (h \log n/R_n)/(h - R_n) \\
 \log a &= 0.080 + 0.481 \log W, & W &= 1 \text{ to } 10^6 \text{ KT} \\
 \log h &= 0.880 + 0.448 \log W, & W &= 1 \text{ to } 28 \text{ KT} \\
 \log h &= 4.226 + 0.104 \log W, & W &= 28 \text{ to } 10^6 \text{ KT} \\
 \log n/R_n &= 1.070 + 0.098 \log W, & W &= 1 \text{ to } 10^6 \text{ KT} \\
 \log R_n &= 2.810 + 0.888 \log W, & W &= 1 \text{ to } 10^6 \text{ KT} \\
 K_n &= (\log n/R_n)/(h - R_n)
 \end{aligned}$$

$$R_n = \frac{1000 + (\alpha_{14,n} + 0.020) R_n}{\alpha_{14,n}}, \quad W = 0 \text{ KT}, \quad V_w = 16 \text{ mph}$$

OR

$$R_n = (h - b), \quad W = 0 \text{ KT}$$

For n or x_n greater than 60,000 feet, the constants 1000 and 0.020 are 1100 and 0.080, respectively. The parameters n_n , x_n , and v_n are assumed to be independent of the wind speed.

$\log X_5$	$= 0.044 + 0.407 \log W, \quad W = 1 \text{ to } 28 \text{ KT}, \quad \sigma_n \approx \text{a/h}$ $= 4.049 + 0.180 \log W, \quad W = 28 \text{ to } 10^3 \text{ KT}, \quad \sigma_n \approx \text{a/h}$
X_5	$= 5.88 \times 10^3 W^{0.040} - 1.24 \times 10^4 W^{0.180} \sqrt{1 + 0.300 W^{0.000}}$ $W = 1 \text{ to } 28 \text{ KT}, \quad \sigma_n \approx \text{a/h}$
X_5	$= 1.484 \times 10^4 W^{0.250} - 1.24 \times 10^4 W^{0.300} \sqrt{1 + 0.300 W^{0.000}}$ $W = 28 \text{ to } 10^3 \text{ KT}, \quad \sigma_n \approx \text{a/h}$
$\log X_6$	$= 0.850 + 0.451 \log W, \quad W = 1 \text{ to } 28 \text{ KT}$ $= 4.200 + 0.200 \log W, \quad W = 28 \text{ to } 10^3 \text{ KT}$
$\log X_7$	$= 0.002 + 0.300 \log W, \quad W = 1 \text{ to } 28 \text{ KT}$ $= 4.308 + 0.305 \log W, \quad W = 28 \text{ to } 10^3 \text{ KT}$
$\log X_8$	$= 4.008 + 0.306 \log W, \quad W = 1 \text{ to } 28 \text{ KT}$ $= 4.410 + 0.315 \log W, \quad W = 28 \text{ to } 10^3 \text{ KT}$
$\log X_9$	$= 5.190 + 0.310 \log W, \quad W = 1 \text{ to } 28 \text{ KT}$ $= 5.302 + 0.311 \log W, \quad W = 28 \text{ to } 10^3 \text{ KT}$
$\log Y_5$	$= 3.228 + 0.400 \log W, \quad W = 1 \text{ to } 10^3 \text{ KT}$

Values of Y_n for yields other than those given can be obtained from a plot of the listed values against yield.*

The scaling functions for the high intensity ridge near ground zero, the intensity at the shoulder in the cloud pattern, and the intensity of the downwind pattern features, are:

$$\log I_{Y_{n,a}} = k_{1,a}(X_a - X_1)/0.300$$

where

$$\log k_{1,a} = 0.308 - 0.404 \log W, \quad W = 1 \text{ to } 28 \text{ KT}$$

$$= 2.100 - 0.037 \log W, \quad W = 28 \text{ to } 10^3 \text{ KT}$$

* See Tables 5.2 above and 5.3 below.

or

$$\log I_{\mu,\alpha} = \log k_{\mu,\alpha}(1)\bar{\Lambda}_f + \log \Delta \pi_{\mu,\alpha}$$

and

$$\log I_4 = \log k_4(1)\bar{\Lambda}_f + \log \Delta \pi_4$$

where

$$\log \Delta \pi_{2,3} = \log \Delta \pi_{2,3}^0 + n \log v_w \quad (\text{See Table 5.1})$$

and

$$\log \Delta \pi_4 = 0.280 + 0.040 \log W - \log v_w, \quad W = 10^4 \text{ to } 10^6$$

also,

$$\log K_{\mu,\alpha}\bar{\Lambda}_f = 2.088 - 0.408 \log W, \quad W = 10^4 \text{ to } 10^6 \text{ KT}$$

$$\log K_4\bar{\Lambda}_f = 2.080 - 0.404 \log W, \quad W = 10^4 \text{ to } 10^6 \text{ KT}$$

For $\ell = 5$ through D :

$$I_\ell = 4.000n K_\ell \bar{\Lambda}_f \log \phi_\ell, \quad \alpha_\ell \geq n/h$$
$$= 4.000n K_\ell \bar{\Lambda}_f \log \phi'_\ell, \quad \alpha_\ell < n/h$$

where

$$\log n/h = -0.481 - 0.014 \log W, \quad W = 1 \text{ to } 28 \text{ KT}$$
$$= -0.887 + 0.267 \log W, \quad W = 28 \text{ to } 10^6 \text{ KT}$$

and

$$\phi_\ell = \frac{(\alpha_\ell + n/h) + \sqrt{(n/h)^2 + (\alpha_\ell + n/h)^2}}{(\alpha_\ell - n/h) + \sqrt{(n/h)^2 + (\alpha_\ell - n/h)^2}}, \quad \alpha_\ell \geq n/h$$

$$\phi'_\ell = \frac{(\alpha_\ell + n/h) + \sqrt{(n/h)^2 + (\alpha_\ell + n/h)^2}}{\alpha_{\ell,n} + \sqrt{(n/h)^2 + \alpha_{\ell,n}^2}}, \quad \alpha_\ell < n/h$$

where

$$\log (n/h)^2 = 0.486 + 0.262 \log W$$

$$\log n = 3.389 + 0.481 \log W$$

and where

$$\log K_0 \bar{A}_\alpha = -0.280 + 0.808 \log W, W = 1 \text{ to } 28 \text{ KT}, \alpha_0 > n/h \\ = -0.280 + 0.072 \log W, W = 28 \text{ to } 10^6 \text{ KT}, \alpha_0 > n/h$$

$$\log K_0 \bar{A}_\alpha = -0.185 + 0.408 \log W, W = 28 \text{ to } 10^6 \text{ KT}, \alpha_0 < n/h$$

$$\log K_0 \bar{A}_\alpha = -1.184 + 0.074 \log W, W = 1 \text{ to } 10^6 \text{ KT}, \alpha_0 > n/h \\ \log K_0 \bar{A}_\alpha = -1.225 + 0.022 \log W, W = 1 \text{ to } 10^6 \text{ KT}, \alpha_0 < n/h$$

$$\log K_0 \bar{A}_\alpha = -0.989 + 0.037 \log W, W = 1 \text{ to } 10^6 \text{ KT}, \alpha_0 > n/h \\ \log K_0 \bar{A}_\alpha = -1.070 + 0.020 \log W, W = 1 \text{ to } 10^6 \text{ KT}, \alpha_0 < n/h$$

$$\log K_0 \bar{A}_\alpha = -2.106 + 0.052 \log W, W = 1 \text{ to } 10^6 \text{ KT}, \alpha_0 > n/h$$

The values of the fallout pattern features from the above scaling functions are given in Table 5.8 for several weapon yields.

The scaling functions for α_1 and $K_1(1)\bar{A}_\alpha$, derived from the scaling system suggest that (1) the distribution of the activity in the different particle-size groups tends to broaden with yield, and (2) the distribution shifts to smaller particle sizes with increasing weapon yield. Because the highest intensities are near X_0 , the particle-size groups having the highest value of A_α are those of the size group designated by α_1 . None of the more complicated fallout models in use at the present time considers a change with yield in either the activity particle size or the activity fall-velocity distributions, as this result suggests.

The product $(x(1) + 0.02)C(1)$ for the scaling system varies from about 0.4 to 0.8 between 1-KT and 10^6 -KT (for integrations out to the 1 r/hr at 1 hr contour). These results indicate, at least for the larger yields where the fraction of the activity on the ground but outside the 1 r/hr at 1 hr contour is very small, that both the over-all fractionation and the fraction contributed to world-wide fallout decrease with increasing yield. These indications are in accord with (1) the shift of the activity particle size distribution mentioned above, and (2) the slower cooling of the fireball with yield. Both factors should contribute to a more complete scavenging of the vaporized fission products by soil particles. For comparison with similar values in DNW and other publications, the values of $C(1)K(1)$ in terms of r/hr at 1 hr per KT/sq mi for the six selected yields, 1 to 10^6 -KT, are 850, 1140, 1280, 1380, 1480, and 1600, respectively.

TABLE 5-3

SUMMARY OF FAIRING PATTERN FEATURES AND FAIRING SCALE'S SENSITIVE
PARAMETER VALUES FOR AN INERTIAL EFFECTIVE WIND SPEED OF 15 MPH^a

Parameter	WIND SPEED			INPUT
	15 MPH	30 MPH	45 MPH	
X ₁	-2.69	-6.20	-15.99	-69.30
X ₂	206	1,710	3,731	3,359
X ₃	1,659	5,128	11,309	46,359
X ₄	7,720	22,610	59,330	73,600
X ₅	4,339	13,800	35,466	52,800
X ₆	7,659	21,500	45,209	57,100
X ₇	7,250	25,000	75,320	111,600
X ₈	35,319	38,319	118,409	131,400
X ₉	355,600	323,010	987,009	915,000
X ₁₀	1,619	4,210	10,209	25,309
X ₁₁	6,659	12,210	31,209	56,700
X ₁₂	1,710	22,510	55,309	342,000
X ₁₃	1,659	212	595	1,439
X ₁₄	355	317	863	15,300
X ₁₅	5,300	14,910	22,309	5,679
X ₁₆	0.43	0.33	0.63	0.73
X ₁₇	1.0000000000000002	1.0000000000000002	2.4500000000000003	2.5000000000000002

^a Parameters are in feet. Input values are in 1/16 ft.^b at 1 ft. increments.

^b The value of 1 ft. per second is 0.02778 ft.

5.5 Illustrative Computations for the Use of the Simplified Fallout Scaling System

5.5.1 Construction of Idealized Fallout Patterns

The use of the scaling functions and of the simplified fallout scaling system is illustrated in this section by some calculations for a 1-MT yield surface detonation. The first step in constructing the idealized contours is to plot (or compute) the intensity profiles along the center line of the pattern as $\log I/I_0$ against distance. The second step is to compute or read off the distances from surface zero to a pre-selected set of contour values. The third step is to plot or compute the semilogarithmic line from $(I_{1,0}, 0)$ to $(1, Y_1)$ for the lateral locations of the contours for the stem fallout (see Eqs. 5.48 to 5.49).

The fourth step is to construct the stem-fallout pattern by marking on a rectangular grid the noted distances to each contour along the line $y = 0$. The "ground-zero" circular portion of the pattern is then drawn in, by first drawing the appropriate circles centered at X_0 and then closing them to the lateral distances taken from the $I_{1,0} - Y_1$ plot. At this point, the contours are drawn parallel to the X-axis and closed (with an elliptical shape) if a common point occurs on the X-axis. The remainder are extended to about the distance to the lowest-valued closed contour.

The fifth step is to draw or compute the semilogarithmic line from $(I_1, 0)$ to $(1, \sqrt{Y_1} + (X_1 - X_0))$, to determine the contour locations between $(X_1, 0)$ and (X_0, Y_1) . If the distance between these two locations is designated D , and the distances from $(X_1, 0)$ to the selected contours are D' , then the lateral distance to each one, Y_1 , is determined from $D'Y_1/D$ or directly from Eq. 5.52. The corresponding downwind location, X_1 , is $X_1 + D(X_1 - X_0)/D$ or $X_1 + (X_1 - X_0)(Y/Y_1)$. These are the points through which the elliptical contours of the cloud fallout pass.

The farthest upwind locations at X'_0 are read from the intensity profile between X_0 and X_1 , or computed from Eqs. 5.54 or 5.55. The upwind half-ellipse is given by the equation

$$\frac{(x - X'_0)^2}{(X_1 - X'_0)^2} + \frac{y^2}{Y^2} = 1 \quad (5.63)$$

The downwind half-ellipse is

$$\frac{(x - X_1)^2}{(X_0 - X_1)^2} + \frac{y^2}{Y^2} = 1 \quad (5.64)$$

In which X is the downwind distance to the contour between X_1 and X_2 (see Eq. 5.53). The various intensity-distance lines and profiles for the 1-MT yield are shown in Figure 5.2; the contours derived from them are shown in Figure 5.3, with the distances converted to statute miles.

The pattern of Figure 5.3 is in many respects quite different from those described in ENW. Table 5.4 gives a few comparisons of the two derivations for the 1-MT yield.

Table 5.4

**COMPARISON OF FALLOUT PATTERN DATA FOR A 1-MT YIELD
OBTAINED FROM THE SIMPLIFIED SCALING SYSTEM FUNCTIONS
AND FROM THE ENW METHODS**

	Distance in Miles ^a	
	Simplified System	ENW Method
Upwind Distance to 1 r/hr contour	6.8	17.4
Downwind Distance to 1000 r/hr contour	55	28
Downwind Distance to 100 r hr contour	129	98
Downwind Distance to 10 r hr contour	190	270
Maximum Half-Width, 1 r hr contour	52	89

a. Wind speed of 15 mph.

The major pattern features not recognized in the ENW scaling method are the observed presence of the major downwind peak and the corresponding rapid broadening of the pattern in the region of this peak. Also, the huge ground-zero circle obtained by the ENW method does not agree with observations for yields greater than a few KT; these two scaling systems should give patterns most nearly alike for yields in the region of 1-KT. Comparisons of the fallout pattern features calculated from the simple scaling system presented here with those from other fallout models, are discussed further in Section 5.6.

Figure 5.2
INTENSITY-DISTANCE PLOTS FOR CONSTRUCTION OF AN IDEALIZED FALLOUT PATTERN
FOR A 1-MT YIELD SURFACE DETONATED FOR A WIND SPEED OF 15 MPH

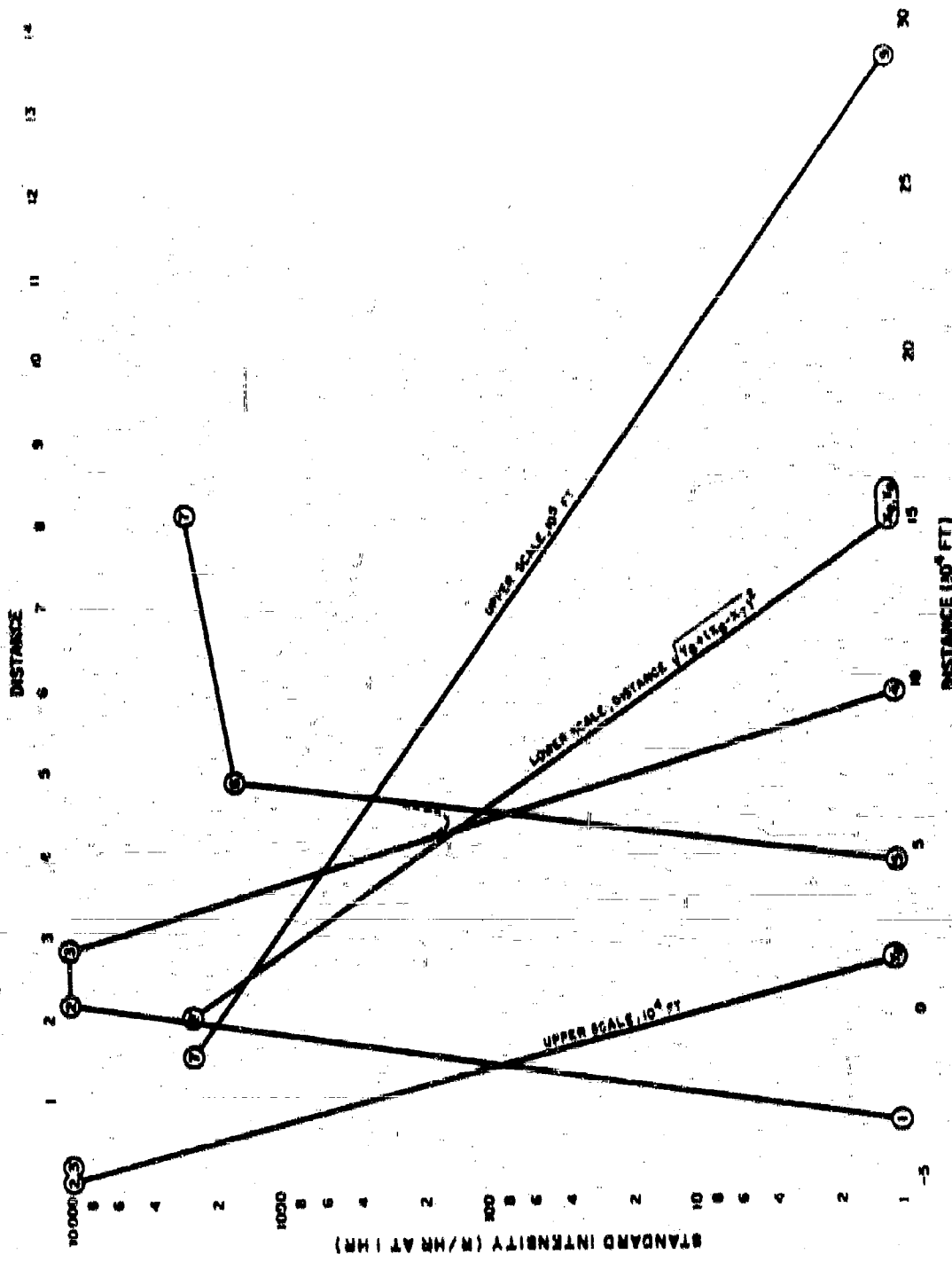
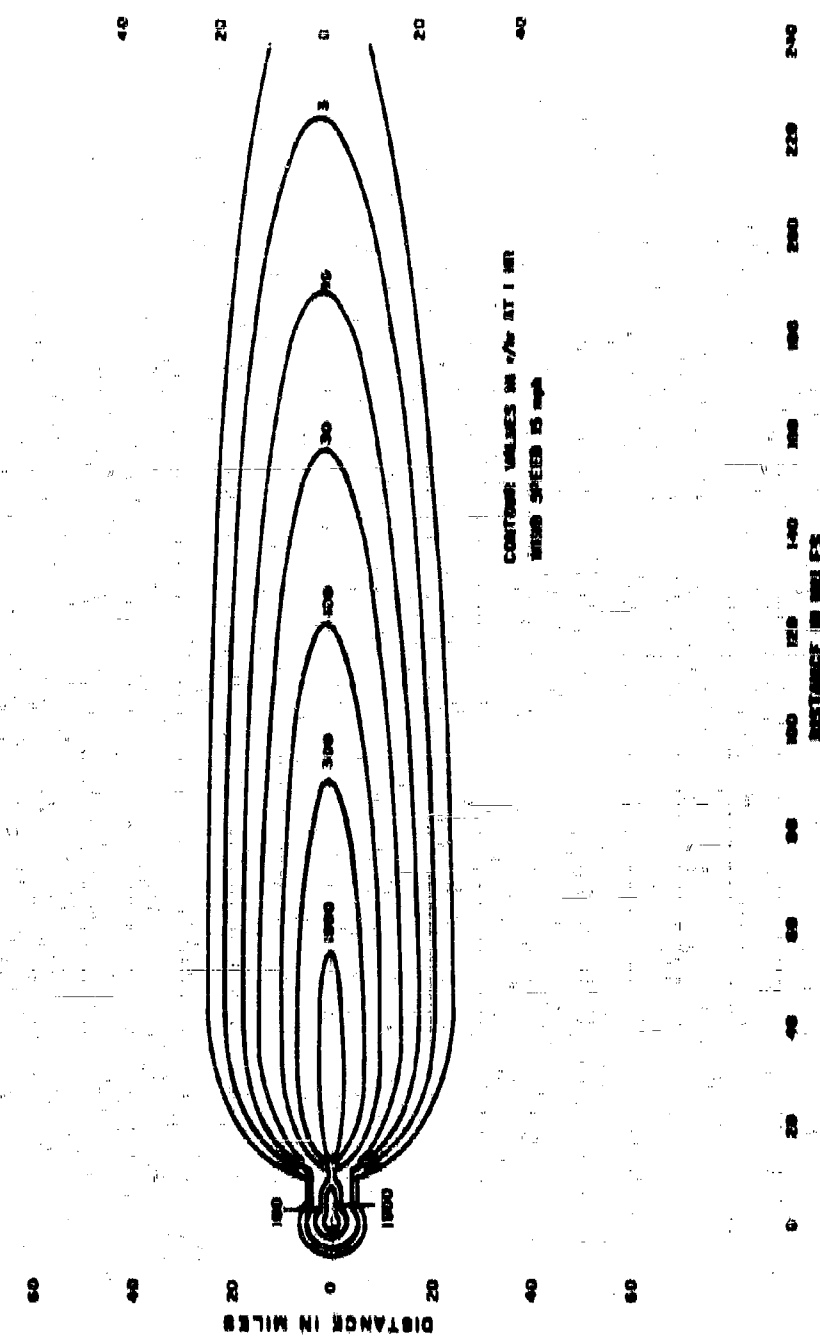


Figure 5.3
IDEALIZED FOLLOUT PATTERN FOR A 1-MT YIELD SURFACE BURST FOR A WIND SPEED OF 15 MPH AND NO PENETRANT EMISSION



5.5.2 Fallout Arrival Rate and Exposure Dose during Fallout Arrival

The method of estimating the times, rates, and duration of fallout arrival, and the resulting exposure dose, is illustrated by calculations for the 1-MT yield. Two locations are selected, one at the downwind distance of 5.85×10^4 ft (6.3 miles) and the other at 1.87×10^5 ft (35.4 miles); both are on the center line of the idealized pattern. The standard intensity at both these locations is 2000 r/hr at 1 hr. At the shorter distance, essentially all the fallout comes from stem altitudes; at the greater distance it all arrives from cloud altitudes. Different methods are applicable to the two cases; the one for the fallout from cloud altitudes is described first.

To make these calculations, estimates of A_α as a function of α are required in order to evaluate the integral of $A_x(\alpha)$ as indicated by Eqs. 4.8 to 4.11. From Eqs. 4.22, 4.66, and 4.75, the first estimate of A_α is given by

$$A_\alpha = \frac{6.17 \times 10^7 I_x(1)}{[r_x(1) + 0.019]} \quad (5.65)$$

However, since $r_x(1)$ is not known, and since the term $(r_x(1) + 0.019)$ will cancel out in adjusting the integral of $A_x(\alpha) d\alpha$ to 2000 r/hr at 1 hr, it is convenient to replace the multiplier of $I_x(1)$ with the constant, $1/K_x(1)$, so that

$$K_x(1) = 1.62 \times 10^{-8} [r_x(1) + 0.019] \frac{\text{r/hr at 1 hr}}{\text{fission/cu ft}} \quad (5.66)$$

In the first estimate of the distribution of $K_x(1)A_\alpha$ with α , the α for a given value of $I_x(1)$ is taken to be equal to X/h . The distribution curve for $K_x(1)A_\alpha$ is shown in Figure 5.4.

The computations for α_{\min} , α_{\max} , h_0 , h_1 , t_0 , $K_x(1)A_\alpha(\alpha)$, and $K_x(1)A_\alpha(\alpha)/\Delta t$ are summarized in Table 5.5. The values of $K_x(1)A_\alpha(\alpha)$ are plotted in Figure 5.5. The peak value is noted to occur at an α of about 3.1, which is less than the value of $\alpha_c = 8.86$ for this distance. The integral under the curve is $K_x(1)A_x = 6.96 \times 10^7$ r/hr at 1 hr-ft, and A_x is $9.98 \times 10^{13} / [r_x(1) + 0.019]$ fissions/sq ft.

The calculated standard intensity, from

$$I_x(1) = 3.90 \times 10^{-13} [r_x(1) + 0.019] A_x \quad (5.67)$$

Figure 5.4
FIRST ESTIMATE OF THE DEPENDENCE OF $K_p(t_{\text{DP}})$ ON (FOR A 1-MT SURFACE)
DETONATION AND INDO SPEED OF 15 MPH

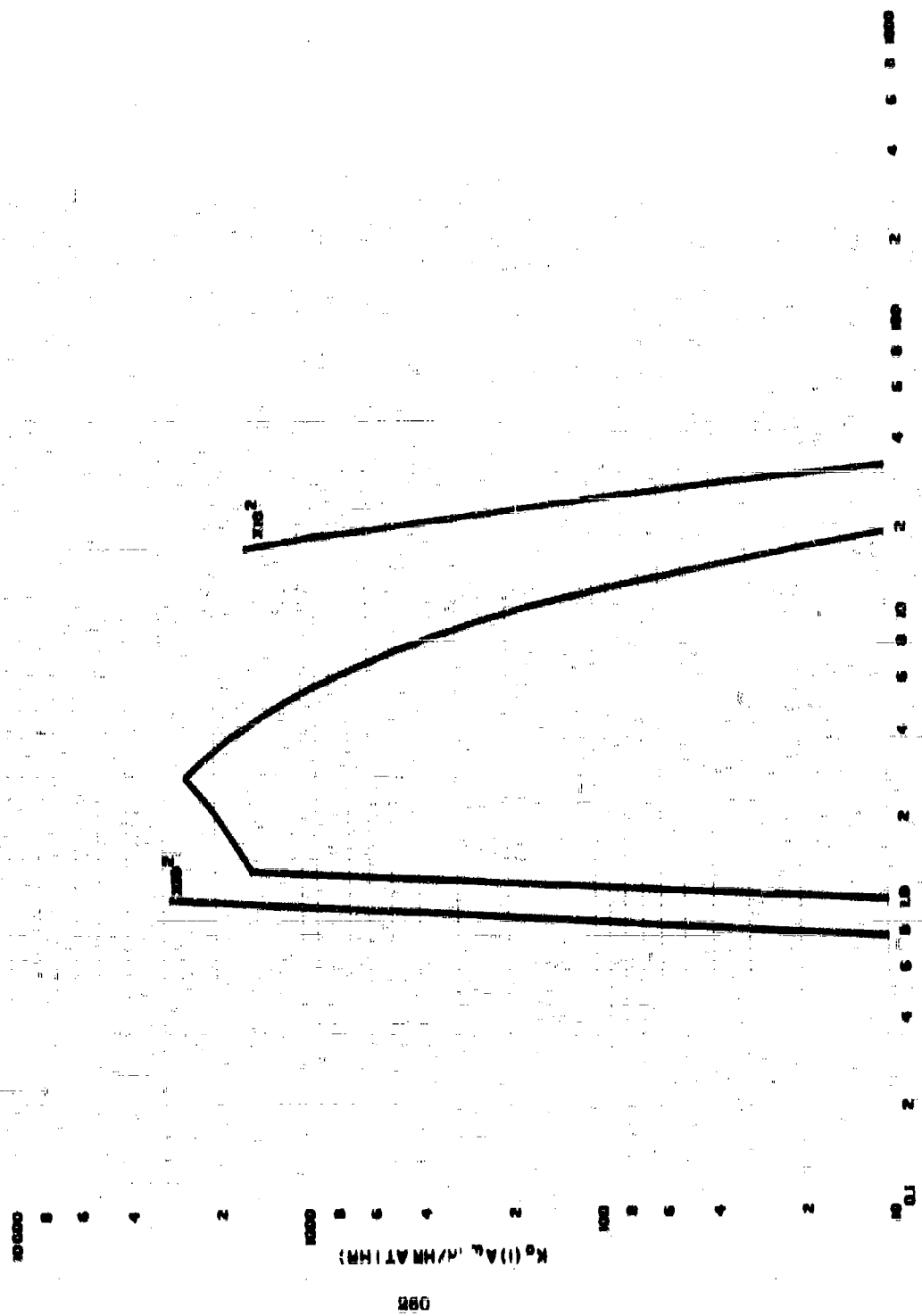


Table 5-5
CALCULATION OF FAILURE ARRIVAL RATE AT $X = 1.67 \times 10^5$ ft, $\beta = 9$
FROM A 1-50 SURFACE TEST FOR A WIND SPEED OF 15 MPH

a	b_2 (ft^2/ft)	b_1 (ft^2/ft)	t_a (sec)	t_c (sec)	Δt (sec)	$K_{CPA-Het}$ ($10^{-7} \text{ ft}^2/\text{sec} \cdot \text{ft}^2 \cdot 1 \text{ hr}^{-1}$)	$K_{CPA-Het}$ ($10^{-7} \text{ ft}^2/\text{sec} \cdot \text{ft}^2 \cdot 1 \text{ hr}^{-1}$)
2.50	5.38	5.08	1.07	1.07	0	0	0
2.6	5.35	5.12	1.09	2.19	0.5	1.79	5.30
2.5	5.37	5.30	1.09	2.35	0.46	2.35	6.37
3.0	4.37	6.22	1.04	2.53	0.49	2.82	6.37
3.2	4.59	6.39	1.07	2.67	0.55	3.43	5.12
3.4	4.55	6.19	2.05	2.75	0.71	2.60	4.35
3.6	4.35	6.46	2.11	2.89	0.78	3.48	4.35
3.8	4.25	5.91	2.18	2.97	0.73	3.86	3.78
4.0	4.39	5.72	2.25	3.03	0.73	2.79	3.36
4.2	4.14	5.35	2.32	3.07	0.71	2.38	3.08
4.4	4.11	5.15	2.32	3.10	0.68	1.95	2.72
4.6	4.10	5.10	2.31	3.10	0.70	1.92	2.41
4.8	4.14	4.94	2.64	3.06	0.12	0.97	2.23
5.0	4.05	4.37	2.99	2.99	0	0	0

$a = 4.39 \times 10^5$ ft

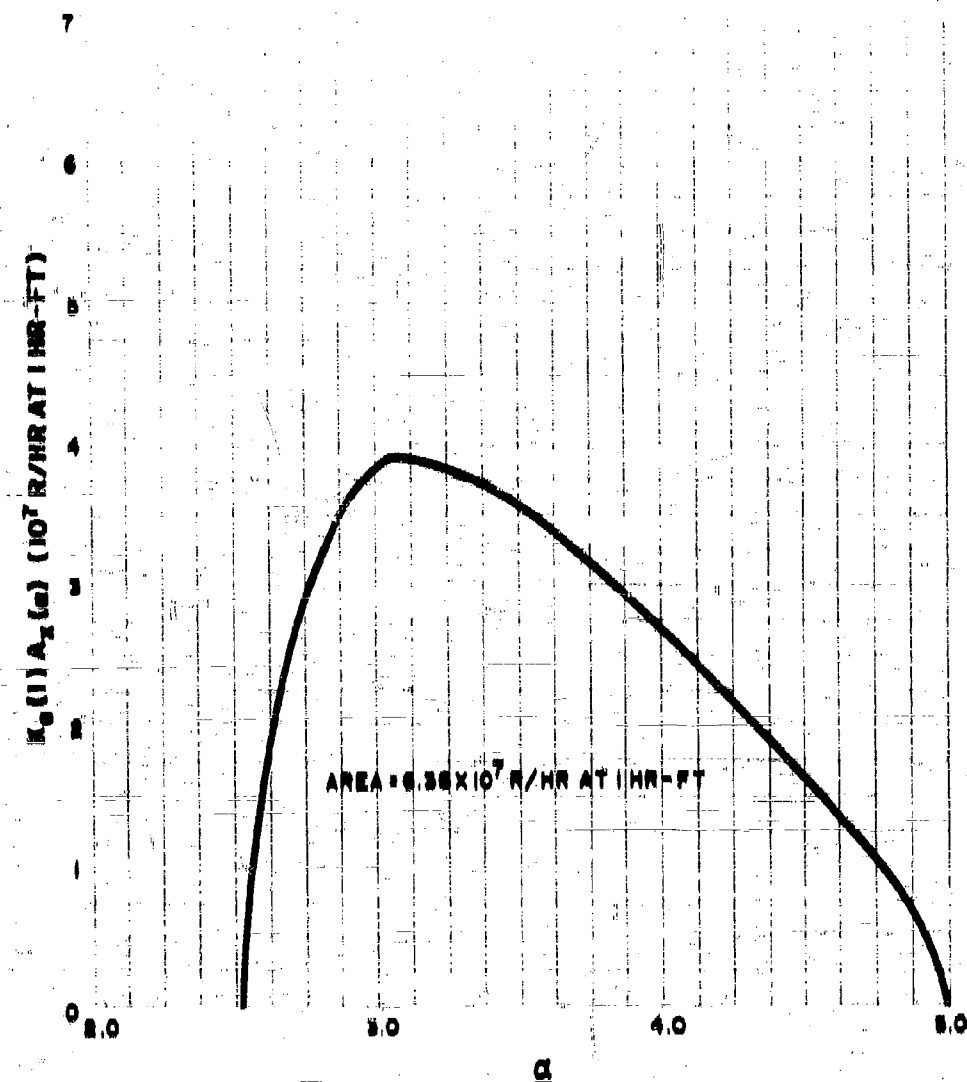
$b = 1.11 \times 10^5$ ft

$b = 5.25 \times 10^5$ ft

$L_D = 3000 \text{ ft}$

$t_c = 1000 \text{ sec}$ or 27.8 min

Figure 5.5
VARIATION OF $K_0(1)A_\alpha(\alpha)$ WITH α AT $x = 1.67 \times 10^5$ FT FOR $W = 10^3$ KT
AND A WIND SPEED OF 18 MPH



is 1080 r/hr at 1 hr. This value is about 76 percent of the pattern value, 2000 r/hr at 1 hr. In order to make the calculation more exact, the distribution curve of $K_n(1)A_n$ should be increased about 31 percent for α values between 2.0 and 5.0. However, since similar calculations at several additional locations would be required to make a complete second estimate of $K_n(1)A_n$, and since these have not yet been done, no correction is made in $K_n(1)A_n$ for this illustration. Instead, the correction was applied as a single multiplier to the final values of $I_n(1)$.

The times of fallout arrival, t_a , and of detonation, t_d , were increased by 0.18-hour (8 minutes) to account for the time of cloud formation. The time of arrival intervals, shown in Figure 5.6 as a function of α , form a closed loop; this curve is used to provide the range of α groups that are landing at any given time. The rate of arrival of the radioactivity carried by each α group in Figure 5.7 shows the highest rate of accumulation for the larger particles (those having the lower α values).

The activity arriving at any given time is the sum of that being deposited by all the α groups that are landing. The indicated summation is shown in part of Table 5.6. First, the sum under the curve of Figure 5.7 was obtained by summing the areas of rectangles. This was done by reading the midpoints of each 0.05 increment of α and accumulating 0.05 times the values directly on an adding machine. The α ranges for selected values of the time were taken from Figure 5.6 and the differences in the summation to the respective values of α_{\max} and α_{\min} arriving at each time were then calculated by direct interpolation of the summation.

The total rate of arrival shown in Figure 5.8 reaches its maximum at about 2.3 hours after detonation. The summation of the activity under this curve is 0.51×10^7 r/hr at 1 hr-ft, which is in agreement with the summation of $K_n(1)A_n(\alpha)$. The $I_n(1)$ values were obtained by adjusting the total to 2000 r/hr at 1 hr and adjusting all the other values by the same factor. The decay correction factors, $d(t,1)$, were calculated from the data of Figure 11.2 (see Volume II, Chapter 11), which includes the contributions of about 0.8 atoms of U-238 produced at zero time for each fission event. The product, $I_n(1)d(t,1)$, is the value of $I_n(t)$ at each time after fission.

The maximum observed intensity indicated is 420 r/hr, occurring at 8 hours after detonation. The shape of the intensity-time curve is shown in Figure 5.9. The exposure dose, D_{ex} , is the summation under this curve times 1.00; this factor corrects for the instrument response contained in the values of $I_n(t)$.

The dose accumulation (true air ionization) over terrain such as existed at the test site is 444 roentgens up to time of detonation (0.11 hours).

Table 5.6
**SUMMATION OF ARRIVAL RATES FOR GROUPS ARRIVING AT THE SAME
 TIME AND ACCUMULATION OF ACTIVITY AND EXPOSURE DOSE DURING
 THE FALLOUT PERIOD**

α	0.051X ₀ (DA ₀)Δt (10 ⁻⁷ r/hr \pm 1 hr \cdot B/μr)	T (hr)	α Range	Σ			$K_0(DA_0)/\Delta t$ (10 ⁻⁷ r/hr \pm 1 hr \cdot B/μr)
				$\alpha = \alpha_{\text{min}}$	$\alpha = \alpha_{\text{max}}$	$\alpha = 2.5$	
2.5	0.9	1.0	2.5-2.8	1.984	2.22	-	0.9
2.6	0.175	1.9	2.52-3.22	4.538	9.079	1.462	
	0.389	2.0		6.186	9.175	6.013	
	0.848	2.1	2.55-3.55	7.34	9.712	5.632	
2.7	1.194	2.2	2.63-3.83	8.358	1.470	6.528	
	1.539	2.3	2.74-4.13	9.104	2.294	6.316	
	1.884	2.4	2.86-4.37	9.571	3.931	6.620	
2.8	2.226	2.5	2.97-4.58	10.804	3.956	6.039	
	2.575	2.6	3.12-4.73	10.315	4.757	5.358	
	2.920	2.7	3.26-4.87	10.494	5.626	4.868	
3.0	3.265	2.8	3.43-5.08	10.532	6.336	5.956	
	3.513	2.9	3.63-5.09	-	-	-	
3.1	3.868	3.0	3.88-4.83	10.442	7.330	2.912	
	4.113	3.1	4.09-4.69	9.700	9.187	8.513	
3.2	4.428	3.1	-	-	-	6.0	
	4.784	-	-	-	-	-	
3.3	4.979	-	-	-	-	-	
	5.229	-	-	-	-	-	

Table 5.6 (continued)

α	$0.052X_c$ (PA, cm/m)	t (cm)	X_c (PA, 10^7 m/m)	$L(1)$ (m^2 /m at 1 fm)	$d\Phi/dt$	$L(t)$ (m^2 /m)	D_{π}^2 (fm)
3.4	5.498						
3.5	5.723	1.88	6.9	0.416	0.0	0.0	
	5.599	1.9	6.016	5.1	0.497	2.1	0.02
3.6	6.198	2.0	6.114	46.	0.394	18	0.53
	6.498	2.0	6.238	187.	0.380	41	2.35
3.7	6.622	2.1	6.591	187.	0.365	68	5.23
	6.839	2.1	6.873	279.	0.353	98	11.58
3.8	7.033	2.2	1.162	378.	0.342	129	19.48
	7.229	2.2	1.518	481	0.330	159	29.23
3.9	7.429	2.2	1.854	587	0.321	188	46.95
	7.684	2.3	2.198	686	0.311	216	54.53
4.0	7.784	2.3	2.544	806	0.303	244	76.06
	7.938	2.4	2.888	915	0.294	269	87.23
4.1	8.128	2.4	3.225	1,022	0.285	291	105.83
	8.294	2.5	3.570	1,128	0.278	314	125.36
4.2	8.454	2.5	3.885	1,231	0.271	334	147.53
	8.609	2.6	4.196	1,330	0.264	351	176.28
4.3	8.760	2.6	4.492	1,423	0.257	365	194.13
	8.916	2.7	4.776	1,513	0.250	378	213.95
4.4	9.065	2.7	5.047	1,599	0.245	392	244.6
	9.187	2.8	5.301	1,680	0.239	401	271.88
4.5	9.321	2.8	5.536	1,756	0.233	409	298.13
	9.451	2.9	5.750	1,822	0.226	415	325.62
4.6	9.577						

Table 5.6 (continued)

	$\theta_{\text{NET}}(D_A, d, t)$ (10^3 r/hr at 1 hr- d hr)	t (hr)	$K_2(D_A)$ (10^7 r/hr at 1 hr- d)	$K_3(D)$ (r/hr at 1 hr)	$d(D, I)$	$I_c(\theta)$ (r/hr)	D_{ex}^2 (θ)
4.6	9.700	3.0	5.389	1.882	0.224	.22	353.45
	9.819	3.9	6.102	1.933	0.219	.23	381.63
	9.936	4.7	6.231	1.974	0.214	.22	409.32
	10.053	5.1	6.339	1.99	0.211	.21	436.63
	10.162	5.11	6.312	2.009	0.210	.20	443.65
	10.272	4					
	10.380	5					
	10.484	6					
	10.582	8					
5.0		10					

2. Separation of Eqn 33

Figure 5.6
TIME OF ARRIVAL OF THE VARIOUS PARTICLE GROUPS DESIGNATED BY α
FOR A WIND SPEED OF 15 MPH



Figure 5.7
RATE OF ACTIVITY DEPOSITION ON THE GROUND AS A FUNCTION OF α AT
 $X = 1.87 \times 10^3$ FT. FOR $W = 10^3$ KT AND A WIND SPEED OF 15 MPH

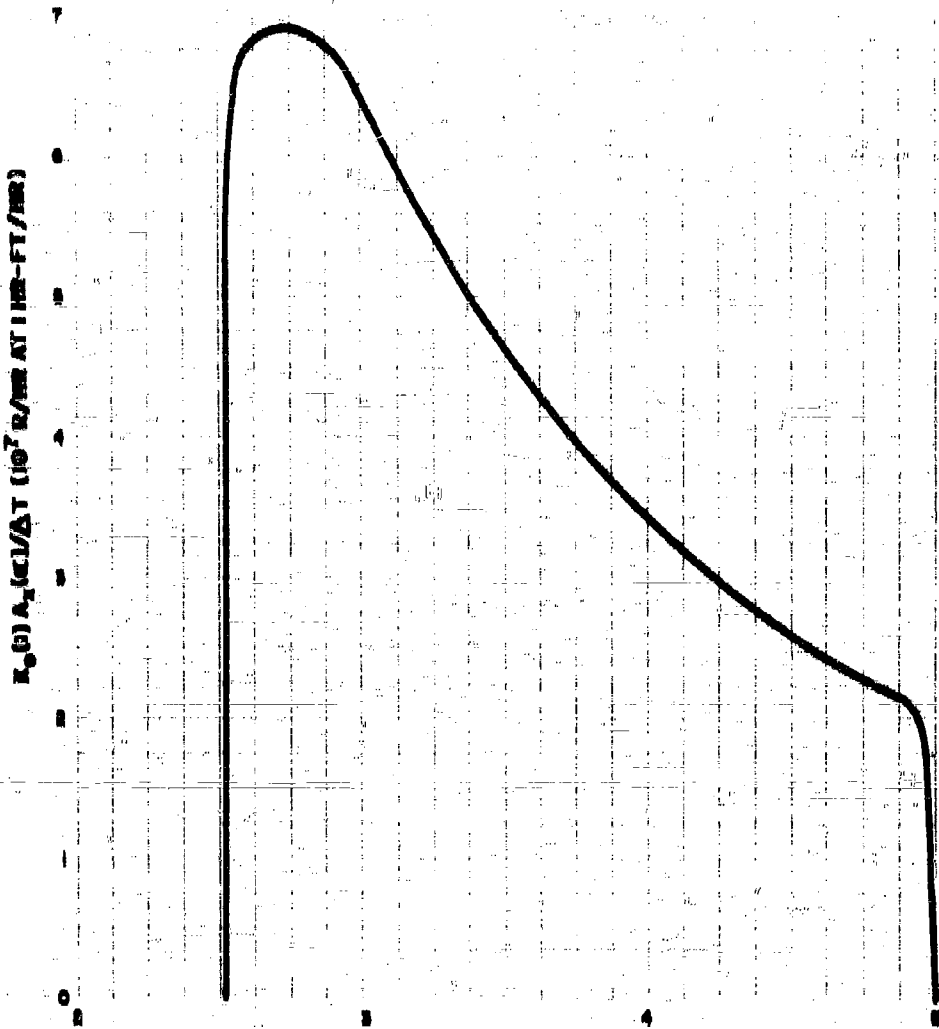


Figure 5.8
RATE OF FALLOUT ARRIVAL AS A FUNCTION OF TIME AFTER DETONATION AT
 $X = 1.87 \times 10^5$ FT FOR $W = 10^3$ KT AND A WIND SPEED OF 15 MPH

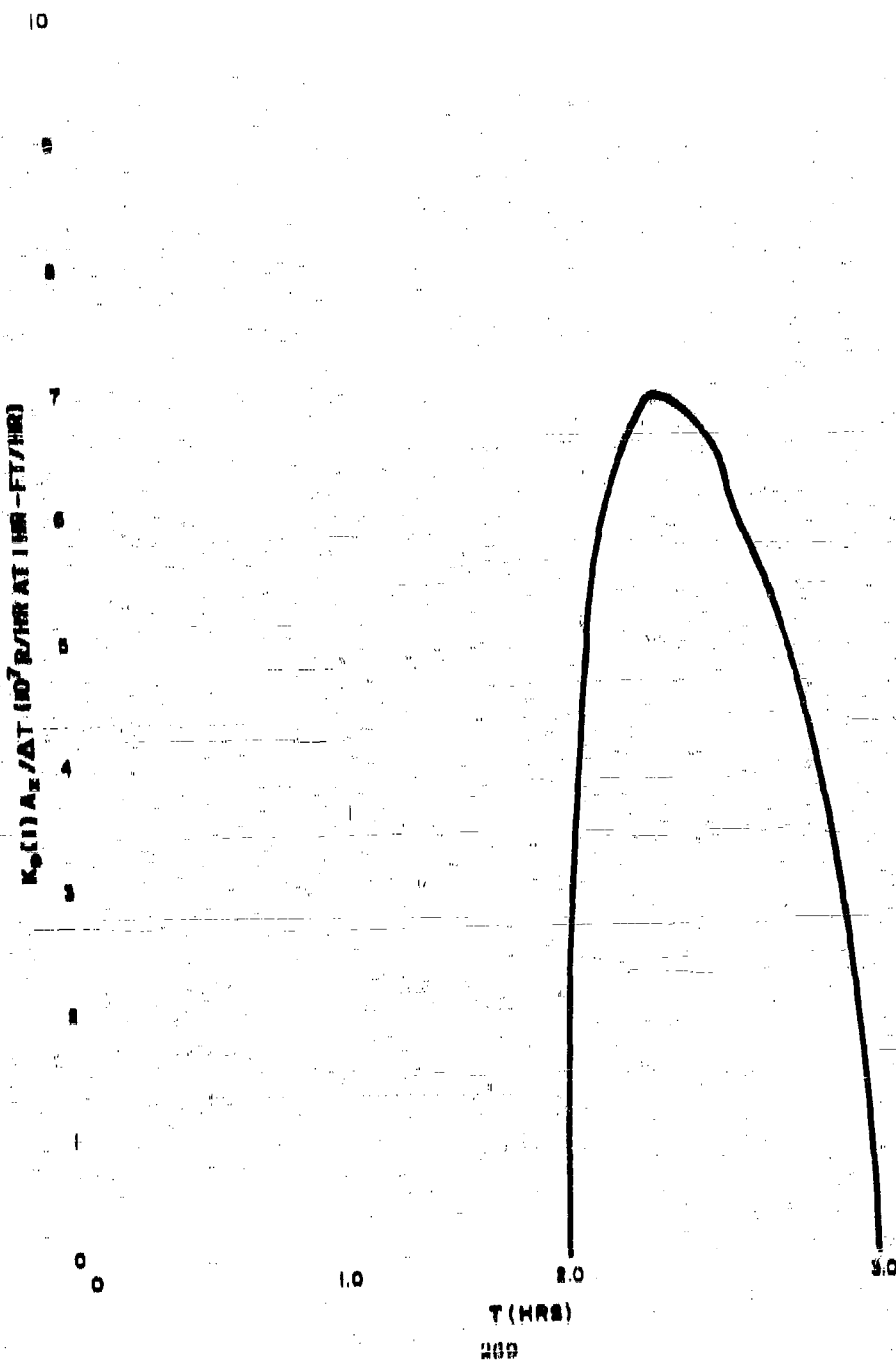
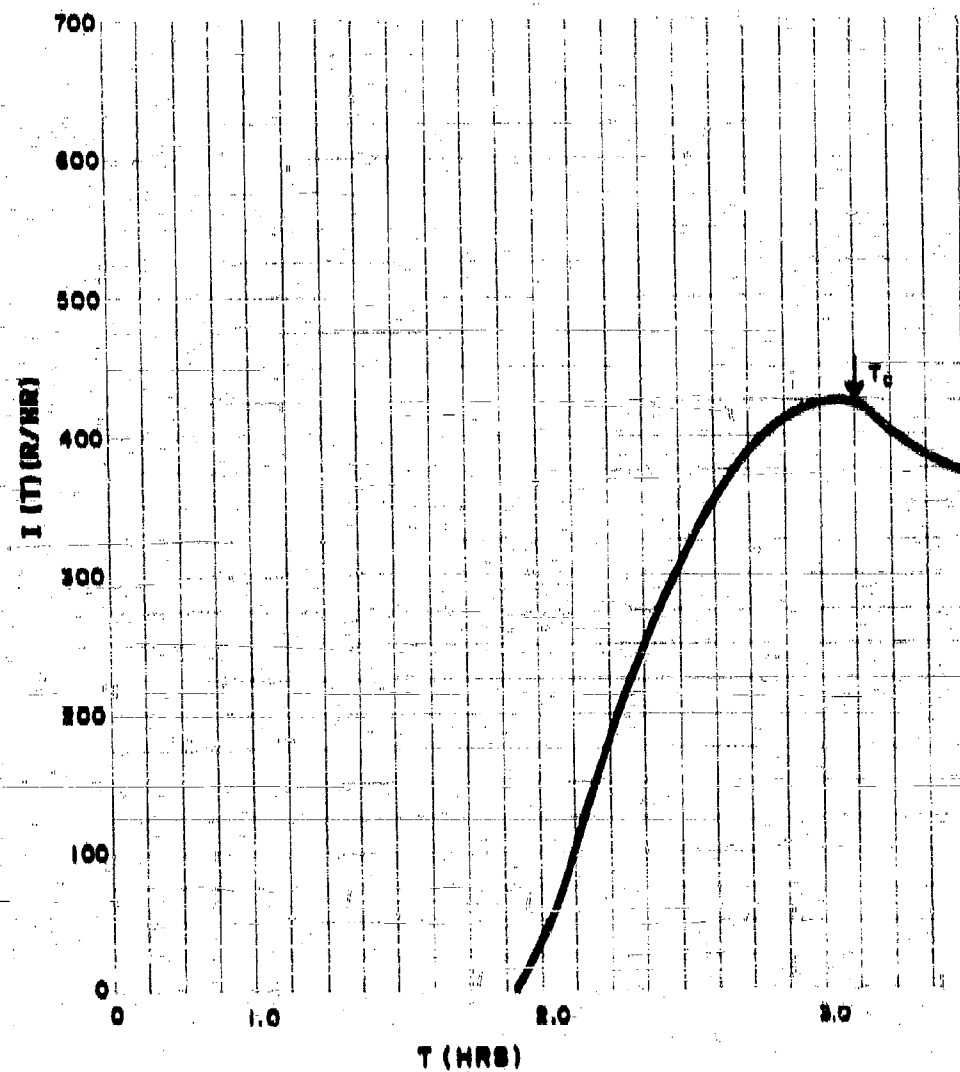


Figure 5.9
VARIATION OF IONIZATION RATE WITH TIME AFTER DETONATION AT
 $X = 1.87 \times 10^3$ FT FOR $W = 10^3$ KT AND A WIND SPEED OF 18 MPH



From the decay curve of Figure 11.2 (see Volume II, Chapter 11) the total exposure dose is 4540 roentgens at 48 hours, 6080 roentgens at 1 week, and 8470 roentgens at 2.8 years (this is the so-called infinity dose).

The contribution to the dose rate from airborne activity can be estimated if it is assumed that the fractionation effect on A_{α} cancels that in A'_{α} . The dose rate from the airborne material should be proportional to the rate of deposition of the activity, so that if it is computed for one time the contribution at other times should be proportional to $K_p(1)A'_{\alpha}/\Delta t$. The time selected for the calculation was 2.8 hours, the time of maximum fallout deposition.

At this time the arriving particle groups have α values between 2.74 and 4.18 (see Table 5.6). From Figure 5.4, the integral, or summation of $K_p(1)A'_{\alpha}d\alpha$, between these α values is 2.82×10^{-6} r/hr at 1 hr; increasing this by 81 percent to correspond to the adjusted deposit level gives 3.86×10^{-6} r/hr at 1 hr (observed). If $(r_s(1) + 0.019)$ is assumed to equal unity, and the value of $A_{\alpha}N_1$ is taken as that for unfractionated fission products, then the integral of $A'_{\alpha}d\alpha$ in Eq. 4.73 is 2.86×10^{11} fissions/cu ft, and $A'_{\alpha}E_t$ is 4.4×10^{-9} Mev/sec/fission. These values give a dose rate of 0.9 r/hr at 2.8 hours.

The contribution to the ionization rate at 8 feet above the surface from the deposited material at this time of 2.8 hours is 216 r/hr, giving a total ionization rate of 250 r/hr. The airborne contribution at 2.8 hours is, therefore, about 4 percent of the total ionization rate. However, at 1.9 hours, just as the fallout is beginning to deposit, the airborne ionization rate is about 2.4 r/hr or just over 50 percent of the total. It is seen from Table 5.6 that, at 2.8 hours, the summation of $K_p(1)A'_{\alpha}/\Delta t$ is slightly less than this value and, since the same summation would apply to the ionization rate from airborne material, the total exposure dose from this source would be less than 0.9 roentgens. This is about 2 percent of the total exposure dose. Therefore, at this selected location, the airborne material is not an important contributor to the total exposure dose.

The first step in making estimates of the arrival times of the various particle groups and the resulting dose rate from stem fallout is to compute the values of α_{\min} and α_{\max} at several downwind distances. The α values are plotted against distance and read off at selected distances as required to make the first estimate of the distribution of A'_{α} as a function of α . To make this estimate, Eq. 4.60 is used, in the form

$$K_p(1)A'_{\alpha} = I_s(1)/(\alpha_{\max} - \alpha_{\min}) \quad (5.68)$$

where $K_p(1)$ is assumed to be constant in lieu of information on the dependence of $r_s(1)A'_{\alpha}$ on α . The average particle-size group at a given downwind distance, α , is calculated from $(\alpha_{\min} + \alpha_{\max})/2$.

The values of α_{\min} and α_{\max} at various downwind distances are most easily determined by calculating the values of α_y and α for different values of y by use of Eqs. 4.31 and 4.48 and then from Eq. 4.82, computing the distance. These equations, for a 1-MT yield detonation, are

$$\log \alpha_y = 3.261 + 2.72 \times 10^{-6} y, \quad (5.60)$$

$$\alpha = \frac{1900 + 0.020 y}{28,900 - y}, \quad (5.70)$$

and

$$X = \alpha y + R_s, \quad (5.71)$$

The values of α_{\min} and α_{\max} obtained from these three equations are plotted in Figure 5.10. The computation of the first estimate of $K_x(1)A'_x$ as a function of X , which is shown in Table 5.7 and is plotted in Figure 5.11, was made by use of the $I_x(1)$ -values of Figure 5.2. The odd shape of the distribution near its maximum is due to the assumption in the scaling system, that the top of the activity ridge is flat from X_s to X_m .

The time of fallout arrival and the distribution function of $K_x(1)A'_x$ should not be applied to distances less than R_s , which is about 2000 feet for the 1-MT yield; however, $K_x(1)A'_x$ should approach zero as α or $\bar{\alpha}$ approaches zero. These distances will not be of much interest for estimating fallout arrival times, since R_s is approximately equal to the crater radius.

For the illustrative computation of the arrival rate of fallout from stem altitudes, the standard intensity of 2000 r/hr at 1 hr was again selected. For the stem fallout, this intensity occurs at $X = 8.80 \times 10^3$ feet, or 6.3 miles, and $y = 0$. The time of arrival of each particle group, selecting 10 mph for the wind speed, can be estimated from Eqs. 4.62 and 4.64. For the 1-MT yield, these arrival times are

$$t_g = 0.0581 [\log (\alpha + 0.020) + 1.182] \quad (5.72)$$

and

$$t_f = \frac{1.26 \times 10^{-3} \alpha (28,900 \alpha - 1900)}{(\alpha + 0.020)} \quad (5.73)$$

for the time in hours. The group arrival time is the sum of t_g and t_f (neglecting the delay-time due to circulation in the fireball). From Figure 5.10, at the selected distance of 6.3 miles, α_{\min} is 0.80, and α_{\max} is 1.60. The arrival times for these groups and for particle groups with intermediate values of α , the calculated activity αu , and the calculated ionization rates, are shown in Table 5.8.

Figure 5.10
VARIATION OF α_{MAX} AND α_{MIN} WITH DOWNWIND DISTANCE FOR A 1-MT YIELD
SURFACE DETONATION AND WIND SPEED OF 15 MPH

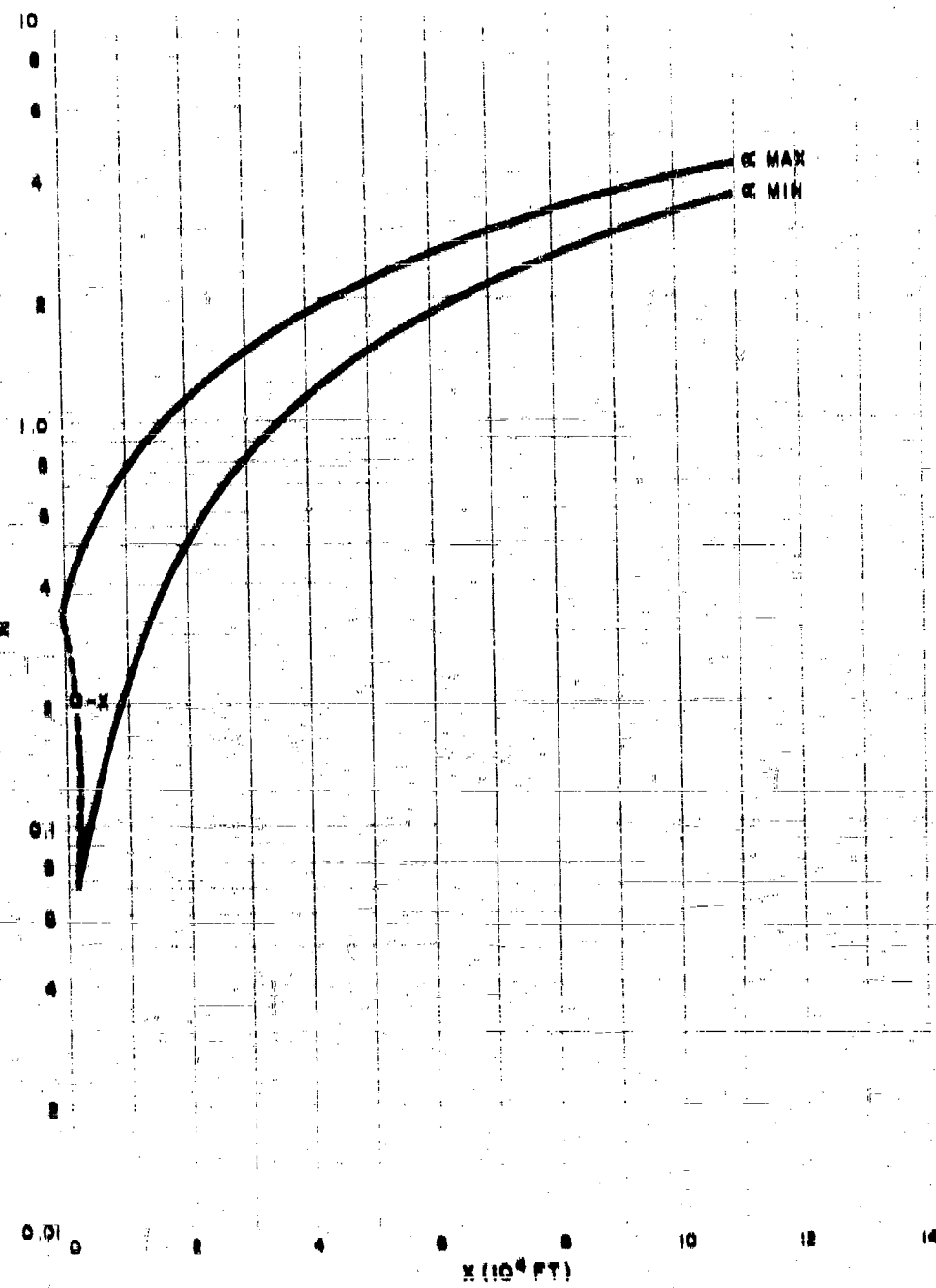


Table 8.7

FIRST ESTIMATE OF $K_x(1)\Delta_\alpha$ AS A FUNCTION OF α
FOR A 1-MT YIELD SURFACE DIPOXATION

X (10^4 ft)	α_{trap}	α_{min}	$\Delta\alpha_m$	$I_x(1)$ (v/hr at 1 hr)	$K_x(1)\Delta_\alpha$ (v/hr at 1 hr)	θ
0	0.32	0	0.32	3800	1.00×10^4	0.16
0.20	0.40	0.07	0.33	0000	1.01×10^4	0.25
0.400	0.50	0.11	0.39	0800	2.38×10^4	0.32
1.0	0.75	0.22	0.53	0800	1.85×10^4	0.48
2.0	1.10	0.40	0.70	0800	1.04×10^4	0.80
2.18	1.15	0.52	0.63	0800	1.00×10^4	0.84
2.5	1.20	0.64	0.56	0700	8.77×10^3	0.90
3.0	1.48	0.80	0.68	0100	4.00×10^3	1.14
4.0	1.84	1.13	0.71	040	1.02×10^3	1.48
5.0	2.10	1.47	0.72	285	390	1.88
6.0	2.58	1.80	0.73	85	110	2.16
7.0	2.00	2.17	0.73	26.5	35	2.54
8.0	3.20	2.81	0.78	7.7	10.7	2.87
9.0	0.00	3.80	0.71	2.00	0.28	3.20
0.7	0.70	0.08	0.71	1.0	1.41	3.44

Figure 5.11
FIRST ESTIMATE OF $K_1(1)A'$ AS A FUNCTION OF α FOR FALLOUT FROM STEM ALTITUDES
FOR A 10^3 KT YIELD SURFACE BURST AND A WIND SPEED OF 15 MPH

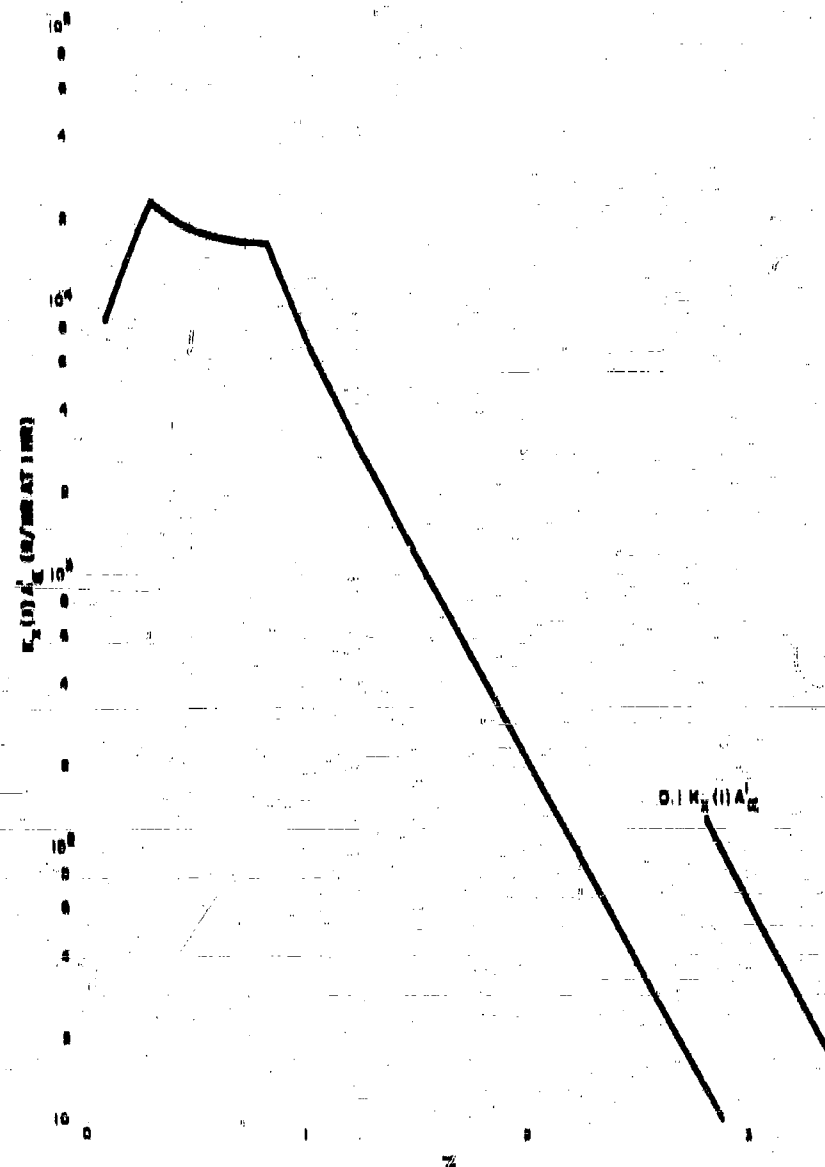


Table B.8

CALCULATED ARRIVAL TIMES AND DOSE RATES DURING THE FALLOUT PERIOD AND UP TO 1.8 HR AT THE DOWNWIND DISTANCE OF 0.3 MILES FROM A 1-MT YIELD SURFACE DTONATION

α	t_p (hr)	t_f (hr)	t (hr)	$K_x(1)\Delta_a'$ (r/hr at 1 hr)	$K_x(1)\Delta_x$ (r/hr at 1 hr)	$I_x(1)$ (r/hr at 1 hr)	$d(t,1)$	$I_x(0)$ r/hr
0.00	0.007	0.208	0.308	1.20×10^4	0	0	2.80	0
0.05	0.008	0.210	0.304	9.7×10^3	800	800	2.08	1,010
1.00	0.060	0.304	0.400	7.0	900	700	2.50	1,700
1.05	0.070	0.308	0.420	0.4	1,340	900	2.13	2,300
1.10	0.073	0.371	0.448	0.2	1,000	1,100	2.04	2,710
1.15	0.073	0.325	0.402	4.8	1,800	1,820	2.25	2,080
1.20	0.074	0.407	0.481	8.0	2,000	1,400	2.17	3,170
1.25	0.070	0.426	0.500	2.00	2,222	1,080	2.00	3,300
1.30	0.070	0.444	0.520	2.48	2,000	1,070	2.01	3,370
1.35	0.077	0.462	0.580	2.08	2,571	1,770	1.94	3,480
1.40	0.078	0.480	0.558	1.70	2,000	1,820	1.80	3,440
1.45	0.078	0.498	0.570	1.47	2,040	1,880	1,820	3,480
1.50	0.070	0.617	0.600	1.20	2,712	1,920	1,700	3,300
1.55	0.080	0.584	0.614	1.00	2,708	1,970	1,700	3,350
1.60	0.081	0.552	0.608	8.7×10^3	2,810	2,000	1,040	3,280
				0.80			1,200	3,680
				1.0			1,000	2,000
				1.2			0.704	1,500
				1.4			0.638	1,280
				1.6			0.520	1,000
				1.8			0.442	881

In the computation, $K_x(1)\Lambda_x$ is the summation of $K_x(1)\Lambda_{\alpha}$ over the α increments. The summation is made by reading off the midpoint values of $K_x(1)\Lambda_{\alpha}$ for each 0.05 α increment, multiplying by 0.05, and summing. Since the model is set up for the arrival of only one α group at a time, the summation can be made by using either α or the arrival time as the independent variable. This procedure actually utilizes α as a designator for a group of particles of a finite particle size range in which α may be considered to be the designator for the average or median size of the particles in that group.

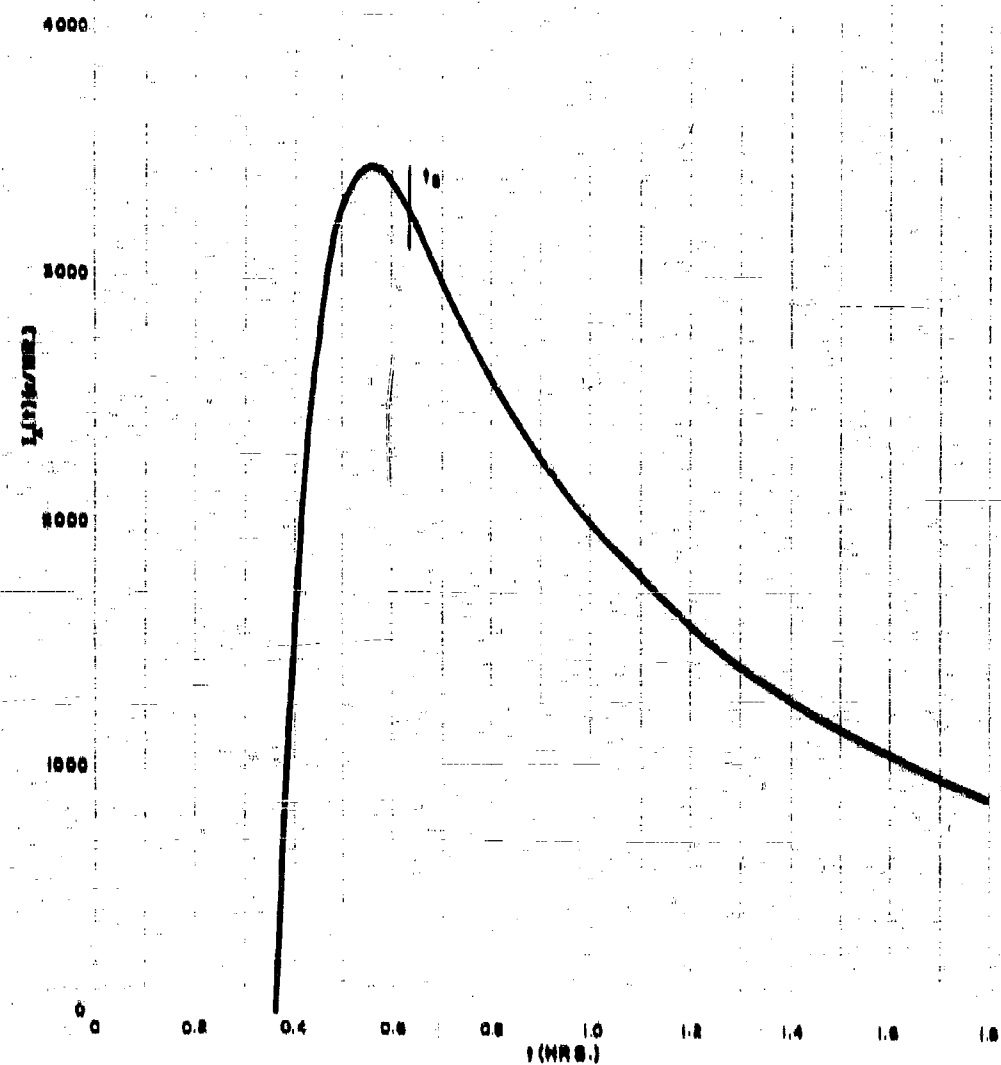
The summation, $K_x(1)\Lambda_x$, up to the time of fallout cessation (0.63 hours), gives a value of 2,816 r/hr at 1 hr rather than the scaled value of 2,000 r/hr at 1 hr; hence the second estimate of $K_x(1)\Lambda_{\alpha}$ for α values between 0.00 and 1.00 would be 71 percent of the values of $K_x(1)\Lambda_x$ shown in Figure 5.11. Since the other calculations necessary for adjusting the whole distribution curve have not yet been made, all the $K_x(1)\Lambda_x$ values were multiplied by 0.71 to obtain the appropriate values of $I_x(t)$. The decay correction factors were obtained, as before, from Figure 11.9.

The variation of the dose rate with time after detonation, at the 0.3 mile distance, is shown in Figure 5.12. Since in this case fallout has stopped before H+1, the curve passes through the 2,000 r/hr at 1 hr point at 1 hour after detonation. Because of the rapid rate of arrival of the larger particles and the rapid decay rate, the intensity rises very rapidly to a peak of about 3,400 r/hr at about 0.56 hours. In the cloud fallout case, by contrast, the peak intensity is relatively nearer the time of fallout cessation and the rate of build-up is not nearly as rapid.

The summation of the area under the $I_x(t)$ curve was made by using 0.02 hour increments. The sum to 0.63 hour is 770 roentgens; the exposure dose itself, therefore, is 1,080 roentgens. At 1 hour the exposure dose would be 2,200 roentgens; at 48 hours it would increase to 8,880 roentgens; at 2 weeks the exposure dose would be 11,000 roentgens; and at about 2 years (the infinity dose) it would increase to 13,800 roentgens.

The most rapid arrival rate occurs at the beginning of fallout. The contribution of the airborne activity to the dose rate at this time should be at a maximum. It can be estimated by use of Eqs. 4.73 and 4.78, if the fractionation is assumed to cancel between A_1 , \bar{W}_1 and $K_x(1)\Lambda_x$, and if $(r_x(1) + 0.010)$ is not equal to unity. The average value of dI_x/dt (i.e., for the corrected values of $K_x(1)\Lambda_x$) from 0.883 to 0.884 hours is about 2.05×10^4 r/hr at 1 hr per hour. Using 3.0×10^{-10} r/hr at 1 hr per fission/mg ft for $K_x(1)$, the value of $d\Lambda_x/dt$ is 0.20×10^{10} fissions/mg ft-hr. At the mid-time of the time interval, particles with an α value of 0.925 are arriving, so that, with a 15 mph wind speed, the value of A_{α} of Eq. 4.73 for these particles is 0.14×10^{11} fissions/cu ft.

Figure 5.12
VARIATION OF THE IONIZATION RATE WITH TIME AFTER DETONATION AT
 $X = 3.35 \times 10^4$ FT FOR $W = 10^3$ KT AND A WIND SPEED OF 18 MPH



The calculations of LaRiviere¹ give $A_t B_t$ at 0.374 hours as 9.5×10^{-4} Mrv/mic-fission. Use of these values in Eq. 4.72 gives 2.0 r/hr at 0.374 hours. Since this is about the maximum airborne contribution to the ionization rate because of the rapid rate of fall and of accumulation of particles on the ground, the contribution of the airborne activity to the total dose during fallout at this location is negligible.

5.5.3 Method for Estimating the Particle Sizes in the Fallout at a Given Location

The particle-size range of the fallout at a given location or locations is an important consideration in the design of fallout shelter ventilation systems as well as in the planning and execution of decontamination operations. For purposes of conducting realistic and meaningful experiments in decontamination and in shelter design, methods for estimating likely particle sizes are necessary for the preparation and use of fallout simulants.

The simplified fallout-system scaling functions, together with particle fall-rate data, can be used to estimate the particle-size groups that fall at any given downwind location. Further, they can be used to make estimates of the fraction of the activity that is carried by the different sizes of particles that fall from both stem and cloud altitudes. This information could also be used in the more sophisticated computer programs for estimating fallout depositions under meteorological conditions other than those of uniform wind speed and direction.

Because the fall velocity of a particle of a given size varies with altitude in falling through the atmosphere, the designator, α , of a given fall vector represents a group of particles, with a spread in diameters that depends on both the thickness of the cloud and the altitude from which the group falls. In Figure 5.18 the size of spherical particles falling through a standard atmosphere from various altitudes is plotted as a function of vector velocity. These curves were prepared by D. B. Clark from data provided by A. D. Anderson.² The estimated diameters of the particles falling at $X = 1.87 \times 10^4$ feet and at $X = 8.35 \times 10^4$ feet for the 1-MT yield detonation used in Section 5.4 are shown in Table 5.9. For $v_w = 10$ mph,

$$v_f = 22/\alpha \text{ ft/sec.} \quad (5.74)$$

The height of fall for the particles falling from stem altitude is

$$z = \frac{(28,900\alpha - 1900)}{(\alpha + 0.020)} \text{ ft.} \quad (5.75)$$

Figure 5.13
VERTICAL COMPONENT OF THE VELOCITY FOR SPHERICAL PARTICLES FALLING
FROM VARIOUS ALTITUDES TO SEA LEVEL

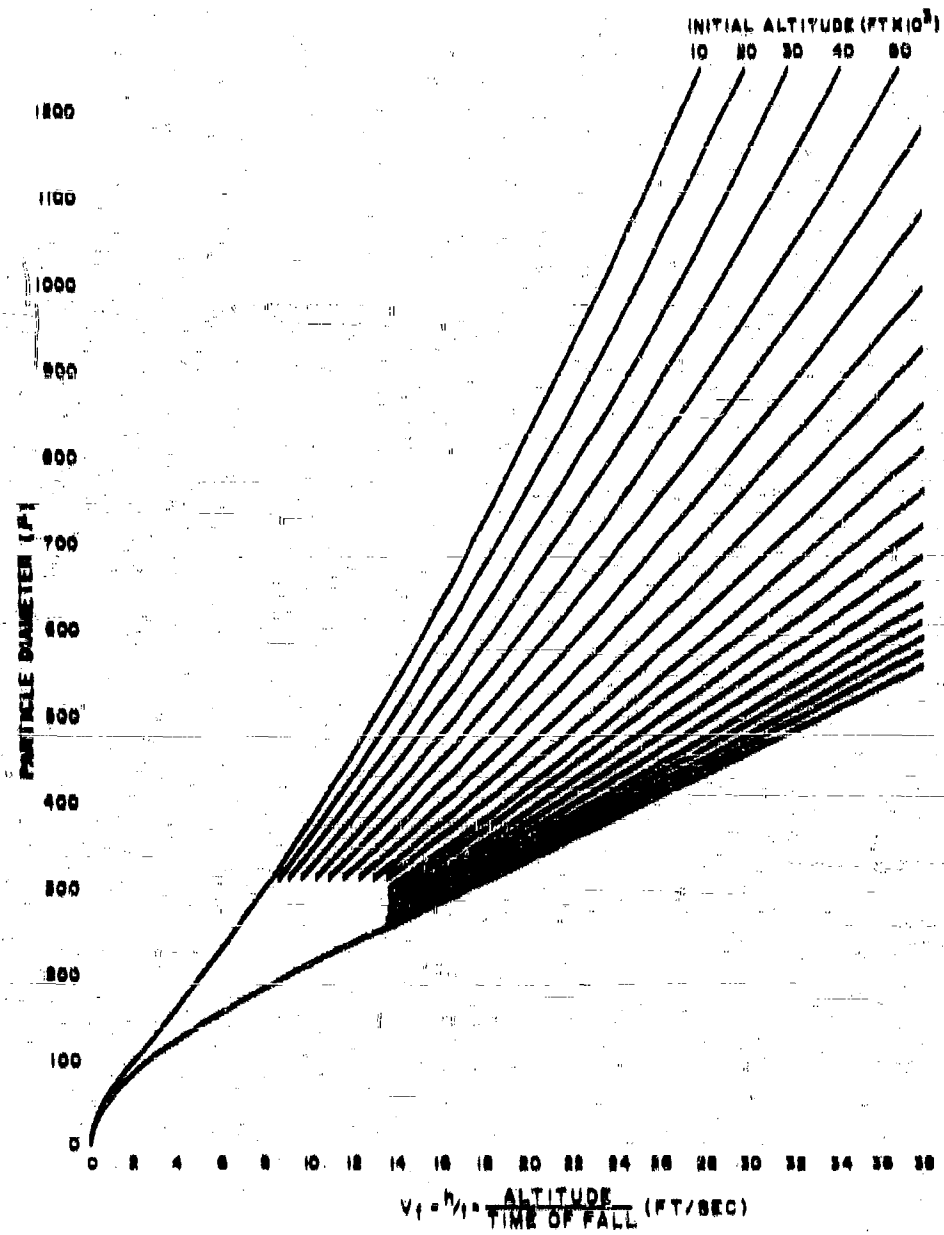


Figure 5.13 (continued)

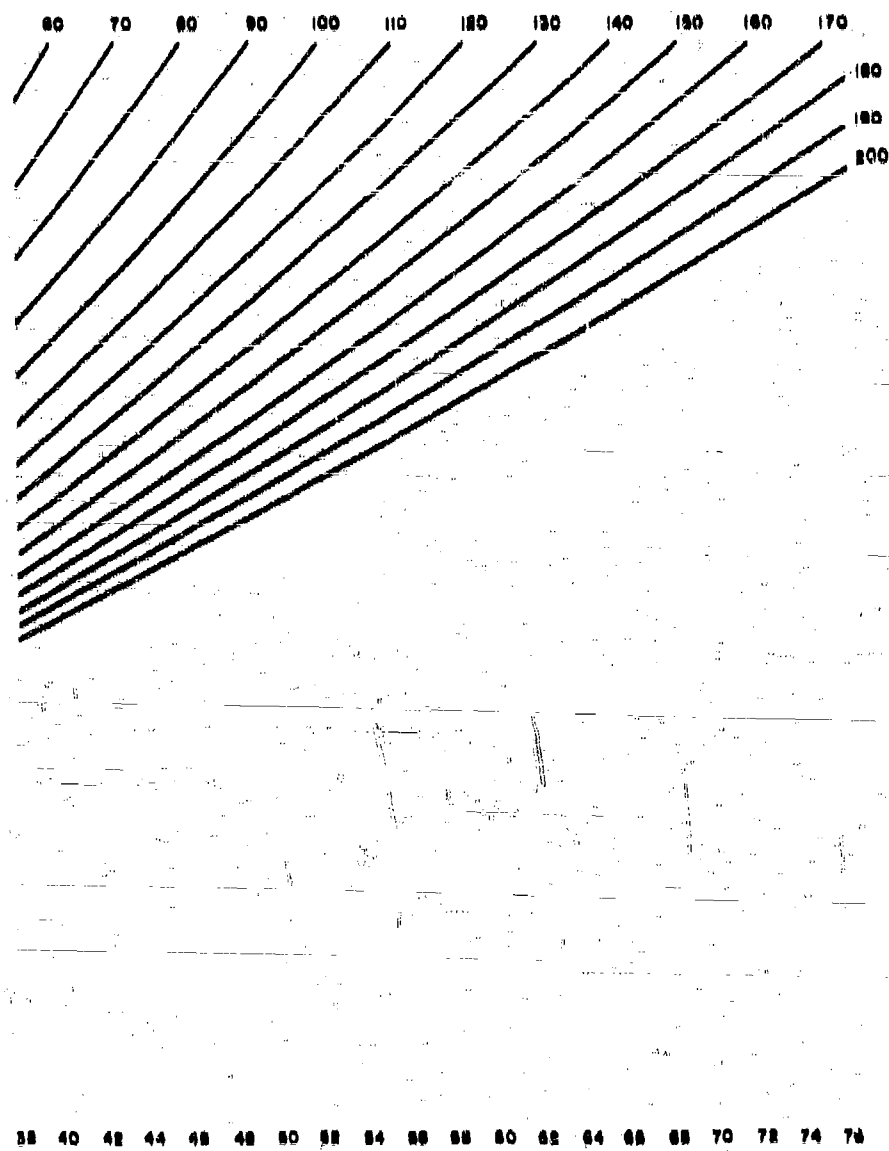


Figure 5.13 (continued)

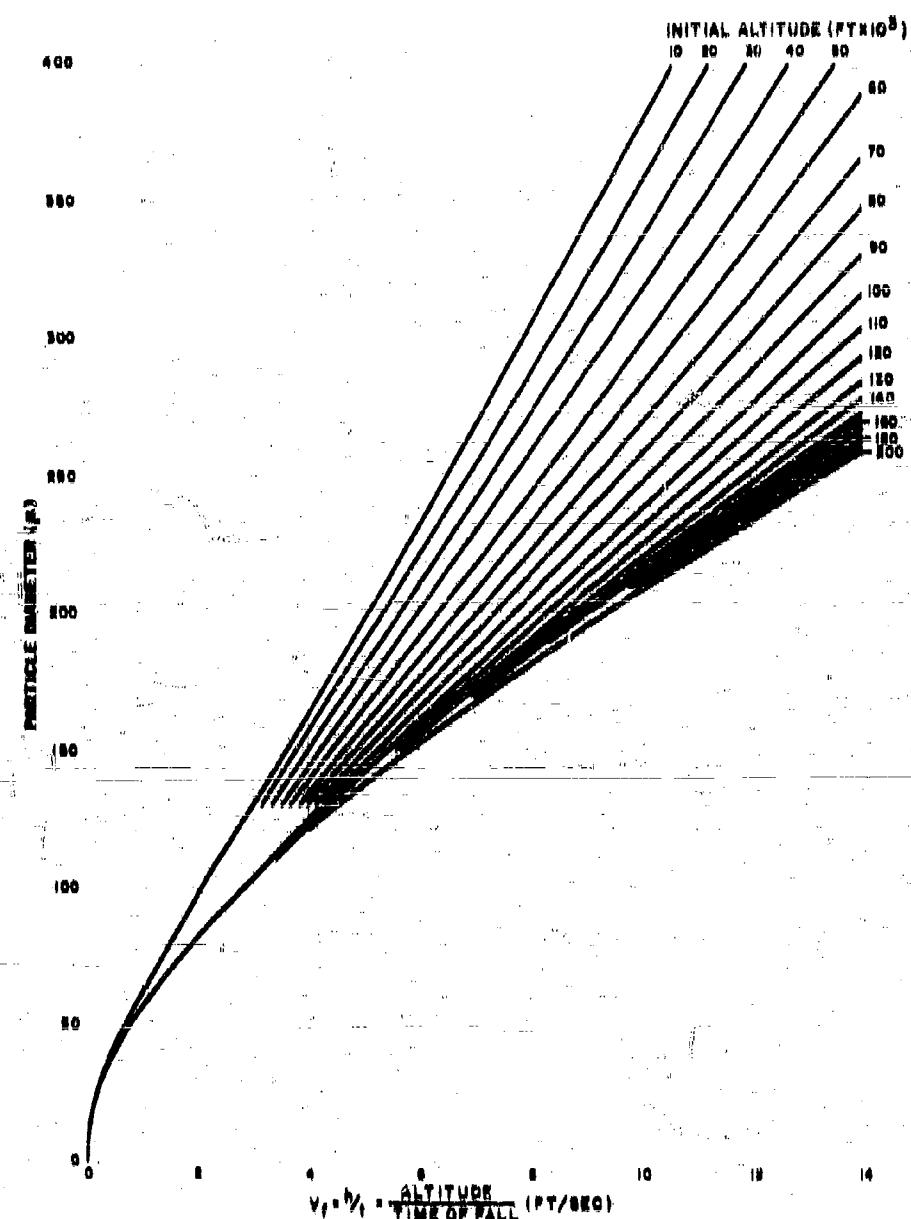


Figure 5.13 (continued)

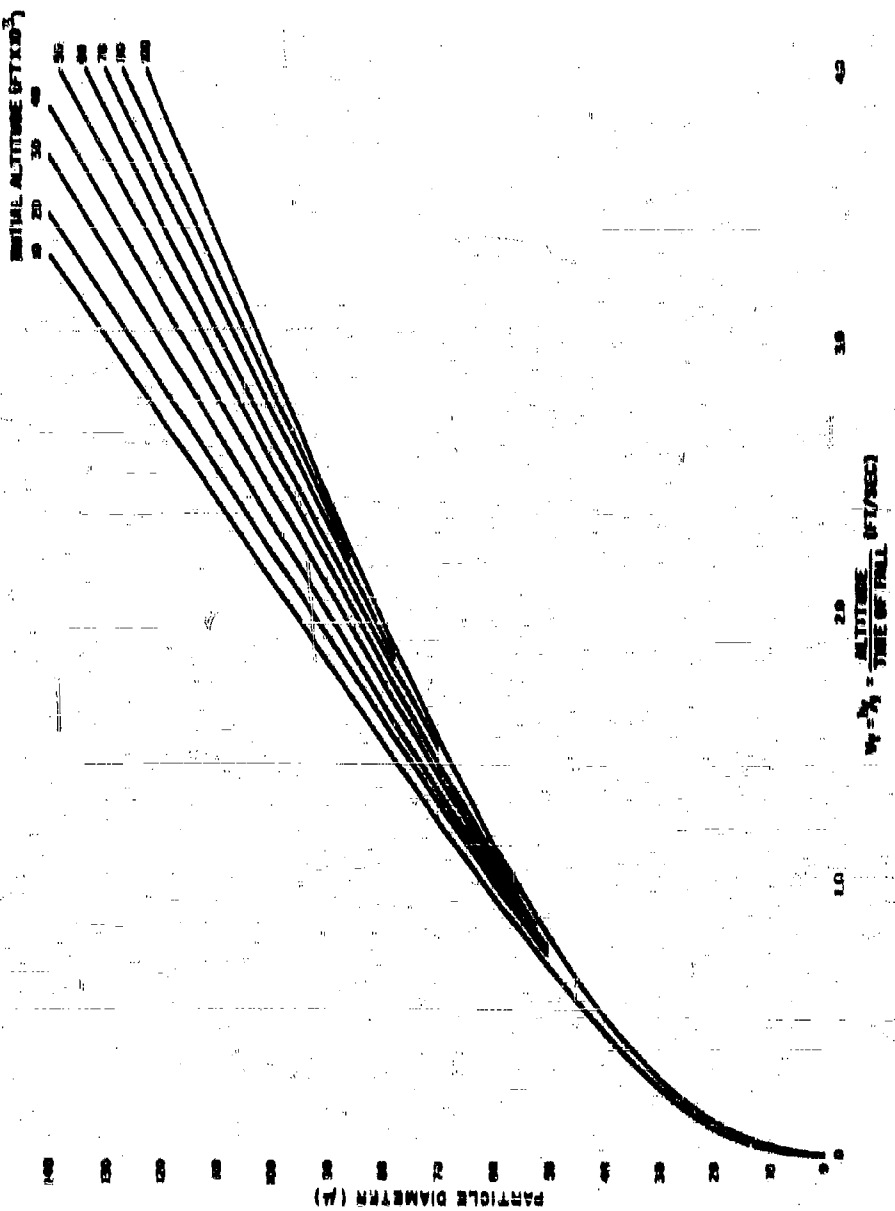


Table 8.0

DIAMETERS OF SPHERICAL PARTICLES FOR VARIOUS GROUP PALETTING
 AT 1.87×10^4 FT AND 8.00×10^4 FT DOWNWIND FROM A 1-MT YIELD
 SURFACE DTONATION ASSUMING A WIND SPEED OF 10 MPH

$X = 1.87 \times 10^4$ ft ($y=0$)							$X = 8.00 \times 10^4$ ft ($y=0$)			
α	v_t ft/sec	h_1 10^3 ft	h_2 10^3 ft	d_1 (μ)	d_2 (μ)	Δd (μ)	α	v_t ft/sec	h 10^3 ft	d (μ)
2.018	8.70	57.8	57.8	252	262	0	0.0	24.4	20.8	910
2.6	8.40	53.0	61.8	252	242	10	1.0	22.0	20.5	800
2.8	7.80	49.0	63.0	240	230	14	1.1	20.0	20.7	720
3.0	7.00	47.7	63.2	229	219	10	1.2	18.8	20.0	680
3.2	6.88	46.0	62.8	219	209	17	1.3	18.0	27.0	600
3.4	6.47	44.0	61.0	209	193	16	1.4	16.7	27.1	545
3.6	6.11	43.0	60.0	200	184	16	1.5	14.7	27.0	500
3.8	5.79	42.0	59.1	192	178	14	1.6	18.8	27.4	470
4.0	5.50	42.0	57.4	184	173	11				
4.2	5.24	41.4	55.5	177	167	10				
4.4	5.00	41.1	53.4	171	160	8				
4.6	4.78	41.0	51.0	165	158	7				
4.8	4.58	41.4	48.4	159	155	4				
4.900	4.40	40.7	46.7	153	153	0				

The spread in particle diameters for each α value for cloud fallout is seen to be quite small; at maximum cloud thickness the spread in diameter is only 17 microns. The spread should be somewhat larger at smaller distances and somewhat smaller at greater distances.

The stem fallout model, as formulated, gives no spread in the diameters of the particles falling from a given altitude. At the 1.87×10^5 foot distance, the over-all spread in particle diameters is about 100 microns; at the shorter distance it is 485 microns. The accumulated activity distributions (in r/hr at 1 hr) at the two locations are shown in Figure 6.14; these were obtained from the respective summations of $K_0(1)A_\alpha(\alpha)$ and $K_X(1)A'_\alpha$ over α .

The gross activity-particle size distribution for the 1-MT yield, calculated from the first approximation of $K_\alpha(1)A_\alpha$ for fallout from cloud altitudes, is shown in Figure 6.15 along with the distributions used in fallout models by Anderson² (NRDL distribution) and by Rapp (RAND distribution) as given by Pugh and Galliano³. If the stem fallout were included and additional approximations of the distribution were made, it is likely that the curve for the simplified fallout model presented here for the 1-MT yield would have slightly higher percentages of the activity on both the small and larger particles. Also, the distribution curve would change somewhat with weapon yield.

The NRDL distribution was obtained from data on sieved fallout sample fractions from a low-yield underground shot in Nevada. The amount of activity not accounted for in the fallout pattern consists of the fractions in the very small particles. Thus, if the NRDL distribution were readjusted to the distribution in the fallout on the ground, the high fractions in the small sizes would be reduced. The same would apply to the RAND distribution. These two distributions are generally used in terms of fraction of the weapon activity (fractions, d/m, etc.) but these units, during computation, are usually not directly proportional to roentgens per hour.

The RAND distribution was obtained from data on a few fallout sample fractions obtained from a high-yield detonation on coral. The absence of a significant amount of large particles in the distribution suggests either a high degree of particle breakage during shipment and sizing of the more fragile coral-based particles (as discussed in Chapter 2) and/or insufficient sampling for obtaining data on the larger particles. Also, even if the activity-size measurements were not subject to question because of bias and particle break-up, some question occurs regarding the use of activity distributions on coral particles in calculations for silicate-type fallout particles.

The noted discrepancies in the three activity-size distributions have not been satisfactorily resolved. The utility of the simplified fallout scaling system to predict shifting of the activity-size distributions with yield has not yet

Figure 5.14
 ACCUMULATED ACTIVITY DISTRIBUTION AS A FUNCTION OF PARTICLE SIZE AT
 $X = 3.35 \times 10^4$ FT AND $L_0 = 35$ FT DOWNTREAM FROM THE 1-MT YIELD
 SURFACE BURST FOR A WIND SPEED OF 15 MPH

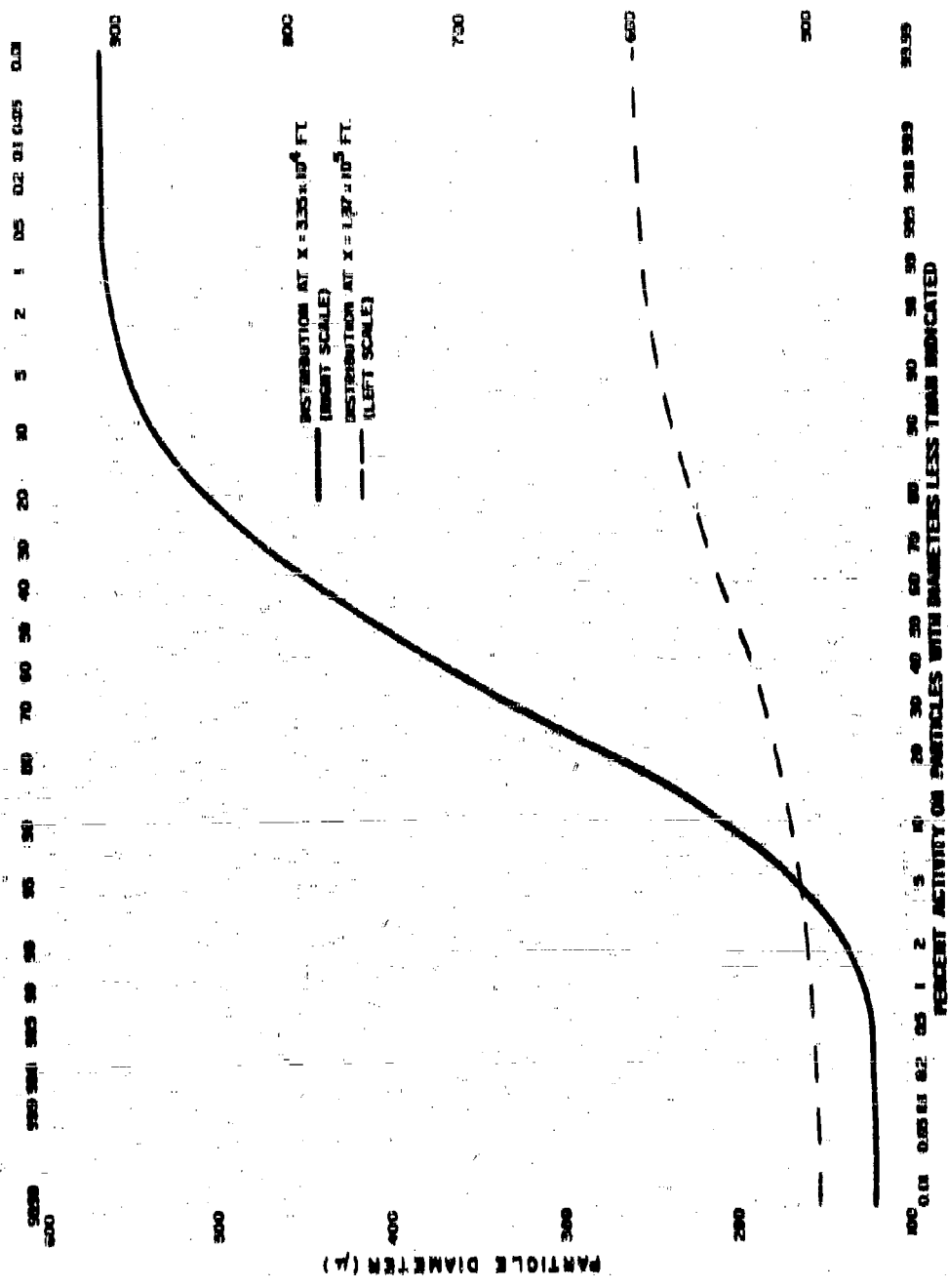
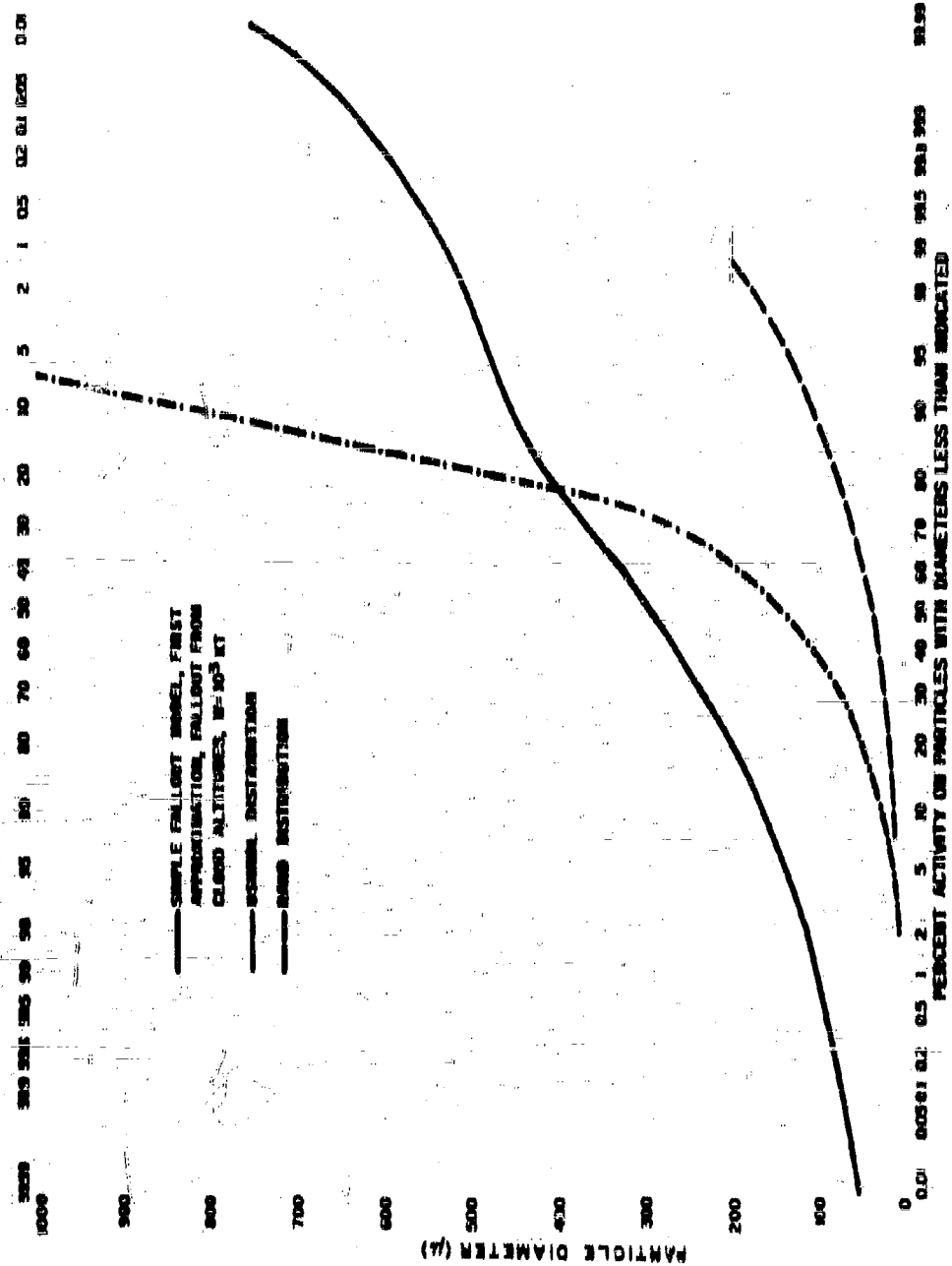


Figure 5.15
COMPARISON OF THE GROSS ACTIVITY DISTRIBUTION ON PARTICLES OF VARIOUS
DIAMETERS DERIVED FROM THE SIMPLIFIED FALLOUT SEALING SYSTEM TO
DISTRIBUTIONS USED IN OTHER MATHEMATICAL FALLOUT MODELS



been used in the more refined models to determine whether the predicted change would result in any significant differences in the predicted fallout patterns. These discrepancies are of less importance when the results of the calculations are used to estimate the general magnitudes of the hazard from fallout and the extent of the area affected than when they are used to predict fallout effects at a given location with respect to a hypothetical burst point. Even in the more general use of the model, however, the maximum estimated hazard will still be sensitive to the shape of the activity-size distribution curve.

5.6 The Effect of Cross-Wind Shear on the Fallout Pattern Scaling System

The simple fallout scaling system contains the effects of some degree of wind shear because the original fallout patterns from which it was derived were formed under real wind conditions in which some shear occurred. The relative shear, or relative pattern spread, can be defined as $(Y_s - a)/Y_s$. This ratio is proportional to the tangent of the angle of the maximum lateral spread of particle trajectories falling from all altitudes to the ground.

For the 1-KT yield, the relative shear of the pattern from the simple fallout-model-scaling method is 0.424. Since this scaling system was derived with use of the fallout data from the Jangle "S" shot whose yield was 1.2 KT, it is of interest to review the wind data for that shot with respect to the effect of the wind shear on the relative pattern spread. The wind data and particle fall trajectories are summarized in Table 5.10.

The lateral distance, Δd , traveled by a particle having a fall velocity, v_f , in a wind speed of v_w , while falling through the altitude increment, Δh , is:

$$\Delta d = v_w \Delta h / v_f \quad (5.70)$$

In Table 5.10, the quantity $v_f \Delta d$ is given since it is independent of particle size. The lateral distance component, Δy , is $\Delta d \sin \Delta \theta$ and the "downwind" distance, Δx , is $\Delta d \cos \Delta \theta$, where $\Delta \theta$ is the angle between the wind direction at the altitude of the top of the 10-minute cloud (12,000 feet) and the wind direction at any lower altitude. The summation of the component distances (starting at ground zero) assumes that v_f is constant from 4,000 to 12,000 feet. The reference direction of 200° was selected because it corresponds closely to the direction of the maximum pattern intensity, the "hot" line, in the fallout area from the Jangle "S" shot.

Table 5.16
WIND DATA AND PARTICLE FALL TRAJECTORY COMPONENTS FOR JANGLE "S" SHUTTLE

Altitude Increment (10 ³ ft)	Wind Direction (degrees)	Wind Speed (knots)	Az (degrees)	10 ³ knot/ft			
				V _x Δd	V _y ΔY	V _x ΔX	V _y ΔZ
11-12	210	37	0	37	0	37.00	32.32
10-11	210	34.5	9	34.5	9	31.50	29.33
9-10	210	32	9	32	9	32.00	29.33
8-9	210	38	0	28	0	28.00	22.23
7-8	190	25	20	25	8.39	24.44	22.33
6-7	190	20	20	20	6.84	18.80	13.34
5-6	170	13	30	13	6.58	11.25	6.50
4 ^a -5	cabs	cabs	—	—	0	0	0

Note: Cloud base at ~ 10 miles; h₂ ~ 9,900 ft.
 Cloud top at ~ 10 miles; h₂ ~ 12,000 ft.

a. Surface (4,230 ft).

The effective, or average, wind speed is

$$\bar{v}_w = \frac{\sum_{i=1}^n t_i v_i}{\sum_{i=1}^n t_i} \quad (6.77)$$

where t_i is the time a particle spends in the i^{th} altitude increment and v_i is the wind speed in that increment ($t_i = h/v_i$). For a constant fall velocity, \bar{v}_w is equal to $\sum_i v_i/n$, where n is the number of altitude increments considered. The data of Table 6.10 give 20.8 knots (20.6 mph) for \bar{v}_w for a constant v_f . The wind shear, S , between the altitude increments m and n is given by

$$S(m,n) = \left[\begin{array}{cc} \frac{\sum_{i=1}^n t_i v_i}{\sum_{i=1}^n t_i} & \frac{\sum_{i=1}^m t_i v_i}{\sum_{i=1}^m t_i} \\ \frac{\sum_{i=1}^n t_i}{\sum_{i=1}^n t_i} & \frac{\sum_{i=1}^m t_i}{\sum_{i=1}^m t_i} \end{array} \right] \frac{1}{(h_n - h_m)} \quad (6.78)$$

For the assumption of a constant v_f , the following values of $S(m,n)$ are obtained from Table 6.10:

$$\begin{aligned} S(5,8) &= 2.14 \text{ (knots/10^4 ft)} \\ S(4,8) &= 2.26 \text{ (knots/10^4 ft)} \\ S(3,8) &= 2.50 \text{ (knots/10^4 ft)} \\ S(2,8) &= 2.88 \text{ (knots/10^4 ft)} \end{aligned}$$

The notation $S(0,8)$ is for the altitude range 0,000-12,000 feet, etc.

The value of wind shear of Eq. 6.78 (for a given particle size or fall velocity) gives the total wind shear rather than just the crosswind shear that spreads out the vertical distribution of particles laterally (from the downwind direction of the center of the pattern). Since Table 6.10 shows that the lateral shear for a given particle size originating from the cloud altitudes (0,000-12,000 feet) is negligible, the only cause of the relative pattern spread is the relative shear of particles of different sizes as they fall through the lower altitudes.

The lateral spread due to changes in v_f with particle size may be represented by the variation of $v_f \sum \Delta y$ with $v_f \sum \Delta x$. The deposition of particles (from

the center line of the source, say) starting from the lower altitudes nearest the origin (i.e., ground zero), proceeds in a lateral direction up to an altitude of 8,000 feet. And, since both coordinates are proportional to v_t , the variation of v_t (i.e., change of particle size) will result in the deposit of a continuous band of particles in the lateral direction bounded by the line (at low values of Δx) with a slope (in Δy) of approximately $22.28/54.34$ or 0.408. This ratio is very near the value of $(Y_n - a)/X_n$, 0.424, for the 1-MT yield that is obtained from the scaling functions.

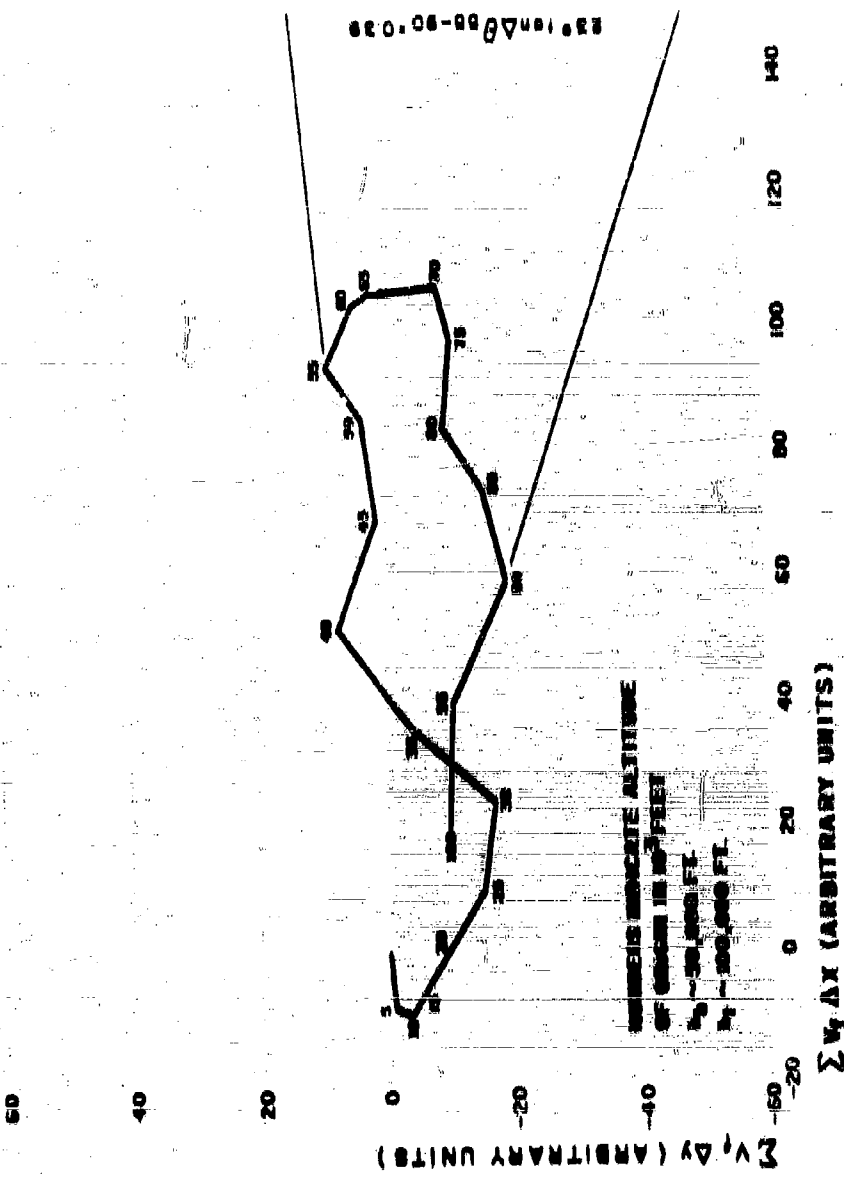
The fallout pattern for the Castle Bravo shot pattern was also used to derive the scaling functions for the simple fallout-pattern scaling system. The particle fall trajectory components (in relative units), with respect to the estimated pattern center (or hot) line for Castle Bravo winds, and for a particle size of about 100 microns, is shown in Figure 5.10. (The effect of these winds on the lateral spread of the derived pattern for the 10-MT yield should be about the same as it was for the Castle Bravo shot pattern which was used to establish the scaling system.) The lateral shear in the Figure 5.10 plot is due to changes of both wind speed and direction over the range of altitudes containing the cloud (at 8-10 minutes after detonation).

It is seen that the maximum spread in particle deposition, for all from altitudes between 50,000 and 90,000 feet (heights of bottom and top of cloud), is equivalent to a shear angle of about 20° ; the tangent of this angle is 0.90. This value of the tangent is reasonably close to $(Y_n - a)/X_n$ for the 1 r/hr at 1 hr contour at the 10-MT yield, which is 0.407.

If, for the Castle Bravo wind conditions, it is assumed that the smaller particles fell from altitudes as high as 100,000 feet, and that the fall trajectory components (for all the smaller particles) are proportional to those of Figure 5.10, then the maximum downwind distance at which the particles would have landed for a single wind direction would have been about 8.0 times greater than for the trajectories of Figure 5.10. Under such conditions, the value of X_p for the 1 r/hr at 1 hr contour would have been no more than 1,200 miles for the 10-MT yield.

The relative pattern spread and "equivalent" uniform wind shear, for the simple fallout scaling system patterns for several yields, are given in Table 5.11. It is interesting that the relative pattern spread (for the 1 r/hr at 1 hr contour) is about the same for both the Jungle "B" and the Castle Bravo fallout patterns, but the shear mechanism by which the spread occurred is very different. Of the two shots, the manner in which the shear occurred in the Bravo shot is more like the assumed uniform lateral shear used by Pugh and Callano

Figure 5-16
PLOT OF PARTICLE FALL TRAJECTORY COMPONENTS RELATIVE TO ESTIMATED PATTERN CENTER LINE FOR CASTLE BRAVO WINDS



In their computations. Thus, for the larger yields, the included lateral shear for the simple fallout scattering system can be related roughly to a uniform wind shear through the cloud of 0.2 and 0.3 knots per 1000 feet when the average wind speed is about 10 mph.

Table 6.11

**SUMMARY OF "EQUIVALENT" UNIFORM WIND
SHEAR FROM INITIATIVE PATTERN SPREAD FOR
THE SIMPLE FALLOUT SCATTERING SYSTEM PATTERNS
(Wind Speed of 10 mph)**

$W(RT)$	$(Y_{n=0})/X_n$	$H_y(\text{knots}/10^6 ft)$
1.0	0.41 ^b	0.88
10	0.14	0.08 ^a
10^0	0.28	0.41 ^a
-10^0	0.60	0.40 ^a
10^4	0.47	0.28 ^a
1.5×10^4	0.80 ^b	0.82 ^a
10^6	0.88	0.15 ^a

^a From plots derived from the computations of Pugh and Gallino⁶ for $(Y_{n=0})/X_n$ as a function of H_y assuming a 10 mph wind and 100% fission yield; the standard intensities given by Pugh and Gallino were multiplied by 0.60 to account for terrain shielding and instrument response.

^b From wind vector data.

6.7 Comparison of Beyond-Fallout Pattern Computations

Methods of computing fallout patterns can be compared, in a gross way, by (1) the relative area that is enclosed within given standard intensity contours, and (2) the differences in the enveloped variation with downwind distance of the standard intensity along the center line of the fallout pattern. Another way of gross comparison involves differences in the contour shapes.

A comparison has been made by Ferber and Hoffer¹ of several fallout models^{2,3,4,5} considering wind effects. The fallout models compared were those developed by

1. Pugh and Galliano⁶ (WSEG-RM10);
2. a revised but as yet unpublished version of the Pugh-Galliano model based on recommended changes by the National Academy of Science Working Group on Fallout Models in 1961 (WSEG-NAS);
3. a model developed by the weather bureau (WB);
4. a model developed by the Air Force Intelligence Center (AFICIN); and
5. a model developed by the RAND Corporation (RAND).

Comparing of fallout pattern computations by means of the areas enclosed within a given standard-intensity contour is a fairly good method because the enclosed areas are not very sensitive to wind speed or wind shear. Because of this, it is possible also to compare the fallout patterns calculated for a 10-MT yield surface detonation and 16 mph wind speed based on the model given in ENW⁷, the WSEG-RM10 model, the model developed by Anderson⁸, and the simple fallout scaling system described here.

The wind shear for the ENW model is unspecified; for the WSEG-RM10 model it is taken at 0.1 knots/1,000 ft; for the Anderson model the wind shear is zero; and for the simple fallout scaling system it is about 0.8 knots/1,000 ft. The comparisons presented by Ferber and Hoffer¹ are for a 1-MT yield surface detonation, a 25 mph wind speed, and a vertical wind shear of 0.2 knots/100 ft. The areas within stated contours, for the two sets of calculations, are given in Table 5.12; the area ratios are relative to the WSEG-RM10 model since it is common to both sets.

Another factor of difference between the two sets of calculations which could have a small effect on the value of the ratios, is that the areas calculated by Ferber and Hoffer are, presumably, for the ionization rate at 8 feet above an ideal plane (except perhaps for the AFICIN model). The calculations presented here are for the observed ionization rate at 8 feet above a plane including a terrain attenuation factor of 0.75 and an instrument response factor of 0.75 for the WSEG-RM10 model and the simple fallout scaling system. It is not clear, from the referenced sources, what the value of these factors are for the ENW and Anderson models.

Table 5.12

**RATIO OF AREAS WITHIN STATED STANDARD INTENSITY
CONTOURS FOR FALLOUT PATTERNS COMPUTED
FROM VARIOUS MODELS RELATIVE TO THOSE
FROM THE WNRG-RM10 MODEL.**

Model Designation	Standard Intensity in $\mu\text{Ci}/\text{hr}$ at 1 hr			
	1	10	100	1000
A. 10-MT Yield, 15 mph Wind Speed (100% Plume)				
ENW	0.66	1.80	0.70	0.62
Anderson	1.40	1.14	1.00	0.98
Simple Fallout Scaling System	0.67	0.71	0.83	1.10
B. 1-MT Yield, 25 mph Wind Speed, 0.2 knots/10^3 ft Vertical Shear (100% Plume)				
ATCIN	0.18	0.18	0.26	0.67
WR	2.16	1.18	0.67	0.49
WNRG-NAS	1.00	1.00	0.87	0.60

Since most of the area within the stated contours is associated with the downwind distance, the ratio values in excess of unity for the lower-valued contours and the values that decrease to less than unity for the higher-valued contours correspond to a higher fraction of the total activity on smaller particles than the values used in the WNRG-RM10 model. This type of trend in the ratios is exhibited most clearly by the ENW and WR models and, to a lesser extent, by the WNRG-NAS and Anderson models. The reverse trend, representative of an activity-particle size distribution having a higher fraction of the total activity on the larger particles than is used in the WNRG-RM10 model, is exhibited by both the ATCIN model and the simple fallout scaling system.

The actual values of the area ratios are related, of course, to the assumed value of the yield-distribution contour ratio; this is given as $K(T)$ or $K(T)C(1)$ in r/hr at 1 hr per KT/mi² in Chapters 2 and 3. For the 10-MT yield patterns, the values of $K(T)C(1)$ are computed, from pattern integration,¹ to be (in r/hr at 1 hr per KT/mi²)

- 1,400 for the ENW model;
- 1,500 for the WBBQ-RM10 model (corrected by 0.50);
- 1,500 for the Anderson model; and
- 1,130 for the simple fallout venting system.

For the other patterns, according to Perker and Hefter,¹ the values of $K(T)$ are:

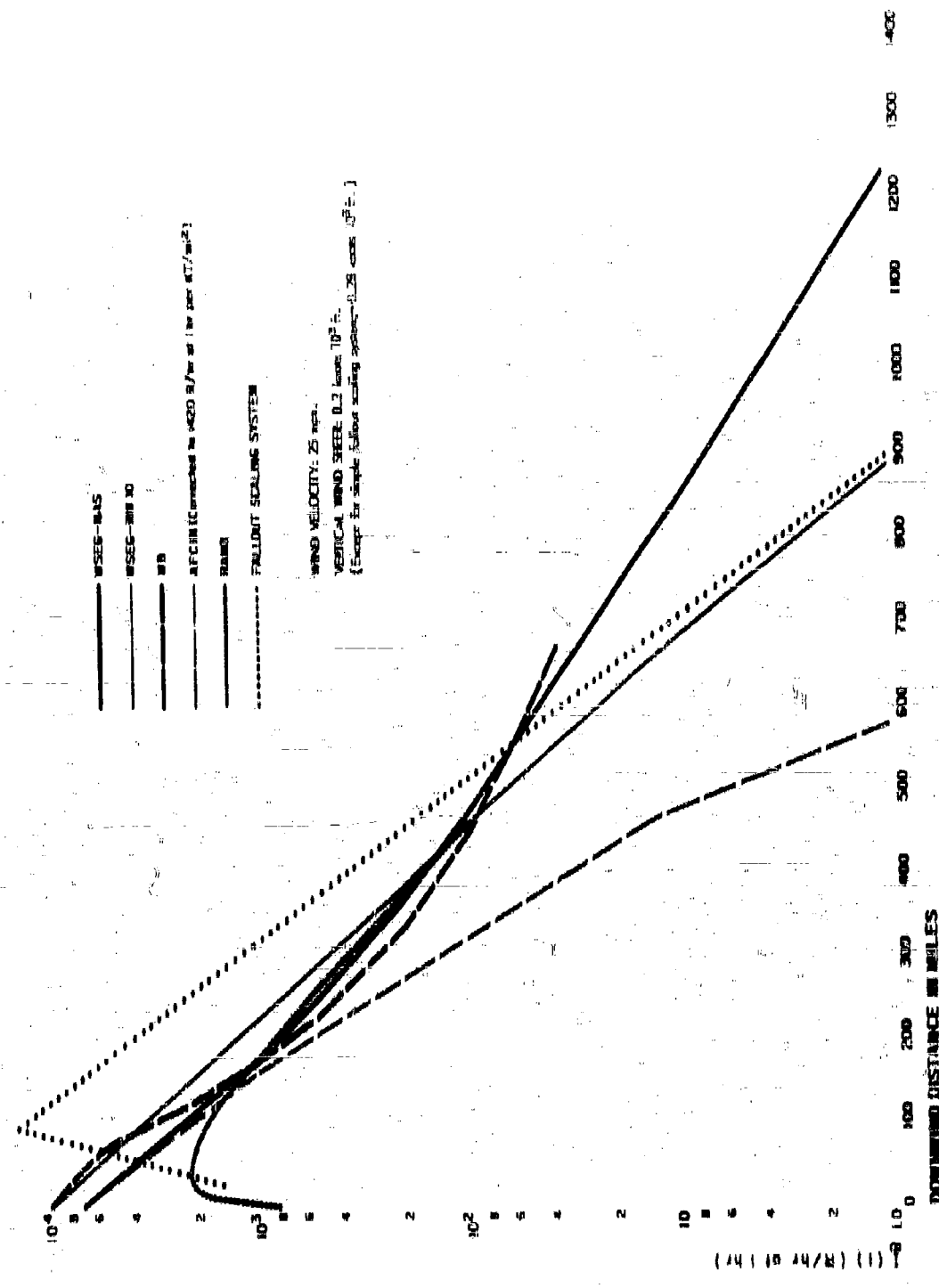
- 2,500 for the WBBQ-RM10 model;
- 2,400 for the WBBQ-NAS model;
- about 2,000 for the WB model; and
- 800 for the AFCIN model.

The low value of $K(T)$ for the AFCIN model suggests that it applies to an observed ionization rate and that it includes terrain attenuation and instrument response factors. The higher values of $K(T)$ for the other models apparently are for fallout deposited on an ideal smooth plane. If this is true, the comparable value of $K(T)$ for the AFCIN model, on the ideal plane, would be about 1,420 r/hr at 1 hour. The value of $K(T)C(1)$ for the simple fallout model pattern, for the ideal smooth plane source and a 10-MT yield, would be about 2,500 r/hr at 1 hour per KT/mi² at 3 feet.

The variation of the calculated-infinite ideal plane standard intensity with downwind distance along the center line of the fallout pattern, for several of the fallout models, is plotted in Figure 5.17, for a 10-MT yield surface detonation assuming a 25 mph windspeed and 100 percent fission yield. The simple fallout venting system and the RAND model are the only two methods that predict the observed downwind major peak.

A portion of the higher rate of decrease in the standard intensity with downwind distance, for the simple fallout venting system, may be due to the higher degree of vertical shear. But most of the higher standard intensities in the first 500 miles downwind, and the high ratio of decrease with distance, is due to the higher fraction of the total activity implied as being associated with

Figure 5.17
VARIATION OF THE CALCULATED INFINITE IDEAL PLANE STANDARD INTENSITY
WITH DOWNGRADED DISTANCE (Center Line of Pattern) FOR A 10-MT YIELD SURFACE
DETONATION (URE Fission)



the larger particles. The curve for the AFCIN model implies an even sharper decrease in the fraction of activity with decreasing particle size.

The curve for the WB model implies an activity-particle size distribution in which the largest fractions of the activity are on the small particles. The development of fallout models for tower and balloon detonations⁸ quite likely had an influence on the development of the WB surface-burst fallout model. The WSEG-NAS model curve also implies a larger fraction of the activity on the smaller particles.

Since the simple fallout scaling system is adjusted to the Castle Bravo fallout pattern, for which the yield and wind conditions were not very different from the conditions used in the calculations for the curves of Figure 8.17, it appears that the AFCIN model does not account for enough of the total activity, and that the WB and WSEG-NAS models give too much weight to the activity carried by the smaller particles. If factors for the type of soil at the point of detonation are taken into account, these factors could be responsible for some of the indicated differences. However, none of the models explicitly consider soil type; therefore, no explanation of the difference on this basis is possible.

Further work on the fallout distribution models and their connection with the fallout-formation process is discussed in Chapter 6. A thorough study of the early-time condensation and other dynamic processes that take place during the rise of the fireball is required before significant progress is possible in the development of improved fallout models. It is clear that, when differences of a factor of 10 to 50 occur in the calculated standard intensities, one or more of the models has been poorly calibrated to the available observed fallout data.

CHAPTER 6 REFERENCES

1. LaRiviere, P.D., Early-Time Gamma-Ray Properties of U-235 Fission Products, USNRDL-TM-80, 1958.
2. Clark, D.E., and A.D. Anderson, Private communication, USNRDL, July 1960.
3. Pugh, G.E., and R.J. Galasso, An Analytic Model of Close-In Deposition of Fallout for Use in Operational-Type Studies.
4. Research Memorandum No. 10, Weapons Systems Evaluations Group, 1969.
5. Ferber, Gilbert J., and Jerome L. Hoffer, A Comparison of Fallout Model Predictions With a Consideration of Wind Effects, U.S. Weather Bureau, 1961.
6. Battin, E.H., D.L. Ingelhart, and R.R. Rapp, Derivation of Two Simple Methods for the Computing of Radioactive Fallout, RM-2B00, 1960.
7. Nagler, K.M., L. Macht, and F. Pooler, Jr., A Method of Fallout Prediction for Tower Bursts at the Nevada Test Site, TID-5480, OTB, Department of Commerce, Washington 25, D.C., 1955.
8. U.S. Government, Nuclear Weapons Employment Handbook, Air Force Manual 200-8, 1961 (Classified).
9. The Effects of Nuclear Weapons, U.S. Government Printing Office, Washington, D.C., 1957.
10. Anderson, A.D., Scaling Relations for Fallout Dose-Rate Patterns from Land-Surface Nuclear Bursts, USNRDL-TR (in publication, 1961).

Chapter 8

IONIZATION RATE CONTOUR RATIOS AND COMPOSITION OF FALLOUT

6.1 Definition and Use of Ionization Rate Contour Ratios

These contour ratios are defined as the ratio of the surface density of some property of fallout to the ionization rate at 8 feet above an extended open area covered with fallout. The three fallout properties of most interest in radiological countermeasures are:

1. The mass of fallout per unit area,
2. The number of atoms or moles of fission products per unit area, and
3. The fraction of the weapon yield deposited per unit area.

At a given location in the fallout area, the contour ratios for these quantities are defined by

$$M_r(t) = \frac{m_r}{I_x(t)} \quad (6.1)$$

$$FP_r(t) = \frac{n_{fp}}{I_x(t)} \quad (6.2)$$

and

$$FD_r(t) = \frac{FD}{I_x(t)} \quad (6.3)$$

where $M_r(t)$ is the mass contour ratio, m_r is mass of fallout per unit area at the location, $FP_r(t)$ is the fission product or activity contour ratio, n_{fp} is the number of atoms or moles of fission products per unit area, $FD_r(t)$ is the fraction of device contour ratio, FD is the fraction of device per unit area, and $I_x(t)$ is the observed ionization rate.

Knowledge of the values of these contour ratios makes possible estimates of the amount of fallout particles, fission products, or other components of the weapon that are present, given the level of the ionization ratio. These estimates are necessary in the design of realistic experiments using synthesized fallout materials, in the operational use of radiological countermeasures, and in general evaluations of radiological hazards from fallout.

The reverse procedure is equally useful; knowledge of the chemical or physical behavior of particles or of the fission-product elements as a function of their surface density can, through the contour ratios, be associated with the level of the radiation hazard. For example, decontamination data based on the mass of particles can be readily converted into reduction in radiation hazard by means of the contour ratio. Use of the contour ratios and their scaling functions allows extrapolation of a modest amount of experimental data to innumerable operational cases because the contour ratios are not constants; they are point functions whose value depends on many variables. Thus a single value of m_x , for example, may be associated with many values of $I_x(t)$.

The final use of the contour ratios is to permit estimates of m_x , n_{fp} , and FD to be made, for use in radiological countermeasure operations, from observations of $I_x(t)$. In such estimates, additional information is required, along with the value of $I_x(t)$, before a reliable estimate of the quantity of interest can be made. This particular use of the contour ratio may be the only method available for estimating one of the desired quantities when fallout areas are monitored with portable survey instruments. The additional information needed for these estimates is discussed in the following paragraphs.

4.8 Dependence of the Mass Contour Ratio on Detonation Conditions and Other Parameters

4.8.1 Dependence on Weapon Type and Yield

Because the mass contour ratio is inversely proportional to the specific activity of fallout, its value or range of values must depend on the amount of radioactive materials produced in the detonation. The fission product yield is proportional to BW where B is the ratio of fission to total yield; hence, for the usual amount of induced activities, the total gross activity from Eq. 4.74 is

$$I_x(t)\Delta \text{rea} = 5.46 \times 10^{10} [r_x(t) + 0.019] \text{ BW } \mu/\text{hr at 1 hr} \times \text{sq ft} \quad (4.4)$$

where $r_x(t)$ is the gross ionization rate fractionation number at H+1 and 0.019 is the ratio of the ionization rate from a nominal yield of induced activities to that of the fission products (both at H+1). The multiplier, $5.46 \times 10^{10} \mu/\text{hr}$ at

1 hr per NT/sq ft, contains an instrument response and a terrain roughness attenuation factor. The value of $r_x(1)$ will vary with downwind distance, or particle size, as well as with time after detonation. The value of the ratio, 0.019, for the induced activity will depend on the construction materials of the weapon, the environmental elements at the point of detonation, and, to some degree, on the height of burst and on the values of B . For example, if B is very small (the definition of the so-called "clean" bomb), then the relative induced activity yield could be much higher than is indicated by the 0.019 of Eq. 6.4. Except for the possible dependence of $r_x(1)$ and induced activity ratio on yield, the total area activity of Eq. 6.4 is directly proportional to W .

If it is assumed that the total crater mass becomes uniformly mixed with the radioactive material in the fallout formation, then the expected maximum value of $M_r(1)$ should be given by $M_r(1) \times A_{\text{crat}}$ which (from Eqs. 8.18B and 6.4) is

$$M_r(1)_{\max} = \frac{93.6 W^{-0.083}}{B \cdot r_x(1) + 0.019} \frac{\text{mg}/\text{sq ft}}{\text{r/hr at 1 hr}} \quad (6.5)$$

If, on the other hand, it is assumed that only the soil that is melted at 1400°C, as in the case of the ideal surface burst, becomes uniformly mixed with the radioactive elements, then only the mass equivalent of the $n(t)$ moles of liquid soil would be considered. The yield dependence of this quantity, from Table 8.18, can be represented by

$$n(t) = 1.92 \times 10^{11} W^{1.018} \frac{\text{mg soil}}{\text{r}} \quad (6.6)$$

On the average, the mass represented by $n(t)$ should result in an expected minimum value of $M_r(1)$, which is

$$M_r(1)_{\min} = \frac{3.52 W^{0.018}}{B \cdot r_x(1) + 0.019} \frac{\text{mg}/\text{sq ft}}{\text{r/hr at 1 hr}} \quad (6.7)$$

The two limiting values of $M_r(1)$ indicate that (1) the dependence on the total yield should be rather small, (2) the values are inversely proportional to the fraction of fission yield of the detonation, and (3) the real values are most likely to be in the range 1 to 100 (mg/sq ft)/(r/hr at 1 hr) for $B=1$. With respect to the fraction of fission yield, B , the type of weapon is apparently a more important parameter in determining the value of $M_r(1)$ than is the yield itself. Because both melted and unmelted particles are found in fallout, more soil is involved in the fallout formation process than is indicated by $n(t)$, but the amount involved should certainly be less than that removed from the whole (apparent) crater -- even for the larger yield where essentially no crater lip remains.

Actually, the values of M_r (1) show a tendency to decrease with yield that is more or less proportional to the apparent crater index. Therefore, the crater index per RP associated with fallout formation, $m(n, W)$, is assumed to have the form

$$m(n, W) = f(n)W^{-0.083} \text{ mg/RP} \quad (6.8)$$

where $f(n)$ is the mass per kiloton of yield for each particle group to be evaluated from available measurements of M_r (1). With the assumed dependence of $m(n, W)$ on yield, the relative abundance of melted particles increases with yield, since $n(t)$ increases with yield, and the average value of M_r (1) decreases with yield.

6.2.2 Dependence on Downwind Distance from Shot Point

The variation of M_r (1) with downwind distance from shot point is best considered in terms of the particle group size parameter, α . To represent this dependence, r_α (1) is redesignated r_α (1) for evaluation as a function of both α and the yield. Appropriate values of r_α (1) along with observed values of M_r (1) are then used to evaluate $f(n)$.

In estimating r_α (1), the assumption is made that an abundance of solid surface (as particles) is present in the rising fireball and cloud at all times to facilitate the condensation of the gaseous radioactive species. With this condition, the amounts of each element condensed during the second period of condensation may be estimated by the method outlined in Chapter 2. In the simple process where all the particles are present at the end of the first period of condensation, differences in the radioactive composition on the various particles at a later time can occur only if some of the particles are removed from the volume before further condensation occurs. The particles that remain in the volume the longest time, providing a large number are always present, will then condense more of the volatile radioactive elements. In the fallout formation process, where the larger particles are falling out or leaving the gas volume at earlier times, the fraction of total available activity that is condensed on particles of various sizes should increase with decreasing particle size. Hence the fraction of the total activity condensed up to a given time after detonation should be described by an accumulative distribution curve that increases to a stated amount for a given particle size, or a value for a group of particles. Such a representation cannot consider discrete values of the fraction condensed for a given particle size but may be given in terms of an average value for each of the particle groups.

In the next process, unmelted and melted particles become mixed during the second period of condensation. Since the unmelted particles have entered the fireball after it has cooled below their melting point, they can only condense radioactive materials not previously condensed. However, since these unmelted particles fall in the same areas as the melted particles of the same fall vector, the over-all radioactive composition of the group should not be changed. The main effect of the presence of the unmelted particles in condensing some of the remaining volatile radioactive materials is to reduce the specific activity of the whole group of smaller particles.

The fraction that each nuclide of a mass chain condensed in the second period of condensation, $r_s(\Lambda)$, is estimated from

$$r_s'(\Lambda) = \frac{\sum_j N_j(\Lambda, t) k_j^0 / (1 + k_j^0)}{\sum_j N_j(\Lambda, t)} - \frac{V}{0.23RTBW} \cdot \frac{\sum_j N_j^f(\Lambda, 0) p_j^0 / y_j(t)}{\sum_j N_j^f(\Lambda, t')} \quad (6.9)$$

In which the first term contains the parameter values for the first period of condensation (see Eq. 3.40); V is the fireball or cloud volume at $t' = 0.28$; N_j is the number of fission-moles per atom; k_j^0 ; $y_j(t')$ is the number of atoms per fission of element j that are present at t' ; p_j^0 is the sublimation pressure of element j ; and $N_j^f(\Lambda, t')$ is the number of atoms of each element of mass chain Λ per 10^4 fissions not condensed in the first period of condensation, doony-corrected to t' .

In other words, $p_j^0 V / RT$ is the number of moles of element j in the vapor phase and $0.23RTBWy_j(t')$ is the total number of moles of the element produced and in existence at t' . The first term gives the fraction not condensed in the liquid particles during their existence, and the second term gives the fraction in the vapor state, the difference being the fraction condensed to the solid state on or in the solid particles by the sublimation process.

In making the computations for $r_s(\Lambda)$, the yields of 84-KT and 14-MT were selected since the $r_s(\Lambda)$ values were already available (see Table 8.15). The times of the beginning of the second period of condensation are 9 seconds and 60 seconds, respectively. The Inter Umax selected are 208 seconds and 406 seconds for the 84-KT yield, and 174 seconds and 408 seconds for the 14-MT yield. The mid-time points were derived in previous estimates of the time when the top of the cloud is near h-h for the respective yields the longer time for when the cloud is near full expansion. These relatively late times were selected to simplify the computations of $r_s(\Lambda)$; in both cases, the temperatures at the indicated times should be less than 300 to 350°K, at which time the second term of Eq. 6.9 is essentially zero for most fission product elements.

However, there are two general cases where the vapor pressures are still significant with respect to $r_n(\Lambda)$ values at these temperatures. The first is for the rare gas elements which are normal gases at these temperatures, and the second is for elements in very low abundance having slight vapor pressures at normal temperatures. For both yields, $\sqrt{0.28RTBW}$ (B-1) is about 3×10^{-11} at the second altitude point; thus $p_j^2/y_j(t')$ values less than about 10^{-10} make the term negligible with respect to unity. The only elements indicating relative pressures larger than this, except the rare gases, are the oxides of Se and As; for these $p_j^2/y_j(t')$ values of 10^{-8} to 10^{-9} are obtained, indicating that they would be entirely in the vapor state (since $r_n(\Lambda)$ cannot have values less than zero). With these exceptions, Eq. 6.0, for the temperature conditions of the computations, reduces to

$$r_n'(\Lambda) = 1 - r_n(\Lambda) \quad (6.10)$$

For the rare gases, $r_n(\Lambda)$ is taken to be zero, although some fraction of these gases would surely be absorbed on the surfaces of the particles. In this case, it is assumed that the fraction would be small and that the rare gas atoms formed from precursors previously condensed on the surface of the particle would sputterate (those formed inside the particle are assumed to remain in the particle). The $r_n(\Lambda)$ values calculated for the indicated times and described conditions are summarized in Table 6.1.

The independent nuclide yield data for the calculations were read from plots of the atom-yields for each nuclide calculated by Dolles and Ballou¹ based on the Glendenin postulate, and a set of calculations for both U-238 fission (thermal-neutrons) and Th-232 fission (8-Mev neutrons) was made. For U-238 fission, the calculations were carried out as described in Chapter 2. For U-235 fission, the nuclide fractionation numbers were multiplied by the air ionization rates per fission/sec ft at 3 feet above a uniformly contaminated plane, as tabulated by Miller and Loeb² at 48.8 minutes and 1.12 hour after fission, and then summed. The sum obtained by use of the $r_n(\Lambda)$ fractionation numbers were then added to each of the sums for the later times obtained by the respective $r_n(\Lambda)$ sets. These were then used to evaluate the constants of

$$I = I_0 t^n \quad (6.11)$$

were I_0 is the air ionization rate at 1 hr, t is the time-in hours, and n is a constant applicable from 48.8 minutes to 1.12 hour. The results of the computations are shown in Table 6.2 along with the fraction of the ionization rate condensed up to the indicated times defined by the ratio, I_n (condensed mixture) / I_0 (normal mixture), for r_n (1).

Table 6.1
SUMMARY OF FISSION PRODUCT NUCLIDE ν_{γ}^{f} (A) VALUES
FOR 84-KT AND 14-MT YIELD SURFACE DTONATIONS

Nuclide	84-KT		14-MT	
	200K	400K	174K	100K
Co-75	0.058	0.058	0.895	0.866
Co-77	0.826	0.826	0.854	0.854
Co-78	0.670	0.670	0.925	0.920
As-77	0.106	0.130	0.883	0.940
As-78	0.002	0.040	0.890	0.872
As-79	0.00124	0	0.00000	0
Ba-81	0	0	0	0
Ba-82	0	0	0	0
Ba-83	0	0	0	0
Br-83	0.047	0.018	0.470	0.012
Br-84	0.742	0.800	0.020	0.800
Kr-83	0	0	0	0
Kr-85	0	0	0	0
Kr-86	0	0	0	0
Kr-87	0	0	0	0
Kr-88	0	0	0	0
Pb-88	0.0298	0.0310	0.0200	0.0322
Rb-80	0.588	0.752	0.487	0.748
Rb-81	0.071	0.071	0.050	0.050
Sr-80	0.012	0.780	0.800	0.778
Sr-80	0.002	0.008	0.817	0.800
Sr-81	0.800	0.800	0.740	0.740
Sr-82	0.005	0.005	0.070	0.070
Sr-88	0.202	0.282	0.002	0.002
Y-80	0.002	0.008	0.817	0.830
Y-81	0.803	0.803	0.740	0.740
Y-82	0.803	0.803	0.740	0.740
Y-82	0.002	0.002	0.075	0.075
Y-83	0.270	0.270	0.002	0.002
Y-84	0.060	0.000	0	0

Table 6.1 (continued)

Nuclide	84-KTP		14-MTP	
	200m	400m	174s	400s
Zr-90	0.011	0.011	0	0
Nd-105	0.011	0.014	0	0
Nb-95	0.011	0.011	0	0
Mo-90	0.043	0.043	0.230	0.230
Mo-101	0.480	0.480	0.070	0.070
Mo-102	0.001	0.001	0.000	0.000
Ta-99	0.043	0.043	0.230	0.230
Ta-101	0.487	0.487	0.000	0.000
Ta-102	0.000	0.000	0.020	0.020
Ru-100	0.047	0.047	0.404	0.404
Ru-105	0.470	0.470	0.800	0.800
Ru-106	0.000	0.000	0.070	0.070
Rh-103	0.047	0.047	0.404	0.404
Rh-105	0.470	0.470	0.800	0.800
Rh-106	0.000	0.000	0.070	0.070
Rh-107	0.007	0.007	0.800	0.800
Pd-109	0.001	0.001	0.001	0.001
Pd-111	0.100	0.100	0.002	0.002
Pd-112	0.087	0.087	0	0
Ag-109	0.001	0.001	0.001	0.001
Ag-111	0.100	0.100	0.004	0.004
Ag-112	0.080	0.080	0	0
Ag-113	0.082	0.082	0.000	0.000
Ag-115	0.000	0.000	0.074	0.074
Cd-115	0.037	0.037	0.005	0.005
Cd-116	0.037	0.037	0.005	0.005
Cd-117	0.153	0.153	0.502	0.502
Cd-118	0.257	0.257	0.747	0.747
Cd-120	0.000	0.000	0.010	0.010

Table 8.1 (continued)

Nucleus	84-KT		14-MT	
	200n	400n	17-n	400n
In-115	0.030	0.030	0.074	0.074
In-117	0.158	0.158	0.581	0.581
In-118	0.257	0.257	0.747	0.747
In-119	0.080	0.080	0.715	0.715
In-120	0.048	0.048	0.850	0.850
Sn-121	0.016	0.016	0.182	0.182
Sn-123	0.077	0.077	0.011	0.011
Sn-125	0.131	0.131	0.004	0.004
Sn-126	0.041	0.041	0.004	0.004
Sn-127	0.007	0.007	0.004	0.004
Sb-125	0.131	0.131	0.004	0.004
Sb-126	0.055	0.055	0.020	0.020
Sb-127	0.050	0.050	0.050	0.050
Sb-128	0.450	0.450	0.007	0.007
Sb-129	0.704	0.704	0.082	0.082
Sb-131	0.018	0.018	0.080	0.080
Tc-125	0.131	0.131	0.004	0.004
Tc-127	0.050	0.050	0.050	0.050
Tc-127	0.050	0.050	0.050	0.050
Tc-129	0.704	0.704	0.082	0.082
Tc-130	0.708	0.708	0.082	0.082
Tc-131	0.010	0.010	0.084	0.084
Tc-131	0.025	0.025	0.084	0.084
Tc-132	0.004	0.004	0.088	0.088
Tc-133	0.087	0.087	0.080	0.080
Tc-133	0.080	0.080	0.088	0.088
Tc-134	0.002	0.002	0.080	0.080
I-131	0.020	0.020	0.084	0.084
I-132	0.005	0.005	0.088	0.088
I-133	0.080	0.080	0.080	0.080
I-134	0.001	0.001	0.080	0.080
I-135	0.000	0.000	0.080	0.080

Table 6.1 (continued)

Nuclide	84-KT		14-MT	
	208n	408n	174n	400n
Xe-101	0	0	0	0
Xe-103	0	0	0	0
Xe-105	0	0	0	0
Xe-106	0	0	0	0
Xe-108	0	0	0	0
Cm-107	0.475	0.677	0.809	0.078
Cm-108	0.207	0.285	0.0102	0.285
Cm-109	0.988	0.988	0.988	0.080
Ba-137	0.475	0.677	0.809	0.078
Ba-139	0.988	0.988	0.988	0.008
Ba-140	0.982	0.982	0.982	0.008
Ba-141	0.424	0.424	0.000	0.000
Ba-142	0.144	0.144	0	0
La-140	0.982	0.982	0.982	0.558
La-141	0.418	0.418	0.000	0.000
La-142	0.130	0.100	0	0
La-143	0.015	0.015	0	0
Co-141	0.418	0.418	0.000	0.000
Co-147	0.014	0.014	0	0
Pr-148	0.014	0.014	0	0

For all Nuclides not listed, $r_0'(A) = 0$, $r_0(A) = 1.0$

Table 6.2

EQUATION CONSTANTS FOR AIR IONIZATION RATES FROM 0.70 TO 1.12 HOURS AFTER FISSION AND FRACTION OF THE TOTAL IONIZATION RATE AT 1-HR FROM FISSION PRODUCTS CONDENSED ON PARTICLES AT GIVEN TIMES AFTER DETONATION OF AN 84-KT AND A 14-MT YIELD LAND SURFACE BURST

Source of Fission Product Mixture	I_0 ($\mu/\text{hr at 1 hr}$) fission/sq ft	n	$F_n(1)$
1. U-235 (thermal neutrons)			
Normal Fission Product Mixture	7.10×10^{-10}	1.108	1.00
84-KT, 0 sec	2.47×10^{-10}	1.001	0.848
84-KT, 268 sec	6.48×10^{-10}	1.108	0.780
84-KT, 400 sec	6.61×10^{-10}	1.109	0.784
14-MT, 00 sec	2.50×10^{-10}	1.280	0.849
14-MT, 174 sec	0.20×10^{-10}	1.148	0.788
14-MT, 400 sec	0.01×10^{-10}	1.180	0.784
2. U-238 (8-Mev neutrons)			
Normal Fission Product Mixture	0.90×10^{-10}	1.084	1.00
84-KT, 0 sec	2.57×10^{-10}	1.007	0.800
84-KT, 268 sec	6.57×10^{-10}	1.107	0.800
84-KT, 400 sec	6.68×10^{-10}	1.108	0.810
14-MT, 00 sec	2.40×10^{-10}	1.281	0.840
14-MT, 174 sec	0.32×10^{-10}	1.181	0.764
14-MT, 400 sec	0.04×10^{-10}	1.109	0.810

Two rather significant conclusions about the radioactive compositions of fallout are indicated by the results of the computations (providing the assumptions used in setting up the calculation were not inappropriate). The first conclusion is that no large effect of yield is indicated, either for the gross fraction of the ionization rate (or of the number of fission product atoms) condensed in the liquid particles or for the total fraction condensed at a given later time. The second conclusion is that in local fallout the gross fraction of the ionization rate at 1 hour has a maximum value of about 0.8, since most of the particles falling in the local regions will have left the gas cloud by 400 seconds (0.8 minutes). The values of n vary from about 1.1 to 1.4; however, these n values apply only to the short time interval, 0.70 to 1.12 hours, without consideration of induced activation. The differences in the values in Table 6.2 between the two fission nuclides are rather small.

The calculated ionization rates for the U-238 fission (8 Mev neutrons) are summarized in Table 6.3, and those for the 14-MT yield are plotted as a function of time after detonation in Figure 6.1. The values for the 0 second (84-KT) and 60 second (14-MT) condensations that were given in Chapter 2 are included for comparison. It may be noted that the mid-times selected (208 and 174 seconds) are not particularly good choices for obtaining differences in the decay curves as a function of condensation times. However, the differences shown between the mid-times and 400 seconds are mainly due to the net gain in condensed rare gas daughter products on the particle surfaces for the indicated time interval; this gain is rather small for both yields.

The fractionation numbers relative to the ionization rate from the normal fission-product mixture from thermal neutron fission of U-235 are given in Table 6.4 for the condensations at the end of the first period of condensation and at 400 seconds. The fractionation numbers in the table are not the ones applicable to $r_{\alpha}(t)$ because they include differences due to fission yields. The values of the fractionation numbers, however, do show that the fractionation number can vary by a factor or two or more during the second period of condensation (i.e., as a function of particle size) and can also vary with time after detonation, depending on the relative abundances of the condensed radionuclides.

In all cases, the computations of the particle sizes, or the α values, from the simple fallout scaling system based on the particle group fall-times, when compared with fractionation data of different particle groups of fallout from test devices of various yields, indicated that a time delay of considerable length must be taken into account before the computed $r_{\alpha}(1)$ values agree with the observed values. This time delay may be associated with the air circulation, presumably toroidal, in and about the rising cloud.

In this type of circulation (as discussed in Chapter 8), the particles entering the bottom of the cloud (or those within the volume when the circulation begins) apparently condense out gaseous radioactive elements and small previously condensed particles as they sweep through the gas volume. The larger particles circulate to the edge of the cloud, are accelerated downward and then continue to fall when the pull of gravity exceeds the upward force of the air circulating back into the bottom center of the fireball. In a circulation of this general type, the condensations that occurred at a given time in the central region of the circulation would be in evidence on particles whose apparent exit time, based on free fall from the bottom of the cloud, is much later.

From the few data of Chapter 2 and the lower shot data of Reference 9, the best agreement between the calculated and observed $r_{\alpha}(1)$ values and the observed time of arrival of a given particle size group is obtained by using a delay-time of about 180 seconds together with the apparent rate of rise scaling

Table 6.11
CALCULATED IONIZATION RATES OF CONDENSED Fission PRODUCT MIXTURES FROM U-238 (8-Mev NEUTRONE) FISSION AT SELECTED CONDENSATION TIMES^a

Time After Detonation			84-MT			14-MT		
Years	Days	Hours	0 sec	200 sec	400 sec	00 sec	174 sec	400 sec
		0.700	0.71	7.00	7.77	0.46	7.80	7.74
		1.14	0.80	4.00	5.00	2.10	4.60	4.04
		1.48	1.18	3.00	5.04	1.18	3.86	3.00
		2.40	0.640	1.70	1.81	0.007	1.70	1.70
		3.00	0.000	1.07	1.08	0.480	1.04	1.00
		3.10	0.274	0.000	0.004	0.010	0.030	0.005
		7.00	0.107	0.422	0.422	0.201	0.417	0.417
		11.1	0.107	0.283	0.283	0.101	0.288	0.288
		16.0	(1) 000 ^b	0.180	0.180	0.108	0.180	0.180
		20.8	(1) 544	0.107	0.107	(1) 580	0.107	0.107
	1.48	047.0	(1) 020	(1) 020	(1) 020	(1) 020	(1) 020	(1) 020
	2.10	01.1	(1) 100	(1) 004	(1) 004	(1) 180	(1) 000	(1) 000
	0/12	74.0	(2) 000	(1) 000	(1) 000	(1) 100	(1) 220	(1) 221
	4.07	100.7	(2) 000	(1) 140	(1) 140	(2) 001	(1) 140	(1) 140
	6.70	101.	(2) 000	(2) 040	(2) 040	(2) 008	(2) 047	(2) 048
	8.82	200	(2) 100	(2) 040	(2) 040	(2) 050	(2) 040	(2) 040
	14.4	040	(2) 110	(2) 427	(2) 427	(2) 101	(2) 427	(2) 427
	21.1	500	(2) 000	(2) 280	(2) 280	(2) 141	(2) 280	(2) 281
	26.0	748	(2) 000	(2) 178	(2) 178	(2) 100	(2) 177	(2) 177
	45.0	1087	(2) 000	(2) 100	(1) 100	(2) 078	(2) 105	(2) 105
	69.4	1504	(2) 000	(2) 011	(2) 011	(2) 480	(2) 010	(2) 011
	97.0	2000	(2) 000	(2) 070	(2) 070	(2) 011	(2) 070	(2) 070
	148	0400	(2) 000	(2) 280	(2) 201	(2) 000	(2) 200	(2) 200
	208	4000	(2) 000	(2) 120	(2) 120	(2) 107	(2) 125	(2) 125
	301	7200	(4) 470	(4) 008	(4) 008	(4) 408	(4) 008	(4) 008
1.80	488	10820	(4) 170	(4) 020	(4) 021	(4) 120	(4) 021	(4) 021
1.78	650	18800	(5) 577	(5) 000	(5) 000	(5) 810	(5) 048	(5) 040
0.60	040	28,700	(5) 070	(5) 010	(5) 000	(5) 188	(5) 008	(5) 040
0.80	1087	50,000	(5) 100	(5) 000	(5) 000	(5) 000	(5) 000	(5) 000
0.88	2007	48,000	(5) 070	(5) 104	(5) 104	(5) 004	(5) 120	(5) 120
0.10	2000	71,700	(5) 000	(5) 002	(5) 002	(5) 101	(5) 700	(5) 102
12.0				(5) 104	(5) 004	(5) 000	(5) 111	(5) 000
17.0				(5) 100	(5) 000	(5) 000	(5) 007	(5) 004
20.7			(7) 000	(5) 400	(5) 000	(7) 007	(5) 000	(5) 001

a. Values are for the ionization rates in 10^{-10} r/hr per electron/mg ft at 0 ft above a smooth ideal plane uniformly contaminated with the mixture.

b. Number in parentheses is the number of zeros between the decimal point and first digit.

Figure 6.1
CALCULATED IONIZATION RATE AS A FUNCTION OF TIME AFTER DETONATION FOR
ASSUMED CONDENSAITERS OF TD 62, 174, AND 426 SECONDS AFTER FISSION OF
FISSION PRODUCTS FROM 235-U NEUTRON FISSION OF U-235 AND AN ASSUMED SURFACE
BURST TOTAL YIELD OF 14.1 MT

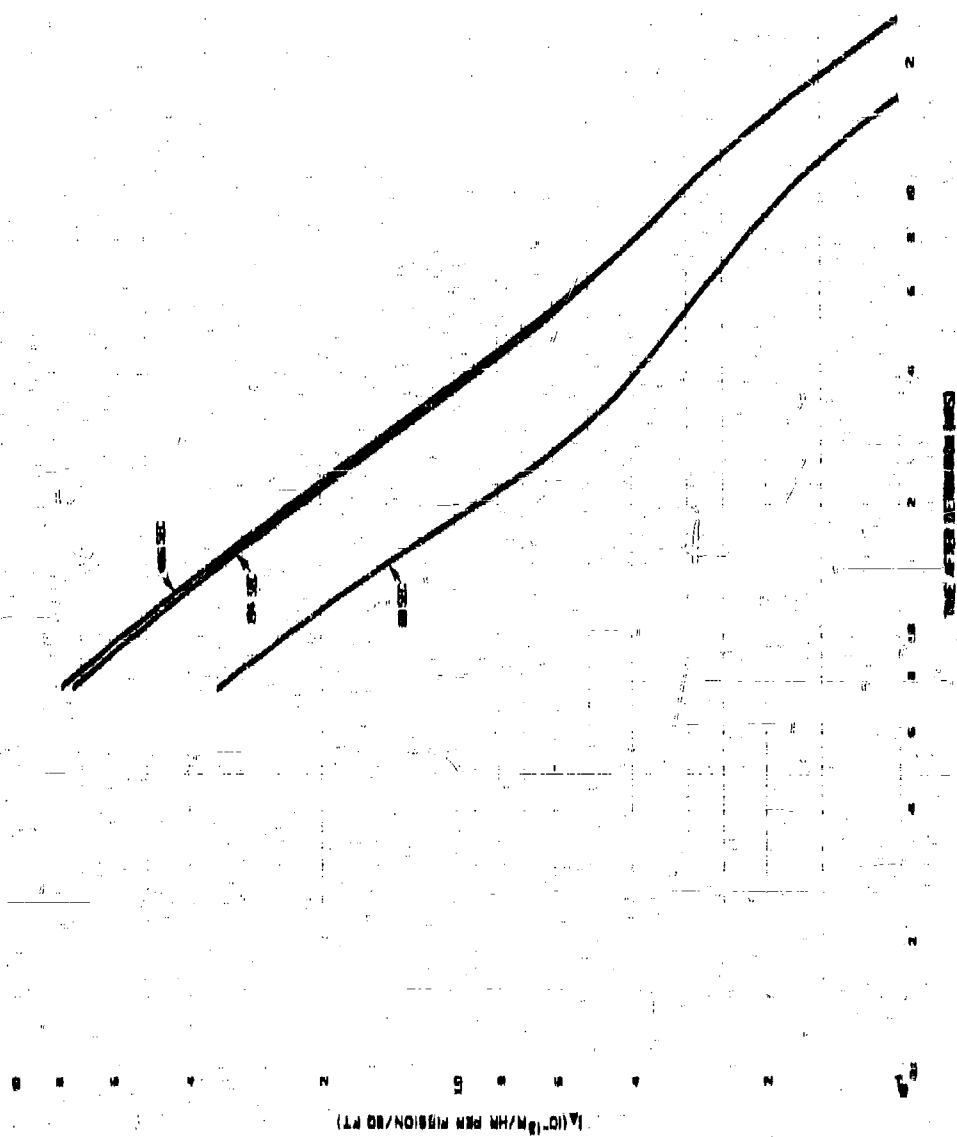


Figure 6.1 (continued)

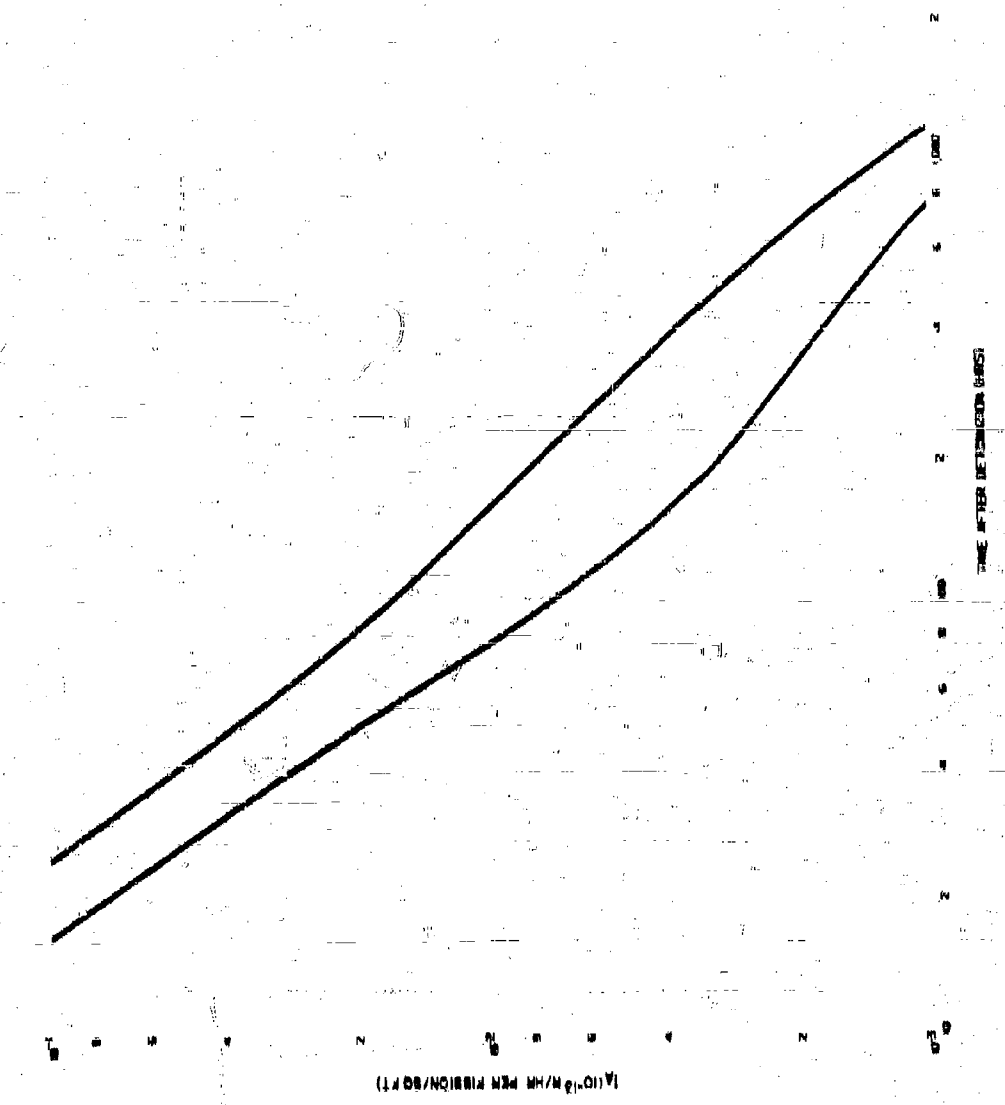
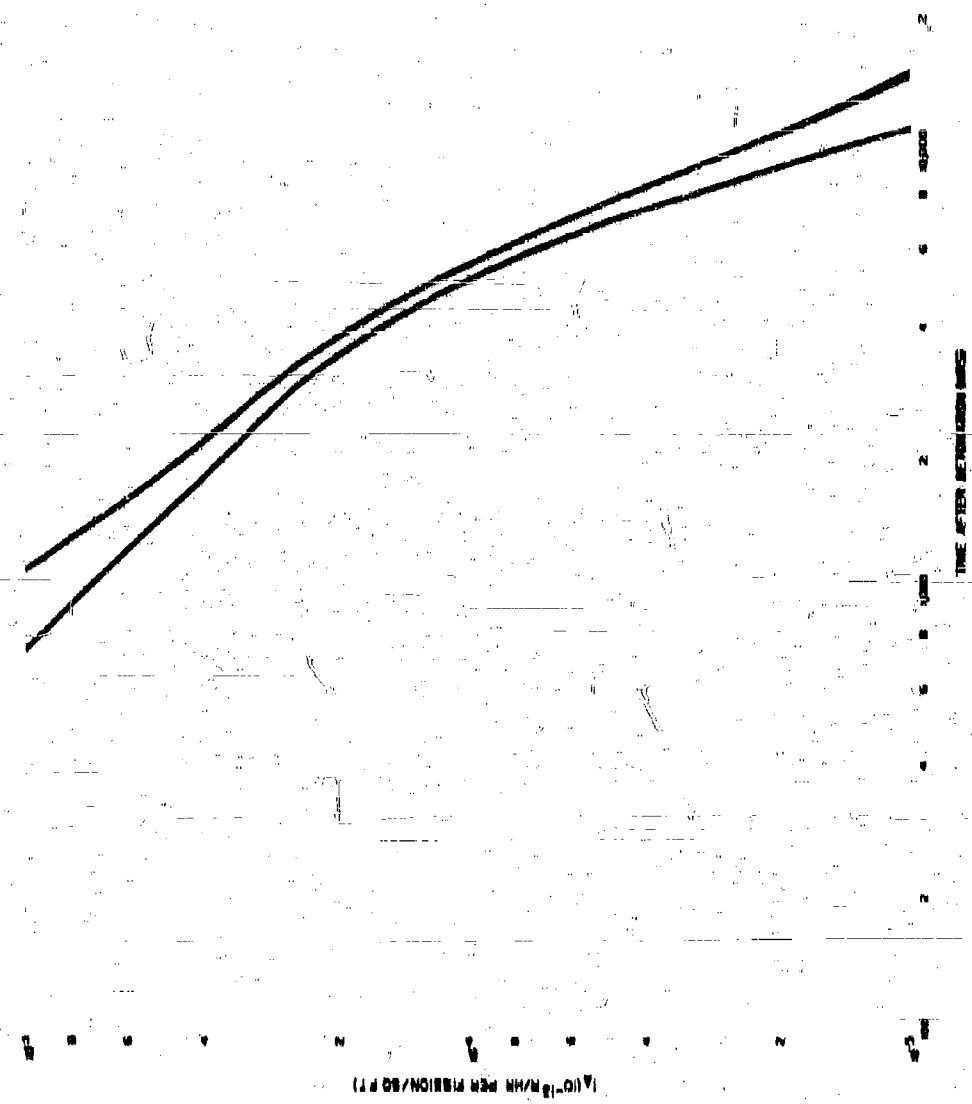


Figure 6.1 (continued)



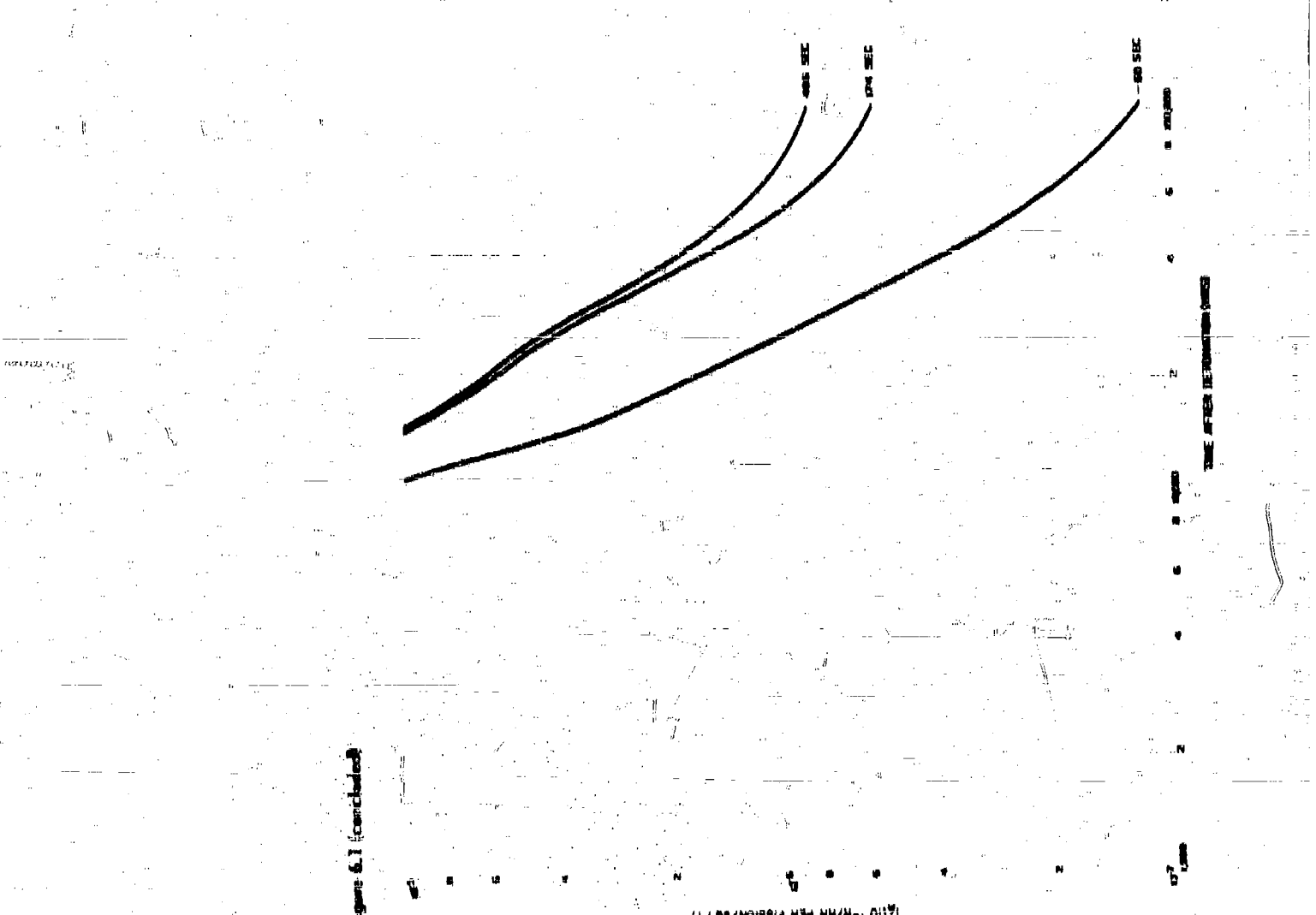


Figure 6.1 (continued)

(L10/N10000 NH/NH₂O)^{1/2}

Table 6.4

FRACTIONATION NUMBERS FOR U-238 (8 Mev NEUTRONS) FISSION PRODUCTS
RELATIVE TO THE NORMAL MIXTURE OF U-238 (THERMAL NEUTRONS) FISSION
PRODUCTS AS CALCULATED FOR THE END OF THE FIRST PERIOD OF CONDEN-
SATION AND AT 400 SEC AFTER DETONATION.

Time After Detonation			84-KT		14-MT	
Year	Days	Hours	0 Mev	400 Mev	00 Mev	400 Mev
		0.700	0.072	0.778	0.010	0.774
		1.12	0.001	0.701	0.010	0.749
		1.64	0.287	0.733	0.281	0.720
		2.40	0.202	0.730	0.272	0.730
		3.52	0.270	0.705	0.304	0.752
		5.10	0.000	0.810	0.088	0.798
		7.00	0.412	0.882	0.480	0.874
		11.1	0.402	0.000	0.010	0.002
		16.2	0.400	1.000	0.000	1.000
		20.8	0.000	1.10	0.007	1.10
		24.4	0.012	0.084	0.000	0.084
		28.1	0.401	0.070	0.507	0.074
		31.1	74.0	0.000	0.450	0.071
		4.07	100.7	0.000	0.000	0.004
		6.70	101.	0.000	0.040	0.048
		8.52	200.	0.000	0.048	0.040
		10.4	340.	0.000	0.051	0.061
		21.1	500.	0.000	0.480	0.000
		30.0	742.	0.002	0.082	0.001
		45.0	1,087.	0.000	1.000	0.000
		60.4	1,004.	0.000	1.000	0.700
		67.0	8,885.	0.702	1.015	0.840
		145.	0,400.	0.010	1.000	0.000
		208.	4,000.	0.021	1.047	0.800
		301.	7,220.	0.002	1.100	0.808
1.00	438.	40,620.	1.215	1.000	0.922	1.004
1.78	650.	15,000.	1.480	2.022	0.821	2.022
2.00	640.	22,780.	1.070	2.000	0.680	2.000
2.80	1087.	30,000.	0.021	2.000	0.415	2.000
5.08	2037.	48,000.	0.498	1.884	0.240	1.820
8.18	2080.	71,700.	0.285	0.004	0.107	0.004
12.0			0.200	0.870	0.118	0.878
17.0			0.100	0.830	0.007	0.834
30.7			0.130	0.784	0.086	0.781

functions of the simple fallout scaling system. It might be expected that the delay-time should be dependent on both yield and particle-size (or on the true time after burst), but no reliable trends with these variables could be established with the few unclassified data available. Therefore, the same time-delay is used to estimate all the 10 mph α -values for each of the condensation times of Table 0.1. The calculations of the α values corresponding to the particle groups leaving the fireball or cloud at the selected times, for the 180-second delay time, are shown in Table 0.8.

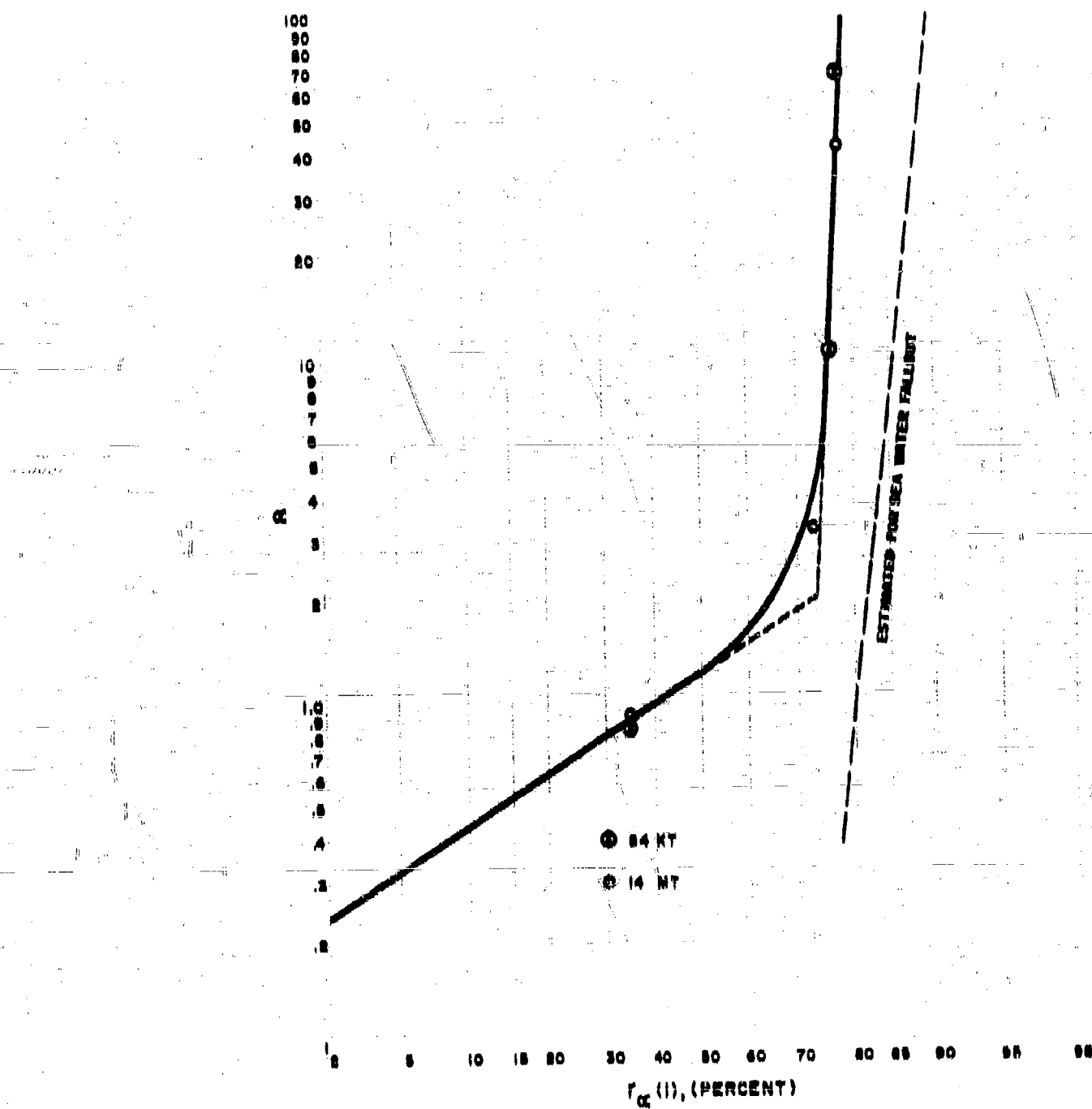
Table 0.8

COMPUTATION OF PARTICLE SIZE PARAMETERS FOR VARIOUS CONDENSATION TIMES OF THE 84-KT AND 14-MT YIELD LAND SURFACE DETONATIONS

Time (sec)	R (ft)	A (ft/sec)	V _t (ft/sec)	α
1. 84-KT, $r_0 = 2.18 \times 10^4$ ft				
9	1.01x10 ⁴	80.0	26.2	0.84
900	2.18x10 ⁴	2.40	2.08	10.0
400	2.18x10 ⁴	0.382	0.025	67.6
2. 14-MT, $r_0 = 4.09 \times 10^4$ ft				
90	3.60x10 ⁴	82.1	24.0	0.92
174	4.01x10 ⁴	0.16	0.76	9.26
400	4.00x10 ⁴	0.710	0.584	42.0

The R_α (1) values are plotted as an accumulated distribution curve, as a function of α , in Figure 0.2; the dotted line applies to sea water fallout (see Subsection 0.2.4). The slope of the curve for α values between 0.0 and 2.0 was determined with the aid of some observed fractionation data on several single nuclides relative to Zr-90 and Co-144. A single curve was drawn through the points to indicate that, within the uncertainties in the calculations and data, no real differences in the function have been established to make certain that the small differences are due only to yield. As can be seen, the curve appears to approach a value of about 80 percent of the r/hr at 1 hr condensed, for α values in excess of 100.

Figure 6.2
ESTIMATED PERCENT OF THE FISSION PRODUCT ACTIVITY IN 1 hr AT 1 HR FROM THE
FISSION PRODUCTS CONDENSED ON PARTICLE GROUPS WITH α VALUES
(15 MPH Wind Speed) LESS THAN A STATED VALUE



The concept of the accumulated distribution curve for the fraction of the total radionuclides condensed up to a given time as a function of the particle groups still present in the volume is a valid one, irrespective of the accuracy with which it can be calculated by using the thermodynamic data and the dynamic aspects of the fallout model. The use of the distribution curve in a precise way, however, requires information about the number distribution of the particles with respect to both their sizes and the fraction of the activity that is carried away by each size group. Details of this nature still need to be worked out before satisfactory estimates can be made; for example, of the fraction of I-131 or Sr-90 that is fused inside of particles of a given size and the fraction that is condensed on their exterior. The amount or fraction of each nuclide on the smaller particles depends on the fraction of the chain in question that is carried away by the larger particles.

In the following treatments of the data in which the distribution curve is used, no account is made of the fraction of the activity (in terms of r/hr at 1 hr) that is carried away by the larger particles. The implied assumption is that the effect is small, due to the large abundance of smaller particles relative to the larger ones. For the gross ionization rates, this assumption may not involve very large errors, simply because the limit of the fraction condensed increases rapidly to about 70 percent and never increases beyond about 80 percent for the small-particle sizes of interest. But even if this is the case, and the effect is small, further study is needed of the relationships mentioned above, to estimate the fate of single radionuclides.

The curve of Figure 6.8 was used in conjunction with some observed $M_r(1)$ values from Operation Jangle Shot "G" to establish the dependence of $f(\alpha)$ on α . The calculation of the values of $f(\alpha)$ from the data is presented in Table 6.6; the values were obtained from

$$f(\alpha) = 5.46 \times 10^{10} \cdot [r_g(1) + 0.019] \cdot M_r(1) \cdot W^{0.083} \quad (6.12)$$

The fallout collectors nearest shot point collected considerable amounts of debris and dust from the desert, kicked up in the vicinity of the collectors by the blast wave. This extraneous grit accounts for the exceedingly high observed $f(\alpha)$ values at those locations. Although it is likely that all the recovered samples contained some extraneous dust, the amount collected should have decreased with distance from shot point. Since this source of dust would not contribute to the fallout in other less desert-like regions, nor at the same relative distances from large yield detonations, it would be desirable to eliminate its contribution to $f(\alpha)$; unfortunately, there are no means for estimating the amounts of extraneous debris in the samples and for correcting the total mass to the mass of "pure" fallout.

Table 6.6

CALCULATION OF $f(\alpha)$ FROM $M_r(1)$ DATA FROM
OPERATION JANGLE SHOT "B"

X (ft)	$M_r(1)$	α_{\min}	α_{\max}	$\bar{\alpha}$	$v_n(1)$	$(v_n(1) + 0.018)$	$f(\alpha)$ (mg/RT)
	$(\frac{\text{mg/mg ft}}{\text{r/hr at 1 hr}})$						
200	24,000	0.082	0.474	0.428	0.100	0.110	1.81×10^{14}
800	818	0.416	0.625	0.550	0.550	0.100	7.00×10^{12}
1,110	158	0.516	0.680	0.598	0.100	0.200	1.77×10^{12}
1,720	108	0.020	0.800	0.710	0.250	0.272	1.00×10^{12}
1,940	800	0.085	0.800	0.700	0.280	0.200	0.22×10^{12}
2,000	22.5	0.770	1.00	0.885	0.845	0.804	4.47×10^{11}
2,820	28.0	0.804	1.04	0.922	0.502	0.881	4.70×10^{11}
3,040	47.8	0.85	1.09	0.970	0.887	0.400	10.0×10^{11}
3,480	31.8	0.024	1.18	1.082	0.480	0.440	7.80×10^{11}
3,600	25.0	0.96	1.20	1.005	0.448	0.407	6.88×10^{11}
3,010	37.1	1.00	1.27	1.185	0.470	0.470	9.00×10^{11}
7,400	17.8	1.68	1.08	1.805	0.025	0.044	0.08×10^{11}
9,120	17.8	1.04	2.02	2.180	0.687	0.070	0.88×10^{11}
12,000	10.0	2.00	0.00	2.80	0.000	0.714	0.80×10^{11}

The variation of the function, $f(\alpha)$, with α can be indicated in a very general sort of way by making an analogy between what may occur in the fallout formation process to what should occur in an idealized condensing system. If the idealized system consists of a group of suspended drops in equilibrium with a dissolved gas, the concentration of the condensing gas should be the same in all particles whose diameter is larger than a few tenths of a micron. For these particles, the concentration is independent of the particle diameter and, therefore, independent of the parameter, α .

In a system where the particles are rapidly heated and cooled over a short period of time; only the surface of the particles having diameters larger than the same size will be melted; those larger particles should, in a given period of time, condense amounts of vapor that are proportional to their surface area or to the square of their diameters. The same result should occur for particles of all sizes that do not melt at all. If the particles are very large, only part of the surface may be melted (see discussion in Chapter 2); the amount that is condensed will not be proportional to their surface area.

Thus, in an ideal system where particles are exposed for the given period of time to a uniform concentration of condensing gas, the ratio of the particle mass to the amount condensed on each particle (m/a) should: (1) remain constant for smaller liquid particles; (2) be proportional to the particle diameter, d , for the larger surface-melted particles and for all solid particles; and (3) increase more rapidly than the particle diameter for very large partially-melted particles.

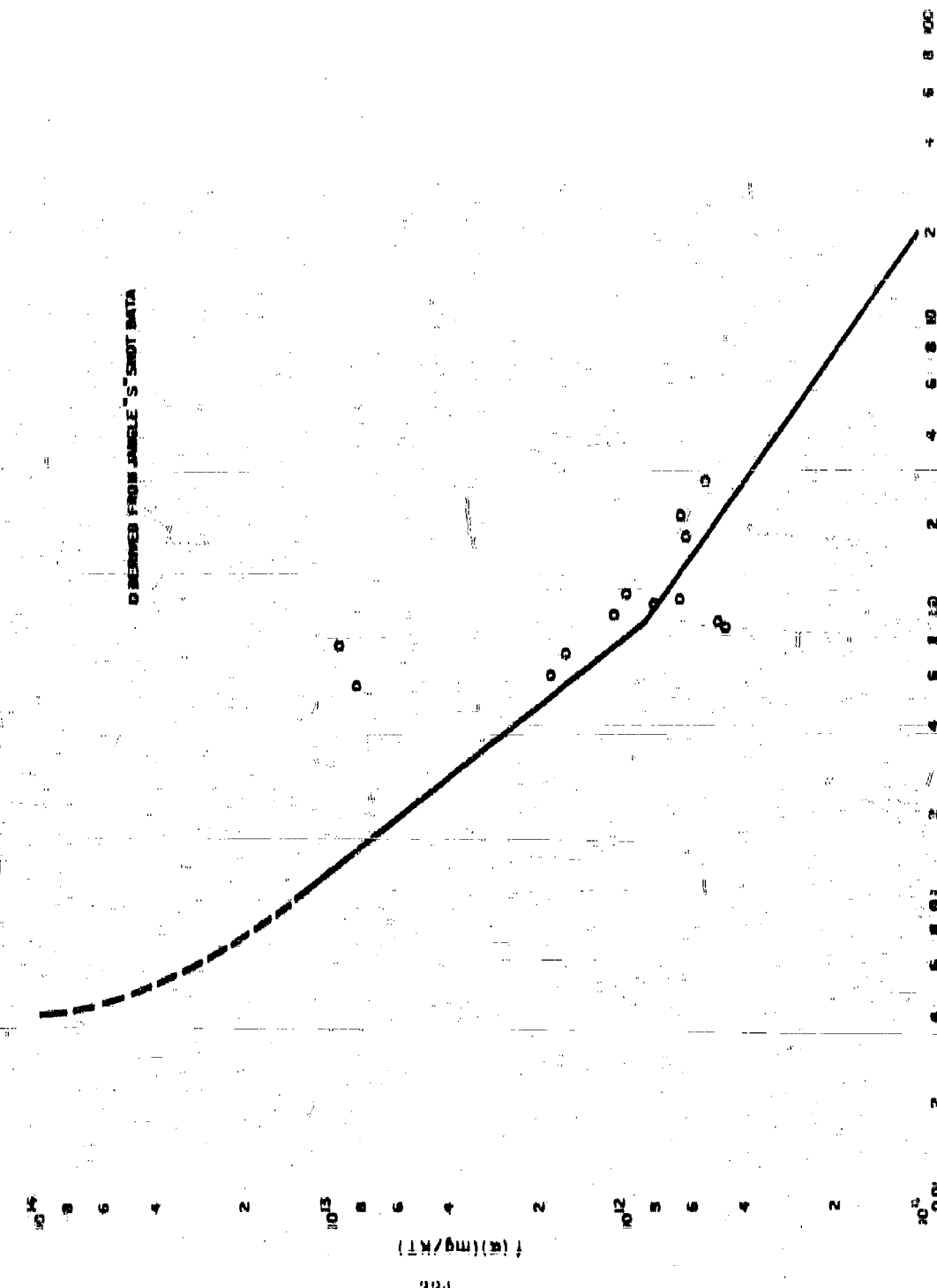
However, in the fallout formation process some of the smaller liquid particles can remain in the gas volume after they solidify, and condense material on their surfaces in addition to that contained in their volumes; these particles could carry more activity than would be indicated by (1) above. Smaller particles, with diameter less than about 80 microns, have terminal fall velocities proportional to the square of their diameter (Stokes' law). For these, the particle diameter is proportional to v_w/α . Hence, for a mixture of small spherical (previously melted) and irregular particles, the ratio, (m/a) , should not decrease with α more rapidly than does $1/\alpha^2$. If the amount of small unmelted particles that enter the cloud at late times is large, it would be possible for the average value of (m/a) actually to increase with α . For particles with diameters from about 80 to 1000 microns that have fall velocities roughly proportional to their diameter, their diameters are proportional to v_w/α . The dependence of the ratio, (m/a) , for these particles on α should lie between being proportional to α and $1/\alpha$.

If $f(\alpha)$ roughly follows this admixture of behaviors, it should decrease very rapidly with α at low values of α ; also, its rate of decrease with α should also decrease with the value of α . At high values of α , $f(\alpha)$ may decrease slowly with α , have a constant value, or even pass through a minimum and increase again.

In Figure 6.3 a proposed curve for the variation of $f(\alpha)$ with α is shown; it is based mainly on the Jangle "B" data. The slope of the curve from $\alpha=0.1$ to 0.9 was determined with the aid of single-particle activity data of fallout from low yield detonations where the specific activity was roughly proportional to the diameter of the particles and, for larger sizes comparable to α values less than 0.1, increased less and less rapidly with size. The line from $\alpha=0.9$ to 20 was based on a geometric mean value of the plotted data in the range $\alpha=0.85$ to 2.5, and on several values of M , (1) from higher yield detonations which, when corrected by use of Eq. 6.12, gave a mean value of $f(\alpha)$ of 1×10^{-1} and an average α value of 20. No data were available for estimating $f(\alpha)$ at α values larger than 20; hence a constant value of 1×10^{-1} was assumed for α values larger than 20.

The lack of available data for establishing more accurate values of $f(\alpha)$ at the higher α values is not of too much concern for many uses of $f(\alpha)$ because of the lower levels of fallout that are associated with the smaller particles. This lack of data is of much more concern in evaluating the longer-

Figure 6.3
PROPOSED CURVE FOR THE VARIATION OF τ_{d} WITH t FOR A 15-MPH WIND SPEED



term hazards that are associated with the uptake of certain long-lived radionuclides by plants and animals, since much of the surface-contaminated, biologically available elements will be carried by the smaller particles.

The mathematical expressions for portions of the proposed function for $f(\alpha)$ are

$$\begin{aligned} f(\alpha) &= 7.46 \times 10^{11} \alpha^{-1.25} \text{ mg/RT, or} \\ &= 5.33 \times 10^{-18} \alpha^{-1.25} \text{ mg/fission, } \alpha = 0.1 \text{ to } 0.9 \end{aligned} \quad (0.13)$$

and

$$\begin{aligned} f(\alpha) &= 7.90 \times 10^{11} / \alpha - 0.690 \text{ mg/RT, or} \\ &= 5.64 \times 10^{-18} \alpha - 0.690 \text{ mg/fission, } \alpha = 0.9 \text{ to } 20 \end{aligned} \quad (0.14)$$

$$\begin{aligned} f(\alpha) &= 1.0 \times 10^{11} \text{ mg/RT, or} \\ &= 7.14 \times 10^{-18} \text{ mg/fission, } \alpha < 20 \end{aligned} \quad (0.15)$$

In which the wind speed associated with the α values is approximately 10 mph.

The general equation for estimating $M_p(1)$ for a land surface burst, from the above treatment of the data, is

$$M_p(1) = \frac{f(\alpha)W - 0.083}{D(1)q_s B [r_\alpha(1)]l_{T_p}(1) + l_1(1)} \quad (0.16)$$

In which $f(\alpha)$ is the ideal (or unfractionated) inverse specific activity in mg/fission, $D(1)$ is an instrument response factor, q_s is the terrain attenuation factor, B is the ratio of fission to total yield, $r_\alpha(1)$ is the gross fission-product ionization rate fractionation number at RT, $l_{T_p}(1)$ is the true air ionization rate at RT at 0 feet above an ideal plane uniformly contaminated with the radionuclides from a normal (unfractionated) mixture of fission products at a surface density equivalent to one fission per sq ft, and $l_1(1)$ is the true air ionization rate per fission contributed by induced activation.

By substituting 0.75 for $D(1)$, 0.75 for q_s , 0.04×10^{-13} (r/hr at 1 hr)/fission/sq ft for $l_{T_p}(1)$; and 0.18×10^{-18} (r/hr at 1 hr) (fission/sq ft) for $l_1(1)$, the mass contour scaling function for the land surface burst is

$$M_p(1) = \frac{1.83 \times 10^{11} f(\alpha)W - 0.083}{B [r_\alpha(1) + 0.019]} \frac{\text{mg/sq ft}}{\text{r/hr at 1 hr}} \quad (0.17)$$

6.2.3 Dependence on Height or Depth of Burst

When an explosive charge is detonated below the surface of the ground, the apparent crater volume increases in size until a maximum amount of soil is thrown out. As the charge depth increases beyond this point, the amount of soil thrown out begins to diminish and, at some depth, the explosive force is no longer sufficient to break through the surface of the ground. When the height of burst is increased, the apparent crater from the explosion rapidly decreases until no crater is formed.

However, in nuclear explosions, the updraft of air following the rising fireball usually forms a column of loosened soil particles even when no real crater is formed. The height of burst at which the local fallout becomes insignificant occurs for detonations in which the rising dust column just fails to catch up with the rising cloud. Instead of specifying the requirement for entrainment of soil particles to form fallout, ENW gives a fireball radius of 1800^{0.1} feet as the minimum height of burst for negligible fallout; this height is supposedly associated with the height for contact of the fireball with the earth's surface.

Since the gross specific activity of the fallout for surface detonations has been found to be more or less proportional to the mass of soil removed from the crater, it seems that the same trend should occur with change of depth or height of burst. Thus, the value of $M_r(1)$ is expected to increase with depth of burst and decrease with height of burst, at least if the depths and/or heights of burst are not large. As the depth of burst becomes very large, only a small amount of activity should escape with most of the radioactivity remaining in or beneath the crater; that which does escape is on very small particles which could be dispersed over relatively large areas, so that no high levels of fallout would occur. However, the specific activity of these very small particles may still be higher than it is for the particles from detonations at intermediate depths.

As the height of burst is increased (by small distances) the smaller amounts of loosened (or melted) soil particles would result in increases in the specific activity of the fallout. However, as the height of burst becomes large, the size of the particles that can actually enter the cloud decreases. Since those that enter do so at later times (because of the height involved), and since, by this time, the concentration of the condensing radioactivity has decreased, due to both expansion of the cloud and depletion by vapor condensation to form very small solid particles, the amount of radioactivity collected by each soil particle that enters the fireball or rising cloud should be small. Therefore the specific activity of particles in the fallout should first increase and then decrease as the height of burst increases.

A proposed curve for a mass correction to $M_p(1)$ is shown in Figure 6.4 in which the mass-correction factor, K_λ , is defined by

$$M_p^\lambda(1) = M_p(1)/K_\lambda \quad (6.18)$$

where $M_p^\lambda(1)$ is the mass contour ratio at the nuclear-scaled depth given by

$$\lambda_N = h/W^{1/3} \quad (6.19)$$

and h is the depth of burst ($>h$ is the height of burst) and W is the total yield in KT rather than in pounds of TNT as usually defined.

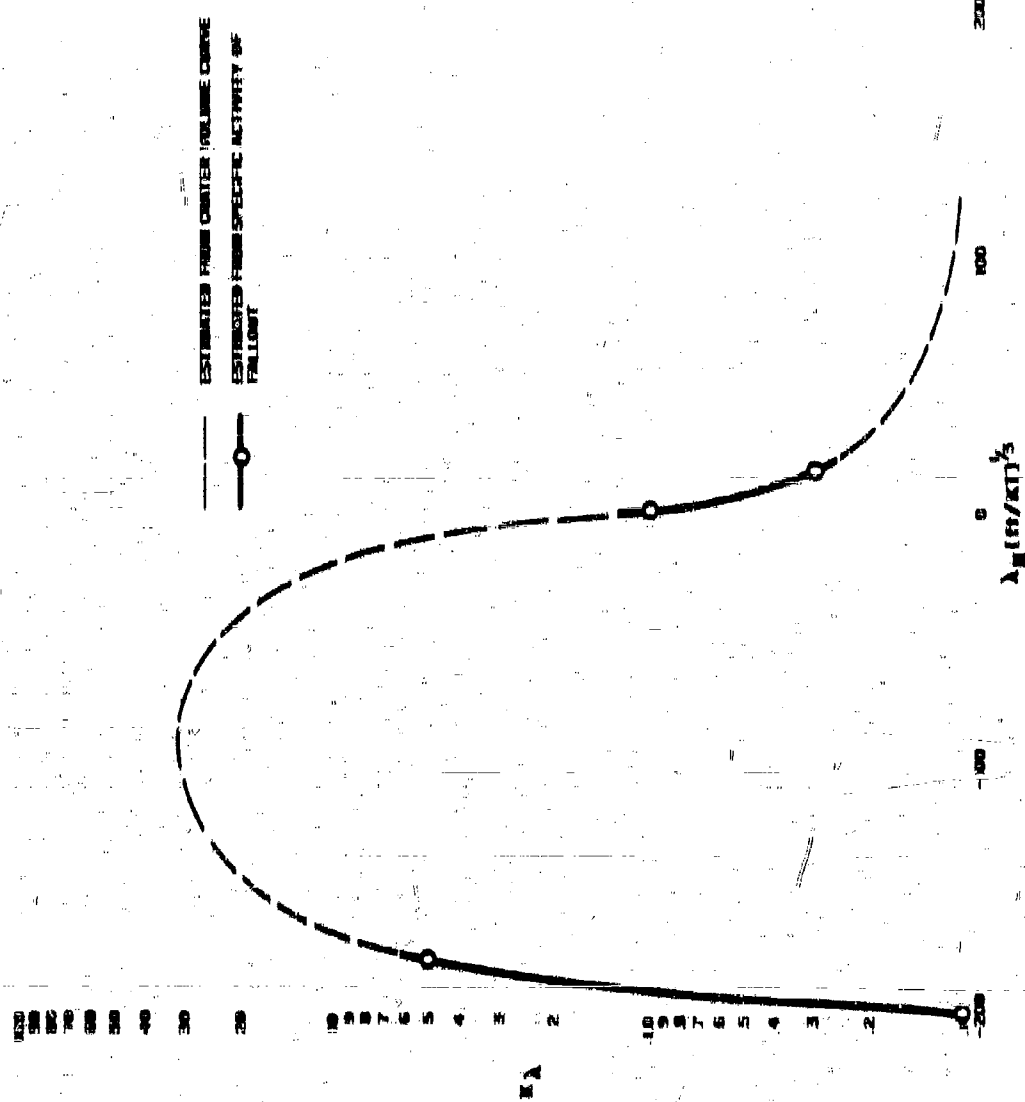
The point of $K_\lambda = 0.8$ was obtained, from the $M_p(1)$ data of Reference 4 for the Operation Jungle "W" shot, by comparing the measured values with those from the Jungle "B" shot at the same downwind distance. At the larger heights of burst one of the two points was derived from the specific activity and contour ratio data of fallout from a tower detonation; the other point was derived from the specific activity data of fallout from a balloon detonation. The values of K_λ are ratios of the average values of $M_p^\lambda(1)$ in each case. The remainder of the curve was determined from high-explosive crater-volume data.

In using the proposed curve, the assumption is implied that the crater volume or mass that forms fallout varies as $W^{0.017}$ for all heights and depths of burst represented by the curve. This assumption is valid, within the accuracy of most crater data, for a fairly wide variation in soil-type media, and for λ_N values between about -100 and +75. In estimating $M_p^\lambda(1)$ for a low-air-burst or shallow underground-burst, $M_p(1)$ at selected values of the downwind distance is to be computed for the same yield surface-burst and then corrected by use of Eq. 6.18. This procedure is indicated because K_λ was determined by comparison to the $M_p(1)$ values at the same downwind distances. However, without methods for correcting the fallout contours themselves for height or depth of burst, the contour ratio $M_p^\lambda(1)$ is of less immediate general use than $M_p(1)$.

6.2.4 Mass Contour Ratio for Fallout from a Surface Detonation on Deep Fresh Water

No unclassified data are available from which $M_p(1)$ for sea water detonations can be computed; however, rough estimates may be made, using the data in ENW, if it is assumed that (1) the mass of water thrown up is proportional to the yield, (2) K_λ holds for a detonation in water as well as in soil, and (3) fractional mixing of the environmental material and fission

Figure 6.4
PROPOSED MASS CORRECTION CURVE TO THE MASS CONTOUR RATIO AS A FUNCTION
OF THE NUCLEAR SCALED DEPTH OF BURST



products is larger for a water shot. In ENW, p. 46, it is estimated that approximately 10^6 tons of water were ejected into the air by the 20-kT Bldm1 Baker detonation. This is equivalent to 4.5×10^{18} mg/kt. Taking the depth of burst as approximately half the depth of the lagoon, K_X is about 0.21. Therefore, the amount of water thrown up for a sea water surface detonation may be approximated by

$$M_w = 9.6 \times 10^{18} W \text{ mg sea water.} \quad (0.20)$$

If α_f is used to estimate an average value of $f(\alpha)$ for the fallout from a land-surface detonation, the fractional mixing of the soil can be estimated from $f(\alpha)/M_r$ which, from Figure 0.3 and Eq. 0.100, is found to be approximately given by $0.14W^{-0.014}$, or about 10 to 14 percent of the total soil thrown out of the crater. For the surface water burst, the fractional mixing was assumed to be about 50 percent of the water thrown up or about 8 to 8 times larger than that of the surface land detonations.

Because the end of the first period of condensation for a water shot occurs at about 0°C , very little fractionation of the fission products (with possible exception of the rare gas elements) should occur, especially for the larger yield detonations. This longer period of condensation for the water before the final sea water fallout particles are formed by vapor condensation should result in more thorough mixing of the water and the fission products, as well as in rather uniform concentrations of the radioactive elements in all fallout particles or drops. For these reasons, $f'(\alpha)$ for the water shot was taken to be independent of α , or droplet size, and equal to 4.5×10^{18} mg/kt or 0.4×10^{11} mg/fission. The mass contour ratio, in terms of the mass of original sea water, is then

$$M_r(1) = \frac{3.4 \times 10^{11}}{D(1)c_{in} B [I_{fp}(1) + I_f(1)]} \text{ mg sea water/eq ft} \quad (0.21)$$

where no fractionation of the radionuclides in the fallout is assumed.

The no-fractionation assumption is essentially valid for yields greater than about 5-MT. For lower yields than this, a gross estimate of the gross fractionation number for a surface water detonation, $r'_f(1)$, can be made from a log-normal distribution curve of $r'_f(1)$ in which the cumulative distribution curves passes through $r'_f(1) = 0.8$ at $\alpha = 1$, and through $r'_f(1) = 0.0$ at $\alpha = 100$ (see dotted line of Figure 0.2). The simple fallout scaling system for the land surface burst can be used to provide a gross estimate of the fallout areas from sea water detonations. No large or experimentally observed significant differences in the areas of heavy fallout at sea have been found between the land and sea types of detonations for large yields.

For non-water fallout that is deposited on land areas where the previous values of $D(1)$ and η_0 apply, the mass contour ratio for the fallout of a large yield detonation on the surface of the water reduces to

$$M_r(1) = \frac{8.8 \text{ mg/kg water}}{D} \text{ sq ft} \quad (0.218)$$

When completely dried, the non-water salt residue, at 0.8 percent of the initial non-water mass, is only $8.8/D(\text{mg/kg ft}^2)/(\text{r/hr at 1 hr})$.

Because the fallout drops apparently full most of the distance from the high altitude in the solid state through temperatures where the sublimation pressure of the water is rather low, the change in droplet-size with time is probably rather slow. At the lower and warmer altitudes, where the particles exist in the liquid-state, they either grow larger or decrease in size by evaporation, depending on the relative humidity of the surrounding air. Thus, the true value of $M_r(1)$ for the arriving particles could be almost as low as the $8.8/D$ value or could be even larger than the $8.8/D$ value. In dry (warm) climates and over land areas where the $M_r(1)$ value of the arriving material would be low, the fallout pattern would extend much farther downwind than would be estimated from use of the simple fallout scaling system for land surface detonations. This is simply because the droplets, decreasing in size and density as the water evaporates, would be carried to greater distances and dispersed over a larger area. Under these conditions, the deposit levels would all be decreased.

0.2.5 Mass Contour Ratio for Fallout from Detonations in Harbors

The mass contour ratio from detonations in shallow water should depend on (a) the height or depth of the burst point with respect to the water surface, (b) the depth of the water, and (c) the effective depth of the crater in the bottom of the harbor. Equations for estimating the contour ratio were derived from the assumption of proportional mixing of the soil and water contained in a set of assumed cone-shaped crater volumes.

For detonations in which the water depth, d_w , is small enough so that a significant amount of bottom material is removed, the crater depth, d_c , measured from the surface of the water to the bottom of the crater in the harbor bottom, is assumed to approach the crater depth of a detonation in dry soil. Using the data of ENW (0.213) for a land surface detonation, the crater depth is given by

$$d_c = \frac{25W^{0.25}}{R_A} \text{ ft} \quad (0.219)$$

where δ_λ is the ratio of the center depth for a surface burst to the center depth for a burst at the nuclear scaled depth, x_N . An estimating curve for δ_λ , based on high-explosive data, is shown in Figure 6.6.

It is convenient to use the mass solid-to-liquid ratio, designated S , as a composition variable for the relative amounts of harbor bottom material and sea water as the two major constituents of this type of fallout. The same relative mixing ratios of the total material removed from the soil crater and the water volume lifted up to form fallout are assumed to occur in the harbor detonation as occur for each type of shot separately; the ratios would then depend on the relative masses of water and soil that are drawn up. Accordingly, the ratios (of the masses of each constituent) would be roughly proportional to $f(x)W^{0.006}/f'(x)$; the proportionality factor (soil) must be related to the initial amounts of soil and water dislocated by the detonation. The initial amounts of each constituent involved must, in turn, depend on the depth of the water and the size of the crater in the harbor bottom.

Data are not available for establishing the proportionality factor on an empirical basis, so geometrical considerations were used to develop a model for estimating its values. The geometrical crater-shapes assumed were two inverted cones both having the same radius, R_1 at the water surface. The height of the cone involving the harbor bottom material is the depth of the water, d_w plus the depth of the crater in the harbor bottom, d_b^* . With this geometry, the volume of the harbor bottom material (solids) removed is

$$V_s = (\pi/3)R_1^2(d_b^*)^2 / (d_b^* + d_w)^3 \quad (6.24)$$

where it, for a land surface detonation, according to ENW, is $0.2W^{1/3}$ ft.

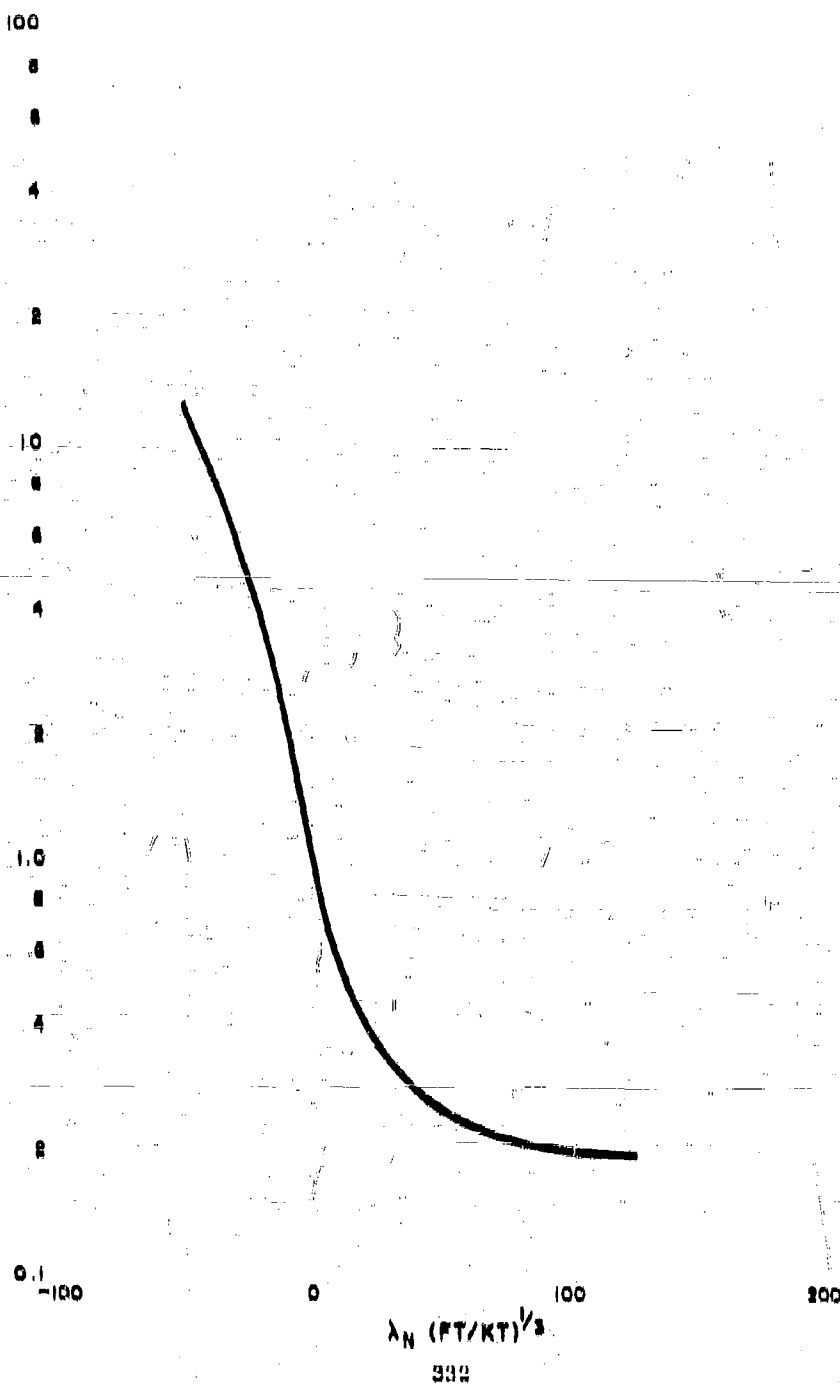
The depth (or height) of the cone for the water component, d_b^* , was taken to be equal to the depth of the water involved in the explosion for the case in which the water is sufficiently deep so that no crater is formed in the harbor bottom. For this geometry, the volume of water involved is

$$V_L = (\pi/3)R_1^2 [d_b^* - (d_b^* + d_w)^2 / (d_b^*)^2] \quad (6.25)$$

By assuming the ratio of the bulk density of the bottom material to that of the sea water to be $\bar{\rho}$, the proportionality factor is given by

$$S_0 = \frac{2(d_b^*)^2}{d_b^*(d_b^* + d_w)^2 [1 - (d_b^* + d_w)^2 / (d_b^*)^2]} \quad (6.26)$$

Figure 4.5
PROPOSED CRATER DEPTH CORRECTION CURVE FOR THE MASS CONTOUR RATIO AS A FUNCTION OF THE NUCLEAR SCALED DEPTH



Since d_b should decrease with depth of water, a first-order approximation of d_b^* may be obtained from a function of the form

$$d_b^* = d_b^0 \left[1 + d_b(W) d_w \right] \quad (0.27)$$

where $d_b(W)$ is a yield dependent parameter that might be evaluated from available data. It was not possible to evaluate $d_b(W)$ from the data of ENW (pp. 226 and 227) because, for yields of about 10-KT and greater, that data gives larger craters in a harbor bottom (clay mud) under water than for a land surface detonation. Because such results are not in accord with observations, the data in ENW are presumably extrapolated incorrectly from high explosive data; hence they are not directly applicable to the higher yield nuclear explosions. Correcting some of the ENW data to an equivalent nuclear yield (see Chapter 2 for fraction of energy in blast) gives

$$d_b(W) = 0.017 W^{0.16} \text{ ft.} \quad (0.28)$$

The appropriate value of d_b^* is obtained from Eq. 0.27 for the water depth at which d_b^* becomes zero; for a water surface detonation this is

$$d_w = d_b^* = 89 W^{0.16} \text{ ft.} \quad (0.29)$$

From Eq. 0.29, the value of d_b^* obtained by assuming the involvement of a hemispherical volume of water is $89 W^{1/5}$ ft. On the other hand, if the shape of the water volume thrown up is assumed to be the same as that of a crater in soil, then d_b^* , from a linear increase in all the soil crater dimensions to the volume of the water removed, would be $38 W^{0.370}$ ft. Thus the value of d_b^* found for Eq. 0.29 suggests that the ratio of the radius to the depth for the water "crater" increases more rapidly with yield than it does for a crater in dry soil.

With S_o defining the solid-to-liquid ratio weighting factor, the liquid mass fraction weighting factor is $1/(1 + S_o)$ and the solid mass fraction weighting factor is $S_o/(1 + S_o)$. With these weighting factors, the total mass of material per unit of yield for the fallout from a harbor detonation on the surface of the water, is

$$f_{sf}(a) = \frac{f(a) + S_o f(a) W^{0.081}}{1 + S_o} \quad (0.30)$$

The solid-to-liquid mass ratio at a given location in the fallout area is, then,

$$S = \frac{B_0 f(\alpha) W^{0.083}}{f'(\alpha)} \quad (0.81)$$

and the mass contour ratio for this harbor detonation type of fallout may be estimated from

$$M_r(1) = \frac{7.1 \times 10^{-11} f_{st}(\alpha)}{d(1) q_x K_X D [r_\alpha^*(1) r_{tp}(1) + l_t(1)]} \quad (0.82)$$

for $r_{tp}(1)$ and $l_t(1)$ in (r/hr at 1 hr)/(fission/sq ft), $f_{st}(\alpha)$ in mg/kt, and in which $r_\alpha^*(1)$ is the gross fractionation number for the slurry.

For shot geometries where B_0 has values less than about one, a large amount of water and non-water solids are present in the fireball. Under such conditions the use of the $r_\alpha(1)$ values for fallout from a surface land detonation is not appropriate--even for the solid fraction--because of differences in vapor pressures between the oxides and hydroxides of many of the fission product elements. However, as the water content decreases (B_0 becomes larger) the use of $r_\alpha(1)$ for the solids becomes more applicable, and, as the B_0 values decrease, the $r_\alpha^*(1)$ values for the water fallout apply. To account, in gross way, for these interactions, it is suggested that $r_\alpha^*(1)$ be estimated from

$$r_\alpha^*(1) = \frac{r_\alpha(1) + B_0 r_\alpha(1)}{1 + B_0}, \quad B_0 > 1 \quad (0.83)$$

and

$$r_\alpha^*(1) = r_\alpha(1), \quad B_0 < 1 \quad (0.84)$$

For large-yield detonations ($W \geq 1-MT$) on the surface of the harbor water (where $r_\alpha^*(1)$ is essentially unity for all α , B_0 is less than unity, and $D(1)$, q_x , $f_{tp}(1)$, and $l_t(1)$ have the standard values), the mass contour ratio is

$$M_r(1) = \frac{1.8 \times 10^{-11} (4.8 \times 10^{18} + B_0 f(\alpha) W^{0.083})}{(1 + B_0) D} \frac{\text{mg slurry/sq ft}}{\text{r/hr at 1 hr}} \quad (0.85)$$

and, for lower yields, the multiplier would be $1.88 \times 10^{-11} = M_r^1(1) + 0.09$ instead of 1.8×10^{-11} .

Because the functions were derived from data on fallout from land surface detonations, and because the simple fallout model applies only to land surface detonations, use of the scaling functions at other depths of burst will introduce errors among the distance, standard intensity, and particle size parameters. These errors should, of course, increase as the nuclear scaled depth (or height) shifts farther away from zero.

For burst heights or depths that are a small deviation from a surface burst, the error in the extent of the fallout pattern itself should not be large since the cloud height and size are not very sensitive to either height or depth of burst or type of medium at the point of detonation. However, the value of the mass contour ratio is very sensitive to the depth of burst; this is indicated by the rapid change of K_λ and δ_λ with λ_N when λ_N is small. Considering the general trends and accuracy of the source data, the fallout model scaling functions for a surface detonation could be used, without significant increase in error for all types of detonations characterized by λ_N values up to ± 5 , and it is likely that consistent errors would become increasingly large for λ_N values larger than ± 10 . By use of K_λ and δ_λ , however, the scaling function for $M_r^1(1)$ values appears to be as reliable as the original data up to λ_N values of ± 20 .

0.2.0 Mass Contour Ratio for Fallout from a 1-MT Detonation at Several Detonation Geometries

To illustrate the use of the scaling functions for the mass contour ratio and how its value depends on the various parameters, computations for $M_r^1(1)$ were made for: (1) a land surface detonation, (and detonations on the) (2) water surface, and (on the) (3) water bottom, for depths of 20, 50, and 100 feet. The calculation results for K_λ are shown in Table 0.7.

The value of d_p^1 indicates that, for water depths in excess of about 180 feet, the fallout, from a surface detonation, would be a pure-water type of fallout. It may be noted that d_p^1 has been corrected for depth of burst by $1/\delta_\lambda$ in the same way as d_p and d_p^2 .

For computing $M_r^\lambda(1)$, the parameters B , q_α , and $D(1)$ were taken to be 1.0, 0.70 and 0.70, respectively. With these values, the mean contour ratio scaling function becomes

$$M_r^\lambda(1) = \frac{1.26 \times 10^{-11} f_{BL}(\alpha)}{K_\lambda [6.93 \times 10^{-11} r_\alpha^\lambda(1) + 0.13 \times 10^{-11}]} \cdot B_0^{-1} \quad (0.86)$$

and

$$M_r^\lambda(1)^e = \frac{1.83 \times 10^{-11} f_{BL}(\alpha)}{K_\lambda}, \quad S_n < 1 \quad (0.87)$$

Table 0.7
COMPUTATION OF S_n FOR SEVERAL DETONATION CONDITIONS OF A 1-MT FUSION WEAPON

Depth of Burnt (ft)	λ_N	d_w (ft)	δ_λ	K_λ	d_n (ft)	d_n' (ft)	d_n'' (ft)	S_n
0	0	20	1.0	1.0	140	124	178	0.48
20	2.0	20	0.80	0.80	100	108	198	0.80
0	0	50	1.0	1.0	140	101	178	0.808
50	5.0	50	0.74	0.60	189	106	240	1.20
0	0	100	1.0	1.0	140	91	178	0.108
100	10.0	100	0.07	0.07	240	108	318	0.272

The $M_r^\lambda(1)$ values at various downwind distances are given in Table 0.8.

The values for $r_\alpha^\lambda(1)$ were calculated by use of Eq. 0.88 for $S_n = 0.48$, 0.80, and 1.20. At distances where both stem and cloud fallout occur, the overall $M_r^\lambda(1)$ values were calculated by multiplying the individual ratios by the respective Lytton, adding the masses obtained, and then dividing the total by the sum of the two I values.

Selection of the surface-water and bottom detonations was made so as to give the spread in $M_r^\lambda(1)$ values for detonations anywhere in the water layer; this spread is not large for 20 and 50 foot depths, but at 100 foot the spread is

TABLE 6.8
COMPUTATIONS OF $M^2(0)$ FOR SEVERAL DEFORMATION CONDITIONS OF A 1-MI FIELD PERSON WEAPON
AT SELECTED DISTANCES

X (in. m)	$\sigma_{\text{def}} \cdot S_0$	r_{eff}	I (hr^{-1} at 1 km)	$M^2(0)$ Long slanting/ $S_0 \cdot 10^3$ / (hr^{-1} at 1 km)					
				$S_0 = 1.00$	$S_0 = 1.25$	$S_0 = 1.50$	$S_0 = 1.75$	$S_0 = 2.00$	$S_0 = 2.25$
0.1	6.38	0.124	3600	74.5	123	102	82.7	105	110
0.2	6.39	0.20	3600	5.36	31.7	37.3	76.8	102	90.1
0.3	1.15	0.35	31.30	3.95	11.2	34.6	55.1	75.0	73.9
0.4	1.35	0.35	31.30	1.38	10.7	35.7	32.0	74.2	78.5
0.5	1.34	0.33	2.50	2.50	8.22	32.9	35.8	73.6	78.7
0.6	0.95	0.35	0.3	4.37	2.59	30.3	38.6	74.1	73.6
0.7	2.19	0.35	0.65	4.36	10.3	33.3	38.6	73.6	73.6
0.8	1.15	0.35	0.70	2.14	10.2	31.9	38.1	74.2	73.6
0.9	1.54	0.35	0.70	3.20	10.2	31.9	38.1	74.2	73.6
1.0	1.02	0.55	0.70	2.04	7.83	32.0	35.6	73.6	75.3
1.2	2.02	0.70	0.70	2.13	5.42	33.8	38.2	72.8	78.5
2	3.94	0.70	0.70	1.76	4.45	27.4	39.3	72.4	69.1
3	5.76	0.71	0.70	1.34	3.22	26.4	38.5	72.3	67.5
4	7.18	0.75	0.70	1.19	2.35	25.5	32.7	71.5	67.1
5	9.25	0.76	0.70	0.92	2.21	25.5	37.9	71.5	66.1
6	11.5	0.76	0.70	0.835	1.95	25.2	36.8	72.2	66.1
7	13.4	0.76	0.70	0.74	1.74	24.7	36.5	71.2	65.3
8	15.4	0.77	0.70	0.677	1.58	24.7	36.2	71.0	65.3
9	17.3	0.77	0.70	0.622	1.47	24.5	36.0	71.0	65.3
10	19.2	0.77	0.70	0.581	1.35	24.5	36.0	71.0	65.3
11	21.1	0.77	0.70	0.554	1.21	24.5	36.0	71.0	65.3
12	22.0	0.77	0.70	0.534	1.09	24.5	36.0	71.0	65.3
13	24.9	0.77	0.70	0.521	1.09	24.5	36.0	71.0	65.3
13.6	25.1	0.77	0.70	0.521	1.09	24.5	36.0	71.0	65.3

about a factor of 3. The large change in $M_r(1)$ from dry-salt fallout to that for the fallout from a detonation on the surface of 30 feet of water is, of course, due to the larger amounts of water thrown up. No absolute accuracy can be stated for any of the numbers for the harbor-shot fallout; however, the values for the water-surface detonations are more accurate, taken relative to each other, than are the absolute values of the mass contour ratios.

6.3 Fission-Product and Fraction-of-Delayed Contour Ratios

Since two fission-product atoms are produced in each fission event, there are 8.82×10^{-14} moles of fission products formed per fission, or 0.405 moles of fission products produced per kiloton of yield. The distribution of these products over an extended area would result in an air ionization rate at 3 feet above the area given by $I_{p_0}(t)$ in r/hr per fission/kg ft. Thus the fission-product-contour ratio for a fractionated mixture, including induced activation, from a land-surface detonation, is given by

$$FP_p(1) = \frac{3.32 \times 10^{-14} \sum_j A_j r_j \lambda(\alpha)}{D(1) q_\alpha [r_\alpha(1) I_p(1) + I_f(1)]} \text{ moles fp/kg ft} / \text{r/hr at 1 hr} \quad (6.08)$$

where $r_j \lambda(\alpha)$ is the fraction of each nuclide condensed on the particle group designated by α relative to the total number of fissions, and is defined by

$$r_j \lambda(\alpha) = \frac{1}{2} [r_\alpha(\Lambda) + r_\alpha^*(\Lambda)] y_\Lambda \quad (6.09)$$

In which $r_\alpha(\Lambda)$ is the fraction of the mass chain for a given element (or chain mass number) condensed when the particles were in the liquid state, $r_\alpha^*(\Lambda)$ is the fraction condensed on the surface of the particles of size α , y_Λ is the yield of the mass chain in atoms per fission, and the factor 2 is for the total yield of 2 atoms per fission. If no fractionation occurs the sum of the $r_j \lambda(\alpha)$ for all α is unity.

Using the standard values of $D(1)$, q_α , and $I_f(1)$, $FP_p(1)$ is given

$$FP_p(1) = \frac{8.61 \times 10^{-10} \sum_j A_j r_j \lambda(\alpha)}{[r_\alpha(1) + 0.019]} \quad (6.10)$$

For non-water or harbor-type fallout, $r_\alpha(1)$ is replaced by $r_\alpha^*(1)$ or $r_\alpha^f(1)$; thus the value of $FP_p(1)$ is dependent on the conditions of detonation only through the gross fractionation number.

The fraction-of-device contour ratio, in terms of the total number of fission events, is

$$FD_r(t) = \frac{7.1 \times 10^{-14}}{D(t)q_nBW \left[r_n(t)t_p(t) + t_p(t) \right]} \quad (\text{r/hr} \cdot \text{st} \cdot \text{hr} \cdot \text{sq ft})^{-1} \quad (6.41)$$

or, for the standard values of $D(t)$, q_n , and $t_p(t)$,

$$FD_r(t) = \frac{1.83 \times 10^{-11}}{BW [r_n(t) + 0.019]} \quad (6.42)$$

The fraction-of-device contour ratio has two uses. The first is that it is used to estimate the surface density of constituents that are assumed to mix uniformly with the more refractory fission products. The second is that it is used in conjunction with observed fallout patterns when the latter are integrated for the total fraction of the weapon contained within a stated ionization rate contour. The use of both contour ratios is illustrated in Chapter 7, Volume II.

For a land surface burst, the average concentration of the fission products is estimated from the ratio of $FP_r(t)$ to $M_r(t)$; this is

$$C_{fp} = \frac{3.12 \times 10^{-14} BW 0.08^3 D_J A r_j \Lambda(\alpha)}{f(\alpha)} \frac{\text{mole} \cdot \text{fp}}{\text{mg fallout}} \quad (6.43)$$

6.4 Foliage-Contamination Factor Contour Ratio

In Chapter 2, the foliage-contamination factor, w_f , was defined as the ratio of the number of fissions in the fallout on foliage per gram of dry plant (or foliage) to the number of fissions in the total deposited fallout, per sq ft of soil. Also, the foliage-surface density, w_L , (subject to contamination) was defined as the grams of dry foliage per sq ft of soil. Therefore, the foliage-contamination factor contour ratio is defined by

$$FC_r(t) = \frac{w_L w_f \text{ Fissions on foliage/ft}^2 \text{ of soil area}}{K_\alpha(t) \text{ r/hr}} \quad (6.44)$$

The contour ratio, evaluated as of II + 1, is

$$FC_r(1) = \frac{E_{LW_L}}{K_\alpha(1)} \frac{\text{Electrons on foliage}/\text{ft}^2 \text{ of soil area}}{\text{r/hr at 1 hr}} \quad (0.46)$$

where

$$K_\alpha(1) = 3.90 \times 10^{-13} [r_\alpha(1) + 0.019] \frac{\text{r/hr at 1 hr}}{\text{fission}/\text{ft}^2} \quad (0.46)$$

when the standard values of $D(1)$ and q_1 are used. It is seen that multiplication of $FC_r(1)$ by $I(1)$ gives the number of fissions on foliage per sq ft of soil area.

The "zero-time" number of atoms of a given radionuclide (at least for the end member of a mass chain) in the fallout is given by

$$N_A^0 = Y_A FC_r(1) I(1) \frac{\text{atoms on foliage}}{\text{ft}^2 \text{ of soil area}} \quad (0.47)$$

in which Y_A is the mass chain yield in atoms per fission of mass number A.

The major interest in the contamination of foliage by fallout is related to the fact that the consumption of the foliage by animals and humans may produce an internal radiological hazard. Therefore, generalization and extensions of the foliage contamination factor data from tower-and balloon-detonation fallout are needed for making estimates of the potential biological availability of the radionuclides in the fallout from other types of nuclear explosions and for various foliage contamination conditions.

When contaminated foliage is consumed, some of the radionuclides or some fraction of each nuclide ingested is dissolved in the stomach fluids; the remainder stays with the particles and passes through the digestive tract. Many of the dissolved nuclides are assimilated into the blood and concentrate in specific body organs. The factors involved in this distribution and the methods for estimating the resulting internal doses are given by K. Z. Morgan and others.¹

However, methods are needed for estimating the relative amount of each nuclide that is soluble in the stomach fluids. Evaluations of the internal hazard can be made (for fallout conditions in a nuclear war, for example) from the generalizations of the foliage contamination factor together with estimates of the solubilities of the radionuclides.

The amount of radionuclides that pass through the digestive tract may be considered separately because a large fraction of certain radionuclides in the fallout will be insoluble. For these radionuclides, only the gross amount passing through need be considered. However, for the case of the assimilation of the soluble nuclides in other body organs, each radionuclide must be considered separately.

8.4.1 Insoluble-Nuclide Fractions

A gross estimate of the radioactivity of insoluble nuclides passing through the digestive tract from ingestion of contaminated foliage can be made if it is assumed that the gross solubility of the radioactivity is the same in the stomach as it is in 0.1N HCl. If the soluble fraction of the gross activity is defined as $S(t)$, the number of moles of fission product atoms ingested that pass through the digestive tract with the particles is given by

$$FP_s = 3.32 \times 10^{-24} [1 - S(t)] A_p C_s(t) \frac{\text{moles of fission products}}{\text{day}} \quad (8.48)$$

where A_p is $PC_r(t)/t^2$ in fractions on foliage/ t^2 of net area, and $C_s(t)$ is in t^2 of foliage consumed/day. Equation 8.48 can be written in terms of dLW/sec , as

$$FP_s = [1 - S(t)] A_p C_s(t) a_{fp}(t) \frac{\text{dLW/sec}}{\text{day}} \quad (8.49)$$

where $a_{fp}(t)$ is in dLW/sec per fission at the time, t , after detonation. It may be noted that if $C_s(t)$ is defined in terms of grams of dry foliage per day, w_t , may be eliminated from the definition of $PC_r(t)$ in Eqs. 8.44 and 8.45.

Theoretical estimates of the fractional amount of insoluble activities may be made from the data of Chapter 4 if it is assumed that all the fission-product nuclides on the exterior surface of the particles dissolve in the stomach fluids. The fraction not dissolved is then given by the $r_0(\Lambda)$ values for each of the fission-product nuclides. If these fractionation numbers are redefined as $r_{j\Lambda}$, where j designates the element and Λ the mass number (isotope), then Eqs. 8.48 and 8.49 can be written as

$$FP_s = A_p C_s(t) \sum_{j\Lambda} r_{j\Lambda} N_{j\Lambda}(t) \frac{\text{moles of fission products}}{\text{day}} \quad (8.50)$$

and

$$ED_{\text{I}} = \Delta_F C_0(t) N_{JA}(t) \frac{\text{dis/sec}}{\text{day}} \quad (8.51)$$

where $N_{JA}(t)$ is the number of atoms of element I with the mass number A per fission at the time, t, after fission, and $n_{JA}(t)$ is the netivity in dis/sec per fission of the nuclide (the indices A and J define the nuclide in terms of its mass number and its atomic number, or elemental designation).

8.4.2 Soluble-Nuclide Fractions

The solubility in digestive fluids of each element, radionuclide, carried by the fallout particles deposited on edible foliage must be known before estimates of the amounts of each that concentrate in the tissues of (specific) body organs can be made. If the nuclide solubilities in 0.1 normal HCl solution are the same as in digestive fluids, then measurements of the solubilities in the field can be used in such estimates. If the solubility in the 0.1 normal HCl solution is defined as S_j , for the jth element, the amount and radioactivity of the jth radionuclide (of element I) dissolved is

$$N_{JA}^* = 1.66 \times 10^{-11} \Delta_F C_0(t) S_j N_{JA}(t) \text{ moles/day} \quad (8.52)$$

and

$$r_{JA}^* = \Delta_F C_0(t) S_j n_{JA}(t) \frac{\text{dis/sec}}{\text{day}} \quad (8.53)$$

In which r_{JA}^* is the fraction of element I that is soluble. Theoretical upper-limit values of $N_{JA}^*(t)$ and r_{JA}^* can be estimated by substituting the appropriate values of $r_p^*(A)$, redefined as r_{JA}^* , given by Eq. 8.9 for S_j .

It should be emphasized that, for general applicability, the values of $S(t)$ and S_j must be known as a function of particle diameter. For the smaller particles, the values of $R_b(A)$, or r_{JA} , are independent of particle size, but the values of $r_p^*(A)$, or r_{JA}^* , are not.

8.4.3 Variation of the Foliage-Contamination Factor with Particle Size

The values of a_{f} and $K_a(t)$ depend on particle size. The dependence of the latter on the particle-size designator, α , is represented by Eq. 8.46. The dependence of a_{f} on α was derived from the data of Romijoy and coworkers⁶ presented in Chapter 2.

The values of α_0 that are applicable to the various measured values of a_{15} were calculated from

$$\alpha_0 = 5/h \quad (6.4)$$

where X is the distance from ground zero and h is the mid-height of the cloud. The values of α_0 can be used to estimate the median particle-diameter of the particles deposited at the distance X by the methods described in Chapter 5. When v_f (the fall velocity) can be determined for the median particle diameter, as obtained from particle-size data, then the 15 mph value of α_0 can be determined from

$$\alpha_0 = 22.0/v_f \quad (6.5)$$

for v_f in feet per second. The values of h and other data, for the detonations for which values of a_{15} are available, are given in Table 6.0.

Table 6.0

SUMMARY OF SHOT CONDITIONS FOR ESTIMATING THE MEDIAN PARTICLE-DIAMETER DENOMINATOR

Shot	(Yield (kT))	Height of Burst (feet)	h (feet)	Type of Shot
Tuska	7	800	24,000	Tower
Apple I	14	500	27,000	Tower
Mof	22	400	36,000	Tower
Apple II	20	800	38,500	Tower
Projectile	37	700	34,500	Balloon
Disable	17	800	20,000	Tower
Shasta	17	800	24,000	Tower
Smoky	44	700	32,000	Tower

The values of the median particle size, with respect to the distribution of activity on the particles, for two locations each on Shots Apple II and Smoky, along with the computations of α_0 , are given in Table 6.10. The α_0 values calculated by the two methods are nearly the same.

Table 6.10
CALCULATION OF α_0 FOR SOME FALLOUT LOCATIONS FROM
BUCH APPLET AND HMOKY

Shot	X (miles)	d _m (inches)	v _f (ft/sec)	α_0	X/h	$\alpha_0 \cdot 22.0/v_f$
Apple II	7	-	-	-	0.000	(0.000)
	48	120	0.24	0.08	0.00	0.00
	100	70	1.00	14.0	10.8	10.8
Hmoky	132	50	0.04	21.8	20.4	20.4
	200	47	0.07	34.0	32.8	32.8
	250	-	-	49.8	(41.8)	(41.8)

The values of α_1 given in Table 2.18 (see Chapter 2) are plotted in Figure 6.6 as a function of α_0 values computed by use of Eq. 6.54. This set of data for the retention of fallout by native plants is widely scattered; however, the general trend of the values of α_1 from individual shots is to increase with increasing α_0 . Part of the difference in the observed variation of α_1 with α_0 from one detonation to another is undoubtedly due to the fact that differences in wind speed occurred. Other causes of the differences in the variation with α_0 could be due to differences in humidity conditions and in the predominant types of foliage that were collected for analyses.

The values of α_1 calculated from the data of Table 2.18 (see Chapter 2) for the forage crops (clover, alfalfa, wheat, and mixed grasses) are plotted in Figure 6.6 as a function of the α_0 values that were corrected to an average wind speed of 10 miles per hour (see Table 6.10). Since the absolute accuracy of the source data is probably not better than 50 percent, a single line was drawn through the plotted data, neglecting one point. The suggested representation of α_1 for these four forage crops is therefore given by

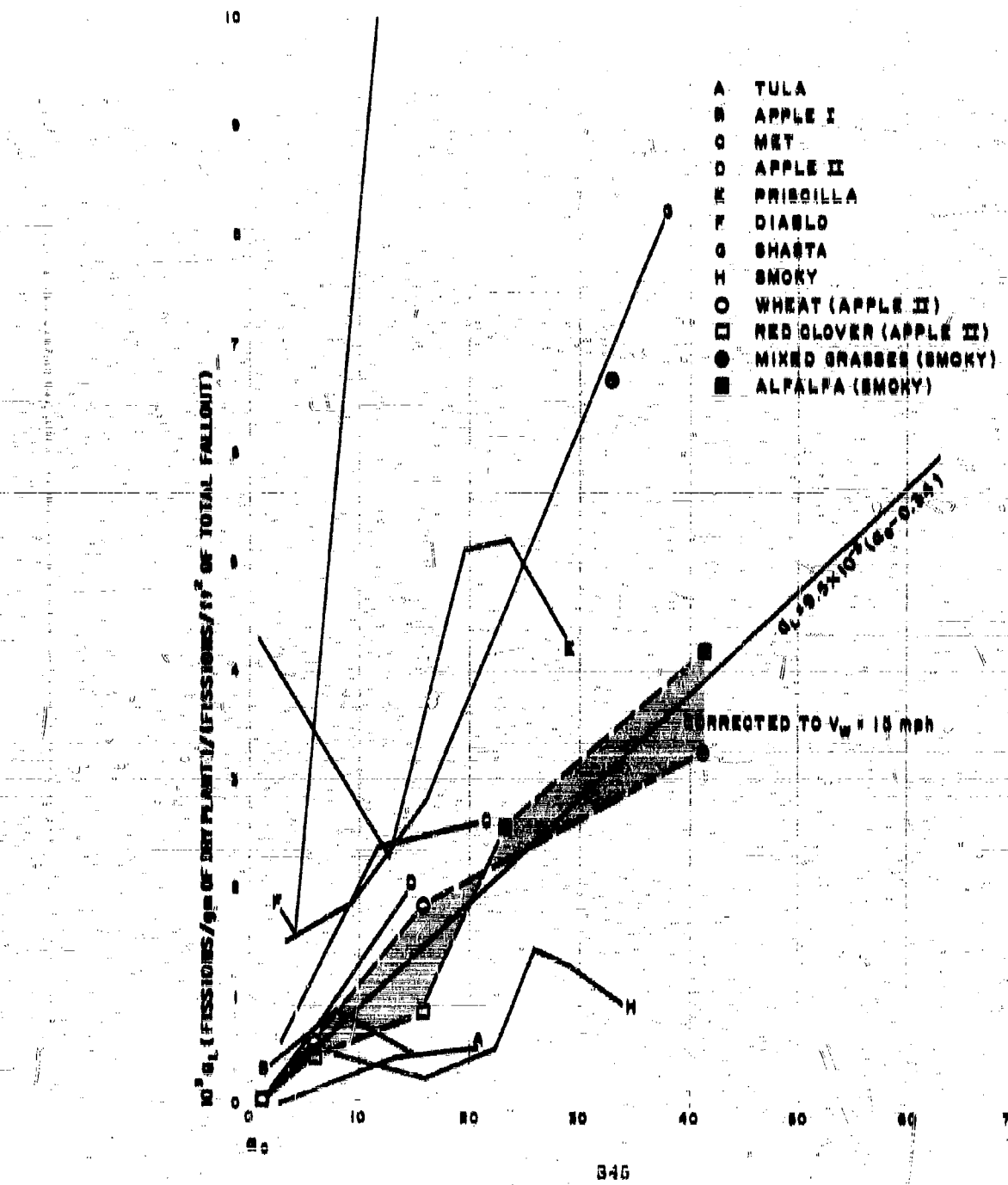
$$\alpha_1 = 9.5 \times 10^{-6} (\alpha_0 - 0.34); \quad \alpha_0 \geq 0.34 \quad (6.56)$$

The complete representation of the foliage contamination factor contour ratio for evaluation at 10.1 hour is then

$$FC_F(1) = \frac{2.44 \times 10^6 w_L (\alpha_0 - 0.34)}{(\alpha_0(1) + 0.019)}; \quad \alpha_0 \geq 0.34 \quad (6.57)$$

The value of $FC_F(1)$ for α_0 values less than 0.34 is taken to be zero.

Figure 6.6
VARIATION OF a_1 WITH CALCULATED VALUES OF χ_0



If it is assumed that the surface densities of the clover and wheat foliage in the flats used on Apple II detonation were higher than the average for such crops, then a range of values of w_L may be suggested. These are:

Red Clover	: $w_L = 5$ to 25 gm. dry plant/ ft^2 of soil surface
Wheat	: $w_L = 10$ to 40 gm. dry plant/ ft^2 of soil surface
Alfalfa	: $w_L = 10$ to 50 gm. dry plant/ ft^2 of soil surface
Mixed Grasses	: $w_L = 5$ to 25 gm. dry plant/ ft^2 of soil surface

Wide variations in w_L from these ranges might occur in various sections of the country.

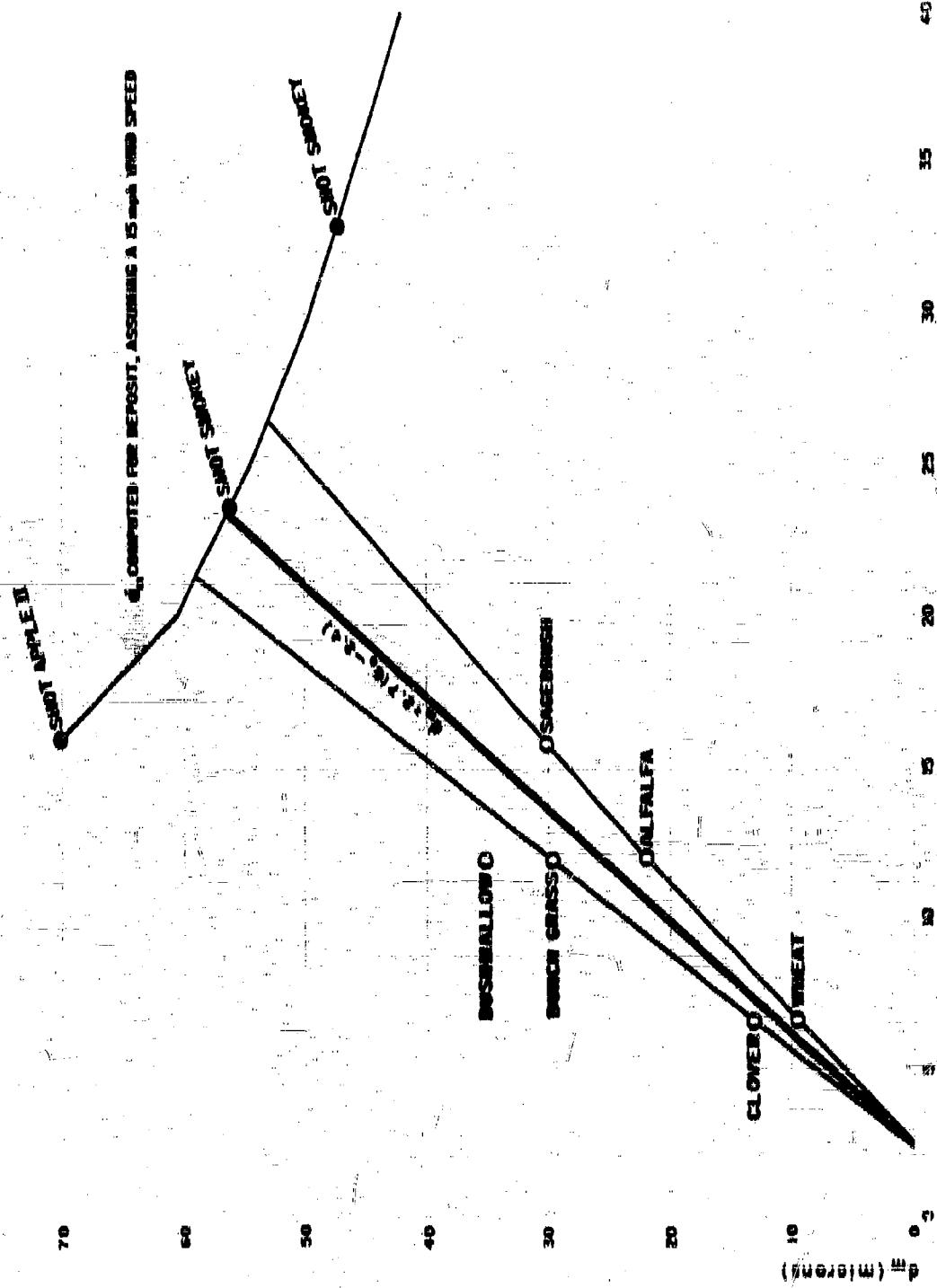
The fraction of the total fallout that is retained on foliage can be estimated from the product $a_L w_L$. Thus, for a w_L value of 20 , the fraction retained is 1.9×10^{-3} ($a_0 = 0.84$). In Table 6.6, the value of a_0 at the 1 r/hr at 1 hr contour farthest downwind from ground zero is 26.1 ; at this location, $a_L w_L$ is then 0.049 , or about 5 percent, and the calculated value of $r_n(1)$ is 0.77 . Hence, from Eq. 6.57, the value of $FC_r(1)$, is 1.6×10^{11} (fissions on foliage/ ft^2 of soil area)/(r/hr at 1 hr).

Estimates of the median size (or size-range) of particles retained on foliage may be made if the variation with a_0 of the median diameter of the particles in the deposited fallout is known. In Figure 6.7 the values of the median diameters of the fallout lodged on foliage, taken from Table 2.15, are plotted as a function of a_0 . For these data, the median diameter of the fallout particles on the foliage increases with a_0 ; thus, the median diameter of the retained fallout increases as the median diameter of the deposited fallout decreases.

Clearly this trend in the median diameter of the retained particles with a_0 could not continue indefinitely since at some point, when the diameters of the deposited fallout particles become very small, all the particles could be retained by the foliage. To illustrate this aspect, calculated values of the median diameter (d_m) for the deposited fallout are also plotted as a function of a_0 in Figure 6.7. Extrapolation the linear representation of the data for d_m of the foliage-retained particles as a function of a_0 to the curve for d_m of the deposited fallout gives a maximum value of about 57 microns.

The various functional representations of the foliage contamination factor contour ratio, as derived from the data of Romney and coworkers⁶, are based on information obtained from nuclear detonations of tower and balloon-mounted devices. However, in the treatment of that data the emphasis was placed on the particular mathematical functions that could be used in making estimates of internal hazard from fallout produced by land-surface detonations.

Figure 6.7
VARIATION OF THE MEDIAN PARTICLE DIAMETER OF FALLOUT ON FOLIAGE
WITH 10^6 OF THE DEPOSITED FALLOUT



This application should be valid for any condition of deposition since the same physical phenomena must be involved in particle retention by foliage irrespective of the source of the depositing particles. When more data become available, the proposed representations of the processes can be altered to be either more specific for different types of foliage or otherwise more complicated depending on the observed variations in the data.

CHAPTER 6 REFERENCES

1. Bolles, R.C., and N.E. Ballou, Calculated Abundances of U-235 Fission Products, USNRDL-456, 1956.
2. Miller, C.F., and P. Loeb, Ionization Rate and Photon Pulse Decay of Fission Products From the Slow Neutron Fission of U-235, USNRDL-TR-247, 1958.
3. Strope, W.E., Evaluation of Countermeasure System Components and Operational Procedures, Operation Plumbbob WT-1464, 1958.
4. Miller, C.F., Analysis of Fallout Data, I. The Jangle "S" and "U" Shot Fallout Patterns, USNRDL-TR-220, Del. 1959.
5. Morgan, K.Z., et al., Report of ICRP Committee II on Permissible Dose For Internal Radiation (1959), Health Physics, Vol. 8 (1960).
6. Romney, E.M., R.C. Lindberg, H.A. Hawthorne, B.G. Bystrom, and K.H. Larson, Health Physics (to be published).

MAJOR SYMBOLS

<u>Symbol</u>	<u>Definition</u>
--A--	
A	Mass number of a nuclide
Δ_0	Effective gross attenuation factor for decontamination equipment operator
Δ_F	Defined by $FC_r(t)I(t)$; in fissions on foliage per sq ft of soil area
Δ_h	Effective attenuation factor for streetsweeper operator from radiation sources in the hopper
Δ_s	Attenuation factor for streetsweeper operator from surrounding radiation sources
Δ_a	Cloud radioactivity concentration in fissions per cubic foot
Δ'_a	Stem radioactivity concentration in fissions per sq ft
a	Nuclear explosion cloud radius at 6 to 8 minutes after detonation
a, a_j , or a_{Fj}	Decontamination equation constant for absorption interaction (seawater and slurry type fallout)
a_L	Foliage contamination factor; fissions per gram of dry foliage divided by fissions per sq ft of soil area
a_x	Radium of stem or fireball at the altitude, x
$a_i(t)$	Radioactivity of the i^{th} nuclide at the time, t, after fission; in dis/sec per fission

Symbol	Definition
R_0	Blow-off cloud radius at time of earliest fallout particle ejection
α	Particle size parameter, defined as v_w/v_t
re_0	Size parameter for particles from cloud center, defined as X/h
B	B
B	(1) Ratio of fission to total yield (2) Freundlich adsorption equation constant for elements in slurry type fallout
b	(1) Nuclear explosion cloud half-thickness at 0 to 8 minutes after detonation (2) Ratio of mass of solids to number of moles of radioactive element
C(A)	C
$C_n(t)$	Ratio of number of neutron captures to number of fissions (to form a nuclide of mass number A)
C_{fp}	Voltage evaporation rate; in sq ft of foliage (dry), consumed per day
C_p	Concentration of fission products in fallout, in moles of fission products per mg of fallout
C_d	Radioelement concentrations in liquid phase of slurry type fallout, in moles per mg of liquid
$(ef)_j$	Radioelement concentrations in seawater fallout drops
R_j	Radiation contribution factor of area j

Symbol	Definition
C_s	Concentration of radionuclides entrained in the manometric solution in manometry-type fallout, or, concentration of radionuclides in the solid (sooty) fallout particles, in moles per mg of sootde
	D
D^T	Planning dose or allowable dose; in roentgens
$D_{or} B_{ok}$	Potential exposure dose; usually defined for a location at 3 foot above an extended plane source of radioactivity
$D_{or} D_x(I)$	Instrument response factor
DRM	Dose-rate, or ionization rate, multiplier; defined as $D/I_x(I)$
d	(1) Particle diameter (2) Density of solids in separator fallout
d_a	Crater depth (soils)
d_a'	Apparent crater depth (water)
d_m	Median diameter of fallout particles
d_w	Water depth (harbor detonation)
d_{bb}	Crater depth in harbor bottom
$d(t, t_1)$	Density-correction factor (to standard time after detonation, $t=1$)
ΔDRM	Δ
ΔE_D	Dissociation energy
ΔE_{sp}	Change in internal energy
ΔF°	Change in standard free energy of chemical reactions

<u>Symbol</u>	<u>Definition</u>
ΔH_v	Heat of vaporization
δ_λ	Ratio of crater depth for surface detonation(s) to crater depth for detonation(s) at other depths or heights of burst
--E--	
E	(1) Energy, of photons, etc. (2) Decontamination method effort, or energy expended; in man- or equipment-hours per unit area
e_n	Efficiency coefficient for (some) decontamination methods; in fraction of fallout mass removed per cycle
--F--	
F, F_j or F_{rj}	Decontamination ratio, or fraction of fallout, or of a radioelement in fallout, remaining after decontamination
$FC_r(t)$	Foliation-contamination factor contour ratio; in fractions on foliation/sq ft of soil area per r/hr at time, t, after detonation
FD	Fraction of device per unit area
$FD_r(t)$	Fraction of device contour ratio; in $(r/\text{hr})^{-1}$
F_m	Fraction of mass of fallout remaining after decontamination
F_r	Fraction of ionization remaining after decontamination
FP_g	Amount of ingested nuclides on particles passing through digestive tract (gut); in moles of fission products per day or dim/sec per day
$FP_r(t)$	Fission product contour ratio; in moles of fission products/sq ft per r/hr at time, t, after detonation

Symbol	Definition
$f_{\text{H}}(\alpha)$	Total mass of solids and liquids per unit of yield for harbor-detonation fallout
$f(\alpha)$	Ideal (or unfractionated) inverse specific activity of land-type fallout; in mg/fission
$f'(\alpha)$	Ideal (or unfractionated) inverse specific activity of seawater fallout; in mg/fission
ϕ or ϕ'	-- ϕ -- Fallout model scaling parameter for computing standard intensities -- ϕ' --
G^*	Constant for referenced free energy change
γ	-- γ -- Surface tension of drop of liquid
h	-- H -- (1) Altitude of center of cloud at 6 to 8 minutes after detonation (2) Depth or height of burst -- l --
$I(1)$	Standard intensity; observed ionization rate decay-corrected to H+1; in r/hr at 1 hr, at 8 feet above an open, uniformly contaminated, field
$I_a(t)$	Air ionization rate; in r/hr at time, t , after detonation
I_l	The initially deposited amount of an element in the liquid phase of slurry fallout; in moles per sq ft
I_m	Initial mass level of fallout deposit; in gm/sq ft
I_s	Source intensity of a contaminated surface

<u>Symbol</u>	<u>Definition</u>
I, I_p , etc.	Ionization rate, radiation intensity, or other representation of the initial fallout deposit level
I	Number of moles of a given element in a drop of seawater fallout
--K--	
K or K_1	Decontamination equation parameter for seawater type fallout; in C-Level units
K_{eq}^I	Decontamination parameter for seawater fallout; in mg/sq ft
K_p	Decontamination parameter for seawater fallout; in r/hr at 1 hr
K_a, K_b, K_s	Thermodynamic equilibria constants and/or solubility products
K_n	Various equation constants; for $n = 1, 2, 3$, etc.
$K(1), K_{\alpha^+}(t)$	Yield distribution contour ratio, same units as $K(1)C(1)$; in r/hr per fission/sq ft or in r/hr per K/sq mi
$K(E)$	Efficiency coefficient, wet decontamination methods
K_{AB}	Equilibrium constant for formation of compound designated AB
K_I	Equilibrium constant for exchange reaction of an element
K_p	Equilibrium, or dissociation, constant in terms of partial pressures
K_λ	Mass-correction factor (surface detonation)
$K_{\lambda H}$	Fallout model scaling system parameter
k_j	Henry's law constant
k_f	Mixing coefficient for the insoluble elements with the soil particles in slurry type fallout

<u>Symbol</u>	<u>Definition</u>
k_1	Cloud or fireball rate-of-rise equation constant
	--L--
\bar{L}_g	Relative partial molar heat content of element in gas phase
\bar{L}_l	Relative partial molar heat content of element in liquid phase
	--λ--
λ_N	Nuclear-scaled depth; defined by $h/W^{1/3}$ where h is in feet and W is in kilotons
	--M--
M	(1) Molecular weight (2) Mass of fallout particles remaining after decontamination; in gm/sq ft
$M_p^\lambda(t)$	Mass contour ratio; in mg/sq ft per r/hr at time, t, after detonation (for the fallout from a detonation at a nuclear scaled depth of λ_N)
M^*	Mass of particles remaining after decontamination after expending an excess of energy (i.e., infinite effort)
	--μ--
μ_A	Klein-Nishina absorption coefficient for air
μ_I	Compton absorption or scattering coefficient
	--N--
N_A^0	"Zero time" number of atoms/sq ft of radionuclide of mass number A
N_j	Mole fraction of element j in liquid phase
N_j^v	Mole fraction of gaseous species of element j in vapor phase

<u>Symbol</u>	<u>Definition</u>
$N_j(A,t)$	Number of atoms of element j of mass chain A per 10^4 fissions
n_{fp}	Number of atoms or moles of fission products per unit area
n_j^g	Number of moles of element j in gas phase
n_j	Number of moles of element j condensed on or into liquid soil particle surfaces
$n(\ell,p)$	Number of moles of melted carrier in surface layer of particle
$n_c(p)$	Total number of moles of carrier in particle
$n(\ell)$	Moles of liquid carrier
n_α	Number of particles having size parameter α per unit volume of cloud
n_T	Total number of moles of gas molecules in fireball
--P--	
P	(1) Total pressure, in atmosphere (2) Kinetic power of a water stream
P_0	Initial pressure, in atmosphere
P_j	Ionization rate weighting factor for radionuclides of element j
PF_j	System protection factor
p	(1) Overpressure, in psi (2) Pressure, over the surface of a drop of liquid

Symbol	Definition
p_j	Partial pressure of element j over liquid phase
p_j^*	Sublimation pressure of element j
p_n	Vapor pressure of carrier material
$\sim Q \sim$	
Q	Water-flow rate through nozzle
Q_1	Energy in blast wave
Q_2	Energy in fireball
q_n	Terrain attenuation factor
$\sim R \sim$	
R	Molar Boltzman, or gas, constant
R_M	Remaining mass of fallout particles after decontamination, for infinite effort and a high initial level fallout deposit; in mg/sq ft
R_m	Remaining mass of fallout particles after decontamination, for infinite effort and a low or intermediate initial level fallout deposit; in mg/sq ft
R_N	Residual number: ratio of exposure dose with a radiological countermeasure to the potential exposure dose (i.e., without a radiological countermeasure)
$R_p(r)$	Ionization rate remaining after decontamination, for a contact time of τ ; in r/hr at 1 hr
$R_p(t)$	Ionization rate at time, t , after detonation (and after decontamination)
r	Fireball radius
$r_{\beta}(1), r_x(1),$ or $r_\alpha(1)$	Gross fission-product ionization-rate fractionation number at H+1
$r_{JA}(\alpha)$	Fraction of a nuclide of element j and mass number A that is condensed on particles, or particle groups, designated by α

<u>Symbol</u>	<u>Definition</u>
r_m	Maximum fireball radius
$r_o(A)$	Fraction of an element of mass chain A condensed into liquid particles at the time that they solidify; a fractionation number
$r'_o(A)$	Fraction of an element of mass chain A condensed on the surface of solid particles; a fractionation number
$r_i(A)$ or $r'_i(A)$	Same as $r_o(A)$ and $r'_o(A)$, respectively, for a radionuclide designated by i
ρ	-- ρ -- (rho) Density of liquid (or solids)
s	-- s -- Solid-to-liquid mass ratio
s_i	Solubility of an element or nuclide in 0.1 normal HCl
s_0	Solid-to-liquid ratio weighting factor
$S(t)$	Fraction of gross amount of radioactivity that is soluble in 0.1 normal HCl at time, t , after detonation -- S --
T	Absolute temperature in degrees Kelvin
t_a	Fallout arrival time; time after detonation
t_c	Fallout cessation time; time after detonation
t_e	Time of entry into a contaminated area; time after detonation
t_{dec}	Decontamination starting time; time after detonation

Symbol	Definition
t_f	Time, in days, of contact of fallout with a surface
V	Fireball (or cloud) gas volume
V_0	(1) Original volume of heated air molecules (in fireball) (2) Initial liquid volume of a drop (seawater fallout)
V_a	Fireball volume at second temperature maximum
V_b	Volume of harbor-bottom crater
v_w	Wind velocity; a vector quantity for a particle group from its point of origin in the cloud to its location on the ground surface
v_t	Terminal fall-velocity vector of a particle or particle group
v_0	Particle fall-rate equation constant
W	Total weapon explosive yield; in kilotons (of TNT)
w_L	Fallout surface density; in grams of dry fallout per sq ft of land area
w_0	Particle fall-rate equation constant

Symbol**Definition****--X--****X** Downwind distance from ground zero**x** A distance or coordinate variable**x_h** Distance between sweeper operator and hopper**--Y--****y_A** Chain fission yield of mass number A;
in atoms or moles per fission**y_s** Half-width of stem fallout pattern to the
1 r/hr at 1 hr contour**y** Mass surface density of fallout particles
(identical with I_m for land-type fallout);
in mg per sq ft**y_j(t)** Number of atoms per fission of element j
(all mass numbers) at time, t, after fission**y_{A'}** Fractional chain yield; in atoms per fission**--Z--****z** Altitude coordinate; apparent altitude of
fallout particle origins**z₀** Parameter defining cloud and particle
rate-of-rise function; upper limit in h-h**z_c** Characteristic altitude at which first
large particles fall away from
rising fireball or cloud

XXX

INDEX

--A--

- Abram, J.O., 28
Absorption, energy, 5, 52, 114
Accumulated dosage, 357, 371, 547-
549
Actions, defense, see Counter-
measures
Active countermeasures, see Methods
Activity, see Radioactivity
thermodynamic, 188, 400-407
Adams, C.E., 28, 31, 38, 41, 151,
488
Adsorption, particle
chemisorption, see Chemical
systems
curves, 306
equation variables, 423
equilibrium, 394, 401
interactions, see Surfaces
isotherm, 394
process, 52, 80, 114, 388; see
also Methods reactions, see
Chemical systems, fallout
AFCIN, 298, 294
Affected area,
perimeter, 354
Agglomeration, see Particles
Agricultural area,
decontamination, 508
Air
burst, 4, 74, 114, 180, 360
circulation, 312
concentration, 322
see Ionization
velocity, 215
ventilation, see Shelters
Air jets,
high pressure, 484
Alfalfa, 87, 349
Allowed dose, see Planning factors
Alamogordo, N.M., 1
Albite, 188
Alcock, C.B., 159, 163
Alexander, L.T., 28
Alpha particles, 72, 84
Altitude, see Cloud
Ambrose clay, 486, 504
Anderson, A.D., 201, 203, 218, 214,
293, 299
Animals, see Human
Anorthoclase, 188
Apple Shot, 78, 84, 91, 340
Applicable countermeasures, see
Planning factors
Applied effort, see Planning factors
Area(s),
affected, 354, 547-549
boundary, 351-354
characteristic, 358
clean, 368
Damaged, 355
decontamination, coverage rate,
358-471, 478, 479
disposal, 475, 504
exposed, 78-74, 327
Free, 352
gross, 355
identification, 354-356
land-, see Surfaces
lawn-, 500
major, 354
paved, 488, 570
perimeter, 351-356
protective, 507

INDEX

Area(s), (Cont.)

Rural, 309
residential, 354-359
roof, 400
rural, 367
source, 355
staging, 369-377
see Surfaces
target, 348
test, *see Field tests*
unaffected, 358
unpaved, 357

Asphalt, *see Surfaces*

Attack, nuclear war, 368-369

Attenuation, exposure *see Shelter, Shielding, Terrain*

--B--

Backyard contributions, *see Radioactivity*

Badger, F.S., 465
Baker Shot, Bikini, 326, 405
Balloon-mounted devices, 72-77, 91,
297, 324-327

Ballou, N.D., 17, 23, 25, 50, 165, 176,
183, 328, 365, 347, 400

Band, Red, 356

Batten, D.R., 203

Batten, E.M., 298

Bellamy, A.W., 72

Belt, Gray, 356

Berkowitz, J., 163

Beta decay, 18, 50, 78, 81

Bigger, (Molurphy and), 465

Bikini Atoll, 46, 326, 405

Biological effects, *see Hazard*

Biological elimination period, 372,
375

Biological systems, *see Hazard*

Biosphere, 354

Birefringence, 71

Blackbody conditions, 125

Black Zone, 358, 362, 368

Blade angle, 508

Blast,

damage, 350

protection, 354

wave, 114, 318, 351, 358

Blume, J.M., 28

Boiling point, 164

Boles, R.C., 17, 28, 50, 165, 176,
183, 223, 309, 347, 400, 405

Bomb

"clean", 27, 101

components, 407

structure, 3, 400

warhead, *see Yield, weapon*

Bone, effects on, 75

Bottom harbor, 324, 325

Bravo, Shot, *see Shot*

Breakaway time, 117, 118, 125

Brewer, L., 159, 168

Broom, rotary, 500

Broomed concrete, 400

Brushing, 322

Bucket scraper, 509

Building,

surface, 486, 498, 499

Buildings,

houses, 490

Buildings,

small, 490

Bulldozer, *see Method(s)*

Bunchgrass, *see Foliage*, 87

Bunney, L.R., 28

Burns, K.P., 159, 168

Burst

air, 4, 76, 329, 360

hypothetical, 290

land-surface, 328

multiple, 395

near-surface, 328

single, 395

yield, 362

INDEX

Bushmallow, 87
Buster, Operation, 1
Bystrom, B.G., 78, 79, 81

--C--

Callahan, E.D., 208
Camp Parks, 80, 561, 573, 595, 597
Camp Stoneman, 470, 485, 486
Capabilities of Atomic Weapons, 202
Carr, W.J., 465
Carrier, fallout
 materials, 8, 15, 62, 68, 106-110
 matrix, 393
 properties, 380
 sea water, 405
 surface tension, 112
 total, 402-407
Castle, Operation, 1, 78
Chains, mass, 8-17, 68, 106-109, 146
 165, 214, 305, 387, 386, 414-418,
 490
Chandrasekhariah, M.S., 159, 168
Charge-distribution curves, 28
Chemical systems, fallout
 additives, 388, 407
 see Adsorption
 assay, radiochemical, 17, 50
 chemisorption, 388, 401
 contact time, 407
 contamination process, 52, 72, 80,
 417
 interactions, 10, 48, 52, 72, 80-85,
 97-108, 159, 205, 349-351,
 379-388, 398, 402, 417, 425,
 429, 445, 460, 465; see also
 Methods, Surfaces
 oxide matrix, 393
 parameters, 388
 polymerization, 159
 radiochemical standards, 16
 reactions, 378-390, 392, 422-424

Chemical systems, fallout (Cont.)
 reference nuclide, 68
 slurry, 417-420
 solubility interactions, 78-89,
 113, 340, 401-403
Chilton, A.B., 551, 599
Chupka, W.A., 159, 168
Civil defense,
 information, 378
 operations, 358, 368
 options, 356
 organization, 353, 362
 planning, see Planning
Clark, D.C., 511
Clark, D.E., 299
Clay soil, 496, 504
Clean area, 500, 507
Clean-up operations, 307
"Clean" weapon, 27, 101
Cleaning agent, Orvus, 426
C-Level unit, 400
Clothing, crew, 80, 866, 456
Cloud, fireball
 altitude, 154, 205, 215-218, 208-
 244, 294
 atmosphere effects, 117-121,
 379-382
 chemistry, 10, 99, 308, 429, 464
 expansion, energy, 218
 formation, 10, 201-221, 304
 internal pressure, 155
 model parameters, 115, 180-182,
 146-148, 207
 radium, 205, 230, 304
 rise rate, 218, 312
 size, 15, 205, 237, 301
 stem altitudes, 293, 295
 stem configuration, 206
 stem geometry, 218, 232, 237
 sublimation pressure, 98, 109, 305
 surface, 142, 152

INDEX

- Cloud, fireball (Cont.)
 temperature(s), see model
 parameters
 volume, 15, 95, 109, 184, 141,
 208, 304
- Clover, see Foliage
- Coagulation process, 45
- Cole, R., 382, 388, 391, 400, 408,
 409, 411, 414, 420, 424, 428, 433
- Collection, see Fallout
- Colloidal particles, see Chemical
 system interactions
- Complexing agent, EDTA, 407, 426
- Compounds
 chemical, 10, 99, 305
 final, 429
- Computations
 computer, 202, 211
 illustrative, 358, 363, 514
 manual, 204, 210, 211, 218
 see Planning factors
- Concrete surfaces, 414, 436
- Condensation equilibrium, 99, 102
- Condensation process, see Particles
- Contact time, 407
- Contamination process, see Chemical
 systems, fallout
- Contamination reduction, see
 Planning factors
- Contour,
 see Fallout
 ground zero, 387
 idealized, 253
 isointensity, 9, 227, 241, 256,
 297, 327, 349
 mass, see Fallout
 ratio, 10, 85, 109, 164, 207, 228,
 241, 301, 315, 324, 382, 388,
 349
 ridge, 230, 243
 standard, 235
- Conventional flusher, 494, 498, 499
- Coral, 31-38, 150, 284
- Corrosion, 382
- Coryell, C.D., 17
- Cost-effectiveness, 470
- Coughlin, J.P., 150, 169
- Countermeasures
 action options, 363, 550
 actions, 365, 372, 520
 active, 350, 364
 applicable, 351
 basic concepts, 513
 communication, 365
 composition, 351
 cost-effectiveness, 470
 crews, 364, 478, 486-490, 501-509
 see Decontamination
 defense actions, see Planning
 factors
 design, 362
 dispersal, 351, 362-368
 distance effects, see Wind
 distribution, 366
 see Effectiveness
 equipment, see Methods
 evacuation, 351, 362, 368
 see Fallout
 feasibility, 204, 596
 see Hazard
 major, 353-360
 objectives, 351, 371
 operational use, 352
 organization, 363
 passive, see Shelters
 see Planning factors
 population distribution, 368
 preventive, 300, 362, 548
 priority, 366, 367-369
 problems, 366
 protective, 547-549
 receptive, 351
 recovery, 355-375, 529, 547-549
 repair, 360

INDEX

Countermeasures (Cont.)

remove, 369
see Shelters
see Shielding
specification, 349-370
supplies, 361, 362, 365, 596
system analysis, 580
system development, 580
teams, 368
work times, see Time

Crater(s)

depth
materials, 14, 81, 114, 152, 303, 328
radius, 158
soil, 417

Crew, see Decontamination, see Methods

Criteria, planning done, 470

Crooks, R.N., 195

Crossroads, Operation, 1

Crosswind

direction, 358
distance, 360
shear, see Wind shear

Crystals

hydrated, 391
salt, 394, 396

Curie units, 81

Curtis, H.B., 470, 485, 511

Curve(s)

adsorption, 396
assumed decay, 9, 50, 80, 229, 318, 380, 386, 518
average decay, 514
calibration, 72, 486
charge distribution, 25
correction, 108-110, 107, 221, 324, 352
decay rate, 58, 229, 386, 416, 518, 524
delivery, 259, 355-366, 472, 547

Curve(s) (Cont.)

distribution, 324
DRM, 514
efficiency, 541
intensity, 877; see Radioactivity
ionization, see
rate-time, 513
reference, 183
temperature, 117, 121, 129, 148
yield, 16, 68, 142

Cycle, equipment,

area coverage, 508
crew exposure, 579
overlap, 475
pass-width, 478, 504
ratio, decontamination, 474
speed, 478, 496, 500

--D--

Damage,

biological, 356
physical, 354, 358
property, 353, 365

Damaged area, 353, 356, 363, 370

Decay

correction, 108, 110, 157, 221, 329
curve, see Curves
see Ionization
radioactivity, see Radioactivity
rate, see Curves

Debris, non-fallout, 69, 369

Decay, "normal", see Curves

Decontaminated area

as protection, 507
entry time, minimum, 537

Decontamination

active, 370
agents, 407-412
agricultural, 508
analysis, 500
area, 471-480, 498-504

INDEX

- Decontamination (Cont.)
building grounds, 509
building surfaces, 486
constants, 410
contm., 470
see Countermeasures
crew, 304, 473, 480, 532, 535,
539, 551-559
critical parameters, 451-476
effectiveness, 382, 393, 410, 451,
471, 489, 508, 550, 572-599
efficiency, see Method
equation constants, 384, 405, 484,
494, 498, 538
see Equipment
equipment cycles, 472, 485, 500,
see Pass
experiments, 481, 485, 486, 490,
577
feasibility, 204, 598
see Field tests
see Harbor
Hazard, see Dose, exposure
ion changes in, 386
land area, see Soil
manual, 494
mass fractions remaining, 480
see Methods
objectives, 10, 84, 871
paved area, see Surfaces
planning, see Planning factors
procedures, 382, 472, 489, 496
rates, see Method, Efficiency
removal, see Fallout
residential area, 554-590
see Residual number
scheduling, 488
see Seawater fallout
serial methods, use, 508
soil, coral, see Fallout
solubility, 401
start time, 535, 558
- see Surfaces
times, see Method, Efficiency
vertical surfaces, 486
waste disposal, 376, 504, 508
water washing, see Method
wet method, 382, 472, 486
work times, 535, 553, 552
Decontamination solution, 401
Defense actions, see Countermeasures
Defense Planning, see Planning
Dehydration, 382
DeMaria, G., 159, 168
Density, see Particle
Density, liquid, 112, 308
Deposit level, see Fallout
Deposition, see Fallout
Desert surface, 488
Design, countermeasure system, 388
Designator, particle,
median diameter, 341
Desired dose, see Planning dose
Desorption rate, 391, 396
Detector, see Instruments
Detergents, 388
Detonation effects,
blast, 10, 114, 118, 316, 351-350,
360-366
cumulative, 354
see Crater
see Harbor
land-surface, see Soil
magnitude, 10, 56-72, 114, 227,
304-324, 337
materials, see Yield, weapon
multiple, 358, 360-380
overpressure, 118, 360, 368
point, 361, 417
sea water surface, 48, 60-71,
320-330, 405
thermal, 366
underground, 486
see Yield

INDEX

- Dhain, R., 466
Diablo, Shot, *see* Shot, 80, 81
Diamotor,
 see Cloud,
 Particle
Diesel equipment, 508
Differential coefficient, 473, 484
Differentiation of fallout 3
Diffraction, 31, 48, 71
Diffusion, 38, 118, 395
Diffusion process, 118
Digestive tract, 887
Dilution, 48, 99
Direct Intake, *see* Fallout
Dimes, *see* Particles
Discing, *see* Soil
Disintegration multipliers, *see*
 Radioactivity
Dispersal, 861, 862, 868
Disposal area, 875, 894
Dissociation, 118, 119, 120, 126, 136,
 137, 159
Distance, effect on location,
 see Wind, Countermeasure
Distribution,
 energy, 801, 880, 402
 equilibrium, 120, 400
 fractional mass, 203-205
 NRDL, 887
 population, 869
 RAND, 887
 relative, mud-*sea* water, 427
 particle size, 884
 smearing of, 885
Dolan, P.T., 170
Donovan, L.K., 881, 880
Dose, exposure
 accumulated, 887, 872, 847-848,
 878
 allotted, "allowed", 886, 470, 489,
 821, 828
Dose, exposure (Cont.)
 biological, *see* Hazard, 16, 46,
 79, 80-114, 104, 202, 837-854,
 864-876, 489, 503, 832-834, 855,
 871, 881
 crew, 881, 879-899
 critique, 886
 critical, 808, 400, 813-815
 decontamination crew, 864, 470,
 480, 881-890
 "desired", 886, 470, 489, 814, 822,
 828, 832, 844
 early, 886, 848
 incremental, 887, 872, 848, 878
 infinity, 886, 808, 820
 lethal, 868, 409
 levels, 886, 848
 limit, 470
 maximum, 884, 828
 motor equipment operator, 880
 observed, 887
 planning, *see* Planning factors
 potential, 6, 884, 860, 821, 828
 property, 884
 rate, *see* Curve, decay
 ratio, RN, 814-844
 reduction, 881
 received, 89, 818, 891
Dose Rate Multiplier (DRM), 813-844
Downwind location, *see* Wind
Drainage systems, 870-883, 489
 available, 880
 pit, 480
 storm, 880
 surface, 475, 489
DRM, dose rate multiplier, 813-844
Drowart, J., 169, 163
Drop (droplet)
 fireball, 14, 72, 112
 interactions in, 394
 see Radioactivity
 see Seawater
 volume, 895

INDEX

- Dry conditions
desert, 80, 330, 382
see Methods
see Soil
- Drying period, *see* Particles
- Dump truck, 508
- Dumping area, 504, 508, 530
- Dunning, G.M., 78
- Dynamics, deposition, 218, 301
- Dust, 818
- E--
- Earth-cover, *see* Fallout
- Earth-hauling, *see* Method
- Ecological consequences,
nuclear war, 300
- EDTA, complexing agent, 426
- Edwards, R.R., 17
- Effectiveness
volv., 470
see Countermeasure
decontamination, 382, 398, 416,
481, 471-473, 489, 508, 550,
572-599
desired, 486
measure, 471, 476, 489, 508, 514
method, 480, 508, 520, 547
operational, 471, 508
over-all, 480, 507
parameters, 451-470
see Planning factors
recovery, 507
relative, 370, 407
removal, 10, 375, 380-386, 427,
507, 509
requirements, 470, 500
see Residual number
- Shelter, D, 81, 382, 386-388, 538
shielding, 520
variables, 451
variation, 451, 483
- Efficiency
coefficient, 472, 477
concept, 409
curves, 541
decontamination, 480, 507-508, 544
differential coefficient, 473, 484
effectiveness, method, 382-398,
410, 461-471, 489, 508, 550,
572-599
man-hours per unit area, 473
parameters, 451-470
work-time, 470, 502
- Effects of Nuclear Weapons (ENW),
18, 115, 125, 153, 186, 202, 210,
203, 323, 328, 330, 350
- Effort, work
applied, 470, 508
expenditure, 486, 507
infinite-, 471
least, 503-508
rate, 471, 508, 533, 558
time parameter, 471, 508, 501-502
- Electronic computers, 202-211
- Elements,
see Ionization, Particles,
Radioactivity
nonradioactive, 426
refractory, 8-14, 48-74, 111-119,
184
separating, 258
trapped, 401
- Elimination period, biological, 353
- Emergency period,
centers, 380-382
hospitals, 371-373, 540
see Shelters
- Empirical data relationships, 204, 228
- Emulsifier, 407
- Energy, *see* Radioactivity
absorbed, 5
balance, 74, 117, 144-148, 152
lost, 110
released, 13, 115-141

INDEX

- Kwajalein Proving Grounds, 50, 60, 78
Entry time, 502, 507, 508, 509
Environment effects, 30, 62, 340,
 370, 481
ENW, *see* Effects of Nuclear Weapons
Equipment; countermeasure
 availability, 500
 capability, 301, 474, 480, 508
 communication, 360
 crew, 304, 473, 501-500
 design, 476
 diesel, 508
 firehosing, 480, 575
 fuel requirements, 508
 motorized, 360, 508, 570
 requirements, 500
 shovels, 480-491, 500
 speed, 400
 set-up, 508, 578, 582
 work-time, 502
Estimates, *see* Planning factors
Evaluation, 301, 302, 308
Experimental decontamination, *see*
 Field Tests
Exposure, *see* Dose; Hazard
External
 radiation hazard, 301, 304
- F--
- Facilities,
 protective, 840
 recoverable, 350-360
Fallout,
 aging, decay, *see* Curves, decay
 areas, 207-204, 355-358, 301-370,
 347
 arrival rate, 250, 305-304, 308-
 306, 472
 arrival time, 300, 304, 513
 burying, 375, 504
 cessation time, 513
 chemistry, *see* Chemical system
 collection, 71, 81-84, 113, 318, *see*
 Field tests
 colloidal, 308
 composition, 71-97, 301-324, 392-
 393, 425-429, 514, 583, *see*
 Chemical systems
 contributions, contamination, *see*
 Radioactivity
 coral, 31-42, 63-63, 67-78, 98,
 156, 284
 coverage, area, 471
 density, 38, 61, 113, 370, 380, 384,
 386, 391, 406, 517
 deposition rates, 80, 118, 156, 218,
 235, 284, 324-340, 384
 desert, 480
 disposal, 375, 504
 distribution, 7, 32, 73, 78, 104, 106
 201, 204-272, 310, 324-341,
 360, 427, 471, 480-480
 earth-fill, cover, 500
 formation, 111-114
 fraction removed, *see* Decontam-
 ination
 in body organs, *see* Hazard
 initial mass, 300, 400
 intake, direct, 78, 85, 420
 pattern, 202-217, 227-241, 252-260,
 300-321, 330, 484
 precipitate, 401
 properties, 370-380
 removal, 270-280, 470-480, 504-
 508, 570-583, 602-600
 removal effectiveness, 380, 507
 residual mass, 471-490
 retention, 340
 sealing system, 125-130, 202-227,
 205-201, 315-320, 513
 solids, *see* Particles
 See Surfaces
 synthetic, 400, 471-486, 507

INDEX

- Fallout (Cont.)
 types, see Harbor detonation,
 Land surface detonation, Sea
 water surfac, detonation
 vaporization effects, 6-42, 76-98,
 114-133, 169, 251, 306, 393
- Fallout levels, see Particles, density
- Farlow, N.H., 32, 45, 71, 151, 388
- Farmers, 387
- Fatalities, see Hazard, Planning
 factors, Dose, lethal
- Feasibility, countermeasure, 204, 599,
- Ferguson, G.J., 293, 299
- Field tests,
 fallout collection, 71, 81-84, 118,
 318-324
 decontamination, 560, 469, 485-
 486, 489, 496, 504
- Film, x-agent, 45, 71
- Filtration, 78
- Fire(s)
 control, 369
 duration, 369
 ignition, 352
 large-hole, 356-360, 548
 secondary, 351, 548
 thermal, 547-549
- Fireball, see Cloud
- Fireball, formation process, 16, 80,
 42
- Firehose,
 crew, 488
 standard, 481, 488
- Firehosing
 automatic washdown, 491
 concrete surfaces, 488, 489
 crew arrangement, 488, 490
 crew RN, 480, 575
 distance, effect, 489
 land surfaces, 482, 485, 498, 499
 leaking procedure, 490
 nozzle team, 489
- Firehosing (Cont.)
 roof surfaces, 480, 587
 runoff, 489
- First aid, 362, 369
- Fischer, E.M.R., 195
- Fission materials, see Materials
- Fission(s)
 chains, see Mass chains
 concentration in seawater, 401
 number of, 217, 248
 tracer, 56, 414
- Fission products, 8-31, 50-77,
 97-102, 151-164, 186, 217, 245
 251, 301-319, 379, 391-394, 414,
 514
- Flash,
 thermal, 389
- Flame, thermal, 389
- Fluid stream energy, 456
- Flushing method, 494-500
- Foliage contamination
 alfalfa, 87, 348
 bushmallow, 87
 clover, 79-84, 87, 348
 rabbit brush, 89
 sagebrush, 83, 87
 wheat, 79, 84, 348
- Food chain, see Hazard
- Ford, M.R., 7
- Fraction condensed, 164, 315
- Fraction remaining, see Fallout,
 Particles, Radioactivity
- Fractional yields, see Yields
- Fractionated mixture, 168, 195, 221
 305, 317, 328, 392, 514
- Fractionation, 8, 16, 50, 80, 89, 78,
 81, 112, 120, 134, 169, 221, 251,
 514
- Fractionation number, 54, 60, 76, 108,
 110, 221, 318, 341

INDEX

- "Free" area, 355, 363
Free energy
 equation, 402
 relationship, 399
Freiling, E.C., 62, 63, 195
Fukuryu Maru, 50
Fuller, R.K., 78, 408, 409, 414
Fuel consumption, 508
Fuel requirements,
 equipment, 508
 operation total, 508
Function, temperature-time, 189
 countermeasure, 352
 ENW scaling, 180, 328
 scaling, 134, 189, 141, 216, 309,
 step, 208
Fused particles, see Particles
Fusion,
 process, 13, 108
 see Thermonuclear reactions

--G--
Galiano, R.J., 205, 207, 284, 292
Gamma rays, see Hazard
Gas
 cooling, 146, 149, 319
 phase, 49, 97, 106, 111, 120, 304,
 311
Gaseous species, 392
Gasoline engines,
 fuel requirements, 508
Geometry, sources, see Radioactivity
Gilfillan, E.S., 28
Glassy particles, see Particles,
 fused
Glendenin, L.E., 17, 25, 67, 165, 176,
 188, 308
Gloves,
 firehosing, 486
Gradient, 305
Graham, L.J., 408, 409, 414
Grass-cover soil, 504
Gravel, roof,
 removal, 490
Gravity, 201, 210, 383
 effect on fallout, 475
Greenfield, S.M., 201
Greenhouse, Operation, 1
Gray Belt, 358
 survivors, 362
 width, 362
Grimley, R.T., 159, 168
Ground, distribution on, 78
Grounds,
 near buildings, 809
Ground zero, see Wind direction

--H--
Habitability, shelter, 378
Harbor detonation, 327, 417
Haul distance, 509
Hawkins, M.B., 465
Hawthorne, H.A., 78, 79, 81
Hazard,
 beta, 5
 biological, 15, 45, 72-85, 114-164,
 308, 328, 337-334, 364, 425,
 469, 508, 532-534, 535, 571, 581
 contact, 3
 countermeasure, 471-489, 513-544,
 547-549
 critical dose, 365, 469, 513-516
 decontamination crew, 364, 478,
 480, 551-559
 degree, 78, 372, 470, 552
 external, 349-351, 364, 366
 fallout, see Radioactivity, Dose
 gamma, 5, 6-13, 56-70, 78, 189,
 306, 373, 389, 469, 547-549
Ingestion, 72-78, 85, 301, 328,
 345, 373, 549
Intensity, 10, 35, 109-115, 164-207,
 228-241, 304, 337, 341-349, 354,
 420, 485, 494, 534-544, 551-559

INDEX

- Hazard (Cont.)
 internal, 85, 363-368, 375, 549
 lethal, 368, 469, 549
 potential, 5
 protection, see Countermeasures,
 Planning factors
 radiation sickness, 384, 469
 residual radiation, 349, 381, 469
 rural area, 368
 thermal radiation, 351-360
 X-ray, 4, 5, 8, 204
Health service centers, 381
Heffter, J.L., 298, 299
Height,
 burst, 4, 76, 328
 cloud, 311
 optimum, 351
Helman, W.T., 78, 380, 382, 389,
 391, 400, 411, 420, 424, 428, 438
Heimkell, R., 311
Henry's law, 98, 187, 189
Herrington, A.C., 25
Hiroshima, 361
Highway,
 surface, 469
Holden, F.R., 311
Hooper, G.W., 159, 168
Hepper, fallout collecting, 500, 804
Horizontal surface, 494
Hose,
 hook-up, 490
 size, 490
Hoisting,
 see Firehosing
 high-pressure, 484
House,
 roofs of, 490, 555
Howell, J., 481, 511
Human, see People
Humidity, 88, 89, 382, 387, 389
Humidity chamber, 387

Hydrants, availability, 539
Hydrous
 oxides, 418
 solids, 401, 428
Hygroscopic, see Particles
Hypothetical attack, 360

--J--
Ideal soil, see Soil
Identification methods, see Particles
Illustrative
 analysis, 554-560
 computations, 268, 305, 514-544
Impaction, see Particles
Impaction process, 48, 100
Impurity, see Particles
Improvised motor flusher, 494, 498,
 499
Incandescence, 115, 117, 128
Incident neutrons, 16, 108
Independent yields, 17, 67, 107
Induced activity, see Radioactivity
Industry, national, 381
Inert materials, 15
Infinite effort, 471
Infinity dose,
 criterion, 358
Initial
 fallout level, 386, 414, 472, 480,
 486
 mass, 386, 414, 496
 radiation, 381, 380, 382, 386, 414,
 472, 488, 496
 survival, 386, 371, see Planning
 factors
Ingestion hazard, 378
Ingram, M.G., 159, 168
Inglehart, D.L., 298, 299
Inhabited area, 480
Instrument(s)
 NaI(Tl), 58, 70

INDEX

- Instruments(s) (Cont.)
portable, 9, 70, 180, 195, 196, 220,
 DBB, 850
radio AN/PDR/-39(TIB), 189,
 195, 220
radiation detector, 366
response factor, 156, 171, 195, 220
scintillation counter, 86
- Intensity
 see Contour
contributions, see Radioactivity
gradient, 229, 339, 361-367
 see Hazard
levels, 230-240
magnitude, 349-351
observed, 208, 357
pattern, 227, 241, 252, 259, 290-
 300, 321-336
radiation, 368
ridge, 230, 240
standard, 9, 227, 235, 247, 304
- Intensity profile,
 downwind, 241
 standard, 247
 upwind, 235
- Interactions, see Chemical systems
- Interface,
 surface-liquid, 895
 vapor-liquid, 895
- Interference color, 71
- Internal energy change, 117
- Internal emitters, 370
- Internal pressure, see Cloud
- Ion chamber, 189, 418
- Ion concentration, see Radioactivity
- Ion current, 50-50
- Ionization
 air, 397, 400, 471
 contribution, 494, 551-552
 fraction remaining, see Particles,
 Radioactivity
 gross fractionation, 464, 494
- Ionization (Cont.)
maximum reduction, 391
rate, 5-14, 50-51, 116-196, 291-
 297, 304-314, 372, 391, 411,
 464, 471, 485, 515-524, 552
ratio 493, 301-305, 471, 518
reduction, 471
weighting factor, 464
- Irregular particles, see Particles
- Inointensity
 contour, 9
 patterns, 349
- Isotopes, 24, see Radioactivity
- Ivy, Operation, 31
- J--
- James, P.R., 508, 511
- Jangle, Operation, 1, 28, 70, 156,
 "5" Shot, 156, 288, 310
 "U" Shot, 156, 324
- Jeep, 508
- Jefferson, M.E., 28
- Jet, water, 114, 476
- Jones, J.W., 56
- K--
- Kaplan, J.D., 208
- Katcoff, S., 17, 176
- Kehrer, W.S., 511
- Kelley, K.K., 120, 186, 189, 168
- Kellogg, W.W., 201
- Kimura, K., 50, 51, 70, 195
- Kinetic energy, 118
- Kinetic power,
 water stream, 476
- King, R.W., 51
- Knapp, H.A., 80
- Knothole, Operation, 38
- Kaanda, C.F., 202

INDEX

--L--

Land area, see Surface
Land area methods, see Decontamination, Soil
Land surface detonation, see Soil, Methods, Planning factors
Lane, W.B., 582, 408, 414, 418, 419,
 425, 426
Lapp, R.E., 78
Lapple, C.E., 198
LaRiviere, P.D., 174, 228, 270, 511
Larson, K.H., 72, 78, 74, 78
Lateral distance, see Distance, Wind
Laughlin, R.A., 481, 511
Laumetz, N., 222
Laurino, R., 202, 470, 549
Lawn areas,
 soil cutting, 509
Layer, soil, 504
Ledges, fallout on, 494
Lee, H., 470, 473, 475, 485, 500,
 511, 532, 549
Lethality, see Hazard
Level, attack, 566
Level, ionization, see Radioactivity
Levels, fallout, see Particles, density
Lindberg, R.G., 72, 78, 74, 81
Liquid
 condensation, 417
 -phase, 14, 46, 57, 106, 508, 582
 -surface interface, 595
 -vapor interface, 595
Loading, mass, see Fallout
Loam soil, 498, 504
Lobbing method, 485-491
Location, 84, 378, 514
Loeb, P., 6, 81, 167, 174, 189, 306,
 347, 377, 437, 555
Love, D., 56, 198

--M--

McDonald, D., 56, 198

--M--
Machta, L., 288, 299
Mackin, J., 56, 60, 62, 189, 198, 382
Magnetic particles, 481
Maloney, J.C., 485
Manpower, trained, 365
Manual decontamination methods, 494
Margrave, J.L., 159, 165
Marshall Islanders, 2
Mass, see Fallout, Particles
Mass fraction remaining, 566
 Particles
Materials, fallout
 balance of, 106, 164
 see Carrier
colloidal, 395
dense, 378, 552
environmental, see Soil(s), Water
handling of, 469
inert, 15, 379-381
released, 469
structural, 381, 486
 -surface, 470
Mather, J.R., 50
Matrix, carrier, 398
Maxwell, R.D., 28
Medical service centers, 368
Menzel, R.G., 408, 511
Met Whot, 78, 85, 91
Meter response, see Instruments
Method(s), countermeasure
 analytical, 549
 application procedure, 476, 489,
 588
approximations, 208, 216, 547
bulldozer, 485, 489, 506, 508, 588
combination of, 506, 538, 547
crew, 384, 478, 486, 581-599

INDEX

Method(s) (Cont.)

decontamination, *see* Decontamination, Planning factors
distance effects, 489
dry, 382, 472, 484
earth-hauling, 504
effectiveness, 382, 388, 416, 451,
471, 489, 505, 520, 547
efficiency, 489, 507, 508, 544
efficiency coefficient, 472
efficiency differential coefficient,
473, 484
firehosing, 388, 458, 578
fuel requirements, 508
see Hazard
immersion stirrer, 387
land areas, 504
lobbing, 488, 491
manual, 489, 494
motor grader, 485
motorized sweeper, 485, 588, 574
operational effectiveness, 471,
588, 592
pick-up, 472
pile-up, 472, 475, 508
plowing, 500
procedural aspects, 486
recovery, 387
residual levels, 471, 489
residual number, 520
roof-washdown, 490
scraper, tractor, 480
scrubbing, 382
serial use of, 508
set-up time, 508, 578, 582
simple washing, 482, 496
soil removing, 480, 507
spillage effects, 474
stirrer, 412
streets, 489
sweeping, 472, 538
water flushing, 472, 494

Method(s) (Cont.)

water spray, 387
water washing, 451, 491
wet, 382, 474, 485
work times, 592
Mike Shot, 31
Miller, C.F., 6, 78, 80, 81, 167, 174,
189, 308, 324, 348, 377, 382, 388,
391, 400, 405, 408, 413, 414, 417,
418, 420, 424, 428, 433, 437, 484,
485, 511, 514, 558
Miller, J.R., 80
Minvielle, L., 202
Missile, *see* Yield, weapon
Mixing coefficient, slurry, 447
Mixture, particle
fractionated, 8, 112, 186, 198, 221,
505, 517, 528, 592, 514
slurry, 425, 429
soil, 588
Model
air burst, 181, 189
condensation process, 187
mathematical, 202-210
scaling, *see* Scaling system
surface burst, 181-189, 147-149,
153-175, 167, 227
Moist soil, grass cover, 504
Molumphy and Bigger, 488
Morgan, K.Z., 7, 387
Moskin, A., 202
Motorgrader, 485, 508
Motorized methods, 481-510
Multiple detonations, 358, 360-368

INDEX

--N--

- Nagasaki, 301
Nagler, K. M., 203, 200
Nakamura, J. K., 80
NAVDOCKS, 411, 416, 470, 514
Neel, J. W., 72, 74, 76, 78, 80
Neutron(s)
activation, see Radioactivity
capture, 3, 8, 15, 56
emission, 6, 59, 114, 189
excess, 26
fission product, 3, 8, 15, 27, 56,
73, 97, 150, 164, 186, 261, 301,
310, 379-391, 514
incident, 16, 26, 108
Nevada Test Site, 69, 73, 74, 77, 78,
80, 91, 213, 386, 486
New Mexico, 78
Nishita, H., 72, 73
Nozzle, firehosing
bar, 491
calibration data, 486, 500
pressure, 476, 486, 489
size, 476, 486
time, 486, 490, 577
tip, area of, 476, 486
NRDL, 28, 30, 41, 56, 284, 298
Nuckolls, M., 408, 412, 414, 417
Nuclear devices, see Yield, weapon
Nuclides, see Radioactivity

--O--

- OCDM, National Plan Appendix Series,
581
O'Connor, J. D., 41
Open area entry time, 504
Open field rate, see Ionization
Operation(s), test
Buster-Jangle, 1
Cratlo, 1, 78
Crossroads, 1

- Operation(s) (Cont.)
Greenhouse, 1
Ivy, 31
Jangle, 48, 484
Knothole, 38
Plumbbob, 75, 486, 507, 551
Redwing, 41
Streetweep, 481
Teapot, 72, 73, 74, 78
Upshot, 1, 28, 31, 38, 41, 101, 486
Organization, civil defense
command and control structure,
384, 566
countermeasure options, 800
Planning factors
plans, 361, 366, 362, 550
program, 553-566
Orvus, cleaning agent, 426
Outdoor surfaces, 491
Overman, R. T., 58
Overpressure, blast, 16, 118, 360, 368
Owen, W. L., 40, 440, 470, 475, 486,
488, 494, 500, 511, 561, 573, 586,
587

--P--

- Pacific Proving Grounds, 440
Packing-fraction curves, 28
Painted surfaces, 491
Pappas, A. C., 25
Parameters, effectiveness, 481-470
Parks, Camp, 30, 501, 573, 595, 597
Particle(s), fallout
adsorption, see Chemical systems
agglomeration, 38, 380, 392
albite, 135
altitudes, source, see Cloud
anorthoclase, 135
collection, see Fallout, Field tests
collisions, 30-49, 113

INDEX

- Particle(s), fallout (Cont.)
 colloidal, 302, 407
 condensation, 90-102, 310, 302,
 417, 514
 coral, 31-38, 150, 284
 crystalline, 41-49, 71-98, 150,
 382-391
 density, 38, 81, 113, 218, 301, 370-
 380, 391, 414, 472, 483, 547
 depth, surface layer, 113, 391
 designator, 288
 diameters, 288, 481
 dikes, 203
 disposal, see Fallout removal
 distribution, 204, 384, 427
 drainage discharge, 489
 drying, 445
 fall time, 220-230, 387
 fall trajectory, 191-201, 218-241,
 288
 see Fission products
 flow lines, 38
 fluffy, 36-38
 form, 392
 formation process, 111-114
 fraction remaining, 380, 416-420,
 474-489, 494
 fraction removed, see Fallout
 fused, 28-38, 56-60, 72-80, 85-117,
 165, 379-389, 417
 glassy-bead, grains in, 98, 223-251,
 380, 425
 groups, 228, 251, 305, 380
 hydrated crystal, 401, 428
 hydrous oxido, 418
 hydrous solid, 401, 428
 hygroscopic, 383-397
 identification methods, 70
 Impaction, 30, 48
 Initial deposit levels, 414, 471-
 472, 483, 490
 insoluble hydroxide, 402
Particle(s), fallout (Cont.)
 interactions in, see Chemical
 systems, Slurry
 ionic, 393
 irregular, 30-38, 41-62, 97, 157,
 383
 levels, see density
 liquid, see Sea water, Slurry
 magnetic, 481
 median diameter, 288, 481
 melted, 97, 114, 303
 metal oxides, 112
 see Mixture
 molar concentration, 400
 nonreactive, 420
 prewetted, 387, 401, 496
 purity, 40
 remaining, 391, 471, 485-489, 490
 removal, 380, 470-477, 481
 removal methods, see Methods
 residual, 471, 490
 retention, 7, 81-88, 340, 391, 401,
 471-491
 saturation level, 489
 silicates, 28, 38, 40, 45, 60, 70, 111,
 196, 208, 280, 304, 380, 384,
 471, 481
 size distribution, 384
 size effects, 480, 485
 slurry, 420
 smearing, 381-386
 solid, 8, 14, 28, 30, 45, 72-78, 97-
 108, 150, 301, 320
 solid phase, 98, 420
 soluble crystal, 392, 401
 source, see Radioactivity
 spheronit, 30-38, 59-60, 98-112,
 283, 380
 structure, 28, 48, 71
 surface density, 384, 404, 472

INDEX

- Particle(s), fallout (Cont.)
tagged, 480
thin section analysis, 71
transport, 402, 470
travel distance, 401, 480
unmelted, 417
vaporization, 8-42, 70-88, 114-138, 169, 261, 306, 308
velocity, 40, 204, 218, 283, 288, 287, 295, 340
voids, 80, 88
volume, solid phase, 401
- Pass, decontamination
exposure, 570
method-, 478, 570, *see* Cycle
multiple, 485, 504
speed, 478, 481
- Passive countermeasures, *see*
Shelters, Planning factors
- Pattern, isotonicity
center, 217, 239
contour, 227-241, 262-269, 290-300, 321-336, 349
idealized, 247, 258
variation, 471
- Paved surface decontamination, 466, 570
- Pay-loader, 598
- Perkins, J.F., 81
- Pestana, J.F., 400, 414
- Petrography, 28, 81, 69, 71
- Pettijohn, F.J., 81
- Phase, attack, 368
- Phenomena, detonation, 380-388
- Pick-up method, 472
- Pick-up truck, 508
- Pile-up method, 473; 475, 583
- Pit, drainage, 480, 504
- Planning, countermeasure, *see*
Planning factors
- Planning dose, criteria, 470
- Planning factors,
- Planning factors, (Cont.)
"acceptable" dose level, 470, 480
action options, 352-354, 363, 367-381, 513, 547, 570
affected areas, 363-369, 368
allowable dose, 356, 470, 480, 514, 521, 528, 532, 544
applied effort, 470-471
applicable countermeasures, 327, 354, 417, 532
attenuation, shielding, 81, 189-198, 322-324, 378
burst altitude, 210-237
calculations, 26, 67, 117, 188, 202-211, 216, 258, 305, 356, 470, 489, 514, 522, 528, 532, 544
contamination, *see* Surfaces,
Methods, Chemical systems
contamination reduction, 327, 354, 417, 470, 509
conversion data, 26, 67, 117, 188, 221
cost-effectiveness, 470
crew assembly, 539
crew, maximum exposure, 582-585, 581-579
criteria, 470
decay rate, fallout, 56, 80, 108, 167, 321, 329, 318, 330, 352, 360-386, 513
decontaminated area, 387, 588
decontamination method analysis, 586
"desired" dose, 470
dose rate, max linear
dose restriction, 470, 521, 534
see Effectiveness
see Efficiency
see Entry time
see Environmental effects
see Equipment
explosion phenomena, 15, 27, 65, 201, 324

INDEX

- Planning factors, (Cont.)
exposure dose, *see* Hazard
see Fallout; *see also*, Particles,
Radiactivity
feasibility, countermeasure, 204,
598; *see* Chemical systems
harbor detonation, 327-417, *see*
also Slurry
instrument response, 186, 198,
221, 324; *see also* Instruments
ionization rate, *see* Curves
land-area detonation, *see* Soil,
Surfaces, Methods
location, *see* Wind
mass correction, 324
minimum shelter stay, 324; *see*
also Shelters, Planning
meteorological effects, 79-84,
202, 350-362; *see also* Wind
operational estimates, 489
operational parameters, 553
organization program, 358
preventive measures, 350
priority, action, 356, 367, 369
protection aspects, 356, 370,
486, 547-549
"R" factor, 16, 128, 168
recovery feasibility, 365, 367,
369
recoverable facilities, 358-360
repair operations, 367
requirements, 470-548-549, 596
scheduled, 480, 547
shelter exit time, *see* Shelters
see Shielding
survival actions, 366, 371
target areas, 547
temperature effects, 117-121,
129, 148, 365
terrain, 156, 159, 195, 221, 322-
323
training program, 366
- Plowing method, 40, 308
Plumbbob, Operation, 75, 485, 507,
551
- Point-location analysis, 548
- Polymerization, 150
- Population distribution, *see*
Countermeasures
- Pooler, F., Jr., 203, 209
- Poppoff, I.G., 28, 31, 202
- Portable survey meter, *see*
Instruments
- Porter, R.F., 173
- Portland cement, 480
- Potential dose,
definition, 6, 354
- Precipitate, fallout, 401
- Present, R.D., 17, 188
- Pressure, *see* Cloud, Ionization,
Radiactivity
- Preventive countermeasure, 360
- Planning factors
- Priscilla, shot, 91
- Properties, fallout, *see* Fallout
- Property damage, 358, 368
- Protection factor, system, 356, 370
- Protection requirements, *see*
Planning factors
- Postattack period, 366; *see also*
Planning factors
- Pugh, G.E., 203, 207, 254, 392
- Pump, firehosing, 480

--Q--

- Quantity,
see Fallout
see Particles(s)
see Radiactivity

INDEX

--R--

Rabbit brush, 89
Rabbits, 74
Radep areas, 366, 358, 361, 364
Radio, see Instruments
Radiation, see Radioactivity
Radiation sickness, 354, 469
Radioactivity
 accumulated, 221, 351, 348
 amounts of elements, 15, 45, 72,
 114, 164, 304-308, 341-355,
 393, 401-408
 atoms, 8, 5
 back yard, 388
 colloid, 393, 400
 contributions, 195, 222, 351-357,
 455-494, 534, 555-559, 571, 587
 decontamination effects, 324-366,
 376-398
 deposition, 50, 118, 166, 218-288,
 284, 324-340, 384
 detector, see Instruments
 disintegration multipliers, 168
 exposure, see Hazard
 fraction remaining, 303, 450, 471,
 490
 fractional distribution, 205, 248,
 301-311
 gamma ray, 8-18, 24, 50-78, 159
 366-389, 469, 547-549
 Induced, 8, 99, 195, 221, 308, 391
 ionic elements, 8, 45, 72, 97, 385,
 395, 400, 471, 485, 484
 insoluble elements, 425, 460
 intensity, 10, 55, 109-207, 225-241,
 341-349, 534-544, 551-559
 long-lived elements, 371
 neutron capture, 8, 8, 15, 58
 neutron emission, 8, 59, 114, 189
 nuclides, 10-35, 50, 62-68, 106-110,
 387
 point source, 350

Radioactivity (Cont.)
 radiation, 15, 45, 72, 114, 181-188,
 184-207, 226-241, 304-337, 354,
 425, 485, 494, 503, 534, 555, 571,
 587
 refractory elements, 8, 14, 48, 58,
 74, 111, 112, 154
 residual radiation, 471, 489-490
 scavenging elements, 253
 sources, 5, 10, 99, 201-243, 201-
 332, 353-313, 549, 552, 561
 source geometry, see Cloud,
 fireball
 specific, 357, 464, 471
 vaporization, 8-48, 76-96, 114-188,
 189, 201, 306, 398
Radioelements, see Radioactivity
Radiography, 26, 81, 42, 69, 71
Radiological countermeasures, see
 Planning factors
Radionuclides, see Radioactivity
Radiotantalum particles, 481
Radishes, contaminated, 78
"Rad-safe" concept, 469
Rain, effects, 79-84, 380-382
Rainey, C.T., 72, 74
RAND distribution, 284
Raoult's law, 164, 165, 166
Rapp, R.R., 201, 305, 398, 399
Rate count, decay, 307
Rate, drying, 382
Rats, contaminated, 74
Reactions, see Chemical systems,
 fallout
Reagent film, 72
Recovery period, 351, 372, 548
 actions, 367, 529
 see Countermeasures
crew, see Methods
feasibility, see Planning factors
of industries, 363
Radep area, 366

INDEX

- Recovery period, (Cont.)
survival and, 802
teams, 804, 807
- Red Band, 808-809
- Redwing, Operation, 41
- Rehabilitation centers, 808
- Refammeter, R.F., 80
- Refractory elements, 8, 14, 48, 68,
74, 111, 118, 354
- Relative effectiveness, 870, 407
- Removal effectiveness, 10, 875-884,
420, 507, 509
- Removal, fallout, *see* Methods
- Removal, particle, *see* Decontamination
- Repair operations, 807
- Requirements, *see* Planning factors
- Rasouo operations, 802, 809
- Residential area decontamination,
804-806
- Residual mass, *see* Fallout
- Residual number, RN
combination, 814
components, major, 814-821
maximum, 820, 809
minimum, 809
ratio, 410-427
Requirements, 820
- Residuum radiation, *see* Radioactivity
- Resources, nonhuman, 800
- Response levels, 801
humans, 808
inanimate objects, 808
instruments, 150
- Retention, dose, *see* Planning
factors
- Roxford, W., 400
- Riley, Intensity, 210, 240
- Retention, particle, *see* Surfaces
- RN, residual number; *see* Planning
factors
- Ridge entry, cloud, 213, 312
- Rodents, *see* Biological system, 74
- Roentgen(s), *see* Dose, Ionization
definition, 8
r/hr, 822
- Rongelap Atoll, 2
- Romney, R.M., 72, 78, 79, 81, 84
- Rosenblum, I., 203
- Root decontamination, 80, 400-401;
see also Surfaces, Methods
- doughnuts, surfaces, 480, 504
- Runoff, stripwashing, 480, 491
- Rural area decontamination, 808
- 8-
- "8" Shot, 150
- Safety procedures, *see* Countermeasures, Planning factors
- Scrubbrush, 83, 87
- Salt crystals, 807
- Sam, D., 80, 100, 400, 414
- San Francisco Bay mud, 420
- Sandbags, 870
- Shovelblasting, 882
- Short, J.D., 80, 470, 478, 480, 480,
494, 500, 511, 501, 573, 580, 507
- Saturation level, *see* Particles
- Searden, R.M., 20
- Sealing system, model, 125-140, 802-
808, 808-809, 815-816, 810-814,
820
- Scheduling, *see* Planning factors
- Sehell, W.R., 101, 821, 888
- Sehorr, M.C., 28
- Schmidt, B.A., 201, 207, 210
- Sensitivity counter, *see* Instruments
- Sedapor method, motorized, 472-800
prime mover, 804
spillage, blade, 474, 485, 504
tractor, 480, 800
- Scrubbing method, 882

INDEX

- Non-water fallout, 203, 301-307, 408-410
characterization, 303
C-Level unit, 405, 408
components, 301-307
concentration, 303
contamination, 406
decontamination, 410, 450
residue, 72, 327
salt, 72, 327, 398
surface density, 402
surface interactions, 307, 408-409
Serial use, see Method(s)
Survivor center, survivor, 301-302
Set-up time, equipment, 508, 578, 582
Sowers, particle drainage, 409
Shallow water detonation, 417
Sheath, Shot, 85, 91
Shear effects, see Wind
Shelter
adequate, 307
blast, 308, 348-349
buried, 308
characterization, 348
communication, 308
design, 308, 348
effectiveness, 0, 31, 302, 308-309,
372, 320, 398
exit time, 308
"fallout", 308, 348
fireproof, 370
habitability, 308, 340
inadequate, 307, 348
requirements, 308, 340
see Residual number
Soaking, 348
see Shielding
Stay times, 322
ventilation, 348
Shielding,
attenuation, 31, 300, 308, 373, 382
countermeasure, see Shelter
- Shielding (Cont.)
effectiveness, 320
requirements, 304
terrain, 180, 185, 221, 328, 508
Ships, target, 0, 30, 381, 397
Shock phenomena
effects, 14, 114, 124, 133, 301, 308
wave energy, 118, 124, 340
waves, 114-115
Shovels, see Equipment, countermeasure
Shot(s); test
Apple, 78, 84, 91, 340
Baker, 40, 306, 405
Bravo, 1, 00, 200, 207
Diablo, 85, 340
Mot, 78, 340
Miko, 31
Priscilla, 01, 340
Jungle "B", 100, 200, 318
Smoky, 70, 84, 340
Tsun, 01, 340
Trinity, 1, 78
Jungle "U", 100, 324
Shrub, in decontamination, 500
Shock, radiation, 304, 480
Showerhead, in decontamination, 300
Surfaces
Silicates, see Particles
Simulated-fallout, 471, 480, 507
Single-particle analysis, 70
Sinker, G.C., 180, 186, 189, 198
Sintered soil grains, see Particles
Simple washing method, 400
skip loader, 480, 500
slurry
bulk solution, 482
interactions, 417, 485, 486
talc apatite in, 410
liquid phase, 482
mixing coefficient, 447
mixtures, 427, 480
mud, 423

INDEX

- Slurry (Cont.)
phase concentrations, 426
solid phase, 420-429, 460
surface interactions, 386
volume-to-area ratio, 428
- Smearing coefficient, 472, 496
- Smoky, shot, 73, 84, 91
- Soaps, 382
- Sod, lawn-cutting, 509
- Soil(s)
characteristics, 480, 504-505
clay, 388, 498, 504
clean, 489, 500
cohesion, 474, 507
concentrations on, 146, 148
contaminated, 504
coral, see Surfaces
see Crater
decontamination, see Methods
desert, 488
detonation, 303-309
dry, 504
excavated, 504
grass covered, 504
ideal, 185-188, 198, 474, 508
in fallout, see Particles
layer, 504
liquid, 147-151
loam, 490
loose, 508
mixture, 498, 500
moist, 504
properties, 386, 478, 504
removal of, 474, 504-507, 508
scrapping, 505
shear strength, 504
shrubs on, 509
sod, 509
spilled, 474
subsoil drainage, 480
surface layer, 478, 504
tagged, 480, 498, 507
- Soil(s) (Cont.)
tilted, 504
-type, 504
uniform, 474
wet, 504
- Solid particles in slurry, 429
- Solid-to-liquid mass ratio, 428
- Solution, decontaminating, 157, 401
- Soulen, J.R., 159, 163
- Source(s), fallout, see Cloud, Radioactivity
- Special clothing, crews, 486
- Speed(s), equipment, 496, 500, 508, 576
- Spillage, fallout, 474, 485, 504
- Spray, water, method
angle, 472, 486
chamber, 412, 498
high pressure, 472, 490
nozzle, 475
operating parameters, 475, 490-496
pattern, 490
- Spreading coefficient, particle removal, 472, 484
- Staging areas, survivor rescue, 361
- Steinberg, E.P., 17
- Stem, see Cloud
- Stetson, R.L., 78
- Stewart, K., 30, 59, 108
- Sthapitpanonda, P., 159, 163
- Stirrer method, 412
- Stokes' law, 380
- Stoneman, Camp, 470, 486, 488, 496, 504, 511
- Stream, water, method, 475, 476, 486-488, 498
- Street sweeper, motorized, 481, 500, 508, 574
- Stripping films, 71
- Strope, W.E., 187, 470, 484, 485, 491, 511, 540, 551

INDEX

Structure(s)

- destruction of, 361
 - particle-, 28, 48, 71; *see* Particles
 - shielding effectiveness of, 620
 - surfaces of, 401; *see* Surfaces
 - test device, 30, 48
 - undamaged, 361
- Stull, D.R., 120, 136, 159, 163
- Sublimation pressure, *see* Cloud, fireball
- Subsoil drainage, 489
- Supplies, countermeasure, 361, 365, 590
- Surface contributions, *see* Radioactivity
- ### Surface(s)
- Ambrose clay, 496, 504
 - asphaltic concrete, 414, 486
 - broomed, 489
 - building, 486, 490
 - burnt, 118, 132, 169, 380, 370, 398
 - carker-, 99, 109
 - chemical interactions, 375
 - clay, 496, 504
 - concrete, 481-494
 - condition, 489
 - contaminated, 16, 380, 418, 476
 - coral-, 31-38, 156, 234
 - decontaminated, 418
 - density, 384, 471
 - desert, *see* Soil(s)
 - deterioration, 476
 - drainage, 476
 - earth-, 340, 500
 - exposed, 380
 - fractional coverage of, 384-385
 - galvanized iron, 414
 - highway, 489
 - horizontal, 400, 494
 - irregular, 418
 - land type, 80, 485, 504, 585
- ### Surface(s) (Cont.)
- ledge, 404
 - liquid interface, 398
 - microdam, 481
 - mass density, 384
 - micro porosity of, 407
 - most difficult, 508
 - orientation of, 381
 - outdoor, 491
 - painted, 491
 - paved, 480, 570
 - Portland cement, 486, 494
 - reactions with, 375
 - removal of, 486, 585
 - road, 481
 - roof-, washdown, 490
 - roofing, 490
 - roughness of, 486, 489
 - saturation level of, 381, 385, 472
 - sidewalks, 486, 570
 - smoothness of, 489
 - tension, 118
 - types, 407
 - unpaved, 587
 - vertical, 491
 - water angle on, 486
 - window frame, 494

Surface-method combination, 479, 489, 584

Surface-removal methods, 486

Surprise attack, 360

Survival

- initial, 366, 371
 - elements, 364
 - Gray Bolt, 360
 - problems, 360-366, 268-271
 - population, 360
 - rate, 369-382
 - resources, 347

Sweeping method

- hand, 481
 - motorized, 382, 479, 484

liv

INDEX

Synthetic fallout, 400, 471-480, 507
System protection factor, 370

--T--

Tagged soil, 485, 496, 507
Tantalum particles, 481
Tar and gravel road, 400, 401
Target
 analysis, 547, 586, 597
 complex, 351, 547, 580
 distribution, 355
 materials, 476
 prime-, 582
 -ship, 507
 spatial, 585
 -unit, 547, 586, 587
Team, hose, 490
Team, nozzle, 489, 490
Techniques, removal
 manual, 484
 motorized, 472-508
Temperature(s), see Ionization,
 Fallout
Tennant vacuum sweeper, 500, 508
Terrain shielding, 156, 195, 221, 320
Tesla, Shot, 91
Test series, see Field tests, Oper-
 ations(s), Shot(s)
Thermodynamic equilibrium, 597
Thermodynamic model, 87, 100, 110,
 124, 187, 210
Thermonuclear reactions, 26-27
Thin section analysis, 71
Thorntithwaite, C.W., 80
Thyroid, 74
Tilled soil, 504
Time
 arrival, fallout, 74, 81, 183, 214,
 311, 386, 370, 518
 breakaway, 117
 deposition, fallout, 216, 222, 513

Time, (Cont.)
 condensation, 87, 106, 300
 control, 407
 critical, 514, 547-549
 entry, 522, 537, 538, 553
 decontamination start, 535, 553
 fall, particle, 220, 230, 387, 518
 ionization, 0, 13, 49, 62, 519
 measurement, 76, 81
 operating, 508
 reference, 116
 relative, 370
 rise, 232
 scale, 504
 set-up, 508, 578, 582
 shelter exit, 522
 shelter stay, 365, 365, 522, 548
 thermal balance, 116
 Working, 386, 508
Tissue, 7, 78
Tower-mounted devices, 38-49, 72-
 84, 91-113, 151-158, 297, 324
Tracer, fission product, 58, 414
Toroidal circulation in cloud, 215, 230,
 312
Tractor
 scraper, 480
 wheel, 500
Training
 manpower, 308
 program, 508
Trajectory, particle-fall, 201, 241,
 288, 491
Transattack period, 360, 364, 366
Transport, see Particles
Tripolyphosphate, 407, 412
Trinity Shot, 1, 78
Turbulence, 118
Truck
 pay-loader, 508
 pick-up, 508

INDEX

--U--

Unpaved area recovery, 587

"U" Shot, 186, 324

Underground,

detonation, 77, 185, 485

shelter, 361

Unit-average analysis, 549

Unmelted particles, 303

Unpaved surfaces, 80

Unshielded operations, 364

Updrafts, 184

Upshot, Operation, 72, 74

Uptake, see Hazard, Ingestion

--V--

Vacuum cleaning method, 382, 472, 484, 500

Van Horn, W.H., 470, 476, 485, 486, 494, 500, 511

Vapor-liquid interface, 395

Vaporization, 3-42, 76-98, 114-133,

109, 251, 306, 309

process, 3-42, 76-98, 114-133,

158-169, 251, 300-303

Ventilation, 373

Vertical surfaces, 491

Volatile elements, 8, 40, 60, 70, 112

Volume, fallout drop, 72

--W--

Wahl, A.C., 26

Wallace, N.R., 28, 31

War, nuclear, 1, 340

Warhead, bomb

missile, 4, 381, 391, 400

Warning, attack, 368

Washing method, 451, 400-401

Waste disposal, see Fallout removal

Water

bulk, 330, 475

countermeasure use, 302, 530, 596

expenditure, 485

-flow, volume, 451, 475

-flushing, 472-494

hydrants, available, 539

jet, 114, 476

-lobbing, 485-491

pressure, 486

sea water, synthetic, 392, 400

shallow, 327, 417

shelters, in, 355, 367

source, availability, 539

spray angle, 472, 486

spray chamber, 494

runoff, 490

vapor, 302

-washing, simple, 496

Water stream,

kinetic power, 407, 476

surface impingement, 475, 489

volume, 330, 475

Wayne streetsweeper, 500, 539

Weapon, see Yield

Weapons tests, see Field tests,

Operation(s), Shot(s)

Wet methods, 382, 472, 485

Weathering, 78, 381

Well-crystal (WC) counter, 58

Wheat, 70, 84-87, 343

Wheel barrow, 500, 500

Wheel tractor, 500

Width, equipment pass, 473

Width, Grey Belt, 300

Best Available Copy

INDEX

Wind

crosswind area, 244
direction effects, 202, 237, 300,
382
downwind location, 9, 63-91, 112,
105, 217, 227-245, 276-304,
362-370
shear, 228, 242, 290, 301
upwind location, 360
vector, 81, 218
velocity, 80, 202, 205, 218, 235,
242, 292

Wittman, J.P., 38

Work-effort, see Effort

World War II, 361

WSEG, 293, 294, 297

--X--

X-rays, 4, 8, 204

--Y--

Yield, weapon

attack level, 366-367
effects, 8, 27, 45, 56, 62, 67,
87, 101-115, 135-139, 157,
165, 183, 202-204, 230, 305,
327, 397, 355-366, 381, 392
Independent, 17, 67, 107

--Z--

Zone, Black, 350

Zigman, P., 56, 180, 195, 223

Best Available Copy

**STANFORD
RESEARCH
INSTITUTE**

**MENLO PARK
CALIFORNIA**

Regional Offices and Laboratories

Southern California Laboratories
820 Mission Street
South Pasadena, California

Washington Office
200 17th Street, N.W.
Washington 3, D.C.

New York Office
270 Park Avenue, Room 1770
New York 17, New York

Detroit Office
The Stevens Building
1025 East Maple Road
Birmingham, Michigan

European Office
Polikantstrasse 37
Zurich 1, Switzerland

Representatives

Honolulu, Hawaii
Finance Factors Building
195 South King Street
Honolulu, Hawaii

London, Ontario, Canada
88 Wychwood Park
London 14, Ontario, Canada

London, England
15 Abbotbury Close
London W. 14, England

Milan, Italy
Via Macedonio Melloni 40
Milano, Italy

Tokyo, Japan
911 Iino Building
22, 2-chome, Uchisaiwai-cho, Chiyoda-ku
Tokyo, Japan

Best Available Copy